

28th Benelux Meeting
on
Systems and Control

March 16 – 18, 2009

Spa, Belgium

Book of Abstracts

Welcome

It is a pleasure to welcoming you to the *28th Benelux Meeting on Systems and Control*, at the "Domain Sol Cress" in Spa, Belgium.

The secretariat of the conference has been ensured by Céline Dizier and Michèle Delville from the A.I.M. (Association des Ingénieurs de Montefiore). They are gratefully acknowledged for their first-class support.

The scientific organization of the conference would not have been possible without the hard work of Michel Journée (conference website, program, and book of abstracts) and Alain Sarlette (program). They are gratefully acknowledged for a full commitment in the midst of writing their PhD thesis.

The meeting is financially supported by the following organizations :

- FRS-FNRS (Belgian National Fund for Scientific Research)
- Belgian Programme on Interuniversity Attraction Poles DYSCO (Dynamical Systems, Control, and Optimization), initiated by the Belgian State, Science Policy Office.

Rodolphe Sepulchre and Michel Gevers
Conference organizers
March 2009

Aim

The aim of the Benelux Meeting is to promote research activities and to enhance cooperation between researchers in Systems and Control. This is the twenty-eighth in a series of annual conferences that are held alternately in Belgium and The Netherlands.

Overview of the Scientific Program

1. Plenary lectures by invited speakers

Navin Khaneja (Harvard University, USA)

Control of ensembles

René Vidal (Johns Hopkins University, USA)

Binet-Cauchy Kernels for the Recognition of Visual Dynamics

2. Mini course

Jorge Cortés and *Sonia Martínez* (University of California at San Diego, USA)

Distributed control of Robotic Networks

3. Contributed short lectures, see the list of sessions for the titles and authors of these lectures.

Scientific Committee

The Scientific Committee of the 28th Benelux Meeting consists of

P.-A. Absil (Univ. catholique de Louvain), D. Aeyels (Univ. Gent), V. Blondel (Univ. catholique de Louvain), O. Bosgra (Technische Univ. Delft), G. De Cooman (Univ. Gent), M. Gevers (Univ. catholique de Louvain), M. Kinnaert (Univ. libre de Bruxelles), P. van den Hof (Technische Univ. Delft), G. Meinsma (Univ. Twente), B. de Moor (Katholieke Univ. Leuven), H. Nijmeijer (Technische Univ. Eindhoven), R. Pintelon (Vrije Univ. Brussel), A. van der Schaft (Rijksuniv. Groningen), J. Scherpen (Rijksuniv. Groningen), J. Schoukens (Vrije Univ. Brussel), M. Steinbuch (Technische Univ. Eindhoven), S. Stramigioli (Univ. Twente), A. Stoorvogel (Univ. Twente), P. Van Dooren (Univ. catholique de Louvain), G. van Straten (Wageningen Univ.), R. Sepulchre (Univ. de Liège), H. Stigter (Wageningen Univ.), A. Vande Wouwer (Faculté Polytechnique de Mons), L. Wehenkel (Univ. de Liège), J. Winkin (Facultés Univ. Notre-Dame de la Paix, Namur), J. Willems (Katholieke Univ. Leuven), S. Weiland (Technische Univ. Eindhoven).

Instructions for speakers

For a contributed lecture the available time is 25 minutes. Please leave a few minutes of this period for discussion and room changes and adhere to the indicated schedule. In each room beamers will be available. Computers are not provided.

Best junior presentation award

Continuing a tradition begun in 1996, the Benelux meeting will close with the announcement of the winner of the Best Junior Presentation Award. This award is given for the best presentation at the meeting given by a junior researcher (*i.e.*, someone working towards a PhD degree). The award is specifically given for quality of presentation rather than quality of research, which is judged in a different way. At the meeting, the chairs of sessions will ask three volunteers in the audience to fill out an evaluation form. After the session, the evaluation forms will be collected by the Prize Commissioners who will then compute a ranking. The winner will be announced on Wednesday, March 18, immediately after the final lectures of the meeting and he or she will be presented with the award, which consists of

a trophy that may be kept for one year and a certificate. The evaluation forms of each presentation will be returned to the junior researcher who gave the presentation. The Prize Commissioners are Joseph Winkin (University of Namur-FUNDP), and Peter Heuberger (Delft University of Technology) . The organizing committee is counting on the cooperation of the participants to make this contest a success.

Conference location

The conference takes place in the Solcress seminar center, at walking distance from the center of the city of Spa located in the Belgian Ardennes. The Domain Sol Cress is situated at the edge of a 1300 hectar forest. The town of Spa is only 10 minutes away by foot or 1 minute by funicular (railway). The Spa's new Thermal Baths are just up the road.

Domain Sol Cress
Spaloumont, 5
B-4900 Spa
Belgique

Website

An *electronic version* of the Book of Abstracts can be downloaded from the Benelux Meeting web site :
[http ://www.montefiore.ulg.ac.be/~beneluxmeeting09/](http://www.montefiore.ulg.ac.be/~beneluxmeeting09/)

Part 1

Programmatic Table of Contents

Monday, March 16, 2009

Pierre le Grand
Welcome and opening

Chair: Rodolphe Sepulchre 11.25–11.30

Plenary Pierre le Grand
Binet-Cauchy Kernels for the Recognition of Visual Dynamics
René Vidal (Johns Hopkins University, USA)
Chair: Paul Van Dooren 11.30–12.30

Binet-Cauchy Kernels for the Recognition of Visual Dynamics 179
René Vidal (Johns Hopkins University, USA)

MoA01 Pierre le Grand
Identification 1
Chair: Paul Van den Hof 14.00–16.30

MoA01-1 14.00–14.25
Identification of a distillation column for PLC control purposes 21
B. Huyck KaHo Sint-Lieven
F. Logist Katholieke Universiteit Leuven
B. De Moor Katholieke Universiteit Leuven
J. De Brabanter, Jan Van Impe

MoA01-2 14.25–14.50
Effects of Overlapping and Windowing on the Estimation of the Frequency Response of a System using White Noise 22
Dr W. D. Widanage Vrije Universiteit of Brussels
Professor J. L. Douce University of Warwick
Professor K. R. Godfrey University of Warwick

MoA01-3 14.50–15.15
Linear regressive realizations of LTI state space models : an advection-reaction case study 23
Karel Keesman Wageningen University
Nurulhuda Khairudin Wageningen University

MoA01-4 15.15–15.40
System Identification of a Spindle with Active Magnetic Bearings 24
Ir. R.S. Blom Delft University of Technology
Prof. dr. ir. P.M.J. Van den Hof Delft University of Technology
Dr.ir. H.H. Langen Delft University of Technology
Prof. ir. R.H. Munnig Schmidt

MoA01-5 15.40–16.05
Towards Automatic Control of Scanning Transmission Electron Microscopes : System Identification Issues 25
Dr Arturo Tejada Delft University of Technology

MoA01-6 16.05–16.30
Estimating a Power-Scalable Linearized Model for Amplifiers 26
Koen Vandermot Vrije Universiteit Brussel
Yves Rolain Vrije Universiteit Brussel
Gerd Vandersteen Vrije Universiteit Brussel
Rik Pintelon

MoA02 Source de la Reine
Synchronization and clustering
Chair: 14.00–16.30

MoA02-1 14.00–14.25
A synchronization criterion for delay-coupled systems based on absolute stability 27
Toshiki Oguchi Tokyo Metropolitan University
Henk Nijmeijer Eindhoven University of Technology
Noriko Tanaka Tokyo Metropolitan University

MoA02-2 14.25–14.50
Recent advances and open questions on Peskin model for coupled oscillators 28
Alexandre Mauroy University of Liège
Rodolphe Sepulchre University of Liège

MoA02-3 14.50–15.15
A first-order phase transition in a multi-dimensional clustering model 29
Filip De Smet Ghent University
Dirk Aeyels Ghent University

MoA02-4 15.15–15.40
Semi-passivity and synchronization of diffusively coupled neuronal oscillators 30
Erik Steur Eindhoven University of Technology
Ivan Tyukin University of Leicester
Henk Nijmeijer Eindhoven University of Technology

MoA02-5 15.40–16.05
On the influence of positive and negative feedback loops on the phase response curve of biological oscillators. 31
Pierre Sacré University of Liège
Rodolphe Sepulchre University of Liège

MoA02-6 16.05–16.30
Bursting modeling in dopaminergic neurons 32
G. Drion University of Liège
R.Sepulchre University of Liège
V.Seutin University of Liège

MoA03 Wellington
Control for teleoperation
Chair: Thomas Delwiche 14.00–16.30

MoA03-1 14.00–14.25
Haptic Feedback in Telesurgery 33
D. van Raaij Eindhoven University of Technology
M. Steinbuch Eindhoven University of Technology

MoA03-2 **14.25–14.50**
User Adapted Control of Force Feedback Teleoperators : Evaluation and Robustness Analysis 34
 L. Barbé University of Strasbourg
 B. Bayle University of Strasbourg
 E. Laroche University of Strasbourg
 M. de Mathelin

MoA03-3 **14.50–15.15**
A Passivity Study of the Classical Position-Force Teleoperation controller 35
 B. Willaert K.U.Leuven, Belgium
 B. Corteville
 D. Reynaerts
 H. Van Brussel, E.B. Vander Poorten

MoA03-4 **15.15–15.40**
Robust 4-channel Teleoperation Controller Design 36
 E. B. Vander Poorten Katholieke Universiteit Leuven
 D. Reynaerts Katholieke Universiteit Leuven
 H. Van Brussel Katholieke Universiteit Leuven
 T. Kanno and Y. Yokokohji

MoA03-5 **15.40–16.05**
Optimization of a static output feedback controller for teleoperation 37
 Thomas Delwiche Université Libre de Bruxelles
 Samir Aberkane Université Henri Poincaré
 Michel Kinnaert Université Libre de Bruxelles
 Laurent Catoire, Serge Torfs

MoA03-6 **16.05–16.30**
Passivity and Transparency in Bilateral Telemanipulation 38
 Ir. M.C.J. Franken University of Twente
 Prof.dr.ir. S. Stramigioli University of Twente

MoA04	Pouhon Pia
Estimation for biochemical processes	
Chair: Alain Vande Wouwer	14.00–16.30

MoA04-1 **14.00–14.25**
Stabilizing the baseline current of a microbial fuel cell-based biosensor 39
 Nienke Stein Wetsus, centre of excellence for sustainable water technology
 Hubertus V.M. Hamelers Wageningen University
 Hans Stigter Wageningen University
 Cees Buisman

MoA04-2 **14.25–14.50**
Identification of Biochemical Reaction Systems using a Dissipative Observer 40
 Dirk Fey University of Strathclyde
 Eric Bullinger University of Strathclyde

MoA04-3 **14.50–15.15**
Input and state estimation of a microalgae culture using a linear quasi unknown input observer 41
 E. Rocha-Cózatl Faculté Polytechnique de Mons
 A. Vande Wouwer Faculté Polytechnique de Mons

MoA04-4 **15.15–15.40**
On the comparison of OED/PE strategies for the accurate identification of microbial kinetics 42
 Eva Van Derlinden KULeuven
 Kristel Bernaerts KULeuven
 Jan F. Van Impe KULeuven

MoA04-5 **15.40–16.05**
Stochastic Observers for Industrial Seeded Batch Crystallization Processes 43
 A. Mesbah Delft University of Technology
 I. Mora Moreno Delft University of Technology
 A. Huesman Delft University of Technology
 P. Van den Hof

MoA04-6 **16.05–16.30**
Model analysis for individual-based modelling 44
 A.J. Verhulst Katholieke Universiteit Leuven
 K. Bernaerts Katholieke Universiteit Leuven
 J.F.M. Van Impe Katholieke Universiteit Leuven

MoA05	Groesbeeck
Computational methods	
Chair: Wim Michiels	14.00–16.30

MoA05-1 **14.00–14.25**
Nonlinear projection on manifolds 45
 Victor Onclinx Université catholique de Louvain
 Michel Verleysen Université catholique de Louvain
 Vincent Wertz Université catholique de Louvain

MoA05-2 **14.25–14.50**
Fitting Curves on Riemannian Manifolds Using Energy Minimization 46
 Chafik Samir Université catholique de Louvain
 Pierre-Antoine Absil Université catholique de Louvain
 Anuj Srivastava
 Erik Klassen

MoA05-3 **14.50–15.15**
Algorithms for nonsmooth optimization on manifolds 47
 C. Lageman Université de Liège
 R. Sepulchre Université de Liège

MoA05-4 **15.15–15.40**
*Optimal H₂-design with the smoothed spectral abs-
 cissa* 48
 Joris Vanbiervliet KULeuven
 Wim Michiels KULeuven
 Stefan Vandewalle KULeuven

MoA05-5 **15.40–16.05**
Computing H-infinity norm of time-delay systems 49
 Suat Gumussoy K. U. Leuven
 Wim Michiels K. U. Leuven

MoA05-6 **16.05–16.30**
Robust stability assessment in high-speed milling 50
 Niels van Dijk Eindhoven University of Technology
 Nathan van de Wouw Eindhoven University of Technology
 Henk Nijmeijer Eindhoven University of Technology

MoB01	Pierre le Grand
Model reduction	
Chair: Pierre-Antoine Absil	17.00–18.40

MoB01-1 17.00–17.25

Model Reduction and Controller Synthesis for L2 Systems 51
 Mark Mutsaers Eindhoven University of Technology
 Siep Weiland Eindhoven University of Technology

MoB01-2 17.25–17.50

Model reduction for Lur'e type systems 52
 Bart Besselink Eindhoven University of Technology
 Nathan van de Wouw Eindhoven University of Technology
 Henk Nijmeijer Eindhoven University of Technology

MoB01-3 17.50–18.15

Nonlinear model approximation using block structured models 53
 Omar Naeem Technische Universiteit Delft
 A.E.M. Huesman Technische Universiteit Delft
 O. H. Bosgra Technische Universiteit Delft

MoB02	Source de la Reine
Model-free control	
Chair: Vincent Wertz	17.00–18.40

MoB02-1 17.00–17.25

Inferring bounds on the performance of a control policy from a sample of one-step system transitions . . . 54
 Raphael Fonteneau University of Liège
 Susan Murphy University of Michigan
 Damien Ernst University of Liège
 Louis Wehenkel

MoB02-2 17.25–17.50

Fixed Structure Controller Synthesis Using Non-Parametric Plant 55
 Irmak Aladagli Technische Universiteit Eindhoven
 Arjen den Hamer Technische Universiteit Eindhoven
 Maarten Steinbuch Technische Universiteit Eindhoven
 Georgo Angelis

MoB02-3 17.50–18.15

Adaptive extremum-seeking control of fed-batch cultures of micro-organisms exhibiting overflow metabolism 56
 L. Dewasme Faculté Polytechnique de Mons
 A. Vande Wouwer Faculté Polytechnique de Mons
 B. Srinivasan Ecole Polytechnique de Montréal
 M. Perrier

MoB02-4 18.15–18.40

Model-free Optimal Control Synthesis 57
 Arjen den Hamer Eindhoven University of Technology
 Siep Weiland Eindhoven University of Technology
 Maarten Steinbuch Eindhoven University of Technology

MoB03	Wellington
Fault detection applications	
Chair: Jan Van Impe	17.00–18.40

MoB03-1 17.00–17.25

Lazy online batch-end quality estimation : is less more? 58
 Geert Gins Katholieke Universiteit Leuven
 Jef Vanlaer Katholieke Universiteit Leuven
 Jan F.M. Van Impe Katholieke Universiteit Leuven

MoB03-2 17.25–17.50

Fault detection in a biochemical fed-batch process . . . 59
 Jef Vanlaer K.U.Leuven
 Geert Gins K.U.Leuven
 Jan F.M. Van Impe K.U.Leuven

MoB03-3 17.50–18.15

A control system for suppression of magnetic islands in a fusion plasma 60
 Bart Hennen FOM-Institute for Plasma Physics Rijnhuizen
 Dr. E. Westerhof FOM-Institute for Plasma Physics Rijnhuizen
 Dr. Ir. P.W.J.M. Nuij Technische Universiteit Eindhoven
 Dr. M.R. de Baar, Prof. Dr. Ir. M. Steinbuch

MoB03-4 18.15–18.40

Detection and isolation of sensor faults in induction machines 61
 Manuel Gálvez Université Libre de Bruxelles
 Michel Kinnaert Université Libre de Bruxelles

MoB04	Pouhon Pia
Humanoid robotics	
Chair: Philippe Lefèvre	17.00–18.40

MoB04-1 17.00–17.25

Motion control of the Twente Humanoid Head . . . 62
 L.C. Visser University of Twente
 R. Carloni University of Twente
 S. Stramigioli University of Twente

MoB04-2 17.25–17.50

A gaze saccade model based on separate head and gaze controllers. 63
 Pierre Daye UCLouvain
 Lance Optican National Institut of Health
 Philippe Lefèvre UCLouvain
 Gunnar Blohm, Queens University/CompNeurosci Lab,
 blohm@biomed.queensu.ca

MoB04-3 17.50–18.15

Motor commands are optimized in the gravity field . . . 64
 Frédéric Crevecoeur Université catholique de Louvain
 Jean-Louis Thonnard Université catholique de Louvain
 Philippe Lefèvre Université catholique de Louvain

MoB04-4 18.15–18.40

Control of walking robots using virtual springs . . . 65
 Gijs van Oort University of Twente
 Stefano Stramigioli University of Twente

MoB05	Groesbeeck
Distributed control	
Chair: Dragan Kostic	17.00–18.40

MoB05-1 17.00–17.25

A Jacobi algorithm for distributed model predictive control of dynamically coupled systems 66
 Dang Doan Delft University of Technology
 Tamas Keviczky Delft University of Technology
 Bart De Schutter Delft University of Technology
 Ion Necoara, Moritz Diehl

MoB05-2 17.25–17.50

An application of distributed control : the segmented primary mirror for the European Extremely Large Telescope 67

Christian Bastin University of Liège
Alain Sarlette University of Liège
Rodolphe Sepulchre University of Liège
Martin Dimmler, Toomas Erm, Babak Sedghi, Bertrand Bauvir

MoB05-3 17.50–18.15

Modeling and Control of Inkjet Printhead 68

Mohammed Ezzeldin Technische Universiteit Eindhoven
Dr. A. Jokic Technische Universiteit Eindhoven
Prof.dr.ir. P.P.J. van den Bosch Technische Universiteit Eindhoven

MoB05-4 18.15–18.40

A comparison between different state estimation methods in a nonlinear distributed parameter system 69

C. Retamal Université Libre de Bruxelles
A. Vande Wouwer Faculté Polytechnique de Mons
M. Kinnaert Université Libre de Bruxelles
C. Vilas

Tuesday, March 17, 2009

TuA01	Pierre le Grand
Stochastic estimation and decision making	
Chair:	8.30–10.35

TuA01-1 8.30–8.55

Risk-aware sequential decision making and dynamic programming 70

Boris Defourny University of Liège
Damien Ernst University of Liège
Louis Wehenkel University of Liège

TuA01-2 8.55–9.20

Estimating distributions from censored microbiological contamination data for use in quantitative risk assessment 71

P. Busschaert Katholieke Universiteit Leuven
A.H. Geeraerd Katholieke Universiteit Leuven
J.F.M. Van Impe Katholieke Universiteit Leuven
M. Uyttendaele

TuA01-3 9.20–9.45

The Kalman Filter applied to Hydrologic Systems 72

ir. Douglas Plaza University of Ghent
Prof.Dr.ir. Robin De Keyser Ghent University - Faculty of Engineering
Dr.ir. Gabriëlle De Lannoy University of Ghent
Prof.Dr.ir. Valentijn Pauwels

TuA01-4 9.45–10.10

Multi-armed bandit based decision making for cognitive radio 73

Wassim Jouini SUPELEC
Damien Ernst University of Liège
Christophe Moy SUPELEC
Jacques Palicot

TuA01-5 10.10–10.35

Formal Verification and Improved Analysis Tools for Agent-Based Simulations 74

Dr. Arturo Tejada Ruiz Delft University of Technology

TuA02	Source de la Reine
Nonlinear control 1	
Chair: Alain Sarlette	8.30–10.35

TuA02-1 8.30–8.55

Passivity-based tracking control of port-Hamiltonian mechanical systems with only position measurements 75

D.A. Dirks University of Groningen
J.M.A. Scherpen University of Groningen

TuA02-2 8.55–9.20

Feedback stabilisation of a pool-boiling system 76

Rob van Gils Technische Universiteit Eindhoven
Michel Speetjens Technische Universiteit Eindhoven
Henk Nijmeijer Technische Universiteit Eindhoven

- TuA02-3** **9.20–9.45**
Stabilization via positive invariance for linear distributed parameter systems with constraints on both control and its rate 77
 B. Abouzaid CESAME, Université catholique de Louvain, LLN, Belgium
 V. Wertz CESAME, Université catholique de Louvain, LLN, Belgium
 M. E. Achhab Université Chouaib Doukkali, Morocco

- TuA02-4** **9.45–10.10**
Control of the exothermic CSTR : the power-shaping approach 78
 Audrey Favache Université catholique de Louvain
 Denis Dochain Université catholique de Louvain

- TuA02-5** **10.10–10.35**
A Study of Stability Conditions for Haptics 79
 I. Polat Technische Universiteit Delft
 Prof. Dr. C.W. Scherer Technische Universiteit Delft

TuA03	Wellington
Advanced actuation and sensing	
Chair: Herman Ramon	8.30–10.35

- TuA03-1** **8.30–8.55**
Automatic control of microscope alignment 80
 Dr Ir S. W. van der Hoeven Technische Universiteit Delft

- TuA03-2** **8.55–9.20**
Characterization of hysteresis within magnetic electron lenses 81
 P.J. van Bree Eindhoven University of Technology
 C.M.M. van Lierop Eindhoven University of Technology
 P.P.J. van den Bosch Eindhoven University of Technology

- TuA03-3** **9.20–9.45**
Pneumatic circuit assessment in Pneumatic Artificial Muscle applications 82
 Tri Vo-Minh KULeuven
 Herman Ramon KULeuven
 Hendrik Van Brussel KULeuven

- TuA03-4** **9.45–10.10**
Load Dynamics in Piezoelectric Actuation 83
 J.R. van Hulzen Delft University of Technology
 P.M.J. Van den Hof Delft University of Technology
 G. Schitter Delft University of Technology
 J. van Eijk

- TuA03-5** **10.10–10.35**
Control of a moving magnet planar actuator at industrial specifications 84
 J. Achterberg Technische Universiteit Eindhoven
 C.M.M. van Lierop Technische Universiteit Eindhoven
 P.P.J. van den Bosch Technische Universiteit Eindhoven

TuA04	Pouhon Pia
Biochemical processes	
Chair: Hans Stigter	8.30–10.35

- TuA04-1** **8.30–8.55**
Input design for PWA biological cell systems 85
 Dirk Vries Delft University of Technology
 Peter Verheijen Delft University of Technology
 Arjan den Dekker Delft University of Technology

- TuA04-2** **8.55–9.20**
A systematic procedure to develop dynamic models of bioprocesses 86
 J. Mailier Faculté Polytechnique de Mons
 A. Vande Wouwer Faculté Polytechnique de Mons

- TuA04-3** **9.20–9.45**
Macroscopic modeling as a tool for gaining insight in AI-2 dynamics of Salmonella Typhimurium 87
 Astrid M. Cappuyns K.U.Leuven
 Kristel Bernaerts K.U.Leuven
 Jan F. Van Impe K.U.Leuven
 Sigrid C. De Keersmaecker, Jos Vanderleyden

- TuA04-4** **9.45–10.10**
Three ways to do temperature reconstruction based on Bivalve-proxy information 88
 Maite Bauwens Vrij Universiteit Brussel
 Henrik Ohlsson Linköping University
 Kurt Barbé Vrij Universiteit Brussel
 Johan Schoukens, Frank Dehairs

- TuA04-5** **10.10–10.35**
Quantitative characterization of Streptomyces lividans batch fermentations 89
 P.-J. D'Huys Katholieke Universiteit Leuven
 K. Bernaerts Katholieke Universiteit Leuven
 J.F.M. Van Impe Katholieke Universiteit Leuven
 J. Anné

TuA05	Groesbeeck
Control in networks	
Chair: Bram de Jager	8.30–10.35

- TuA05-1** **8.30–8.55**
A simplified model for urban traffic network control 90
 S. Lin Delft University of Technology
 B. De Schutter Delft University of Technology
 Y. Xi Shanghai Jiao Tong University

- TuA05-2** **8.55–9.20**
Distributed control of urban traffic networks using hybrid models 91
 Ir. Nicolae Marinica Universiteit Gent
 Dr. Ir. Rene Boel Universiteit Gent

- TuA05-3** **9.20–9.45**
Optimal control in hybrid vehicles using route information 92
 Thijs van Keulen Technische Universiteit Eindhoven
 Bram de Jager Technische Universiteit Eindhoven
 Maarten Steinbuch Technische Universiteit Eindhoven

- TuA05-4** **9.45–10.10**
Tracking in WiMAX Networks depending on RSS-based measurements 93
 Mussa Bshara Vrije Universiteit Brussel
 Leo Van Biesen Vrije Universiteit Brussel

TuA05-5 **10.10–10.35**
Stability Analysis of Networked Control Systems using a Switched Linear Systems Approach 94
 M.C.F. Donkers Eindhoven University of Technology
 L. Hetel Ecole Centrale de Lille
 W.P.M.H. Heemels Eindhoven University of Technology
 N. v.d. Wouw, M. Steinbuch

Mini Course **Pierre le Grand**
Distributed control of Robotic Networks
Jorge Cortés and Sonia Martínez
(University of California at San Diego, USA)
Chair: Dirk Aeyels **11.00–12.30**

Distributed control of Robotic Networks 193
 Jorge Cortés and Sonia Martínez (University of California at San Diego, USA)

Pierre le Grand
DISC PhD Thesis Award 2008 and DISC Certificates
Chair: Paul Van den Hof **14.00–14.15**

Mini Course **Pierre le Grand**
Distributed control of Robotic Networks
Jorge Cortés and Sonia Martínez
(University of California at San Diego, USA)
Chair: Dirk Aeyels **14.15–15.45**

Distributed control of Robotic Networks 213
 Jorge Cortés and Sonia Martínez (University of California at San Diego, USA)

TuB01 **Pierre le Grand**
Modeling, simulation and control of distributed parameter systems
Chair: Joseph Winkin **16.15–18.45**

TuB01-1 **16.15–16.40**
Spatial discretization of a 1D Euler-Bernoulli beam model 95
 T. Voss Rijksuniversiteit Groningen
 J.M.A. Scherpen Rijksuniversiteit Groningen

TuB01-2 **16.40–17.05**
Model based optimisation of tubular reactors for the production of low-density polyethylene. 96
 Peter M.M. Van Erdeghem Katholieke Universiteit Leuven
 Filip Logist Katholieke Universiteit Leuven
 Jan F. Van Impe Katholieke Universiteit Leuven

TuB01-3 **17.05–17.30**
Modeling and Validation of the parameters of a quad cable for DSL applications 97
 Wim Foubert Vrije Universiteit Brussel
 Carine Neus Vrije Universiteit Brussel
 Leo Van Biesen Vrije Universiteit Brussel
 Yves Rolain

TuB01-4 **17.30–17.55**
Model based kinetics estimation for crystallization processes 98
 J.A.W.Visser Technische Universiteit Eindhoven
 S.Weiland Technische Universiteit Eindhoven
 T.Backx Technische Universiteit Eindhoven

TuB01-5 **17.55–18.20**
Compartmental model of a bubble column 99
 S. Djordjevic Delft University of Technology
 P.M.J. Van den Hof Delft University of Technology
 O.H. Bosgra Delft University of Technology
 D. Jeltsema

TuB01-6 **18.20–18.45**
Modeling and simulating the sawtooth instability in Nuclear Fusion 100
 Ir. G. Witvoet Technische Universiteit Eindhoven
 Dr. E. Westerhof FOM
 Prof.dr.ir. M. Steinbuch Technische Universiteit Eindhoven
 Dr.ir. N.J. Doelman

TuB02 **Source de la Reine**
Nonlinear control 2
Chair: **16.15–18.45**

TuB02-1 **16.15–16.40**
PRC-based phase resetting for nonlinear oscillators 101
 D. Efimov University of Liège
 R. Sepulchre University of Liège

TuB02-2 **16.40–17.05**
Dynamical positioning of ship motion; a nonlinear regulation problem 102
 S. Muhammad Delft University of Technology
 J.W. van der Woude Delft University of Technology

TuB02-3 **17.05–17.30**
State predictor based on synchronization applied to a mobile robot 103
 Alejandro Alvarez-Aguirre Eindhoven University of Technology
 Henk Nijmeijer Eindhoven University of Technology
 Toshiki Oguchi Tokyo Metropolitan University

TuB02-4 **17.30–17.55**
Improving the performance of a Drop-on-Demand Inkjet Printhead 104
 A. A. Khalate Delft University of Technology
 Dr.Ir. X.J.A. Bombois Delft University of Technology
 Prof. Dr. R. Babuška Delft University of Technology

TuB02-5 **17.55–18.20**
On the robustness of feedback linearizing control schemes for multiple-input/multiple-output bioreactors 105
 Daniel Coutinho Faculté Polytechnique de Mons
 Alain Vande Wouwer Faculté Polytechnique de Mons

TuB03 **Wellington**
Aerospace
Chair: Jonathan Rogge **16.15–18.45**

TuB03-1 **16.15–16.40**
Global nonlinear optimization using interval analysis 106
 E. van Kampen Delft University of Technology
 E. de Weerd Delft University of Technology
 Q.P. Chu Delft University of Technology
 J.A. Mulder

TuB03-2 **16.40–17.05**
Fuel optimization for constrained rotations of space-craft formations using interval analysis 107
 E. de Weerd Delft University of Technology
 Q.P. Chu Delft University of Technology
 J.A. Mulder Delft University of Technology

TuB03-3 **17.05–17.30**
Feasibility of thrust vectoring in large passenger aircraft 108
 H. Yu Delft University of Technology

TuB03-4 **17.30–17.55**
Aerodynamic Model Identification and Flight Control Design with Multivariate Splines 109
 C.C. de Visser Delft University of Technology
 J.A. Mulder Delft University of Technology

TuB03-5 **17.55–18.20**
Nonlinear analysis of flutter 110
 Mattijs Van de Walle Vrije Universiteit Brussel
 Johan Schoukens Vrije Universiteit Brussel
 Steve Vanlanduit Vrije Universiteit Brussel

TuB04	Pouhon Pia
Biomedical robotics	
Chair: Maarten Steinbuch	16.15–18.45

TuB04-1 **16.15–16.40**
Design and control of a teleoperated palpation device for minimally invasive thoracic surgery 111
 Angelo Buttafuoco Université Libre de Bruxelles
 Thomas Delwiche Université Libre de Bruxelles
 Michel Kinnaert Université Libre de Bruxelles

TuB04-2 **16.40–17.05**
Haptic control of a tele-operated ultrasound probe 112
 Kees-Jan Zandsteeg Philips Applied Technologies
 Dennis Bruijnen Philips Applied Technologies
 Boudewijn Verhaar Philips Applied Technologies
 Peter Frissen, George de Fockert, Dennis Bos

TuB04-3 **17.05–17.30**
Influence of the skin moisture at fingertip on the static grip force during object manipulation 113
 T. André Université catholique de Louvain
 P. Lefèvre Université catholique de Louvain
 J-L. Thonnard Université catholique de Louvain

TuB04-4 **17.30–17.55**
Modeling of friction in a trocar for minimally invasive surgery 114
 J. Verspecht, Université Libre de Bruxelles
 T. Delwiche Université Libre de Bruxelles
 M. Kinnaert Université Libre de Bruxelles

TuB04-5 **17.55–18.20**
Novel Dexterous robotic finger concept with controlled stiffness 115
 Martin Wassink University of Twente
 Raffaella Carloni University of Twente
 Dannis Brouwer University of Twente
 Stefano Stramigioli

TuB05	Groesbeeck
Consensus and cooperative control	
Chair: Ming Cao	16.15–18.45

TuB05-1 **16.15–16.40**
The arithmetics of average consensus 116
 J-C Delvenne Université catholique de Louvain
 M. Branicky Case Western Reserve University
 K H Johansson KTH, Stockholm
 S. Zampieri

TuB05-2 **16.40–17.05**
Second-order Consensus Algorithms 117
 Wenwu Yu City University of Hong Kong
 Ming Cao University of Groningen

TuB05-3 **17.05–17.30**
Infinite Horizon Cooperative Differential Games - Necessary Conditions for Pareto Optimality 118
 Puduru Viswanadha Reddy Tilburg University
 Jacob Engwerda Tilburg University

TuB05-4 **17.30–17.55**
Collision-free coordination of a group of unicycle mobile robots 119
 D. Kostic Technische Universiteit Eindhoven
 S. Adinandra Technische Universiteit Eindhoven
 J. Caarls Technische Universiteit Eindhoven
 H. Nijmeijer

TuB05-5 **17.55–18.20**
Cooperative Adaptive Cruise Control 120
 Gerrit Naus Eindhoven University of Technology
 Jeroen Ploeg TNO, Business Unit Automotive
 Rene' v.d. Molengraft Eindhoven University of Technology

TuB05-6 **18.20–18.45**
Multi-robot coverage to locate fixed and moving targets 121
 Dr Ir J. Rogge Ghent University
 Dr. Ir. D. Aeyels Ghent University

Wednesday, March 18, 2009

WeA01	Pierre le Grand
Identification 2	
Chair: Rik Pintelon	8.30–11.00

WeA01-1	8.30–8.55
<i>Identification method for time-varying ARX models</i> 122	
Quentin Rentmeesters	Université catholique de Louvain
P.-A. Absil	Université catholique de Louvain
Paul Van Dooren	Université catholique de Louvain

WeA01-2	8.55–9.20
<i>Extracting information on time-varying systems using multisines</i> 123	
John Lataire	Vrije Universiteit Brussel
Rik Pintelon	Vrije Universiteit Brussel

WeA01-3	9.20–9.45
<i>Blind maximum likelihood identification of Wiener systems with measurement noise</i> 124	
Laurent Vanbeylen	Vrije Universiteit Brussel
Rik Pintelon	Vrije Universiteit Brussel
Pieter de Groen	Vrije Universiteit Brussel

WeA01-4	9.45–10.10
<i>Comparison of two nonlinear optimization methods for black box identification</i> 125	
Anne Van Mulders	Vrije Universiteit Brussel
Marnix Volckaert	Katholieke Universiteit Leuven
Prof. Dr. Ir. Jan Swevers	Katholieke Universiteit Leuven
Moritz Diehl, Johan Schoukens	

WeA01-5	10.10–10.35
<i>System realization of generalized model structures</i> 126	
Edwin Reynders	K.U.Leuven
prof. Guido De Roeck	K.U.Leuven

WeA01-6	10.35–11.00
<i>Finite record effects of the errors-in-variables estimator for linear dynamic systems</i> 127	
Kurt Barbé	Vrije Universiteit Brussel
Rik Pintelon	Vrije Universiteit Brussel
Gerd Vandersteen	Vrije Universiteit Brussel

WeA02	Source de la Reine
System Theory	
Chair: Gerard van Willigenburg	8.30–11.00

WeA02-1	8.30–8.55
<i>Stability analysis in continuous- and discrete-time, using the Cayley transform</i> 128	
Niels Besseling	University of Twente
Hans Zwart	University of Twente

WeA02-2	8.55–9.20
<i>Identifiability of the parametrizations of polynomial and rational systems</i> 129	
Jana Nemcova	Centrum Wiskunde & Informatica, Amsterdam

WeA02-3	9.20–9.45
<i>Energy equipartition and the second law of thermodynamics</i> 130	
Gerard van Willigenburg	Wageningen University

WeA02-4	9.45–10.10
<i>Extension of the behavioral approach to linear parameter-varying systems</i> 131	
R. Tóth	Delft University of Technology
J. C. Willems	Katholieke Universiteit Leuven
P. S. C. Heuberger	Delft University of Technology
P. M. J. Van den Hof	

WeA02-5	10.10–10.35
<i>An IQC Approach to Robust Estimation against Perturbations of Smoothly Time-Varying Parameters</i> . 132	
Ir J. Veenman	Technische Universiteit Delft
Dr H. Köroğlu	Technische Universiteit Delft
Prof Dr C. W. Scherer	Technische Universiteit Delft

WeA02-6	10.35–11.00
<i>The Optimal Linear Quadratic Feedback State Regulator Problem for Index One Descriptor Systems</i> 133	
Engwerda J.C.	Tilburg University
Salmah	Gadjah Mada University, Yogyakarta, Indonesia
Wijayanti I.E.	Gadjah Mada University, Yogyakarta, Indonesia

WeA03	Wellington
Automotive applications	
Chair: Bayu Jayawardhana	8.30–11.00

WeA03-1	8.30–8.55
<i>Improving Pushbelt Continuously Variable Transmission Efficiency via Extremum Seeking Control</i> . . . 134	
Stan van der Meulen	Eindhoven University of Technology
Bram de Jager	Eindhoven University of Technology
Erik van der Noll	Bosch Business Unit CVT

WeA03-2	8.55–9.20
<i>Model predictive control for the reduction of traffic emissions</i> 135	
S. K. Zegeye	Delft University of Technology
B. De Schutter	Delft University of Technology
J. Hellendoorn	Delft University of Technology

WeA03-3	9.20–9.45
<i>Minimum-fuel control of combustion engine powertrains</i> 136	
Bart Saerens	Katholieke Universiteit Leuven
Eric Van den Bulck	Katholieke Universiteit Leuven

WeA03-4	9.45–10.10
<i>Controlling an active cabin suspension for commercial vehicles</i> 137	
Willem-Jan Evers	Technische Universiteit Eindhoven
Arjan Teerhuis	TNO Automotive
Igo Besselink	Technische Universiteit Eindhoven
Henk Nijmeijer	

WeA03-5	10.10–10.35
<i>Global chassis control based on load sensing</i> 138	
Mathieu Gerard	Delft University of Technology
Michel Verhaegen	Delft University of Technology
Edward Holweg	Delft University of Technology

WeA03-6	10.35–11.00
<i>Development of a belt force actuator for controlled seat belt systems</i> 139	
E.P. van der Laan	Technische Universiteit Eindhoven
A.G. de Jager	Technische Universiteit Eindhoven
F.E. Veldpaus	Technische Universiteit Eindhoven

WeA04	Pouhon Pia
Methods for computational biology	
Chair: Georges Bastin	8.30–11.00

WeA04-1	8.30–8.55
<i>Estimating the parameters of a Rice distribution using a Bayesian approach</i> 140	
Lieve Lauwers	Vrije Universiteit Brussel
Kurt Barbé	Vrije Universiteit Brussel
Wendy Van Moer	Vrije Universiteit Brussel
Rik Pintelon	

WeA04-2	8.55–9.20
<i>Reverse-engineering genetic networks without prior knowledge</i> 141	
Jimmy Omony	Wageningen University
Dr.ir. A.J.B. van Boxtel	Wageningen University
Prof.dr.ir. G. van Straten	Wageningen University
Dr.ir. L.H. de Graaff	

WeA04-3	9.20–9.45
<i>Stochastic learning of fixed-rank positive semidefinite matrices</i> 142	
Gilles Meyer	University of Liège
Silvère Bonnabel	University of Liège
Rodolphe Sepulchre	University of Liège

WeA04-4	9.45–10.10
<i>Metabolic Flux Interval Analysis of CHO Cells</i> 143	
Francisca Zamorano	Service d'Automatique
Alain Vande Wouwer	Service d'Automatique
Georges Bastin	Université catholique de Louvain

WeA04-5	10.10–10.35
<i>Generalized power method for sparse principal component analysis</i> 144	
M. Journée	University of Liège
Y. Nesterov	Université catholique de Louvain
Peter Richtarik	Université catholique de Louvain
R. Sepulchre	

WeA04-6	10.35–11.00
<i>An initialization procedure for parameter estimation problems using simultaneous Gauss-Newton method</i> 145	
Julian Bonilla	Katholieke Universiteit Leuven
Moritz Diehl	Katholieke Universiteit Leuven
Bart De Moor	Katholieke Universiteit Leuven
Jan Van Impe,	Katholieke Universiteit Leuven,
CIT/BioTeC	

WeA05	Groesbeeck
Optimization for learning and control	
Chair:	8.30–11.00

WeA05-1	8.30–8.55
<i>Predictive input shaping prefilters</i> 146	
L. Van den Broeck	K.U.Leuven
M. Diehl	K.U.Leuven
J. Swevers	K.U.Leuven

WeA05-2	8.55–9.20
<i>Extending iTaSC to support inequality constraints</i> . 147	
Wilm Decré	Katholieke Universiteit Leuven
Ruben Smits	Katholieke Universiteit Leuven
Herman Bruyninckx	Katholieke Universiteit Leuven
Joris De Schutter	

WeA05-3	9.20–9.45
<i>Directional repetitive control of a metrological AFM</i> 148	
Michael Ronde	Technische Universiteit Eindhoven
Roel Merry	Technische Universiteit Eindhoven
René van de Molengraft	Technische Universiteit Eindhoven
Maarten Steinbuch, Richard Koops, Marijn van Veghel	

WeA05-4	9.45–10.10
<i>Iterative Learning Control by Linear Repetitive Processes Theory</i> 149	
Wojciech Paszke	Eindhoven University of Technology

WeA05-5	10.10–10.35
<i>A constrained Gauss-Newton method for model inversion in iterative learning control</i> 150	
M. Volckaert	Katholieke Universiteit Leuven
A. Van Mulders	Vrije Universiteit Brussel
M. Diehl	Katholieke Universiteit Leuven
J. Swevers	

WeA05-6	10.35–11.00
<i>Iterative optimization of parameterized trajectories for complex mechatronic systems</i> 151	
Bruno Depraetere	Katholieke Universiteit Leuven
Jan Swevers	Katholieke Universiteit Leuven
Wim Symens	Flanders Mechatronics Technology Centre
Gregory Pinte, Walter Verdonck	

Plenary	Pierre le Grand
Control of ensembles	
Navin Khaneja (Harvard University, USA)	
Chair: Rodolphe Sepulchre	11.30–12.30

<i>Control of ensembles</i> 233
Navin Khaneja (Harvard University, USA)

WeB01	Pierre le Grand
Advanced application modeling	
Chair: Yves Rolain	13.50–15.55

WeB01-1	13.50–14.15
<i>Robust beyond-rigid-body control of next generation wafer stages</i> 152	
Robbert van Herpen	Eindhoven University of Technology
Tom Oomen	Eindhoven University of Technology
Marc van de Wal	Philips Applied Technologies
Okko Bosgra	

WeB01-2 14.15–14.40

Model development for propofol and remifentanyl induced anesthesia in ICU patients 153
 ir. Ramona Hodrea Ghent University
 ir. Bogdan Nour Ghent University
 Drd.ir. Clara Ionescu Ghent University
 Prof.Dr.ir. Robin De Keyser

WeB01-3 14.40–15.05

Dynamical Modeling of Micro-Assembly Systems . 154
 Dr B. Jayawardhana Rijksuniversiteit Groningen

WeB01-4 15.05–15.30

Modeling and Control of a Wobble Yoke Stirling Engine : Application to a Micro-Cogeneration System 155
 M. Kuindersma Rijksuniversiteit Groningen
 E. Garcia-Canseco Technische Universiteit Eindhoven
 J.M.A. Scherpen Rijksuniversiteit Groningen

WeB01-5 15.30–15.55

Modeling the baseband output envelope of a microwave detector 156
 Liesbeth Gommé Vrije Universiteit Brussel
 Yves Rolain Vrije Universiteit Brussel
 Johan Schoukens Vrije Universiteit Brussel
 Rik Pintelon

WeB02	Source de la Reine
Modeling and control of chemical processes	
Chair: Karel Keesman	13.50–15.55

WeB02-1 13.50–14.15

Identification of Low Order Model for Large Scale Systems 157
 S.K. Wattamwar Technical University of Eindhoven
 Siep Weiland Technical University of Eindhoven

WeB02-2 14.15–14.40

Efficient multiple objective optimal control : (bio)chemical engineering applications 158
 F. Logist Katholieke Universiteit Leuven
 P.M.M. Van Erdeghe Katholieke Universiteit Leuven
 J.F.M. Van Impe Katholieke Universiteit Leuven

WeB02-3 14.40–15.05

An Efficient Methodology for Model Predictive Control of SMB Plants Based on the Wave Theory and Reduced Order Models 159
 Vilas Carlos Faculté Polytechnique de Mons
 Vande Wouwer Alain Faculté Polytechnique de Mons

WeB02-4 15.05–15.30

The effect of imperfect maintenance on deterioration processes 160
 Samira S. Farahani Technische Universiteit Delft
 J. A. M. van der Weide Technische Universiteit Delft
 M. J. Kallen HKV Consultants
 R. P. Nicolai

WeB02-5 15.30–15.55

Very fast temperature pulsing : catalytic reactor design 161
 Jasper Stolte Technische Universiteit Eindhoven
 Ton Backx Technische Universiteit Eindhoven
 Okko Bosgra Technische Universiteit Eindhoven

WeB03	Wellington
Power systems	
Chair: René Boel	13.50–15.55

WeB03-1 13.50–14.15

Using multidimensional scaling to represent a power system according to the electric distances between nodes 162
 Florence Fonteneau-Belmudes University of Liège
 Damien Ernst University of Liège
 Louis Wehenkel University of Liège

WeB03-2 14.15–14.40

LMI formulation for optimal control of coal fired power plants 163
 E. Simon Ecole Polytechnique de Louvain
 V. Wertz Ecole Polytechnique de Louvain

WeB03-3 14.40–15.05

Non-centralized model predictive control of power networks 164
 A.C.R.M. Damoiseaux Technische Universiteit Eindhoven
 R.M. Hermans Technische Universiteit Eindhoven
 A. Jokic Technische Universiteit Eindhoven
 M. Lazar, P.P.J. Van den Bosch

WeB03-4 15.05–15.30

Power Factor Compensation in Nonsinusoidal Systems Based on Cyclodissipativity 165
 D. del Puerto-Flores Rijksuniversiteit Groningen
 J. M. A. Scherpen Rijksuniversiteit Groningen
 R. Ortega SUPELEC

WeB03-5 15.30–15.55

Using the event-driven Petri net in complex distributed systems design 166
 Alexandre Skrylnik Faculté Polytechnique de Mons

WeB04	Pouhon Pia
Artificial and living vision systems	
Chair: Raffaella Carloni	13.50–15.30

WeB04-1 13.50–14.15

Biological Motion boosts the oculomotor response 167
 Sebastien Coppe Université catholique de Louvain
 Jean-Jacques Orban de Xivry Johns Hopkins University
 Marcus Missal Université catholique de Louvain
 Philippe Lefevre

WeB04-2 14.15–14.40

Controlling a moving camera setup for humanoid gaze emulation 168
 R. Reilink University of Twente
 S. Stramigioli University of Twente
 F. van der Heijden University of Twente

WeB04-3 14.40–15.05

The visuomotor transformation of velocity signals for visually guided arm movements 169
 Guillaume Leclercq Université catholique de Louvain
 Gunnar Blohm Queen's University
 Philippe Lefèvre Université catholique de Louvain

WeB04-4 15.05–15.30*How To Obtain a 1 kHz Visual Servoing Setup?* . . . 170

Jeroen de Best Technische Universiteit Eindhoven

René van de Molengraft Technische Universiteit Eindhoven

Maarten Steinbuch Technische Universiteit Eindhoven

WeB05	Groesbeeck
Control of vibrations	
Chair: Jan Swevers	13.50–15.55

WeB05-1 13.50–14.15*Active chatter control for high-speed milling using* *μ -synthesis* 171

T.A.C. Verschuren Eindhoven University of Technology

N.J.M. van Dijk Eindhoven University of Technology

N. van de Wouw Eindhoven University of Technology

H. Nijmeijer

WeB05-2 14.15–14.40*A modular bearing with internal piezoshunt damping* 172

Dr. Ir. Gregory Pinte Flanders' Mechatronics Technology Center

Dr. Ir. Steven Devos Flanders' Mechatronics Technology Center

Dr. Ir. Wim Symens Flanders' Mechatronics Technology Center

Bert Stallaert, Jan Swevers, Paul Sas

WeB05-3 14.40–15.05*Self-sensing actuation and damping of a Piezoelec-**tric Tubescanner* 173

S. Kuiper Delft University of Technology

G. Schitter Delft University of Technology

WeB05-4 15.05–15.30*Black box identification of a semi-active damper* . . 174

Maarten Witters K.U.Leuven

Jan Swevers K.U.Leuven

WeB05-5 15.30–15.55*Stabilization & Vibration Control of Gaussmount**Suspension System* 175

C. Ding Technische Universiteit Eindhoven

A.A.H. Damen Technische Universiteit Eindhoven

P.P.J. van den Bosch Technische Universiteit Eindhoven

Pierre le Grand
Best Junior Presentation Award ceremony
16.15–16.30

Part 1 : Programmatic Table of Contents 5

Overview of scientific program

Part 2 : Contributed Lectures 19

One-page abstracts

Part 3 : Plenary Lectures 177

Presentation materials

Part 4 : List of Participants 245

Alphabetical list

Part 5 : Overview Program 261

Part 2

Contributed Lectures

Identification of a Distillation Column for PLC Control Purposes

Bart Huyck, Jos De Brabanter

KaHo Sint Lieven - Department Industrieel Ingenieur

Email: bart.huyck@kahosl.be jos.debrabanter@kahosl.be

Filip Logist, Jan Van Impe

K.U.Leuven - Department of Chemical Engineering (CIT)

Email: filip.logist@cit.kuleuven.be jan.vanimpe@cit.kuleuven.be

Bart De Moor

K.U.Leuven - Department of Electrical Engineering (ESAT - SCD)

Email: bart.demoor@esat.kuleuven.be

1 Introduction

In a world where economic and environmental issues become more and more important, efficient control systems have become indispensable. When dealing with complex processes, Model Predictive Control (MPC) is one of the possible control strategies[1]. In practice, current linear and non-linear MPC algorithms require powerful computers. However, since Programmable Logic Controllers (PLCs) with less computational power are used a lot in industry for control, it might be interesting to explore the possibilities and limitations of these devices for MPC. For this purpose, a 6 m high pilot scale binary distillation column, is selected as an industrial example.

2 Goal

The column is currently controlled by PI controllers, but the goal is to upgrade the control system with a linear MPC running on a PLC. However, before a model based controller can be used on a PLC, an accurate (but simple) process model has to be constructed. Therefore linear parametric MIMO black-box models (e.g., ARX, ARMAX, and output error) are adopted.

3 Experimental set-up

In this set-up, four variables can be manipulated: the reboiler duty Q_r , the feed rate F_v , the duty of the feed heater Q_v and the distillate flow rate F_d . Measurements are available for the distillate flow rate F_d , the feed flow rate F_v and nine temperatures, i.e., the temperature at the top of the column T_t , the temperatures in the center of every packing section (T_{s1} , T_{s2} and T_{s3} , respectively), the temperature between section 1 and 2 T_{v1} , the ambient temperature T_{amb} , the temperature in the reboiler of the column T_b , and the temperatures of the feed before and after heating (T_{v0} and T_v , respectively).

4 Model identification procedure

A parametric model is fitted following the Box-Jenkins modelling procedure using the Matlab System Identification Toolbox [2, 3]. An experiment with PRBN input signals is performed for 20000 seconds. From these recorded signals, 5 inputs (Q_r , F_v , Q_v , F_d and T_{amb}) and 5 outputs (T_{s1} , T_{s2} , T_{s3} , T_t and T_b) are selected to create a model. Two datasets are prepared: one with sampling rate of 5 seconds and an other with sampling rate of 60 seconds. Both sets are split up in an identification and validation part. MIMO ARX, ARMAX and OE models are fitted and validated. The AIC criterium is adopted to select the correct model order. Additional model reduction is performed with the help of Hankel Singular Values.

5 Results

Only ARX and ARMAX models predict the output accurately, but the best performing models are ARMAX models. After model reduction and conversion, these models result in a 6th order state space model for both datasets. The authors believe that these models (despite their low complexity) will predict the output accurately enough to be employed in an MPC algorithm which can be implemented on a PLC.

6 Acknowledgements

Work supported in part by Projects OT/03/30 and EF/05/006 (Center-of-Excellence Optimization in Engineering) of the Research Council of the Katholieke Universiteit Leuven, and by the Belgian Program on Interuniversity Poles of Attraction, initiated by the Belgian Federal Science Policy Office. The scientific responsibility is assumed by its authors.

References

- [1] S. J. Qin and T. A. Badgwell. "A survey of industrial model predictive control technology," *Contr Eng Pract*, 11:733764, 2003.
- [2] L. Ljung. *System Identification: Theory for the User*, Second Edition. Prentice Hall, Upper Saddle River, New Jersey, 1999.
- [3] L. Ljung. *System Identification Toolbox Users Guide*. The MathWorks, Inc, Natick, 2008.

Effects of Overlapping and Windowing on the Estimation of the Frequency Response of a System using White Noise

W. D. Widanage
Department ELEC
Vrije Universiteit of Brussels
Pleinlaan 2. 1050.
Belgium

Email: wwidanag@vub.ac.be

J. L. Douce and K. R. Godfrey
School of Engineering
University of Warwick
Coventry. CV4 7AL
U.K.

Email: John.Douce@btinternet.com

Email: K.R.Godfrey@warwick.ac.uk

1 Abstract

Errors are introduced when estimating the frequency response of a system, when using random inputs with block overlap and time windowing. The sources of these errors are studied in the absence of external noise. The sources of errors for the bias and variance of the frequency response are identified to be due to the Fourier transforms of the end effects that arise due to nonperiodic signals, and a time varying error over the period of a block that is dependent on the type of window. Using a pure time delay as an example for the system, it is shown that there is a limit to the improvement achievable in reducing the variance as the block overlap is increased.

2 Introduction

Consider an input and output pair of blocks with the system being a pure time delay. The first D samples (this will be termed the header of the output) in each measured output block $y_l(n)$ is uncorrelated with the entire measured input $x_l(n)$. Similarly, the last D samples of $x_l(n)$ (this will be termed the tail of the input) is reproduced at the start of the next output block, $y_{l+1}(n)$. Therefore for a given pair of $x_l(n)$ and $y_l(n)$, the block $y_l(n)$ does not capture the full response to $x_l(n)$ and contains a term that is correlated with $x_l(n)$ and a further term uncorrelated with it. This uncorrelated term, which can be treated as a noise source, leads to the variance of the estimate.

The composition of the error between the measured output and the modelled output from an estimated frequency response is considered to explain the effects of block overlap. There are two factors involved. The first factor arises from the periodic assumption of the Discrete Fourier Transform. The modelled output includes in the header the response to the tail of the input signal, while the true output includes the response to the input over the preceding block $x_{l-1}(n)$. This factor introduces errors in the estimated frequency response function (FRF) due to the header signal diverging from the signal produced by the nonperiodic input block. The second factor is due to the distortion introduced by the time vary-

ing gain of the window. With any such window, the gain from input to output varies with time over the duration of the block. It leads to the suggestion that distortion occurs due to windowing, and the position of this distortion relative to other blocks affects the performance of the overlapping procedure.

3 Simulation Results

The effect of overlap on the variance of an estimated frequency response is illustrated, with a pure time delay of 10% of the block length and Hanning windowing. The input is a zero mean white noise process and the statistics of the estimate are obtained over 1000 repeated simulations. With

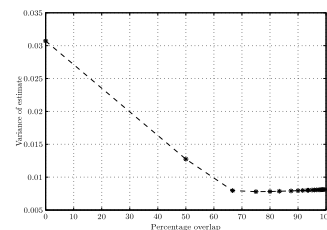


Figure 1: The variance of the FRF against percentage overlap with Hanning window.

Hanning windowing no significant improvement in variance is achieved for an overlap of more than 65%. This phenomenon is also observed with other types of systems.

4 Conclusions

The sources of errors and their effects on the estimated frequency response using overlapping blocks are discussed and illustrated. The errors are due to 1) the response of the tail of the input, 2) the response from the preceding input block, and 3) the time-varying gain of the window function. By considering the distribution of these errors over the length of a block, it leads to the conclusion that the predominant factor in the source of variance and, hence, the performance of the overlapping operation is the characteristic of the window function and not of the dynamics of the system.

Linear regressive realizations of LTI state space models: an advection-reaction case study

K.J. Keesman and N. Khairudin

Systems and Control Group, Wageningen University

THE NETHERLANDS

karel.keesman@wur.nl

1 PROBLEM FORMULATION AND SOLUTION

Estimation of physical parameters in continuous-time linear time-invariant state-space models generally leads to nonlinear estimation problems. It is well known that nonlinear estimation problems frequently lead to local minima solutions. Furthermore, solving these problems can be very (computer) time consuming, especially when multi-start procedures are used. Since the global solution is not known beforehand, no characterization of the systematic error in the estimates can be given.

In this presentation, our aim is to uniquely estimate model parameters in state-space model structures while preserving the (original) physical model structure. Our approach, for continuous-time systems, is to handle the parameter estimation problem via discretization and a linear regressive parametric realization of the dynamical system. Unlike ‘data based’ methods such as subspace identification, we will conserve the physical model structure.

In particular, we will consider the class of finite LTI state space systems $\mathcal{S}(\Sigma)$. By the properties of this class, we are able to find another realization of Σ which is suited for linear estimation and prediction. It will be shown later on, that the resolvent of the system matrix ($R(A)$) of the discrete-time system, plays a key role in this. In specific cases, the discrete-time system matrix ($I + A(\vartheta)$), with ϑ a vector with physical parameters, becomes a bidiagonal matrix or a symmetric tridiagonal matrix. For the latter case, explicit solutions to $R(A)$ are known (see [1]). The goal here is to unravel the structure of $R(A)$, in such a way that we may write the system as a linear regressive set of equations: $\theta^T \phi = \gamma$. Herein, $\theta_i = \xi_i(\vartheta)$ are known reparametrization functions that are not confounded with coefficients that originate from either the discretization step or from constants in A . From here, it is rather straightforward to arrive at an ordinary least-squares estimate $\hat{\theta}$ and at an explicit expression for the output at time instant k .

The key objective of the presentation is twofold: to show the derivation of linear regressive model structures from LTI state space models, while conserving the physical model structure, and to illustrate this to an advection-reaction system.

2 CONCLUDING REMARKS

The proposed procedure allows the conservation of the underlying physical model structure in combination with linear regressive parameter estimation. The realization of a linear regressive system $\tilde{\Sigma}$ from a state space system Σ is based on linearity of the system and linearity in the parameter ϑ of $A(\vartheta)$ and $B(\vartheta)$.

References

- [1] Vries, D. Estimation and Prediction of Convection-Diffusion-Reaction Systems from Point Measurements. PhD Thesis, Wageningen University. pp. 170, 2008.

System Identification of a Spindle with Active Magnetic Bearings

Rogier S. Blom ^{a,b,*}, Paul M.J. Van den Hof ^a, H.H. Langen ^b, R.H. Munnig Schmidt ^b

^a Delft Center for Systems and Control, ^b Precision and Microsystems Engineering

Delft University of Technology

* Corresponding author, email: r.s.blom@tudelft.nl

1 Introduction

The problem addressed in this presentation has its roots in the area of micro-manufacturing. In particular micromilling is considered, which entails the scaling of conventional milling into the microdomain. Active Magnetic Bearing (AMB) spindle technology is a promising technology for the micro-milling process. Not only are high rotational speeds attainable, but the active nature of these spindles can be used for monitoring and control purposes, resulting in a more stable cutting process and better manufacturing results.

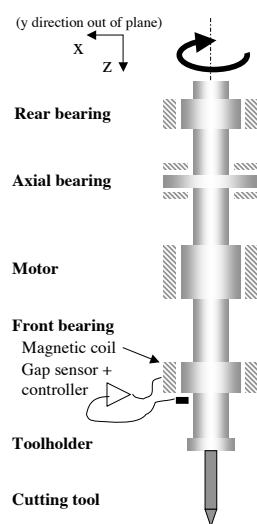


Figure 1: Schematic of an AMB spindle

2 Problem statement

Availability of an accurate model of the dynamics of the AMB spindle is of crucial importance to develop the process monitoring and control techniques mentioned in the introduction. Here, identification of the AMB spindle system from measured data sequences is considered. This problem can be characterized by the following aspects (see fig. 1):

- The dynamics are multivariable. The coupling between the inputs (the currents through the coils of the actuators) and outputs (the position of the rotor shaft at the bearings) varies with the rotational speed;

- The dynamics are unstable, hence experiments need to be performed in closed-loop;
- The flexural modes of the rotor are very lightly damped and modes split due to gyroscopy;
- The AMB spindle exhibits nonlinear behavior, caused by the electromagnetic actuators.

3 Approach

A frequency domain approach is used to identify the dynamics of the AMB spindle. This approach consists of two stages. In the first step, a non-parametric estimate of the multivariable frequency response function (FRF) is made. Orthogonal odd random phase multisine excitation signals are selected for their favorable effect on the variance of the FRF estimate [1]. To ensure that for the chosen excitation the effect of the nonlinearities present in the system is negligible, tests are performed to measure the level of nonlinear distortion. The second step involves estimation of a parametric model of the plant dynamics from the frequency response data obtained in the first step. Using the approach in [2], models in matrix fraction description are fit to the estimated FRF.

Results will be presented for a high-speed micro-milling AMB spindle (120,000 rpm). Estimated models will be compared for different rotational speeds.

4 Acknowledgement

This research is supported by MicroNed and the Delft Center for Mechatronics and Microsystems.

References

- [1] T. Dobrowiecki, J. Schoukens, P. Guillaume. Optimized Excitation Signals for MIMO Frequency Response Function Measurements. *IEEE Transactions of Instrumentation and Measurement*, Vol. 55, No. 6, Dec. 2006, 2072-2079.
- [2] R.A. de Callafon, D. de Roover, P.M.J. Van den Hof. Multivariable least squares frequency domain identification using polynomial matrix fraction descriptions. *Proc. 35th IEEE Conference on Decision and Control*, Kobe, Japan, 11 - 13 December 1996, 2030-2035.

Towards Automatic Control of Electron Microscopes: System Identification Issues

Dr. Arturo Tejada Ruiz
Delft Center for Systems and Controls
Delft University of Technology
Mekelweg 2, 2628 CD, Delft, The Netherlands
Email: a.tejadaruiz@tudelft.nl

1 Introduction

Scanning transmission electron microscopes (STEMs) are the tools of choice for material science research, since they provide information on the internal structure of a wide range of specimens. These complex machines are operated by skilled technicians, who execute repetitive tasks (e.g., alignment, particle counting, etc.) following long scripted manual procedures and using mainly visual feedback. Automating such procedures is a crucial step towards transforming the STEMs from qualitative tools into flexible quantitative nano-measuring tools. This is the goal of the CONDOR project, which is managed by the Embedded Systems Institute (www.esi.nl). To enable this automation, STEM dynamical models of enough fidelity are needed. Unfortunately, to the best of our knowledge, such models are not available in the literature. The first steps toward developing such dynamical models were reported in recently [1]. In here, we outline our most recent efforts towards deriving those models.

2 STEM Modeling

Figure 1 shows a simplified STEM dynamical model. As explained in [1], a STEM can be divided into two section:

- **Electronics:** This represents the STEM's electronics. The value of an operator-controlled "knob", $u(t)$, sets the value of an optical parameter, $p(t)$. For instance, $u(t)$ could represent the voltage applied to an electromagnetic lens, while $p(t)$ could represent the corresponding focal distance
- **Optics + Algorithm:** This represents the STEM image formation process and a feature extraction algorithm. Note that the image formation process on *bright field mode* is a time independent process, while the algorithm is time dependent.

The dynamics of the electronics are given by the (possibly nonlinear) function $f: \mathbb{R}^2 \rightarrow \mathbb{R}$. That is, $\dot{p}(t) = f(p(t), u(t))$. The dynamics of the optics + algorithm block are more difficult to establish. Using bright field images (BFI), these dynamics are given by $I(r) = |\phi(r) * h(r, p)|^2$, where $\phi(r)$ is

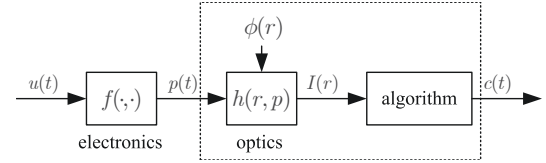


Figure 1: Simplified STEM model.

a two-dimensional complex signal that represents the sample electrical potential, $h(r, p)$ represents the microscope's two-dimensional transfer function, which is parameterized by p , and $*$ represents the convolution operator (over r).

The algorithms used to measure p vary depending on the nature of p . For focal distance measurement, algorithms are readily available based on BFI analysis. Their outputs, c , are static functions of the parameter p . That is, $c = g(p)$, where $g: \mathbb{R} \rightarrow \mathbb{R}$ is usually a polynomial function. Hence, the optics + algorithm block can be modeled as follows: $c(t) = g(p(t - \Delta)) + \eta(t)$, where Δ denotes the delay introduced by the algorithm and $\eta(t)$ represents measurement noise. The overall system model is the

$$\begin{aligned}\dot{p}(t) &= f(p(t), u(t)) \\ c(t) &= g(p(t - \Delta)) + \eta(t),\end{aligned}$$

Thus, $c(t)$ is a nonlinear observation of the state variable $p(t)$. The function g has been recently characterized via simulated images and will soon be validated through experiments with STEM microscopes.

Acknowledgements

This research was sponsored by the Condor project at FEI company, under the responsibilities of the Embedded Systems Institute (ESI). This project is partially supported by the Dutch Ministry of Economic Affairs under the BSIK program.

References

- [1] A. Tejada, S. van der Hoeven, A. den Dekker, and P. van den Hof, "Towards automatic control of scanning transmission electron microscopes," in *Proc. of the Conference of Control Applications*, Saint Petersburg, Russia, 2009, p. under review.

Estimating a Power-Scalable Linearized Model for Amplifiers

Koen Vandermot, Yves Rolain, Gerd Vandersteen, Rik Pintelon

Vrije Universiteit Brussel, dep. ELEC, Pleinlaan 2, 1050 Brussels, BELGIUM

e-mail: koen.vandermot@vub.ac.be

Abstract - The input-output behavior of RF amplifiers is not only function of the frequency but also shows an input power dependency. Here a linearized 2-dimensional model will be estimated by a Maximum Likelihood Estimator.

I. INTRODUCTION

For the design of telecommunication systems, designers rely on models of the different components of their system. For amplifiers there exists already a linearized and non-parametric model that is easy to create out of input and output signals: the Best Linear Approximation (BLA) [1]. However, this approximation is only valid for the chosen class of signals: the class of the gaussian noise signals with a fixed power spectrum (rms value and coloring are fixed) [2]. A consequence of this approach is that the BLA will be different for another RMS value of the input signal. Since the input power is one of the tuning parameters in the design of a communication system, the model for the amplifier has to predict the behavior also for a variation of the input power. In this abstract, a 2D rational model will be identified by a maximum likelihood estimator (MLE). The reason for this choice of estimator are its properties: consistency, asymptotic normality and asymptotic efficiency. Due to these statistical properties, a measure for the quality of the obtained model as the uncertainty bounds on the estimates are known.

II. ESTIMATING THE MODEL FROM MEASUREMENTS

By measuring the S_{21} parameter for every chosen couple of the frequency f_k and the power of the input signal P_l , one gets the complex value of the S_{21} transfer function. Since this is a linearization of the input-output behavior of the RF amplifier under the considered operation condition, this gives a nonparametric BLA for each power level separately:

$$G_m(j\omega_k, P_l) = \frac{Y(j\omega_k, P_l)}{U(j\omega_k, P_l)} = S_{21}(j\omega_k, P_l) \quad (1)$$

The goal is to get a 2-dimensional rational parametric model in the frequency and the power, that is valid for every couple of the frequency and the input power within the considered frequency and input power range. A parametric model for this 2-dimensional rational form will be estimated by a MLE. However, this estimator is only able to reach the global minimum when “good” starting values for the parameters are given. For this reason, a method is proposed that combines a good minimization procedure with the good statistical properties of the MLE [1]. To do so, one starts by estimating the starting values with a Weighted Generalized Total Least Squares (WGTLs) [1]. Next, these starting values are used for a Bootstrapped Total Least Squares estimation (BTLS) [1]. This estimation procedure will give the starting values for the final estimation: a Maximum Likelihood Estimation (MLE). With this last

estimator the parameters \hat{a}_{m_a, n_a} and \hat{b}_{m_b, n_b} of the parametric model are found:

$$\hat{G}(j\omega, P) = \frac{\sum_{(m_b, n_b) = (0, 0)}^{(M_b, N_b)} \hat{b}_{m_b, n_b}(j\omega)^{m_b} P^{n_b}}{\sum_{(m_a, n_a) = (0, 0)}^{(M_a, N_a)} \hat{a}_{m_a, n_a}(j\omega)^{m_a} P^{n_a}} \quad (2)$$

With (M_a, N_a) and (M_b, N_b) the orders of respectively the denominator and the numerator of this model. When a low order is chosen, it is possible that the model is not capable to explain all the measured dynamics. For an high order, the estimated model will also capture the noise disturbances. Furthermore, choosing higher orders results in models that are not stable over the power and frequency range. For these reasons, a selection of the model order is needed.

III. MODEL VALIDATION

The norm of the residuals (measurements-model) over the frequencies and powers is taken and compared with its 95% uncertainty level. When circular complex distributed noise is assumed, it is proven that the 95% uncertainty level corresponds with the $\sqrt{3}\sigma$ level, where $\sigma^2(f_k, P_l)$ is the variance on the measurements for a given frequency f_k and a given input power P_l . Hence, making this comparison (see Fig. 1) will give an idea about the quality of the obtained parametric model. This is the major advantage of this modelling procedure.

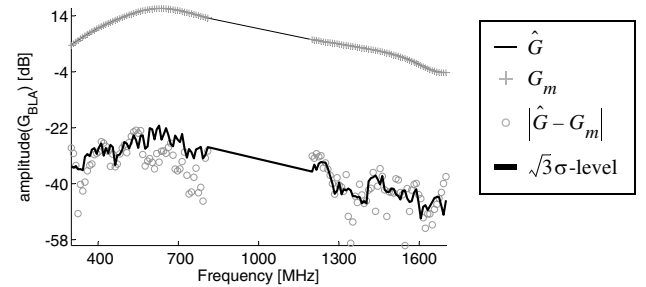


Fig. 1. The order of the numerator and denominator are chosen: $M_b = M_a = 8$ and $N_b = N_a = 8$. Note that an input power slice $P = -6.2\text{dBm}$ of the model is considered.

IV. CONCLUSION

The proposed method estimates a parametric 2-dimensional rational model that takes into account the frequency as well as the input power dependency and allows to find a measure for the quality of the obtained model.

REFERENCES

- [1] R. Pintelon, J. Schoukens (2001). *System Identification. A frequency domain approach*. IEEE Press, New Jersey.
- [2] Y. Rolain, W. Van Moer, R. Pintelon, J. Schoukens. Experimental Characterization of the Nonlinear Behavior of RF Amplifiers, *IEEE Transactions on Microwave Theory and Techniques*, vol. 45, no. 8, pp.3209-3218, August 2006.

A Synchronization Criterion for Delay-coupled Systems based on Absolute Stability

Toshiki Oguchi¹⁾, Henk Nijmeijer²⁾, Noriko Tanaka³⁾

1) Graduate School of Science & Engineering, Tokyo Metropolitan University
1-1, Minami-Osawa, Hachioji-shi, Tokyo 192-0397 Japan

Email: t.oguchi@tmu.ac.jp

2) Department of Mechanical Engineering, Eindhoven University of Technology
P.O. Box 513, 5600 MB Eindhoven, The Netherlands

3) Department of Precision Engineering, Tokyo Metropolitan University
1-1, Minami-Osawa, Hachioji-shi, Tokyo 192-0397 Japan

Synchronization in networks of chaotic systems has been widely investigated in applied physics, mathematical biology, social sciences and control science and interdisciplinary fields since the early work by Fujisaka and Yamada [1] and by Pecora and Carroll [2]. The study on synchronization of coupled systems [3, 4] has extensively dealt with coupled systems with delay-free coupling. In addition, from a viewpoint of control science and engineering, the synchronization problem has been also investigated via control theory. More recently the interest is spreading to synchronization phenomena of chaotic systems with time-delay and the effect of time-delay in synchronization [5, 6]. In practical situations, time-delays are caused by signal transmission between coupled systems and affect the behavior of coupled systems. It is therefore important to study the effect of time-delay in existing synchronization schemes. The effect of time-delay in synchronization of coupled systems has been investigated both numerically and theoretically by a number of researchers, these works concentrate on synchronization of systems with a coupling term typically described by $u_i(t) = \sum_{j=1, j \neq i}^N K_{ij}(x_i(t - \tau) - x_j(t - \tau))$ and there are few results for the case in which the coupling term is described by $u_i(t) = \sum_{j=1, j \neq i}^N K_{ij}(x_i(t) - x_j(t - \tau))$. In either case, the synchronization error dynamics can be described by a difference-differential equation, and the synchronization problem can be reduced to the stabilization problem for the origin of the error dynamics with suitable conditions on the coupling gain and the time-delay. However most existing conditions for synchronization are based on the Lyapunov-Krasovskii functional approach and are given by linear matrix inequalities (LMIs), and these criteria tend to have conservative results due to the -almost inherently- conservativeness of the Lyapunov-Krasovskii approach.

In this paper, we propose a less conservative criterion for synchronization of coupled systems with time-delay. Throughout, we assume that the error dynamics can be rewritten by a feedback connection of a linear delay system with multiple inputs and outputs and nonlinear elements

which are decentralized and satisfy the sector condition. Then, we derive a synchronization condition for coupled systems with delay by applying the multivariable circle criterion [8] which is an extension of the result by Popov and Halanay [7]. Unlike the conventional synchronization criteria, the derived criterion is based on a frequency-domain condition and avoid the Lyapunov-Krasovskii approach. As a result, the condition does not contain the conservativeness caused by the Lyapunov-Krasovskii approach. The effectiveness of the proposed criterion is shown by examples of coupled Chua systems with delay coupling. The condition obtained by the criterion is less conservative than the conventional LMI condition, and the boundary condition for synchronization is relatively close to the result by numerical simulations.

References

- [1] H. Fujisaka and T. Yamada "Stability theory of synchronized motion in coupled-oscillator systems," *Prog. Theor. Phys.* **69**-1, 32-47, 1983.
- [2] L. M. Pecora and T. L. Carroll "Synchronization in chaotic systems," *Phys. Rev. Lett.*, **64**-8, 821-825, 1990.
- [3] A. Pikovsky, M. Rosenblum, and J. Kurths "Synchronization - A universal concept in nonlinear sciences-," Cambridge University Press, 2001.
- [4] C. W. Wu "Synchronization in coupled chaotic circuits and systems," World Scientific, 2002.
- [5] T. Oguchi and H. Nijmeijer "Prediction of chaotic behavior," *IEEE Trans. on Circ. and Sys. I*, **52**-11, 2646-2472, 2005.
- [6] T. Oguchi, H. Nijmeijer, and T. Yamamoto "Synchronization in networks of chaotic systems with time-delay coupling," *Chaos*, **18**, 037108, 2008.
- [7] V. Popov and A. Halanay "On the stability of nonlinear automatic control systems with lagging argument," *Automation and Remote Control*, **23**, 783-786, 1962.
- [8] P. A. Bliman "Extension of Popov absolute stability criterion to non-autonomous systems with delays," *Int. J. Control*, **73**-15, 1349-1361, 2000.

Acknowledgments: This work was partially supported by the Japan Society for the Promotion of Science (JSPS) Grant-in-Aid for Scientific Research (No. 20560424).

Recent advances and open questions on Peskin model for coupled oscillators

Alexandre Mauroy and Rodolphe Sepulchre

Departement of Electrical Engineering and Computer Science,

University of Liège, B-4000 Liège, Belgium

Email: alexandre.mauroy@ulg.ac.be, r.sepulchre@ulg.ac.be

1 Introduction

Clustering and synchronization are ensemble phenomena commonly observed in natural and artificial populations of interacting oscillators. The Peskin model [3] is a seminal and simple model to study such populations. For each oscillator, the evolution of the state variable obeys a differential equation (linear for LIF oscillators, quadratic for QIF oscillators, ...) and is comprised between two threshold values. When the high threshold level is reached, the variable is reset to the low one (the oscillator is said to fire). The coupling between the oscillators is impulsive: if a firing occurs, the state of every connected oscillators will be increased by a constant value.

The behaviors exhibited by identical and all-to-all coupled Peskin oscillators are well-known. For instance, synchronization of the network was proved under some conditions in [2] and clustering phenomena were highlighted in [4]. On the other hand, there exists no mathematical tool to understand, in an extensive way, the behaviors of heterogeneous populations of Peskin oscillators. A new approach seems to be necessary.

2 A continuous model

Due to the limitations and issues encountered with the original Peskin model, it is relevant to consider a mean-field approach in which the population of large networks is assimilated to a continuum of oscillators and approximated by a density function. Classical tools of calculus enable the study of this continuous model, through the analysis of a partial differential equation. Furthermore, considering heterogeneous populations, by the introduction of white noise, is mathematically tractable and leads to the study of a Fokker-Planck equation.

The present work deals with the development and the study of such a continuous version of the Peskin model. The pulse discrete coupling is shown to become a continuous coupling, which is proportional to the network firing rate, i.e. the flux of oscillators through the high threshold, and which actually corresponds to a limit case of a model studied in [1].

3 Synchronous and asynchronous states

The continuous model exhibits two distinct stationary behaviors (synchronous and asynchronous states) which are exactly the counterparts of synchronization and clustering phenomena observed in the original Peskin model. The arising of these behaviors depends on the coupling strength and is related, in the Peskin model, to the role of avalanches.

The stability of the (a)synchronous state depends both on the coupling nature and on the curvature of the time evolution of the single oscillator state variable, as it was already pointed out in [4]. Considering both homogeneous and heterogeneous populations, we will report on stability analysis and expectations in the two cases of LIF and QIF oscillators. The results will be related to conjectures originally formulated in the context of the Peskin model.

References

- [1] L. F. Abbott and C. van Vreeswijk, *Asynchronous states in networks of pulse-coupled oscillators*, Physical Review E, 48 (1993), pp. 1483–1490.
- [2] R. E. Mirollo and S. H. Strogatz, *Synchronization of pulse-coupled biological oscillators*, Siam J. Appl. Math., Vol. 50, No. 6, pp. 1645–1662, December 1990
- [3] C. S. Peskin, *Mathematical Aspects of Heart Physiology*, Courant Institute of Mathematical Sciences, New York University, New York, pp. 268–278, 1975
- [4] A. Mauroy and R. Sepulchre, *Clustering behaviors in networks of integrate-and-fire oscillators*, Chaos, 18 (2008), p. 037122.

Acknowledgments

This work was supported by the Belgian National Fund for Scientific Research (FNRS) through a Research Fellowship at the University of Liège. This paper presents research results of the Belgian Network DYSCO (Dynamical Systems, Control, and Optimization), funded by the Interuniversity Attraction Poles Programme, initiated by the Belgian State, Science Policy Office. The scientific responsibility rests with its author(s).

A first-order phase transition in a multi-dimensional clustering model

Filip De Smet and Dirk Aeyels

SYSTeMS Research Group

Department of Electrical Energy, Systems and Automation
Ghent University Technologiepark Zwijnaarde 914, 9052 Zwijnaarde
Belgium

Email: Filip.DeSmet@UGent.be, Dirk.Aeyels@UGent.be

1 Model description

We investigate a multi-agent model describing the formation of clusters, a phenomenon that can be observed in e.g. swarming behavior of animals, opinion formation, or synchronization in systems of coupled oscillators. Each agent belongs to a multi-dynamical state space, and is characterized by an autonomous component and attraction towards the other agents:

$$\dot{x}_i(t) = b_i + K \sum_{j=1}^N \gamma_j f_{ij}(\|x_j(t) - x_i(t)\|) e_{x_j(t) - x_i(t)}, \quad (1)$$

for all $i \in \{1, \dots, N\}$, where $\gamma_j > 0$, $K \geq 0$, $N > 1$, and $x_i(t), b_i \in \mathbb{R}^P$. The differentiable functions f_{ij} are non-decreasing with $f_{ij}(0) = 0$, $f_{ij} = f_{ji}$, and $\lim_{\xi \rightarrow +\infty} f_{ij}(\xi) = F_{ij}$, for all i and j in $\{1, \dots, N\}$, for some symmetric matrix $F \in \mathbb{R}^{N \times N}$. Furthermore, $e_x \triangleq \frac{x}{\|x\|}$, for all x in $\mathbb{R}^P \setminus \{0\}$, with $e_0 \triangleq 0$.

2 Clustering behavior

In [2] we show that the long term behavior of the system (1) can be characterized by a set partition H of $\{1, \dots, N\}$, defining different clusters, such that agents belonging to the same cluster have a common long term average velocity (and agents from different clusters have different long term average velocities). We will refer to this behavior as *clustering behavior* with respect to cluster structure H .

3 Preliminary results for $P = 1$

In [1] we show that, for any choice of the model parameters, the system (1) with $P = 1$ exhibits clustering behavior with respect to some cluster structure H , and we formulate necessary conditions and sufficient conditions (only differing in inequality signs being strict or not) characterizing this cluster structure. Furthermore, if the interaction functions are increasing, then distances between agents from the same cluster approach constant values that are independent of the initial condition.

4 Results for $P > 1$

The case $P > 1$ is harder to analyze, and for the investigation of the emerging cluster structure we focus on two special cases: a system with 3 agents, all-to-all interaction and equal weights, and a system with an infinite number of agents in a spherically symmetric configuration.

In the first case we investigate the transition between a single cluster containing all three agents, and a configuration with three clusters, each containing a single agent, without an intermediate stage with two clusters. For $P > 1$ this may happen for generic values of the model parameters, as opposed to the behavior for the case $P = 1$, where a transition generically involves at most two clusters.

In the second case we calculate a lower and an upper bound for the critical value of the coupling strength corresponding to the origination of a central cluster with velocity zero and containing a non-zero fraction of the population. At this transition value, the central cluster has an initial size different from zero, characteristic of a first-order phase transition.

Acknowledgements

This paper presents research results of the Belgian Network DYSCO (Dynamical Systems, Control, and Optimization), funded by the Interuniversity Attraction Poles Programme, initiated by the Belgian State, Science Policy Office. The scientific responsibility rests with its authors.

During this research Filip De Smet was supported by a Ph.D. fellowship of the Research Foundation - Flanders (FWO).

References

- [1] F. De Smet and D. Aeyels. Clustering in a network of non-identical and mutually interacting agents. Accepted by Proceedings of the Royal Society A, 2008.
- [2] F. De Smet and D. Aeyels. A multi-dimensional model for clustering exhibiting a first-order phase transition. In preparation, 2009.

Semi-passivity and synchronization of diffusively coupled neuronal oscillators

Erik Steur*

e.steur@tue.nl

Ivan Tyukin†

I.Tyukin@le.ac.uk

Henk Nijmeijer*

h.nijmeijer@tue.nl

*Dept. of Mechanical Engineering,
Eindhoven University of Technology,
P.O. Box 513 5600 MB, Eindhoven,
The Netherlands

†Department of Mathematics,
University of Leicester,
University Road, Leicester, LE1 7RH,
United Kingdom

1 Introduction

It is well known that neurons might synchronize their behavior to each other. Examples include synchronous oscillations in the visual cortex, motor cortex and the olfactory bulb. Moreover, epileptic seizures are characterized by an increase of synchronized activity.

We discuss synchronization in networks of electrically coupled neuronal oscillators, i.e. neurons that are linearly coupled via gap junctions. In particular, we present sufficient conditions for asymptotic synchronization of an ensemble of electrically coupled neurons.

Semi-passivity and synchronization

Let the neurons in the network be represented by the systems

$$\begin{pmatrix} \dot{x}_{1,j} \\ \dot{x}_{2,j} \end{pmatrix} = \begin{pmatrix} f_1(x_{1,j}, x_{2,j}) \\ f_2(x_{2,j}, x_{1,j}) \end{pmatrix} + \begin{pmatrix} u_j \\ 0 \end{pmatrix}, \quad y_j = x_{1,j}, \quad (1)$$

where $j \in \{1, 2, \dots, k\}$ denotes the number of the oscillator in the network, output $y_j = x_{1,j} \in \mathbb{R}$ denotes the membrane potential, input $u_j \in \mathbb{R}$ is a current stimulus which the j^{th} neuron receives, state $x_{2,j} \in \mathbb{R}^m$ represents internal, possibly biophysically meaningful variables and \mathcal{C}^1 vectorfields $f_1 : \mathbb{R} \times \mathbb{R}^m \rightarrow \mathbb{R}$ and $f_2 : \mathbb{R}^m \times \mathbb{R} \rightarrow \mathbb{R}^m$. Note that many neuronal models are in this normal form or can be put in this form via some (well-defined) transformation of coordinates.

Definition 1 (Passivity and semi-passivity). *See [1]. A system (1) is semi-passive if there exists a nonnegative storage function $V : \mathbb{R}^{m+1} \rightarrow \mathbb{R}_+$, $V(0) = 0$ such that*

$$\dot{V}(x_j) \leq y_j u_j - H(x_j),$$

where the function $H : \mathbb{R}^{m+1} \rightarrow \mathbb{R}$ is nonnegative outside some ball. If the function $H(\cdot)$ is positive outside some ball, then the system (1) is strictly semi-passive.

The most important property for our purpose is that a semi-passive system, when being interconnected by a feedback $u = \varphi(y)$ satisfying $y^\top \varphi(y) \leq 0$, has ultimately bounded solutions [1].

Define the electrical coupling between the systems (1) as

$$u_j = -\gamma_{j1}(y_j - y_1) - \gamma_{j2}(y_j - y_2) - \dots - \gamma_{jk}(y_j - y_k), \quad (2)$$

where the gains $\gamma_{ji} = \gamma_{ij} \geq 0$ represent the synaptic conductances. Defining the $k \times k$ coupling matrix as

$$\Gamma = \begin{pmatrix} \sum_{i=2}^k \gamma_{1i} & -\gamma_{12} & \dots & -\gamma_{1k} \\ -\gamma_{21} & \sum_{i=1, i \neq 2}^k \gamma_{2i} & \dots & -\gamma_{2k} \\ \vdots & \vdots & \ddots & \vdots \\ -\gamma_{k1} & -\gamma_{k2} & \dots & \sum_{i=1}^{k-1} \gamma_{ki} \end{pmatrix},$$

we can write (2) as $u = \Gamma y$, where $u := \text{col}(u_1, u_2, \dots, u_k)$ and $y := \text{col}(y_1, y_2, \dots, y_k)$. Note that Γ is symmetric, singular and positive semi-definite (Gerschgorin's theorem). Moreover, assuming that the network cannot be divided into two or more disconnected networks, the matrix Γ will have a simple zero eigenvalue. If each system (1) is semi-passive, then the network of electrically coupled systems possesses ultimately bounded solutions.

Theorem 1.1 (Synchronization). *See [1]. Suppose that*

1. *each system (1) is semi-passive;*
2. *each subsystem $\dot{x}_{2,j} = f_2(x_{2,j}, x_{1,j})$ is a convergent system¹.*

Let γ_i be an eigenvalue of Γ and let the eigenvalues be ordered as $0 = \gamma_1 < \gamma_2 \leq \dots \leq \gamma_k$. Then there exists $\bar{\gamma} > 0$ such that if $\gamma_2 \geq \bar{\gamma}$ the systems (1) synchronize asymptotically.

In [2] we show that the neuronal models of *Hodgkin-Huxley*, *Morris-Lecar*, *FitzHugh-Nagumo* and *Hindmarsh-Rose* satisfy both assumptions of the theorem. Hence, for some $\gamma \geq \bar{\gamma}$, i.e. for a given network topology in combination with sufficiently strong coupling, the neurons in the network asymptotically synchronize.

References

- [1] A.Yu. Pogromsky and H. Nijmeijer, Cooperative Oscillatory Behavior of Mutually Coupled Dynamical Systems, IEEE Trans. Circuits Syst. I, vol. 48, pp. 152-162, 2001
- [2] E. Steur, I. Tyukin and H. Nijmeijer, Semi-passivity and synchronization of neuronal oscillators, (submitted)

¹see [1] or [2] for details

On the influence of positive and negative feedback loops on the phase response curve of biological oscillators

Pierre Sacré and Rodolphe Sepulchre

Department of Electrical Engineering and Computer Science,

GIGA-Systems Biology and Chemical Biology,

University of Liège, Belgium.

Emails: Pierre.Sacre@ulg.ac.be, R.Sepulchre@ulg.ac.be

1 Introduction

Rhythmic phenomena are essential to the dynamic behavior of biological systems. They find their roots in the many regulatory mechanisms that control life at the cellular level. Understanding those molecular and cellular mechanisms is crucial to advances in systems biology.

Dynamic models of regulatory mechanisms are made of complex interconnections of feedback loops often described by bloc diagrams. In this research, our goal is to understand how entrainment and synchronization, two important system properties of biological oscillators, depend on the circuitry of these bloc diagrams. The general idea is illustrated on a particular model of cell mitosis [1].

2 Circuitry of oscillators

A single two-component negative feedback system can exhibit damped oscillations but will inevitably approach a stable steady state. Some aspect of the circuit must be altered to convert it into a sustained oscillator. Two basic types of bloc diagrams have been proposed for biological oscillators.

One type contains only negative feedback loop. With sufficient phase delay in the feedback loop, the system repeatedly overshoots and undershoots its steady state, leading to sustained oscillations [2, 3].

A second type of bloc diagrams contains both positive and negative feedback loops. The positive-feedback loop creates a bistable system (a toggle switch) and the negative-feedback loop drives the system back and forth between the two stable steady states [4, 5].

3 Infinitesimal phase response curve

The infinitesimal phase response curve (iPRC) has proven a very useful tool to study the input-output properties of oscillators. The start point is a dynamical system of the form

$$\dot{x} = f(x) + \varepsilon u(t), \quad x \in \mathbb{R}^m, \quad (1)$$

having for $\varepsilon = 0$ a limit cycle attractor $\gamma \subset \mathbb{R}^m$ with period T and frequency $\Omega = 2\pi/T$, and forced by a weak input $\varepsilon u(t)$.

Using an asymptotic method of reduction [6], the system (1) is transformed into the phase model

$$\dot{\theta} = \Omega + \varepsilon Q(\theta) \cdot p(t) \quad (2)$$

with $Q(\theta)$ being the iPRC. The iPRC tabulates the transient change in the cycle period of an oscillator induced by an infinitesimal perturbation as a function of the phase at which it is received.

The characterization of this phase model, especially its equilibria and their stability, is used to study the entrainment and the synchronization of the system. The shape of the iPRC plays thus a leading role in those properties.

4 Shaping the iPRC from the circuitry

We wish to relate the circuitry of the bloc diagram describing the biological oscillator and its iPRC. We illustrate this general question on a model of mitotic oscillations abundantly discussed in the literature [1].

References

- [1] T. Y.-Ch. Tsai, Y. S. Choi, W. Ma, J. R. Pomeroy, Ch. Tang, and J. E. Ferrell Jr. Robust, tunable biological oscillations from interlinked positive and negative feedback loops. *Science*, 321(5885):126–129, Jul 2008.
- [2] B. C. Goodwin. Oscillatory behavior in enzymatic control processes. *Adv Enzyme Regul*, 3:425–438, 1965.
- [3] A. Goldbeter. A minimal cascade model for the mitotic oscillator involving cyclin and Cdc2 kinase. *Proc Natl Acad Sci U S A*, 88(20):9107–9111, Oct 1991.
- [4] J. J. Tyson, K. C. Chen, and B. Novak. Sniffers, buzzers, toggles and blinkers: dynamics of regulatory and signaling pathways in the cell. *Curr Opin Cell Biol*, 15(2):221–231, Apr 2003.
- [5] J. R. Pomeroy, E. D. Sontag, and J. E. Ferrell Jr. Building a cell cycle oscillator: hysteresis and bistability in the activation of Cdc2. *Nat Cell Biol*, 5(4):346–351, Apr 2003.
- [6] F. C. Hoppensteadt and E. M. Izhikevich. *Weakly Connected Neural Networks*. Springer-Verlag, New York, 1997.

Bursting modeling in dopaminergic neurons

Guillaume Drion^{1,2}, Vincent Seutin² and Rodolphe Sepulchre¹

¹Department of Electrical Engineering and Computer Science

²Laboratory of Pharmacology and Research Center for Cellular and Molecular Neurobiology
University of Liège, 9 Place du 20-Août, Liège, Belgium

1 Introduction

Midbrain dopaminergic (DA) neurons profoundly influence behavior by promulgating a reward signal in critical striatal and forebrain structures. In physiological conditions, these cells can switch between tonic, irregular, and burst firing (Grace and Bunney, 1984), which is a critical component of the signalling (Heien and Wightman, 2006).

A particularity of pacemaker cells such as DA neurons is that bursting is not expressed endogenously. Indeed, whereas only regular tonic firing (or pacemaker firing) is observed in *in vitro* conditions, glutamate synaptic inputs (such as NMDA inputs) are required to make the cell to fire in burst. Moreover, the intra-burst firing frequency is much higher (about 15Hz) than the firing frequency in single-spikes (between 0.5Hz and 5Hz). This suggests that the system requires two different mechanisms to regulate intra-burst firing in the one hand (a fast dynamic), and tonic firing, inter-burst time in the other hand (a slow dynamic). Therefore, a common model of noise-induced bursting composed of Hodgkin-Huxley like equations with added stochastic currents would not be sufficient to describe this behavior.

Finally, it has been shown that an inhibition of a calcium-activated potassium current (expressed by SK channels) in *in vivo* conditions induces burst firing in dopaminergic neurons (Waroux et. al., 2005) and in other non-endogenous bursting cells, such as serotonergic neurons (Rouchet et. al., 2008). This suggests a role for the intracellular calcium concentration $[Ca^{2+}]_{in}$ dynamic in the regulation of the firing patterns of this type of cells.

2 Proposed model

A complex model of a dopaminergic neuron was already developed to fit signalling of DA neurons as well as possible (Canavier and Landry, 2006). Here, we propose a basic one-compartmental model that reproduces the mechanisms that regulates firing patterns of pacemaker cells in general. This model can be generalized to all cells that can fire either in tonic firing mode or synaptically induced bursting mode, spontaneously active or not.

In order to be consistent with the experimental data that we mentioned above, the model is composed of two dynamics,

following the common equation

$$C\dot{V} = -I_{ion} \quad (1)$$

The fast dynamic includes a sodium current I_{Na} and a delayed-rectifier potassium current $I_{K,DR}$. These currents are responsible for the creation of action potentials. The slow dynamic describes the fluctuations of $[Ca^{2+}]_{in}$. Calcium entries come from a L-Type calcium current $I_{Ca,L}$, which is voltage-gated and calcium-regulated, and the calcium is pumped out of the cell by calcium pumps, which generate an outward calcium current $I_{Ca,pump}$. Synaptic inputs activate a sodium synaptic current $I_{Na,syn}$, which is a depolarizing current. The background of synaptic activity was modeled through deterministic and stochastic waveforms. A calcium-activated potassium current $I_{K,Ca}$ was also implemented in the model.

3 Results

The proposed model is able to fire spontaneously in single-spike at a low frequency, following the calcium waves. In the presence of synaptic inputs, the modeled neuron can switch from irregular firing to burst firing when blocking $I_{K,Ca}$, with a high intra-burst firing frequency. We observed that burst firing is always accompanied by higher $[Ca^{2+}]_{in}$ fluctuations.

We analyzed the mechanisms underlying this behavior from a non linear dynamic point of view, showing that the system is able to oscillate only if the level of intracellular calcium concentration is under a critical. We also showed that this critical value is dependent on the synaptic inputs, this dependence being attenuated by the presence of a calcium-activated potassium current.

References

- [1] O. Waroux, L. Massotte, L. Alleva, A. Graulich, E. Thomas, JF. Liegeois, J. Scuvée-Moreau, and V. Seutin. *SK Channel Control the Firing Pattern of Midbrain Dopaminergic Neurons in Vivo*. European Journal of Neuroscience, 2005, 22:3111-3121.
- [2] N. Rouchet, O. Waroux, C. Lamy, L. Massotte, J. Scuvée-Moreau, JF. Liegeois and V. Seutin. *SK channel blockade promotes burst firing in dorsal raphe serotonergic neurons*. European Journal of Neuroscience, 2008, 28:1108-1115.
- [3] C. C. Canavier and R. S. Landry. *An Increase in AMPA and a Decrease in SK Conductance Increase Burst Firing by Different Mechanisms in a Model of a Dopamine Neuron In Vivo*. Journal of Neurophysiology, 2006, 96:2549-2563.

Haptic Feedback in Telesurgery

Dennis van Raaij
Department of Mechanical Engineering
Eindhoven University of Technology
P.O. Box 513, 5600 MB Eindhoven
The Netherlands
Email: d.w.j.v.raaij@tue.nl

Maarten Steinbuch
Department of Mechanical Engineering
Eindhoven University of Technology
P.O. Box 513, 5600 MB Eindhoven
The Netherlands
Email: m.steinbuch@tue.nl

Minimally Invasive Surgery

In a master/slave *minimally invasive robotic surgery system* (MIRS system), conventional laparoscopic surgical instruments are separated into two pieces. The instrument interface is embedded in a *master console* where it interacts with the surgeon, the (exchangeable) instrument end-effectors are incorporated in a *slave robot* located next to the patient.

The advantage of such a surgical teleoperation system is twofold. The surgeon will, on one hand, be able to perform surgical tasks in a more natural, intuitive and ergonomic way. On the other hand, the patient's body will experience less trauma which will result in a shorter recovery time.

Bilateral Control

To reobtain the mechanically lost *interaction* between the instrument interface and end-effector, both are recoupled via a virtual link which is simulated by a *bilateral controller* which allows for two-way information exchange (in this case position and/or force in both directions). Today's commercial systems for robot assisted surgery lack the feedback of force information which results in a higher mental load as the surgeon is expected to estimate the interacting forces continuously based on visual feedback.

The difficulty in enabling a natural coupling lies, from a control point of view, in (among others) limitations of sensors and actuators, large uncertainties associated with the (unknown) operator and (unknown) environment and the possible compensation of dynamics that may decrease the usability of the system as a tool (e.g. large inertias or friction).

MIRS Project at the TU/e

A surgical teleoperation system is currently build at the Mechanical Engineering department of the TU/e. The hardware is developed at the Construction Engineering R&D Lab and is proceeding towards a first prototype.

Regarding the development of a control architecture that enables force feedback (a 'haptic controller') some preliminary work has been done. A short overview can be given as follows.

- There has been done some research towards the estimation of external forces (using a *disturbance observer*) for use with an *admittance controller* in case force sensors are not available at either the master side, slave side or both. A controller was designed and implemented on a 1 DOF master/slave lab setup.
- Some experiments were done in which the human lower arm was identified in a specific posture. The goal was to get insight into the (passive) impedance to be expected at the master side. See also figure 1 for an indication of the results.

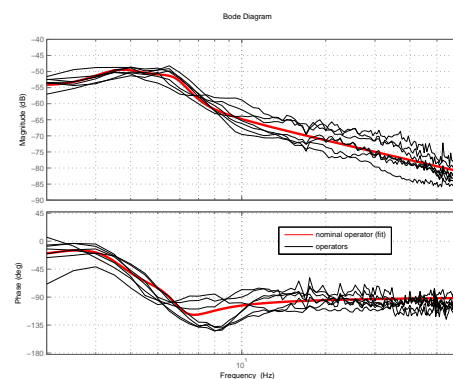


Figure 1: Results of the identification (2 – 60 [Hz]) for the situation with relaxed muscles. Shown are the individual operator FRF estimations $\hat{Y}_{opr} = \hat{Z}_{opr}^{-1}$ (black) and mean FRF (red).

- A first attempt has been made to relate *task execution performance* to *controller performance*. The main objective was to identify a threshold related in a certain representative controller performance measure above which further improvement of the controller performance would not lead to better task execution performance. The task was simple free-air positioning (no force feedback yet). The associated task performance was based on *Fitt's Law*. The controller was a simple position-error controller implemented on a linear 1 DOF setup featuring air-bearings to control the influence of friction.

User Adapted Control of Force Feedback Teleoperators: Evaluation and Robustness Analysis

L. Barbé, B. Bayle, E. Laroche and M. de Mathelin
LSIIT, University of Strasbourg, France.

The main problem in force feedback teleoperation consists in the design of a stable and transparent controller. While the fundamental requirement for any control system is stability, transparency is specific to force feedback teleoperation. It characterizes the operator immersion in the remote environment. Stability and transparency have been extensively studied in the literature [1]. Bilateral controller synthesis has been considered to simultaneously offer stability and optimal transparency in spite of time delays, plant disturbances, measurements noise and modeling uncertainties, etc. This problem is difficult for two main reasons. First, the slave manipulator interacts with an a priori unknown environment. But above all, the interaction between the human operator and the master manipulator, and the behavior of the operator are extremely complex to model. To our knowledge, very few methods deal with the search for an automatic synthesis method of the telemanipulation controller. In the current work we propose an auto-tuning method [2] and a robustness test in order to prove the stability of the system for variations of both the environment and the user behavior. Herein we consider the Force-Position scheme.

1 Automatic tuning method of Master controller

We propose to tune the local force controller of master device with an automatic method based on relay feedback [3]. There are two steps in the method : first, the controller is replaced by a relay (Fig. 1), and secondly, the frequency and the amplitude of the oscillations are measured to derive the parameters of a PID controller.

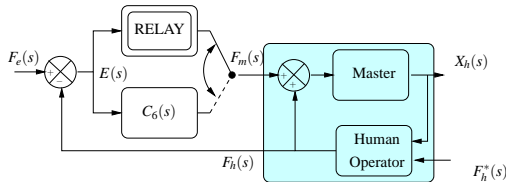


Figure 1: Relay method principle

2 Experimental evaluation

The slave manipulator is a Cartesian robot equipped with a needle. The environment is composed of a Limbs and ThingsTM mannequin. The master manipulator is a PHANTOMTM 1.5/6DOF haptic interface. During the relay

identification the master robot only interacts with the user. Then the relay is replaced by the synthesized controller and the slave is connected using the FP teleoperation scheme. Then the user performs a teleoperated needle insertion into soft tissue.

3 Robustness analysis

We propose to identify several LTI models of a human operator and to develop an uncertain model that encompasses all the identified models. The human arm model can be written as $F_h(s) = F_h^*(s) - Y_h(s)^{-1}V_h(s)$. The uncertain model is chosen of the shape $Y_h(\Delta_h, s) = Y_{h0}(s)(1 + W_h(s)\Delta_h(s))$ where $Y_{h0}(s)$ is the nominal model, $W_h(s)$ is a weighting function and $\|\Delta_{hk}(s)\|_\infty \leq 1$. The slave manipulator interacts with an uncertain environment, that can be modelled by $F_e(s) = (k_e + b_e s)X_e(s)$ where parameters k_e and b_e vary over intervals. The results of the robustness analysis are given in Fig. 2.

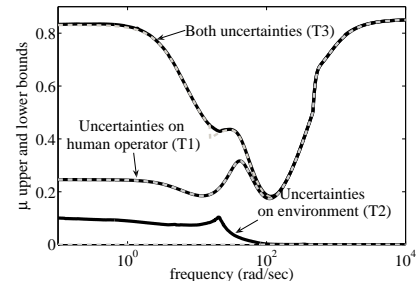


Figure 2: Structured singular values (μ) for the three robustness tests (plain: upper bounds; dashed: lower bounds)

References

- [1] P. Hokayem and M. Spong, "Bilateral teleoperation: An historical survey," *Automatica*, vol. 42, no. 12, pp. 2035–2057, 2006.
- [2] L. Barbé, B. Bayle, E. Laroche, and M. de Mathelin, "User adapted control of force feedback teleoperators: Evaluation and robustness analysis," in *IEEE/RSJ International Conference on Intelligent Robots and Systems*, Nice, France, 2008.
- [3] K. Åström and T. Hägglund, "Automatic tuning of simple regulators with specification on phase and amplitude margins," *Automatica*, vol. 20, no. 5, pp. 645–651, 1984.

A Passivity Study of the Classical Position-Force Teleoperation controller

B. Willaert, B. Corteville, D. Reynaerts, H. Van Brussel and E.B. Vander Poorten

Department of Mechanical Engineering, K.U.Leuven

Celestijnenlaan 300C, B-3001 Heverlee, Belgium

Email: bert.willaert@mech.kuleuven.be

1 Introduction

This work rigourously analyzes the stability properties of the popular Position-Force bilateral teleoperation controller. Firstly, the existing concepts of *two-port passivity* and *absolute stability* are discussed, after which a new method for stability analysis is presented, referred to as *one-port Passivity*.

In the basic configuration of the Position-Force controller, the control inputs for the motors are:

$$\tau_m = -\lambda \cdot F_e, \quad \tau_s = (K_v s + K_p) \cdot (\mu \cdot x_m - x_s) \quad (1)$$

with μ and λ the position and force scaling factor. The analysis is based on simple mass-damper models for the master (M_m, B_m) and the slave (M_s, B_s). x_m and x_s are the position of the master and the slave respectively. F_e is the measured interaction force with the environment.

2 Two-port Passivity and Absolute Stability

Two-port Passivity is a sufficient condition for stable interaction. Absolute stability is a less conservative sufficient condition incorporating the structural knowledge that no direct interaction between operator and environment occurs. However, the authors proved analytically that the Position-Force controller as defined in the introduction is never passive nor absolutely stable for non trivial parameters. These proofs are based on the *Raisbeck passivity criterion* and on *Llewellyn's absolute stability criterion* respectively.

3 One-port Passivity

The new method is based on combining the dynamics of the master, slave, controller and environment into a one-port network $Y_{MS(K_e)}$. The *coupled stability* between any operator and the $Y_{MS(K_e)}$ one-port is now discussed (Figure 1). Coupled stability can be checked by verifying positive realness of the admittance $Y_{MS(K_e)}$ [1]. In order to determine $Y_{MS(K_e)}$, an assumption has to be made about the environment. As stated in [1], pure springs and pure masses can be considered as the *worst* case environments since their admittance is not strictly passive. Since for teleoperation research displaying stiffnesses is in most cases more relevant, the environment considered here is a pure spring (K_e).

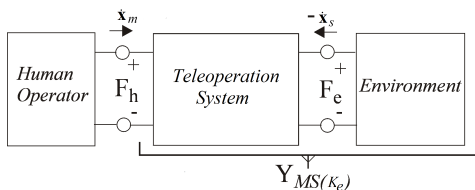


Figure 1: A one-port network $Y_{MS(K_e)}$ representation of a combined teleoperator-environment system.

Through this assumption the admittance of the one-port can be written as:

$$Y_{MS(K_e)} = \frac{s(M_s s^2 + (B_s + K_v)s + (K_p + K_e))}{(M_m s^2 + B_m s)(M_s s^2 + (B_s + K_v)s + (K_p + K_e)) + \mu \lambda K_e (K_v s + K_p)} \quad (2)$$

The $\Re(Y_{MS(K_e)}(j\omega)) \geq 0$ condition results in a rather complicated set of analytic conditions on the parameters of the system. However, the authors found that in most practical cases, the conditions simplify to the following:

$$\mu \lambda \leq \frac{B_m(B_s + K_v)}{M_s K_e K_v^2} \left((B_s + K_v)K_v - 2M_s K_p + 2\sqrt{M_s^2 K_p^2 + M_s K_v^2 K_e - K_p K_v B_s M_s} \right) \quad (3)$$

Figure 2 shows the effect on the maximum allowed $\mu \lambda$ as a function of the selected K_e^{max} and the parameters M_s , B_m and K_p , every time for all other parameters fixed.

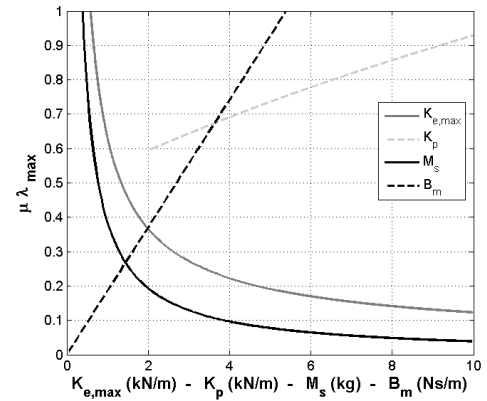


Figure 2: Effect K_e^{max} , M_s , B_m and K_p on $\mu \lambda^{max}$. The nominal parameters are based on an experimental setup: $M_s = 0.6$ kg, $K_p = 4000$ N/m, $K_v = 80$ Ns/m, $B_m = 3.4$ Ns/m, $B_s = 11$ Ns/m. K_e^{max} is set at 1000 N/m.

4 Discussion and Conclusions

The inequality (3) shows the incapability of the Position-Force controller to display arbitrarily large environment stiffnesses. Other fundamental insights obtained from (3) are: the mass of the slave strongly limits the achievable $\mu \lambda^{max}$, an increase of master damping (B_m) allows larger $\mu \lambda^{max}$ and also a tighter position loop at the slave allows larger $\mu \lambda^{max}$ (when the damping ratio is kept constant). In future work the same systematic approach will be followed to analyze other more general teleoperation controllers. ¹

References

- [1] J.E. Colgate "The Control of Dynamically Interacting Systems," Ph.D. Thesis, MIT, August 1988

¹Research funded by a PhD grant from the Institute for the Promotion of Innovation through Science and Technology in Flanders (I.W.T.-Vlaanderen)

Robust 4-channel Teleoperation Controller Design

E.B. Vander Poorten, D. Reynaerts, H. Van Brussel

Dept. of Mech. Eng., K.U. Leuven, Celestijnenlaan 300C, B-3001 Heverlee, Belgium

emmanuel.vanderpoorten@mech.kuleuven.be

T. Kanno, Y. Yokokohji

Dept. of Mech. Eng. & Science, Kyoto Univ., Yoshida Honmachi, Sakyo-ku, Kyoto, 606-8501, Japan

1 Abstract

Controller synthesis for teleoperation boils down to making an adequate trade-off between performance and stability. By incorporating more knowledge of the system or its interacting elements, performance can be gained without compromising stability. Compared to 2- and 3-channel schemes, 4-channel controllers, using force and displacement signals measured at both master and slave, are inherently more powerful. However, the substantial amount of parameters involved in these systems, complicates their understanding, restraining their practical use. This document advocates the use of \mathcal{H}_∞ theory to take care of parameter tuning and introduces methods to incorporate stability requirements and environmental knowledge into the \mathcal{H}_∞ framework.

2 \mathcal{H}_∞ controller formulation for teleoperation

Compared to traditional controller design, the design of teleoperation controllers is complicated by the need to guarantee the performance and stability of a system that interacts with two largely unknown dynamic elements: 1) the human operator and 2) the remote environment. A challenge exists in finding an appropriate way to incorporate these constraints in the \mathcal{H}_∞ controller synthesis. Traditionally, \mathcal{H}_∞ theory foresees in methods to treat bounded uncertainties. However in a general teleoperation setting, the only assumption that is being made about the uncertainties is that they are passive [1], which implies that their impedances belong to the right half complex plane. In order to reshape these unbounded conditions towards \mathcal{H}_∞ compatible equivalents, one can reformulate the interaction between teleoperator and operator/environment towards a wave-variables form. Fig.1 explains this procedure for a system with 1-dimensional master and slave. The operator and environment are replaced by their scattering forms: S_{op} and S_e , for which the passivity property reads as: $\|S_{op}\|_\infty \leq 1$ and

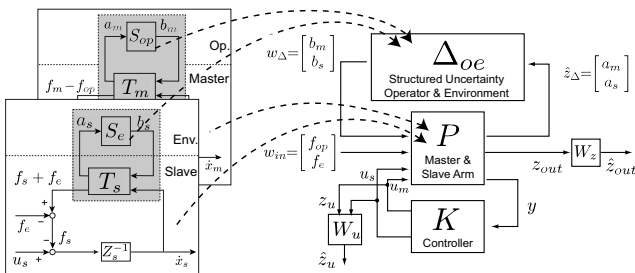


Figure 1: Operator/environment as structured uncertainty

$\|S_e\|_\infty \leq 1$. The transformation matrices \mathbf{T}_m and \mathbf{T}_s are responsible for the transition towards wave variables. The generalized plant \mathbf{P} includes \mathbf{T}_m and \mathbf{T}_s as well as the other elements pertaining to master and slave. \mathcal{H}_∞ theory allows then to derive a controller \mathbf{K} that minimizes a weighted set of performance objectives \mathbf{z}_{out} and control penalties \mathbf{z}_u in the presence of the bounded uncertainty Δ_{oe} .

3 Introduction of operator/environment bounds.

Teleoperation controllers designed according to the passivity property tend to be conservative. By including additional knowledge of operator/environment, performance gains could be achieved. In [2], Hashtrudi-Zaad and Salcudean showed how passive shunts can be placed around the teleoperator to *analyze* the stability of non-passive controllers interacting with operator/environments with known boundaries in impedance. The formalism of section 2 makes it possible to use the idea of passive shunts and *synthesize* less conservative controllers with \mathcal{H}_∞ theory. Fig.2 sketches this for the operator-side. Practically, \mathbf{T}_m and \mathbf{T}_s are reformulated towards \mathbf{T}_{lim}^{op} and \mathbf{T}_{lim}^e and then inserted into \mathbf{P} .

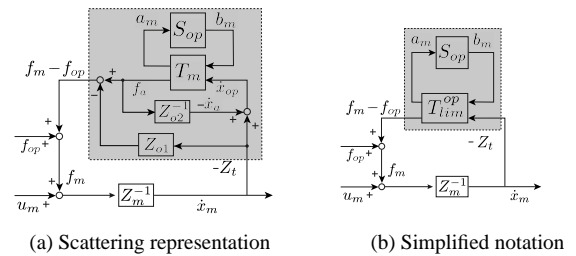


Figure 2: Bounds on the operator dynamics.

4 Conclusion

This paper introduced a framework to design robust 4-channel teleoperation \mathcal{H}_∞ controllers. Further work will deal with the practical implications of the presented approach.

5 Acknowledgements

This research was supported by a Marie Curie International Reintegration Grant within the 7th European Community Framework Programme.

References

- [1] N. Hogan. Controlling impedance at the man/machine interface. *ICRA'89*, pp.1626–1631, Scottsdale, AZ, 1989.
- [2] K. Hashtrudi-Zaad and S.E. Salcudean. Analysis of control architectures for teleoperation systems with impedance/admittance master and slave manipulators. *IJRR*, 20(6):419–445, June 2001.

Optimization of a static output feedback controller for teleoperation

Thomas Delwiche, Laurent Catoire, Serge Torfs and Michel Kinnaert

Dept. of Control Engineering (CP 165/55)

Université Libre de Bruxelles (ULB)

Av. F.D. Roosevelt, 50 1050 Brussels, Belgium

Samir Aberkane

CRAN-UMR 7039 CNRS

Université Henri Poincaré

Nancy I, F-54506 Vandoeuvre-les-Nancy, France

Corresponding author email: Thomas.Delwiche@ulb.ac.be

1 Introduction

Teleoperation consists in performing a remote task with an electromechanical master-slave device. The master part of the system is manipulated by the human operator while the slave part, which is located remotely, reproduces the task imposed by the master. When force feedback is present at the master side to make the user feel the interaction forces between the slave and its environment, one refers to bilateral teleoperation. In this paper we propose to tune a static output feedback (SOF) controller for a teleoperation system using a heuristic approach. Compared to widespread approaches like H_∞ optimization or μ synthesis [1], where the order of the controller is at least as high as the order of the plant, a SOF controller can be easily implemented on the system without requiring order reduction methods.

2 Optimization algorithm

The teleoperation system is characterized by n_y ($n_y \geq 2$) measured outputs and n_u ($n_u = 2$) actuation inputs in the case of a one degree of freedom system. The SOF controller, which will be denoted K , is therefore a matrix with $K \in \mathbb{R}^{n_u \times n_y}$.

Two cost functions are defined, namely $j_p(K)$ and $j_r(K)$ where the first one is related to the performance of the system and where the second one is related to its stability margin. The optimization of these cost functions is performed iteratively, starting from a stabilizing K^0 . At each step, the next controller is calculated using the following algorithm.

$$K^{k+1} = \arg \min_{K \in \mathbb{D}(K^k)} d(K, K^k)$$

where the function $d(K, K^k)$, given by

$$d(K, K^k) \equiv \begin{cases} j_p(K) - j_p(K^k) & k = 2n + 1 \quad n \in \mathbb{N} \\ j_r(K) - j_r(K^k) & k = 2n \quad n \in \mathbb{N} \end{cases}$$

is minimized over a subset of $\mathbb{R}^{n_u \times n_y}$ defined by

$$\mathbb{D}(K^k) = \{K | j_p(K) \leq j_p(K^k), j_r(K) \leq j_r(K^k)\}$$

Constraining the optimization to $\mathbb{D}(K^k)$ allows a monotonical decrease of the cost functions. In practice, the optimization is reduced to a one degree of freedom search along a direction pointing into $\mathbb{D}(K^k)$.

3 Initial solution

Because the optimization problem presents local minima, numerical experiments will be conducted to investigate the variation of the performance as a function of the initial controller setting K^0 .

4 Comparison with other methods

Our algorithm will be compared in terms of quality of the solution and computation time with a well-established LMI approach given in [2].

Acknowledgments

The work of Thomas Delwiche is supported by a FRIA grant. This paper presents research results of the Belgian Network DYSCO (Dynamical Systems, Control, and Optimization), funded by the Interuniversity Attraction Poles Programme, initiated by the Belgian State, Science Policy Office. The scientific responsibility rests with its authors.

References

- [1] K. Kim, M.C. Çavusoglu and W.K. Chung, "Quantitative comparison of bilateral teleoperation systems using μ -synthesis", *IEEE Transactions on Robotics*, vol. 23, no. 4, pp. 776-789, Aug. 2007.
- [2] L. El Gahoui, F. Oustry and M. AitRami, "A cone complementary linearization algorithm for static-output feedback and related problems", *IEEE Transactions on Automatic Control*, vol. 42, no. 8, pp. 1171-1176, Aug. 1997.

Passivity and Transparency in Bilateral Tele-manipulation

Michel Franken
Institute of Technical Medicine
University of Twente
P.O. Box 217, 7500 AE Enschede
The Netherlands
Email: m.c.j.franken@utwente.nl

Stefano Stramigioli
IMPACT Institute
University of Twente
P.O. Box 217, 7500 AE Enschede
The Netherlands
Email: s.stramigioli@utwente.nl

1 Introduction

A tele-manipulation chain is composed of a user, a master system, a communication channel, a slave system and an environment. In a bilateral tele-manipulation chain the control algorithm usually tries to synchronize the motions of the slave device with the motions of the master device enforced by the user and to reflect the interaction forces between the slave device and the environment to the user by means of the master device.

2 Time delays

It is likely to assume that time delays will be present in the communication channel between the master and slave systems. Due to these time delays it is not simply possible to exchange the power variables (forces and velocities) between the master and slave system. A direct exchange of these variables would create “virtual” energy in the presence of time delays turning the communication channel into an active element and this generated energy could let the system become unstable.

3 Transparency and Stability

An extensive overview of various approaches to the tele-manipulation problem is given in [1]. Different approaches are usually compared based on their transparency and stability properties.

Transparency relates to how well the complete system is able to convey to the user the perception of directly interacting with the remote environment. As the time delays in the communication channel might be unknown and/or time-varying it is desirable that stability of the system will be guaranteed in the presence of arbitrary time delays. A solution to the stability problem with respect to time delays can be found in the expression of the communication channel in scattering variables, which makes the system passive. The power variables are “coded” in such a way that no energy is virtually generated in the communication channel [2]. A major criticism on the use of scattering variables is the level of transparency that can be obtained. During steady state operation the appropriate forces will be reflected, but the transient response can be heavily distorted.

4 Proposed algorithm

The presence of time delays will always have a negative influence on the achievable transparency, but in current schemes this limit is the result of the fact that both the energy exchanged between master and slave and the information which should transmit the haptic behavior for transparency are transmitted/coded in the same variables.

A two-layer algorithm is therefore proposed that allows the highest transparency possible whilst guaranteeing passivity and thus stability in the presence of arbitrary time delays. The *Transparency Layer* computes control efforts to satisfy the goals of the tele-manipulation chain: movement synchronization on the slave side and force reflection on the master side. The *Passivity Layer* on the other hand has to make sure that the commands originating from the *Transparency Layer* do not violate the passivity condition. The benefit of this strict separation in layers is that the implemented strategy to ensure optimal transparency does not depend on the implemented strategy to ensure passivity and vice versa.

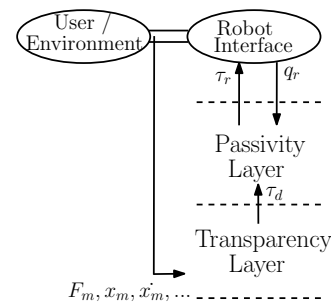


Figure 1: Two layer algorithm

References

- [1] P. Hokayem and M. Spong, “Bilateral teleoperation: An historical survey,” *Automatica*, vol. 42, pp. 2035–2057, 2006.
- [2] S. Stramigioli, A. van der Schaft, B. Maschke, and C. Melchiorri, “Geometric scattering in robotic telemanipulation,” *IEEE Transactions on Robotics and Automation*, vol. 18, no. 4, pp. 588–596, August 2002.

Stabilizing the baseline current of a microbial fuel cell-based biosensor.

STEIN Nienke^{1,2,3}, HAMELERS Hubertus³, BUISMAN Cees^{1,3}, STIGTER Hans²

¹Wetsus, centre of excellence for sustainable water technology

²System and control group, Wageningen University

³Subdepartment of Environmental Technology, Wageningen University

Keywords: biosensor, on-line, Electrochemically active bacteria

It is of crucial importance that drinking water is safe to drink. A fast and economical way to monitor the water quality is through on-line continuous methods using e.g. sensors. The current on-line toxicity sensors have some limitations e.g. low number of individuals, a complicated metabolism or a loss in accuracy due to a two-step translation of the signal. A better sensor is required to overcome these limitations [Hasan 2005].

The aim of this research is to develop a robust, continuous sensor for the integral determination of (toxic) changes in water quality using electricity producing bacteria. Electrochemically active bacteria produce electrical current dependent on their metabolic state. This current therefore represents the quality of the water and can be directly measured. [Kim 2007] Fluctuations in the water composition will lead to fluctuations in electrical current.

The influence of pH, substrate concentration and anode potential on electrical current production by bacteria has been tested. The results show that pH has a major influence on the produced electrical current even at intermediate levels. The bacterial metabolism is not influenced at these levels but pH changes cause a change in overpotential and this is clearly seen in the produced current. Substrate concentrations have a much lower impact on the overpotential and this results in a much lower sensitivity of the sensor for changes in substrate concentration. Only when the substrate concentration decreases very much it affects the bacterial metabolism and so the electrical current.

From the definition of the overpotential it can be seen that pH has a larger influence on the overpotential than the substrate concentration. The overpotential is defined as the difference between the potential of the electron acceptor, the anode, and the potential of the electron donor, the reactor medium with substrate in solution.

$$V_{\text{overpotential}} = V_{\text{anode}} - V_{\text{equilibrium}}$$

$$V_{\text{overpotential}} = V_{\text{anode}} - \left(E_0 + \frac{RT}{nF} \ln \left(\frac{[HCO_3^-]^2 [H^+]^9}{[S^-]} \right) \right)$$

$$I = R_{\text{anct}} * V_{\text{overpotential}}$$

In which:

E_0 = redox potential at standard conditions (V),

R = gas constant ($J \text{ mol}^{-1} \text{ K}^{-1}$)

T = Temperature (K), n = number of electron

involved in the reaction (-), F = Faradays

constant ($C \text{ mol}^{-1}$), S = substrate concentration,

during the experiments acetate was used (mol l^{-1}),

R_{anct} = anodic charge transfer resistance, I = electrical current (A),

The anode potential is linearly related to the electrical current when it changes in a range in which bacteria can easily adapt. A further increase in anode potential will not lead to an increase in electrical current because bacteria can not adapt.

These results show that controlling the overpotential is very important for the control of the sensor in order to distinguish between changes in toxic levels and changes in other environmental parameters in water.

Future research focuses on understanding the mechanisms that build up the overpotential and to model these as to arrive at a model-based toxicity sensor that includes fault-detection algorithms for reliable determination of a toxicity event.

Hasan, J., D. Goldbloom-Helzner, et al. (2005). Technologies and Techniques for Early Warning Systems to Monitor and Evaluate Drinking Water Quality: A State-of-the-Art Review

Kim, M., M. S. Hyun, et al. (2007). "A novel biomonitoring system using microbial fuel cells." *Journal of environmental monitoring* **9**: 1323-1328.

Identification of Biochemical Reaction Systems using a Dissipative Observer

Dirk Fey and Eric Bullinger

Department of Electronic and Electrical Engineering

University of Strathclyde

United Kingdom

Email: dirk.fey@eee.strath.ac.uk

Email: eric.bullinger@eee.strath.ac.uk

Abstract

An essential part of systems biology is dynamic modelling and mathematical analysis, whereby the behaviour of the models depends crucially on its kinetic parameters. Often these parameters can not be measured directly, and must be estimated from indirect measurements, usually in the form of time course data. In spite of numerous estimation methods in the literature, there seems to be a lack of accurate and reliable estimation methods. Certain particularities of biological systems, such as nonlinearity, high number of components and sparse, noisy measurements hinder the straightforward application of common systems theoretical methods (1).

Some of these biological particularities can be exploited in order to develop methods that are particularly tailored to biological systems. Earlier work demonstrated that using structural information only, systems of biochemical reactions can be transformed into a parameter independent form (2; 1). The next step is to estimate the transformed state trajectory from time course measurements using a suitable observer. Earlier designs required expensive Lie-algebraic computations (3). Here we present an alternative design based on a dissipativity argument. Advantages of the dissipative approach are its flexibility and generality.

The method considers reaction kinetic systems of the form

$$\frac{d}{dt}c = Nv(c; k, K), \quad y = h(c; k, K),$$

where c denotes the vector of species concentrations, N the stoichiometric matrix and y the measurement. The vector of reaction rates v , is a nonlinear function depending on unknown kinetic parameters k, K :

$$v_i = k_i \frac{c^{v_{ij}}}{K^{\eta_{ij}} + c^{\eta_{ij}}}.$$

After the system is transformed into a parameter independent form (1), a dissipative observer estimates the trajectory in the new coordinates, from which the parameters can be

calculated easily. The dissipative observer is based on a dissection of the system into a linear and nonlinear part and takes the form

$$\frac{d}{dt}x = Ax + L\Delta y + \Psi(x + N\Delta y),$$

where A and Ψ describe the linear and nonlinear part of the system, x denotes the state estimate, Δy the output error and L and N the observer gain matrices to be designed.

Based on a dissipativity argument we present several sufficient conditions such that the design problem can be formulated in terms of linear matrix inequalities. These matrix inequalities are well studied and efficient computation tools are available to solve them. The result is a globally convergent observer, that guarantees the uniqueness of the state estimate, and subsequently the parameter estimate.

Summarising, the method recast the estimation of kinetic parameters into a state observation problem of an extended system. Using structural information only, an extended system model can be derived that is independent of the parameters and in Lure form. This special structure is advantageous for using a dissipative observer approach. Several sufficient conditions are presented that simplify the design of a dissipative observer.

References

- [1] D. Fey, R. Findeisen, E. Bullinger, "Parameter estimation in kinetic reaction models using nonlinear observers is facilitated by model extensions," *17th IFAC World Congress*, Seoul, Korea, 313–318, 2008.
- [2] M. Farina, R. Findeisen, E. Bullinger, S. Bittanti, F. Allgöwer, P. Wellstead, "Results towards identifiability properties of biochemical reaction networks," *45th IEEE CDC*, San Diego, USA, 2104–2109, 2006.
- [3] D. Fey, R. Findeisen, E. Bullinger, "Identification of biochemical reaction networks using a parameter-free coordinate system," in P. A. Iglesias, B. Ingalls, *Control-Theoretic Approaches in Systems Biology*, MIT press, 293–310, 2009.

Input and State Estimation of a Microalgae Culture using a Linear Quasi Unknown Input Observer

E. Rocha-Cóztatl¹, A. Vande Wouwer

Automatic Control Laboratory. Faculté Polytechnique de Mons.
Boulevard Dolez 31, B-7000 Mons, Belgium.

E-mail: Edmundo.Rocha@fpms.ac.be , Alain.VandeWouwer@fpms.ac.be

1 Introduction

The simultaneous estimation of unmeasured state variables and unknown inputs is particularly relevant in environmental applications, such as biological wastewater treatment or culture of microalgae in open environments. In this paper, a linear Quasi-Unknown Input Observer (QUIO) is designed and applied to state and input reconstruction in a continuous culture of the marine microalga *Dunaliella tertiolecta*, which has the following dynamics [1]

$$\begin{aligned}\dot{X}(t) &= -d(t)X(t) + \bar{\mu} \left(1 - \frac{k_Q}{Q(t)}\right) X(t) \\ \dot{Q}(t) &= \rho_m \frac{S(t)}{S(t)+k_S} - \bar{\mu} (Q(t) - k_Q) \\ \dot{S}(t) &= d(t) [S_{in}(t) - S(t)] - \rho_m \frac{S(t)}{S(t)+k_S} X(t)\end{aligned}\quad (1)$$

where X : biovolume; Q : internal quota (the quantity of nitrogen per unit of biovolume); S : substrate (inorganic nitrogen) concentration; S_{in} : input substrate concentration; $d(t)$: dilution rate. Terms k_S , ρ_m , $\bar{\mu}$ and k_Q are constant.

The QUIO [2] receives its name from the fact that in addition to the decoupling of the effect of the unknown input to the estimated states, some features of the unknown input are indeed known (and then can be called *quasi-unknown inputs*) and can be included in the design by means of an *exosystem*. The present study extends the procedure presented in [2] to the simultaneous estimation of states and inputs.

2 Methodology and Results

Consider that model (1) is linearized around an steady-state operation point. A linear framework is suitable for this class

$$\begin{aligned}\dot{x}_p &= A_p x_p + B_p u + D_p w, & \dot{x}_e &= A_e x_e + D_e v, \\ y &= C_p x_p, & w &= C_e x_e, \\ z_p &= G_p x_p & z_e &= G_e x_e\end{aligned}$$

$$\begin{aligned}\text{Augmented} & \quad \dot{x}_a = A_a x_a + B_a u + D_a v, \\ \text{system:} & \quad y = C_a x_a, \\ & \quad z_a = G_a x_a,\end{aligned}$$

of bioprocesses operated in continuous mode as a linearization around an operating point is valid and sufficiently robust. The dilution rate is the quasi-unknown input since it

¹E. Rocha-Cóztatl is currently on leave from the Departamento de Ingeniería Mecatrónica. Universidad Nacional Autónoma de México. edmundor@dctrl.fi-b.unam.mx

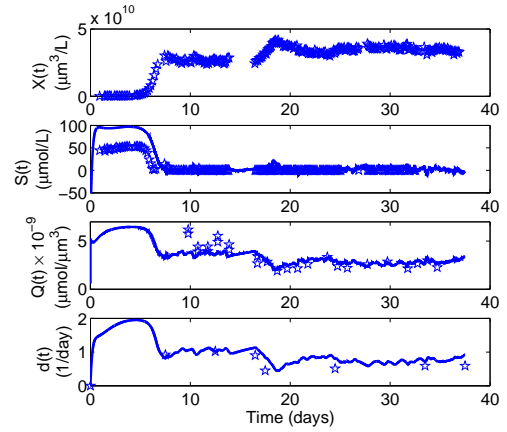


Figure 1: Solid lines: estimated variables. Stars: measurements.

is considered that is piecewise constant (step-like) and then $A_e = 0$, $D_e = 0$, $C_e = 1$, $G_e = 1$. By measuring X , estimations of states S , Q and input $d(t)$ are obtained. With the plant (left) and the exosystem (right) an augmented system can be formed, that is $x_a^T = [x_p^T, x_e^T]$, $z_a^T = [z_p^T, z_e^T]$.

The design of the observer was made in a similar way than in [2] and simulation results as well as off-line processing of real data obtained from a laboratory setup [1] demonstrate the performance of the method (Figure 1).

The estimate of S seems to be good qualitatively; however it is noisy. The estimations of Q and $d(t)$ are very satisfactory.

3 Acknowledgements

This paper presents research results of the Belgian Network DYSCO (Dynamical Systems, Control, and Optimization), funded by the Interuniversity Attraction Poles Programme, initiated by the Belgian State, Science Policy Office. The scientific responsibility rests with its authors.

References

- [1] O. Bernard, A. Sciandra, G. Sallet. A non-linear software sensor to monitor the internal nitrogen quota of phytoplanktonic cells. *Oceanologica Acta* 2001, 24, 435-442.
- [2] J. Moreno. Quasi-unknown input observers for linear systems. *Proceed. 2001 IEEE Int. Conf. on Control Applications*, 2001, pp 732 – 737, 2001. Mexico City, Mexico.

On the comparison of OED/PE strategies for the accurate identification of microbial kinetics

Eva Van Derlinden, Kristel Bernaerts and Jan F. Van Impe

BioTeC - Chemical and Biochemical Process Technology and Control

Department of Chemical Engineering, Katholieke Universiteit Leuven

W. de Croylaan 46, B-3001 Leuven, Belgium

jan.vanimpe@cit.kuleuven.be - kristel.bernaerts@cit.kuleuven.be - eva.vanderlinden@cit.kuleuven.be

1 Introduction

In predictive microbiology, mathematical models are developed to describe and predict the behavior of microorganisms in food. Reliable model predictions ask for accurate model parameters with good statistical properties. This work exploits optimal experiment design for parameter estimation (OED/PE) for the identification of the Cardinal Temperature Model with Inflection (CTMI)[1]. This kinetic model describes the effect of temperature on the microbial growth rate and encloses four parameters. For the estimation of the parameters, three OED/PE strategies are considered. In a first approach, the four parameters are estimated simultaneously from one optimal experiment. In the other strategies, each design focuses on two parameters such that six optimal experiments are obtained. The parameters are then estimated from the experiments in a sequential or global way. In this work, the three design strategies are evaluated based on a simulation study.

2 Simultaneous, sequential and global OED/PE

In the *simultaneous strategy* (SiOED/PE), one optimal experiment is designed from which all model parameters are estimated simultaneously. In the *sequential strategy* (SeOED/PE), the problem is reformulated as a series of two-parameter estimation problems. Taking the CTMI model with four parameters, the approach works as follows. A first optimal experiment focuses on the estimation of parameters p_1 and p_2 while considering p_3 and p_4 perfectly known. After implementation of this experiment, p_1 and p_2 are estimated. Nominal parameters are updated and a new optimal design round is applied, e.g., aimed at the accurate estimation of p_2 and p_3 . At the end of the cycle six experiments are performed and each parameter is considered three times. In the *global strategy* (GIOED/PE), optimal experiments are designed for each parameter combination, based on common nominal values. Next, all six optimal experiments are implemented and new parameter values are globally estimated from all experimental data sets. In contrary to SeOED/PE, nominal values are not intermediately updated. The advantage of SeOED/PE and GIOED/PE is that the error in one (or more) nominal values is not spread over all designs. Moreover, the advantage of taking into account several experiments is that the variability of the system is included in the parameter uncertainty.

3 Results

Simulation study. A comparison of the optimization strategies is based on a simulation study consisting of three steps. (i) D-optimal experiments are designed for a selected temperature profile parameterization. (ii) Corresponding growth curves are simulated based on the true parameters. During simulation, an error, equal to the measurement error variance, is added mimicking the variability on experimental data due to measurement errors and biological variability. (iii) Parameters are identified from the resulting experimental data via the minimization of the sum of squared errors. Based on identical nominal values (\mathbf{p}^o), the procedure is repeated for three sets of true parameters (\mathbf{p}^*). For the SiOED/PE and the GIOED/PE strategy, optimal experiments are calculated with respect to the nominal values. For SeOED/PE, optimal temperature profiles are designed and parameters estimated for a selected order of parameter combinations. During optimal design and parameter identification of (p_1, p_2) , the remaining parameters (p_3, p_4) are set at their latest estimates. The order of parameter couples optimized is different for the three replicates.

Results. Generally, parameter values derived via the SeOED/PE approach deviate more from the true parameters than the simultaneous and global strategy estimates. Both SiOED/PE and GIOED/PE render values very close to \mathbf{p}^* , and differentiating between the two methods is difficult. As SiOED/PE only requires the implementation of one experiment, this method seems most suitable. However, estimating the four parameters from one experiment makes the procedure rather sensitive for experimental errors.

Acknowledgments

Work supported in part by Projects OT/03/30 and EF/05/006 (Center-of-Excellence Optimization in Engineering) of the Research Council of the Katholieke Universiteit Leuven, and by the Belgian Program on Interuniversity Poles of Attraction, initiated by the Belgian Federal Science Policy Office. K. Bernaerts is a Postdoctoral Fellow with the Fund for Scientific Research Flanders. The scientific responsibility is assumed by its authors.

References

- [1] L. Rosso, J.R. Lobry, S. Bajard and J.P. Flandrois (1995) Convenient model to describe the combined effects of temperature and pH on microbial growth. *Appl Environ Microbiol*, 61: 610-616.

Stochastic observers for industrial seeded batch crystallization processes

A. Mesbah, I. Mora Moreno, A.E.M. Huesman and P.M.J. Van den Hof

Delft Center for Systems and Control

Delft University of Technology

Mekelweg 2, 2628 CD Delft

The Netherlands

Email: ali.mesbah@tudelft.nl

Keywords

Batch crystallization, Population balance equation, Real-time control, Stochastic process, Kalman filter

Abstract

Batch crystallization is often used for production of high purity, high added-value materials with tight specifications on crystal properties, i.e. size, purity and morphology. In order to meet these requirements, an effective control strategy is needed.

Real-time model-based control of batch crystallization processes requires estimation of the state of the system, the state vector contains all relevant information required to describe the system under investigation while the output vector represents measurements that are related to the state vector. Estimation is performed using a sequence of inputs and output measurements made on the system and used in parallel with a model of the system. Building a model of a system requires understanding the physics behind the crystallization phenomena, unfortunately real-life systems may present behavior which is not fully understood. This lack of knowledge, in addition to the presence of process disturbances that often exhibit random behavior, lead to the necessity of creating a stochastic model.

Observers allow estimation of state variables based on a system model and measurements of the output vector. Uncertain measurements and/or disturbances may corrupt a system; in order to keep up with this type of imperfections the observer to be used must be a stochastic observer. In crystallization processes, it is complicated to build models that fully represent real-life dynamics in case that no stochastic terms and disturbances are considered in the model. Observation techniques capable of dealing with stochastic models are therefore highly demanded.

As the importance of an observer has been highlighted, this work is intended to present up to date information about theory and applications of stochastic observers in the crystallization process industry. It should be noted that different types of observers can be found in literature; neverthe-

less this work focuses on Kalman Filter variants. Extended Kalman filter (EKF), a variant of the Kalman filter used in nonlinear applications, is widely used in the chemical industry with several results proving that it generally performs well. In the course of several years more Kalman filter variants have appeared, research carried out in this area points towards enhancing properties of the original filter.

In this study, two filters, namely the Unscented Kalman filter (UKF) [1] and the Ensemble Kalman filter (EnKF) [2], are studied in a more detailed manner than other variants since they are regarded as improvements over the EKF. The filters are first applied to a moment model pertaining to a 75-liter draft tube crystallizer in order to investigate the performance of the filters in terms of the estimation accuracy, as well as computational burden; the moment model is a reduced order model obtained from a full population balance equation. The filters are then assessed in terms of their closed-loop performance, namely their capability to deal with plant-model imperfections, uncertain initial conditions and disturbance handling.

In a later stage the filters will be applied to a full population balance equation representing an industrial 1100-liter draft tube baffle crystallizer.

References

- [1] S.J. Julier, and J.K. Uhlman, "A New Extension of the Kalman Filter to Nonlinear Systems," University of Oxford, Dept. of Engineering Science, 1997.
- [2] G. Evensen, "Data Assimilation: The Ensemble Kalman Filter," Springer, book chapter, 2006.

Model analysis for individual-based modelling

A.J. Verhulst, K. Bernaerts and J.F.M. Van Impe
BioTeC - Chemical and Biochemical Process Technology and Control,
Department of Chemical Engineering,
Katholieke Universiteit Leuven,
W. de Croylaan 46, B-3001 Leuven (Belgium)
{anke.verhulst, kristel.bernaerts, jan.vanimpe}@cit.kuleuven.be

1 Introduction

Individual-based modelling (IbM) is widely applied in a number of disciplines, e.g., economy, astronomy, ecology. Recently, IbM is introduced in the field of predictive microbiology. Predictive microbiology is a scientific discipline that aims to condense mathematical and biological knowledge in models describing microbial dynamics (growth, survival and inactivation) in a wide range of environmental conditions. Traditionally, microbial growth is modelled from a macroscopic viewpoint by describing the dynamics of a population parameter (e.g., total cell number) in function of time. These models are able to predict microbial dynamics under uncomplicated environmental conditions, but fail to provide accurate predictions when more complex situations occur. Individual-based modelling considers the individual cell as the modeling unit, circumventing some of these limitations and complementing the traditional approach. Nevertheless, the IbM methodology is still lacking a generic set of tools for model analysis. Model analysis is an important step in the individual-based modeling cycle. In Grimm et al. [1], techniques for IbM model analysis are proposed. This research applies some of the techniques presented, i.e., statistical techniques and robustness analysis, to a basic IbM.

2 Materials and methods

Model

The IbM is designed to model microbial growth dynamics (i.e., lag and exponential phase) in a rich homogeneous liquid medium. It will be the core of a more complex IbM modelling complex microbial dynamics, such as, adaptive behaviour (lag phase), dynamics in structured food and interspecies interactions. The model defines rules for the individual behaviour of the bacteria, e.g., growth and reproduction. In a rich and homogeneous liquid medium, substrate depletion does not take place and diffusion of substrates and substrate limitation can be ignored. Thus, these aspects are not included.

Model Analysis

Model analysis includes learning about the behaviour of the model and the system modelled. IbMs tend to be more com-

plex than classical macroscopic models and are therefore more difficult to understand and learn from. In this study, information is gathered about how the model reacts to changes in the model structure induced by, e.g., different hypotheses about cell division. This is done by a robustness analysis. Robustness analysis is similar to conventional sensitivity analysis only a larger range of parameter values is considered. Not only parameter values are considered, also the outcome of different hypotheses defining the model is evaluated. This analysis provides information about the model and the system modelled. Statistical techniques are used to concisely summarise the data and to compare the different model outcomes.

The model structure is validated by qualitative comparison of the different model outcomes with experimental data found in literature.

3 Results and Conclusions

By comparing the different model outcomes to each other quantitatively and to experimental data in literature qualitatively, a thorough understanding of the model and the system modelled is attained. The analysis reveals the importance of model structure characteristics, such as the time step. Based on the results, some design considerations are formulated.

4 Acknowledgements

Simulations are performed on the VIC cluster of the High Performance Computing (HPC) infrastructure KULeuven. Work supported in part by Projects OT/03/30 and EF/05/006 (Center-of-Excellence Optimization in Engineering) of the Research Council of the Katholieke Universiteit Leuven, and by the Belgian Program on Interuniversity Poles of Attraction, initiated by the Belgian Federal Science Policy Office. K. Bernaerts is a Postdoctoral Fellow with the Fund for Scientific Research Flanders (FWO-Vlaanderen). The scientific responsibility is assumed by its authors.

References

- [1] V. Grimm, S. Railsback (2005). Individual-based modeling and ecology. Princeton University Press.

Nonlinear data projection on manifolds

Victor Onclinx^{1,2,*}, Michel Verleysen² and Vincent Wertz^{1,2}

1- Department of Applied Mathematics, Université catholique de Louvain,

Avenue Georges Lemaître, 4, 1348, Louvain-la-Neuve, Belgium

2- Machine Learning Group, Université catholique de Louvain

Place du Levant, 3, 1348, Louvain-la-Neuve, Belgium

Email : victor.onclinx@uclouvain.be

Abstract

Numerous domains like data mining, machine learning and data analysis have, nowadays, to deal with high dimensional data. The complex structure of such data makes difficult their comprehension and the extraction of relevant information. It is thus of primary importance to develop analysis tools like projection methods that are aimed at visualizing high dimensional data [2].

Projection methods try to minimize the loss of information between the high dimensional data and the projected ones. This work defines the loss of information by the mean of a pairwise distance criterion [2]. However, the data projection methods have to deal with a compromise between *trustworthiness* and *continuity* [4], meaning the risk of flattening and tearing the projection, respectively.

In general, nonlinear projection methods cannot perfectly reach these two objectives simultaneously without strong and often unrealistic hypotheses on the data. This work defines a pairwise distance criterion (1) that implements and controls this trade-off by the introduction of a user-defined parameter $\lambda \in [0, 1]$ [5]:

$$f \equiv \sum_{i=1}^{N-1} \sum_{j>i}^N \lambda \frac{(D_{ij} - \delta_{ij})^2}{D_{ij}} + (1 - \lambda) \frac{(D_{ij} - \delta_{ij})^2}{\delta_{ij}}, \quad (1)$$

where D_{ij} is the distance between the data i and j in the original space, δ_{ij} is the corresponding distance in the projection space and N is the number of data.

However, most current developments aiming at visualizing data project the latter in the Euclidean two-dimensional space. By trying to project on more complex manifolds embedded in a three-dimensional space, we hope that both the trustworthiness and the continuity of the projection can be substantially improved. For example, projecting on a sphere, on a torus or on a cylinder can be more adapted to some more complex structures of data, specially when the data distribution intercepts itself.

The projection is thus achieved by minimizing the criterion (1) on a manifold with respect to the corresponding optimization theory [1]. The gradient descent principle is then adapted to project data living in a three-dimensional space,

with an additional constraint that they have to belong to a two-dimensional manifold. Briefly summarized, the method includes four main steps. The first one consists in the evaluation of the gradient of the criterion. To take into account the manifold constraint, the gradient is then projected on the tangent space. The current locations can thus be translated in this search direction where the step size is determined by the Armijo rule [1]. To ensure that points stay on the manifold after the steepest descent, the last step consists in a deterministic *retraction* on the manifold [1]. The steps are repeated until convergence.

Preliminary experiments show the adequacy of the proposed procedure to complex data that are difficult to project directly in an Euclidean two-dimensional space.

The ideas of this paper are detailed in [3].

References

- [1] P.-A. Absil, R. Mahony, and R. Sepulchre, "Optimization Algorithms on Matrix Manifolds", Princeton University Press, Princeton, NJ, January 2008.
- [2] J.A. Lee and M. Verleysen, "Nonlinear Dimensionality Reduction", Springer Science+Business Media, LLC, 2007.
- [3] V. Onclinx, V. Wertz, and M. Verleysen, "Nonlinear data projection on a sphere with a controlled trade-off between trustworthiness and continuity", In ESANN 2008, European Symposium on Artificial Neural Networks, pages 43-48, Bruges (Belgium), April 23-25 2008, ESANN, d-side publi.
- [4] J. Venna and S. Kaski, "Neighborhood preservation in nonlinear projection methods: An experimental study", In ICANN '01: Proceedings of the International Conference on Artificial Neural Networks, pages 485-491, London, UK, August 21-25 2001. Springer-Verlag.
- [5] J. Venna and S. Kaski, "Local multidimensional scaling with controlled tradeoff between trustworthiness and continuity", In Proceedings of WSOM'05, 5th workshop on self-organizing maps, pages 695-702. WSOM, September 5-8 2005.

Fitting Curves on Riemannian Manifolds Using Energy Minimization

Chafik Samir

P.-A. Absil

Anuj Srivastava

Eric Klassen

Abstract

Given data points p_0, \dots, p_N on a manifold \mathcal{M} and time instants $0 = t_0 < t_1 < \dots < t_N = 1$, we consider the problem of finding the curve γ on \mathcal{M} that best approximates the data points at the given instants. In this work, γ is expressed as the curve that minimizes the weighted sum of a least-squares term penalizing the lack of fitting to the data points and a regularity term defined as the mean squared velocity of the curve. The optimization task is carried out by means of a steepest-descent algorithm on the set of continuous paths on \mathcal{M} . The steepest-descent direction, defined in the sense of the Palais metric, is shown to admit a simple formula based on parallel translation.

1 Introduction

1.1 Motivation

Let p_0, p_1, \dots, p_N be a finite set of points in \mathbb{R}^n , or more generally on a Riemannian manifold \mathcal{M} , and let $0 = t_0 < t_1 < \dots < t_N = 1$ be different instants of time. The problem of fitting a curve γ in \mathcal{M} to the given points at the given times involves two goals of conflicting nature. The first goal is that the curve should fit the data as well as possible, e.g., in the sense of the functional E_d defined by:

$$E_d(\gamma) = \sum_{i=0}^N d^2(\gamma(t_i), p_i),$$

where d denotes the geodesic distance function on the Riemannian manifold \mathcal{M} . (In the case where \mathcal{M} is the Euclidean space \mathbb{R}^n endowed with its canonical metric, $E_d(\gamma)$ is simply $\sum_{i=0}^N \|\gamma(t_i) - p_i\|^2$, where $\|\cdot\|$ denotes the Euclidean norm). The second goal is that the curve should be sufficiently “regular”, in certain sense, e.g., the length of the curve should be as small as possible, or the changes in velocity should be minimized.

1.2 Our approach

In the spirit of the work of Machado and Leite [ML06], we consider the problem of minimizing a functional of the form:

$$E : \Gamma \rightarrow \mathbb{R} \\ \gamma \mapsto E(\gamma) := E_d(\gamma) + \lambda E_s(\gamma)$$

where Γ denotes the set of all continuous paths on \mathcal{M} , i.e.,

$$\Gamma = \{\gamma : [0, 1] \rightarrow \mathcal{M} \mid \gamma \in C^0\}, \quad (1)$$

and where λ is a positive real constant, termed *regularity parameter*. The parameter λ makes it possible to mitigate

between the two conflicting goals mentioned above. When λ is large, the emphasis is laid on the regularity condition and less so on the fitting condition, whereas when λ is small, the fitting condition dominates. Observe that there is no constraint on γ further than belonging to Γ .

In [ML06], the regularity cost function E_s is chosen as

$$\int_0^1 \left\langle \frac{D^2\gamma}{dt^2}, \frac{D^2\gamma}{dt^2} \right\rangle_{\gamma(t)} dt, \quad (2)$$

where $\langle \cdot, \cdot \rangle_x$ denotes the Riemannian metric at $x \in \mathcal{M}$ and $\frac{D^2\gamma}{dt^2}$ denotes the covariant derivative of the velocity vector field, $\dot{\gamma}$, along γ . This is a natural generalization to manifolds endowed with an affine connection. The choice of (2) is motivated by the fact that cubic splines in \mathbb{R}^n can be viewed as extrema under the interpolation condition. The main result in [ML06] is to give a necessary condition of optimality for γ to be a minimizer of $E_d + \lambda E_s$. The necessary condition takes the form of a fourth-order ordinary differential equation for γ involving the covariant derivative and the curvature tensor.

In summary, the function to be minimized, in this work, is

$$E : \Gamma \rightarrow \mathbb{R} : \gamma \mapsto E(\gamma) = E_d(\gamma) + \lambda E_s(\gamma) \\ = \sum_{i=0}^N d^2(\gamma(t_i), p_i) + \lambda \int_0^1 \langle \dot{\gamma}(t), \dot{\gamma}(t) \rangle_{\gamma(t)} dt. \quad (3)$$

Other forms of E_s , such as (2) will be considered in later work. A major advantage of using the Palais metric [SSDK08] in this context is that the gradient of E (whose negative provides the steepest-descent direction) admits a simple expression involving the parallel translation on the manifold \mathcal{M} . The step size of the steepest-descent iteration is selected using an Armijo backtracking procedure, but any other efficient step size selection method would have been suitable.

References

- [ML06] Luís Machado and F. Silva Leite. Fitting smooth paths on Riemannian manifolds. *Int. J. Appl. Math. Stat.*, 4(J06):25–53, 2006.
- [SSDK08] C. Samir, A. Srivastava, M. Daoudi, and E. Klassen. An intrinsic framework for analysis of facial surfaces. *International Journal of Computer Vision*, Accepted, to appear, 2008.

Algorithms for nonsmooth optimization on manifolds

C. Lageman, R. Sepulchre

Systems and Modeling

Department of Electrical Engineering and Computer Science, B28

Université de Liège

B-4000 Liege Sart-Tilman, Belgium.

email: {christian.lageman, r.sepulchre}@ulg.ac.be

1 Introduction

In many applications in engineering and numerical linear algebra one is faced with an optimization problem, i.e. the minimization of a cost function, over state space which has the structure of a nonlinear smooth manifold. In many of these applications the state space is a classical manifold with a well-understood geometry like e.g. the compact Stiefel manifold or one of the classical matrix groups. In the last two decades there has been a considerable interest to develop algorithms which exploit the geometry of the underlying manifold, see [1, 2] for an overview of some results in this area. However, these approaches have mainly focused on smooth cost functions and problems with nonsmooth cost functions have received only very limited attention.

2 Nonsmooth optimization on manifolds

Nonsmooth cost functions arise naturally in many problems and applications, e.g. as a minmax cost function for optimal packings on the Grassmann manifold [4] or as eigenvalue functions [3]. A standard approach to problems with a nonsmooth cost function is approximate the cost with a sequence of smooth cost functions and apply the algorithms for smooth cost functions to these approximations. However, this approach can be computationally expensive and can lead to ill-conditioned problems.

Alternatively one can extend nonsmooth algorithms from Euclidean space to manifolds, an approach which has been applied with great success in the case of smooth cost functions. Generalizations of the subgradient to Riemannian manifolds [5, 6], can be used to construct subgradient-type iterations for convex [5] and nonconvex functions [4]. In a similar way the generalized Newton method on Euclidean space can be extended to Riemannian manifolds [7]. Recent results have demonstrated that for submanifolds of Euclidean space more efficient algorithms can be obtained for convex functions by using the geometry of the embedding space [8].

In Euclidean space some shortcomings of subgradient algorithms for convex functions can be overcome by extending these algorithms to ε -subgradients [9]. This motivates us to consider generalizations of such ε -subgradient algorithms to Riemannian manifolds. Here, we follow the embedding ap-

proach and focus on submanifolds of Euclidean space. The embedding is used to derive an ε -subgradient on the manifold from the ε -subgradient in the embedding space. We propose ε -subgradient descent algorithm on the manifold and illustrate it by an example.

3 Acknowledgements

This paper presents research results of the Belgian Network DYSCO (Dynamical Systems, Control, and Optimization), funded by the Interuniversity Attraction Poles Programme, initiated by the Belgian State, Science Policy Office. The scientific responsibility rests with its authors.

References

- [1] P.-A. Absil, R. Mahony, R. Sepulchre, *Optimization Algorithms on Matrix Manifolds*, Princeton University Press, 2008
- [2] U. Helmke, J. B. Moore, *Optimization and dynamical systems*, Springer Verlag, Berlin, 1994
- [3] A.S. Lewis, *Nonsmooth analysis of eigenvalues*, Mathematical Programming, 84, 1-24, 1999
- [4] C. Lageman, U. Helmke, *Optimization methods for the sphere packing problem on Grassmannians*, In "Taming Heterogeneity and Complexity of Embedded Control: CTS-HYCON Workshop on Nonlinear and Hybrid Control, Paris IV Sorbonne, 10-12 July 2006", 2006
- [5] O. P. Ferreira, P. R. Oliveira, *Subgradient Algorithm on Riemannian Manifolds*, Journal Opt. Theory Appl., 97 (1), 93–104, 1998
- [6] Yu. Ledyayev, Q.J. Zhu, *Nonsmooth analysis on smooth manifold*, Trans. AMS, 359, 3687–3732, 2007
- [7] C. Lageman, U. Helmke, J.H. Manton, *The Nonsmooth Newton method on Riemannian manifolds*, Proceedings of the 18th International Symposium on Mathematical Theory of Networks and Systems (MTNS), 2008
- [8] M. Journée, Y. Nesterov, P. Richtárik, R. Sepulchre, *Generalized power method for sparse principal component analysis*, preprint, arXiv:0811.4724v1 [math.OC], 2008
- [9] C. Geiger, C. Kanzow, *Theorie und Numerik restringierter Optimierungsaufgaben*, Springer Verlag, Berlin, 2002

Optimal H_2 -design and the smoothed spectral abscissa

Joris Vanbiervliet

Wim Michiels

Stefan Vandewalle

Department of Computer Science,
Katholieke Universiteit Leuven,
Celestijnenlaan 200A,
3001 Leuven (Heverlee), Belgium

Email: {joris.vanbiervliet,wim.michiels,stefan.vandewalle}@cs.kuleuven.be

1 Introduction

The stabilization of systems with control laws having a smaller amount of free variables than the system's dimension is a difficult problem, and optimizing the stability robustness is even more challenging. In particular, given a plant matrix A , a control matrix B and an observer matrix C that are all dependent on some parameter vector K , we are interested in finding values for K such that

1. the system matrix A is stable,
2. the H_2 -norm of the system's transfer function \mathbf{T}

$$\mathbf{T}(s;K) = C(K)(sI - A(K))^{-1}B(K),$$

is minimal.

It is assumed that the amount of free parameters is much smaller than the system's dimension, i.e. $\dim(K) \ll \dim(A)$, and that (A, B) is controllable and (C, A) is observable.

Concisely put, we want to solve the minimization problem

$$\min_K \|\mathbf{T}(s;K)\|_{H_2}$$

over the set of stabilizing K . The H_2 -norm, defined as

$$\|\mathbf{T}(s;K)\|_{H_2}^2 = \frac{1}{2\pi} \int_{-\infty}^{\infty} \text{tr}(\mathbf{T}(j\omega;K)^* \mathbf{T}(j\omega;K)) d\omega,$$

is a smooth function and thus relatively easy to optimize. For the H_2 -norm to exist however, the system matrix A must be stable, i.e. all its eigenvalues must reside in the left half complex plane. This is equivalent to demanding that the real part of the rightmost eigenvalue of A , the so-called spectral abscissa $\alpha(A)$, be negative. Objective functions derived from $\alpha(A)$ unfortunately are in general not smooth, so one typically ends up with a nonsmooth optimization problem for the stabilization.

Recently, several nonsmooth optimization approaches have been devised to overcome this difficulty. These methods then result in a two stage approach for the H_2 -minimization problem, with a first step that stabilizes the system, and a second step that subsequently robustifies the system.

We present a framework that, making use of the smoothed spectral abscissa [1], uses only smooth optimization techniques to stabilize a system. If desired, the method can also be adapted to optimize the H_2 -norm, which is performed in a way simultaneously with the stabilization, thus without having to worry about the (nonsmooth) first step of the traditional two-stage approach.

2 Stabilization and optimal H_2 -design

The method is based on the smoothed spectral abscissa. This stability measure, denoted by $\tilde{\alpha}_\varepsilon$, is defined as the shift σ for which it holds that the function f

$$f(A, B, C, \sigma) := \|C(sI - (A - \sigma I))^{-1}B\|_{H_2}^2. \quad (1)$$

is equal to ε^{-1} . The function f is nothing else than the H_2 -norm of a *shifted* transfer function. The larger the shift σ , the easier this function is to optimize. We therefore do a series of optimizations with decreasing σ , where the new, smaller σ is computed as a smoothed spectral abscissa. The algorithm looks as follows.

Algorithm 1 Optimal H_2 algorithm

Require: $E > 1$, $\varepsilon > 0$, initial K^* , $\sigma = +\infty$

- 1: **while** $\sigma > 0$ **do**
- 2: $\sigma \leftarrow \tilde{\alpha}_\varepsilon(A(K^*))$
- 3: Solve

$$f^* \leftarrow \min_K f(A, B, C, \max\{\sigma, 0\})$$

with K^* as initial guess for K .

- 4: Update K^* with the minimizer of step 1.
 - 5: Decrease ε : $\varepsilon \leftarrow \varepsilon/E$
 - 6: **end while**
 - 7: **return** f^* and corresponding minimizer K^*
-

By putting simply σ instead of $\max\{\sigma, 0\}$ on line 3, the algorithm reduces to a pure stabilization method.

References

- [1] J. Vanbiervliet, B. Vandereycken, W. Michiels, S. Vandewalle, M. Diehl, "The smoothed spectral abscissa for robust stability optimization", to appear in SIAM Journal on Optimization.

Computing H-infinity Norm of Time-Delay Systems

Suat Gumussoy

Department of Computer Science

K. U. Leuven

Celestijnenlaan 200A 3001 Heverlee

Belgium

Email: suat.gumussoy@cs.kuleuven.be

Wim Michiels

Department of Computer Science

K. U. Leuven

Celestijnenlaan 200A 3001 Heverlee

Belgium

Email: wim.michiels@cs.kuleuven.be

1 Abstract

We consider the computation of the \mathcal{H}_∞ norm of the stable transfer function G ,

$$G(j\omega) = C \left(j\omega I - A_0 - \sum_{i=1}^m A_i e^{-j\omega\tau_i} \right)^{-1} B + D e^{-j\omega\tau_0} \quad (1)$$

where the system matrices are (A_i, B, C, D) , $i = 0, \dots, m$ are real-valued and the time delays, (τ_0, \dots, τ_m) , are real numbers.

The following theorem is used to compute the \mathcal{H}_∞ norm of a transfer function in the finite dimensional case.

Theorem 1.1 [1] *Let $\xi > 0$ be such that the matrix $R = \xi^2 I - D^T D$ is non-singular. For $\omega \geq 0$, the matrix $G(j\omega) = C(j\omega I - A)^{-1} B + D$ has a singular value equal to ξ if and only if $\lambda = j\omega$ is the imaginary eigenvalue of the Hamiltonian matrix*

$$H_\xi = \begin{bmatrix} A + BR^{-1}D^T C & BR^{-1}B^T \\ -C^T(I + DR^{-1}D^T)C & -(A + BR^{-1}D^T C) \end{bmatrix}.$$

Hence the \mathcal{H}_∞ norm of G can be defined as

$$\|G\|_\infty = \sup \{ \xi > 0 | H_\xi \text{ has eigenvalue on the imaginary axis} \}.$$

Based on this fact, a numerical method is given to calculate \mathcal{H}_∞ norm of finite dimensional systems converging quadratically [2].

In this talk, we extend the computation of \mathcal{H}_∞ norm to the time-delay systems with the transfer function representation (1). The relation between the singular value of the transfer function and the corresponding Hamiltonian matrix is valid. Let $\xi > 0$ be such that the matrix

$$D_\xi := D^T D - \xi^2 I$$

is non-singular. For $\omega \geq 0$, the matrix $G(j\omega)$ has a singular value equal to ξ if and only if $\lambda = j\omega$ is a solution of the equation

$$\det H_\xi(\lambda) = 0, \quad (2)$$

where

$$H_\xi(\lambda) := \lambda I - M_0 - \sum_{i=1}^m \left(M_i e^{-\lambda\tau_i} + M_{-i} e^{\lambda\tau_i} \right) - \left(N_1 e^{-\lambda\tau_0} + N_{-1} e^{\lambda\tau_0} \right)$$

where M_0, N_1, N_{-1} and M_i, M_{-i} $i = 1, \dots, m$ depends on ξ and the system matrices in (1).

We show that the nonlinear eigenvalue problem (2) is equivalent to a linear eigenvalue problem of the infinite dimensional Hamiltonian operator \mathcal{L}_ξ on $X := \mathcal{C}([- \tau_{\max}, \tau_{\max}], \mathbb{C}^{2n})$ which is defined by

$$\begin{aligned} \mathcal{D}(\mathcal{L}_\xi) &= \{ \phi \in X : \phi' \in X, \phi'(0) = M_0 \phi(0) + \\ &\quad \sum_{i=1}^m (M_i \phi(-\tau_i) + M_{-i} \phi(\tau_i)) + N_1 \phi(-\tau_0) + N_{-1} \phi(\tau_0) \}, \\ \mathcal{L}_\xi \phi &= \phi'. \end{aligned}$$

Our approach consists of two steps. In the first step inspired by Theorem 1.1, we compute using the method presented in [2]

$$\max \{ \xi > 0 | \mathcal{L}_\xi^N \text{ has eigenvalue on the imaginary axis} \}$$

where \mathcal{L}_ξ^N is a matrix approximating \mathcal{L}_ξ under mild conditions. This problem can be interpreted as computing the \mathcal{H}_∞ norm of an approximation of G .

In the second step, the approximated results are corrected using Newton iteration on a set of equations which are obtained from the nonlinear eigenvalue problem (2) and characterize the peaks in the singular value plot.

References

- [1] S. Boyd, K. Balakrishnan, and P. Kabamba, "A bisection method for computing the \mathcal{H}_∞ of a transfer matrix and related problems," Math Control Signals and Systems, 2(3), pp. 207-219, 1989.
- [2] O. Bruinsma, and M. Steinbuch, "A fast algorithm to compute the \mathcal{H}_∞ norm of a transfer function matrix," Systems and Control Letters, vol. 14, pp. 287-293, 1990.

Robust stability assessment in High-speed milling

Niels van Dijk*, Nathan van de Wouw and Henk Nijmeijer

Department of Mechanical Engineering, Eindhoven University of Technology

P.O. Box 513, 5600 MB Eindhoven, The Netherlands

Email: *N.J.M.v.Dijk@tue.nl

1 Introduction

In high-speed milling (HSM), the occurrence of chatter vibrations limits the performance of the milling process. The occurrence of chatter results in heavy vibrations of the cutter, increased wear of the cutter, noise and an inferior workpiece quality, see Figure 1. Stability of the milling process is characterised in so-called Stability Lobes Diagrams (SLD) in which the stability boundary is given in terms of two process parameters: the spindle-speed $n \propto 1/\tau$, with delay τ , and depth of cut a_p .

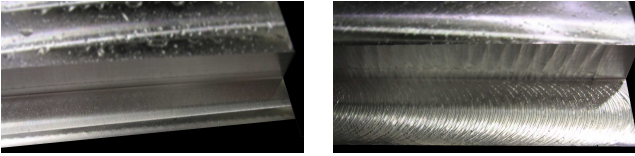


Figure 1: Workpiece without (left) and with (right) chatter marks.

2 Approach

Here, a method is presented to determine robust stability for a certain range in spindle speeds. The uncertain system is represented as a feedback interconnection between the nominal milling system, using a linear cutting force model, $F = a_p \bar{H}(v(t) - v(t - \tau))$, and machine dynamics model, $\dot{x} = Ax(t) + BF(t)$, $v(t) = Cx(t)$, see [1], yielding

$$\begin{aligned} \dot{x}(t) &= A_0 x(t) + A_1 x(t - \tau), \\ v(t) &= Cx(t), \end{aligned} \quad (1)$$

where $A_0 = A + a_p B \bar{H} C$, $A_1 = -a_p B \bar{H} C$, and uncertainties δa_p and $\delta \tau$, in the depth-of-cut and delay, respectively. Using stability characterisations as in [2], it can be concluded that the system is robustly stable if

$$\|\Delta\|_\infty \leq (\sup_{\omega \geq 0} \mu_\Delta P(j\omega))^{-1}, \quad (2)$$

where μ_Δ is the structured singular value of

$$\begin{aligned} P(s) &= \begin{bmatrix} Cs \\ Cs(1 - e^{-s\tau}) \end{bmatrix} [sI - A_0 - A_1 e^{-s\tau}]^{-1} \\ &\quad \begin{bmatrix} \frac{a_p}{w_1} B \bar{H} & \frac{1}{w_2} B \bar{H} \end{bmatrix} + \begin{bmatrix} 0 & 0 \\ \frac{1}{w_1} I & 0 \end{bmatrix}, \end{aligned} \quad (3)$$

with respect to uncertainty

$$\Delta(s) = \begin{bmatrix} w_1 \frac{e^{-s\tau}(1 - e^{-s\delta\tau})}{s} I & 0 \\ 0 & w_2 \delta a_p I \end{bmatrix}. \quad (4)$$

Weighting factors are chosen as $w_1 = 1/\delta\tau_{max}$ and $w_2 = 1/\delta a_{p,max}$ with $\delta\tau_{max}$ and $\delta a_{p,max}$ indicating the area in the SLD for which stability should be assessed.

3 Results

Norm-bounded stability criteria, as used above, introduce conservatism. Therefore, the approach is compared to a SLD determined via the semi-discretisation method, see [1]. Results are depicted in Figure 2 for $w_1 = 4.0945 \cdot 10^4$, $w_2 = 1.040$. It can be seen that the proposed strategy very well predicts a stability region, i.e. the rectangle (almost) touches the SLD at the corner points. Moreover, since there is no need to calculate the entire SLD this strategy for robust stability analysis is computationally efficient.

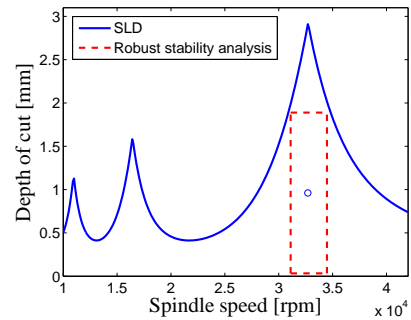


Figure 2: SLD and calculated norm-based stability region.

4 Conclusions

An approach for robust stability assessment for the high-speed milling process is presented. Future work includes the development of controllers that stabilise a predefined region in the stability lobes diagram.

References

- [1] R.P.H. Faassen, Chatter prediction and control for high speed milling: modelling and experiments, Ph.D. Thesis, Eindhoven University of Technology (2007)
- [2] W. Michiels, E. Fridman, and S.-I. Niculescu, "Robustness assessment via stability radii in delay parameters", International Journal of Robust and Nonlinear Control, 2008, Accepted.

Model Reduction and Controller Synthesis for \mathcal{L}_2 Systems

Mark Mutsaers & Siep Weiland

Department of Electrical Engineering, Eindhoven University of Technology

P.O. Box 513, 5600 MB Eindhoven, The Netherlands

E-mail: M.E.C.Mutsaers@tue.nl and S.Weiland@tue.nl

1 Introduction

Control systems that are designed from models described by partial differential equations (PDE's) often follow either of two popular design strategies. The first one being a control synthesis procedure on the basis of a low order plant that is obtained by applying a popular model reduction technique on a high-order discretization of the (spatial) configuration space of the PDE. The technique therefore implies a reduction followed by an optimization. The second one involves a controller synthesis on the basis of a high resolution discretization of the PDE and is followed by a reduction of the controller itself. Although both techniques lead to low order controllers, a major disadvantage of either of these techniques is the lack of guarantees that can be given on closed-loop performance, on closed-loop stability and on robustness of the design.

2 Controller synthesis problem

Our approach starts by describing the desirable closed-loop objectives as a dynamical system, which will have a higher complexity than the plant. Model reduction results in an approximation Σ_K , which contains almost the same dynamical properties as the full-order model. This model will be used in the controller synthesis problem (depicted in Figure 1):

Given: a complex model for the plant Σ_P and a reduced-order model for the desired closed-loop objectives Σ_K .

Find (if they exist): all possible controllers with low complexity Σ_C such that the interconnection of the full-order plant and one of the found controllers results in Σ_K .

Because the controller is obtained from the reduced-order closed-loop objectives, one preserves the desired guarantees when the interconnection with the real plant is made.

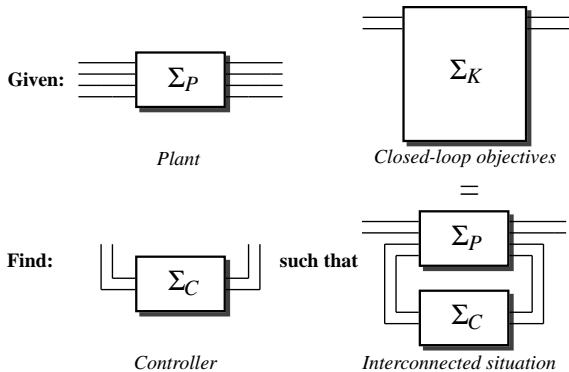


Figure 1: PF: Given Σ_P and Σ_K . Find Σ_C such that $\Sigma_P \wedge \Sigma_C = \Sigma_K$.

3 \mathcal{L}_2 systems / behaviors

A solution to this problem can be given using \mathcal{L}_2 systems: $\Sigma = (\mathbb{C}, \mathbb{W}, \mathcal{B})$, where \mathbb{C} indicates that we work in the frequency domain, \mathbb{W} is the space where the (interconnection) variables of the system, denoted as w , can take their values (e.g. $w(s) \in \mathbb{C}^w$) and \mathcal{B} is the \mathcal{L}_2 behavior of the system. We consider special \mathcal{L}_2 systems represented as kernels of (anti-stable) rational operators $R \in \mathcal{RH}_\infty^-$ (as in [3]) by setting:

$$\mathcal{B} = \{w \in \mathcal{L}_2 \mid R(s)w(s) = 0\} = \ker R(s),$$

This differs from “classical” behaviors [2], where polynomial differential operators are used and where the trajectories are in the time domain. Some advantages of using rational operators for behaviors are that there exists a calculus on Hardy spaces, it is possible to use projections and that it allows us to use state space calculus, which is desired in algorithms.

4 Algorithms

In this presentation, we address the problems of existence and complete parametrization of all \mathcal{L}_2 controller behaviors \mathcal{C} (of the controller Σ_C) such that the interconnection with the plant Σ_P results in the desired closed-loop objectives Σ_K . We moreover give explicit algorithms to determine such \mathcal{L}_2 controllers and analyze their properties. For those algorithms, we will make a distinction between two different types of interconnections, namely:

- *full interconnection:* the closed-loop situation is autonomous, so all variables of the plant are used for the interconnection with the controller. More details on the algorithm for this case can be found in [1].
- *partial interconnection:* the interconnected situation is not autonomous (as in Figure 1), so disturbances can influence the closed-loop dynamics. Details of the algorithm for this situation will be part of my presentation.

References

- [1] Mark Mutsaers and Siep Weiland, *Controller synthesis for \mathcal{L}_2 behaviors using rational kernel representations*, Proceedings of the 47th IEEE Conference on Decision and Control, Cancun, Mexico, pages 5134-5139, 2008.
- [2] Jan Willem Polderman and Jan C. Willems, *Introduction to Mathematical Systems Theory: A Behavioral Approach*, Springer, 1998.
- [3] Jan C. Willems and Y. Yamamoto, *Behaviors defined by rational functions*, Linear Algebra and Its Applications, Volume 425, pages 226-241, 2007.

Model reduction for Lur'e type systems

Bart Besselink, Nathan van de Wouw, Henk Nijmeijer

Department of Mechanical Engineering

Eindhoven University of Technology

P.O. Box 513, 5600 MB Eindhoven

The Netherlands

Email: b.besselink@tue.nl

1 Introduction

In the design of complex high-tech systems, predictive models are typically of high order. Model reduction can be used to obtain a low-order approximation of these models, allowing for efficient analysis or control design. Several methods exist for the reduction of linear systems. Balanced truncation [1] is among the most popular, since it provides guarantees on both stability and error bounds of the reduced-order model. Nonlinear model reduction techniques such as nonlinear balancing or proper orthogonal decomposition lack such an error bound or require simulations of the full-order model. In this work, (linear) balanced truncation is applied as a tool for model reduction of Lur'e type systems, representing a specific class of nonlinear systems. Next, conditions for stability of the reduced-order model are stated and an error bound is presented.

2 Lur'e type systems

A Lur'e type system Σ , as depicted in Figure 1, consists of a linear part Σ_l and a local nonlinearity φ , which is assumed to be scalar. The linear part, with $x \in \mathbb{R}^n$, is described by

$$\Sigma_l : \begin{cases} \dot{x} = Ax + B_u u + B_v v, \\ y = C_y x, \\ z = C_z x, \end{cases} \quad (1)$$

The static nonlinearity is given by $v = -\varphi(z)$ and is assumed to satisfy the incremental sector condition

$$-\mu \leq \frac{\varphi(z_1) - \varphi(z_2)}{z_1 - z_2} \leq \mu. \quad (2)$$

Then, the system Σ is absolutely stable (i.e. stable for any φ satisfying (2)) if A is Hurwitz and the circle criterion condition $\|G_{zv}(s)\|_\infty < \mu^{-1}$ holds, with G_{zv} the transfer function from v to z .

3 Model reduction

In order to find a low-order approximate $\hat{\Sigma}$ of Σ , the linear part is reduced using balanced truncation, introducing an error in the linear dynamics

$$\left\| \begin{bmatrix} G_{yu}(s) & G_{yv}(s) \\ G_{zu}(s) & G_{zv}(s) \end{bmatrix} - \begin{bmatrix} \hat{G}_{yu}(s) & \hat{G}_{yv}(s) \\ \hat{G}_{zu}(s) & \hat{G}_{zv}(s) \end{bmatrix} \right\|_\infty \leq 2 \sum_{i=k+1}^n \sigma_i = \varepsilon, \quad (3)$$

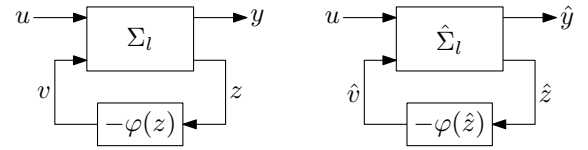


Figure 1: Lur'e type system Σ (left) and reduced-order Lur'e type system $\hat{\Sigma}$ (right).

with σ_i the Hankel singular values and $G_{ji}(s)$ denoting the transfer function from i to j . Since balancing maintains stability of the linear part, the nonlinear reduced-order system is guaranteed to be absolutely stable if the original system satisfies

$$\|G_{zv}(s)\|_\infty < \mu^{-1} - \varepsilon. \quad (4)$$

The error bound for the total nonlinear system is found by analyzing the propagation of the error in the linear dynamics, using a contraction property of the nonlinear loop. Here, it has to be noted that the same scalar nonlinearity is used in the reduced-order system. This leads to an error bound $\|y(t) - \hat{y}(t)\|_2 \leq \alpha \varepsilon \|u(t)\|_2$, with

$$\alpha = 1 + \frac{\mu \|G_{zu}\|_\infty}{1 - \mu \|G_{zv}\|_\infty} + \frac{\mu \|\hat{G}_{yv}\|_\infty}{1 - \mu \|\hat{G}_{zv}\|_\infty} \left(1 + \frac{\mu \|G_{zu}\|_\infty}{1 - \mu \|G_{zv}\|_\infty} \right).$$

Here, the error bound reduces to that of the linear system when $\mu = 0$. Thus, in the limit $\mu \rightarrow 0$ linear model reduction is indeed recovered.

4 Conclusions and recommendations

A model reduction procedure for Lur'e type systems is presented, where well-developed linear balancing techniques are used for reduction. Next, conditions for stability and an error bound are given. Since the nonlinearity is not explicitly taken into account in the model reduction procedure, the results hold for all nonlinearities satisfying the incremental sector condition.

References

- [1] B.C. Moore, Principal component analysis in linear systems - controllability, observability, and model reduction, *IEEE Transactions on Automatic Control*, AC-26, 1981.

Nonlinear model approximation using block structured models

O. Naeem, A. E. M. Huesman and O.H. Bosgra

Delft Center for Systems and Control, Delft University of Technology,

Mekelweg 02, 2628CD Delft, the Netherlands.

Email: O.Naeem@tudelft.nl

1 Introduction

Typically mathematical models of physical and chemical processes are large and complex because of complications and nonlinearities of physical processes. The importance of mathematical models is evident for optimization and control purposes. Large rigorous mathematical models are cause of high computational loads and computational times, restricting the use of such models for online applications. This provides the opportunity to use reduced models, which are match of NL processes within defined 'operational domain' which can achieve low computational loads and faster simulation times.

2 Methodology

Block structured models (in particular Hammerstein structure) have been used for identification purposes efficiently [1], but have not been used for model reduction purposes. Block structured models have advantage in approximation and identification; the approximated or identified block structures give insight to the complex and complicated process, hence providing handle for reduction. In this study, input-state (I/S) Hammerstein block structure is used for the approximation and model reduction of NL process.

Initially input-output Hammerstein block structure has been used for approximation (identification) of NL process [2]. The methodology has been extended to I/S Hammerstein structure. In this work, it is shown that I/S Hammerstein structure can be derived by Taylor series expansion (under trivial assumptions) [3]. Mathematically, I/S Hammerstein structure is given (as in equation 1 and shown in figure 1);

$$\begin{aligned} \dot{x} &= J(x - x_{ss}) + g(u) \\ y &= Cx \end{aligned} \quad (1)$$

where, J = Jacobian; C = output state matrix; y = output; $x_{ss} = g(u)$ is steady-state scheduling (from lookup table); $x^* = x_{ss}$; $u^* = u$.

The accuracy of the I/S Hammerstein approximation structure shown in figure 1, is improved by estimating Jacobian online using state x and input u information [3]. The accuracy of approximation is improved further by including higher order terms; estimation of Jacobians not only using (current) state information but also using steady-state information. The second order approximation block (I/S Hammerstein structure) has been derived from Taylor series [3].

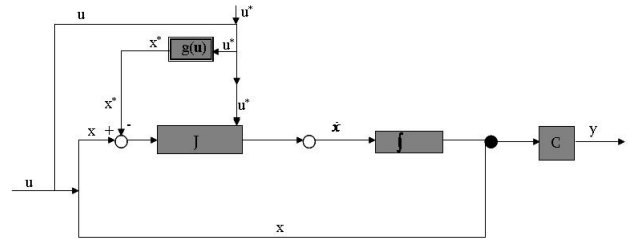


Figure 1: I/S Hammerstein structure

3 Results & Future Perspective

The methodology developed in this study has been implemented on high purity distillation column. Satisfactory results are obtained as far as approximation of the NL process is concerned. The approximation model has potential to be reduced (reduction in states and reduction in Jacobian size). The reduced block structure model is computationally attractive and reduction in computational load is expected. The reduced order I/S Hammerstein structure estimated NL processes adequately [3]. Future work focuses on implementation of reduced model efficiently in professional environment such as C++. Further the original and reduced model has to be compared.

Acknowledgement

This work has been supported by the European union within the Marie-Curie Training Network PROMATCH under the grant number MRTN-CT-2004-512441.

References

- [1] G. Harnischmacher, Wolfgang Marquardt. "A multivariate Hammerstein model for processes with input directionality." Journal of Process Control, Vol.17, 2007 (p539-550).
- [2] O. Naeem, Adrie E. Huesman and Okko H. Bosgra, "Identification based model reduction using block structured models." 27th BENELUX meeting 2007, Heeze.
- [3] O. Naeem, Adrie E. Huesman and Okko H. Bosgra, "Non-linear model order reduction using input to state Hammerstein structures" In the proceedings of REDUCIT Symposium 2008, Frankfurt.

Inferring bounds on the performance of a control policy from a sample of one-step system transitions

Raphael Fonteneau, Susan Murphy, Louis Wehenkel and Damien Ernst
University of Liège - University of Michigan
{fonteneau, lwh, ernst}@montefiore.ulg.ac.be, samurphy@umich.edu

In financial, medical, and engineering sciences, as well as in artificial intelligence, variants (or generalizations) of the following discrete-time optimal control problem arise quite frequently: a system, characterized by its state-transition function $x_{t+1} = f(x_t, u_t)$, $x_t \in X$, $u_t \in U$, $f: X \times U \rightarrow X$, should be controlled by using a policy $u_t = h(t, x_t)$, $h: \{0, \dots, T-1\} \times X \rightarrow U$ so as to maximize a cumulated reward $\sum_{t=0}^{T-1} \rho(x_t, u_t)$, $\rho: X \times U \rightarrow \mathbb{R}$ over a finite horizon $T \in \mathbb{N}$.

Different approaches have been proposed for solving this class of problem, such as dynamic programming [1] and model predictive control [2], reinforcement learning approaches [3, 4, 5] or approximate dynamic programming approaches [6]. Whatever the approach used to derive a control policy for a given problem, one major question that remains open today is to ascertain the *actual* performance of the derived control policy [7] when applied to the *real* system behind the model or the dataset (or the finger). Indeed, for many applications, even if it is perhaps not paramount to have a policy h which is very close to the optimal one, it is however crucial to be able to guarantee that the considered policy h leads for some initial states x_0 to high-enough cumulated rewards on the real system that is considered.

Motivated by these considerations, we have focused on the evaluation of control policies on the sole basis of the actual behaviour of the concerned real system. This has lead us to develop an approach for computing a lower bound on the sum of rewards generated by a policy h based on the sole basis of a sample of one-step system transitions $\mathcal{F} = \{(x^l, u^l, r^l, y^l)\}_{l=1}^{|\mathcal{F}|}$. Each one-step system transition provides the knowledge of a sample of information (x, u, r, y) , named four-tuple, where y is the state reached after taking action u in state x and r the instantaneous reward associated with the transition. The assumptions under which the approach works are similar to those made usually in the dynamic programming literature when studying problems with infinite state-action spaces: the state and action spaces X and U are normed and the functions f , ρ , and h are Lipschitz continuous.

The approach, which is fully detailed in [8], works by identifying in \mathcal{F} a sequence of T four-tuples $[(x^0, u^0, r^0, y^0), (x^1, u^1, r^1, y^1), \dots, (x^{T-1}, u^{T-1}, r^{T-1}, y^{T-1})]$ ($l_t \in \{1, \dots, |\mathcal{F}|\}$), which maximizes a specific numerical criterion. This criterion is made of the sum of the T rewards

corresponding to these four-tuples $(\sum_{t=0}^{T-1} r^{l_t})$ and T negative terms. The negative term corresponding to the four-tuple $(x^{l_t}, u^{l_t}, r^{l_t}, y^{l_t})$ of the sequence represents an upper bound variation of the cumulated rewards over the remaining time steps that can occur by simulating the system from a state x^{l_t} rather than y^{l_t-1} (with $y^{l_t-1} = x_0$) and by using at time t the action u^{l_t} rather than $h(t, y^{l_t-1})$. Once this best sequence of tuples has been identified - something that can be achieved by using an algorithm whose complexity is linear with respect to the optimization horizon T and quadratic with respect to the size $|\mathcal{F}|$ of the sample of four-tuples - a lower bound on the sum of rewards can be computed in a straightforward way. Furthermore, it can be shown that this lower bound converges at least linearly towards the true value of the return with the density of the sample (measured by the maximal distance of any state-action pair to this sample).

References

- [1] D. Bertsekas, *Dynamic Programming and Optimal Control*, 2nd ed. Belmont, MA: Athena Scientific, 2005, vol. III.
- [2] E. Camacho and C. Bordons, *Model Predictive Control*. Springer, 2004.
- [3] R. Sutton and A. Barto, *Reinforcement Learning, an Introduction*. MIT Press, 1998.
- [4] M. Lagoudakis and R. Parr, "Least-squares policy iteration," *Journal of Machine Learning Research*, vol. 4, pp. 1107–1149, 2003.
- [5] D. Ernst, P. Geurts, and L. Wehenkel, "Tree-based batch mode reinforcement learning," *Journal of Machine Learning Research*, vol. 6, pp. 503–556, 2005.
- [6] D. Bertsekas and J. Tsitsiklis, *Neuro-Dynamic Programming*. Athena Scientific, 1996.
- [7] R. Schapire, "On the worst-case analysis of temporal-difference learning algorithms," *Machine Learning*, vol. 22, no. 1/2/3, 1996.
- [8] R. Fonteneau, S. Murphy, L. Wehenkel, and D. Ernst, "Inferring bounds on the performance of a control policy from a sample of trajectories," in *Proceedings of the IEEE Symposium on Adaptive Dynamic Programming and Reinforcement Learning (IEEE ADPRL 09)*, Nashville, TN, USA, 2009.

Fixed Structure Controller Synthesis Using Non-Parametric Plant Models with Uncertainty

Irmak Aladagli¹, Arjen den Hamer¹, Maarten Steinbuch¹, Georgo Angelis²

E-mail: i.aladagli@student.tue.nl

¹ Control Systems Technology Group, Eindhoven University of Technology

² Philips Applied Technologies

1 Introduction

Controller design can be classified into two main methods, norm based designs and manual loopshaping for SISO systems. Norm based control design methods are strong in handling uncertainty and closed-loop (CL) performance specifications giving an optimal or suboptimal controller. However they require a model of the plant and they usually result in high order infeasible controllers. Manual loopshaping on the other hand, does not require a parametric model and the order of the controller is the choice of the designer. However this method does not systematically account for closed-loop performance specifications or uncertainties. Moreover its success depends on the skills of the engineer.

Quantitative Feedback Theory (QFT), developed by Isaac M. Horowitz, is a transparent graphical design tool in frequency domain that offers promising solutions to all above problems (see [2]). It allows design according to the CL performance specifications and it can handle parametric or non-parametric uncertainties. Order of the resulting controllers is the choice of the designer. The only disadvantage of traditional QFT is that there is no systematic design procedure. The objective of this research is to automate the controller design procedure of QFT. Once this is done, the new design procedure has none of the disadvantages listed above. Research has been going on to automate this design step since it was first suggested by [1]. A very nice summary of the research history since then can be found in [3].

2 Problem Definition and Method

Given plant model or frequency response coefficients for an uncertain system, and performance specifications as a discrete mixed sensitivity (MS) problem, the problem is to calculate the allowable parameter space of a fixed structure stabilizing controller. In this research we consider two parameter controllers, however we believe it is possible to extend the suggested method to higher order controller design.

The method can be explained as converting the design specs in the form of a MS problem into bounds on the parameters of the controller. MS specs result in quadratic inequalities (QI's) in terms of the controller parameters. These QI's define bounds in the form of conic sections in controller parameter space and allow the designer or an optimization al-

gorithm to choose from the allowable parameter space according to the needs of the problem. This conversion, done per frequency, translates bounds in the traditional Nichols and/or Nyquist planes into bounds in controller parameter space.

Uncertainty is accounted for by defining a plant set that includes all possible plants. The plant set and frequency range to be analyzed are discretized and corresponding conic sections are calculated for all. The outermost bound is selected to define the allowable parameter space. A stability criteria is employed to define the parameter space that result in a stable system. Controller parameters are chosen according to variable criteria, like minimizing high frequency gain, from the resulting allowable parameter space.

3 Conclusion

Applying the above procedure using plants with multiplicative uncertainty, allowable parameter space of a two parameter controller is calculated, for both numerator and denominator parameters. From the allowable space, controller parameters are chosen according to variable criteria, like stabilizing the feedback system, minimizing high frequency gain, etc.. It is observed that the resulting controller satisfies the performance specs while staying in close range of the optimal solution.

References

- [1] A. Gera and I.M. Horowitz. Optimization of the loop transfer function. *International Journal of Control*, 31:389–398, 1980.
- [2] Isaac M. Horowitz. *A Gourmet QFT Dinner*. QFT Publications, 1993.
- [3] P. S. V. Nataraj and Manoj M. Deshpande. Automated synthesis of fixed structure qft controller using interval constraint satisfaction techniques. In *17th IFAC World Congress*, 2008.

Adaptive extremum-seeking control of fed-batch cultures of micro-organisms exhibiting overflow metabolism

Laurent Dewasme and Alain Vande Wouwer
Laboratoire d'Automatique
Faculté Polytechnique de Mons
Boulevard Dolez, 31 7000 Mons
Belgium

Email: laurent.dewasme@fpms.ac.be
alain.vandewouwer@fpms.ac.be

Bala Srinivasan and Michel Perrier
Département de Génie Chimique
Ecole Polytechnique de Montréal
C.P.6079, Montréal, Québec
Canada

Email: bala.srinivasan@polymtl.ca
michel.perrier@polymtl.ca

1 Introduction

Overflow metabolism characterizes cells strains that are likely to produce inhibiting metabolites resulting from an excess of substrate feeding and a saturated respiratory capacity. The critical substrate level separating the two different metabolic pathways is generally not well defined. This paper proposes two non-model based extremum-seeking strategies preventing a too important accumulation of inhibiting metabolites in fed-batch cultures, by estimating the critical substrate level on the basis of 3 simple measurements related to the feeding, oxygen and carbon dioxide. A simple substrate controller based on Lyapunov stability arguments is then designed and tested in combination with the two extremum-seeking schemes.

2 Adaptive model-free extremum-seeking strategies

Industrial vaccine production is usually achieved using fed-batch cultures of genetically modified yeast or bacteria strains, which can express different kinds of recombinant proteins. From an operational point of view, it is necessary to determine an optimal feeding strategy (i.e. the time evolution of the input flow rate to the fed-batch culture) in order to maximize productivity.

The main encountered problem comes from the metabolic changes of such strains in presence of feeding overflow. This "overflow metabolism", also called "short-term Crabtree effect", is a metabolic phenomenon that is induced when the rate of glycolysis exceeds a critical value, leading to a generally inhibiting by-product formation from pyruvate (for not well understood reasons). It occurs for instance in *S. cerevisiae* cultures with aerobic ethanol formation, in *P. pastoris* with aerobic methanol formation, in *E. coli* cultures with aerobic acetate formation or in mammalian cell cultures with the aerobic lactate formation. To avoid this undesirable effect, a closed-loop optimizing strategy is required, which could take various forms ([1], [2], [3]).

In this study, a non-model based extremum-seeking strategy is chosen (see Figure 1). Two original techniques are proposed and compared. The first one is related to the work of Blackman in the 60's, revisited and improved in [4] while

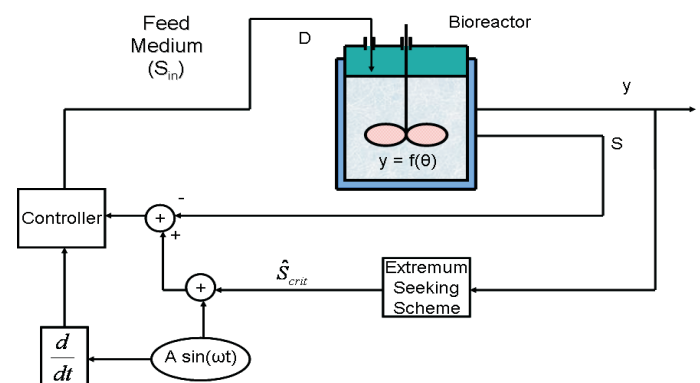


Figure 1: Application of extremum-seeking to fed-batch cultures of microorganisms: D , S , S_{in} and \hat{S}_{crit} are respectively the dilution rate, the substrate concentration in the culture medium, the substrate concentration in the feed medium and the estimation of the substrate critical level.

the second one is based on a simple recursive least squares technique (RLS).

Acknowledgment

This paper presents research results of the Belgian Network DYSCO (Dynamical Systems, Control, and Optimization), funded by the Interuniversity Attraction Poles Program, initiated by the Belgian State, Science Policy Office. The scientific responsibility rests with its authors. The authors also gratefully acknowledge the support of the Wallonie-Bruxelles-Québec commission in the framework of the research project between A. Vande Wouwer and M. Perrier.

References

- [1] Pomerleau, Y. *Modélisation et commande d'un procédé fed-batch de culture des levures à pain*. Département de génie chimique. Ecole Polytechnique de Montréal. PhD Thesis (1990).
- [2] Renard, F. *Commande robuste de bioprocédés opérés en mode fed-batch. Application industrielle à des cultures de S. cerevisiae*. PhD thesis, Faculty of Engineering, Mons, April 2006.
- [3] L. Dewasme, F. Renard, and A. Vande Wouwer. *Experimental investigations of a robust control strategy applied to cultures of S. cerevisiae*. ECC 2007, Kos, Greece, July 2007.
- [4] K. B. Ariyur and M. Krstic. *Real-Time Optimization by Extremum-Seeking Control*. John Wiley & Sons, INC., publication, wiley-interscience edition, 2003.

Model-free Optimal Control Synthesis

Arjen den Hamer¹
a.j.d.hamer@tue.nl

Siep Weiland²
s.weiland@tue.nl

Maarten Steinbuch¹
m.steinbuch@tue.com

¹ Control Systems Technology Group,
Eindhoven University of Technology

² Control Systems Group,
Eindhoven University of Technology

1 Introduction

Experimental data is of unrivalled value for system analysis and controller synthesis. Especially for high performance motion systems, large amounts of experimental data can be obtained with high quality, i.e. with low noise content, and at a low cost.

In order to exploit state of the art norm based control synthesis techniques, a parametric model of the plant has to be extracted from the experimental data. However, the high dynamical order typically found in motion systems and the lack of prior knowledge about the dynamical structure makes system identification a non-trivial task. Choosing a high plant order minimizes misfit but results in high order controller for which numerical tooling may be cumbersome. Constraining the order of the plant model results in misfit for which the consequences for closed-loop performance or even stability are not given in a straightforward manner.

To overcome the problem mentioned above, the goal of this research is to perform norm based controller synthesis from experimental plant data directly. This approach omits identification of the plant and therefore exploits all experimental data with equal importance since no prior assumptions about the system structure are used.

2 Approach

In this presentation, fixed-structure controller synthesis from frequency response data directly is considered. The problem statement can be described as:

Given: a predefined controller structure with parameters θ and given measured frequency response data of a stable plant $P_i = P(j\omega_i)$ at an equally spaced frequency grid $\omega_i \in \Omega$.

Find: the controller parameters θ^* that result in the minimum H_∞ norm of the closed-loop system $M = LFT(P, C)$.

This problem is splitted in two parts: closed-loop stability and closed-loop performance. These parts will be discussed shortly.

2.1 Stability

Since only finite frequency response data of the plant is given, the poles of the closed-loop system are not directly accessible. Within this research, guarantees for closed-loop stability are derived that can be applied on measured frequency response data directly, i.e. without explicit knowledge of the underlying poles [2]. Via assumptions about the relative stability of the system, the following relation can be used to guarantee stability of the closed-loop system:

$$M(\omega_i) = \frac{1}{\pi} \sum_j M(\omega_j) \frac{1}{j\omega_i - j\omega_j} \Delta \quad (1)$$

where Δ represents the frequency grid distance.

2.2 Performance

Due to the lack of an interpolating model, the \mathcal{H}_∞ norm is approximated with a frequency sampled \mathcal{H}_∞ problem. This results in an LMI constraint for every frequency point.

$$\begin{bmatrix} \gamma & P_{1,1i} + P_{1,2i} & Q_i & P_{2,1i} \\ * & & \gamma & \\ & & & \end{bmatrix} \succ 0, \quad \forall \omega_i \in \Omega \quad (2)$$

Where Q_i represents the frequency response coefficients of the Youla parameter.

3 Synthesis

Although both performance and stability constraint are affine in the closed-loop transfer functions, the controller parameters are related to the closed-loop transfer-function in a non-convex manner resulting in non-linear matrix inequalities. Via a local linearization technique, a gradient can be computed that locally minimizes the singular values [1], i.e. the \mathcal{H}_∞ norm of M . Although this a non-convex optimization problem, it is expected that the use of several starting points results in the global minimizer θ^* .

References

- [1] S. Boyd and L. Vandenberghe *Convex Optimization*. Cambridge university press, 2004.
- [2] A.J. den Hamer, S. Weiland, M. Steinbuch and G.Z. Angelis, *Stability and causality constraints on frequency response coefficients applied for non-parametric \mathcal{H}_2 and \mathcal{H}_∞ control synthesis*. CDC, 2008

Lazy online batch-end quality estimation: is less more?

G. Gins, J. Vanlaer, J.F.M. Van Impe

BioTeC - Chemical and Biochemical Process Technology and Control

Department of Chemical Engineering, Katholieke Universiteit Leuven,

W. de Croylaan 46, B-3001 Leuven, Belgium.

{geert.gins, jef.vanlaer, jan.vanimpe}@cit.kuleuven.be

1 Introduction

In (bio)chemical industry, batch processes are commonly used for the production of products with a high added value (e.g., high-performance polymers, pharmaceuticals, ...). To ensure a constant and satisfactory product quality, a close online monitoring of these batch processes is required.

Recently, most research effort has been dedicated towards fault detection and diagnosis using *Principal Component Analysis* (PCA [2]). These PCA models are very powerful tools for detecting abnormal process behavior, but lack the online prediction capability of batch-end quality. Therefore, *Partial Least Squares* models (PLS [3]) are used when such predictions are required [5]. Due to their need for data of a *completed* batch, however, these PLS models cannot be directly employed online [4].

This work compares the use of *Intermediate Models* with *Trimmed Scores Regression* for overcoming this problem.

2 Online batch-end quality estimation

When monitoring a running new batch, the future measurements are unknown at a given time. Hence, the input matrix for the developed full PLS model, which relates the measurements from a *complete* batch with the quality parameters obtained after batch completion, is only partially known. Consequently, the PLS model cannot be employed directly to obtain batch-end quality predictions online. To alleviate this problem, two methodologies are available.

A first methodology for dealing with the unknown measurements is the use of a series of *Intermediate Models* (IMs). Each IM is a newly identified local PLS model, and takes only a part of the full batch duration as input (e.g., the first 10%, 20%, ... of the batch). Hence, it provides an estimate of the final quality at only one specific point in time; a series of IMs yields a pseudo-online estimate of the final quality.

A second methodology compensates for the missing (future) measurements through missing data techniques. García-Munoz *et al.* demonstrated the superiority of *Trimmed Scores Regression* (TSR [4]). TSR first makes an (incorrect) estimate of the batch-end quality variables of the new (running) batch, based only on the available measurements by truncating the model matrices. Next, a regression model is extracted from the historic training data, and used to adjust the incorrect estimate. Because TSR only uses a single PLS model for all times, it yields true online quality estimates.

3 Results & Conclusions

The performance of the IMs and TSR is compared on two different (fed-)batch processes. The first is a penicillin fermentation of which the data is generated using the *Pensim* simulator [1]. The second data set describes an industrial batch polymerization.

It is observed that the accuracy of the TSR estimates is generally slightly less than that of IMs. However, TSR saves a substantial amount of work because it requires the identification of a single PLS model, in contrast with IMs, where a new model must be identified for each time where end quality predictions are requested. The small loss in batch-end quality parameter prediction accuracy (if any) does not outweigh the significant reduction in required workload. Hence, it is concluded that, for the cases studied in this paper, TSR outperforms the IMs: the less work-intensive method is the best.

Acknowledgements. Work supported in part by Projects OT/03/30 and EF/05/006 (Center-of-Excellence Optimization in Engineering) of the Research Council of the Katholieke Universiteit Leuven, Leverage Project IOFHBKP/06/002 (SCORES4CHEM) of the Industrial Research Council of the Katholieke Universiteit Leuven, and the Belgian Program on Interuniversity Poles of Attraction, initiated by the Belgian Federal Science Policy Office. The scientific responsibility is assumed by its authors.

The authors would like to thank J. De Wilde of CYTEC (Drogenbos, Belgium) for the industrial polymerization data set provided for this study.

References

- [1] G. Birol, C. Ündey, and A. Çinar. A modular simulation package for fed-batch fermentation: penicillin production *Comput. Chem. Eng.*, 26:1553-1565, 2002.
- [2] L. Eriksson, E. Johansson, N. Kettaneh, and S. Wold. *Multi- and Megavariate Data Analysis: Principles and Applications* Umetrics Academy, 91-973730-1-X, 2002.
- [3] P. Geladi and B.R. Kowalski. Partial least-squares regression: a tutorial *Anal. Chim. Acta*, 185:1-17, 1986.
- [4] S. García-Munoz, T. Kourti, and J.F. MacGregor. Model predictive monitoring for batch processes *Ind. Eng. Chem. Res.*, 43:5929-5941, 2004.
- [5] P. Nomikos and J.F. MacGregor. Multivariate SPC charts for monitoring batch processes *Technometrics*, 37(1):41-59, 1995.

Fault detection in a biochemical fed-batch process

J. Vanlaer, G. Gins and J.F.M. Van Impe

BioTeC - Chemical and Biochemical Process Technology and Control
Department of Chemical Engineering, Katholieke Universiteit Leuven,
W. de Croylaan 46, B-3001 Leuven, Belgium.
{jef.vanlaer, geert.gins, jan.vanimpe}@cit.kuleuven.be

1 Introduction

In the (bio)chemical industry, products with a high added value are often produced in (fed-)batch reactors. Since product quality is only known at the end of a batch, a close monitoring of these processes is necessary. To detect process behavior that deviates from normal operation, several fault detection techniques, based on a combination of *Principal Component Analysis* (PCA) and *Statistical Process Control* (SPC), have been developed (e.g., [4]).

Compared to continuous process data, (fed-)batch process data exhibit significantly more auto- and cross-correlation. Specific techniques, such as *AutoRegressive PCA* (ARPCA [3]) and *Batch Dynamic PCA* (BDPCA [2]) have been developed to take this inherent cross- and auto-correlation into account. In this work, the fault detection performance of these techniques and a standard Multi-way PCA technique with Variable-wise unfolding (MPCAV) are compared, based on extensive simulation results for a (fed-)batch fermentation process for penicillin production.

2 PCA-based fault detection

For a known history of I batches, each consisting of J variables sampled over K time points, a three-dimensional $I \times J \times K$ data matrix \mathbf{X} is obtained. *Multi-way Principal Component Analysis* (MPCA) deals with this three-dimensional structure by unfolding the 3D matrix. With *variable-wise unfolding* (MPCAV), the variable direction is preserved by placing I slices of size $K \times J$ under each other. On the unfolded matrix \mathbf{X} , a standard PCA model is trained [4].

ARPCA [3] and BDPCA [2] take the inherent auto- and cross-correlation of (fed-)batch process data into account by starting from a time-lagged data matrix. Whereas in ARPCA a PCA model is trained on the residuals of an autoregressive Partial Least Squares (PLS) model, the eigenvector decomposition of the average covariance matrix (computed from the time-lagged data matrices for the different batches) is calculated in BDPCA.

By comparing the process behavior of a new batch with an in-control model, based on a set of normal training batches, abnormal process behavior can be detected. Hereto, three statistics are monitored throughout the batch. The T^2 -statistic is a measure for the difference between the model scores, whereas the SPE (Squared Prediction Error) and Q^2 -statistic measure the instantaneous and total reconstruction error, respectively. When one of these statistics exceeds

its 99.9% control limit (determined based on the statistical properties of the training data) on three consecutive sample instances, an alarm is raised.

3 Case study

200 batches of a fed-batch process for penicillin fermentation with varying initial conditions are simulated as a training set via the `Pensim` simulator [1]. A total of 45 faulty test batches are simulated to compare the fault detection performance of the different techniques. Hereto, two process fault types (a 20% step decrease in agitator power and a gradual decrease of 0.05% per hour in the substrate feedrate) are introduced at different times in the process. Both training and test data are aligned via *indicator variables*.

4 Results

The results of this study corroborate the statement that ARPCA and BDPCA enhance the fault detection capability in batch processes, since these techniques show smaller mean detection times and higher detection rates than MPCAV. ARPCA seems to outperform BDPCA, showing slightly lower mean detection times. However, BDPCA has lower detection times for quite a few batches, so, for this case study, the difference is found to be non-significant.

Acknowledgements. Work supported in part by Projects OT/03/30 and EF/05/006 (Center-of-Excellence Optimization in Engineering) of the Research Council of the Katholieke Universiteit Leuven, Leverage Project IOFHBKP/06/002 (SCORES4CHEM) of the Industrial Research Council of the Katholieke Universiteit Leuven, and the Belgian Program on Interuniversity Poles of Attraction, initiated by the Belgian Federal Science Policy Office. The scientific responsibility is assumed by its authors.

References

- [1] G. Birol, C. Ündey, and A. Çinar. A modular simulation package for fed-batch fermentation: penicillin production. *Comput. Chem. Eng.*, 26:1553–1565, 2002.
- [2] J. Chen and K.-C. Liu. On-line batch process monitoring using dynamic PCA and dynamic PLS models. *Chem. Eng. Sci.*, 57:63–75, 2002.
- [3] S.W. Choi, J. Morris, and I.-B. Lee. Dynamic model-based batch process monitoring. *Chem. Eng. Sci.*, 63:622–636, 2008.
- [4] S. Wold, P. Geladi, K. Esbensen, and J. Ohman. Multi-way principal component and PLS analysis. *J. Chemom.*, 1:41–56, 1987.

A control system for suppression of magnetic islands in a fusion plasma

Bart Hennen, Egbert Westerhof, Marco de Baar
FOM-Institute for Plasma Physics Rijnhuizen,
Association EURATOM-FOM, Trilateral Euregio Cluster,
P.O. Box 1207, 3430 BE Nieuwegein
The Netherlands
Email: B.A.Hennen@tue.nl

Pieter Nuij, Maarten Steinbuch
Department of Mechanical Engineering
Technische Universiteit Eindhoven
P.O. Box 513, 5600 MB Eindhoven
The Netherlands
Email: P.W.J.M.Nuij@tue.nl

1 Introduction

A real-time control system is introduced, which is designed for the stabilization of magneto-hydrodynamic (MHD) events in a present-day experimental fusion reactor, i.e. a so-called tokamak. In the torus-shaped tokamak, a plasma is confined magnetically using helical magnetic fields. The control system presented here, focuses on the suppression of so-called magnetic islands, encountered in such plasmas [1]. Actively controlled suppression is required since these events harm the operational stability of the machine and deteriorate the plasma performance.

2 Suppression of magnetic islands

High power electron cyclotron waves (ECRH or microwaves) are recognized as an ideal tool for control of plasma profiles and instabilities, like magnetic islands, where one exploits their effect on the plasma in terms of localized heating and current drive. Deposition of the ECRH power onto the magnetic instability must be performed precisely within certain accuracy. Misalignment of the ECRH power deposition w.r.t. the magnetic island reduces the effectiveness of its suppression. An island track-and-kill system must therefore deal both with the identification of the magnetic island and its position in the plasma, as well as with the steering of the ECRH beam in order to deposit the power at the magnetic island. Note that such system has a typical feedback control structure where the necessary detection and control actions must be performed in real-time within tenth of milliseconds, while the tracking of the ECRH wave beam w.r.t. the island is subject to disturbances.

3 Real-time control system

The particular control system discussed here is designed and implemented at the TEXTOR tokamak, Forschungszentrum Jülich, Germany. The TEXTOR installation involves a 800 kW source, which produces a 140 GHz ECRH wave beam. This beam can be directed at any location within the plasma by a fast steerable mechanical launcher. Model-based position controllers have been developed and implemented for this launcher, based on analysis of its dynamics. Identifica-

tion of magnetic islands relies on the perturbations caused by their appearance on the magnetic topology and the electron temperature profiles of a plasma. Plasma diagnostics like electron cyclotron emission (ECE) and Mirnov coils are used to identify the magnetic islands. On TEXTOR, the tasks of instability identification and localization and of the steering of the ECRH wave beam are combined in a single system, in which low power (100 pW) Electron Cyclotron Emission is measured along the same sight-line as the high power (800 kW) ECRH wave beam [2]. The ECE spectrum is measured while scanning the combined ECRH/ECE wave beam through the plasma. Localization of a given structure in the ECE spectrum relative to the ECRH frequency is thereby used directly to position the ECRH power relative to this structure. Algorithms to extract relevant control variables such as the location, amplitude and phase of the magnetic island from these fluctuation measurements will be addressed. The generation of control set-points for the launcher steering and control of the ECRH power will be demonstrated. A flexible real-time control and data-acquisition system is currently installed for implementation of the data-processing algorithms, trajectory generation and for real-time execution of the control loops.

4 Model-based control design and experimental validation

The design of controllers for this control problem is aided by the development of a dedicated simulation model of the overall control loop, including magnetic island and plasma dynamics, actuator models, diagnostic models, and models for the data-processing algorithms. A complete control simulation for typical TEXTOR conditions is in progress. Experimental results are used to validate and optimize the functionality of the control system to guarantee stable, accurate and fast positioning of the ECRH wave beam.

References

- [1] R.J. La Haye, "Neoclassical tearing modes and their control," *Phys. Plasmas* 13, 2006.
- [2] J.W. Oosterbeek et al., *Rev. Sci. Instrum.* 79, 093503, 2008.

Detection and isolation of sensor faults in induction machines

Manuel Gálvez and Michel Kinnaert

Université Libre de Bruxelles (U.L.B.)

50, Av. F.D. Roosevelt-CP 165/55, B-1050 Brussels, Belgium

mgalvezc@ulb.ac.be, michel.kinnaert@ulb.ac.be

1 Introduction

In a controlled induction machine, the measured three-phase currents are used for the computation of the control law. A fault in one of these sensors can produce a degradation in the performance and turn into a failure. The proposed fault detection and isolation (FDI) system is based on the model of the three-phase signals, instead of the machine model. It is made of a multi-observer scheme for residual generation and a statistical change detection and isolation algorithm as decision system. Two kinds of faults are considered: additive (offset or slow drift) and multiplicative (gain change) faults. It is assumed that the three currents are measured and that only one fault can occur at a time.

2 Signal-based model

Assume balanced three-phase currents $[y_1, y_2, y_3]^T$, which means that they have the same amplitude (M) and frequency (ω_e), and are shifted $-2\pi/3$ rad from each other. Then:

$$\begin{bmatrix} \dot{x}_1(t) \\ \dot{x}_2(t) \end{bmatrix} = \begin{pmatrix} 0 & \omega_e(t) \\ -\omega_e(t) & 0 \end{pmatrix} \begin{bmatrix} x_1(t) \\ x_2(t) \end{bmatrix} \quad (1)$$

$$\begin{bmatrix} y_1(t) \\ y_2(t) \\ y_3(t) \end{bmatrix} = \begin{pmatrix} 1 & 0 \\ -\frac{1}{2} & -\frac{\sqrt{3}}{2} \\ -\frac{1}{2} & \frac{\sqrt{3}}{2} \end{pmatrix} \begin{bmatrix} x_1(t) \\ x_2(t) \end{bmatrix} \quad (2)$$

is a state-space representation of such signals. An additive and a multiplicative sensor fault can be modelled by:

$$y_i^m(t) = k_i(t)y_i(t) + \eta_i(t) + f_i(t) \quad (3)$$

where y_i^m and y_i are the measured and actual current, respectively, η_i is the measurement noise, f_i is the additive fault magnitude and k_i is the multiplicative gain, for $i = \{1, 2, 3\}$. When an additive fault in the i -th sensor occurs, $f_i(t) \neq 0$, while when a multiplicative fault occurs, $0 \leq k_i(t) < 1$.

3 Residual generation and decision system

For residual generation purposes, a multi-observer approach is used, based on the Generalized Observer Scheme (GOS). In this approach, the i -th observer uses all but the i -th measurement, as shown in Fig. 1. The residual generator is actually a time-varying discrete Kalman filter (KF), based on (1)-(2), of which the innovation is used as residual vector. For the decision system, the multi-CUSUM (Cumulative

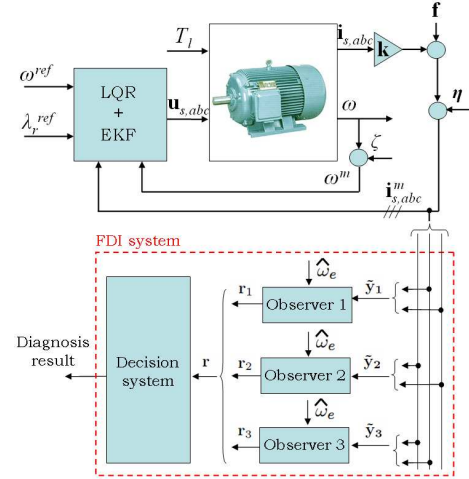


Figure 1: Controlled IM with FDI system.

sum) [1], a statistical change detection and isolation algorithm is used. In this approach, the whole set of residuals signals r_i , for $i = \{1, 2, 3\}$, is combined in a single residual vector. The latter is processed using as many CUSUM algorithms as the number of possible faults. An alarm is then issued when one of the CUSUM decision functions reaches a threshold (h), calculated in order to satisfy a given criterion, namely a required mean detection delay for each fault ($\bar{\tau}_i$), in our particular case. The FDI system has been validated for additive and multiplicative faults respectively. In both cases, the fault has been properly detected and isolated within the required detection delay, even in the presence of disturbances and changes in the references.

Acknowledgments

The work of Manuel Gálvez is supported by the ARC project 'Advanced supervision and dependability of complex processes: application to power systems'. This paper presents research results of the Belgian Network DYSCO (Dynamic Systems, Control and Optimization), funded by the Interuniversity Attraction Poles Programme, initiated by the Belgian State, Science Policy Office. The scientific responsibility rests with its authors.

References

- [1] I. Nikiforov, A simple recursive algorithm for diagnosis of abrupt changes in signals and systems, In *Proceedings of the 1998 American Control Conference*, vol. 3, pp. 1938–1942, Philadelphia, USA, 1998.

Motion Control of the Twente Humanoid Head

L. C. Visser, R. Carloni and S. Stramigioli

IMPACT Institute, Faculty of EEMCS

University of Twente, PO Box 217, 7500 AE Enschede, The Netherlands

{l.c.visser,r.carloni,s.stramigioli}@utwente.nl

1 Abstract

In this work, we present the design and the realization of the motion control algorithm implemented in the Twente humanoid head, a seven degrees of freedom (dof) robotic system. The aim of the project is to have a humanoid head that can serve as a research platform for human-machine interaction purposes. The head should not only be able to perceive its environment and track objects, but also be able to move in a human-like way, i.e. to reproduce the motions of human beings and to mime the human expressions. The Twente humanoid head is presented in Fig. 1.



Figure 1: The Twente humanoid head.

The mechanical design consists of a four dof head-neck structure and a three dof vision system. Two dofs of the neck are combined in a differential drive setup on which the other two dofs are mounted. The cameras of the vision system share a commonly actuated tilt axis and can rotate sideways independently. The mechanical design is treated in detail in [2].

A vision processing algorithm analyzes the camera images and extracts the target information in the image plane, as deeply explained in [3]. This target can be either an object or a particular feature in the image plane and it provides the input of the control algorithm.

The mechanical structure has been translated into kinematic and dynamic models based on screw theory. The relation between the change in perceived 2D target coordinates, de-

noted by $\dot{\mathbf{x}}$, and the generalized joint velocities $\dot{\mathbf{q}}$ is

$$\dot{\mathbf{x}} = \mathbf{F}(\mathbf{q})\dot{\mathbf{q}} \quad (1)$$

where $\mathbf{F}(\mathbf{q})$ is a matrix mapping as function of the generalized joint positions \mathbf{q} . From this relation, given a desired $\dot{\mathbf{x}}$, the joint velocities $\dot{\mathbf{q}}$ can be obtained through the relation

$$\dot{\mathbf{q}} = \mathbf{F}^\# \dot{\mathbf{x}} + (\mathbf{I} - \mathbf{F}^\# \mathbf{F}) \mathbf{z} \quad (2)$$

where $\mathbf{F}^\#$ is a generalized inverse of matrix \mathbf{F} and \mathbf{z} is an arbitrary vector of appropriate dimension which is projected onto the null space of \mathbf{F} , see [1] for more details. Vector \mathbf{z} can be both used to generate human-like motions of the head in the tasks of target tracking and to generate motions in the null-space so to realize certain expressions, or human-like behavior, that can be exploited in human-machine interaction. The controller overview, presented in Fig. 2, has been implemented in 20-sim simulation software [4] for the preliminary tests and, then, in the real setup.

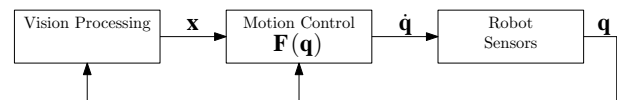


Figure 2: Control scheme.

Finally the expression movements have been coupled to the movement of the eyelids and the eyebrows, realized with a LED system which projects light from the internal part of the plastic cover of the head.

References

- [1] L.C. Visser, R. Carloni and S. Stramigioli, "Vision based motion control for a humanoid head", *Master's Thesis, University of Twente*, 2008.
- [2] D. M. Brouwer, J. Bennik, J. Leideman, H. M. J. R. Soemers and S. Stramigioli, "Mechatronic design of a fast and long range 4 degrees of freedom humanoid neck", *IEEE Int. Conf. Robotics and Automation 2009*.
- [3] R. Reilink, S. Stramigioli, F van der Heijden and G. van Oort, "Saliency-based humanoid gaze emulation using a moving camera setup", *Master's Thesis, University of Twente*, 2008.
- [4] 20-sim, <http://www.20sim.com>, Controllab Products B.V., 2009.

A gaze saccade model based on separate head and gaze controllers.

Daye P.

UCL/CESAME

4, Avenue Georges Lemaitre. 1348 Louvain-la-Neuve. Belgium

Email: pierre.daye@uclouvain.be

Blohm G.

Queens University/CompNeurosci Lab

18, Stuart Street. Kingston, Ontario, K7L 3N6. Canada

Email: blohm@biomed.queensu.ca

Optican L.

NIH/NEI

2020, Vision Place. Bethesda, MD 20892-3655. USA

Email: lmo@lsr.nei.nih.gov

Lefèvre P.

UCL/CESAME

4, Avenue Georges Lemaitre. 1348 Louvain-la-Neuve. Belgium

Email: philippe.lefevre@uclouvain.be

1 Abstract

In everyday life, reorienting our visual axis to a new center of interest generally recruits a rapid combined movement of the eye and head called gaze saccade (gaze=eye with respect to an inertial frame). The interaction and coordination of those two systems to achieve a general accurate movement remains a challenging question.

In trying to model the gaze system, two major theoretical propositions are present in the literature. In a first one (e.g. [3], [1]), the authors proposed that the central nervous system planned the needed displacement of the eye and the head before the gaze saccade execution. Major failure of this kind of model comes from the ability of the central nervous system to get rid of a perturbation that occurred during the execution of the gaze saccade. The second approach is based on a gaze feedback controller (e.g. [4], [2]). Authors proposed that during gaze saccades, eye and head movements are coupled by a shared motor drive and a stabilizing reflex, the vestibulo-ocular reflex (VOR). However, even if those models are able to reject gaze perturbation, experimental evidence has shown that eye and head trajectories can be decoupled because head movement is strongly influenced by the task. "Feedback" theories are facing difficulties to deal with the variabilities present in head movements.

We proposed a model of gaze saccades based on separate controllers for head and gaze. The model is an extension of [5]. We proposed that three main neural pathways are involved in the control. The first one is the main drive provided by the superior colliculus (SC) and is shared by the

eye and the head. This drive gives the general direction of the gaze shift. The second pathway represents the independent controller acting on the head and allows separate goals for head and gaze trajectories. The last pathway is the core of the model and is based on a cerebellum gaze controller. The cerebellum monitors the gaze motor error on the basis of gaze velocity feedback. It provides an additional drive which compensates for deviations coming from the head trajectory during the gaze shift and updates gaze heading dynamically towards the target. As soon as the gaze is on the target, the VOR is on and stabilizes the gaze whatever the remaining head movement.

References

- [1] Freedman, E. G. Coordination of the eyes and head during visual orienting, *Experimental Brain Research*, Vol. 190, 2008.
- [2] Guitton, D., Munoz, D.P. and Galiana H.L. Gaze Control in the Cats: Studies and Modeling of the coupling Between Orienting Eye and Head Movements in Different Behavioral Tasks, *Journal of Neurophysiology*, Vol. 64, 1990.
- [3] Goossens, H. and Van Opstal, A. Human eye-head coordination in two dimensions under different sensorimotor conditions, *Experimental Brain Research*, Vol. 114, 1997.
- [4] Lefèvre, P. and Galiana, H. L. Dynamic feedback to the superior colliculus in a neural network model of the gaze control system, *Neural Networks*, Vol. 5, 1992.
- [5] Lefèvre, P., Quaia, C. and Optican L.M. Distributed model of control of saccades by superior colliculus and cerebellum, *Neural Networks*, Vol. 11, 1998.

Motor commands are optimized in the gravity field

Crevecoeur Frédéric, CESAME
4 Av. Georges Lemaître 1348 Louvain-la-Neuve
frederic.crevecoeur@uclouvain.be

Thonnard Jean-Louis, READ
53 Av. Mounier 1200 Bruxelles
jean-louis.thonnard@uclouvain.be

Lefevre Philippe, CESAME
4 Av. Georges Lemaître 1348 Louvain-la-Neuve
philippe.lefevre@uclouvain.be

1 Introduction

How motor commands are generated to complete smooth and accurate movements is a fundamental field of investigation in movement neuroscience. Many models for motor control are based on the hypothesis that motor actions are optimized with respect to a cost defined along the movement. Optimal feedback control is also currently utilized to model the flexibility and adaptability of human movements to face new dynamics or uncertainty. Whatever the control schemes, the generation of appropriate motor command must rely on an internal representation of the limb position and dynamics. Such internal representations, called internal models [1], have two main functions: (1) to compute motor commands to bring the limb towards a desired goal (e.g. reach to grasp for an object) and (2) to compute a prior estimate of the current state of the limb in order to compensate for time delays in sensory feedback loops. At the neural level, increasing evidence can be found that regions of the brain implement control and estimation related computational issues [2]. Knowing that optimality characterizes motor commands adjustments to artificially altered dynamics, this study aims at understanding whether optimality also applies to the internal models of arm dynamics including the action of gravity, and if yes, how do subjects adapt to changes in gravity.

2 Methods

This study investigates the properties of vertical pointing movements performed in normal gravity and hyper gravity induced by parabolic flights ($\sim 1.8 \times g$). Subjects ($N = 10$) performed arm straight rotation of around the shoulder towards visual targets. Their behavior was compared with an optimal control design based on the following equations:

$$I\ddot{\theta} = f - mgl\cos(\theta) - k_v\dot{\theta}, \quad (1)$$

$$\dot{f} = \frac{1}{\tau}(u - f), \quad (2)$$

with minimum control input:

$$J(u) = \int_{t_0}^{t_f} |u|^2 dt. \quad (3)$$

The mechanical equation (Equation 1) assumes that three torques were acting on the limb: the muscular torque f , the

gravitational torque and a viscous friction torque. This equation was coupled to a physiological model (Equation 2) for torque output as a first order response to control input u with time constant τ equal to 40 ms. Specific inertia, mass and length were estimated for all subjects.

3 Results

In normal gravity, vertical pointing movements typically exhibit skewness in the velocity profiles not observed in horizontal movements, i.e. the relative time to peak velocity is shorter than 0.5. Our data reproduce this property, as do the simulations computed from Equations 1 and 2 at minimum cost (Equation 3). In addition, the simulations with gravity set to $1.8 \times g$ predicted an increase in peak velocity and initial peak acceleration. In accordance with these predictions, the subjects significantly increased the peak acceleration and peak velocity. This was accompanied by a significant reduction in movement duration, despite the fact that the arm weight was nearly doubled (all P values were smaller than 0.01).

4 Conclusion

The results suggest that the action of the gravitational torque on the limb is optimally integrated in the internal models of arm dynamics. In addition, the adaptation of arm movements in hyper gravity is consistent with the hypothesis that learning new dynamics is a re-optimization process. We suggest that a comparison between the actual movement cost and the estimated movement cost from prior expectation can be derived from actual and predicted feedback in order to update the kinematics of the movement in response to a change in the environment.

References

- [1] Kawato (1999), Internal models for motor control and trajectory planning. *Current Opinion in Neurobiology*, 9 : 718 – 727.
- [2] Shadmehr (2008), A computational neuroanatomy for motor control. *Experimental Brain Research*, 185 : 359 – 381.

Control of walking robots using virtual springs

Gijs van Oort, Stefano Stramigioli

Impact Institute, Faculty of EEMCS/University of Twente

g.vanoort@ewi.utwente.nl, s.stramigioli@utwente.nl

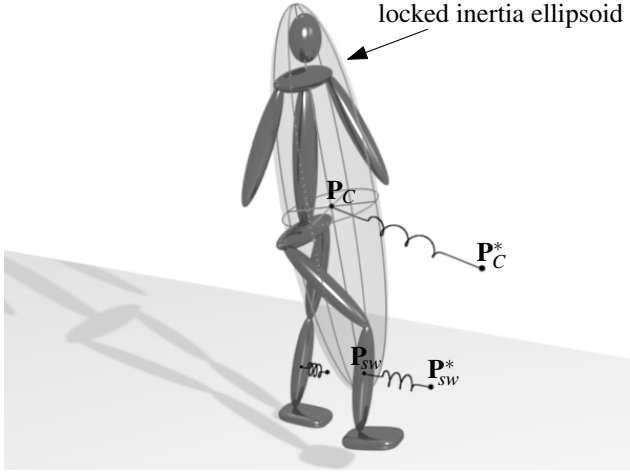


Figure 1: Virtual springs attached to the walking robot. For clarity, distance between \mathbf{P}_C and \mathbf{P}_C^* is exaggerated.

1 Introduction

At the Control Engineering group of the University of Twente, we are conducting research on control of bipedal robots. In our search for robust and energy efficient control, we are making extensive use of simulation. In order to facilitate the development of algorithms, we want to design controllers that work in a space of “meaningful variables”; *i.e.* we don’t control joint angles directly but we control things as “position and velocity of center of mass”, “shape of the robot’s locked inertia ellipsoid” [1] and “foot position”.

2 Controller

We propose a controller for a 3D bipedal robot, based on virtual springs [2]. The idea of a virtual spring is to exert torques on all joints of the robot (called *equivalent joint torques*, τ) in such a way that the robot behaves as if a spring were attached to it.

Instead of attaching the virtual spring (which we actually model as a damped spring with K and D as spring and damping constants respectively) to any of the robot’s links, we connect it to the center of the inertia ellipsoid of the whole robot, called \mathbf{P}_C (see figure 1). This results in some parts of the system accelerating in such a way that the center of the inertia ellipsoid moves as if it were pulled by the virtual spring.

The other end of the spring is attached to a point in space, \mathbf{P}_C^* , which follows a periodic trajectory. Eventually, in our search for a robust and energy efficient controller, this trajectory will be subject to optimization. In this set-up, the virtual (3D) force \mathbf{F}_C exerted by the virtual spring can be

calculated by

$$\mathbf{F}_C = K \cdot (\mathbf{P}_C^* - \mathbf{P}_C) - D \cdot \frac{d}{dt}(\mathbf{P}_C^* - \mathbf{P}_C). \quad (1)$$

Assuming that at least one foot has full contact with the floor, the equivalent joint torques τ are

$$\tau = J^T(q) \cdot \mathbf{F}_C, \quad (2)$$

where $J(q)$ is the the jacobian matrix mapping joint velocities to the velocity of the robot’s center of mass, *i.e.* $\dot{\mathbf{P}}_C = J(q) \cdot \dot{q}$. In the more general 6D case, where \mathbf{F}_C is replaced by a wrench \mathbf{W}_C , the way to proceed is similar, although some extra mathematical steps are needed.

The legs of the robot are also controlled through virtual springs (as shown in figure 1); proper foot placement is achieved by dynamically adjusting the end point \mathbf{P}_{sw}^* of the swing-leg spring.

This strategy would work perfectly if the allowable torques in the joints were unlimited. Unfortunately, the ankle torques of the stance foot are severely limited: a too large torque will inevitably make the stance foot rotate around one of its edges, thereby losing the full contact with the floor. The maximum allowable ankle torque, $\tau_{\text{ankle,max}}$ is dependent on the foot size and the state (q, \dot{q}) and actions (\ddot{q}) of the robot (in particular, on the amount of pressure exerted on the foot).

The limitation in allowable ankle torque leads to an equivalent limitation in allowable \mathbf{F}_C . Therefore, the actually implemented virtual force is linearly scaled down by factor $0 \leq \alpha \leq 1$ such that the ankle torque (one of the elements of τ) stays within the allowable range. This force may not be enough to keep the robot upright, which is actually the reason that walking robots have to take steps at all. In this sense, the best spot to place the swing foot is the spot where the allowable \mathbf{F}_C is maximized.

3 Conclusion

The proposed controller needs some more detailing before it can actually make the robot walk in simulation. For example, determining where exactly to place the foot has not been considered yet. We are working on this, and expect to show the results soon.

References

- [1] G. van Oort and S. Stramigioli, “Geometric dynamics analysis of humanoids – locked inertia,” Benelux meeting, 2008.
- [2] J. Pratt, “Virtual Model Control of a Biped Walking Robot,” Massachusetts Institute of Technology, 1995.

A Jacobi algorithm for distributed model predictive control of dynamically coupled systems

Dang Doan, Tamás Keviczky, Bart De Schutter
Delft Center for Systems and Control
Delft University of Technology
Delft, The Netherlands

Email: {m.d.doan,t.keviczky}@tudelft.nl, b@deschutter.info

Ion Necoara, Moritz Diehl
Department of Electrical Engineering
Katholieke Universiteit Leuven
Leuven, Belgium

Email: {ion.necoara,moritz.diehl}@esat.kuleuven.be

1 Abstract

In this presentation we introduce an iterative Jacobi algorithm for solving distributed model predictive control (MPC) problems, with linear coupled dynamics and convex coupled constraints. The proposed iterative approach involves solving local optimization problems consisting of only few subsystems, depending on the choice of the designer and the sparsity of dynamical and constraint couplings. This algorithm guarantees stability and persistent feasibility, and the solution of the iterative process converges to the centralized MPC solution.

2 Introduction

MPC theory is not yet fully developed for control of large-scale networked systems, due to information exchange requirements and computational aspects. Distributed MPC approaches this problem by decomposing the overall system into small subsystems, and by making use of cooperation between local controllers on the basis of limited information exchange.

A distributed MPC scheme for dynamically coupled systems has been proposed in [1]. This scheme works only for input-coupled linear time-invariant (LTI) subsystem dynamics without state constraints, and is not applicable to problems with constraints between subsystems. In this presentation, we propose an extension of this scheme in order to solve these issues.

3 Method and results

Consider a networked system consisting of input- and state-coupled LTI subsystems with convex coupled constraints. Each subsystem belongs to a “neighborhood” which contains all subsystems that directly influence it through either the coupled dynamics or the coupled constraints.

At first, we formulate a centralized receding horizon control problem, using terminal point constraints. This involves a huge convex optimization problem, which is computationally intensive for a centralized controller. Therefore, one can consider solving the problem in a distributed fashion, where each local controller optimizes the global cost function with regard to the variables inside its neighborhood, subject to the constraints within its neighborhood.

During each sampling step, an iterative procedure then takes place: Each subsystem gets new results from its neighbors (i.e. prediction of states and inputs inside their neighborhoods), updates its own local optimization problem, and solves it for new locally optimal actions. Subsequently, a convex combination of all locally optimal solutions yields a centralized solution. This new centralized solution is the starting point for all subsystems in the next iteration. This procedure is guaranteed to converge asymptotically to the centralized optimal solution.

We show that the convex combination of all locally optimal solutions can be performed using only local communications, therefore the algorithm can be implemented without global communications.

The algorithm and its features are illustrated on a series of interacting spring-mass systems.

While offering very valuable extensions to existing approaches, the drawbacks of this method are the frequent communications (although they are all localized) and the use of terminal point constrained MPC, which is conservative.

References

- [1] A. Venkat, J. Rawlings, and S. Wright, “Distributed MPC Strategies with Application to Power System Automatic Generation Control”, *IEEE Transactions on Control Systems Technology*, vol. 16, no. 6, pp. 1192-1206, 2008.

An application of distributed control: the segmented primary mirror for the European Extremely Large Telescope

Ch. Bastin, A. Sarlette and R. Sepulchre
University of Liège
(ch.bastin, alain.sarlette, r.sepulchre)@ulg.ac.be

M. Dimmler, T. Erm, B. Sedghi, B. Bauvir
European Southern Observatory (ESO)
(mdimmler, term, bsedghi, bbauvir)@eso.org

1 Context and Setting

The European Extremely Large Telescope (E-ELT) is a project to build the largest telescope in the world for optical/infrared astronomical observations. The project is in its detailed design phase and expected to operate in 2018. The diameter of 42 meters for the primary mirror makes it 4 times larger and thereby at least 100 times more sensitive than the largest telescopes currently in operation [1].

The difference in scale is huge between the revolutionary size of the telescope and the extreme precision required for optical observations — the reflecting surface may introduce just a few nanometers error on the wavefront of the incoming light. This poses several challenges for design and construction of the E-ELT. Among others, current technology reaches a limit to build rigid mirrors with the required accuracy around 8 to 9 meters. Therefore larger mirrors are built from smaller segments.

The 42 m diameter E-ELT primary mirror (M1) is composed of 984 hexagonal segments with $\sim 0.7m$ edge length. Each segment is supported by 3 unidimensional position actuators which move perpendicular to the wavefront. This allows to control piston, tip and tilt of each segment separately (i.e. considering that the telescope points to the zenith, the vertical position of a segment and its rotation around horizontal axes). The position of these 3×984 actuators must be controlled such that the overall deformation of the complete mirror surface, with respect to a slightly spherically curved reference surface, does not exceed 10 nm root-mean-squared. Due to this extreme accuracy required over several tens of meters, it is not possible to measure the position of all segments with respect to a sufficiently stable reference. Therefore sensors are placed on the edges of adjacent segments to measure *relative* vertical displacements.

The role of the E-ELT M1 controller studied in the present work is to operate the position actuators as a function of edge sensor measurements in order to maintain the shape of the mirror to the required accuracy, under various perturbations (wind load, temperature and gravity effects) and with real-world operation requirements (robustness, finite noise and resolution, practical feasibility). The complete mirror is a MIMO system with 2952 inputs and 5604 outputs.

2 Main results

For design and analysis of the E-ELT M1 controller, preliminary studies by ESO suggest to decompose the huge MIMO system in modal basis [2]. We also investigate a complementary approach approximating the system as “spatially invariant”; indeed, the authors of [3] propose powerful tools for robust decentralized control design in this context. The following points lead to more general conclusions.

- The “spatially invariant” control method applies very well, despite inhomogeneities and boundary effects; thus “spatial frequency” loopshaping can be as useful as the familiar “time frequency” design based on time-invariance.
- Different deformations inherently have very different observabilities using relative position measurements; this makes robustness an issue, requiring leakage to robustly stabilize a tuned integral controller.
- Overdetermination of measurements allows fast and efficient sensor health monitoring.

Acknowledgments

This paper presents research results of the Belgian Network DYSCO (Dynamical Systems, Control, and Optimization), funded by the Interuniversity Attraction Poles Programme, initiated by the Belgian State, Science Policy Office. The scientific responsibility rests with its authors. The second author is supported as an FNRS fellow (Belgian Fund for Scientific Research). This study is the result of a consulting contract of the Systems & Control research group at University of Liège for the European Southern Observatory.

References

- [1] European Southern Observatory E-ELT project. <http://www.eso.org/sci/facilities/eelt/>. 2009.
- [2] M. Dimmler, A. Wallander, and J. Spyromilio. E-elt programme: M1 control strategies. *ESO internal report E-TRE-ESO-449-0211, issue 1*.
- [3] D. Gorinevsky, S. Boyd, and G. Stein. Design of low-bandwidth spatially distributed feedback. *IEEE Trans. Automatic Control*, 53(2):257–272, 2008.

Modeling and Control of Inkjet Printhead¹

Mohammed Ezzeldin, Andrej Jokic and Paul van den Bosch

Department of Electrical Engineering

Technische Universiteit Eindhoven

P.O. Box 513, 5600 MB Eindhoven

The Netherlands

Email: m.ezz,a.jokic and p.p.j.v.d.bosch@tue.nl

1 Introduction

Inkjet printers are non-impact printers which print text and images by spraying tiny droplets of liquid ink onto paper. Besides the well known small inkjet printers for home and office, there is a market for professional inkjet printers. Inkjet printers are used to form conductive traces for circuits, and color filters in LCD and plasma displays. That makes the printing quality is an important issue. Currently, most inkjet printers use either thermal inkjet or piezoelectric inkjet technology. Thermal inkjet printer uses heating element to heat liquid ink to form vapor bubble, which forces the ink droplets onto the paper through the nozzle. Most commercial and industrial ink jet printers use a piezoelectric material in an ink-filled chamber behind each nozzle instead of a heating element. When a voltage is applied, the piezoelectric material changes shape or size, which generates a pressure pulse in the fluid forcing a droplet of ink from the nozzle. This is essentially the same mechanism as the thermal inkjet but generates the pressure pulse using a different physical principle. Piezoelectric ink jet allows a wider variety of inks than thermal or continuous ink jet but the print heads are more expensive. In my project the piezoelectric inkjet printer is considered.

2 Problem Statement

After a drop is jetted, the fluid-mechanics within an ink channel are not at rest immediately: apparently traveling pressure waves are still present. These are referred to as residual vibrations. These residual vibrations result in changing the speed of the second drop. Usually the fixed actuation pulse is designed under the assumption that a channel is at rest. To guarantee consistent drop properties, one has to wait for these residual vibrations to be sufficiently damped out to fulfill this assumption.

Cross-talk is the phenomenon that one ink channel cannot be actuated without affecting the fluid-mechanics of the neighboring channels. The cross-talk happens due to the fact that the pressure waves within one channel influence other chan-

nels. This type of cross talk is called acoustic cross-talk. Since all piezo-fingers are connected to a substrate, a deformation of one piezo-unit induces a deformation of the neighboring units. Another path is via the deformation of a channel itself. As a result, the volume of the neighboring channels changes also which induces pressure waves in those channels. Residual vibrations and cross-talk result in ink drops with different speed and volume which affect the printing quality. The main goal is to improve the printing quality of the printhead that is achieved by keeping both the speed and volume of the ink drop constant. In other word, to minimize the speed and volume variations occur because of the residual vibration and cross-talk.

3 Identification and Control Approach

Since there are no online measurements for the system variables, a feedforward controller is the most appropriate solution. Although residual vibration and cross-talk effects are large, they are very predictable and reproducible. Hence, a model based feedforward controller can be appropriate for this case. Different approaches for modeling and control are given in [1] and [2]

The main idea of the proposed approach is to identify the dynamics of every channel and also the coupling dynamics with the neighboring channel. In the test setup, both the channel pressure and the meniscus speed can be measured. Hence, the system can be decomposed into two subsystems, the first one represents the dynamics between the input voltage and the channel pressure and the neighboring channel pressure. The second subsystem represents dynamics between the pressure and the meniscus speed. If the identified model represents the system exactly, the controller could be some kind the inverse of the identified model. Hence, the actual drop speed and volume will be almost the same as the desired input speed and volume.

References

- [1] H.M.A. Wijshoff, "Structure- and fluid-dynamics in piezo inkjet printheads," PhD thesis, 2008.
- [2] M. B. Groot Wassink, "Inkjet printhead performance enhancement by feedforward input design based on two-port modeling," PhD thesis, 2007.

¹This work has been carried out as part of the OCTOPUS project with Océ Technologies B.V. under the responsibility of the Embedded Systems Institute. This project is partially supported by the Netherlands Ministry of Economic Affairs under the Bsik program.

A comparison between different state estimation methods in a nonlinear distributed parameter system

Cristina Retamal^{a,b}, Michel Kinnaert^a

^a Control Engineering Department

Université Libre de Bruxelles (ULB)

Avenue F.D. Roosevelt 50, CP 165/55 1050 Bruxelles
Belgium

Email: cristina.retamal.reyes@ulb.ac.be
michel.kinnaert@ulb.ac.be

Carlos Vilas^b, Alain Vande Wouwer^b

^b Automatic Control Laboratory

Faculté Polytechnique de Mons

31 Boulevard Dolez, 7000 Mons
Belgium

Email: carlos.vilas@fpms.ac.be
Alain.VandeWouwer@fpms.ac.be

The state estimation in distributed parameter systems (DPS) is an important and complex problem since complete spatial profiles of the state variables are usually non-measurable and have to be inferred from a limited set of pointwise measurements [7]. On the other hand, in many practical applications, only some of the states involved are available for on-line measurement [3]. Due to this, the design and application of state observers to these systems has been an active area of research [1, 2, 5, 6, 7].

The state estimation problem can be approached from two different perspectives: namely the early and the late lumping approach. In the early lumping, the partial differential model is first approximated by means of a discretization method (finite difference, finite elements, etc), and the observer is then designed on the basis of the approximated system. In the late lumping approach, the distributed nature of the system is kept as long as possible and the state observer is designed using the partial differential equations system [7]. The general design procedure for a state observer requires the choice of a “gain” such that the error dynamics (difference between the estimate and the real (unknown) state) has desired properties. This has resulted in a number of state observers designs [3].

In this study, two state estimation strategies are developed, tested and compared. The first strategy, which is based on an early lumping approach, makes use of a reduced order model of the DPS obtained by a proper orthogonal decomposition (POD) method. The reduced order model, which has been successfully applied in the context of state estimation in DPS (see [4] and references therein), is then used to design an extended Kalman Filter (EKF), taking the measurement noise into account. The second strategy, which is based on a late lumping approach, is an extension of the Luenberger observer for nonlinear DPS. The correction term is design based on a physical interpretation of the error equation [5, 6].

Both observers are tested in simulation in the situation where the complete temperature and concentration profiles in a catalytic fixed-bed reactor have to be estimated using

pointwise measurement of the temperature only [6]. the performance of these observers is assessed in terms of computation time, convergence, robustness to measurement noise and plant-model mismatches.

Acknowledgments

This work presents research results of the Belgian Network DYSCO (Dynamical Systems, Control, and Optimization), funded by the Interuniversity Attraction Poles Program, initiated by the Belgian State, Science Policy Office.

References

- [1] M. Alamir and J.P. Corriou. Nonlinear receding-horizon state estimation for dispersive adsorption columns with nonlinear isotherm. *Journal of Process Control*, 13:517–523, 2003.
- [2] J.P. Corriou and M. Alamir. A hybrid nonlinear state observer for concentration profiles reconstruction in nonlinear simulated moving bed. *Journal of Process Control*, 16:345–353, 2006.
- [3] D. Dochain. State and parameter estimation in chemical and biochemical processes: a tutorial. *Journal of Process Control*, 13:801–818, 2003.
- [4] M. R. García, C. Vilas, J. R. Banga, and A. Alonso. Exponential observers for distributed tubular (bio)reactors. *AIChE Journal*, 54(11):2943–2956, 2008.
- [5] M. Mangold, G. Lauschke, J. Schaffner, M. Zeitz, and E. Gilles. State and parameter estimation for adsorption columns by nonlinear distributed parameter state observers. *Journal of Process Control*, 4:163–171, 1994.
- [6] A. Vande Wouwer, N. Point, S. Porteman, and M. Remy. An approach to the selection of optimal sensor locations in distributed parameter systems. *Journal of Process Control*, 10:291–300, 2000.
- [7] A. Vande Wouwer and M. Zeitz. State estimation in distributed parameter systems. *Control Systems, Robotics and Automation*, 2003.

Risk-Aware Sequential Decision Making and Dynamic Programming

Boris Defourny, Damien Ernst, Louis Wehenkel
 Dept of EECS, University of Liège, Belgium
 {Boris.Defourny, dernst, L.Wehenkel}@ulg.ac.be

This talk, based on [3], considers sequential decision making problems under uncertainty, the tradeoff between the expected return and the risk of high loss, and methods that use dynamic programming [1] to find optimal policies. It is argued that using Bellman's Principle determines how risk considerations on the return can be incorporated. The discussion centers around returns generated by Markov Decision Processes [8] (MDP) and conclusions concern a large class of methods in Reinforcement Learning [10] (RL). It will also interest researchers involved in Robust Control and MPC methods [5, 2].

Incorporating risk sensitivity in RL can serve different purposes: to balance exploration versus exploitation for fast convergence, to protect the agent during the learning process, to increase policy robustness by limiting confidence in the model, or to prevent rare undesirable events. This talk deals with the latter aspect.

Many popular methods in RL such as Temporal Difference learning [9] or Q-learning [11] base the selection of actions on average rewards-to-go, following principles from Monte Carlo estimation [7] and Dynamic Programming. The present talk focuses on the dynamic programming part. It discusses how the use of Bellman's Principle restrains the user from imposing arbitrary requirements on the distribution of the return generated by a Markov Decision Process. It is assumed that the parameters of the MDP are known. Restrictions in that setup will also hold in setups involving estimation issues, observability issues, or complexity issues.

The talk attracts the attention to limitations of dynamic programming beyond the curse of dimensionality, and brings insights on the structure of risk-aware policies. The second point is also of potential interest for non dynamic-programming-based methods, such as policy search methods [6] or scenario-tree-based methods [4].

References

- [1] D.P. Bertsekas. *Dynamic Programming and Optimal Control*. Athena Scientific, Belmont, MA, 3rd edition, 2005.
- [2] D.P. Bertsekas. Dynamic programming and suboptimal control: survey from ADP to MPC. In *Proceedings of the 44th IEEE Conference on Decision and Control and European Control Conference*, page 50, 2005.
- [3] B. Defourny, D. Ernst, and L. Wehenkel. Risk-aware decision making and dynamic programming. In *NIPS-08 Workshop on Model Uncertainty and Risk in Reinforcement Learning*, Whistler, 2008.
- [4] B. Defourny, D. Ernst, and L. Wehenkel. Lazy planning under uncertainty by optimizing decisions on an ensemble of incomplete disturbance trees. In *Recent Advances in Reinforcement Learning, 8th European Workshop, EWRL'08*, LNCS (LNAI) 5323. Springer, 2008.
- [5] P. Li, M. Wendt, and G. Wozny. Robust model predictive control under chance constraints. *Computers and Chemical Engineering*, 24:829–834, 2000.
- [6] S. Mannor, R. Rubinstein, and Y. Gat. The cross entropy method for fast policy search. In *Proc. of the 20th Int. Conf. on Machine Learning*, pages 512–519. Morgan Kaufmann, 2003.
- [7] N. Metropolis and S. Ulam. The Monte Carlo method. *J. Amer. Stat. Assoc.*, 44(247):335–341, 1949.
- [8] M.L. Puterman. *Markov Decision Processes: Discrete Stochastic Dynamic Programming*. Wiley, 1994.
- [9] R.S. Sutton. Learning to predict by the method of temporal differences. *Machine Learning*, 3(1):9–44, 1988.
- [10] R.S. Sutton and A.G. Barto. *Reinforcement Learning, an Introduction*. MIT Press, 1998.
- [11] C.J.C.H. Watkins and P. Dayan. Q-learning. *Machine Learning*, 8:279–292, 1992.

Estimating distributions from censored microbiological contamination data for use in quantitative risk assessment

P. Busschaert⁽¹⁾, A.H. Geeraerd⁽²⁾, M. Uyttendaele⁽³⁾ and J.F.M. Van Impe⁽¹⁾

⁽¹⁾BioTeC - Chemical and Biochemical Process Technology and Control, Department of Chemical Engineering, Katholieke Universiteit Leuven, W. de Croylaan 46, B-3001 Leuven, Belgium

⁽²⁾MeBioS - Mechatronics, Biostatistics and Sensors, Department of Biosystems, Katholieke Universiteit Leuven, W. de Croylaan 42, B-3001 Leuven, Belgium

⁽³⁾Laboratory of Food Microbiology and Food Preservation, Department of Food Safety and Food Quality, Ghent University, Coupure Links 653, B-9000 Ghent, Belgium
{pieter.busschaert - jan.vanimpe}@cit.kuleuven.be

1 Abstract

Outcomes of quantitative microbiological risk assessments in foods are to a large degree dependent on the initial contamination of the micro-organism in the food product, which is generally represented by a distribution. However, the microbiological analyst often has to deal with lower limits of detection, and frequently only qualitative tests instead of quantitative tests are used. Hence, it can be hard to transform the outcomes of these tests into a distribution.

To analyze these kind of data, and potentially combinations of them, maximum likelihood is used. In addition, the bootstrapping technique is applied to separate variability and uncertainty, resulting in a distribution suited for use in a two-dimensional Monte Carlo simulation.

2 Quantitative microbiological risk assessment

In quantitative microbiological risk assessment, the risk associated to a pathogenous micro-organism in a certain type of food is estimated. To determine the concentration of a micro-organism in a food sample, either qualitative or quantitative analyses can be performed. In the case of quantitative measurements, concentrations often are below the lower limit of detection because of the generally low concentrations of pathogens in food, i.e., data are left-censored. However, for several reasons, laboratories often limit their efforts to merely qualitative analyses.

When multiple sample sizes are tested, qualitative analyses can be combined into semiquantitative results. For example, if a 25 g sample is positive and a 0.1 g sample is negative, it can be concluded that the concentration is between 0.04 and 10 CFU/g. These kind of data are called interval-censored data.

3 Maximum likelihood estimation

To assign a distribution to any combination of quantitative, left-censored and interval-censored data, the method of maximum likelihood estimation is used. It is assumed that the initial contamination (\log_{10} CFU/g) is normally distributed. Maximum likelihood estimation results in the parameters of the normal distribution $\theta = (\mu, \sigma)$ which are

most likely to have generated the original data. This distribution can subsequently be used as an input for the Monte Carlo simulation for a probabilistic estimation of the resulting risk.

4 Separation of variability and uncertainty

Variability is inherent to any microbiological system and can not be reduced. Uncertainty is a consequence of limited knowledge, and hence can be reduced by further measurements and observations. As a consequence, it might be valuable to know if the observed variation has been caused mainly due to variability or mainly due to uncertainty.

In risk assessment, this separation is generally obtained by a two-dimensional Monte Carlo simulation. To obtain the hyperparameters needed for a 2D Monte Carlo simulation, a non-parametric bootstrapping technique is applied.

As a result, the microbiologist is able to transform the complex data set into a distribution that is suited for risk assessment. Using these methods, a large amount of valuable data – which would otherwise be ignored – can be integrated to improve the quality of the input distribution, and hence improve the quality of the risk assessment.

5 Acknowledgements

This research is supported in part by the Research Council of the Katholieke Universiteit Leuven (projects OT/03/30 and EF/05/006 Center-of-Excellence Optimization in Engineering), and the Belgian Program on Interuniversity Poles of Attraction, initiated by the Belgian Federal Science Policy Office.

References

- [1] D. Helsel (2005). *Nondetects and data analysis: statistics for censored environmental data*. John Wiley, New York.
- [2] Y. Zhao and H.C. Frey (2004). Quantification of variability and uncertainty for censored data sets and application to air toxic emission factors. *Risk Analysis*, 24(4): 1019-1034.

The Kalman Filter applied to Hydrologic Systems

Plaza D., De Lannoy G. J. M., Pauwels V. R. N.
Laboratory of Hydrology and Water Management
University of Ghent
Coupure Links 653, B-9000 Gent
Belgium
Email: Douglas.PlazaGuingla@UGent.be

Robin De Keyser
Department of Electrical energy, Systems and
Automation - University of Ghent
Technologiepark 913, B-9052 Gent
Belgium
Email: rdk@autoctrl.UGent.be

1 Introduction

The modern burst of development in hydrologic modelling dates from the last decades, when concepts of statistics and systems analysis were applied to hydrology.

The relationship between precipitation and discharge is one of the fundamental research topics in hydrology. The development of information technology allowed hydrologists to increase the complexity of the modelling, following two approaches. A first approach is to better understand the physical processes that influence the relationship between precipitation and discharge, and is referred to as the scientific approach. The second approach, which is known as the engineering approach, focusses on a better prediction of discharge rates.

Hydrologic models can be classified according to the previous approaches, which are referred to as Descriptive and Predictive modelling, respectively. Descriptive models represent all processes of the hydrologic cycle. Different processes like infiltration, evapotranspiration, etc. are represented. All these processes are interdependent, making the construction of descriptive models very complex. For this reason, a number of assumptions must be made, which has lead to the development of a large number of descriptive hydrologic models during the last decades.

Due to the complete process representation these models are called Soil-Vegetation-Atmosphere Transfer Schemes (SVATS) or Land Surface Models (LSM).

The soil moisture and temperature profiles define the state of the land surface model. For every time step, the initial conditions are updated. State estimation is used in order to adapt the results of model simulations, using external observations at every time step where the measurement is available. This process is called Data Assimilation. Although a wide variety of methods can be used for this purpose, the methods based on the Kalman Filter theory are the most frequently used.

Nonlinearities in the system and computational demand must be taken into account for the selection of an assimilation method. The linear Kalman filter is the optimal sequential data assimilation method for linear systems and measurement processes with Gaussian error statistics. The extended Kalman filter (EKF) is a variant of the Kalman filter that can be used for nonlinear problems. Evensen [1] presents the ensemble Kalman filter (EnKF) as a Monte

Carlo approach to the nonlinear filtering problem. The EnKF is based on the approximation of the conditional probability densities of interest by a finite number of randomly generated model trajectories.

This paper presents a comparative study between two state estimation strategies based on the Kalman filter theory, applied to a hydrologic system.

2 The study area

The study area referenced as Bibeschbach subcatchment is located close to Luxembourg city in Luxembourg. The size is 10.8 km². Measurements of volumetric soil moisture content and discharge of water to the river are recorded from this test site. Atmospheric information like precipitation, air humidity, etc. is obtained from a meteorological station located near the catchment.

3 The Hydrologic model

The Hydrologic model chosen for this study is the Community Land Model (CLM) [2], which is a global land surface model, developed through collaboration of experts from different institutes to provide the community with a free model that captures most of the best science currently available for land surface modelling.

4 The State Estimation techniques

Based on soil moisture and discharge measurements from the field, the state estimation technique should use this information in order to improve the model simulations of the discharge. As it was mentioned in section 1, these techniques correspond to the EKF and the EnKF.

References

- [1] G. Evensen, "Sequential data assimilation with a nonlinear quasi-geostrophic model using Monte Carlo methods to forecast error statistics" J. Geophys. Res., 99, 10 143-10 162, 1994.
- [2] K. Oleson, Y. Dai, G. Bonan, M., Dickinson. "Technical description of the Community Land Model (CLM) (Tech. Rep)." NCAR, Boulder, CO. 2004.

Multi-armed bandit based decision making for cognitive radio

Wassim Jouini, Damien Ernst, Christophe Moy, Jacques Palicot

SUPELEC/IETR - University of Liège

{wassim.jouini,christophe.moy,jacques.palicot}@supelec.fr, dernst@ulg.ac.be

Today's radio devices need a specific dedicated electronic chain for each standard. With the growth of the number of these standards (GSM, EDGE, Wi-Fi, etc), the conception and development of these radio devices became a real challenge. Recent hardware advances have offered the possibility to design software solutions to problems which were requiring in the past hardware signal processing devices. These advances are part of a field called Software Defined Radio (SDR). With this added software layer, it is possible now to control a large set of parameters to operate the radio devices with great flexibility and efficiency (e.g., change the bandwidth of the devices, switch from one communication protocol to another, minimize the energy consumption of a device, ...). Soon after the emergence of the SDR field, several scientists have studied ways to control at best these parameters, especially when the radio devices are used in non-stationary and partially unknown environments. This has lead to the emergence of a new research field, named Cognitive Radio, a term introduced by J. Mitola and G. Maguire in 1999 [1].

So far, most of the work in the field of Cognitive Radio has been conceptual. Very few implementable control/optimisation algorithms have indeed been proposed. It is however worth mentioning the evolutionary approach proposed by Virginia Tech [2], as well as the AI approach of Orange Lab [3] which were the two first approaches having lead to some promising simulation results on non-academic cognitive radio problems.

There are many cognitive radio related problems that can be formalized as follows. To a (or many) radio device(s) is (are) associated a performance criterion which is a (finite) sum of terms, named rewards, observed sequentially. Every reward of the sum is the realization of a random function called reward function which is influenced by the value of the parameters of the devices and the environment. The objective is to determine the sequence of values for the parameters to maximize the expected value of the performance criterion, often while having only limited information about the reward function itself. For example, there is poor knowledge on the reward function when one seeks to operate a radio device in a minimum energy consumption mode (under various operational constraints). Indeed, in such a case, it is very difficult to find the 'right' analytical or even algorithmic expression that could model the power consumption. Intuitively, the appropriate way for solving these problems would be to try to overcome this lack of information on the reward function by exploiting past information on the rewards obtained, the en-

vironment and the values of the parameters. Moreover, the parameters should be modified to address at best the trade-off between the exploitation of existing past information to generate immediately as high as possible rewards and the generation of new information which could lead to strategies to get perhaps even better rewards, but probably in a more distant future.

In our research work, solutions for these cognitive radio problems have been built based on research results related to the multi-armed bandit [4, 5]. A multi-armed bandit is a simple machine learning problem based on an analogy with a traditional slot machine (one-armed bandit) but with more than one lever. When pulled, each lever provides a reward drawn from a distribution associated to that specific lever. The objective of the gambler is to maximize the collected reward sum through iterative pulls. It is classically assumed that the gambler has no initial knowledge about the levers. The crucial tradeoff the gambler faces at each trial is between "exploitation" of the lever that has the highest expected payoff and "exploration" to get more information about the expected payoffs of the other levers.

Our simulation results have highlighted that by customizing algorithms developed for solving the multi-armed bandit, efficient engineering solutions to some problems met in cognitive radio can indeed be built.

References

- [1] J. Mitola and G.Q. Maguire. Cognitive radio: making software radios more personal. *Personal Communications, IEEE*, 6:1318, August 1999.
- [2] C.J. Rieser. Biologically Inspired Cognitive Radio Engine Model Utilizing Distributed Genetic Algorithms for Secure and Robust Wireless Communications and Networking. PhD thesis, Virginia Tech, 2004.
- [3] N. Colson, A. Kountouris, A. Wautier, and L. Husson. Cognitive decision making process supervising the radio dynamic reconfiguration. In *Proceedings of Cognitive Radio Oriented Wireless Networks and Communications*, page 7, 2008.
- [4] P. Auer, N. Cesa-Bianchi, and P. Fischer. Finite time analysis of multiarmed bandit problems. *Machine learning*, 47(2/3):235256, 2002.
- [5] S. Mannor, J.N. Tsitsiklis, K. Bennett, and N. Cesa-bianchi. The sample complexity of exploration in the multi-armed bandit problem. *Journal of Machine Learning Research*, 5:623648, 2004.

Formal Verification and Improved Analysis Tools for Agent-Based Simulations

Arturo Tejada Ruiz
 Delft Center for Systems and Controls
 Delft University of Technology
 Mekelweg 2, 2628 CD, Delft
 The Netherlands
 Email: a.tejadar Ruiz@tudelft.nl

1 Introduction

Agent-based models (ABMs) are becoming the de-facto tools for knowledge generation in areas such as environment, health, transportation, energy, aerospace systems and others. As shown in Figure 1, they are used by domain experts to gain understanding on the behavior of systems of interacting elements (e.g. a highway traffic system). The models consist of several time-driven 'agents' that follow a simple set of rules and interact with each other and with their environment. The agents are placed on a virtual world and let free to interact. By analyzing the agent interaction statistics and the 'emergent' group behavior (patterns), the researchers generate new knowledge and insight about the system under study.

ABMs are developed using a programming-oriented paradigm that is more attractive and intuitive for users than the classic equation-based modeling paradigm. Unfortunately, there are no techniques or methods currently available to assess the quality of the simulation results. Also, there are no tools available to systematically determine if the observed simulation outcomes are to be expected from the simulation models, or if they contain artifacts generated by an incorrect software implementation. In addition, the models lack predicting capabilities. That is, the sensitivity of the simulation results to changes in initial conditions or in model parameters can only be determined by running several simulations under different parameter values, without theoretical guidance. These drawbacks make it difficult to verify and validate ABMs, and have reduced their acceptance in the academic community.

The research proposal outlined next aims to address the aforementioned problems by providing researchers with new ABM verification tools based on formal methods and hybrid system theory. The foresaw use of these tools is shown in Figure 1 in blue color.

2 Research Proposal

Most agent-based models are composed of simple agents that interact with each other and their environment follow-

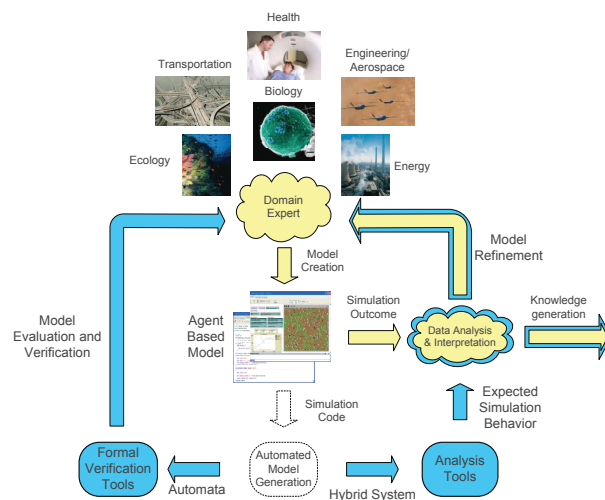


Figure 1: Current ABM methodology (yellow) and planned use for the proposed analysis and verification tools (blue)

ing a set of simple, prescribed rules. Their behavior is determined by the rules and by information stored in their internal memories, which is updated with each interaction with the environment or with other agents. To enable ABM verification, the logical behavior of each agent can be represented by a pushdown automaton. The automata can then be composed together to yield the overall ABM logical model. Finally, the latter can be verified against the ABM model specifications using standard model checkers.

In order to improve the ABM data analysis and interpretation, the ABM software environments (such as NETLOGO) should be equipped with tools to predict the long-term model behavior and the sensitivity of that behavior to changes in initial conditions and model parameters. To do so, the aforementioned automata models must be first augmented to include the continuous dynamics present in most ABMs. This would yield a hybrid system model, which can then be analyzed with the available stability, reachability, and statistical tools.

Passivity-based tracking control of port-Hamiltonian mechanical systems with only position measurements

D.A. Dirksz
University of Groningen
Fac. of Mathematics & Natural Sciences
Nijenborgh 4
9747 AG Groningen
The Netherlands
d.a.dirksz@rug.nl

J.M.A. Scherpen
University of Groningen
Fac. of Mathematics & Natural Sciences
The Netherlands
j.m.a.scherpen@rug.nl

Abstract

It has been shown that port-Hamiltonian mechanical systems can be asymptotically stabilized without velocity measurements by applying a dynamic extension. By interconnecting the system with a (virtual) controller damping is indirectly injected into the system making velocity measurements unnecessary, provided that this damping *propagates* to the mechanical system. The approach has been shown for the case of potential energy shaping and for a class of systems requiring total energy shaping [1]. We now extend this idea to the trajectory tracking problem. Like with the stabilization problem we apply a dynamic extension to avoid having to measure the system velocities and still realize perfect tracking of a desired trajectory. This is done for fully-actuated port-Hamiltonian mechanical systems.

Passivity-based trajectory tracking methods have been presented in [5, 3], for Euler-Lagrange (EL) mechanical systems and port-Hamiltonian systems respectively. With tracking control the energy shaping approach is complicated by having to modify the energy function into a time-varying one which in general spoils passivity. In [2] it was shown how port-Hamiltonian systems are stabilized by canonical transformation. A port-Hamiltonian system is transformed into another one while preserving the structure of the original system. The transformation also includes the time variable, even for time-invariant systems. This canonical transformation theory is used to transform a mechanical system into an *error* system. The trajectory tracking problem then becomes a stabilization problem. The approach then is to shape the energy of the error system to realize a stable equilibrium in the origin. It can be shown that the error system of a mechanical system having constant mass matrix can be asymptotically stabilized by the dynamic extension, which is proven using Barbalat's lemma [4]. Under extra conditions uniform asymptotic stability can be achieved. For the more general case, where the mass matrix is coordinate dependent, (uniform) asymptotic stability can be shown only when some conditions are satisfied. Simulation results for a two degrees of freedom planar manipulator show how the tracking error converges to zero.

For EL systems it has been shown in [5] that semiglobal stability of the the error system can be achieved. Our next step is to show semiglobal tracking for our controller in the port-Hamiltonian framework.

References

- [1] D.A. Dirksz, J.M.A. Scherpen, R. Ortega, 2008, Interconnection and Damping Assignment Passivity-Based Control for port-Hamiltonian mechanical systems with only position measurements, *Proceedings 47th IEEE conference on Decision and Control*, Cancun, Mexico
- [2] K. Fujimoto, T. Sugie, 2001, Canonical transformation and stabilization of generalized Hamiltonian systems, *Systems & Control Letters*, Vol. 42, No. 3, 217-227
- [3] K. Fujimoto, K. Sakurama, T. Sugie, 2003, Trajectory tracking of port-controlled Hamiltonian systems via generalized canonical transformations, *Automatica*, Vol. 39, No. 12, 2059-2069
- [4] H. Khalil, 1996, *Nonlinear Systems*, Prentice Hall, Upper Saddle River
- [5] R. Ortega, A. Loria, P.J. Nicklasson, H. Sira-Ramírez, 1998, *Passivity-based control of Euler-Lagrange systems: mechanical, electrical and electromechanical applications*, London, Springer

Feedback stabilisation of a pool-boiling system

R.W. van Gils^{*,1,2}, M.F.M. Speetjens² and H. Nijmeijer¹

Eindhoven University of Technology, PO Box 513, 5600 MB Eindhoven

Department of Mechanical Engineering,¹Dynamics and Control,²Energy Technology

Email: ^{*}r.w.v.gils@tue.nl

1 Introduction: Electronics cooling

Cutting-edge technologies increasingly require the ability for massive heat removal. Pool boiling affords cooling capacities substantially beyond that of conventional methods, and is as a result emerging as novel cooling technique.

Pool boiling refers to boiling heat transfer by natural convection and admits two stable modes: nucleate and film boiling, for low and high temperatures, respectively. Nucleate boiling is the desired state in cooling applications. However, it transits into undesired film boiling if the heat generation exceeds the so-called “critical heat flux” (CHF) [1]. This causes collapse of the cooling capacity. Hence, optimal cooling performance is a trade-off between efficiency (close to CHF) and low risk (safety margin to CHF).

High uncertainty in predicting CHF and the inability to actively respond to fluctuating cooling conditions result in large safety margins for current applications. Objective is diminishing this margin by stabilisation of the unstable equilibria in the highly unstable transition regime.

2 Pool boiling model description

The model considered, presented in [1], involves only the temperature distribution within the heater, Figure 1 (left). It models the heat exchange with the boiling medium via a nonlinear boundary condition imposed at the fluid-heater interface, which is given by the boiling curve, Figure 1 (right).

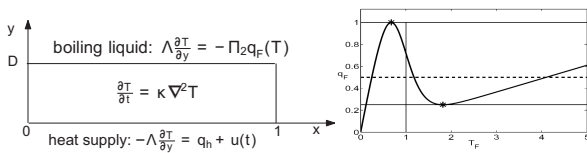


Figure 1 Two-dimensional rectangular heater (left) and boiling curve (heavy) with the constant heat supply (dotted) (right).

This model is spatially discretised using a Fourier-cosine and a Chebyshev-tau expansion in x - and y -direction, respectively [2]. This yields the following nonlinear ODE for T , which represents the temperature profile in the heater,

$$\dot{T} = A_{nl}T + B_{nl}v(u, T_F), \quad T_F(x) = T(x, D) = CT, \quad (1)$$

with constant matrices and a nonlinear vector $v(u, T_F)$. Besides a stable homogeneous (i.e. uniform T_F , $T_F(x) = c$) equilibrium in the nucleate and film boiling region, one homogeneous and several heterogeneous unstable equilibria

exist in the transition boiling regime [1]. Linearisation of (1) around the equilibrium T_∞ considered, allows analysis of the nonlinear model using standard control techniques.

3 Stabilisation of the system

First the unstable homogeneous equilibrium is considered for which the system can be reduced to a one-dimensional (1D) (i.e. x -independent) system. The compact model is found fully controllable and observable and thus a feedback controller in combination with a linear identity observer is introduced. This linear controller-observer pair effectively stabilises the nonlinear system by regulating the heat supply as a function of the internal state. In Figure 2 the interface temperature T_F is given for small (left) and large (right) initial perturbations. Local asymptotic stability is proven (using Lyapunov), while global asymptotic stability is suggested by the large number of simulations with large initial perturbations (see Figure 2). Furthermore, these simulations put forth the state-feedback controller as a viable option for the rapid respond to fluctuating cooling conditions.

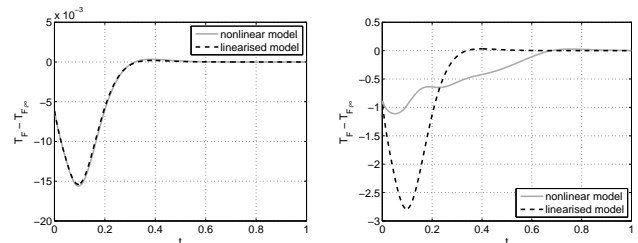


Figure 2 Fluid-heater interface temperature for small (left) and large (right) initial conditions.

4 Future Work

Analyses reveal that some of the unstable equilibria of the pool-boiling system can be stabilised. Therefore future work should comprise: (i) finalisation of the analysis of the 2D system, (ii) extension to 3D pool-boiling system and (iii) experimental validation.

References

- [1] M. SPEETJENS, *et al.* Steady-state solutions in a nonlinear pool-boiling model, Comm. Nonlin. Sci. Numer. Simul., 13 (2008), pp. 1475-1494.
- [2] R.W. VAN GILS, *et al.* 2008 Feedback stabilisation of a pool-boiling system. Submitted

Stabilization via positive invariance for linear distributed parameter systems with constraints on both control and its rate

B. Abouzaid V. Wertz
 CESAME, Université Catholique de Louvain
 4 – 6 avenue G. Lemaitre,
 B-1348 Louvain-la-Neuve,
 Belgium
 bouchra.abouzaid@uclouvain.be
 vincent.wertz@uclouvain.be

M. E. Achhab
 Département de Mathématique et Informatique
 Université Chouaib Doukkali,
 BP-20, El Jadida,
 Morocco
 Email: achhab@menara.ma

1 Abstract

Distributed parameter systems operating under control constraints constitute an important class of infinite-dimensional systems. Any physical system is submitted to limitations induced by physical, technological or even security considerations. These limitations are mainly associated to constraints of actuators and sensors. Hence, controllers developed without taking into account these limitations a priori may lead to undesirable or even disastrous process behavior such as lost of stability. An overview of the state of the art in stabilization problem for linear distributed parameter systems with control constraints is given e.g. in [3] and [4]. This work deals with the stabilization problem for linear infinite-dimensional systems, in the presence of inequality constraints on both the control magnitude and its rate. The approach is developed using semigroup theory and the concept of positive invariance. In the last year, the positive invariance property of polyhedral domains has been used as an interesting theoretical tool to treat the problem of constraints satisfaction for controlled linear finite-dimensional systems [5], [6] and infinite-dimensional systems [3]. The stabilization by a finite-dimensional compensator for a class of infinite-dimensional linear systems with inequality control constraints has been investigated in [2] by combining the approaches of the invariant polyhedral set and the spectral decomposition technique.

The primary objective of this work is to address the stabilization problem with constraints on both control magnitude and its rate assuming complete observation, i.e. the whole state is available,

$$\begin{cases} \dot{x} &= Ax(t) + Bu(t), \quad x_0 \in D(A), \\ -q_2 &\leq u \leq q_1, \quad q_1, q_2 \in \text{int}(\mathbb{R}_+^m), \\ -\Delta_2 &\leq \dot{u} \leq \Delta_1, \quad \Delta_1, \Delta_2 \in \text{int}(\mathbb{R}_+^m). \end{cases}$$

In this case, we propose a stabilizing state feedback $u(t) = Fx(t)$ and we give the necessary and sufficient conditions under which the constraints on both control magnitude and its rate are satisfied by an adequate use of positive invariance concept [1].

Our second objective is to deal with the same problem for a more realistic case, assuming only partial observation, i.e.

we can measure an output that contains only a partial information of the state system,

$$\begin{cases} \dot{x} &= Ax(t) + Bu(t), \\ y(t) &= Cx(t), \\ -q_2 &\leq u \leq q_1, \quad q_1, q_2 \in \text{int}(\mathbb{R}_+^m), \\ -\Delta_2 &\leq \dot{u} \leq \Delta_1, \quad \Delta_1, \Delta_2 \in \text{int}(\mathbb{R}_+^m). \end{cases}$$

So the stabilization was made by an estimated state feedback $u(t) = K\hat{x}(t)$ using a full state observer, which is known as the compensator design. The main results allow to determine some suitable positively invariant polyhedral set of admissible initial states, which is in fact, a stability domain for the closed loop.

These results are illustrated by some numerical example.

References

- [1] B. Abouzaid, M. E. Achhab and V. Wertz, Regulator problem for infinite-dimensional systems with constraints on both control and its rate, submitted.
- [2] B. Abouzaid, M. E. Achhab and V. Wertz, Stabilization of a class of Partially Observed Infinite Dimensional Systems with Control Constraints, to appear in IMA Journal of Mathematical Control and Information.
- [3] M. Achhab and M. Laabissi, Feedback stabilization of a class of distributed parameter systems with control constraints, systems and control letters, vol. 45, no. 1, pp. 163–171, 2002.
- [4] S. Boulite, H. Bouslous and L. Maniar, Invariant sets in Banach Lattices and Linear Differential Equations and Delay, Positivity, vol.8, pp. 127–142, 2004.
- [5] F. Mesquine, F. Tadeo and A. Benzaouia, Regulator problem for linear systems with constraints on control and its increments or rate, Automatica, vol. 40, no. 8, pp. 1387–1395, 2004.
- [6] S. Tarbouriech and C. Burgat, Positively invariant sets for constrained continuous-time systems with cone properties, IEEE Trans. Automat. Control, vol. AC-39, pp.401–405, 1994.

Control of the exothermic CSTR: the power-shaping approach

Audrey Favache^{a,b}, Denis Dochain^{a,b}

^a Université catholique de Louvain, CESAME , B-1348 Louvain-la-neuve

^b Université catholique de Louvain, IMAP , B-1348 Louvain-la-neuve
audrey.favache@uclouvain.be, denis.dochain@uclouvain.be

1 Abstract

Control strategies that are based on the physical phenomena occurring in the considered system have been receiving a growing interest over the past years. Among others, let us mention energy-balancing passivity based control [4] and more recently power-shaping control [3]. Power-shaping control is based on a particular formulation of the system dynamics, namely the Brayton-Moser equations. This particular formulation of the system dynamics can also lead to Lyapunov functions for it. Power-shaping control has first been applied to electric systems, and then to electro-mechanical systems, but in [2] a general formulation has been proposed.

A classical study case of nonlinear systems is the exothermic continuous stirred tank reactor (CSTR). Although it is a low order system, the dynamical behaviour shows complex features, such as multiple equilibrium points. Up to now no exact link with the thermodynamics for this behaviour of the exothermic CSTR has been given [1]. In this study we have applied the power-shaping control approach to the exothermic CSTR case with the aim of bringing more physical insight in its dynamical behaviour. This has led to a "global" Lyapunov function for the adiabatic CSTR case. This Lyapunov function has then be reshaped by the means of a controller in order to stabilize the process at any desired temperature. The obtained controller is also robust against modeling errors in the reaction kinetics and against measurement errors in the concentration.

2 Problem description and general methodology

The system that has been studied here is a CSTR in which an exothermic reaction takes place. The reactor can be cooled by a fluid circulating in an jacket at temperature T_w . Under some assumptions on the physical properties of the mixture, the dynamical model can be written as follows:

$$\begin{cases} \frac{dn_A}{dt} = \delta (C_A^{in} V - n_A) - k(T) n_A \\ \frac{dT}{dt} = \delta (T_{in} - T) + \gamma k(T) n_A + u (T_w - T) \end{cases} \quad (1)$$

where n_A is the quantity of A, T is the temperature, δ is the dilution rate, γ is proportional to the reaction heat, $k(T)$ is the kinetic coefficient and u is the control input. It represents the heat transfer rate coefficient and is linked to the coolant flowrate. It can be shown that the open-loop system (i.e. $u = 0$) can have up to three equilibrium states where one of

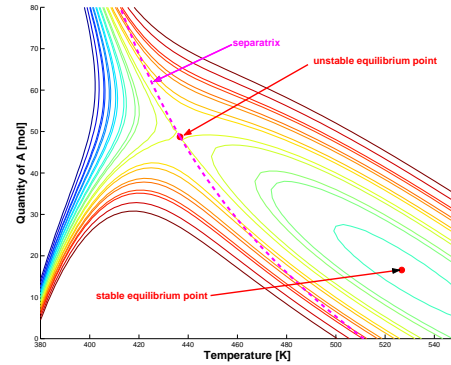


Figure 1: Level curves of the potential function

them is unstable. It can be shown that the system (1) can be written as follows:

$$Q(x) \frac{dx}{dt} = \nabla P(x) + G(x)u$$

where $x = [n_A, T]^T$ and $Q(x)$ is a regular matrix and its symmetric part is positive definite. This formulation of the dynamics is known as the Brayton-Moser equations. The quantity $P(x)$ (the Brayton-Moser potential) is decreasing along the trajectories of the system and has local minima at the asymptotically stable equilibrium states (see Fig. 1).

The Brayton-Moser potential can be reshaped by defining adequately the control input $u(n_A, T)$ to a new potential function $P_d(x)$ that has a local or a global minimum at the desired closed-loop equilibrium. The effects of modeling errors on the kinetics or of measurement errors on the concentration have also been analyzed.

References

- [1] Favache, A., Dochain, D., "Thermodynamics and chemical systems stability: the CSTR case revisited", *Journal of Process Control*, doi: 10.1016/j.jprocont.2008.07.007
- [2] Garcia-Canseco, E., Jeltsema, D., Scherpen, J., and Ortega, R., "Power-based control of physical systems", in *Proc. 17th IFAC World Congress*, Seoul (Korea), 2008
- [3] Ortega, R., Jeltsema, D., and Scherpen, J., "Power-shaping: a new paradigm for stabilization of nonlinear RLC-circuits", *IEEE Transactions on Automatic Control*, 48 (2003), 1762–1767
- [4] Ortega, R., van der Schaft, A., Mareels, I., Maschke, B., "Putting energy back in control", *IEEE Control Systems Magazine*, 21 (2001), 18–33

A Study of Stability Conditions for Haptics

İlhan Polat and Carsten W. Scherer

Delft Center for Systems and Control (DCSC), TUDelft

Mekelweg 2, 2628 CD, Delft, The Netherlands

{i.polat,c.w.scherer}@tudelft.nl

1 Abstract

Haptics, in general, refers to the technology and devices thereof, that present the touch sense or force-feedback to a human operator from a remote site or from a simulated environment. This type of feedback is used for creating an artificial touching feel at the operator side so that tasks which are beyond human capabilities, not feasible to fully automate and/or necessitates exposure to harsh environments, are undertaken. The goal is to be as realistic as possible i.e. the user experiences the remote site as if he is on site. This is denoted as *Telepresence*.

The stability and performance of an haptic device is now an active area of research from the control theory point of view, since it embodies different types of control structures namely, the human user which is highly nonlinear, band-limited and/or gain limited and assumed to be passive, the environment again usually passive, the quantization and sampling. The problem is considered in continuous time e.g. [1], discrete time or hybrid [5], also as special cases of classical results [4],[5] and many more. Recent publications [3], [2] and references therein, indicate the interest in obtaining numerical algorithms for the analysis problem with the contemporary control methodologies.

The purpose of this research is to assess the conservatism of these methods exist in the literature and try to improve if possible via using the Integral Quadratic Constraints and use of Dynamic Multipliers for analysis.

2 Acknowledgements

This work is supported by the MicroNed program (a part of the BSIK program of the Dutch government), The Netherlands.

References

- [1] Hannaford, B. and Ryu, J.H., "Time-domain passivity control of haptic interfaces", *IEEE Transactions on Robotics and Automation*, Vol.18(1), pp.1–10, 2002
- [2] Bianchini G., Orlandesi M. and Prattichizzo D., "Analysis and Design of Multi-Contact Haptic Systems: an LMI approach", *In Proc. IEEE Conference on Decision and Control*, New Orleans, USA, 2007
- [3] Naghshtabrizi, P., Hespanha, J.P., "Designing transparent stabilizing haptic controllers", *In Proc. IEEE Conference on Decision and Control*, Minneapolis, USA, 2006.
- [4] Colgate, J. E., "Robust impedance shaping telemanipulation", *IEEE Transactions on Robotics and Automation*, Vol.9(4), pp. 374–384, 1993
- [5] Colgate, J. E., "Passivity of a Class of Sampled-Data Systems: Applications to Haptic Interfaces", *Journal of Robotic Systems*, Vol.14(1), pp. 37–47, 1997

Automatic Control of Microscope Alignment

S.W. van der Hoeven

Delft Center for Systems and Control

Delft University of Technology

Mekelweg 2, 2628 CD, Delft, NL

E-mail: s.w.vanderhoeven@tudelft.nl

1 Introduction

The alignment of the beam through the electron microscope is a manual, tedious and lengthy process, due to the complicated nature of the machine and its electromagnetic lenses. Automation of the alignment would be a great benefit to the microscope community, especially since current methods are dependent on the skills of the microscopist, and alignment quality and thus image quality will vary user to user.

2 Method

The Ronchigram (also called shadow image) is a diffraction image recorded with a convergent beam on the sample [3]. The physical description of the formation of a Ronchigram, using an amorphous sample which introduces a random phase shift [2], is available [4] and has been used to simulate the diffraction images. The Ronchigram image is formed by convolving the sample function with the probe that illuminates the sample. This probe is formed by the lenses above the sample and contains information about the lens quality and the alignment of the microscope. If the lenses and alignment were ideal, the probe would be a point on the sample. Lens imperfections (aberrations) which result in e.g. spherical aberration and astigmatism, will reduce the maximum possible resolution. In the Ronchigram the influences of the aberrations become directly visible [4] and can therefore be used to adjust and optimise the alignment.

The image simulations are done to gain insight into how the aberrations influence the Ronchigram (forward modelling). This information can then be used to extract information from actual images, which in turn can be used for model-based control of the alignment. Extracting the aberration information is an important issue. It can for example be done using shape detection or with correlative or Fourier based methods. The extracted information can then be used as initial conditions for nonlinear least-squares analysis.

The transfer from microscope parameters to optical parameters is unclear, since the optical parameters, which are used in the simulations, are not measurable. System identification will need to be done to learn the transfer from the microscope parameters to the images or to the extracted parameters. Once a model is available, a control algorithm can be developed that optimises the alignment and minimises the

influence of the lens aberrations.

3 Results and Future Work

The analysis of the Ronchigram formation has given the following results: the central disk of the Ronchigram is dependent on the defocus: the larger the defocus (overfocus), the smaller the central disk. The maximum size is reached when the defocus is such that the spherical aberration is partially compensated for (Scherzer defocus [1]). If astigmatism is present, the central disk in the image becomes an ellipse. The ratio of the long and short axes can be used to find the value of the astigmatism if the spherical aberration is known. The angle of the ellipse is connected to the x-y distribution of the astigmatism.

Several methods have been found that can extract this information out of the images. This will be used to control and minimise the aberrations. The above results are for simulated images, the developed algorithms will be tested on experimental Ronchigrams. Since the Ronchigram images are very noisy in nature, averaging methods or multiple image comparisons might be needed. Alignment control in this case is done separately from the image taking, making any control not concurrent.

References

- [1] M. De Graef. *Introduction to Conventional Transmission Electron Microscopy*. Cambridge University Press, 2003
- [2] G.Y. Fan and J.M. Cowley. The simulation of high resolution images of amorphous thin films. *Ultramicroscopy* 1987; **21**: 125-30
- [3] J.M. Rodenburg and E.B. Macak. Optimising the Resolution of TEM/STEM with the Electron Ronchigram. *Microscopy and Analysis* 2002; **90**: 5-7
- [4] H. Sawada et. al. Measurement method of aberration from Ronchigram by autocorrelation function. *Ultramicroscopy* 2008; **108**: 1467-75

This research was sponsored by the Condor project at FEI company, under the responsibilities of the Embedded Systems Institute (ESI). This project is partially supported by the Dutch Ministry of Economic Affairs under the BSIK program.

Characterization of hysteresis within magnetic electron lenses

P.J. van Bree, C.M.M. van Lierop, P.P.J. van den Bosch
Control Systems, Department of Electrical Engineering
Eindhoven University of Technology
Email: P.J.v.Bree@tue.nl

1 Electron Microscopy

Reproducibility of settings for magnetic electron lenses is complicated because of hysteresis present in the ferromagnetic material of the lens-yoke. In an electron microscope, an electron beam is positioned on a sample with the help of a magnetic field of which the amplitude is controlled by the current applied to the lens coils. As a first principle, electron optics depend on the magnetic flux density, the velocity of the electrons and the position of the specimen. Hysteresis is characterized by means of experiments on a electromagnetic setup and by analysis of obtained electron microscope images (Fig. 1).

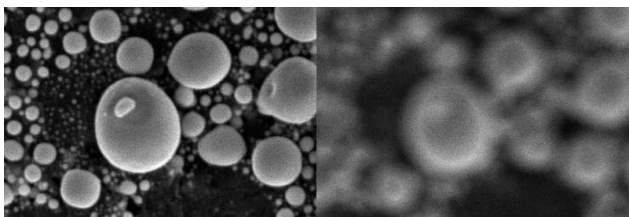


Figure 1: Illustration of the effect of hysteresis on image-quality. Two images obtained with the same lens excitation can be completely different.

2 Hysteresis

Hysteresis can be expressed as a multi-valued input-output relation that depends on its previous trajectory and still holds for quasi-dc inputs [1]. The response to periodic inputs shows transient effects; the minor loops stabilize after a few periods. This effect is often called accommodation [2]. The influence of the history can be wiped out by sufficiently large excitations. However, such a procedure is time demanding.

An illustration of hysteresis (Fig.2) is generated with an implementation of a Duhem-class hysteresis model [1], [3]. Unfortunately, this model does not describe accommodation as observed from experiments [2].

3 Control

Various applications within electron microscopy are involved with repeated variation of the lens excitation between extremes: automated zooming in-out-in, on-off-on with in

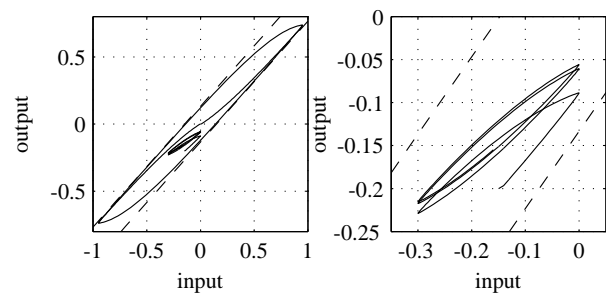


Figure 2: Illustration of hysteresis. **left.** The virgin curve, the stationary response to a periodic oscillation with amplitude 0.95, and accommodation of a minor loop. **right.** Accommodation of a minor loop (zoomed)

dual-beam systems. Here accommodation comes into play. It is observed that the response stabilizes within < 10 cycles. In first instance we focus on feed-forward control and do not consider image-quality and magnetic flux density as possible quantities for feedback control.

The settling-time after single switch is in the order of seconds, but can be reduced by choosing a proper input trajectory. However, dynamics and hysteresis are coupled which means the steady state after overshoot or undershoot will be different. The way to connect dynamics with hysteresis is under study.

4 Acknowledgement

This work is carried out as part of the Condor project, a project under the supervision of the Embedded Systems Institute (ESI) and with FEI company as the industrial partner. This project is partially supported by the Dutch Ministry of Economic Affairs under the BSIK program.

References

- [1] J. Oh and D.S. Bernstein. Semilinear duhem model for rate-independent and rate-dependent hysteresis. *IEEE Transactions on Automatic Control*, 2005.
- [2] S.E. Zirka, Y.I. Moroz, and E. Della Torre. Combination hysteresis model for accommodation magnetization. *IEEE Transactions on Magnetics*, 41(9):2426 – 2431, 2005.
- [3] B.D. Coleman and M.L. Hodgdon. On a class of constitutive relations for ferromagnetic hysteresis. *Archive for Rational Mechanics and Analysis*, 99(4):375–396, 1987.

Pneumatic circuit assessment in Pneumatic Artificial Muscle applications

Tri Vo-Minh

Email: tri.vominh@student.kuleuven.be

Prof. Herman Ramon

Faculty of Bioscience Engineering

Department of Biosystems (BIOSYST)

KULeuven

Kasteelpark Arenberg 30 - bus 2456, 3001

(Heverlee), Belgium

Email: Herman.Ramon@biw.kuleuven.be

Prof. Hendrik Van Brussel

Faculty of Engineering

Department of Mechanical Engineering

Division of Production Engineering, Machine

Design & Automation (PMA)

Celestijnenlaan 300B, B-3001 Leuven

(Heverlee), Belgium

Tel : (+32)16 32 26 47

Hendrik.VanBrussel@mech.kuleuven.ac.be

1. Introduction

Pneumatic artificial muscles (PAMs) or McKibben-based pneumatic artificial muscles have become desirable actuators alternative to hydraulic or electric actuators for the development of humanoid robots. Two main challenges in using such actuator are the nonlinearity of the compressed air and the nonlinearity of the PAM dynamics. In this study, the former challenge is assessed incorporating to the latter, which is completely solved by using hysteresis model. The study results will give the overall solution for improving the PAM control performance.

2. Pneumatic circuit in PAM control applications

In controlling a PAM, the mass of air is charged into or discharged out of the muscle bladder in order to inflate or deflate the muscle (simply called for a PAM) respectively. Due to the limitation of the PAM arrangements, there is only one port for pressurizing or depressurizing the muscle. No matter how the valve is used to feed through and control the mass of air, the mass flow rate through a none-ideal orifice is governed by the nonlinear function as follows:

$$\dot{m} = P_u C \frac{1}{\sqrt{T_1}} \Psi \left(\frac{P_d}{P_u} \right),$$

where:

\dot{m} is the mass flow rate

P_u, P_d are the upstream and the downstream pressure

C is the sonic conductance

T_1 is the temperature in the upstream supply, and

$\Psi(\cdot)$ is the flow function.

The properties of the flow function are determined as:

- two-stage flow such as sonic flow and subsonic flow
- a switching flow since the upstream and downstream are connected to different media during its functioning

The buildup pressure P in a muscle volume is obeying the first-order system as the following equation:

$$\dot{P} = \frac{\gamma}{V} \left(\dot{m} R T - P \dot{V} \right),$$

where:

γ, R are the process exponent and the air gas constant respectively.

In PAM control system, the pressure is known as the only input whereas the muscle force or muscle length can play a role as an input or an output and the way around. Assume that the volume V , the process temperature T are constant, the buildup pressure is very dependent on the high nonlinearity of the flow function. Furthermore, the air leakage in the control valve is difficult to model. The buildup pressure is thus preferable to Proportional-Integral control architecture.

3. Results and Discussion

The study results show that the buildup pressures are asymmetric as inflation and deflation due to the switching property of the flow function. The leakage shows a predominant and unidirectional effect.

For tracking the pressure precisely, the valve control signal is used as a reference for tuning control gains based on the level of the leakage influence. The optimal gain is chosen based on the asymmetric and switching flow assessment.

The sonic conductance plays an important role as an amplifier in the pneumatic circuit of the PAM control. It is used to select the control valve size with a compromise between the flow friction damper and the bandwidth of the overall system.

ACKNOWLEDGEMENT

The author gratefully acknowledges the DGDC (Directorate- General for Development Cooperation), from Belgium Government for funding this research.

Load Dynamics in Piezoelectric Actuation

J. van Hulzen^{1,2}, P.M.J. Van den Hof¹, G. Schitter¹, J. van Eijk²

¹Delft Center for Systems and Control

²Precision and Microsystems Engineering Department, Mechatronics

Delft University of Technology, Mekelweg 2, 2628 CD, Delft, The Netherlands

Email: j.r.vanhulzen@tudelft.nl

1 Introduction

In high speed atomic force microscopes (AFM), the dynamics of loads such as sample carriers can be an important limitation to performance of the vertical axis used for imaging. To investigate the impact of load flexibility on control performance, the actuator and load are modeled by simple low order models. Using these models, the mechanical design can be optimized to achieve maximum control performance.

2 The impact of load flexibility

The dynamics of an unloaded piezoelectric actuator (PEA) consists of an alternating series of resonances and anti-resonances[1]. To study the influence of flexible loads we consider the case where the actuator is fixed on one side and loaded on the other, see Fig 1. Modal expansion is used to model the steady state response to harmonic excitation by a piezoelectrically induced force $F = F_p e^{j\omega t}$ acting on the free end of the actuator.

$$P_a(\omega) = \frac{x_1}{F} = \sum_{i=1}^{n_m} \frac{\phi_i^2(L)}{\mu_i (\omega_i^2(L) - \omega^2)} + \frac{L}{EA} - \sum_{i=1}^{n_m} \frac{\phi_i^2(L)}{\mu_i \omega_i^2}$$

For a fixed-free configuration, the resonant modes ω_i , the modal mass μ_i and the mode shapes ϕ_i are given by the partial differential equation

$$EA \frac{\partial^2 u(x,t)}{\partial x^2} + f(x,t) = A\rho \frac{\partial^2 u(x,t)}{\partial t^2}, \quad 0 < x < L$$

and boundary conditions $u(0,t) = 0$ and $\frac{\partial u(L,t)}{\partial x} = 0$ giving

$$\omega_i = \frac{\lambda_i}{L} \sqrt{\frac{E}{\rho}}, \quad \mu_i = \frac{\rho AL}{2}, \quad \phi_i(L) = \sin \phi_i, \quad i = 1, 2, \dots, \infty$$

The dynamics of a piezoelectric actuator and load are

$$P_{l1}(\omega) = \frac{F_i}{x_1} = \frac{-\omega^2 (P_a(\omega) P_{l2}(\omega))}{1 + P_a(\omega) P_{l1}(\omega)}$$

with the load modeled as a fourth order system

$$P_{l1}(\omega) = \frac{F_i}{x_1} = \frac{-\omega^2 (km_1 + km_2 - m_1 m_2 \omega^2)}{k - m_2 \omega^2}$$

$$P_{l2}(\omega) = \frac{x_2}{x_1} = \frac{k}{k - m_2 \omega^2}$$

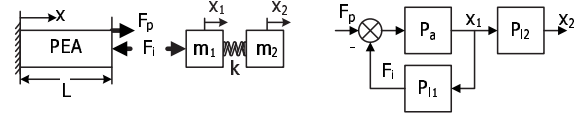


Figure 1: FRF of piezoelectric actuator loaded by a flexible load.

3 Experimental verification

The influence of load flexibility was investigated on a commercial AFM (Veeco E-scanner) based on a piezoelectric tube scanner. The effect of changing loads was studied by adding an additional mass to the cap at the free end of the piezoelectric tube. As can be seen from Fig 2, the flexible load introduces an additional mode causing phase lag in excess of 180 degrees. Compensation by phase lead increases the feedback gain leading to poor noise performance.

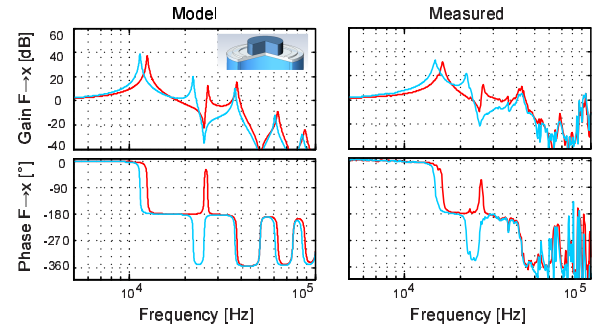


Figure 2: Model and measurement of the z-axis of an AFM without additional load (red) and with an increased load-mass attached at the center of the cap terminating the piezoelectric tube (blue).

4 Acknowledgment

This work is sponsored by the Delft Centre for Mechatronics and Microsystems and by the National Institutes of Health under Award RO1 GM 065354.

References

- [1] H. J. M. T. A. Adriaens, W. L. de Koning, and R. Banning, Modeling piezoelectric actuators, IEEE/ASME Trans. Mechatron., vol. 5, no. 4, pp. 331 to 341, Dec. 2000.

Control of a moving magnet planar actuator at industrial specifications

Jaron Achterberg, C.M.M. van Lierop, P.P.J. van den Bosch
Eindhoven University of Technology, Department of Electrical Engineering
P.O.Box 513, 5600 MB Eindhoven, The Netherlands
E-mail: J.Achterberg@tue.nl

1 Introduction

In today's wafer scanners xy -positioning stages, consisting of multiple stacked linear actuators, are being used to position the wafer accurately in the xy -plane. Developments in lithographic technologies such as extreme UV, require stages that can operate in a vacuum environment. Classical linear actuators are not suitable, since they use mechanic (lubricated) or air bearings which contaminate the vacuum. Therefore planar actuators with active magnetic bearing, a single stage that has a stroke in two degrees of freedom with the remaining four degrees magnetically beared, is being researched for these applications.

These planar actuators can be divided into two main topologies, a moving coils with stationary permanent magnets topology and a moving magnets with stationary coils topology. The former needs a cable slab to supply the translator coils with power and cooling, introducing very unpredictable disturbance forces onto the carrier. The inverse topology does not encounter this problem, yet to operate it completely wireless introduces a lot of extra challenges in the design [3].

2 Goal

Recently this concept of a moving magnet planar actuator has been shown to stably operate in six degrees of freedom, both by Eindhoven University of Technology [1] [2] and Philips Applied Technologies. To use these devices into a wafer stage the accuracy has to be improved a lot. To operate these devices at nanometer-accuracy, a lot of research has to be done on all physical aspects of the machine and the sensitivity of the control to machine imperfections. It is supposed that the rigid body assumption of the carrier will not hold at nanometer-scale, thermal deviations inside the carrier will affect its dimensions and machine (production) tolerances will be limiting model and control accuracy.

3 Approach

There are more active coils that act on the translator than the amount needed to control the six degrees of freedom. Excess input freedom can be used for controlling extra dynamics of the platform. Instead of considering only rigid body dynam-

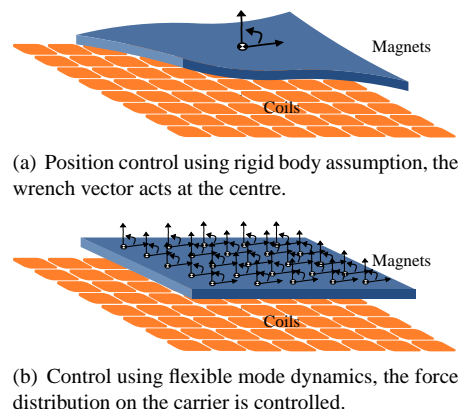


Figure 1: Control of flexible modes in the translator

ics, the flexible modes of the carrier can also be controlled by using overactuation, this is illustrated in Figure 1.

To increase performance, the machine design will be optimised for closed loop performance. So closed loop performance will be expressed as a function of the machine parameters.

4 Conclusion

A challenging research topic has been formulated. From a control point of view it is being characterised by both spatial and temporal phenomena and overactuation.

References

- [1] J. W. Jansen, Magnetically Levitated Planar Actuator with Moving Magnets: Electromechanical Analysis and Design, Ph.D. dissertation, Eindhoven University of Technology, Nov 2007.
- [2] C.M.M. van Lierop, Magnetically Levitated Planar Actuator with Moving Magnets: Dynamics, Commutation and Control, Ph.D. dissertation, Eindhoven University of Technology, Jan 2008.
- [3] J. de Boeij, Multi-Level Contactless Motion System, Ph.D. dissertation, Eindhoven University of Technology, Jan 2009.

Input design for PWA biological cell systems

Dirk Vries^{a,b}Peter Verheijen^aArjan den Dekker^b

^aDepartment of Biotechnology
Delft University of Technology
Julianalaan 67, 2628 BC Delft
The Netherlands

^bDelft Center for Systems and Control
Delft University of Technology
Mekelweg 2, 2628 CD Delft
The Netherlands

Abstract

A procedure for input design is proposed for (micro)biological systems which can be described by PieceWise-Affine Output-Error (PWA-OE) models. The identification approach is based on the calculation of control-to-facet input signals such that all modes are excited and parameter estimation is improved.

1 Introduction

The ability of a micro-organism to react on environmental changes and trigger a particular biological mechanism abruptly when a certain threshold has been reached, i.e. like a switch, can help the organism to survive or outgrow other microbial species. Here, a PieceWise Affine approximation of the deterministic hybrid biological system in [2] is written in OE form and is subsequently used for input design.

2 PWA-OE model class

The following discrete time model class \mathcal{M} is considered:

$$\mathcal{M} : \begin{cases} w(k+1) &= f(x(k), \theta) \\ y(k) &= w(k) + e(k) \end{cases} \quad (1)$$

with

$$f(x, \theta) = \begin{cases} \theta_1^\top \begin{bmatrix} x^\top \\ 1 \end{bmatrix} & \text{for } x \in \mathcal{X}_1 \Leftrightarrow q_0 \\ \theta_s^\top \begin{bmatrix} x^\top \\ 1 \end{bmatrix} & \text{for } x \in \mathcal{X}_s \Leftrightarrow q_s \end{cases} \quad (2)$$

where $x(t_k) := (w(k) \ w(k-n_a+1) \ u(k) \ \dots \ u(k-n_b+1))^\top$ denotes the regressor vector. Note that a transition from one mode $q_i \in Q$ to another $q_j \in Q$, $i \neq j$, Q the set of discrete modes, is induced by crossing the boundaries of bounded polytopic regions of the regressor space \mathcal{X}_i . Furthermore, $w(t_k)$ denotes the state vector corresponding to nutrient, biomass and nucleic acid (mRNA) concentrations, $u(k) \in \mathcal{U} = [0, u_{\max}]$ an inlet nutrient feed concentration, $y(k)$ the measured observations and $e(k)$ a Gaussian white noise signal. The boundaries of \mathcal{X}_i , i.e. the linear hyperplanes $M(x^\top \ 1)^\top = 0$, correspond to (nutrient) concentration thresholds.

It is proposed to excite all, or as much as possible, modes of the hybrid space ($\mathcal{X} = \{\mathcal{X}_i\}_{i=0}^s$ and for $i \neq j$, $\mathcal{X}_i \cap \mathcal{X}_j = \emptyset$) by computing a control-to-facet feedback law $\{u^*\}_{k=0}^N$ to a predetermined route from facet-to-facet. This way, an approximately equal amount of data points in every mode can be collected. The procedure is roughly as follows.

3 Input design procedure

It is assumed that initial estimates of parameters in M , i.e. $\hat{\theta}_0^M$, and $\hat{\theta}_0$ are available. Using tools from [3, 1] it is proposed to:

1. Verify if all modes are reachable in h time steps from the initial point \hat{x}_0 by control-to-facet feedback laws $\{u^*\}_{i=0}^s$. If not, choose different exit facets.
2. Perturb u^* with PRBS with small amplitude and check if conditions in (1) still hold.
3. Collect data set \mathcal{D} and estimate $\{\theta^M, \theta\}$ by a clustering parameter estimation technique. Return to 2 until predetermined identification criterion is met.

4 Results and Conclusions

Further details, results and concluding remarks will be discussed and presented during the BeNeLuX meeting.

References

- [1] P. Collins, L. Habets, A. Kuut, M. Nool, M. Petreczky, and J.H. (van Schuppen). ConPAHS - A Software Package for Control of Piecewise-Affine Hybrid Systems. In *IEEE Conference on Computer-Aided Control Systems Design*, pages 76–81, Munich, Germany, October 2006.
- [2] J. Hu, W.-C. Wu, and S. Sastry. Modeling subtilin production in *Bacillus subtilis* using stochastic hybrid systems. In R. Alur and G.J. Pappas, editors, *HSCC, LNCS*, volume 2293, pages 417–431. Springer-Verlag, Berlin, Germany, 2004.
- [3] M. Kvasnica, P. Grieder, M. Baotić, and M. Morari. Multi-Parametric Toolbox (MPT). In *LCNS*, volume 2993 of *Hybrid Systems: Computation and Control*. Springer Berlin, 2004.

A Systematic Procedure to Develop Dynamic Models of Bioprocesses

Johan Mailier *
Automatic Control Laboratory
Faculté Polytechnique de Mons
B-7000 Mons, Belgium
Johan.Mailier@fpms.ac.be

* Aspirant du F.R.S. - FNRS

Alain Vande Wouwer
Automatic Control Laboratory
Faculté Polytechnique de Mons
B-7000 Mons, Belgium
Alain.VandeWouwer@fpms.ac.be

Abstract

The derivation of dynamic macroscopic models of bioprocesses has received an increasing attention in recent years, with a view to the development of monitoring and control strategies. Two main approaches can be distinguished. The first one makes use of the available knowledge about a detailed metabolic network, and reduces this network to a 'minimal' set of macroscopic reactions, which link external substrates and cellular products. The other one tries to directly establish a macroscopic reaction scheme, from experimental measurements of the time evolution of several substrates and external cellular products.

The second approach, on which attention is focused in this study, is of great interest in situations where prior information about the metabolism is incomplete or unavailable, a frequent situation in the bioproduction of pharmaceuticals, where genetically manipulated strains are used for expressing products of interest, and in environmental or agro-food processes, where a large range of populations of microorganisms are involved.

In this study, a fast and systematic macroscopic model development procedure is developed and tested. This procedure, which makes use of and extends recent results, proceeds in three steps: (a) the determination of the number of biological reactions following a method based on PCA, proposed in [1, 2], (b) the estimation of a candidate biological scheme, which benefits from a C-identifiability property [3], but which might lack a biological interpretation, (c) the projection of this reaction scheme onto a biologically consistent scheme (using a projection matrix to be determined and the concept of equivalence discussed in [4, 5]).

The main contribution of the present paper lies in the formulation and numerical implementation of step (c), which consists of two simultaneous optimization problems, one for estimating the projection matrix while satisfying constraints on the pseudo-stoichiometric coefficients (thus incorporating prior knowledge, if available), and the other for estimating the coefficients of a kinetic model while satisfying constraints on these coefficients (in the event where some prior knowledge on the kinetics is also available). The strong point of this procedure is that it does not require the

repetitive numerical solution of the mass balance ordinary differential equations (i.e. the dynamic model of the bioprocess), as in conventional identification procedures, and it is therefore computationally efficient (the procedure is coded in Matlab using standard functions and allows the development of dynamic models within a few minutes of computation). The performance of the method and software is demonstrated on several application examples.

Acknowledgment

This paper presents research results of the Belgian Network DYSCO (Dynamical Systems, Control, and Optimization), funded by the Interuniversity Attraction Poles Program, initiated by the Belgian State, Science Policy Office. The scientific responsibility rests with its author(s).

The authors are also very grateful to FNRS (Fonds de la Recherche Scientifique), the Belgian Fundation, for his support.

References

- [1] O. Bernard and G. Bastin. *On the estimation of the pseudo-stoichiometric matrix for macroscopic mass balance modelling of biotechnological processes*. *Mathematical Biosciences*, 193:51-77, 2005a.
- [2] O. Bernard and G. Bastin. *Identification of reaction networks for bioprocesses: determination of an incompletely known pseudo-stoichiometric matrix*. *Bioprocess and Biosystems Engineering*, 27(5):293-301, 2005b.
- [3] L. Chen and G. Bastin. *Structural identifiability of the yield coefficients in bioprocess models when the reaction rates are unknown*. *Mathematical Biosciences*, 132:35-67, 1996.
- [4] J.-L. Delcoux, R. Hanus, and Ph. Bogaerts. *Equivalence of reaction schemes in bioprocesses modelling*. In *proceedings of the 4th International Symposium on Mathematical Modelling and Simulation in Agricultural and Bio-Industries*, Haifa, Israel, 2001.
- [5] Ph. Bogaerts, M. Rooman, V. Vastemans, and A. Vande Wouwer. *Determination of macroscopic reaction schemes: towards a unifying view*. In *proceedings of the 17th World Congress of IFAC*, Seoul, Korea, July 2008.

Macroscopic modeling as a tool for gaining insight in AI-2 dynamics of *Salmonella* Typhimurium

A.M. Cappuyns¹, K. Bernaerts¹, S.C. De Keersmaecker², J. Vanderleyden², J.F. Van Impe¹

¹ BioTeC - Chemical and Biochemical Process Technology and Control

Department of Chemical Engineering, Katholieke Universiteit Leuven

W. de Croylaan 46, B-3001 Leuven (Belgium)

astrid.cappuyns@cit.kuleuven.be - kristel.bernaerts@cit.kuleuven.be - jan.vanimpe@cit.kuleuven.be

²Centre of Microbial and Plant Genetics, K.U.Leuven

Kasteelpark Arenberg 20, B-3001 Leuven (Belgium)

1 Introduction

Over the last few decades, research on bacterial cell-cell communication (quorum sensing) has been quite intense. Quorum sensing controls microbiological functions of medical, agricultural and industrial importance and a better understanding of the underlying mechanisms and the conditions under which the signaling occurs, offers possibilities for new applications. In this research, different hypotheses concerning the dynamics of AI-2 signaling of *Salmonella* Typhimurium are investigated.

2 Results & Discussion

Based on experimental observations from dedicated bioreactor experiments and mechanistic knowledge concerning the uptake mechanism for AI-2, three different candidate models for AI-2 dynamics are presented and evaluated. The different hypotheses are introduced below.

Hypothesis A. A first hypothesis assumes that AI-2 production is related to preferential substrate metabolism and that AI-2 production is proportional to the specific substrate consumption rate. The AI-2 concentration measured in the growth medium is assumed to be the result of simultaneous production and uptake.

It has been reported that AI-2 uptake is repressed by phosphatransferase sugars through catabolite repression [1]. Repression of the transporter is causing the maintenance of AI-2 level in the presence of glucose (or galactose). The following two hypotheses incorporate catabolite expression as regulation mechanism for AI-2 uptake.

Hypothesis B. Surette and Bassler [2] conclude from their results that the AI-2 signal in *E. coli* and *S. Typhimurium* serves two functions, i.e., communicating information concerning both their growth phase and the metabolic potential of the environment to one another. In hypothesis B, AI-2 is modeled as a reflection of the growth phase by linking AI-2 to the specific growth rate on preferential substrate.

Hypothesis C. According to the original definition of quorum sensing, bacteria coordinate behavior based on cell density. In hypotheses C, the original definition of quorum sensing is followed and AI-2 production is linked to quorum or biomass solely.

Evaluation. Despite the fact that hypotheses A and B are based on different assumptions, simulations with these models provide similar qualitative results which are in agreement with the experimental data for the continuous experiment. Hypothesis C, in which AI-2 production is modeled as a reflection of cell density and in which uptake is regulated by catabolite repression, is not able to describe the qualitative AI-2 profile of the continuous experiment. The high peak in AI-2 observed in the first hours of the experiments, i.e., during exponential growth, cannot be described by hypothesis C. Based on this observation, hypothesis C can be rejected. Hypotheses A and B have no problem with the description of peak accumulation of AI-2 during the first hours of the continuous experiment and with the description of the steady states during the continuous experiment.

3 Conclusions

Based on a qualitative comparison of the simulations with the experimental data, one of the hypothesis could be rejected, namely the hypothesis that AI-2 production is linked to quorum solely. Two candidate models are retained. With the available AI-2 measurement at this moment, it is not possible to discriminate between the two remaining candidate models. A more quantitative and more accurate measurement for AI-2 is a necessity for further model structure discrimination.

Acknowledgements

Work supported in part by IWT-GBOU-20160 Project, Projects OT/03/30 and EF/05/006 (Center-of-Excellence Optimization in Engineering) of the Research Council of the Katholieke Universiteit Leuven, and by the Belgian Program on Interuniversity Poles of Attraction, initiated by the Belgian Federal Science Policy Office. K. Bernaerts is a Postdoctoral Fellow with the Fund for Scientific Research Flanders (FWO). The scientific responsibility is assumed by its authors.

References

- [1] K.B. Xavier and B.L. Bassler, Regulation of uptake and processing of the quorum-sensing autoinducer AI-2 in *Escherichia coli*, *J. Bacteriol.*, vol. 187, 2005, pp 238-248.
- [2] M.G. Surette and B.L. Bassler, Quorum sensing in *Escherichia coli* and *Salmonella typhimurium*, *Proc. Nat. Acad. Sci. USA.*, vol. 95, 1998, pp 7046-7050.

Three ways to do temperature reconstruction based on Bivalve-proxy information

Maite Bauwens^{1,2}, Henrik Ohlsson³, Veerle Beelaerts², Kurt Barbé², Johan Schoukens² and Frank Dehaers¹

¹ Department of Analytical and Environmental Chemistry, ² Department of Fundamental Electricity and Instrumentation
Vrij Universiteit Brussel, Pleinlaan2, 1050 Brussel, Belgium

³ Division of Automatic Control, Department of Electrical Engineering,
Linköping University, SE-581 83 Linköping, Sweden

e-mail: Maite.Bauwens@vub.ac.be

Introduction

The reconstruction of seasonal variations in the paleo-environment is possible thanks to the bivalve shells that are commonly found back in archeological sites and that are sensitive environmental recorders [1]. To do these reconstructions we look to the chemical composition of a shell along his growth axis. When a certain element or isotope can be related to an environmental parameter it is called a proxy for that parameter.

Problem statement

Many elemental and isotopic have been proposed as potential temperature proxy. But the same problem is showing up over and over again: a certain elemental shows a good linear correlation with temperature, but at the moment that the intrinsic variation has to be explained, the incorporation of the proxy seems to be much more complex than assumed in the first instance.

Two observations gave us the idea to use a new type of models to reconstruct temperature. In first instance we observed that all proxy incorporations were always influenced by more than one environmental parameter, which automatically implicate that the reconstruction of an environmental parameter should be done with more than one proxy input. A second observation is that some proxy-environment relations seemed to be non-linear. We propose to do climate reconstructions based on Non-linear multi-proxy models. Here we present our own intuitive approach to do temperature reconstructions and then we compare our results to two recognized engineering techniques: Manifold learning and Supported vector machines.

Data

These three methods are validated on shell data of Scheldt estuarine environment using high resolution measurements of Mg, Mn, Ba, Sr and Pb on a LA-ICP-MS. The site specificity is tested for all methods using shell-data from 4 different sites along the Scheldt. Time specificity is checked by reconstructing the temperature corresponding to a shell that grew in another year.

Results

An intuitive approach: This approach consists in the construction of a model based on splines or polynomials in a multi-dimensional space to describe the variation in the chemical signature of the shell during a one year cycle.

The shortest distance from another measurement (e.g. in an archeological shell) to the model will give a time estimation, which can be linked in a second step, to several environmental parameters. [2] With this intuitive approach we have good reconstructions with a precision of 0.4°C for shells of a same site, grew in the same year, to moderate reconstructions with a precision of 0.9°C for shells that grown on another site, in another year.

Manifold learning: The manifold learning approach that is a very similar high-dimensional regression technique and is implemented on our data by Ohlsson et al. [3] and gave similar results. Very good reconstructions were obtained for shells of the same site, and the same year, (a precision of 0.35°C) and moderate reconstructions were obtained for shells that grown on another site, in another year (a precision of 1.9°C).

Supported vector machines: The reconstructions generated by the least square supported vector machines toolbox of Espinosa et al [4] were less satisfying since the reconstructed temperature profiles were very scattered and the precision was lower (from 1.1°C to 3.7°C)

Conclusions

The best reconstructions are computed with the manifold learning algorithms, but the simplicity and high precision of the intuitive approach made it a very attractive alternative in the paleoclimatology research field. The study shows also that temperature reconstruction seems possible, but with a moderate precision due to chemical variability in shells from one site to the other.

References

- [1] Klünder M. H., et al. 2008, Laser ablation analysis of bivalve shells – archives of environmental information, GEUS. *Geological Survey of Denmark and Greenland Bulletin* 15, 89–92.
- [2] Bauwens M. et al., 2008 Climate reconstruction based on archaeological shells: a non-linear multi-proxy approach, Benelux abstract book pp.69
- [3] Ohlsson H. , 2008, Regression on Manifolds with Implications for System Identification, Linköping studies in science and technology. Thesis.No. 1382
- [4] Espinosa M. et al 2004, A Comparative Study of LS-SVM's Applied to the Silver Box Identification Problem, *6th IFAC Symposium on Nonlinear Control Systems (NOLCOS 2004)*, Stuttgart, Germany

This research was funded by a grand of the Vrije Universiteit Brussel (HOA-9) and a grand of the Flemish government (CALMAR's)

Quantitative characterization of *Streptomyces lividans* batch fermentations

P.-J. D'Huys¹, K. Bernaerts¹, J. Anné² and J.F.M. Van Impe¹

¹BioTeC - Chemical and Biochemical Process Technology and Control, Department of Chemical Engineering,
Katholieke Universiteit Leuven, W. de Croylaan 46, B-3001 Leuven, Belgium

{pieterjan.dhuys, kristel.bernaerts, jan.vanimpe}@cit.kuleuven.be

²Bacteriology Section, Department of Microbiology and Immunology,
Katholieke Universiteit Leuven, Minderbroedersstraat 10 blok x - bus 1030, B-3000 Leuven, Belgium

1 Introduction

Streptomyces are worldwide used for the commercial production of antibiotics (e.g., by CIPAN s.a.) and industrial enzymes (e.g., Danisco-Genencor International). Recently several genera of Gram-positive bacteria are being tested as host for the production of heterologous proteins due to their ability to efficiently secrete proteins in the culture medium. Among them *Streptomyces lividans* is the host of choice for the secretory production of heterologous proteins [1]. This research aims at a quantitative understanding of the fermentation characteristics of *S. lividans*. In particular we are interested in fluxes in the central carbon and nitrogen metabolism which are directly linked to recombinant protein production. The complexity of the research will be build up gradually. In the current first stage, experiments are done with the wild type strain. Later on, in a second stage, the recombinant strain is examined. Mouse tumor necrosis factor alpha is used as target protein.

2 Materials and methods

Microorganism

S. lividans 66 strain TK24 (John Innes Centre, Norwich, UK) and *S. lividans* pIJ486rmTNF- α are used. All DNA manipulations are performed as described in [2].

Bioreactor experiments

Batch experiments are performed in a computer controlled 5 L BioFlo 3000 benchtop fermentor (New Brunswick Scientific, USA) with a working volume of 3 L. As medium the minimal liquid NMMP medium is used [2]. PID cascade controllers ensure that the fermentation temperature is kept constant at 30°C, pH at 7. The dissolved oxygen concentration is not controlled.

Measurements

Samples collected periodically from the fermentor are evaluated for biomass and extracellular metabolites (i.e., glucose, organic acids, amino acids, ammonium and phosphate).

3 Results and Conclusions

Growth, substrate consumption and metabolite production data are collected. Conversion rates and yields are calculated from these measurements. The accuracy of these measured rates is improved by data reconciliation and gross error diagnosis [3, 4]. The improved conversion rates form a consistent data set which will be used in metabolic flux analysis (MFA). The metabolic network models for the wildtype and recombinant strain, necessary for the MFA, are currently being developed. These are based on the metabolic models of [5] and [6].

Acknowledgements. Work supported in part by Projects OT/03/30 and EF/05/006 (Center-of-Excellence Optimization in Engineering) of the Research Council of the Katholieke Universiteit Leuven, by the Belgian Program on Interuniversity Poles of Attraction, initiated by the Belgian Federal Science Policy Office and by the Fund for Scientific Research Flanders (FWO-Vlaanderen) (project G.0352.09 and the Postdoctoral Fellowship of K. Bernaerts). The scientific responsibility is assumed by its authors.

References

- [1] C. Vallin, E. Pimenta, A. Ramos, C. Rodriguez, L. Van Mel-laert and J. Anné (2005). *Streptomyces* as a host for the secretion of heterologous proteins for the production of biopharmaceuticals. *Journal of Business Chemistry*, 2(3): 107-111.
- [2] T. Kieser, M. Bib, M. Buttner, K. Chater and D. Hopwood (2000). *Practical Streptomyces Genetics*. The John Innes Foundation.
- [3] R.T. van der Heijden, J.J. Heijnen, C. Hellinga, B. Romein and K.C. Luyben (1994). Linear constraint relations in biochemical reaction systems: I. Classification of the calculability and the balanceability of conversion rates. *Biotechnology and Bioengineering*, 43(1): 3-10.
- [4] R.T. van der Heijden, B. Romein, J.J. Heijnen, C. Hellinga and K.C. Luyben (1994). Linear constraint relations in biochemical reaction systems: II. Diagnosis and estimation of gross errors. *Biotechnology and Bioengineering*, 43(1): 11-20.
- [5] E. Daae and A. Ison (1999). Classification and sensitivity analysis of a proposed primary metabolic reaction network for *Streptomyces lividans*. *Metabolic Engineering*, 1: 153-165.
- [6] I. Borodina, P. Krabben and J. Nielsen (2005). Genome-scale analysis of *Streptomyces coelicolor* A3(2) metabolism. *Genome Research*, 15: 820-829.

A Simplified Model for Urban Traffic Network Control

Shu Lin^{*,†,1}, Bart De Schutter^{†,*}, Yugeng Xi^{*}

^{*} Department of Automation, Shanghai Jiao Tong University
No. 800 Dongchuan Road, Minhang District, Shanghai, P. R. China
Email: lisashulin@gmail.com; ygxi@sjtu.edu.cn

[†] Delft Center for Systems and Control, Delft University of Technology
Mekelweg 2, 2628 CD Delft, The Netherlands
Email: b.deschutter@dcsc.tudelft.nl

^{*} Maritime and Transport Technology department, Delft University of Technology

Abstract

In recent years, the number of vehicles has grown larger and larger, and the requirements for traveling by vehicles are getting more and more stringent. To reduce traffic jams and to promote efficiency in traveling, effective traffic control algorithms are necessary. Many control theories have been applied to control traffic, like fuzzy control, PID control, model predictive control, and multi-agent control, in combination with different control structures like centralized, distributed, and hierarchical control.

We focus on model-based control methods, and on model predictive control (MPC) in particular. For different model-based control approaches, there exist different requirements for the control model. Some models just need to express the relation between the input values and the output performance, but some are more detailed so as to depict the dynamics of the traffic evolution; some models are more precise in modeling the dynamics, while some are simpler so as to be fast for on-line computing. As a result, there exists a wide variety of traffic models with different levels of detail. For different control methods, appropriate traffic models with the required modeling power need to be established.

In principle, a centralized MPC method guarantees globally optimal control actions for traffic networks. It can maximize the throughput of the whole network, and provide network-wide coordination of the traffic control measures. However, the problem is that the on-line computational complexity for centralized MPC grows significantly, when the network scale gets larger, the prediction time span gets longer, and the traffic model becomes more complex or gets a higher modeling power. There are two main approaches to address this problem: (1) simplifying the traffic model in order to reduce the computational complexity, and (2) cutting the traffic network into small sub-networks or even intersections, which are then controlled using distributed control or the multi-agent control. In this presentation we consider the first

approach, i.e., we develop simplified yet sufficiently accurate traffic models, in particular for urban traffic networks.

We start with an urban traffic model based on previous work [1–3]. To reduce the computational burden, the simplified model enlarges the simulation time interval to one cycle time. During each simulation time interval, traffic states are updated once in each link according to the average input and output traffic flow rates in the current cycle. To add flexibility, every intersection in the network can have a different cycle time, and the intersections share the same control time interval. This control time interval is the least common multiple of all the cycle times of the intersections in the network. It is necessary to define this common control time interval to keep the model running and communicating synchronously under both centralized control and distributed control. For a given link the average input traffic flow rates are provided by the upstream links, which transform their own output traffic flow rates into input flow rates for the given link taking the different simulation time intervals into account.

This simplified traffic model provides a good trade-off between modeling accuracy and computational complexity for model-based control purposes. To test the model, a simulation is executed to compare it with the other traffic models [1, 3]. Moreover, conclusions are drawn on which model to use in centralized or distributed MPC methods.

References

- [1] H. Kashani and G. Saridis. Intelligent control for urban traffic systems. *Automatica*, 19(2):191–197, 1983.
- [2] S. Lin and Y. Xi. An efficient model for urban traffic network control. In *Proc. 17th World Congress of the International Federation of Automatic Control*, pages 14066–14071, Seoul, Korea, July 2008.
- [3] M. van den Berg, A. Hegyi, B. De Schutter, and J. Hellendoorn. A macroscopic traffic flow model for integrated control of freeway and urban traffic networks. In *Proc. 42nd IEEE Conference on Decision and Control*, pages 2774–2779, Maui, Hawaii USA, 2003.

¹ Visiting researcher at the Delft Center for Systems and Control, Delft University of Technology.

Distributed control of urban traffic networks using hybrid models

Nicolae Marinica and René Boel

*

Abstract

Urban traffic control poses a challenging problem in terms of coordinating the different traffic lights that can be used in order to influence the traffic flow. Model based control requires hybrid systems models consisting of interacting fluid flow Petri net models for controlled and uncontrolled intersections, and cell transmission models for links connecting the intersections. This paper proposes a simulation based distributed model predictive control algorithm for solving this problem.

1. Introduction

Classical traffic light controllers use a fixed red/green schedule that tries to optimize the system behavior under normal operating conditions, hopefully achieving green waves most of the time. Recently many intersections have been equipped with more or less sophisticated vehicle detectors that could be used for implementing a feedback control that only gives a green light to a side road when there are cars waiting there. This feedback policy may however destroy the green wave of the open loop controller. The challenge is to coordinate the feedback actions at neighboring intersections so that no green time is wasted when no cars are waiting, but at the same time so that green waves are preserved.

2. Model

An traffic network consists of many interacting components, like controlled and uncontrolled intersections, and road links connecting those intersections. In-

tersections are best modeled by as a queueing model considering the road space as a service station, that is assigned to different traffic streams according to some priority rule. In order to obtain a simulations model that is sufficiently fast to be applied in an MPC controller we propose a fluid Petri net model of these queues [2]. For short links connecting the intersections a simple time delay may be a sufficiently accurate model, but for longer links a cell transmission model [1] is proposed. Together these different components leads to a hybrid systems model of the plant.

3. Coordinating Control

The size of the model makes imposes a distributed approach to the optimal coordination control problem. This means that the local controller for an intersection will use local measurements on queue lengths, arrival rates, and other local state information, together with summarized data that coarse describing the state at neighboring intersections, and some control parameters generated by a supervising controller. Each local controller should not even have to know the detailed model of its neighbors, since this could not be reliably updated anyway. Each local controller could not even interpret detailed data from neighbors. The supervising controller also knows only this coarse model of each intersection.

To obtain the optimal coordinator the distributed Model predictive Control, as proposed by Krogh et al. [3] is used. The model predictions required for this controller are obtained by running the distributed simulator developed for the urban network.

References:

[1] Boel, R., and L. Mihaylova, *A compositional Stochastic model for real time freeway traffic simulation*, in *Transportation Research. Part B*, vol.40 (2006), pp.319-334.

[2] J. Ilvez and R. Boel: *Modelling and controlling traffic behaviour with continuous Petri nets*, *Proc. 16th IFAC World Congress on Automatic Control*, Prague 2005

[3] E. Camponogara, D. Jia, B. H. Krogh, and S. Talukdar, *Distributed model predictive control*, *IEEE Control Systems Magazine*, vol. 22, no. 1, pp. 44-52, Feb. 2002

*The authors ((nicolaeemmanul.marinica@ugent.be, rene.boel@ugent.be) are with the SYSTeMS Research Group, Gent University, Technologiepark 914, B-9052 Zwijnaarde, Belgium; this work was supported by the European Commission via the Con4CORD project. This paper presents research results of the Belgian Network DYSCO (Dynamical Systems, Control, and Optimization), funded by the Interuniversity Attraction Poles Programme, initiated by the Belgian State, Science Policy Office. The scientific responsibility rests with its author(s).

Optimal Control in Hybrid Vehicles Using Route Information

Thijs van Keulen, Bram de Jager, Maarten Steinbuch
 Department of Mechanical Engineering, Technische Universiteit Eindhoven
 P.O. Box 513, 5600 MB Eindhoven, The Netherlands.
 Email: T.A.C.v.Keulen@tue.nl

1 Introduction

Hybrid Electric Vehicles (HEVs) employ several power sources instead of one. The main advantage of HEVs is that the vehicle's kinetic and potential energy can be (partially) recovered and stored during braking or when driving down-hill. The power request in HEVs is influenced widely by, e.g., changing vehicle mass and route characteristics. However, an increasing number of sensors and information systems enable prediction of the future power requirements, such that the energy usage can be optimized.

2 Problem Definition

The Energy Management Strategy (EMS) governs the power split of the driver power request between the engine, electric machine and service brakes, fulfilling

$$P_{request}(t) = P_{EM}(t) + P_{engine}(t) + P_{brake}(t). \quad (1)$$

Objective of the EMS in HEVs is twofold; i) maximize kinetic and potential energy recovery, ii) optimally use the stored energy. For an upcoming route, energy optimal deceleration trajectories are constructed. Optimal energy usage can be obtained by solving

$$\min_{P_{EM}(t)} \int_0^{t_f} \dot{m}_{fuel}(P_{EM}, t) dt, \quad (2)$$

$$s.t. : \int_0^{t_f} P_{battery}(P_{EM}, t) dt = SOC_{end} - SOC_{initial}. \quad (3)$$

Besides (3), (2) is subject to several component size limitations. Using the method of Lagrange, (2) and (3) can be rewritten by introducing the Lagrange multiplier $\hat{\lambda}$

$$\min_{P_{EM}(t), \hat{\lambda}} \left(\dot{m}_{fuel}(P_{EM}) + \hat{\lambda} P_{battery}(P_{EM}) \right). \quad (4)$$

3 Predictive Energy Management

Figure 1 shows a schematic representation of the setup proposed in [1]. Route information can be derived from Geographical Information Systems (GIS) in combination with a routeplanner and GPS. Using a *trajectory builder*, the future power request trajectory $\hat{P}_{request}(t)$ can be predicted. Hereby, it is assumed the current vehicle mass \hat{m} , and road load force $\hat{F}_{rl}(v)$ can be estimated.

Dynamic Programming (DP) is used to solve the constraint

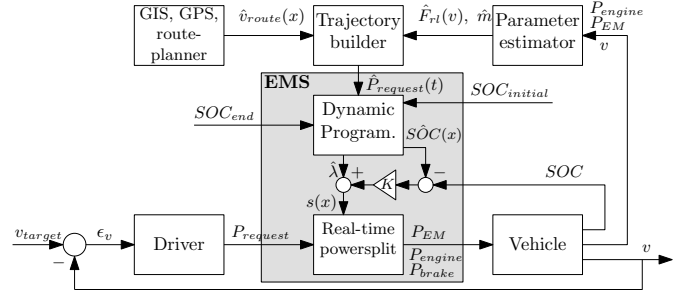


Figure 1: Energy management topology.

equation (2) for $\hat{P}_{request}(t)$. Output of the DP algorithm is $\hat{\lambda}$ and a predicted battery state-of-charge $\hat{SOC}(x)$ trajectory as function of distance x . DP calculations are computationally heavy and the actual $P_{request}$ is not exactly known in advance. Therefore, $\hat{\lambda}$ is calculated iteratively and $\hat{\lambda}$ is adjusted for changing conditions by feedback on the actual battery state-of-charge SOC

$$s(x) = \hat{\lambda} + K(\hat{SOC}(x) - SOC). \quad (5)$$

Here, K is a constant feedback gain. Substitution of $\hat{\lambda}$ in (4) by $s(x)$ is proposed, providing a real-time power split determination with little computational effort, just solving (4) for the next $P_{EM}(t_{k+1})$ only.

4 Simulation Results

The table below shows the hybrid fuel saving potentials, compared to a conventional vehicle on a city route. Route optimization provides a large improvement in obtainable savings. Besides, the vehicle mass has considerable influence on the energy saving potential. The proposed control structure enables adaption to changing operating conditions.

	original route	optimized route
empty vehicle 9 Mg	-7.7 %	-11.7 %
loaded vehicle 18 Mg	-8.9 %	-17.0 %

References

- [1] T. van Keulen, B. de Jager, A. Serrarens, M. Steinbuch. Energy Management in Hybrid Electric Trucks Using Route Information. *Les Rencontres Scientifiques de l'IFP - Advances in Hybrid Powertrains*, Rueil-Malmaison, France, 25-26 November 2008.

Tracking in WiMAX Networks depending on RSS-based measurements

Mussa Bshara

Vrije Universiteit Brussel, dept. ELEC,
Pleinlaan 2, B1050 Brussels, BELGIUM
mbshara@vub.ac.be

Leo Van Biesen

Vrije Universiteit Brussel, dept. ELEC,
Pleinlaan 2, B1050 Brussels, BELGIUM
lvbiesen@vub.ac.be

1 Abstract

Tracking in WiMAX networks is gaining a lot of interest; especially after the mobile WiMAX became one of the emerging technologies that promote low-cost deployment and evolving to provide IP-based services of high mobility including providing location-based services (LBS). The SCORE values are RSS-based values, used by the standard WiMAX modems to evaluate the connection quality between the subscriber station (SS) and the available base stations (BSs). The advantage of using the SCORE values is the possibility to obtain them for all the available BSs simultaneously and without adding any extra software or hardware. But the disadvantage lies in their low accuracy comparing to the received signal strength (RSS) values.

2 Tracking using particle filters

Two particle filters were used to track the target (user) [1],[2]. The first one exploited the target dynamic information and the second filter exploited the public road network information in addition to the dynamic information.

2.1 State Models

The first particle filter uses a classical (nearly) constant velocity model with state $x_k = [p_{k+1}^x p_{k+1}^y v_{k+1}^x v_{k+1}^y]^T$ where variables p and v denote the position and velocity of the target respectively. The motion model is given

$$\begin{bmatrix} p_{k+1}^x \\ p_{k+1}^y \\ v_{k+1}^x \\ v_{k+1}^y \end{bmatrix} = \begin{bmatrix} \mathbf{I}_2 & T_{k+1}\mathbf{I}_2 \\ \mathbf{0} & \mathbf{I}_2 \end{bmatrix} \begin{bmatrix} p_k^x \\ p_k^y \\ v_k^x \\ v_k^y \end{bmatrix} + \begin{bmatrix} \frac{T_{k+1}^2}{2}\mathbf{I}_2 \\ T_{k+1}\mathbf{I}_2 \end{bmatrix} w_{k+1} \quad (1)$$

where w_k is a two dimensional white Gaussian noise with zero mean. The second particle filter makes use of the road database information and uses a reduced order motion model [3]. The state of the particle filter is denoted by x_k^r where r stands for emphasizing road-information. The following model is used for the dynamics of x_k^r .

$$\begin{bmatrix} p_{k+1}^r \\ v_{k+1}^r \\ i_{k+1}^r \end{bmatrix} = f^r \left(\begin{bmatrix} p_k^r \\ v_k^r \\ i_k^r \end{bmatrix}, \mathcal{J}_{RN}, w_{k+1}^r \right) \quad (2)$$

where

$$\begin{bmatrix} p_{k+1}^r \\ v_{k+1}^r \end{bmatrix} = \begin{bmatrix} 1 & T_{k+1} \\ 0 & 1 \end{bmatrix} \begin{bmatrix} p_k^r \\ v_k^r \end{bmatrix} + \begin{bmatrix} \frac{T_{k+1}^2}{2} \\ T_{k+1} \end{bmatrix} w_{k+1}^r \quad (3)$$

2.2 Measurement Models

The measurement update is the same for both particle filters. At a single time instant t_k , the measurement vector is in the following form.

$$y_{t_k} = [V_1 \ V_2 \ \dots \ V_{N_{BS}}]^T \quad (4)$$

N_{BS} is the number of base stations. The values V_j is the corresponding scalar RSS (SCORE) value detected from the j th base station. the results are shown in figure 1.

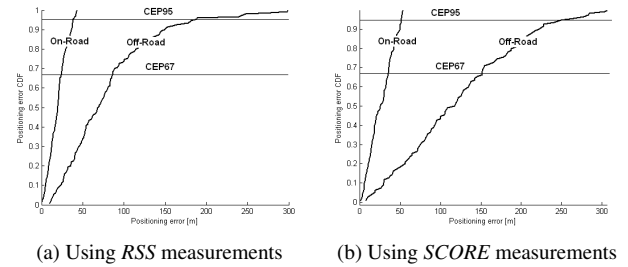


Figure 1: Using motion model with road information (on-road) and without road information (off-road)

References

- [1] M. Nabaee, A. Pooyafard, and A. Olfat, "Enhanced object tracking with received signal strength using kalman filter in sensor networks", International Symposium on Telecommunications, pp. 318-323, 2008.
- [2] A. Doucet, N. de Freitas, and N. Gordon, Eds., Sequential Monte Carlo Methods in Practice. Springer Verlag, 2001.
- [3] Y. Bar-Shalom, X. R. Li, and T. Kirubarajan, Estimation with Applications to Tracking and Navigation. New York: Wiley, 2001.

Stability Analysis of Networked Control Systems using a Switched Linear Systems Approach

M.C.F. Donkers¹, L. Hetel², W.P.M.H. Heemels¹, N. van de Wouw¹, M. Steinbuch¹

¹Department of Mechanical Engineering

Eindhoven University of Technology

P.O.Box 513, 5600 MB Eindhoven, The Netherlands

{m.c.f.donkers,w.p.m.h.heemels,n.v.d.wouw,m.steinbuch}@tue.nl

²Automatic Control Laboratory

École Centrale de Lille

Cité Scientifique - BP 48, 59651 Villeneuve d'Ascq Cedex, France

laurentiu.hetel@ec-lille.fr

1 Introduction

A Networked Control System (NCS) is a system that operates over a shared real-time network. Because of typical network characteristics, the control system has to deal with (i) quantisation of the signals, (ii) varying transmission delays (iii) varying sampling intervals, and (iv) communication constraints, i.e., not all sensors and control values can be transmitted at any time.

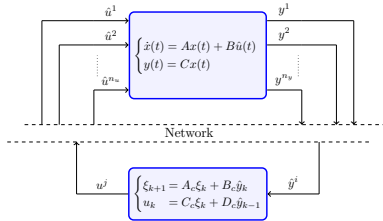


Figure 1: Networked Control System block diagram

Stability of the NCS subject to (iii) and (iv) can be guaranteed if the controller stabilises the non-networked system and the sampling intervals are sufficiently small (see, e.g., [?, ?]). By explicitly exploiting the linearity of the systems under study and taking a discrete time switched systems approach for the purpose of stability analysis, we obtain less conservative results.

2 NCS Model

Consider the NCS as given in Fig. 1, in which a continuous time plant is controlled by a discrete time controller. Because of the network imperfections the actual input of the plant \hat{u} and the controller \hat{y} are not equal to u and y , respectively.

Which sensor or actuator communicates its values is dictated by the protocol. We consider the so-called Try-Once-Discard (TOD) protocol, i.e.,

$$\sigma_k = \arg \max(\|y_k^1 - \hat{y}_k^1\|, \dots, \|y_k^{n_y} - \hat{y}_k^{n_y}\|, \|u_k^1 - \hat{u}_k^1\|, \dots, \|u_k^{n_u} - \hat{u}_k^{n_u}\|).$$

where y_k and u_k denote the measured output and the controller output, respectively, at transmission k and \hat{y}_k and \hat{u}_k the previously sent values. By combining the

plant, controller and the network effects, we obtain an uncertain switched closed loop system of the following form:

$$\bar{x}_{k+1} = \tilde{A}_{h_k, \sigma_k} \bar{x}_k,$$

where \bar{x}_k denotes the state of the NCS, h_k the sampling interval, and σ_k the protocol.

3 Convex Overapproximation

Since verifying stability for all $h \in [h, \bar{h}]$ would require to check stability for infinitely many possible sequences of (h_0, h_1, \dots) , we tightly overapproximate the system by

$$\bar{x}_{k+1} = \left(\sum_{l=1}^M \alpha_l \bar{A}_{l, \sigma} + \alpha_l \bar{B}_l \Delta \bar{C}_\sigma \right) \bar{x}_k,$$

where $\alpha \in \mathcal{A} = \{\alpha \in \mathbb{R}^M \mid \sum_{l=1}^M \alpha_l = 1, \alpha_l \geq 0\}$ and $\Delta \in \mathbf{\Delta} = \{\Delta \in \mathbb{R}^{n \times n} \mid \|\Delta\| \leq \gamma\}$, are both time-varying, such that

$$\{\tilde{A}_{h, \sigma} \mid h \in [h, \bar{h}]\} \subseteq \{\sum_{l=1}^M \alpha_l \bar{A}_{l, \sigma} + \alpha_l \bar{B}_l \Delta \bar{C}_\sigma \mid \alpha \in \mathcal{A}, \Delta \in \mathbf{\Delta}\}.$$

For these systems, we can guarantee stability by verifying a finite number of matrix inequalities [?].

4 Illustrative Example

To illustrate the theory, we consider the benchmark example of a batch reactor. The results are shown in Table 1.

Table 1: Allowable Range of Transmission Intervals

Method	Range
Simulation based, obtained in [?]	$h \in (0, 0.06]$
Theoretical, obtained in [?]	$h \in (0, 10^{-5}]$
Theoretical, obtained in [?]	$h \in (0, 0.0108]$
Newly obtained theoretical bound [?]	$h \in [10^{-4}, 0.032]$

References

- [1] D. Carnevale, A.R. Teel, D. Nešić: A Lyapunov proof of improved maximum allowable transfer interval for networked control systems. *IEEE Trans. on Autom. Contr.*, 2007.
- [2] M.C.F. Donkers, L. Hetel, W.P.M.H. Heemels, N.v.d. Wouw, M. Steinbuch: Stability analysis of networked control systems using a switched linear systems approach. in *Hybrid Systems: Comp. and Contr.*, 2009.
- [3] G.C. Walsh, H. Ye, L.G. Bushnell: Stability analysis of networked control systems. *IEEE Trans. on Contr. Syst. Tech.*, 2002.

Modeling for control of an inflatable space reflector

T. Voß, J.M.A Scherpen

University of Groningen, Faculty of Mathematics & Natural Sciences,
Nijenborgh 4, 9747 AG Groningen, The Netherlands
t.voss@rug.nl, J.M.A.Scherpen@rug.nl

1 Introduction

In this paper we show how to discretize a distributed model of the dynamics of an inflatable space reflector in port-Hamiltonian (pH) form. This model can then be used to design a controller for the shape of the inflatable structure. Inflatable structures have very nice properties, suitable for aerospace applications. We can construct e.g. a huge light weight reflector for a satellite which consumes very little space in the rocket since a reflector can be inflated when the satellite is in the orbit. The starting point of the control design is modeling for control, in this case lumped pH modeling, since these models offer a clear structure for control design. We will show how to derive a nonlinear finite dimensional pH model of a 1-D Euler-Bernoulli beam with piezo actuation. In the future we will also focus on 2-D models.

2 Infinite dimensional Model

The infinite dimensional model of a piezo-electric Euler-Bernoulli beam is given as

$$\begin{bmatrix} \dot{\mathbf{p}} \\ \dot{\mathbf{u}}' \\ \dot{E} \end{bmatrix} = \mathbf{J}\nabla H + \mathbf{B} \begin{bmatrix} \mathbf{f}_u \\ \mathbf{f}_w \\ I_e \end{bmatrix} \quad (1)$$

$$\mathbf{y} = \mathbf{B}^\top \nabla H,$$

where

$$\mathbf{J} = \begin{bmatrix} 0 & \frac{\partial}{\partial x} \mathbf{I}_3 & \mathbf{g} \\ \frac{\partial}{\partial x} \mathbf{I}_3 & 0 & 0 \\ -\mathbf{g}^* & 0 & 0 \end{bmatrix}, \mathbf{g} = [g_1(y), g_2(y), g_3(y)]^\top$$

$$\mathbf{B}^\top = \begin{bmatrix} 2d_b & 0 & -2d_b h_b & 0 & 0 & 0 & 0 \\ 0 & 2d_b & 0 & 0 & 0 & 0 & 0 \\ 0 & 0 & 0 & 0 & 0 & 0 & \frac{1}{\varepsilon^e A_e} \end{bmatrix}$$

This system is an infinite dimensional port-Hamiltonian model. To design a controller for this system we have now two possibilities. We can design the controller for the infinite dimensional model and then spatially discretize the controlled system. Or we can first spatially discretize the system to end up with a finite dimensional model of the system and then design a controller for the system. Here we want to apply the later idea.

3 Spatial discretization

The spatial discretization of the system has to be done in such a way that the discretization of the system preserves

the structure of the system. This makes it impossible to use standard discretization techniques like finite element or finite difference methods. Instead we use an adapted discretization method [1] which preserves the structure of the system. The method uses some ideas of the finite element method. The idea behind this method can be described in the following way.

First we rewrite our equations of motion in terms of differential geometry. Then we identify all one and zero forms. For example the strain is a one form because we have to integrate over an interval to derive the elongation (strain) of the interval, while the stress is a zero form because we can measure the force acting at any point. This one forms are then approximated by a combination of functions and one/zero forms, e.g. we approximate the strain (one form) on the interval $Z_{ab} = [a, b]$ in the following way

$$\varepsilon(z, t) = \varepsilon_{ab}(t) \omega_{ab}^\varepsilon(z)$$

where it holds that

$$\int_a^b \varepsilon(z, t) = \varepsilon_{ab}(t)$$

The stress (zero form) can be approximated as

$$\sigma(z, t) = \sigma_a(t) \omega_a^\sigma(z) + \sigma_b(t) \omega_b^\sigma(z)$$

where it holds that

$$\sigma(a, t) = \sigma_a(t), \sigma(b, t) = \sigma_b(t)$$

This gives certain constraints on the approximating one/zero forms. The next step is to integrate the approximated functions over the interval Z_{ab} . Then we have to define ports at the boundaries where the finite element exchanges energy with connected finite elements. This makes it then possible to define an interconnection structure of the system such that the final system is an finite dimensional approximation of the dynamics on the interval Z_{ab} . The so derived finite dimensional system is still in port-Hamiltonian form.

4 Acknowledgments

We would like to thank the MicroNed programme for the funding of the research.

References

- [1] G. GOLO, V. TALASILA, A.J. VAN DER SCHAFT, B.M. MASCHKE, *Hamiltonian discretization of boundary control systems*, Automatica, 40, pp. 757-771, 2004

Model based optimisation of tubular reactors for the production of low-density polyethylene

Peter Van Erdeghem, Filip Logist and Jan F. Van Impe
BioTeC - Chemical and Biochemical Process Technology and Control
Department of Chemical Engineering
Katholieke Universiteit Leuven
W. de Croylaan 46, B-3001 Leuven, Belgium
Email: {peter.vanerdeghem, filip.logist, jan.vanimpe}@cit.kuleuven.be

1 Introduction

Due to market saturation, global competition and a worldwide financial crisis, today's chemical industry strives for more efficient processes in order to reduce the production costs without disregarding safety and environmental limitations. Mathematical process models and model based optimisation techniques have proven over the past decades to be extremely valuable tools for optimising the operation, control and design of chemical processes, resulting in the desired profit improvement within the given safety and environmental restrictions. Application of these model based techniques to tubular reactors, important workhorses in process industry, e.g., for the production of low-density polyethylene (LDPE), paves the way to improved operation policies and enhanced tubular reactor designs.

2 Project

This project deals with a model based optimisation and design of tubular reactors for the production of low-density polyethylene. Based on information received from the industrial partner and found in literature ([2, 3, 7, 8]) a complex model with numerous (un)correlated differential and algebraic equations is obtained. This complex model consists of mass and energy balances, as well as of detailed relations for reaction kinetics [4, 5], heat transfer phenomena [6] and physical properties [1]. Based on model reduction techniques or by doing an extensive sensitivity analysis on the unknown model parameters, the model is first condensed to a basic model which still contains sufficient essential information and characteristics of the LDPE production process. Depending on the different research objectives, in which the emphasis can be put on either the heat transfer, the reaction kinetics or specific design specifications, this reduced model will be further adjusted to the required level of detail. These adjustments result inevitably in the re-increase of the model complexity, but also yield tailored and well defined optimisation problem.

3 Acknowledgments

Work supported in part by SABIC-Europe (The Netherlands) and Projects OT/03/30 and EF/05/006 (Center-of-Excellence Optimization in Engineering) of the Research Council of the Katholieke Universiteit Leuven and the Belgian Program on Interuniversity Poles of Attraction, initiated by the Belgian Federal Science Policy Office. The scientific responsibility is assumed by its authors.

References

- [1] C.P. Bokis, S. Ramanathan, J. Franjione, A. Buchelli, M.L. Call, and A.L. Brown. Physical properties, reactor modeling and polymerization kinetics in the low-density polyethylene tubular reactor process. *Industrial and Engineering Chemistry Research*, 41(5):1017–1030, 2002.
- [2] A. Brandolin, M.H. Lacunza, P.E. Ugrin, and N.J. Capiati. High pressure polymerization of ethylene. An improved mathematical model for industrial tubular reactors. *Polymer Reaction Engineering*, 4(4):193–241, 1996.
- [3] A. Brandolin, E.M. Valles, and J.N. Farber. High pressure tubular reactors for ethylene polymerization optimization aspects. *Polymer engineering and science*, 31(5):381–390, 1991.
- [4] M. Häfele, A. Kienle, M. Boll, C.-U. Schmidt, and M. Schwibach. Modeling and analysis of a plant for the production of low density polyethylene. *Computers and Chemical Engineering*, 31(2):51–65, 2006.
- [5] C. Kiparissides. Polymerization reactor modeling: a review of recent developments and future directions. *Chemical Engineering Science*, 51(10):1637–1659, 1996.
- [6] M.H. Lacunza, P.E. Ugrin, A. Brandolin, and N.J. Capiati. Heat transfer coefficient in a high pressure tubular reactor for ethylene polymerization. *Polymer Engineering and Science*, 38(6):992–1013, 1998.
- [7] F.Z. Yao, A. Lohi, S.R. Upreti, and R. Dhib. Modeling, simulation and optimal control of ethylene polymerization in non-isothermal, high-pressure tubular reactors. *International Journal of Chemical Reactor Engineering*, 2(2), 2004.
- [8] B.J. Yoon and H.K. Rhee. A study of the high-pressure polyethylene tubular reactor. *Chemical Engineering Communications*, 34(6):253–265, 1985.

Modeling and validation of the parameters of a quad cable for DSL applications

Wim Foubert, Carine Neus, Leo Van Biesen, Yves Rolain

Vrije Universiteit Brussel, Pleinlaan 2, 1050 Brussels, Belgium
Department of Fundamental Electricity and Instrumentation (ELEC),
Email: wfoubert@vub.ac.be

1 Introduction

New digital subscriber line (DSL) technologies are developing in order to meet the ever increasing bandwidth demand of the users. One very promising approach injects 'common mode' signals that superimpose a signal on two regular differential pairs. This technique requires new reliable models for the telephony cables. The models are based on the Multiconductor Transmission Lines theory. In this abstract it is shown how the parameters of a quad (cable with four conductors in a square formation) can be modelled. Measurements have been done for the validation.

2 Modeling of the parameters

The Multiconductor Transmission Lines theory is used to model a transmission line. Figure 1 shows the schematic diagram associated to the telegraph equation.

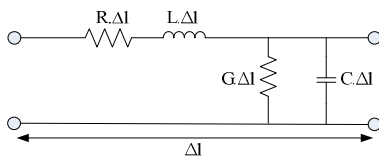


Figure 1: Infinitesimal section of length Δl of a transmission line

Good approximations for the different physical parameters R , L , G and C are indispensable. This problem is decoupled.

First we consider the longitudinal propagation to determine the resistance R and the inductance L . An analytical expression, based on the distributed character, has been derived by Belevitch [1]. This series impedance has been validated with measurements as described in [2].

For the transversal problem, different orders of magnitude are involved. No analytical expression exists to characterize the conductivity G and the capacitance C . A quasi-stationary approximation is made in the transversal plane. Both C and G are independent of the frequency.

Since G depends only on the dielectric, and since this medium is considered to be uniform, we can safely assume that G is constant.

To determine the capacity C , we follow the method as described in [3]. Since the charge Q is related to the voltage V by the capacitance matrix, we need good approximations for Q and V . To describe the charge

distribution around the i -th wire, a Fourier series in the peripheral angle θ_i is used (figure 2).

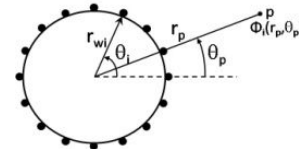


Figure 2: Determination of the charge on a conductor

The total charge q_i on the i -th conductor is obtained by integrating the charge density around the wire periphery. The voltage V_i is defined as the difference between the potential Φ_i and a reference potential Φ_0 . The ratio of the matrices Q and V is given by the capacitance matrix C .

3 Validation

Since the four parameters are known, we will use them to model the S_{11} parameter of a quad. The simulated S_{11} curve can be verified with S_{11} measurements. Therefore, a setup, consisting of four parallel copper wires, was built. To measure the S_{11} curve, we put a signal on two wires. The two other conductors will serve as return path. Figure 3 shows the S_{11} measurement for an open termination that will be used for the validation.

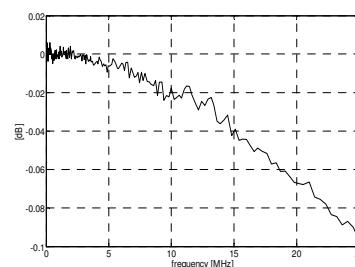


Figure 3: S_{11} measurement for an open termination

4 Conclusions

This abstract explains how the physical parameters of a quad cable should be calculated. Those parameters are necessary to set up a full transmission line model for a quad which take also the common mode signals into account. This will lead to faster DSL technology.

References

- [1] V. Belevitch, Philips Research Reports "Theory of the proximity effect in multiwire cables", pp. 16-43, 1977
- [2] W. Foubert, P. Boets, L. Van Biesen, C. Neus, "Modeling the Series Impedance of a Quad Cable for Common Mode DSL Applications", Proceedings I2MTC-08, pp. 250-253, May 2008, Victoria, Canada
- [3] C.R. Paul, "Analysis of Multiconductor Transmission Lines", John Wiley & Sons, Inc., 1994

Model based kinetics estimation for crystallization processes

Jochem Visser

Department of Electrical Engineering
Technische Universiteit Eindhoven
P.O. Box 513, 5600 MB Eindhoven
The Netherlands
Email: j.a.w.visser@tue.nl

Siep Weiland

Department of Electrical Engineering
Technische Universiteit Eindhoven
P.O. Box 513, 5600 MB Eindhoven
The Netherlands
Email: s.weiland@tue.nl

1 Introduction

Batch crystallization processes form the most important technology used for separation of the Active Pharmaceutical Ingredients from solutions in pharmaceutical industries. The process is widely known as irreproducible and sensitive to environmental conditions and forms bottleneck in the production process. Within this project model based control technology will be employed to improve conditioning and therefore improve reproducibility these processes. The growth rate of crystals is assumed to be a important quality parameter of the process. This presentation considers an attempt to estimate of the crystal growth rate based on line measurements of the crystal size distribution.

2 Problem Description

A batch crystallizer is a multi-phase system, which can be modeled using physical relations for the solid phase, liquid phase and energy balance. The state of the solid phase is characterized by the crystal properties. Typically a number density function $n(L, t)$ for the characteristic crystal length L is introduced and its evolution is described by the partial differential equation:

$$\frac{\partial n(L, t)}{\partial t} + G(C(t), T(t)) \frac{\partial n(L, t)}{\partial L} = 0 \quad (1)$$

$$n(L, 0) = n_0(L), \quad n(0, t) = b(t) \quad (2)$$

Here G is the unknown growth rate function, which depends on the concentration $C(t)$ and temperature $T(t)$. The concentration and temperature are assumed to be measurable. The function b represents the birth of crystals, but is assumed to be zero for simplicity. By use of modern sensors it is possible to obtain an on-line estimate $\hat{n}(L, t)$ of the number density function $n(L, t)$. For research purposes datasets $n(L, t)$ have been generated by use of the CE/SE method [1]. A possible measured $n(L, t)$ is shown in figure 1.

3 Model based approach

The measurement of $n(L, t)$ is usually unreliable at small crystal sizes and distorted by noise. The goal of our research is to develop a method for estimation of $G(t)$ which takes the conservative properties of the underlying dynamic sys-

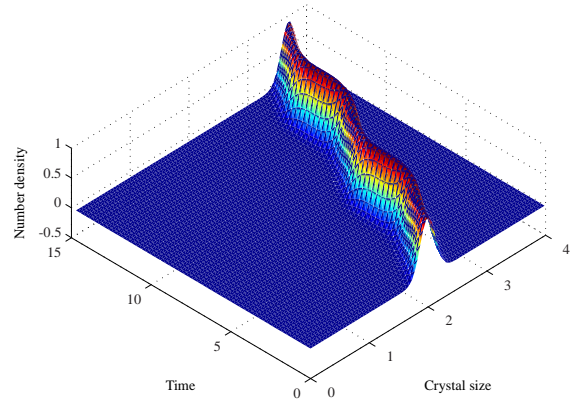


Figure 1: Time dependent number density distribution with $G(t) = 0.1 + 0.1 \sin(t)$.

tem into account. When this is done we attempt to find a functional relation between $G(t)$, $C(t)$ and $T(t)$.

The function $n(L, t)$ can be approximated by a series expansion on finite number of basis functions $[\phi_0(L), \phi_1(L) \dots]$ i.e. $n(L, t) = \sum_{i=0}^{\infty} \alpha_i(t) \phi_i(L)$. By use of Galerkin projection the system 1 can be approximated by a finite dimensional time variant state space system with the structure:

$$\dot{\alpha}(t) = G(t)A\alpha(t) + Bu(t) \quad (3)$$

This representation of the system can be analyzed by use of traditional methods for time variant systems.

4 Acknowledgments

This project is carried out in cooperation with the Delft University of Technology, Groups P&E and DSCS and the Dutch Separation Technology Institute.

References

- [1] SC. Chang, The Method of Space-Time Conservation Element and Solution Element-A New Approach for Solving the Navier-Stokes and Euler Equations, J. Comp. Phys. 1995, vol 119, p295-324

Compartmental model of a bubble column

S. Djordjevic, P.M.J. Van den Hof, O.H. Bosgra, D. Jeltsema
Delft Center for Systems and Control, Delft University of Technology
Mekelweg 2, 2628 CD Delft, The Netherlands
Email: S.Djordjevic@tudelft.nl

1 Introduction

Over the last few decades, control of fluid dynamics has become a problem of high interest in the control community [1]. This interest is due to the variety of industrial applications (e.g., transport of fluids in pipes, mixing of fluids in chemical reactors). The goal of flow control is to lower the operational expenses and improve the process performances. In general, the motion of fluids is described by an enormous number of states in order to model a microscopic behaviour of the flow. However, there is a number of complex issues underlying the microscopic flow control problem such as implicit modelling, input-output structure, numerical stability and simulation time. In this work, we introduce a macroscopic observation of fluids in a bubble column as an initial research for deriving a compartmental model for fluid flows. The model can be used to investigate model-based control strategies for bubble columns and can be beneficial for many practical implementations.

2 The dynamical model

For a bubble column, the flow model is usually formulated in terms of two sets of conservation equations for each fluid separately, after which the equations are coupled via interactive terms [2]. A one-dimensional form of the model is based on the conservation equations only in the x -direction and can be written in matrix form as follows [3]

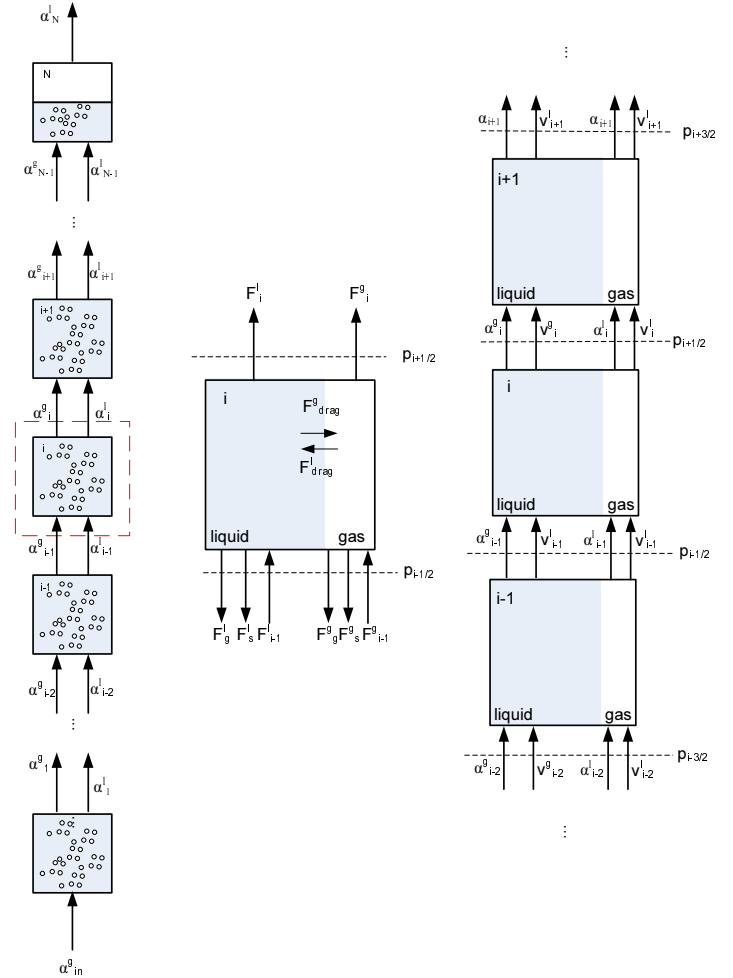
$$\mathbf{E} \frac{\partial \Phi}{\partial t} + \mathbf{A} \frac{\partial \Phi}{\partial x} = \mathbf{c}, \quad (1)$$

with $\Phi = [\alpha_g \ v_g \ v_l]^T$ where α_g is the volume occupied by the gas phase, v_g is the velocity of the gas phase and v_l is the velocity of the liquid phase. The system matrices are given as

$$\mathbf{E} = \begin{bmatrix} 1 & 0 & 0 \\ 1 & 0 & 0 \\ 0 & \rho_g & -\rho_l \end{bmatrix}, \quad \mathbf{A} = \begin{bmatrix} v_g & \alpha_g & 0 \\ v_l & 0 & -1 + \alpha_g \\ 0 & \rho_g v_g & -\rho_l v_l \end{bmatrix},$$

$$\mathbf{c} = \begin{bmatrix} 0 \\ 0 \\ g(\rho_g - \rho_l) + \beta(v_g - v_l)(\frac{1}{\alpha_g} + \frac{1}{1 - \alpha_g}) \end{bmatrix}.$$

The compartmental model of the bubble column is obtained by dividing the total volume into a several compartments which are connected in a series.



In this presentation, we introduce the compartmental model of bubbly flow and discuss some stability issues of the derived model.

References

- [1] T.R. Bewley, Flow control: New challenges for a new renaissance, *Progress in Aerospace Sciences*, vol. 37, pp. 21-58, 2001.
- [2] D.A. Drew, Mathematical modeling of two-phase flow, *Ann. Rev. Fluid Mech.*, vol. 15, pp. 261-291, 1983.
- [3] J.W. Park, D.A. Drew, and R.T. Lahey, Jr., The analysis of void wave propagation in adiabatic monodispersed bubbly two-phase flows using an ensemble averaged two-phase model, *International Journal of Multiphase Flow*, vol. 24, pp. 1205-1244, 1998.

Modeling and simulating the sawtooth instability in Nuclear Fusion

Gert Witvoet

Technische Universiteit Eindhoven

Email: G.Witvoet@tue.nl

Maarten Steinbuch

Technische Universiteit Eindhoven

Email: M.Steinbuch@tue.nl

Egbert Westerhof

FOM - Institute for Plasma Physics

Email: E.Westerhof@rijnhuizen.nl

Niek Doelman

TNO Science and Industry

Email: Niek.Doelman@tno.nl

Introduction

Nuclear fusion plasmas are subject to various instabilities, one of which is the *sawtooth instability*: the repetitive phenomenon of central plasma temperature increases, followed by sudden crashes, see Figure 1. These crashes limit the central plasma temperature, but also removes helium ash from the plasma core. By **controlling the sawtooth period** we can optimize between these effects. Understanding the dynamics of the sawtooth is then a first but crucial step.

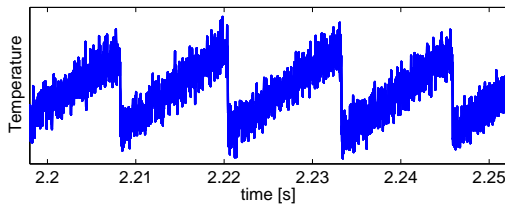


Figure 1: Sawteeth in central temperature measurements

Sawtooth modeling

In a tokamak fusion reactor the hot plasma is confined using toroidal and poloidal magnetic fields \vec{B}_{tor} and \vec{B}_{pol} , see Figure 2. The sawtooth instability is believed to be related to these fields. The most important parameters in explaining sawteeth are the *safety factor* q (magnetic ‘twist’ in \vec{B} or ratio between \vec{B}_{tor} and \vec{B}_{pol}) and *magnetic shear* (radial derivative of the ‘twist’).

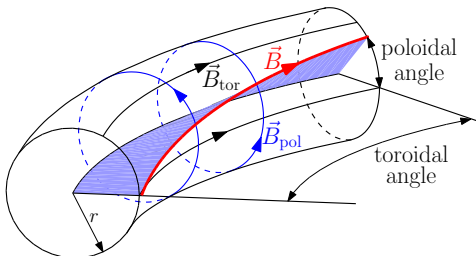


Figure 2: Toroidal and poloidal field lines

Porcelli’s model [1] predicts the occurrence of a sawtooth crash, which can be related to a critical shear value at $q = 1$. Kadomtsev’s model [2] describes what happens at such a crash, i.e. B_{pol} and the temperature T are ‘reset’, such that both are flattened over r . In between crashes B_{pol} and T evolve according to a diffusion and energy PDE respectively.

The TEXTOR environment

The derived sawtooth model is focussed on the TEXTOR tokamak in Jülich, where experiments will be done in the near future. On TEXTOR sawteeth are detected using 6 temperature measurements, while actuation is done via a local current drive J_{CD} (which influences B_{pol} , q and the shear).

Sawtooth simulations

This TEXTOR-focussed model has been implemented in Matlab Simulink. The simulations show realistic sawtooth periods of around 17ms. Figure 3 shows the effect of the current drive J_{CD} on the steady state sawtooth period. Actuation inside the plasma core reduces the period, whereas current drive outside the core increases the period. Similar behavior can be observed in past TEXTOR experiments.

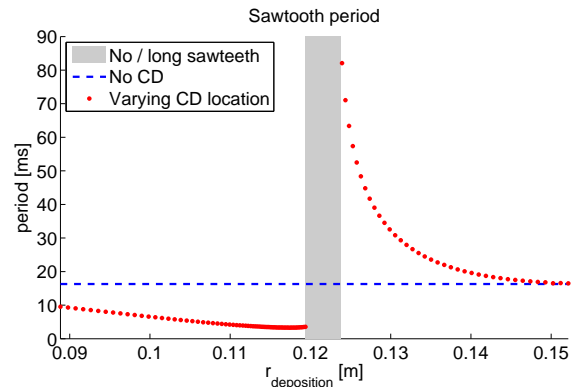


Figure 3: Effect of the current drive deposition location on the sawtooth period

Future research

More simulations and analyses will be performed to gain insight in the system. TEXTOR experiments will be done to check the model and perform system identifications. Ultimately, a controller will be defined and tested (in simulation and on TEXTOR) to regulate the sawtooth period.

References

- [1] O. Merkulov, *Control of plasma profiles and stability through localised ECCD*, PhD thesis, 2006.
- [2] J.A. Wesson, *Tokamaks (third edition)*, Oxford, 2004.

PRC-BASED PHASE RESETTING FOR NONLINEAR OSCILLATORS

Efimov D., Sepulchre R.

Systems and Control @ Systems and Modeling
Department of Electrical Engineering and Computer Science,
B28 Université de Liège, B-4000 Liege Sart-Tilman, Belgium
efimov@montefiore.ulg.ac.be, r.sepulchre@ulg.ac.be

1. Introduction

The problems of phase resetting by external (periodical) input consists in assignment of a desired value for phase applying some (may be periodical) control input [2, 4, 5]. This problem is frequently addressed in oscillators synchronization framework, when external input is an output of another oscillator, which phase becomes desired for resetting [5].

This problem is rather old and practically important [6]. In control theory literature there exist a few approaches to the problem, among them it is necessary to mention master-slave synchronization framework, optimal or predictive control application for phase resetting [1, 3], weak coupling approach [5], *phase resetting curve* (PRC) with Poincaré phase map approach [4]. The purpose of this work is to extend the latter one proposing new control strategy for impulses timing based on PRC.

2. Phase resetting map

Consider the following system:

$$\dot{\mathbf{x}} = \mathbf{f}(\mathbf{x}, u), \quad (1)$$

where $\mathbf{x} \in R^n$ is the state, $u \in R$ is the input, $\mathbf{f} : R^{n+1} \rightarrow R^n$ is a smooth function. It is assumed that for $u(t) \equiv 0$, $t \geq 0$ the system has asymptotically stable T -periodical solution $\gamma(t) = \gamma(t+T)$. The image of this solution in the state space is called limit cycle, for which we can define a scalar phase variable $\nu : R \rightarrow [0, 2\pi)$, that uniquely determines any solution of the system (1) on the cycle [2, 4, 5], $\dot{\nu} = \omega = 2\pi/T$. Thus, any solutions starting on the limit cycle can be characterized by initial phase $\nu_0 \in [0, 2\pi)$, then $\nu(t) = \omega t + \nu_0$.

Let initial conditions belong to the limit cycle with some $\nu_{old} \in [0, 2\pi)$, the input be an “impulse” with properties $u(t) \neq 0$, $0 \leq t \leq t_0 < T$ and $u(t) \equiv 0$, $t \geq t_0$. Then due to stability of the cycle the trajectory will return back with probably new phase $\nu_{new} \neq \nu_{old}$. The map, which tabulates the difference between values ν_{old} and ν_{new} , for all $\nu_{old} \in [0, 2\pi)$ and for the given “impulse” input, is called PRC [4, 5], i.e.

$$\nu_{new} = \nu_{old} + PRC(\nu_{old}). \quad (2)$$

Analytically PRC can be computed using linearization of the system (1) on the limit cycle [4].

Now assume that this “impulse” input is applied periodically with period T (note that $t_0 < T$), then from (2) the phase dynamics is described by the following discrete

nonlinear system [4]:

$$\nu_{i+1} = \nu_i + PRC(\nu_i), \quad \nu_0 = \nu_{old}, \quad (3)$$

where $i=1, 2, 3, \dots$ is the number of the current “impulse”. The map (3) is called Poincaré phase map, it ensures convergence of the phase to some zeros of (3) or PRC if any, i.e. to solutions $\nu_e \in [0, 2\pi)$ such, that $PRC(\nu_e) = 0$ [4].

3. New PRC control

Now assume that the “impulse” is repeated not with the fixed period T but with phase shifts $u_i \in [0, 2\pi)$, then

$$\nu_{i+1} = \nu_i + PRC(u_i), \quad \nu_0 = \nu_{old}, \quad (4)$$

and this is a controlled nonlinear scalar system. Applying control theory it is possible to design controls u_i providing resetting of the phase ν to any desired value.

We propose and examine two strategies: open loop (when u_i for all $i=1, 2, 3, \dots$ are calculated a-priori basing on the model (4) for derived PRC) and feedback one (when u_i are calculated for the model (4) basing on derived PRC and on-line measured ν_i).

Both strategies are successfully tested on several examples of biological oscillators (circadian oscillators, modified van der Pol oscillator). The advantage of the proposed approach consists in low dimension of PRC (it is a scalar map of scalar argument, which completely describes phase resetting dynamics by “impulse” input) and that PRC can be measured experimentally even for oscillators which have not well investigated detailed models.

References

1. Bagheri N., Stelling J., Doyle F.J. Circadian phase resetting via single and multiple control targets. *Comp. Biology*, 7(4), 2008, pp. 1–10.
2. Blekhnman I.I. *Synchronization in Science and Technology*. New York: ASME Press, 1988.
3. Forger D.B., Paydarfar D. Starting, stopping, and resetting biological oscillators: in search for optimum perturbations. *J. Theor. Biol.*, 230, 2004, pp. 521–532.
4. Izhikevich E.M. *Dynamical Systems in Neuroscience: The Geometry of Excitability and Bursting*. The MIT press, 2007.
5. Pikovsky A., Rosenblum M., Kurths J. *Synchronization. A Universal Concept in Nonlinear Sciences*. Cambridge: Cambridge University Press, 2001.
6. Tass P.A. *Phase Resetting in Medicine and Biology. Stochastic Modeling and Data Analysis*. Berlin: Springer Verlag, 1999.

Dynamical Positioning of Ship Motion; A nonlinear Regulation Problem

Shah Muhammad and Jacob van der Woude

Delft Institute of Applied Mathematics, Delft University of Technology

Mekelweg 4, 2628CD Delft, the Netherlands

E-mail: s.muhammad@tudelft.nl

1 Introduction

We study the nonlinear regulation problem of ship motion dynamics [1] in surge, sway, and yaw directions. We use a state space model. We write our state space model in the linear state dependent coefficient (SDC) form. Now the system matrices are state dependent. Specifically, our system matrices have a state dependency due to a single state component. The state space description of the system is given by

$$\begin{bmatrix} \dot{\boldsymbol{\eta}} \\ \dot{\mathbf{v}} \end{bmatrix} = \begin{bmatrix} O_3 & J(\boldsymbol{\psi}) \\ O_3 & -M^{-1}D \end{bmatrix} \begin{bmatrix} \boldsymbol{\eta} \\ \mathbf{v} \end{bmatrix} + \begin{bmatrix} O_3 \\ -M^{-1} \end{bmatrix} \mathbf{u}, \mathbf{x}_0 = \mathbf{x}(0). \quad (1)$$

Here $\boldsymbol{\eta}$, \mathbf{v} , and \mathbf{u} describe the position, velocity and control, respectively. $J(\boldsymbol{\psi})$ is the coordinate transformation matrix and M and D denote the inertia and damping matrices. This description of the system accounts for only the forces due to damping, inertia, and external control effects. At the moment we are not taking into account the environmental forces like affects of wind, waves etc. The first aspect that we consider is the global asymptotic stability. This means that we look for a control which can regulate the states to the stable equilibrium point of the system dynamics from any where in the state space of the system.

2 Global Asymptotic Stability Analysis

We know that a linear constant coefficients system is (globally) asymptotically stable if and only if the system matrix is Hurwitz (asymptotically stable). We extend this idea to nonlinear systems. From the literature we know that the assumption that the system matrix is Hurwitz is not enough, and we require additional assumptions to establish the global asymptotic stability of the nonlinear system. We control the system described in (1) by means of an LQ based feedback. The resulting closed loop system is continuous, periodic and Hurwitz for all $\boldsymbol{\psi}$. Based on simulation experiments, we believe that a nonlinear system whose system matrix satisfies the three assumptions, will have global asymptotic stability. We combine the Lyapunov stability theory and the LMI's to establish the global asymptotic stability of the special type of the nonlinear systems where the system matrices depend periodically on a single state component in a continuous way.

3 Fourier Series Interpolation Method

The second aspect that we consider arises from the aforementioned work. We find that the SDARE¹ based control law yields a continuous, Hurwitz, and periodic system matrix in the feedback dynamics corresponding to (1). The use of the SDARE based control law requires the online computation of the solution of the matrix Riccati equation. This is computationally an expensive job. We utilize the fact that the system matrix is piecewise smooth and periodic and give a Fourier series based method for the solution of the special type of the SDARE. We call our method as the Fourier series interpolation method. This method reduces the online computation cost by offline computing the Fourier coefficients.

4 Results and Perspectives

We study the global asymptotic stability of a nonlinear system whose system matrices depend on a single state component. We assume three conditions on the system matrices; continuity, being Hurwitz, and periodicity. The simulation results point out that these assumptions are sufficient for the global asymptotic stability of the nonlinear systems. However, the lyapunov theory and LMI based approach that we propose to establish the global asymptotic stability, prove to be a heuristic approach. It works fine for some systems but does not help for the system given in (1). More investigation into the details of the procedure are intended. We propose a Fourier series based interpolation method for the solution of the SDARE associated with the system dynamics given in (1). This method is useful in reducing the online computation cost for the solution of SDARE in an SDARE based feedback control law.

References

- [1] J. Snijders. Wave Filtering and Thruster Allocation for Dynamic Positioned Ships. Master thesis, Delft Institute of Applied Mathematics, 2005.

¹State dependent algebraic Riccati equation

State predictor based on synchronization applied to a mobile robot

Alejandro Alvarez-Aguirre*, Henk Nijmeijer
 Department of Mechanical Engineering
 Eindhoven University of Technology
 P.O. Box 513, 5600 MB Eindhoven
 The Netherlands
 Email: *a.a.alvarez@tue.nl

Toshiki Oguchi
 Department of Mechanical Engineering
 Tokyo Metropolitan University
 192-0397 Tokyo
 Japan

1 Introduction

The performance and stability of a control system can be directly affected by a time-delay located either in the inputs, the outputs or both. In the case of mobile robots, an input time-delay may become critical in different situations, such as when vision is used as the localization technique and a high frame per second rate is demanded, or when centralized control of multiple agents is desired, or even if very accurate regulation or tracking is required. Since the control laws derived from the mathematical models that include a time-delay are of a noncausal nature, a state predictor becomes necessary to implement them.

2 Application of a predictor based on synchronization

In [1], a state prediction method for nonlinear systems has been proposed. This method is based on anticipated synchronization exhibited by chaotic systems with time-delay and does not require numerical integration. The predictor estimates the future value of the system and the predictor's output $z(t)$ is used in place of the actual state of the system $q(t)$ in the feedback $u(t) = \gamma(\cdot)$. The prediction error is defined as $e(t) \triangleq z_\tau(t) - q(t)$, where $z_\tau(t) \triangleq z(t - \tau)$. The proposed control scheme is shown in Figure 1.

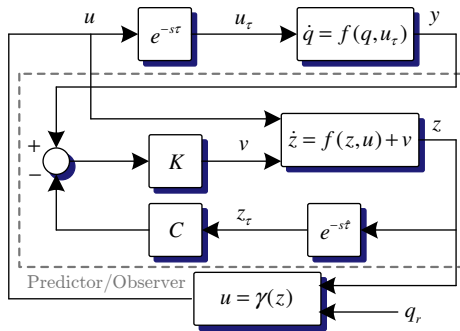


Figure 1: Predictor based on synchronization control scheme.

The predictor is applied to the posture kinematic model of a unicycle-type mobile robot, given by,

$$\dot{x} = v \cos \theta, \quad \dot{y} = v \sin \theta, \quad \dot{\theta} = \omega, \quad (1)$$

where the forward velocity v and the angular velocity ω are established as inputs.

Numerical simulations considering the control law proposed in [2] are shown in Figure 2.

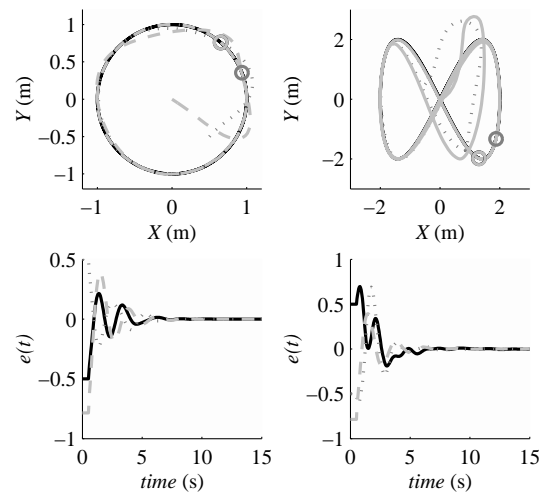


Figure 2: Workspace behavior and prediction error plots.

The upper plots show the reference (solid), predictor (dashed) and robot (dotted) behavior in the X-Y plane. The lower plots show the prediction error of each state for these trajectories, i.e. x (solid), y (dashed) and θ (dotted).

3 Conclusions and future work

The state predictor based on synchronization is capable of coping with disturbances and model or delay mismatches, and does not require numerical integration. Future work includes a formalization of the stability proofs in the current context and the implementation of the control scheme in an experimental setup.

References

- [1] T.Oguchi and H.Nijmeijer. Control of nonlinear systems with time-delay using state prediction based on synchronization. In *ENOC 2005*, pages 1150-1156, Eindhoven, The Netherlands, August 7-12, 2005.
- [2] E.Panteley, E.Lefeber, A.Loria, and H.Nijmeijer. Exponential tracking control of a mobile car using a cascaded approach. In *Proc. of the IFAC Workshop on Motion Control*, pages 221-226, Grenoble, France, 1998.

Improving the performance of a Drop-on-Demand Inkjet Printhead

Amol A. Khalate, Xavier Bombois, Robert Babuška

Delft Center for Systems and Control

Delft University of Technology, Mekelweg 2, 2628 CD Delft, The Netherlands

Email: {a.a.khalate,x.j.a.bombois,r.babuska}@tudelft.nl

1 Abstract

The ability of Inkjet technology to deposit materials with diverse chemical and physical properties on substrate has made it an important technology for industry. Apart from conventional document printing, Inkjet technology has been successfully applied to manufacture e.g. solar panels, PCBs and flat panel displays. Typically, a drop-on-demand (DoD) inkjet consists of several ink channels in parallel. Each channel is provided with a piezo-actuator, which on application of standard actuation voltage pulse can generate pressure oscillations inside the ink channel to push the ink drop out of the nozzle. The volume of the jetted drop is very small compared to the volume of the ink channel, hence the ink channel dynamics can be considered linear. It is possible to experimentally obtain dynamic models from the input voltage of piezo actuator to the pressure inside the channel and also from the input voltage of piezo actuator to the meniscus velocity [1]. The meniscus is the ink and air interface in the nozzle.

The print quality delivered by an inkjet printhead depends on the properties of the jetted drop, i.e. the drop velocity, the positioning and the drop volume. To meet the challenging performance requirements posed by new applications, the drop properties have to be tightly controlled. The productivity and performance of the inkjet printhead is limited by two operational issues. The first issue is the *residual pressure oscillation*. The actuation pulses are designed to provide ink drop of specified volume and velocity under the assumption that the ink channel is at steady state. Once the ink drop is jetted the pressure oscillations inside ink channel takes several μs to decay. If the next ink drop is jetted before settling of these residual pressure oscillations, the resulting drop properties will be different compared to earlier drop. This can degrade the printhead performance. The second operational issue is the *cross-talk*. The drop properties through an ink channel are affected when its neighboring channels are actuated simultaneously. The two major sources of cross-talk are acoustic and structural cross-talk [2]. It is possible to tackle these issue with system and control approach. Given the fact that printhead dynamics is very predictable and the bitmaps to be printed are priori known, feedforward control can be used to improve the performance of the DoD printhead. The possibility to use feedback control is ruled out due to the following limitations of the actuation system

- The driving electronics limit the range of actuation pulses that can be generated in practice. One possible choice of the actuation pulse is the trapezoidal waveform [3].
- No sensor is provided for real-time measurement of the channel pressure or the meniscus velocity.
- The time interval between two drops is very small.

As a first step we will attempt to minimize the residual pressure oscillations within one single channel. In order to reduce the residual pressure oscillations we will proceed as follows. We suppose that the plant transfer function $H(z)$ between the actuation pulse and the pressure in the ink channel is known and that we can design a template $y_{ref}(t)$ for the channel pressure which is desired as the output i.e. a pressure profile with fast decaying oscillations. Based on this template $y_{ref}(t)$ and the transfer function $H(z)$ an optimal actuation pulse $u(t)$ will be determined as the one minimizing the following objective function

$$\mathcal{J} = \sum_{t=0}^T w(t)(y_{ref}(t) - H(z)u(t))^2 \quad (1)$$

with $w(t)$ some user chosen time-domain weighting. In this optimization problem, the class of input signals is limited to trapezoidal actuation pulses since these are the pulses that can be generated in practice.

References

- [1] Matthijs Groot Wassink, "Inkjet printhead performance enhancement by feedforward input design based on two-port modeling," *PhD Thesis, Delft University of Technology*, February, 2007.
- [2] Herman Wijshof, "Structure and fluid-dynamics in piezo inkjet printheads," *PhD Thesis, University of Twente*, January, 2008.
- [3] Kuang-Chao Fana, Jhih-Yuan Chena, Ching-HuaWanga, Wen-Chueh Panb, "Development of a drop-on-demand droplet generator for one-drop-fill technology," *Sensors and Actuators A: Physical*, vol.147, pp.649-655, 2008.

Acknowledgements : This work has been carried out as part of the Octopus project with Océ Technologies B.V. under the responsibility of the Embedded Systems Institute. This project is partially supported by the Netherlands Ministry of Economic Affairs under the Bsik program.

On the Robustness of Feedback Linearizing Control Schemes for Multiple-Input/Multiple-Output Bioreactors

Daniel F. Coutinho¹ and Alain Vande Wouwer

Service d'Automatique – Faculté Polytechnique de Mons

31 Boulevard Dolez B7000 – Mons – Belgium

E-mails: Daniel.Coutinho(Alain.VandeWouwer)@fpms.ac.be

1 Introduction

Traditionally, the control of bioreactors in industrial applications is restricted to the regulation of pH and temperature at constant levels to provide appropriate conditions for microbial growth [1]. In the last years, much research has been carried out to optimize the productivity of biomass by regulating the level of biological variables such as biomass, substrate, and product concentrations. However, the dynamics of these variables are modeled by uncertain nonlinear differential equations making the control synthesis problem much more involved. One of the first attempts to control biological variables was based on a feedback linearizing strategy, but this method has two major drawbacks: (1st) it relies on the exact knowledge of the model parameters yielding poor robustness properties, and (2nd) the on-line measurement of key biological variables is required, which is not always possible. To overcome these problems, several researchers have applied adaptive schemes to estimate uncertain parameters, reaction kinetics and even some unavailable state variables. However, adaptive strategies often lack a guarantee of convergence of the adaptation scheme and a systematic procedure to tune some key parameters. Contrasting with the latter, we follow in this work a different strategy. Firstly, we consider the standard feedback linearizing control technique applied to the nominal system dynamics, where the reaction kinetics is described by rational functions of the biological variables (such as Monod law). Secondly, the resulting linear dynamics is designed to guarantee closed-loop stability assuming convex bounded parameter uncertainty. In addition, we propose a robust Luenberger-like observer to estimate unavailable state variables needed to implement the control strategy.

2 General Setup

Consider the following state space representation for the bioreactor

$$\begin{bmatrix} \dot{y} \\ \dot{\xi} \end{bmatrix} = K(\delta)\psi(y, \xi, \delta) - D(y, \xi)u - Q(y, \xi, \delta) \quad (1)$$

where $y \in \mathcal{Y} \subset \mathbb{R}^n$ and $\xi \in \Xi \subset \mathbb{R}^{n_\xi}$ are the state vector, $\delta \in \Delta \subset \mathbb{R}^{n_\delta}$ is the vector of uncertain parameters, $\psi(\cdot) \in \mathbb{R}^{n_\psi}$ is a rational vector function of (y, ξ, δ) standing for the reaction kinetics, $K(\cdot) \in \mathbb{R}^{m \times n_\psi}$ is an affine matrix of δ representing the yield coefficients with $m = n + n_\xi$,

$D(\cdot) \in \mathbb{R}^{m \times n}$ is a rational matrix function of (y, ξ) , $u \in \mathbb{R}^n$ is the vector of dilution rates, and $Q(\cdot) \in \mathbb{R}^{m \times n_q}$ is a rational matrix function of (y, ξ, δ) representing the mass outflow in gaseous form. We assume \mathcal{Y}, Ξ and Δ are given polytopic sets with known vertices. The control objective is to drive the state y to a given set-point y^* . To this end, we suppose a feedback linearizing control law $u = u(y, \xi, y^*)$ is designed for the nominal system (i.e., $\delta = 0$) leading to the following error system

$$\dot{x} = Ax + f(x, \xi, \delta, y^*) \quad (2)$$

where $x := y^* - y$ is the tracking error, $f(\cdot) \in \mathbb{R}^n$ is a rational matrix function of (x, ξ, δ, y^*) representing the terms that are not canceled by the linearizing control law, and $A \in \mathbb{R}^{n \times n}$ is a constant matrix to be designed representing the free linear dynamics of the control strategy. The above system is analyzed using the DAR framework [2] to ensure closed-loop stability and performance. In addition, we propose the following observer to estimate the state variable vector ξ

$$\begin{bmatrix} \hat{y} \\ \hat{\xi} \end{bmatrix} = \hat{K}\hat{\psi} - \hat{D}u - \hat{Q} + L(y)(y - \hat{y}) \quad (3)$$

where $\hat{K} = K(0)$, $\hat{\psi} = \psi(y, \hat{\xi}, 0)$, $\hat{Q} = Q(y, \hat{\xi}, 0)$, and $L(y) \in \mathbb{R}^{m \times n}$ is an affine matrix function of y to be determined (e.g., following the ideas in [3]).

A numerical example on the simultaneous control of biomass and metabolite concentrations in a perfusion/chemostat bioreactor will be presented at the conference.

3 Acknowledgment

This paper presents research results of the Belgian Network DYSCO (Dynamical Systems, Control, and Optimization), funded by the Interuniversity Attraction Poles Programme, initiated by the Belgian State, Science Policy Office. The scientific responsibility rests with its authors. D. Coutinho is beneficiary of a fellowship granted by the Federal Science Policy Office.

References

- [1] G. Bastin and D. Dochain, *On-line Estimation and Adaptive Control of Bioreactors*, Elsevier, 1990.
- [2] D. Coutinho et al, "L2-gain analysis and control of uncertain nonlinear systems with bounded disturbance inputs", *Int'l J. Robust Nonlinear Contr.*, 18(1):88-110, 2008.
- [3] D. Coutinho et al, "Robust Observer Design for a Class of Nonlinear Systems", in *Proc. CDC-ECC'05*, Dec. 2005.

¹On leave from the Group of Automation and Control Systems, PPGE-PUCRS, Av. Ipiranga 6681, Porto Alegre/RS, 90619-900, Brazil.

Global Nonlinear Optimization using Interval Analysis

E. van Kampen, E. de Weerd, Q. P. Chu, J. A. Mulder

Delft University of Technology, Department of Control and Simulation

P.O. Box 5058, 3600 GB Delft, The Netherlands

E.vanKampen-, E.deWeerd-, Q.P.Chu- and J.A.Mulder@TUDelft.nl

Nonlinear optimization problems occur frequently in nonlinear control system design and system identification. This paper will explain how Interval Analysis can be used to solve these nonlinear optimization problems and it will provide some relevant examples of applications of this method.

Nonlinear optimization

Nonlinear optimization problems, and in particular non-convex optimization problems, are characterized by the existence of multiple local minima of the costfunction. Gradient based optimization techniques can get stuck in a local minimum and their solution depends on the chosen initial conditions. Alternative methods such as simulated annealing or genetic algorithms can increase the chance of ending up in the global minimum, but they cannot guarantee that the optimal solution is found.

Interval Analysis

Interval analysis (IA) deals with intervals of numbers instead of crisp numbers and was developed in the 1960's to evaluate how rounding errors propagate through systems [1, 2]. Interval numbers have a lower and upper bound and there is a special set of arithmetic operators for intervals. An important feature of interval computations is that the result of a computation that is performed on any crisp number inside a given interval will be included in the interval result that is obtained when performing the same computation for the whole interval using interval arithmetic (intervals are indicated by brackets):

$$J = f(p); p \in [p] \rightarrow J \in [J] = [f]([p]) \quad (1)$$

Applications

Three aerospace related applications are used to show the benefits of IA for nonlinear optimization. The first application is pilot model identification, where the goal is to make a mathematical model of a human pilot [3]. This model can then be used to design flight simulators and control systems. The model is created by fitting a number of model parameters onto an input-output dataset of a real human operator in either an aircraft or a simulator. This parameter fitting process is a nonlinear optimization problem, for which it can be proved that multiple local minima exist. By using IA, the true global minimum is found.

The second application is finding the trim points of a nonlinear aircraft model [4]. Trim points are defined as a collection of states and control inputs for which there are no linear or rotational accelerations on the aircraft. As an example, an aircraft in a horizontal level flight with a fixed thrust setting has two trim points: one at low speed and high angle of attack and one at high speed and low angle of attack. Traditional gradient based optimization methods find only one trim point at a time, while IA can find all trim points at once and can also prove that all trim points have been found.

The third application is in the field of Global Navigation Satellite Systems such as GPS [5]. Traditionally the phase-modulated codes on the GPS signals are used as indicators of time of travel of the signal and thus distance between satellite and receiver. For higher accuracy it is also possible to use the phase of the carrier wave as a measurement, but unfortunately the receiver cannot distinguish the individual cycles from each other, resulting in the well known integer ambiguity problem. IA has been applied to solve this integer ambiguity problem by geometric modeling of the problem and by encapsulating the inherent phase measurement noise with an interval. The IA method has been successfully applied to the problem of determining the orientation of a baseline between two receivers using GPS signals.

References

- [1] Ramon E. Moore. *Interval Analysis*. Prentice-Hall, Inc., 1966.
- [2] Eldon Hansen and G. William Walster. *Global Optimization using Interval Analysis*. Marcel Dekker, Inc., second edition, 2004.
- [3] E. van Kampen, P.M.T. Zaal, E. de. Weerd, Q. P. Chu, and J. A. Mulder. Optimization of Human Perception Modeling using Interval Analysis. In *AIAA Modeling and Simulation Technologies Conference*, number AIAA-2008-7108, 2008.
- [4] E. van Kampen, Q. P. Chu, J. A. Mulder, and M. H. van Emden. Nonlinear aircraft trim using interval analysis. In *AIAA Guidance, Navigation, and Control Conference*, volume 4, pages 4073–4087, 2007.
- [5] E. de Weerd, E. van Kampen, Q.P. Chu, and J.A. Mulder. New approach for integer ambiguity resolution using interval analysis. *ION Journal of Navigation*, Winter edition, 2008.

Fuel optimization for constrained rotations of spacecraft formations using interval analysis

E. de Weerd, Q.P. Chu, J.A. Mulder

Kluyverweg 1, 2629 HS Delft, The Netherlands

E.deWeerd@TUDelft.nl, Q.P.Chu@TUDelft.nl, J.A.Mulder@TUDelft.nl

1 Abstract

Future missions in space are more and more directed toward formations of spacecraft. Using multiple spacecraft in formations has several big advantages over using a single spacecraft. The individual spacecrafts in formation can be made smaller since not all functionality needs to be on one spacecraft. Moreover, when using multiple spacecraft more mission possibilities arise. For example, the NASA has planned the Terrestrial Planet Finder mission similar to the ESA Darwin mission where the functionality of a very big telescope is mimicked using several small(er) satellites. Compared to the Hubble telescope the new 'synthetic' telescopes will have much larger resolutions. These levels of resolution can only be obtained using spacecraft formations. Another big advantage of spacecraft formations is that in case of a failure in one of the spacecraft, the mission can in most cases be continued with full or reduced capacity while a failure in one spacecraft mission usually means the end of the mission.

The control systems complexity increases when having multiple satellites in formation. Dependent on the type of mission, i.e. requiring tight/loose formation control, planet orbiting/free space, the control system can be extremely complex. The topic of this paper is fuel optimization for satellite formation reconfiguration. The goal is to develop a planning algorithm which determines the optimal trajectory for each satellite such that at the end of the reconfiguration the total fuel consumption is as low as possible while the difference between fuel levels among spacecrafts is as low as possible. The cost function which represents this goal is given by:

$$J = \sum_{i=1}^N (f_i(t_f) - f_i(t_0))^2 + \mu \sum_{i=1}^N \left[\frac{f_i(t_f)}{\sum_{j=1}^N f_j(t_f)} \log \frac{f_i(t_f)}{\sum_{j=1}^N f_j(t_f)} \right]$$

where f_i is the fuel level of satellite i , t_0 is the start time and t_f is the time when the reconfiguration is complete. The μ factor is used to put more or less weight on the fuel equalization in comparison to the fuel minimization. Literature has shown that these goals are conflicting.

The optimization of the cost function for arbitrary formations in arbitrary orbits about a planet can become a very

non-linear problem and can be hard to describe in analytic form. To solve the problem the final fuel levels need to be expressed in terms of the trajectories per satellite. The number of free variables of the optimization problem can become numerous if much flexibility in the trajectories is allowed increasing the complexity of the optimization problem. Common practice is to parameterize the trajectories to reduce the problem complexity. Adding to the complexity of the problem there can be several constraints such as maximal thrust capabilities per spacecraft, maximal reconfiguration time, collision avoidance, fuel limitations.

To limit the complexity, the problem is confined to free space and constrained spacecraft formations. For the current research the formation is considered as a rigid body which needs to be rotated about a given axis and a given rotation angle similar as in done in [1]. The remaining free variable is the rotation point about which the entire formation rotates. This reduced problem is still non-linear with non-linear constraints. To guarantee that the correct solution is found interval analysis is used instead of gradient based methods as in [1]. Interval analysis is a very powerful global non-linear optimization technique which can solve non-linear (dis)continuous problems with (non)linear inequality and equality constraints [3, 4, 2].

Future work is directed to trajectory planning of planet orbiting spacecraft formations using interval analysis. Typically these planning problems are highly non-linear and dynamic: challenging problems which can be solved rigorously with interval analysis.

References

- [1] R.W. Beard, T.W. McLain, and F.Y. Hadaegh. Fuel optimization for constrained rotation of spacecraft formations. *Journal of Guidance, Control, and Dynamics*, 23(2):339–346, March 2000.
- [2] E. Hansen and G.W. Walster. *Global Optimization Using Interval Analysis*. Marcel Dekker, Inc. and Sum Microsystems, Inc., 2 edition, 2004.
- [3] L. Jaulin, M. Kieffer, O. Didrit, and E. Walter. *Applied Interval Analysis*. Springer, 2001.
- [4] R.E. Moore. *Interval Analysis*. Prentice-Hall, Inc., 1966.

Feasibility of Thrust Vectoring in Large Passenger Aircraft

Hui Yu

Faculty of Aerospace Engineering
Delft University of Technology
Postbus 5058, 2600 GB Delft
The Netherlands
Email: H.Yu@tudelft.nl

1 Abstract

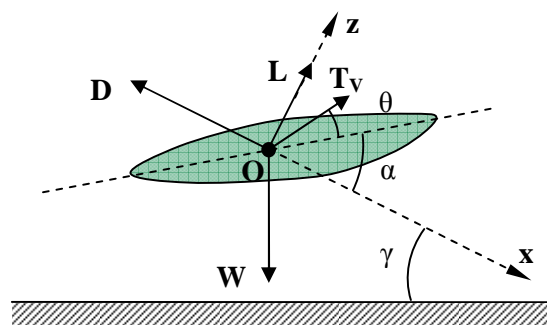
Based on the CleanEra project, research is carried out to investigate the feasibility of the application of thrust vectoring in large passenger aircraft. The goal of the research is to optimize the thrust vector angle in order to reduce the required thrust as much as possible with the view of reducing the fuel consumption. The problem is simplified into a two-dimensional problem, which means that only the pitch movement is taken into account. The parameters to be determined include the vectored thrust and the thrust vector angle. An aerodynamic model is built with the assumption that all the forces acting on the aircraft act through its center of gravity. Parameters according to a Boeing747-100/200 model are provided to represent a wide-body passenger aircraft and optimization is developed to find the minimum thrust for three trim points in climb, cruise and approach respectively. Results show that the technology can not be applied to a passenger aircraft with a single goal of reducing fuel consumption due to the insignificant potential on thrust reduction. However, thrust vectoring is still a candidate for an unconventional passenger aircraft because of its possible contributions to design some special climb and approach trajectories with the hope of reducing noise impact on the perimeter of the airports.

2 Introduction

The CleanEra project, initiated by the faculty of Aerospace Engineering at Delft University of Technology, sets the goal of developing new technologies for a revolutionary conceptual aircraft design(s) optimized for environment and passenger friendliness and investigating the feasibility of these technologies and their integration. CleanEra stands for cost-effective low emissions and noise efficient revolutionary aircraft and the project includes researchers who are working on acoustics, aerodynamics, engines, structures, integration, etc. The research of CleanEra will result in a significant decrease on the noise impact upon the human beings and a noteworthy reduction of CO₂ and NO_x emission to the environment. This research presents the feasibility of thrust vectoring within different flight phases of a wide-body passenger aircraft, including climb, cruise, and approach.

3 Equations of Motion

All the forces acting on the aircraft are assumed to act through the center of gravity such that the moments can be left out of the optimization, including the weight (W), the vectored thrust (T_v) and the aerodynamic lift (L) and drag (D). The model built based on these assumptions are used as a demonstration to investigate the feasibility of thrust vectoring.



Aircraft within climb, cruise, and approach phases can be considered as steady-state flight, so the resulting equations of motion with thrust vectoring can be simplified as follows:

$$T_v \cos(\theta + \alpha) + W \sin(\gamma) - D = 0$$

$$T_v \sin(\theta + \alpha) - W \cos(\gamma) + L = 0$$

4 Results

Because of the limited space, the detailed results are only give for the trim point in climb. The thrust reduction is about 1,000.602 N and the reduction percentage is around 0.212%, which are both the biggest among all the three trim points.

Parameters	Climb
Thrust Required without Thrust Vectoring, T (N)	470,895.057
Minimum Thrust with Thrust Vectoring, T _v (N)	469,894.455
Thrust Vector Angle, θ (°)	-3.7
Thrust Reduction, (N)	1,000.602
Reduction Percentage, (%)	0.212

Aerodynamic Model Identification and Flight Control Design with Multivariate Splines

Coen de Visser

Department of Control & Simulation
Technische Universiteit Delft
P.O. Box 5058, 2600 GB Delft
The Netherlands

Email: c.c.devisser@tudelft.nl

Bob Mulder

Department of Control & Simulation
Technische Universiteit Delft
P.O. Box 5058, 2600 GB Delft
The Netherlands

Email: j.a.mulder@tudelft.nl

1 Abstract

The identification of high quality aerodynamic models for aircraft, based on flight data, is a difficult problem. Aircraft dynamics are highly nonlinear and coupled, which means that the effects of individual dimensions like angle of attack and Mach number on the aerodynamic force and moment coefficients are difficult to separate. The current consensus in aerodynamic model identification is to assume a low order polynomial model structure for a force or moment coefficient, after which parameter estimation techniques are employed to estimate the parameters of the polynomials [1]. The estimation process makes use of data points recorded during flight test maneuvers specifically designed to reduce the effects of dimensional couplings and high order nonlinearities, which is necessary because the polynomial model is of insufficient order to model these effects. The flight test maneuvers are of relatively short duration, i.e. shorter than 10 seconds, which limits the amount of data that can be recorded for every maneuver. In order to obtain sufficiently accurate estimates of the polynomial parameters, a large set of data points is required, especially when the modeled force or moment coefficient is a high order nonlinear function in many dimensions. Together with the short duration of the flight test maneuvers this requires many, sometimes hundreds of maneuvers that must be flown.

High quality aerodynamic models are essential for the adequate functioning of flight control systems based on nonlinear dynamic inversion (NDI). In an NDI control system, the plant output is linearized by multiplying it with the inverse of a model of the plant dynamics. The resulting linearized state can then be controlled with simple linear controllers. The advantage of NDI based control over classic nonlinear control systems is twofold. First, it greatly reduces the cost and effort of developing controllers for complex nonlinear systems. Second, it facilitates the design of a fault tolerant control system which is reconfigured online to maintain control authority in the event of aircraft damage. NDI control systems, however, are highly sensitive to errors in the plant model. Any practical NDI control system is therefore equipped with a robust outer loop which compensates for modeling errors. The robust loop tends to reduce control

performance; the higher the quality of the plant model, the higher the performance of the NDI control system.

We present a new identification method based on multivariate simplex splines inside a linear regression framework. The multivariate simplex splines are a new spline type [2] which can fit scattered data [3] and have an arbitrarily high approximation power. Consequently, the approximation power of the simplex splines is superior to single low order polynomials. The new identification method greatly simplifies the identification of aerodynamic models for aircraft and subsequent flight controller design. Flight test maneuvers are not required to be so strictly designed and executed, as the spline functions are capable of modeling the dimensional couplings and high order nonlinearities. The result is that longer maneuvers can be flown, resulting in higher data volumes, and thus in a smaller total number of maneuvers. From the control perspective, the spline models identified with the new identification method are of higher quality than the polynomial models, and are therefore better suited for use in NDI based flight control systems.

The new identification method was used to create a multivariate simplex spline based aerodynamic model for the F-16 based on simulated flight test data. The spline based aerodynamic model was validated against the original data table based model. Results from the validation showed a $< 1\%$ error RMS in the aerodynamic force and moment coefficients for the spline based aerodynamic model. An NDI flight control system for the F-16 was created based on the inverted spline based aerodynamic model.

References

- [1] V. Klein and E.A. Morelli, Aircraft System Identification, AIAA, 2006.
- [2] M.J. Lai and L.L. Schumacher, Spline Functions over Triangulations, Cambridge University Press, 2007.
- [3] G. Awanou, M.J. Lai, and P. Wenston. The multivariate spline method for scattered data fitting and numerical solutions of partial differential equations, Wavelets and Splines, 2005.

Nonlinear analysis of flutter

Mattijs Van de Walle, Johan Schoukens, Steve Vanlanduit
 Vrije Universiteit Brussel, Pleinlaan 2, 1050 Brussels, Belgium
 Department of Fundamental Electricity and Instrumentation (ELEC),
 Email: mattijs.van.de.walle@vub.ac.be

1 Introduction

Flutter is an aerolastic phenomenon that makes structures oscillate when surrounded by a moving fluidum. Flutter can lead to fatigue and/or failure on the wings, flaps and fuselage of an airplane. Laborious testing needs to be done on aircraft to ensure safe operation within a certain flight envelope. While flutter is inherently nonlinear, most models use a linear framework to predict the critical speed at which oscillations might occur. The aim of this work is the construction of a nonlinear model to more accurately predict the onset of oscillatory behavior, on the basis of wind tunnel test measurements.

2 Experimental setup

In a first step, we built an experimental setup with which we can create flutter under controlled conditions. This first setup, shown in figure 1, is a cantilevered airfoil. The sections we use for this experiment are hotwire-cut out of polystyrene. To keep the sections from producing lift at zero angle of attack, we solely use symmetrical NACA airfoils. Because the velocity of the wind tunnel we have at our disposal is limited to 50 m/s and because of safety reasons, we want the wing to get unstable at as low a wind speed as possible. Therefore, a system has been devised that allows the modal properties of the wing to be altered. It consists of a rail on which small weights can be fixed. By tuning the distance from the weights to the aerodynamic centre of the airfoil, the frequency of the first torsional mode can be brought closer to the frequency of

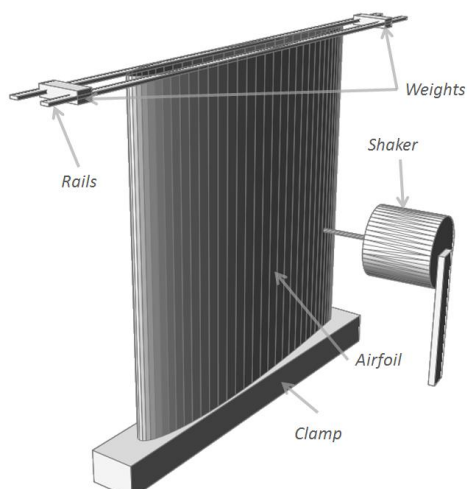


Figure 1: Cantilevered setup

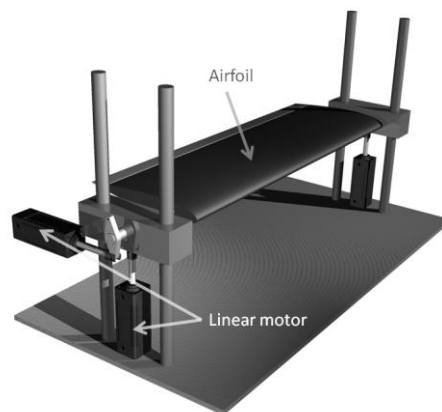


Figure 2: Actively controlled two DOF setup

the first bending mode. When wind is applied, these modes get even closer to one another and because flutter occurs when these modes start to couple, a lower flutter speed is achieved through the use of this tunable system. To measure and tune the modal parameters of the setup, a shaker and laser vibrometer are used. When actually under test, the shaker cannot be used because once the airfoil gets unstable, the vibration would damage the shaker.

In the second step, we will build a setup that also allows the use of forced excitations. The setup is shown in figure 2. Conceptually it is closely tied to a standard two degrees of freedom (DOF) configuration that is often used for flutter research. The advantage of the proposed setup is that instead of using linear springs to characterize the airfoil's pitch and plunge stiffness, it uses linear motors. Not only does this allow us to choose the stiffness of the pitch and plunge motion, but the linear motors enable us to impose an arbitrarily chosen excitation signal upon the airfoil. In doing so, we hope to better understand the flutter phenomenon and characterize its nonlinear behavior [1].

3 Conclusions

We are able to create flutter in a reproducible manner with the cantilevered setup. We also have control over the speed at which it occurs. At the moment of writing the actively controlled setup has not been finalized.

References

- [1] R. Pintelon and J. Schoukens, System Identification: a Frequency Domain Approach, IEEE Press, 2001.

Design and control of a teleoperated palpation device for minimally invasive thoracic surgery

Angelo Buttafuoco, Thomas Delwiche and Michel Kinnaert

Dept. of Control Engineering and System Analysis

Université Libre de Bruxelles (U.L.B.)

50, Av. F.D. Roosevelt-CP 165/55, B-1050 Brussels, Belgium

Angelo.buttafuoco@ulb.ac.be

1 Introduction

Minimally invasive surgery (MIS) consists in operating through small incisions in which a camera and adapted instruments are inserted. It is becoming a standard procedure for many interventions in thoracic surgery, where it is also used to ablate peripheral pulmonary nodules with reduced trauma for the patient[1].

Nevertheless, the means for detecting a nodule during MIS are limited. In fact, because of the loss of direct contact with the organ, the surgeon cannot palpate the lung to find invisible lesions, as he would do in classical open surgery. As a result, only clearly visible nodules can be treated by MIS at the moment.

2 Palpation device

Our work aims at the design, realization and control of a palpation device, in order to extend the possibilities of MIS in the thoracic field. The most intuitive method consists in restoring the haptic sensations by means of a bilateral teleoperation apparatus[2].

In collaboration with the thoracic surgeons of the Erasmus hospital, different experiments were carried out on realistic lung simulators designed within this project. The main goals were to model the palpation, to identify the surgeons' most efficient gestures and the kind of information needed when looking for hidden nodules, and to quantify the force applied on the organ during the procedure.

The results showed that, for instruments presenting 2 dof or more, kinaesthetic feedback alone is sufficient to find hidden nodules efficiently. Moreover, the forces applied on the lung do not exceed 11.5N, which can be reached with classical low power DC motors.

As a first step, a 1 dof master-slave test bench has been realized and a position-position regulation has been set to provide kinaesthetic feedback. Notice that miniaturization issues for MIS have not been taken into account at this point.

3 Future work

The following steps will see further experiments with surgeons to validate the test bench and its regulation scheme, the extension to a second dof and the development of control laws that best suit the needs of palpation[3]. The last part of the project will be dedicated to the miniaturization of the device to meet MIS exigences.

Acknowledgements

The work of Angelo Buttafuoco and Thomas Delwiche is supported by FRiA grants. The experimental setup is financed by the FNRS. This paper presents research results of the Belgian Network DYSCO (Dynamical Systems, Control and Optimization), funded by the Interuniversity Attraction Poles Programme, initiated by the Belgian State, Science Policy Office. The scientific responsibility rests with its author.

References

- [1] J. Lin , M.D. Iannettoni, The role of thoracoscopy in the management of lung cancer, In *Surgical Oncology*, vol. 12, pp. 195–200, 2003.
- [2] P.F. Hokayem, Bilateral teleoperation : An historical survey, In *Automatica*, vol. 42, pp. 2035–2047, 2006
- [3] M.C. Cavusoglu, Bilateral Controller Design for Telemanipulation in Soft Environments, In *Proceedings of the 2001 IEEE International Conference on Robotics and Automation*, 2001

Haptic control of a tele-operated ultrasound probe

Kees-Jan Zandsteeg, Dennis Bruijnen, Boudewijn Verhaar, Peter Frissen, George de Fockert, Dennis Bos

Philips Applied Technologies

High Tech Campus 7, 5656 AE Eindhoven

The Netherlands

Email: boudewijn.verhaar@philips.com

Since the early history of mankind, humans use tools to replace or enhance manual labour. When time went by, tools became more and more developed and more advanced.

Nowadays tele-operation is used as a tool in many areas, for example in the automotive industry, aerospace, nuclear waste management and medical systems. In tele-operation the operator feels no interaction with the environment. Therefore tele-operation cannot be used in tasks in which force information of the environment is necessary.

In the last decades, researchers tried to enhance tele-operated systems with perception, by developing haptic tele-operation control. Haptic tele-operation explores a new area of applications for tele-operation in which force information is necessary.

Ultrasound is used in echo-cardiography during minimal invasive heart surgeries. Echo-cardiography and also X-ray provide images to the surgeon. To be able to obtain a good ultrasound image, sonographers

use their perception of force to locate ribs and tissue to optimize the quality of the image. Therefore perception is necessary to do the ultrasound task.

Performing ultrasound tasks is physically very intensive due to the restricted workspace between the other equipment used and the patients' body combined with the duration of the surgery. Hence work related injuries are unfortunately very common for sonographers. Furthermore during specific interventional procedures, sonographers are often also exposed to X-ray.

To reduce the occupational- and x-ray- hazards of sonographers, a master-slave robotic system with haptic control is developed within Philips Applied Technologies. The so-called Tele-Operated Ultrasound Probe (TOUP) system will be presented in this paper. The focus will be system identification and validation of the TOUP system elements: slave, master, operator, and environment. Furthermore, an introduction of haptic control applied to the TOUP system will be given.



Influence of the skin moisture at fingertip on the static grip force during object manipulation

T. Andre

Readaptation Unit (READ)

53 (5375) Avenue Mounier, 1200 Bruxelles

Thibaut.Andre@UCLouvain.be

P. Lefevre

CESAME

4 Avenue Georges Lemaitre, 1348 Louvain-La-Neuve

Philippe.Lefevre@UCLouvain.be

J-L. Thonnard

Readaptation Unit (READ)

53 (5375) Avenue Mounier, 1200 Bruxelles

Jean-Louis.Thonnard@UCLouvain.be

1 Introduction

In everyday life, humans constantly manipulate small and light objects by using precision grip. Holding an object consists in applying an adapted grip force (GF), which is the normal force exerted by the thumb and index finger on the object, to counteract the tangential load force (LF). In order to prevent the object from slipping, a minimal GF is required, which depends on the coefficient of friction (CF) at fingertip [1]. Humans are able to modulate the GF according to LF variations due to object acceleration. Indeed, the central nervous system (CNS) can predict these variations in order to exert the required GF. When performing different tasks like oscillations, collisions or point-to-point movements, it has been shown that the CNS can adapt this modulation according to the mass of the object, the coefficient of friction at the interface finger/object [2] or a new environment like weightlessness [3]. Other studies have demonstrated that subjects are able to code the friction of the skin in contact with the object and that the cutaneous feedback is needed to perform such a task.

In the present work, we propose to study the evolution of the fingertip moisture during a manipulation task and to analyze the adaptation of the subjects to different moisture conditions.

2 Methods and Results

Ten naive subjects performed point-to-point movements which direction and amplitude were randomly determined by visual targets (LEDs). The object manipulated was a manipulandum equipped with force-torque sensors (Mini40, F/T transducer; ATI Industrial Automation) and custom moisture sensors. The subjects were requested to align the manipulandum with the current target and stay next to it until the next one turned on. The grip force and the moisture at the fingertips were recorded during this task.

The results show a strong relationship between GFs and the moisture of the skin at fingertips. Subjects whose moisture increased along the blocks of trials presented an associated

decrease in GFs. In contrast, subjects with a constant level of skin hydration didn't show any change in their level of GFs.

3 Discussion

Our results showed that subjects with low or high level of moisture exerted ranges of GFs larger than subjects with an intermediate moisture level. This perfectly matches the results presented in Andre et al. [4] where the CF is maximum (in the range of GF investigated in this study) for intermediate moisture values. So the range of moisture that minimizes the GFs also maximizes the estimated CF.

Finally, results also showed that subjects adapted the GFs exerted with moisture across trials when performing the task. Indeed, when the skin hydration increased (resulting from the occlusion), the GFs exerted was adapted to take into account CF modifications.

References

- [1] Johansson, R.S. and G. Westling: Roles of glabrous skin receptors and sensorimotor memory in automatic control of precision grip when lifting rougher or more slippery objects. *Exp Brain Res*, 1984. 56(3): p. 550-64.
- [2] Westling, G. and Johansson, R.S.: Factors influencing the force control during precision grip. *Exp Brain Res*, 1984. 53(2): p. 277-84.
- [3] Augurelle, A.S., Penta, M., White, O., Thonnard, J.L.: The effects of a change in gravity on the dynamics of prehension. *Exp Brain Res*, 2003. 148(4): p. 533-40.
- [4] Andre, T., White, O., Lefevre, P. and Thonnard, J.L.: The effects of grip force and skin moisture on the friction during dextrous manipulations. 17th Annual Meeting of the Society for Neural Control of Movements, Sevilla, Spain (2007).

Modeling of friction in a trocar for minimally invasive surgery

J. Verspecht, T. Delwiche and M. Kinnaert
Control Engineering and System Analysis Department
Université Libre de Bruxelles (U.L.B.)
jonathan.verspecht@ulb.ac.be

1 Introduction

Teleoperation consists in performing a remote task with an electromechanical master-slave device. When force feedback is present at the master side to make the user feel the interaction forces between the slave and its environment, one refers to bilateral teleoperation. Most of the controller design techniques proposed in the teleoperation literature require linear models. However, in most cases, friction makes the linearity assumption invalid. Friction compensation systems (FCS) are used in teleoperation to recover the linearity of the system. In this paper, a specific application of teleoperation is considered, namely the minimally invasive surgery (MIS). In MIS, one of the friction sources is the sealing mechanism of the trocar. The friction of the trocar depends on the type of trocar, the movement velocity, and the movement direction [3]. For some types of trocar, the friction force can be as large as the slave-environment interaction. In this paper we propose an hybrid model to describe the friction in trocars.

2 Friction model of the trocar

A FCS can be based either on a friction model (FM) or a friction observer (FO). It has been shown [2] that FCS based on a FO have better performance at lower frequencies while FCS based on a FM have better performance at higher frequencies. In order to design a model based FCS, an accurate friction model is required.

Some friction models are presented in the literature[1],

present in trocars. The static friction models do not deal with deformation, and the dynamical ones only include the deformation of microscopic asperities. The major assumption in a dynamical friction model is that one of the two surfaces in contact can be taken as fixed. Accordingly, the measured velocity corresponds to the relative velocity between the two surfaces. In the case of a macroscopic deformation, this assumption does not hold anymore. Indeed, the measured velocity is composed of the relative velocity, but also the deformation velocity.

In this paper, we propose the use of an hybrid friction model characterized by two modes (represented on figure 1). A sticking mode where the friction force is governed by a deformation model and a slipping mode, where the friction force is governed by a friction model. The model chooses as output force, the mode leading to the minimum resistance to the motion.

The experimental validation and the identification of this model require a setup which is still under construction. The measurements will be completed for February 2009.

Acknowledgments

The work of Jonathan Verspecht and Thomas Delwiche is supported by FRiA grants. The experimental setup is financed by the FNRS. This paper presents research results of the Belgian Network DYSCO (Dynamical Systems, Control and Optimization) funded by the Interuniversity Attraction Poles Program, initiated by the Belgian State, Science Policy Office. The scientific responsibility rests with its authors

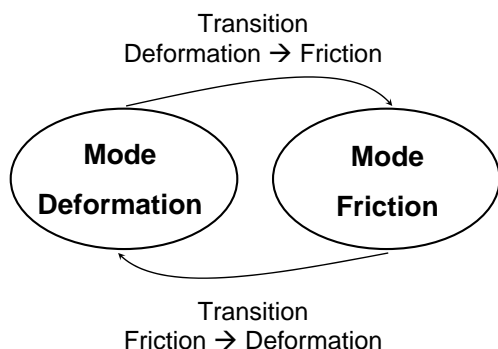


Figure 1: 2-states hybrid model

but none of them can describe the deformation of the seal

References

- [1] B. Bona and M. Indri. Friction compensation in robotics: an overview. *IEEE conference on decision and control, and the European control conference, Seville*, 2005.
- [2] T. Delwiche, L. Catoire, M. Kinnaert, J. Lataire, L. Vanbeylen, and J. Schoukens. Performance evaluation of friction compensation systems in frequency domain. *Internal Report*, 2008.
- [3] J.J. Van den Dobbelsteen, A. Schooleman, and J. Dankelman. Friction dynamics of trocars. *Surgical endoscopy and other interventional techniques*, 21:1338–1343, 2007.

Novel Dexterous Robotic Finger Concept with Controlled Stiffness

Martin Wassink, Raffaella Carloni, Dannis Brouwer and Stefano Stramigioli

Faculty of EEMCS, Control Engineering, University of Twente

P.O. Box 217, 7500 AE Enschede, The Netherlands

{m.wassink, r.carloni, d.m.brouwer, s.stramigioli}@utwente.nl

1 Introduction

These days, robotic research is shifting focus towards robots for applications in human environments. This can be either robots for household tasks as well as flexible robots for unstructured and diverse industrial tasks. Many of these tasks deal with object grasping (and releasing) and object manipulation, while often interacting with some environment as done by our human hands.

The challenge is to develop a robotic hand that can execute the unstructured and varying hand tasks as well as deal with a wide variety of object shapes and materials. The human hand uses its dexterity for manipulability and to be flexible w.r.t. (object) shapes. Furthermore, the human fingers possess adjustable stiffness. This research project aims to develop a robotic hand based on the here presented novel robotic finger concept that resembles the dexterity and controlled stiffness properties of the human hand. The adjustable mechanical stiffness allows to adapt the mechanics (without relying on high bandwidth feedback control loops) for either force (e.g. grasping) or position (e.g. manipulation) sensitive tasks or combinations of the two.

Current state of the art presents robotic hands that have full dof control at the cost of controller and design complexity, reliability and costly components, e.g the DLR Hand [1]. Also under-actuated hands are found, based on the well known ‘Soft Gripper’ [2]. The under-actuated coupled mechanism naturally adapts to object shapes. Hence, at the cost of controlled stiffness and dexterity, this concept can easily handle a wide variety of object shapes, without requiring complex control strategies.

2 Novel Grasper Concept

Figure 1 presents our novel robotic finger concept. The concept combines 3 key features: 1- a coupled antagonistic under-actuated tendon driving mechanism, 2- series elastic tendon actuation with non-linear springs and 3- active joint locking mechanisms on the joints. The under-actuated principles are used to reduce control complexity, while keeping dexterity (by modulating the joint locks) and introducing controlled mechanical stiffness.

The relative position of x_1, x_2 determines the equilibrium (no external force) finger configuration space Q_e , i.e. all $\bar{q} \in Q_e$ that minimize the potential energy ($E(x_1, x_2, \bar{q})$) of the unconstrained finger:

$$\frac{\partial E}{\partial \bar{x}} = 0 \Rightarrow (x_1, x_2, \bar{q} \in Q_e) \quad (1)$$

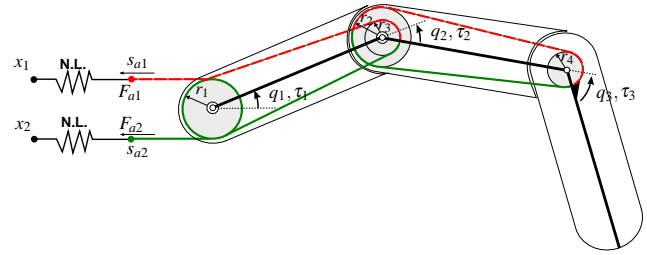


Figure 1: Novel robotic finger concept (N.L. = non-linear spring, $\bar{q} = (q_1, q_2, q_3)$). Pulley 1, 2 rotate freely on joint axes. Pulley 3 is fixed to 3rd phalanx. Joint locks can be switched on to constrain the relative motion of the two attached phalanxes.

Also the apparent mechanical stiffness is a function of the positions x_1, x_2 . Choosing two proper and identical non-linear spring functions makes sure that with x_1, x_2 both the stiffness and Q_e can be set without interfering.

Grasping is executed in 2 stages; *pre-shaping* and *object fixturing*. Pre-shaping (and finger manipulation) is done by moving x_1, x_2 and modulating the joint locks, s.t. the finger moves to a desired configuration $\bar{q}_p \in Q_e$ without getting in contact with the object. Then the object can be fixtured by moving x_1, x_2 , s.t. Q_e changes. If Q_e is chosen properly, the phalanxes will move to, but not reach, Q_e . Instead, the phalanxes naturally adapt their configuration around the object. The resulting contact forces follow from the deviation of the established constrained finger configuration w.r.t. Q_e and the preset mechanical stiffness.

Hence, the finger is controlled by simple low bandwidth position control for x_1, x_2 and joint lock modulation. Only angular position sensors are needed to measure \bar{q} and derive $\bar{\tau}$. Modeling and control of the novel finger for robotic grasping will be the topic of the presentation.

References

[1] J. Butterfaß, M. Grebenstein, H. Liu, and G. Hirzinger, “Dlr-hand ii: Next generation of a dextrous robot hand,” in *IEEE International Conference on Robotics and Automation*, 2001, pp. 109–114.

[2] S. Hirose and Y. Umetani, “The development of soft gripper for the versatile robot hand,” *Mechanism and Machine Theory*, vol. 13, pp. 351–359, 1978.

This project is partially supported by the Dutch government (BSIK03021, <http://www.esi.nl/falcon>).

The arithmetics of average consensus

Jean-Charles Delvenne
 Universit catholique de Louvain
 jean-charles.delvenne@uclouvain.be

Michael Branicky
 Case Western Reserve University
 mb@case.edu

Kalle Johansson
 KTH, Stockholm
 kallej@ee.kth.se

Sandro Zampieri
 Universit di Padova
 zampi@dei.unipd.it

1 Abstract

The average consensus problem arises when N agents moving in the space must communicate in order to gather at the barycentre of the initial positions of the agents.

Using a De Bruijn's communication topology, it is possible (in discrete time) to reach the average consensus in finite time [REF]. Moreover, the time of convergence is in $\log N$, which is optimal.

However, for a maximum degree ν , this only happens for N an exact power of ν .

On the other side, for any number of agents, it is trivial to make a communication topology of degree $\nu = 1$ that reaches consensus at the initial position of one 'leader agent' (everybody observes the leader, who does not move) in one step. The consensus position is potentially far from the average consensus.

This suggest the following general question: Depending on the number theoretic properties of the number of agents, how close can a finite-time strategy get to the average consensus?

First we show that if N has small factors, it is still possible to converge in logarithmic time with a small degree of the communication topology. Namely, if $N = 2_2^e 3_3^e \dots p_p^e$, then we converge to consensus in time $\max e_2, e_3, e_p$ with degree $\nu = 2.3 \dots p$.

On the other side, we show that for any N , there is a strategy reaching consensus, based on the De Bruijn strategy, that reaches a consensus $\sum^N \alpha_i x_i$ relatively close to the average consensus. Here x_i is the initial position of agent i . The weight discrepancy (maximum ratio α_i/α_j) is at most two. If the initial positions of the agents are distributed according to i.i.d. random variables, the typical error on the true average consensus is at most 11%.

2 Acknowledgements

This article presents research results of the Belgian Programme on Interuniversity Attraction Poles, initiated by the

Belgian Federal Science Policy Office. This research has been also supported by the ARC (Concerted Research Action) "Large Graphs and Networks", of the French Community of Belgium. The scientific responsibility rests with the authors. J.-C. D. holds a FNRS fellowship (Belgian Fund for Scientific Research).

References

- [1] J.-Ch. D., R. Carli and S. Zampieri, Optimal strategies in the average consensus problem in *Proceedings of the 46th IEEE Conference on Decision and Control*, New Orleans, Louisiana, Dec. 2007

Second-order Consensus Algorithms

Wenwu Yu

Department of Electronic Engineering
City University of Hong Kong
Hong Kong SAR, China
Email: wwyyu@ee.cityu.edu.hk

Ming Cao

Faculty of Mathematics and Natural Sciences
ITM, University of Groningen
The Netherlands
Email: m.cao@rug.nl

1 Introduction

In the study of cooperative behavior of groups of mobile autonomous agents, it is of great interest to construct conditions under which an agreement can be achieved in a dynamically changing environment. In particular, there is a growing interest [1, 2] in consensus algorithms where each agent is governed by second-order dynamics. It has been shown that, in sharp contrast to first-order consensus problems, consensus may fail to be achieved for agents with second-order dynamics even if the network topology contains a directed spanning tree. Although some sufficient conditions have been derived for reaching second-order consensus [2], it is still a challenging and unsolved problem to identify the key factor for reaching second-order consensus in a multi-agent system. One contribution of this paper is that a necessary and sufficient condition is given to ensure second-order consensus in the network containing a directed spanning tree. It is found that both the real and imaginary parts of the eigenvalues of the Laplacian matrix of the network play key roles in reaching second-order consensus.

2 Second-order consensus in directed networks

We consider the following consensus algorithm:

$$\begin{aligned}\dot{x}_i(t) &= v_i, \\ \dot{v}_i(t) &= \alpha \sum_{j=1, j \neq i}^N G_{ij}(x_j(t) - x_i(t)) \\ &+ \beta \sum_{j=1, j \neq i}^N G_{ij}(v_j(t) - v_i(t)), \quad i = 1, 2, \dots, N\end{aligned}\quad (1)$$

where $x_i \in R^n$ and $v_i \in R^n$ are the position and velocity states of the i th agent, and the positive constants α and β are the coupling strengths. Let $x = (x_1^T, x_2^T, \dots, x_N^T)^T$, $v = (v_1^T, v_2^T, \dots, v_N^T)^T$, and $y = (x^T, v^T)^T$. Then system (1) can be rewritten in a compact matrix form

$$\dot{y}(t) = (\tilde{L} \otimes I_n)y, \quad (2)$$

where L is the Laplacian matrix of the network, $\tilde{L} = \begin{pmatrix} 0_N & I_N \\ -\alpha L & -\beta L \end{pmatrix}$, and \otimes denotes the Kronecker product.

Let μ_i , $1 \leq i \leq N$, be the eigenvalues of L and set μ_1 to be the zero eigenvalue. The main result that we have obtained is as follows:

Theorem 1 *The second-order consensus in system (2) can be achieved if and only if the network contains a directed spanning tree, and*

$$\frac{\beta^2}{\alpha} > \max_{2 \leq i \leq N} \frac{\mathcal{I}^2(\mu_i)}{\mathcal{R}(\mu_i)[\mathcal{R}^2(\mu_i) + \mathcal{I}^2(\mu_i)]}. \quad (3)$$

In addition, as $t \rightarrow \infty$, $v_i(t) \rightarrow \sum_{j=1}^N \xi_j v_j(0)$ and $x_i(t) \rightarrow \sum_{j=1}^N \xi_j x_j(0) + \sum_{j=1}^N \xi_j v_j(0)t$, where ξ is the nonnegative left eigenvector of L associated with eigenvalue 0 and $\xi^T 1_N = 1$.

Remark 1 *It is easy to check that if all the eigenvalues of the Laplacian matrix L are real, then (3) holds.*

Remark 2 *From (3), it is easy to see that both real and imaginary parts of the eigenvalues of the Laplacian matrix play important roles in reaching second-order consensus. Let $2 \leq k \leq N$ be that index for which the maximum value $\max_{2 \leq i \leq N} \frac{\mathcal{I}^2(\mu_i)}{\mathcal{R}(\mu_i)[\mathcal{R}^2(\mu_i) + \mathcal{I}^2(\mu_i)]}$ is obtained. Then in order to reach consensus, the critical value β^2/α increases as $|\mathcal{I}(\mu_k)|$ increases and decreases as $\mathcal{R}(\mu_k)$ increases.*

Corollary 1 *Second-order consensus in multi-agent system (2) can be achieved if the network contains a directed spanning tree, and*

$$\frac{\beta^2}{\alpha} > \max_{2 \leq i \leq N} \frac{1}{\mathcal{R}(\mu_i)}. \quad (4)$$

Remark 3 *While Theorem 1 provides a necessary and sufficient condition for reaching second order consensus, Corollary 1 gives a sufficient condition which depends only on the real parts of the eigenvalues of L .*

References

- [1] Olfati-Saber, R. (2006). Flocking for multi-agent dynamic systems: algorithms and theory. *IEEE Trans. Auto. Contr.*, 51, 401–420.
- [2] Ren, W. (2008). On consensus algorithms for double-integrator dynamics. *IEEE Trans. Auto. Contr.*, 58(6), 1503–1509.

Infinite Horizon Cooperative Differential Games - Necessary Conditions for Pareto Optimality

Puduru Viswanadha Reddy, Jacob Engwerda
 Department of Econometrics and Operations Research
 Tilburg University
 P.O. Box 90153, 5000 LE Tilburg
 The Netherlands
 Email: {P.V.Reddy, J.C.Engwerda}@uvt.nl

1 Abstract

We consider an N-person cooperative infinite horizon differential game with costs exponentially discounted in time. We give necessary conditions for Pareto optimality for a general class of cooperative games.

2 Introduction

Cooperative differential games involve situations where several persons decide to cooperate while trying to realize their individual objectives, with players acting in a dynamic environment. We consider cooperative games with no side payments. The dynamic environment is modeled as:

$$\dot{x}(t) = f(x(t), u_1(t), u_2(t), \dots, u_N(t)), \quad x(0) = x_0 \in \mathbb{R}^n \quad (1)$$

where $u_i(t)$ is the control strategy/action of player i , $(u_1, u_2, \dots, u_N) \in \mathcal{U}$, with \mathcal{U} being the set of admissible controls. Each player tries to minimize the objective function

$$J_i(u_1, u_2, \dots, u_N) = \int_0^\infty e^{-\rho t} g_i(x(t), u_1(t), u_2(t), \dots, u_N(t)) dt \quad (2)$$

for $i = 1, 2, \dots, N$, where the discount factor $\rho \geq 0$. For the above problem to be well-defined we assume that $f : \mathbb{R}^n \times \mathcal{U} \rightarrow \mathbb{R}^n$ and $g_i : \mathbb{R}^n \times \mathcal{U} \rightarrow \mathbb{R}$, $i = 1, 2, \dots, N$, are continuous; all the partial derivatives of f and g_i w.r.t x and u_i are continuous. Pareto optimality plays a central role in analyzing these problems. Due to co-operation, the cost incurred by a single player cannot be minimized without increasing the cost incurred by other players. So, we consider (Pareto optimal) solutions which cannot be improved upon by all the players simultaneously. We call the controls $(\hat{u}_1, \hat{u}_2, \dots, \hat{u}_N) \in \mathcal{U}$ *Pareto optimal* if the set of inequalities $J_i(u_1, u_2, \dots, u_N) \leq J_i(\hat{u}_1, \hat{u}_2, \dots, \hat{u}_N)$, $i = 1, 2, \dots, N$, (with at least one of the inequalities being strict) does not allow for any solution in $(u_1, u_2, \dots, u_N) \in \mathcal{U}$.

A well known way to find Pareto optimal controls is to solve a parametrized optimal control problem. In [1], necessary conditions for Pareto optimality for the finite horizon cooperative differential game were derived in the spirit of Pontryagin's maximum principle. The transversality conditions,

given as a part of necessary conditions, allow us to select an optimal candidate. The transversality conditions for the finite horizon optimal control problems, in general, do not extend naturally to the infinite horizon case. [2] gives certain counterexamples to illustrate this behavior. So, extra care is necessary while formulating the necessary conditions for infinite horizon optimal control problems. For a general class of infinite horizon optimal control problems, [3] gives an approximating technique, where the infinite horizon problem is approximated with a series of finite horizon problems. Further, with dominating discount condition, [3] shows that transversality conditions for the finite horizon case extend naturally to the infinite horizon case. In this paper we use a similar approach to derive necessary conditions for Pareto optimality for a general class of infinite horizon co-operative differential games.

3 Approach

We consider a general class of dynamic games which guarantee the existence of Pareto optimal controls. Inspired by the approach given in [3], we approximate the infinite horizon co-operative game with a series of finite horizon cooperative games. We impose growth conditions on state trajectories and cost functions of the players as suggested in [3]. Further, by a certain choice of the discount factor we show that the necessary conditions of Pareto optimality for the finite horizon case, as derived in [1], extend naturally to the infinite horizon case.

References

- [1] J. C. Engwerda, "Multicriteria Dynamic Optimization Problems and Cooperative Dynamic Games," *Proceedings SEAMS*, 24-27, July 2007, Yogyakarta, Indonesia.
- [2] H. Halkin, "Necessary conditions for optimal control problems with infinite horizons," *Econometrica* (42), pp. 267-272, 1974.
- [3] S. Aseev and V. Kryazhimskiy, "The Pontryagin maximum principle and transversality conditions for a class of optimal control problems with infinite time horizons," *SIAM Journal on Control and Optimization*, 43, No. 3, 1094-1119, 2004.

Collision-free coordination of a group of unicycle mobile robots

Dragan Kostić,¹ Sisdamanto Adinandra,² Jurjen Caarls,³ and Henk Nijmeijer⁴

Department of Mechanical Engineering
Technische Universiteit Eindhoven
P.O. Box 513, 5600 MB Eindhoven
The Netherlands

Email: {¹D.Kostic, ²S.Adinandra, ³J.Caarls, ⁴H.Nijmeijer}@tue.nl

Abstract

We propose a method for collision-free coordination of a group of unicycle mobile robots, which can be used for transportation tasks in large warehouses. A supervisory system assigns to each robot its reference path, together with the preferable velocity profile as a function of position along the path. The reference paths and velocity profiles do not necessarily prevent collisions among the robots. Feedback controllers of individual robots coordinate the robot motions along the assigned paths to ensure collision-free movements.

To design a collision-free tracking control scheme, we make use of a standard kinematic model of unicycle robots in Cartesian space [1]. From this model we derive equations of tracking error dynamics. Unlike the error equations that are often used in the literature, e.g. [1], we present equations such as to reveal some intrinsic properties of the error dynamics. By making use of these properties, we simplify derivation of tracking motion controllers using Lyapunov's direct method. While explicitly accounting for constraints on input signals, these controllers ensure global asymptotic convergence of the tracking errors to zero values. Although derivation of the control law mimics approach proposed in [2], in our work we modify Lyapunov function in order to improve performance of the resulting motion controllers.

To accommodate specific layouts of robot trajectories in the warehouses, we prove that our controller guarantees global asymptotic convergence of the tracking errors even if the reference angular robot speeds are discontinuous. This is relaxation with respect to [2], where the uniform continuity of the angular speeds was required.

We suggest an effective feedback method for collision-free robot coordination. This method employs penalty functions to reduce reference speeds of robots of lower priority. Feedback variables are the arguments of the penalty functions. To avoid deadlocks in the transportation, all mobile robots must have non-equal priorities during execution of their tasks. Quality of the collision-free robot coordination has been verified both in simulations and in experiments. At the top in Fig.1 we present a layout of robot paths that we used in the experiments. Apparently, starting robot positions were away of the reference paths. Despite the initial errors, all the

robots converge to their references and proceed along without collisions. Nonzero values of experimentally recorded distances to collision, shown at the bottom in Fig. 1, confirm collision avoidance.

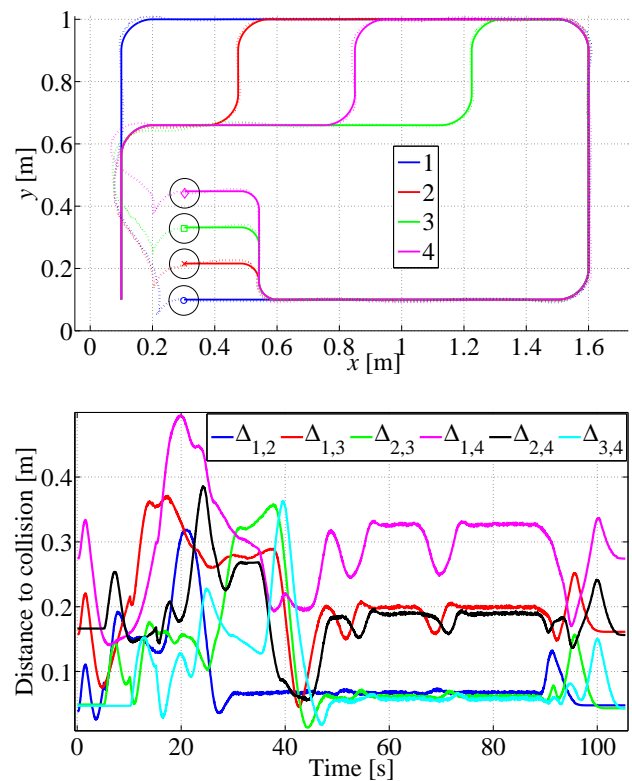


Figure 1: Top: reference (solid) and actual (dotted) paths; bottom: evolution of measured distances to collision.

References

- [1] Y. KanayamaL, *et al.*, "A Stable Tracking Control Method for an Autonomous Mobile Robot," *Proc. IEEE Int. Conf. Robotics and Automation*, pp. 384-389, 1990.
- [2] Z.-P. Jiang, E. Lefeber, H. Nijmeijer, "Saturated Stabilization and Tracking of a Nonholonomic Mobile Robot," *Systems & Control Letters*, Vol. 42, pp. 327-332, 2001.

Cooperative Adaptive Cruise Control

Gerrit Naus, René v.d. Molengraft
Dept. of Mechanical Engineering
Eindhoven University of Technology
P.O. box 513, 5600 MB, Eindhoven,
The Netherlands. Email: g.j.l.naus@tue.nl

Jeroen Ploeg
Business Unit Automotive
Advanced Driver Assistance (ADA)
TNO Helmond, The Netherlands

1 Introduction

Adaptive Cruise Control (ACC) enables automatic following of a preceding vehicle, based on measurements of the inter-vehicle distance $x_{r,i}$ and the relative velocity $\dot{x}_{r,i}$. Commonly, a radar is used for these measurements, see Figure 1. Decreasing the inter-vehicle distance to a small value of only several meters is expected to yield an increase in traffic throughput [1]. To enable this for a string of vehicles, a platoon, inter-vehicle communication is required besides the radar data [2]. This is called Cooperative ACC (CACC).

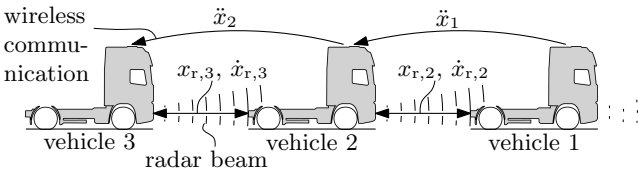


Figure 1: Schematic representation of a platoon of vehicles.

2 CACC problem setup

Consider a string of three vehicles. For more vehicles, the analysis is analogous to that of the third vehicle. Communication with the directly preceding vehicle only is considered, see Figure 1. The primary control objective is to follow the preceding vehicle. A constant time-gap policy is used, which is translated into a desired distance $x_{r,d,i} = r_i + h_{d,i} \dot{x}_{r,i}$, where $h_{d,i}$ the desired time gap or so-called time headway and r_i the desired distance at standstill. The CACC controller consists of a feedback and a feedforward part; the 'standard' ACC controller K_i is implemented as a feedback controller, and the communicated acceleration of the preceding vehicle is used as a feedforward signal. This yields the control output $u_i = K_i e_i + F_i \ddot{x}_{i-1}$, where $e_i = x_{r,d,i} - x_{r,i}$ and F_i a feedforward filter. The resulting control setup for the i^{th} vehicle in the platoon is depicted schematically in Figure 2.

3 String stability analysis

Focusing on heterogeneous traffic, i.e. $G_i \neq G_{i-1}$, $K_i \neq K_{i-1}$, etc., the so-called string stability of a platoon indicates whether velocity or acceleration oscillations are amplified downstream the platoon, i.e. from vehicle one to three [2].

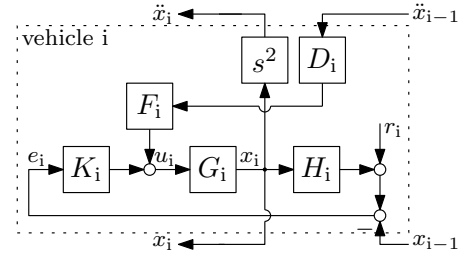


Figure 2: Setup of the CACC control structure for the i^{th} vehicle, where G_i the vehicle dynamics, K_i the ACC feedback controller, F_i the feedforward controller, D_i communication delay and $H_i = 1 + h_{d,i}s$ the spacing policy dynamics.

Using the setup shown in Figure 2, the corresponding string-stability transfer SS_X equals

$$SS_X(s) = \frac{X_i}{X_{i-1}} = \frac{G_i S_i (F_i D_i s^2 + K_i)}{1 + K_i G_i}, \quad \text{for } i \geq 2 \quad (1)$$

where $X_{i(-1)}$ the Laplace transform of $x_{i(-1)}$. String stability is defined as $|SS_X(j\omega)| \leq 1$, $\forall \omega$.

4 Research objective

This research considers the design of a CACC system, focusing on the feasibility of implementation in actual traffic. Hence, communication with the preceding vehicle only and heterogeneous traffic are considered, communication delay is accounted for, and the communicated signal is used in a feedforward setting. A frequency-domain analysis of the string of vehicles regarding string stability and the sensitivity for parameter variations is employed. The presented setup and analysis could be used as a basis for a robust controller synthesis.

References

- [1] B. Van Arem, C.J.G. Van Driel and R. Visser, The impact of co-operative adaptive cruise control on traffic flow characteristics, *IEEE Transactions on Intelligent Transportation Systems*, Vol. 7, No. 4, pp. 429–436, Dec. 2006.
- [2] D. Swaroop and J.K. Hedrick, String stability of interconnected systems, *IEEE Transactions on Automatic Control*, Vol. 41, No. 3, pp. 349–357, March 1996.

Multi-robot coverage to locate fixed and moving targets

Jonathan Rogge
SYSTeMS Research Group
Ghent University
Ghent, Belgium
Jonathan.Rogge@UGent.be

Dirk Aeyels
SYSTeMS Research Group
Ghent University
Ghent, Belgium
Dirk.Aeyels@UGent.be

1 Introduction

The problem statement of this paper belongs to the category of coverage missions using robot formations. Our aim is to locate all targets (fixed or moving) with the robots' sensors within an unknown area, with a 100% certainty that all free space has been covered by the sensors at the end of the procedure. We assume an open space containing disjoint, convex obstacles sparsely spread throughout. Communication is limited: two robots sense each other if their line-of-sight is not obstructed and if the inter-robot distance is sufficiently small.

The algorithm we propose is applicable to situations like search-and-rescue of snow avalanche victims, using specialized transceivers. When a skier is the victim of an avalanche the signal of his transceiver is picked up by receivers of the rescue team. In our setting, the rescue team consists of robots each of which is equipped with a receiver. This scenario may be transposed to similar situations, such as areas prone to earthquakes. Other applications include mine field clearance, where the robots are able to detect the chemical vapor signature of the explosives emanating from the land mines. When a mine is detected a specialized robot can be sent out into the field to remove the mine.

Our algorithm has the nice feature that it can be used for so-called *intercept missions*. This is not true for the existing coverage algorithms in the literature [1]. The use of a robot formation is crucial to this problem. The mission task is to locate and intercept a number of *moving* targets inside an area enclosed by solid obstacle boundaries. Depending on the application these targets can be humans, animals, robots, or simply objects which move under influence of external forces. A robot formation is created to scan the entire area in one sweep, leaving no gaps for the targets to escape.

Preliminary versions of this paper have been described in [2] and [3], containing a sensor coverage algorithm applicable to restricted situations. The present paper describes a novel, more versatile algorithm, which fundamentally differs from the previous versions. The present algorithm uses a different formation configuration, is more rigid, and allows a proof of 100% coverage.

2 Concept of the algorithm

Assume for simplicity that the area to be explored is a rectangular strip $S \subset \mathbb{R}^2$. The robot group will cover all free space by sweeping the strip. Each robot i , with $1 < i \leq N$, is assigned an Individual Leader with index $i - 1$. Robot i maintains a constant distance d with its Individual Leader and observes it at an angle of $\pi/2$ with respect to its forward direction. The forward direction of each robot is imposed at the initialization of the algorithm and is the same for all robots. The resulting set-up is a line formation transversal to the direction of motion.

Consider the case with no objects. The leftmost robot follows the left strip boundary at a constant distance d at a constant velocity v . The remaining robots maintain the formation and follow. This implies that each robot scans a narrow strip, parallel to the strip boundaries, called a basic robot track. Since the sensor ranges of the robots overlap when in formation, the basic robot tracks overlap as well and fill the entire scanning strip. Coverage of all free space is guaranteed.

In the presence of obstacles, the algorithm ensures that the only paths followed by the robots are either paths clockwise along obstacle boundaries, or the aforementioned basic robot tracks. At the start of the algorithm each robot is assigned to one specific robot track, but under the influence of obstacles robots may exchange tracks, altering the initial leader-follower structure. The algorithm we propose ensures that each basic robot track is traced by precisely one robot, yielding complete coverage of the strip S .

References

- [1] H. Choset. Coverage for robotics – a survey of recent results. *Annals of Mathematics and Artificial Intelligence*, 31:113–126, 2001.
- [2] J. Rogge and D. Aeyels. A novel strategy for exploration with multiple robots. In *Proc. of the 4th Intl. Conference on Informatics in Control, Automation and Robotics*, Angers, France, 2007.
- [3] J. Rogge and D. Aeyels. Sensor coverage with a multi-robot system. In *Proc. of the 2007 IEEE Intl. Symposium on Intelligent Control*, Singapore, 2007.

Identification method for time-varying ARX models

Quentin Rentmeesters P.-A. Absil Paul Van Dooren
 quentin.rentmeesters@uclouvain.be absil@inma.ucl.ac.be vdooren@csam.ucl.ac.be
 Department of Mathematical Engineering
 Université catholique de Louvain (UCL)
 Bâtiment Euler, Avenue Georges Lemaître 4, B-1348 Louvain-la-Neuve, Belgium

1 Introduction

In this talk, we are interested in time-varying systems identification using an ARX model of order N :

$$\sum_{i=0}^{N-1} y(t-i)\alpha_i(t) = \sum_{i=0}^{N-1} u(t-i)\beta_i(t)$$

where y is the output of the time-varying system, u is the input and $\alpha_i(t)$ and $\beta_i(t)$ are the coefficients of the model at time t . Time-varying processes appear in many applications such that speech processing, time-varying behaviour detection (fault detection or wear detection) or more generally when some parameters of a linear system vary over time.

Several approaches have been adopted to deal with time-varying modelling problems. One of the most popular approaches to identify a time-varying system is to use an adaptive algorithm which computes iteratively the coefficients of the model; see, e.g., [1]. This approach works quite well under the assumption that the time-variations are slow.

An other approach is to expand the coefficients of the model as a finite set of basis functions [2]. The problem then becomes time-invariant with respect to the parameters in the expansions and is hence reduced to a least squares problem. The two main problems, which are encountered when this approach is applied to general time-varying systems, are how to choose the basis functions, and how to select the significant ones from the family of the basis functions.

Here, we consider a method which identifies the time-varying coefficients in a fixed time window. This method is not recursive and does not impose hard constraints on the evolution of the coefficients of the model. Moreover, at each time step, we identify a value for the coefficients of the model. Thus, we do not have to find a basis to expand these coefficients which is an important practical advantage.

2 Our approach

We propose a method to find the coefficients of the model such that they do not vary too much over time and such that the prediction errors are minimized. This yields a cost func-

tion which is composed of two terms :

$$\min \sum_{t=1}^{T-1} \|X(t) - X(t-1)\|_2^2 + \mu \sum_{t=0}^{T-1} \|\phi^t(t)X(t)\|_2^2$$

s.t. $\alpha_0(t) = 1 \quad \forall t$

where T is the size of the time window where the identification is performed, $\phi(t) = [\alpha_0(t)\beta_0(t)\dots\alpha_{N-1}(t)\beta_{N-1}(t)]$ is the coefficients matrix and $X(t) = [y(t) - u(t)\dots y(t-N+1) - u(t-N+1)]$ is the data matrix. The first term imposes that the coefficients do not vary too fast and the second term corresponds to the prediction error. A parameter μ can be chosen to find a trade-off between fitting the data and enabling the coefficients to vary.

This problem is a least squares problem and we show how to solve it efficiently and how we can adapt it if we know that the true coefficients of the system are periodic functions of time.

Afterwards, we present some methods to select or gain some insights in the μ parameter value and the order of the system.

3 Applications

To illustrate the potential applications of the method presented, we have identified a model of the relation between the measured rain and the river flow in the Meuse river basin and we have tried to detect a seasonal behaviour of the identified coefficients. Finally, we show in which way the method presented is useful to identify a time-varying parameter of a band-pass filter from input-output data.

References

- [1] L. Guo and L. Ljung, Performance analysis of general tracking algorithms, 33rd Conference on Decision and Control, pages 2851–2855, 1994.
- [2] H.L. Wei and S.A. Billings, Identification of time-varying systems using multiresolution wavelet models, International Journal of Systems Science, 2002.

Acknowledgement. This paper presents research results of the Belgian Network DYSCO (Dynamical Systems, Control, and Optimization), funded by the Interuniversity Attraction Poles Programme, initiated by the Belgian State, Science Policy Office. The scientific responsibility rests with its author(s).

Extracting Information on Time-Varying Systems using Multisines

John Lataire and Rik Pintelon

Department ELEC, Vrije Universiteit Brussel, Belgium, e-mail: j.lataire@vub.ac.be

1 Introduction

In this work, some advantages of using multisines as excitation signals for the identification of time-varying systems are highlighted. The systems considered are described by linear differential equations whose coefficients are varying linearly with time. Their equivalent block schematic is given in Figure 1.

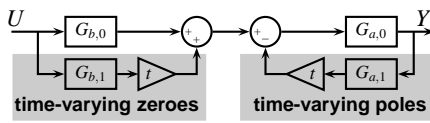


Figure 1: Block schematic of systems described by ordinary differential equations with time-varying coefficients.

Systems that are well described by this schematic within a time window which is significantly larger than the largest typical time constants of the system are further denoted as Linear Slowly Time-Varying (LSTV) systems. When such a system is excited by a multisine, its output signal's spectrum consists of peaks and valleys, as shown in Figure 2. The peaks (given by the black arrows) are centered around the excited frequency lines. They mostly contain information on the time-invariant part of the system. Since, for linear time-invariant (LTI) systems, no signal would be present in between these excited frequencies, the time-varying part is the cause of the valleys at the non-excited lines (given by the grey dots).

These observations are intuitively explained as follows. Applying a multisine to the LSTV system of Figure 1 involves the multiplication of a multisine with a linear ramp at the output of $G_{b,1}$. In the frequency domain, this is equivalent with a convolution of Dirac functions (the multisine's spectrum) with a skirt-like spectrum (the linear ramp's spectrum). This convolution scales, shifts and copies the skirt around each excited frequency line, which explains the presence of valleys and peaks at the output spectrum.

2 The instantaneous transfer function

At a time instant t^* , the frozen system is defined as the system one obtains by freezing the coefficients of the differential equation describing the system at that time instant, or, equivalently, by freezing the time-varying gain in Figure 1

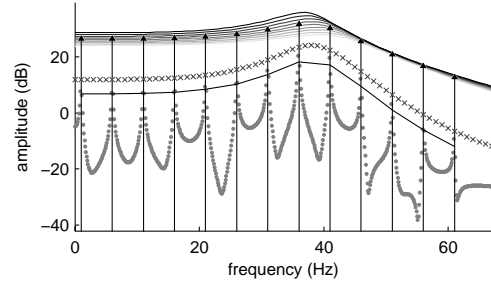


Figure 2: Estimating the speed of variation of a time-varying system's frozen FRF from its output spectrum.

at t^* . The instantaneous transfer function is estimated from the ratio of the second difference of the input and the output spectra, evaluated at the excited frequencies. For $t^* = T/2$ (i.e. the center of the measured time record) a good estimate is shown to be given by [1]: $\bar{F}RF_{\text{instant}} = \Delta^2 Y / \Delta^2 U$, where $\Delta^2 X(k) = -2X(k) + X(k-1) + X(k+1)$, and U and Y are the DFT spectra of the input and output signals over the whole time record.

3 The speed of variation

An interesting knowledge about a time-varying system is the rate at which the instantaneous Frequency Response Function (FRF) varies with time. For slowly time-varying systems, this knowledge is easily extracted from the non-excited frequency lines. The skirts are namely proportional to $G_{b,1}$ and $G_{a,1}$ in Figure 1, which in turn are representative for the time variation of the system. By connecting the tops of the skirts and comparing these with the amplitude of the signal at the excited frequencies, one gets a rough idea of the frequency dependent speed of variation. This is illustrated in Figure 2, where the tops of the skirts are connected by the black full line, and calculated as the corrected mean [1]:

$$Y_{\text{top skirt}}(k_{\text{exc}}) = (Y(k_{\text{exc}} + 1) - Y(k_{\text{exc}} - 1)) / 2. \quad (1)$$

The instantaneous FRF at equidistant time instants is given by the shaded grey to black full lines. Its variance is given by the black crosses. Note that the tops of the skirts are clearly in agreement with the variation of the instantaneous FRF.

References

- [1] J. Lataire, R. Pintelon (2009) "Extracting a Non-parametric Instantaneous FRF of a Linear, Slowly Time-Varying system using a Multisine Excitation", submitted as regular paper to SYS ID 2009.

Acknowledgement - This work is sponsored by the Fund for Scientific Research (FWO-Vlaanderen), the Flemish Government (Methusalem: METH1) and the Belgian Federal Government (IUAP VI/4). J. Lataire is on a Ph. D. fellowship from the Research Foundation - Flanders (FWO)

Blind Maximum Likelihood identification of Wiener systems with measurement noise

L. Vanbeylen¹, R. Pintelon¹, P. de Groen²

Vrije Universiteit Brussel, Depts. ELEC¹ and DWIS², Pleinlaan 2, B-1050 Brussels, Belgium

e-mail: laurent.vanbeylen@vub.ac.be

1 Introduction

This paper is concerned with the maximum likelihood identification of discrete-time Wiener systems from noisy output measurements only (blind identification). It extends the prior developed methods for the blind identification of Wiener (and Hammerstein) systems in a noiseless situation, which, applied to noise-corrupted (output) data unavoidably results in biased estimates. Due to the presence of an extremely high dimensional integral in the expression of the likelihood function, the problem seems very hard at the first glance. The ‘curse of dimensionality’ is avoided by approximating this integral by Laplace’s method for integrals. It turns out that the method works successfully.

2 Model structure

Consider the nonlinear block structure as represented in Fig. 1. It consists of a white, Gaussian input $e(t)$, passing through a cascade connection of a linear, dynamic, LTI system H_0 and a static nonlinearity f_0 . The output measurements are corrupted by additive, white, Gaussian noise $w(t)$, assumed independent of $e(t)$. The linear part is parameterized as a stable, inversely stable, monic rational form $H(q, \theta_L)$ (of known numerator and denominator orders) in the backward shift operator q^{-1} . The nonlinearity is assumed to be described by a function of a known parametric form $f(u, \theta_{NL})$, and is invertible in u . θ_L and θ_{NL} are parameters to be identified, together with the variances of both noise sources $e(t)$ and $w(t)$. All these unknown parameters are collected into a single vector ϑ .

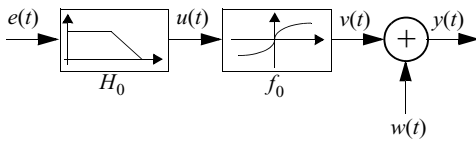


Fig. 1. Block schematic representation of the Wiener system, to be identified from noisy output measurements $y(t)$ only.

3 Integration problem and solution:

Laplace’s integration method

Our task is now, given a vector of N noisy output observations $\mathbf{y}_N^T = [y(0), \dots, y(N-1)]$, to identify ϑ in a maximum likelihood setting, i.e. we need to maximize the likelihood that the measurements \mathbf{y}_N occur given ϑ . The latter is nothing but the probability density function (pdf) $f_{\mathbf{y}}$ of the random vector of observations, evaluated at the data \mathbf{y}_N . The summation at the output results in a

convolution integral over the N -dimensional pdf’s of $v(t)$ and $w(t)$ (denoted by f_v and f_w respectively).

$$f_{\mathbf{y}}(\mathbf{y}_N) = \int_{-\infty}^{+\infty} f_v(\mathbf{v}) f_w(\mathbf{y}_N - \mathbf{v}) d\mathbf{v} \quad (1)$$

Notice that the integral runs over as many dimensions as the number of measurements N . Obviously, due to the fact that N may be (very) high, the classical numerical integration techniques are of no help. It can be shown that after some rearrangements, (1) involves:

$$\int_{-\infty}^{+\infty} \exp(-F(\mathbf{x}, \vartheta)) d\mathbf{x} \quad (2)$$

with $\mathbf{x} \in \mathbb{R}^N$ a vector of integration variables, and $F(\mathbf{x}, \vartheta)$ not specified in this short abstract. In this discussion, the ϑ -dependency is omitted for notational convenience. Laplace’s integration method goes as follows. Since $F(\mathbf{x})$ has a minimum at \mathbf{x}^* , $\exp(-F(\mathbf{x}))$ has a much sharper peak, and the integral will therefore mainly consist of the contribution of the integrand around \mathbf{x}^* . Therefore, it suffices to restrict the evaluation domain to a neighbourhood of \mathbf{x}^* , where we may use a second order Taylor expansion of $F(\mathbf{x})$. Finally, it is observed that the approximate integrand can be seen as a Gaussian pdf. Hence, only the result of this analytic integral has to be evaluated numerically.

4 Results

Laplace’s integration method has given us a minimization to be performed in a N -dimensional domain in exchange to the N -dimensional integration. Moreover, the analytic expression of $F(\mathbf{x}, \vartheta)$ indicates that the approximation error tends to zero as the signal to noise ratio tends to infinity (in which case the estimator coincides with the old method ignoring the presence of noise in the data). An algorithm has been developed to efficiently calculate (involves the minimization of $F(\mathbf{x}, \vartheta)$ over \mathbf{x}) and minimize the approximate negative log-likelihood function over ϑ . The table below shows the very promising results of the described method with 50 Monte Carlo simulations, indicating its superiority compared to the old method.

old method	noiseless data	MSE = 0.062
old method	SNR = 14 dB	MSE = 0.207
new method	SNR = 14 dB	MSE = 0.083

Table 1. The presence of output noise in the data causes a severe bias, indicated by a dramatic increase of the mean squared error (MSE) on the parameters. The latter is significantly reduced by the new method.

This research was funded in part by the Flemish government (METH-1), the Belgian government (IUAP VI/4 - Dysco), and the research council of the VUB (OZR).

Comparison of two nonlinear optimization methods for black box identification

A. Van Mulders¹, M. Volckaert², J. Swevers², M. Diehl³ and J. Schoukens¹

Email: anne.van.mulders@vub.ac.be

¹ Vrije Universiteit Brussel, Dept. ELEC, Pleinlaan 2, B-1050 Brussels, BELGIUM

² K.U.Leuven, Dept. MECH, Celestijnenlaan 300B, B-3001 Heverlee, BELGIUM

³ K.U.Leuven, Dept. ESAT, Kasteelpark Arenberg 10, B-3001 Heverlee, BELGIUM

1 Introduction

Since most real-life systems are to some extent nonlinear, linear models are not always sufficient for users purposes such as Iterative Learning Control (ILC). The black box model structure used here is capable of describing a broad class of nonlinear systems. The maximum likelihood estimation of the model involves the minimization of a nonlinear cost function. Two optimization methods are proposed. The first method (unconstrained) estimates the parameters without estimating the states explicitly, while the second (constrained) estimates both states and parameters by adding an extra constraint equation.

The model structure is a conventional discrete-time state-space model extended with polynomial nonlinear terms. It is called a Polynomial Nonlinear State-space Model (PNLSS) [1]. The PNLSS model equations are shown below:

$$\begin{aligned} x(t+1) &= Ax(t) + Bu(t) + E\zeta(x(t), u(t)) \\ y(t) &= Cx(t) + Du(t) + F\eta(x(t), u(t)) \end{aligned} \quad (1)$$

ζ and η contain monomials in $x(t)$ and $u(t)$. The matrices E and F contain the coefficients associated with these monomials.

2 Identification

The parameters of this nonlinear model are estimated, given the exact input u and the noisy output measurements $y + n_y$ with n_y white noise. The states are assumed to be unknown and in order to solve the problem we minimize the least square error between the measured and modelled output. For both methods, the initial estimates for the linear parameters (A, B, C, D) are found by a two-step procedure [1]. First, the Best Linear Approximation (BLA) of the system is estimated. The BLA minimizes the output error in least squares sense. Secondly, this nonparametric model is converted into a linear parametric state-space model using the Frequency Domain Subspace identification method. The nonlinear parameter matrices (E and F) are initialized to zero.

The two nonlinear optimization methods intend to minimize the same least square cost function $V = \varepsilon^T \varepsilon$ with ε the difference between the modelled and measured output.

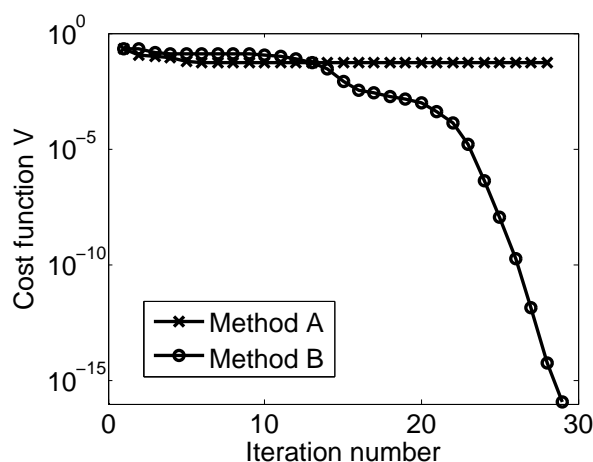


Figure 1: Cost function V versus iteration number for a "nearly" unstable system: methods A and B.

In the unconstrained method (A), the free variables are only the model parameters, optimized with the Levenberg-Marquardt method [2]. In the constrained method (B), both the model parameters and the states are free variables. A constrained Gauss-Newton method based on [2] is used to iteratively update the parameters and states. The Gauss-Newton method is modified in order to overcome singularity problems. Unfortunately, the modification may cause convergence problems. The increased number of search variables of method B (compared to method A), slows down the method and can cause computer memory problems if the number of data points is too high (for instance 10000). On the other hand, method B has the advantage over method A to be robust in case of "nearly" unstable or even unstable models because the constraint equations prohibit the states to diverge. An example illustrating the different convergence behaviour is shown in Fig. 1.

References

- [1] J. Paduart, *Identification of Nonlinear Systems using Nonlinear Polynomial State Space Models*, PhD Thesis, Vrije Universiteit Brussel, 2007.
- [2] R. Fletcher, *Practical methods of optimization*, John Wiley and Sons, 1991.

System realization of generalized model structures

Edwin Reynders and Guido De Roeck

Department of Civil Engineering, Katholieke Universiteit Leuven

Kasteelpark Arenberg 40, B-3001 Leuven, Belgium

Email: edwin.reynders@bwk.kuleuven.be, guido.deroeck@bwk.kuleuven.be

1 Introduction

An algorithm is proposed for the subspace identification of a generalized discrete linear time invariant model structure, composed of a deterministic and a stochastic subsystem that share only part of their poles. Following the terminology of [1], ARMAX, ARARMAX, and Box-Jenkins models can be considered as special cases of the generalized model structure. In a first step, the impulse response of the deterministic subsystem and the correlation function of the stochastic subsystem are estimated in a statistically consistent way. The second step consists of system realization, where a specific choice of the state space basis, that reveals the deterministic and the stochastic dynamics and their coupling, is imposed.

2 Consistent estimation of impulse responses and stochastic output correlations

Let $\mathcal{H}_{0|2i-1}$ and $\mathcal{L}_{1|2i-1}$ denote the matrix consisting of the impulse response matrices \mathbf{H}_k and the stochastic output correlation matrices $\mathbf{\Lambda}_k$ of interest, respectively:

$$\begin{aligned}\mathcal{H}_{0|2i-1} &\triangleq [\mathbf{H}_0^T \ \mathbf{H}_1^T \ \dots \ \mathbf{H}_{2i-1}^T]^T \\ \mathcal{L}_{1|2i-1} &\triangleq [\mathbf{\Lambda}_1^T \ \mathbf{\Lambda}_2^T \ \dots \ \mathbf{\Lambda}_{2i-1}^T].\end{aligned}$$

In [2] it is shown that if (i) the measured inputs can be considered as noise-free, (ii) the considered system is controllable, (iii) the stochastic outputs are uncorrelated with the inputs, and (iv) a persistency of excitation condition on the inputs is satisfied, a strongly consistent estimate of $\mathcal{H}_{0|2i-1}$ can be obtained from projected data matrices. Under the same assumptions, a strongly consistent estimate of $\mathcal{L}_{1|2i-1}$ is obtained from sample correlations, where a Hankel matrix of measured outputs is projected onto the orthogonal complement of a Hankel matrix of measured inputs.

3 Consistent realization of the generalized model structure

Once $\mathcal{H}_{0|2i-1}$ and $\mathcal{L}_{1|2i-1}$ are estimated, it follows from deterministic and stochastic realization theory that their corresponding Hankel matrices can be decomposed into an observability matrix and respectively a deterministic and stochastic controllability matrix:

$$\mathbf{G}_{1|i} \triangleq [\mathbf{H}_{1|i} \ \mathbf{\Lambda}_{1|i}] = \mathcal{O}_i [\mathbf{C}_i^D \ \mathbf{C}_i^S].$$

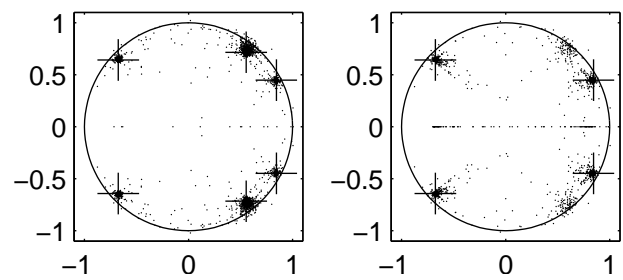
When a specific choice of the state-space basis is imposed, the following generalized state-space model can be obtained from \mathcal{O}_i , \mathbf{C}_i^D , and \mathbf{C}_i^S :

$$\begin{aligned}\begin{bmatrix} x_{k+1}^1 \\ x_{k+1}^2 \\ x_{k+1}^3 \end{bmatrix} &= \underbrace{\begin{bmatrix} A_{11} & 0 & 0 \\ A_{21} & A_{22} & A_{23} \\ 0 & 0 & A_{33} \end{bmatrix}}_A \underbrace{\begin{bmatrix} x_k^1 \\ x_k^2 \\ x_k^3 \end{bmatrix}}_{x_k} + \underbrace{\begin{bmatrix} B_1 \\ B_2 \\ 0 \end{bmatrix}}_B u_k + \underbrace{\begin{bmatrix} 0 \\ K_k^2 \\ K_k^3 \end{bmatrix}}_{K_k} e_k \\ y_k &= \underbrace{[C_1 \ C_2 \ C_3]}_C \begin{bmatrix} x_k^1 \\ x_k^2 \\ x_k^3 \end{bmatrix} + D u_k + e_k,\end{aligned}$$

where $x_k^1 \in \mathbb{R}^{n_1}$ is the part of the state vector $x_k \in \mathbb{R}^n$ that describes the purely deterministic dynamics, $x_k^2 \in \mathbb{R}^{n_2}$ describes the common dynamics and $x_k^3 \in \mathbb{R}^{n_3}$ describes the purely stochastic dynamics.

4 Simulation example

A SISO ARARMAX model, where $n_1 = 0$, $n_2 = 4$, and $n_3 = 2$ in the above decomposition, was used to generate 1000 Monte Carlo simulations of output series of 1000 samples, with equal deterministic and stochastic contributions, i.e., an SNR of 0dB. The figures below show the system poles of the complete system (left) and of the deterministic subsystem (right), identified with the above algorithm for each of the simulations. The true poles are indicated with crosses.



References

- [1] L. Ljung. System identification: theory for the user. Prentice-Hall, Upper Saddle River, NJ, 2nd ed., 1999.
- [2] E. Reynders, R. Pintelon, and G. De Roeck. Consistent impulse response estimation and system realization from noisy data. *IEEE Transactions on Signal Processing*, 22(3):617-637, 2008.

Finite record effects of the errors-in-variables estimator for linear dynamic systems

Kurt Barbé, Rik Pintelon and Gerd Vandersteen,
Vrije Universiteit Brussel, Dept. ELEC, Pleinlaan 2, B-1050 Brussels, Belgium.
Email: Kurt.Barbe@vub.ac.be

1 Problem Statement

Transfer function modeling is a key step in many practical engineering problems such as: the measurement and design of amplifiers, the calibration of sensors, the (physical) modeling of devices from (noisy) input-output data The identification of such systems is generally formulated as a weighted least squares (WLS) problem, [1].

To estimate the transfer function $G_0(j\omega_k)$, with $\sqrt{-1} = j$, a parametric estimate $\hat{G}(j\omega_k, \theta)$ is considered. The Errors-In-Variables (EIV) estimator $\hat{\theta}$ of the parameters θ is found by minimizing the following quadratic cost function, with respect to the parameters θ ,

$$K_L(\theta|\hat{U}, \hat{Y}) = \sum_{k=1}^{L-1} \frac{|\hat{Y}(k) - G(j\omega_k, \theta)\hat{U}(k)|^2}{\sigma_{\xi, \theta}^2(k)} \quad (1)$$

with L the length of one period, $\hat{U}(k), \hat{Y}(k)$ the sample mean of the discrete Fourier transform (DFT) spectra of P periods of the steady state response to a periodic input, \bar{A} the complex conjugate of A and where $\sigma_{\xi, \theta}^2(k)$ equals the variance of the residual $\hat{Y}(k) - G(j\omega_k, \theta)\hat{U}(k)$ at frequencies ω_k .

The good properties of the WLS estimator are only guaranteed asymptotically ($F \rightarrow \infty$). For finite record lengths, the denominator of (1) is not equal to the variance of the numerator due to the non-periodicity of the noise, [2]. This non-periodicity results in a leakage contribution in the numerator of the cost function (1).

2 Proposed Solution

2.1 Modified numerator

Let us consider the Fourier coefficients over blocks of two periods,

$$U_{w_2}^{[i]}(k) = \sum_{n=0}^{2L-1} u_2^{[i]}(n)w(n)e^{-j\frac{\pi k}{L}n} \quad (2)$$

where $u_2^{[i]}(n)$ denotes the i th block of 2 periods of the input signal u . Averaging (2) over the different blocks i is used as the numerator in the cost function (1) where the window $w(n)$ is chosen to suppress the noise leakage errors.

2.2 Modified denominator

If the noise (co)variances are unknown, the (co)variances are to be estimated from the data. Classically, in the case of unknown noise (co)variances these are estimated from the data,

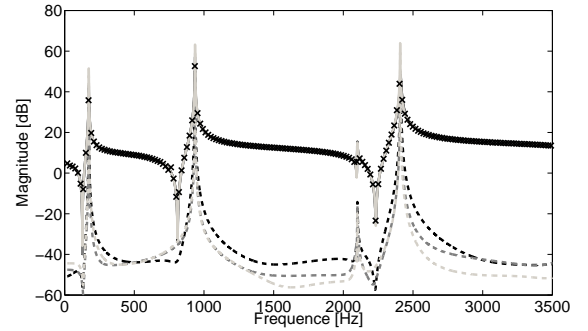


Figure 1: The FRF (crosses), transfer function estimate (solid lines) and its uncertainty (dashed curves) is shown for different windows. Black indicates the rectangular window, dark gray indicates the Hanning window, gray is in some sense the optimal window.

[1], by using the sample (co)variance of the Fourier coefficients over the different blocks. Unfortunately, noise leakage errors are present in the estimated noise (co)variances, such that a strategy similar to the numerator is applied on the residual.

3 Measurement example

A mechanical system was excited with a periodic signal part (50 periods, 1 period is 1024 data points). Figure 1 shows that the transfer function uncertainty can be significantly reduced in the frequency band where the noise leakage errors are the dominant disturbance.

References

- [1] R. Pintelon and J. Schoukens, *System Identification A Frequency Domain Approach*. New York: IEEE press, 2001.
- [2] R. Pintelon, J. Schoukens, and G. Vandersteen, "Frequency domain system identification using arbitrary signals," *IEEE Transactions on Automatic control*, vol. 42, no. 12, pp. 1717–1720, 1997.

Stability analysis in continuous- and discrete-time, using the Cayley transform

Niels Besseling

Department of Applied Mathematics
University of Twente
P.O. Box 217, 7500 AE Enschede
The Netherlands

Email: n.c.besseling@math.utwente.nl

Hans Zwart

Department of Applied Mathematics
University of Twente
P.O. Box 217, 7500 AE Enschede
The Netherlands

Email: h.j.zwart@math.utwente.nl

1 Introduction

Consider the linear differential equation

$$\dot{x}(t) = Ax(t), \quad x(0) = x_0, \quad (1)$$

with the state x in the Hilbert space X . A standard way of solving this differential equation is the Crank-Nicolson method [3]. In this method the differential equation (1) is replaced by the difference equation

$$x_d(n+1) = \left(I + \frac{\Delta A}{2}\right) \left(I - \frac{\Delta A}{2}\right)^{-1} x_d(n), \quad x_d(0) = x_0, \quad (2)$$

where Δ is the time step. The operator $(I + \Delta A/2)(I - \Delta A/2)^{-1}$ is known as the Cayley transform of A , and we denote it by A_d .

The solutions of the differential equation (1) are given via the semigroup $(e^{At})_{t \geq 0}$; i.e. $x(t) = e^{At}x_0$. If we know that a semigroup is exponentially stable, so $\|e^{At}\| \leq M_1 e^{-\omega t}$, with $\omega > 0$, what can be said about the solutions of the difference equation (2), and hence $\|A_d^n\|$?

It is known, that if e^{At} is a contraction semigroup, i.e. $\|e^{At}\| \leq 1$, or if it is an analytic semigroup, then $\|A_d^n\| \leq M_2$, for all $n > 0$. Thus, in these cases the solutions of (2) are bounded, see [1] and [2].

2 Bounded Haar measure difference

We can extend the class of semigroups which behave nicely with respect to the Cayley transform, by introducing the new notion of *bounded Haar measure difference*. We say that two semigroups, e^{At} and $e^{\tilde{A}t}$, have a *bounded Haar measure difference* if the following two inequalities are satisfied for all $x_0 \in X$:

$$\int_0^\infty \|(e^{At} - e^{\tilde{A}t})x_0\|^2 \frac{1}{t} dt < \infty, \quad (3)$$

$$\int_0^\infty \|(e^{A^*t} - e^{\tilde{A}^*t})x_0\|^2 \frac{1}{t} dt < \infty. \quad (4)$$

For example, if $F \in \mathcal{L}(X)$ is a bounded perturbation of A and $\tilde{A} = A + F$, then the semigroups e^{At} and $e^{\tilde{A}t}$ have a bounded Haar measure difference.

For Cayley transforms, A_d and \tilde{A}_d , we say they have a *bounded Haar measure difference* if the following two inequalities are satisfied for all $x_0 \in X$:

$$\sum_{k=1}^\infty \frac{1}{k} \|A_d^k x_0 - \tilde{A}_d^k x_0\|^2 < \infty, \quad (5)$$

$$\sum_{k=1}^\infty \frac{1}{k} \|A_d^{*k} x_0 - \tilde{A}_d^{*k} x_0\|^2 < \infty. \quad (6)$$

One of our main results is, that the Cayley transform conserves the bounded Haar measure difference property. Moreover, the following equality holds:

$$\int_0^\infty \|(e^{At} - e^{\tilde{A}t})x_0\|^2 \frac{1}{t} dt = \sum_{k=1}^\infty \frac{1}{k} \|A_d^k - \tilde{A}_d^k\|^2 x_0. \quad (7)$$

3 Stability

Operators with bounded Haar measure difference have similar stability properties. If A_d and \tilde{A}_d have a bounded Haar measure difference and A_d is *strongly stable*, i.e. $A_d^n x \rightarrow 0$ as $n \rightarrow \infty$, then also \tilde{A}_d is strongly stable. Combining this with equation (7), it leads to the following Theorem:

Theorem 3.1. *Let e^{At} and $e^{\tilde{A}t}$ have a bounded Haar measure difference. Then A_d is strongly stable if and only if \tilde{A}_d is strongly stable.*

Furthermore, the other way around also holds. If A_d and \tilde{A}_d have a bounded Haar measure difference, then e^{At} and $e^{\tilde{A}t}$ have similar stability properties.

References

- [1] B.Z. Guo and H. Zwart, On the relation between stability of continuous- and discrete-time evolution equations via the Cayley transform, *Integral Equations and Operator Theory*, **54**, (2006), 349–383.
- [2] E. Hille and R.S. Phillips, “Functional analysis and semi-groups,” American Mathematical Society, 1957.
- [3] R.D. Richtmyer and K.W. Morton, “Difference methods for initial-value problems,” John Wiley & Sons, Inc., 1967.

Identifiability of the parametrizations of polynomial and rational systems

Jana Němcová

Centrum Wiskunde & Informatica (CWI)

Science Park 123, 1098 XG Amsterdam, The Netherlands

J.Nemcova@cw.nl

1 Abstract

Identifiability is a property of a parametrization of a system. A parametrization is a map from a parameter set to a parametrized system. It maps parameter values to systems derived from the parametrized system by substituting the parameter values to the parameters. We say that a parametrization is globally identifiable if the parameter values can be uniquely determined from the data which are modeled by the parametrized system. It is structurally identifiable if this holds for almost all parameter values. Therefore verifying structural or global identifiability of a parametrization precedes determination of numerical values of the parameters. In this talk, we derive necessary and sufficient conditions for the parametrizations of parametrized polynomial and parametrized rational systems to be structurally or globally identifiable. These results are applied to study the identifiability properties of a system modeling a chain of two enzyme-catalyzed reactions.

2 Introduction

Polynomial and rational systems are used in economy, physics, and engineering. Within systems biology they are used to model for example gene expression, metabolic networks, and enzyme-catalyzed reactions. Since the models of these biological phenomena are usually not fully specified systems but systems with parameters, the problems concerning system identification arise. In this talk we restrict our attention only to the identifiability of parametrizations. This problem deals with the question whether the parameters of the system can be uniquely determined from the measurements.

We study the problem of identifiability for deterministic continuous-time parametrized systems whose dynamics is given by polynomial or rational vector fields and whose output function is componentwise given by a polynomial or a rational function. Our approach, which is related to similarity transformation or state isomorphism approach, strongly relies on the results of realization theory for polynomial and rational systems. For these results which deal with equivalence relations of canonical realizations of the same map see [1, 2]. Many concepts of identifiability of certain parametrized systems are present in the literature. We treat

only global and structural identifiability of parametrized polynomial and rational systems.

3 Main results

In the talk, we introduce the concepts of parametrized and structured polynomial and rational systems. We also introduce the properties of parametrized systems such as structural canonicity and structural distinguishability of parameters. Then the main result can be formulated as follows:

Theorem Let $\Sigma(P)$ be a structured polynomial (rational) system with the parametrization $\mathcal{P} : P \rightarrow \Sigma(P)$. Assume that $\Sigma(P)$ is structurally canonical and denote by CO the smallest strict subvariety of P so that $\Sigma(p) \in \Sigma(P)$ is canonical for all $p \in P \setminus CO$. Assume also that $\Sigma(p)$ is distinguishing parameters for every $p \in P \setminus D$ where D is the smallest strict subvariety of P such that this holds. Then the following are equivalent:

- (a) the parametrization \mathcal{P} is structurally identifiable,
- (b) there exists a strict subvariety S of P such that $CO \cup D \subseteq S$ and for any $p, p' \in P \setminus S$ an isomorphism (birational isomorphism) of the systems $\Sigma(p), \Sigma(p') \in \Sigma(P)$ is the identity.

Global identifiability of the parametrizations of structured polynomial systems is characterized as structural identifiability in the theorem above but with $CO, D, S = \emptyset$. For global identifiability of the parametrizations of structured rational systems we exclude only the parameters $p \in W$ for which the systems are not well-defined, i.e. $CO, D, S = W$.

The results presented in this talk and the motivation for further research are discussed in [3].

References

- [1] Z. Bartosiewicz, *Minimal polynomial realizations*, MCSS, vol.1, 1988, p. 227-237.
- [2] J. Němcová, J.H. van Schuppen, *Realization theory for rational systems: Minimal rational realizations*, to appear in Acta Applicandae Mathematicae.
- [3] J. Němcová, *Structural identifiability of polynomial and rational systems*, submitted.

Energy equipartition and the second law of thermodynamics

Gerard van Willigenburg
Systems and Control Group
Wageningen University
P.O. Box 17, 6700 AA Wageningen
The Netherlands
Email: gerard.vanwilligenburg@wur.nl

Willem de Koning
Kroeskarper 6
2318 NG Leiden
The Netherlands
Email: wilros@planet.nl

1 Introduction

If one demystifies entropy the second law comes out as an emergent property entirely based on the simple dynamic mechanical laws that govern the motion and energies of system parts on a micro-scale. No statistical mechanics is needed. The emergence of the second law is illustrated in this paper through the development of a new, very simple and highly efficient technique to compare and compute time-averaged energies in isolated conservative linear large scale dynamical systems. Entropy is replaced by a notion that is much more transparent and more or less dual called ectropy. Ectropy has been introduced before but we further modify the notion of ectropy such that the unit in which it is expressed becomes the unit of energy. The second law of thermodynamics in terms of ectropy states that ectropy decreases with time *on a large enough time-scale* and has an absolute minimum equal to zero. Zero ectropy corresponds to *energy equipartition*. Basically we show that by *enlarging* the dimension of an isolated conservative linear dynamical system and the dimension of the system parts over which we consider time-averaged energy partition, the tendency towards equipartition increases while equipartition is achieved in the limit. This illustrates that the second law is an *emergent property* of these systems.

2 Energy equipartition

Consider a Hamiltonian conservative system with state x of dimension $2n$. Energies $E_i(t)$ associated to system parts $i=1,2,\dots,N$ are represented by,

$$E_i(t) = x^T(t) S_i x(t), \quad S_i > 0, \quad S_i = S_i^T \quad (1)$$

If the system is *linear, diagonalizable and represented using normal modes* then the following holds for the time-averaged energies [1],

$$\bar{E}_i = \lim_{T \rightarrow \infty} \frac{1}{T} \int_0^T E_i(t) dt = \sum_{j=1,3,5,\dots}^{2n-1} (S_{i,j,j} + S_{i,j+1,j+1}) (x_j^2(0) + x_{j+1}^2(0)) \quad (2)$$

From (2) energies of system parts equipartition, i.e. their time-averages are equal, if and only if all corresponding 2x2 diagonal blocks of S_i have identical traces. This provides a very simple and efficient energy equipartition

test. So far only sufficient conditions, that are also more complicated, have been presented [2], [3].

3 The second law of thermodynamics

The second law of thermodynamics states that entropy always increases towards a maximum. Ectropy is dual to entropy and much more closely related to energy [4]. When modified further ectropy even gets the unit of energy [1]. The following ectropy measure is central to our results,

$$U = \sum_{i=1}^N |\bar{E}_i - \bar{E}|, \quad \bar{E} = \frac{H}{N} \quad (3)$$

where H represents the constant total energy of the conservative linear system. U is nonnegative and measures how far the system is removed from *energy equipartition* among the system parts $i=1,2,\dots,N$ that together make up the whole system. Using (2), (3) in [1] we show that, as the dimensions of a large scale linear conservative Hamiltonian system *divided into equal parts* $i=1,2,\dots,N$ increase, U decreases towards zero. This is consistent with the second law and reveals that this law is an *emergent property*. No statistical mechanics is involved.

The second law of thermodynamics is actually about equipartition of *temperature*, not energy. By introducing thermal capacities however the transition to equipartition of energy of systems divided into equal parts is justified [4]. The results in [1] are restricted to linear large scale one dimensional systems having a homogeneous composition (identical masses and springs). Currently we are investigating if similar results can be produced for linear systems having a non homogeneous composition (different masses and springs).

References

- [1] L.G. van Willigenburg, W.L. De Koning, 2008, "Can the second law of thermodynamics be derived?" Submitted.
- [2] Bhat S.P., Bernstein D.S., 2004, "Average-Preserving Symmetries and Equipartition in Linear Hamiltonian Systems", 43rd Conference on Decision and Control, Atlantis, Paradise Island, Bahamas, December 14-17, 2155.
- [3] Rapisarda P., Willems J.C., 2005, "Conserved- and zero-mean quadratic quantities in oscillatory systems. Mathematics of Control Signals and Systems, 17, 173.
- [4] Haddad W.M., Chellaboina V.S., Nersisov S., 2005, Thermodynamics: A Dynamical Systems Approach, Princeton N.J.: Princeton University Press, Princeton Series in Applied Mathematics.

Extension of the Behavioral Approach to Linear Parameter-Varying Systems

R. Tóth¹, P.S.C. Heuberger¹, and P.M.J. Van den Hof
 Delft Center for Systems and Control
 Delft University of Technology
 Mekelweg 2, 2628 CD Delft
 The Netherlands
 Email: r.toth@tudelft.nl

J.C. Willems
 Department of Electrical Engineering
 Katholieke Universiteit Leuven
 B-3001 Leuven-Heverlee
 Belgium
 Email: Jan.Willems@esat.kleuven.be

1 Introduction

Many physical/chemical processes exhibit parameter variations due to non-stationary or nonlinear behavior, or dependence on external variables. For such processes, the theory of *Linear Parameter-Varying* (LPV) systems offer an attractive modeling framework. LPV systems can be seen as an extension of the class of *Linear Time-Invariant* (LTI) systems. In LPV systems, the signal relations are considered to be linear, but the model parameters are assumed to be functions of a time-varying signal, the so called *scheduling variable* $p: \mathbb{R} \rightarrow \mathbb{P}$, with $\mathbb{P} \subseteq \mathbb{R}^{n_p}$. As a result of this parameter variation, the LPV system class can describe both time-varying and nonlinear phenomena. Practical use of this framework is stimulated by the fact that LPV control design is well worked out, extending results of optimal and robust LTI control theory to nonlinear, time-varying plants.

2 Gaps of the LPV system theory

LPV systems are often described in different representation forms like *Input-Output* (IO), *State-Space* (SS), or *Impulse Response*, where the parameters are functions of the instantaneous value of p . However, representations with such, so called *static dependence*, are inequivalent, which means that generally, there exists no SS realization of an LPV-IO model and vice-versa [2]. As the concept of LPV systems is often defined in terms of these representations, it becomes apparent that there is a lack of basic understanding about the definition of an LPV system. An additional question is how results connected to these different representations can be brought to a common ground. It can be shown that – to establish equivalence of the representations – it is required to introduce *dynamic dependence* of the parameters, dependence on derivatives/time-shifts of p . However, it is not known how to handle such dependencies, and how to formulate algorithms that provide transformations between the representation forms.

3 Behavioral view on LPV systems

A common ground between the several representations and concepts of LPV systems can be found by considering a

behavioral approach to the problem. In this framework, a discrete-time parameter-varying system \mathcal{S} is defined as a quadruple

$$\mathcal{S} = (\mathbb{T}, \mathbb{P}, \mathbb{W}, \mathfrak{B}), \quad (1)$$

where $\mathbb{T} = \mathbb{Z}$ is called the time axis, \mathbb{P} denotes the scheduling space (i.e. $p(k) \in \mathbb{P}$), \mathbb{W} is the signal space and $\mathfrak{B} \subset (\mathbb{P} \times \mathbb{W})^{\mathbb{T}}$ is the *behavior* of the system, defining the trajectories that are possible according to the system model ($\mathbb{X}^{\mathbb{T}}$ stands for all maps from \mathbb{T} to \mathbb{X}). We call \mathcal{S} an LPV system if \mathbb{W} is a vector-space, \mathfrak{B} is time-invariant, and for any valid scheduling trajectory p of \mathcal{S} , $\mathfrak{B}_p = \{w \in \mathbb{W}^{\mathbb{T}} \mid (w, p) \in \mathfrak{B}\}$ is a linear subspace of $\mathbb{W}^{\mathbb{T}}$.

4 System representations

Considering the previous concept of LPV systems, an algebraic structure of polynomials is introduced to define parameter-varying difference equations as representations of the system behavior \mathfrak{B} . Based on the resulting non-commutative polynomial ring $\mathcal{R}[\xi]$, *kernel* (KR), IO, and SS representations of LPV systems are defined with dynamic dependence and the concepts of IO partitions, latent and state-variables are established [1].

5 Equivalence classes and transformations

Using the behavioral framework, equivalence of the introduced representations is investigated via equality of the represented behaviors. It is shown that left-multiplication of the polynomials, associated with these representations, by unimodular matrices on $\mathcal{R}[\xi]$ does not change the behavior while right multiplication results in an isomorphic behavior [1]. These results enable the definition of minimality and the introduction of algorithms to solve the transformation between SS and IO representations via state-elimination and state-map construction.

References

- [1] R. Tóth. *Modeling and Identification of Linear Parameter-Varying Systems, an Orthonormal Basis Function Approach*. PhD thesis, Delft University of Technology, 2008.
- [2] R. Tóth, F. Felici, P.S.C. Heuberger, and P.M.J. Van den Hof. Discrete time LPV I/O and state space representations, differences of behavior and pitfalls of interpolation. In *Proc. of the European Cont. Conf.*, pages 5418–5425, 2007.

¹Support by the Netherlands Organization for Scientific Research (NWO) is gratefully acknowledged.

An IQC Approach to Robust Estimation against Perturbations of Smoothly Time-Varying Parameters

Joost Veenman* and Hakan Koroğlu* and Carsten W. Scherer*

*Delft Center for Systems and Control, Delft University of Technology
Technische Universiteit Delft
P.O. Box 2628 CD Delft
The Netherlands

Email: {j.veenman,h.koroglu,c.w.scherer}@tudelft.nl

Abstract

During the last decade, the robust \mathcal{H}_2 -estimator synthesis problem for linear systems that are subject to white-noise disturbances and norm-bounded parameter uncertainties has been studied intensively. The problem can be formulated as the design of a linear time-invariant estimator that guarantees a norm-bound on the asymptotic variance of the estimation error. Some early works proposed solutions based on Riccati equations and later in e.g [1] methods based on LMI techniques were introduced for systems with parametric uncertainties that can be captured by a polytopic region. It is well known that these methods might lead to rather conservative solutions since the uncertain parameters are allowed to vary arbitrarily fast. For this reason, there have been various attempts to reduce conservatism by using parameter-dependent Lyapunov functions (PDLF). In e.g [2], methods were suggested for systems that depend affinely on uncertain time-invariant parameters. Only recently, in [3] and the references therein, these methods were generalized to the case in which the parameters are allowed to be time-varying. However, despite the fact that the results were considerably improved, they all still might yield conservative results. A second drawback is that the system matrices are restricted to depend affinely on the uncertain parameters.

An alternative framework for stability and performance analysis is the dynamic integral quadratic constraint (IQC) approach, which was initially established in [4]. IQCs are very useful in describing different types of uncertainties. One could for example think of uncertain time-delays, multiple static nonlinearities or uncertain LTI dynamics. Our special attention is devoted to IQC tests for smoothly time-varying parametric uncertainties with bounded rates-of-variation, on which some recent developments are found in [5]. Until very recently, the dynamic IQC-framework was mostly suitable for analysis purposes only. The essential difficulty in synthesis based on dynamic IQCs was the characterization of stability of the closed-loop system. Recently this problem was completely resolved in [6]. A necessary and sufficient positivity condition was derived that can be imposed on the synthesis LMIs in order to enforce stability

of the corresponding closed-loop system. It was also shown in [6] that this result yields convex solutions for the \mathcal{L}_2 -gain and \mathcal{H}_2 -estimator synthesis problems if the uncertainties are described by dynamic IQCs.

The first goal of this work is to merge the new results of [6] with the most recent IQC test for uncertain smoothly time-varying parameters from [5] and to show that we can systematically reduce conservatism with respect to the PDLF based approaches for a broader class of systems. The second goal is to show that the estimator synthesis problem from [6] can be further generalized with the inclusion of a weighting filter at the output. With this filter, we can improve performance in a desired frequency band of interest at the cost of a possible degradation of performance outside the desired frequency band.

References

- [1] J. C. Geromel, "Optimal linear filtering under parameter uncertainty," *IEEE Transactions on Signal processing*, vol. 47, pp. 168–175, 1999.
- [2] K. A. Barbosa, C. E. de Souza, and A. Trofino, "Robust \mathcal{H}_2 filtering for uncertain linear systems: LMI based methods with parametric Lyapunov function," *System & Control Letters*, vol. 54, pp. 251–262, 2005.
- [3] X. Jun and X. Lihua, "An improved approach to robust \mathcal{H}_2 and \mathcal{H}_∞ filter design for uncertain linear system with time-varying parameters," *Proceedings of the 26th Chinese Control Conference*, pp. 668–672, 2007.
- [4] A. Megretski and A. Rantzer, "System analysis via integral quadratic constraints," *IEEE Transactions on automatic and control*, vol. 42, p. 12, 1997.
- [5] H. Koroğlu and C. W. Scherer, "Robust stability analysis against perturbations of smoothly time-varying parameters," *Proceedings of the 45th IEEE Conference on Decision & Control*, pp. 2895–2900, 2006.
- [6] C. W. Scherer and I. E. Köse, "Robustness with dynamic integral quadratic constraints: An exact state space characterization of nominal stability with applications to robust estimation," *Automatica*, vol. 44, pp. 1666–1675, 2008.

The Optimal Linear Quadratic Feedback State Regulator Problem for Index One Descriptor Systems.

Engwerda J.C.

Tilburg University, P.O. Box 90153, 5000 LE Tilburg, The Netherlands
engwerda@uvt.nl

Salmah, Wijayanti I.E.

both Gadjah Mada University, Yogyakarta, Indonesia
syalmah@hotmail.com

1 Abstract

In this paper we present both necessary and sufficient conditions for the existence of a linear static state feedback controller if the system is described by an index one descriptor system. A priori no definiteness restrictions are made w.r.t. the quadratic performance criterium. It is shown that in general the set of solutions that solve the problem constitutes a manifold. This feedback formulation of the optimization problem is natural in the context of differential games and we provide a characterization of feedback Nash equilibria in a deterministic context.

References

- [1] Engwerda J.C., Salmah and Wijayanti I.E., 2008. The Optimal Linear Quadratic Feedback State Regulator Problem for Index One Descriptor Systems. CentER DP 2008-90, Tilburg University, The Netherlands.

Improving Pushbelt Continuously Variable Transmission Efficiency via Extremum Seeking Control

Stan van der Meulen and Bram de Jager
Eindhoven University of Technology
Department of Mechanical Engineering
P.O. Box 513, 5600 MB Eindhoven
The Netherlands

Email: {S.H.v.d.Meulen,A.G.de.Jager}@tue.nl

Erik van der Noll
Bosch Business Unit CVT
Department of Advanced Engineering
P.O. Box 500, 5000 AM Tilburg
The Netherlands

Email: Erik.vanderNoll@nl.bosch.com

1 Background

The infinite number of transmission ratios in a continuously variable transmission (CVT) provides more freedom to match the engine operating conditions to the variable driving conditions in comparison with power transmission devices with a fixed number of transmission ratios. This improves the fuel consumption of the vehicle. The transmission ratio is realized by the variator, a friction drive, see Fig. 1, which consists of a metal V-belt that is clamped between two pairs of conical sheaves. The research is concerned with the variator control design, where the objective is to further improve the variator efficiency, while the variator functionality is preserved.

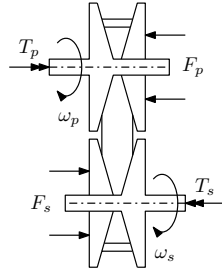
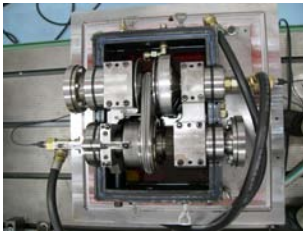


Fig. 1: Pushbelt CVT variator (Left: Test rig; Right: Illustration).

2 Variator Control Design

2.1 Actuators and Sensors

In production CVTs, the clamping forces F_p and F_s (Fig. 1) are applied by the hydraulic actuation system, which includes two servo valves. The manipulated variables are the servo valve currents I_p and I_s . The measured variables are the secondary clamping force F_s and the angular velocities ω_p and ω_s (Fig. 1). Furthermore, T_p and T_s (Fig. 1) denote the torques.

2.2 Control Objectives

The control objectives are: 1) track a prescribed speed ratio reference $r_{s,\text{ref}}$ ($r_s = \omega_s/\omega_p$) and 2) optimize the variator efficiency η ($\eta = T_s\omega_s/T_p\omega_p$). Clearly, the variator efficiency is a performance variable that is not measured. Hence, a measured variable is required that indicates performance.

3 Experimental Results

In the experiments, the primary moveable conical sheave is fixed. This isolates the problem of optimizing the variator efficiency and neglects the problem of tracking a prescribed speed ratio reference. In Fig. 2 (Left), open loop experiments are shown in which F_s decreases. Conclusions are: 1) a global maximum exists in the F_s - η map, 2) a global maximum exists in the F_s - r_s map, and 3) the extrema in 1) and 2) occur for nearly the same value of F_s . Hence, the speed ratio r_s indicates performance.

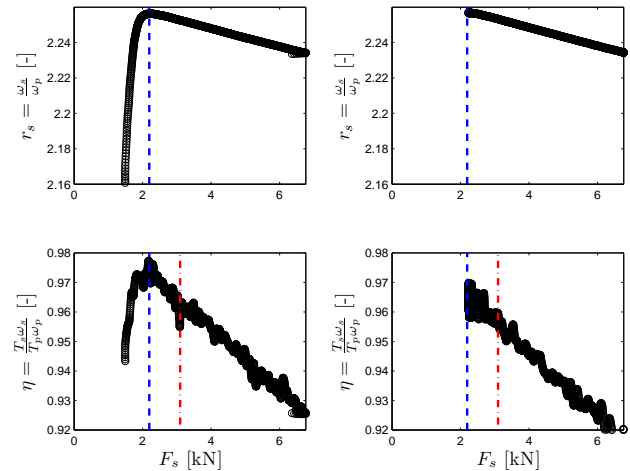


Fig. 2: Experiments (Left: Open loop; Right: Closed loop) (solid: Measurement; dashed: Extremum in F_s - r_s map; dashed-dotted: Conventional variator control design).

The extremum in the F_s - r_s map is found by means of extremum seeking control (ESC) [1] in a stable way. In Fig. 2 (Right), closed loop experiments are shown in which F_s decreases. The ESC algorithm converges towards a small neighborhood of the extremum in the F_s - r_s map and outperforms a conventional variator control design.

References

- [1] M. Krstić and H.-H. Wang, "Stability of extremum seeking feedback for general nonlinear dynamic systems," *Automatica*, vol. 36, no. 4, pp. 595–601, 2000.

Model predictive control for the reduction of traffic emissions

S. K. Zegeye, B. De Schutter¹, and J. Hellendoorn

Delft Center for Systems and Control

Delft University of Technology, Mekelweg 2, 2628 CD Delft, The Netherlands

Email: {s.k.zegeye, j.hellendoorn}@tudelft.nl, b@deschutter.info

1 Introduction

Nowadays, traffic jams are constantly affecting our mobility. Moreover, the frequent traffic jams are also responsible for the enormous increase of fuel consumption and emissions by the road traffic. For example, traffic emissions account for 40% of volatile organic compounds, more than 70% of NO_x, and over 90% of CO in most European cities [4].

Although the demand to reduce emissions and the desire to decrease travel times are two conflicting requirements of traffic control [1], we show that a model-based control approach can be used to address these challenges. In the sequel we describe and demonstrate our approach to tackle the traffic control problem.

2 Approach

Since traffic flow is a very nonlinear and complex system, designing a simple linear controller that can take the constraints of the system into account is infeasible. In this sense, and to predict the effect of applied control measures on the evolution of traffic system states, a model-based traffic control is a sensible approach. Particularly, model predictive control (MPC) is used to reduce both emissions and travel times. In this approach we use models to predict the emissions and travel times of various control measure settings over a certain prediction horizon. The most optimal settings are then selected using numerical optimization and applied to the traffic system. At the next control time step the current traffic condition is assessed again through new measurements and updated predictions of demands, etc., and the whole process is repeated. For this approach we use GHR[3] traffic flow model and VTmicro [2] emission model.

3 Case study

The approach is implemented on a single-lane one-way 8 km freeway. As shown in Fig. 1, the roadway is divided into three sections, and two speed limit controls are applied in the last two sections. The section of the freeway from 3.5 km to 5.5 km is assumed to be congested. We define two objective

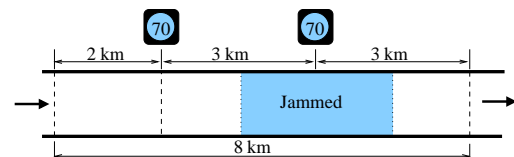


Figure 1: Layout of the case study

Table 1: Simulation results

	Control objective	TE (kg)	TTS (veh·h)
1	Uncontrolled	13.24	383.1
2	Travel time	14.92	210.4
3	Emissions	8.29	340.6

functions, one as the total time spent (TTS) and the other as the total emissions (TE).

4 Results and conclusions

Tab.1 summarizes the simulation results for three different control objectives. We can see that under congested traffic conditions, traffic control aiming at either emissions or travel time can have a negative effect on respectively travel time or emissions. It can also be seen that with the considered case study MPC traffic control reduces the emissions by 37.5% and the travel time by 11.2% when emissions is considered as the objective of the MPC optimization.

References

- [1] K. Ahn and H. Rakha. The effects of route choice decisions on vehicle energy consumption and emissions. *Transportation Research Part D*, 13(3):151–167, May 2008.
- [2] K. Ahn, A. A. Trani, H. Rakha, and M. Van Aerde. Microscopic fuel consumption and emission models. In *Proceedings of the 78th Annual Meeting of the Transportation Research Board*, Washington DC, USA, January 1999. CD-ROM.
- [3] D. Gazis, R. Herman, and R. Rothery. Nonlinear follow the leader models of traffic flow. *Operations Research*, 9(4):545–567, 1961.
- [4] S. Schmidt and R. P. Schäfer. An integrated simulation systems for traffic induced air pollution. *Environmental Modeling & Software*, 13(3-4):295–303, 1998.

¹B. De Schutter is also with the Maritime and Transport Technology Department.

Research supported by the Shell/TU Delft Sustainable Mobility program, the BSIK project “Transition towards Sustainable Mobility (TRANSUMO)”, and the Transport Research Center Delft.

Minimum-fuel control of combustion engine powertrains

Bart Saerens

Department of Mechanical Engineering
Katholieke Universiteit Leuven
Celestijnenlaan 300A, 3001 Heverlee
Belgium

bart.saerens@mech.kuleuven.be

Eric Van den Bulck

Department of Mechanical Engineering
Katholieke Universiteit Leuven
Celestijnenlaan 300A, 3001 Heverlee
Belgium

eric.vandenbulck@mech.kuleuven.be

1 Introduction

Operation optimization of combustion engine powertrains is mainly done based on a given powertrain rotation speed trajectory. A big potential for lowering the energy consumption lies in the optimization of these speed trajectories themselves. This method has been widely used in aerospace applications and for the optimal operation of trains. On the other hand, speed trajectory optimization is hardly researched for road vehicles. For combustion engine powertrains, predictive cruise control (PCC) [1] uses a kind of speed trajectory optimization. To the authors' best knowledge, only Stoicescu [4] published a basic work on minimum-fuel speed trajectories of combustion engine powertrains. Due to assumptions about the fuel consumption modeling, Stoicescu's optimal control is a bang-off-bang control. Although this type of control is typical for simple fuel-optimal control problems [2], it is not practical as shown by Saerens et. al. [3].

2 Problem formulation

Consider a powertrain with an internal combustion engine and a basic driveline (clutch with no dynamics, no gearbox). The dynamics are given by:

$$\frac{d\omega}{dt} = \frac{T - \ell(\omega)}{I}, \quad (1a)$$

$$\frac{d\theta}{dt} = \omega, \quad (1b)$$

with ω the rotation speed of the powertrain shaft, θ its position, T [Nm] the engine brake torque, $\ell(\omega)$ [Nm] the load function and I [Nm.s²/rad] the rotation inertia. The optimal control problem that is considered, is changing the rotation speed of the shaft of the powertrain from ω_s to ω_e with a minimum of fuel consumption. The total time t_e and the total amount of rotations θ_e (\sim distance) can be fixed or subject to optimization.

The authors propose a new generic model of the fuel consumption of the combustion engine:

$$\dot{m}_f = \begin{cases} \dot{m}_{f0}(\omega) + \text{esfc}(\omega, T)\omega T, & \text{if } T > 0, \\ \dot{m}_{fb}(\omega), & \text{if } T \leq 0, \end{cases} \quad (2)$$

with $\dot{m}_{f0}(\omega)$ [kg/s] the fuel mass flow rate at zero torque, $\dot{m}_{fb}(\omega)$ [kg/s] the fuel mass flow rate at idling or braking

torque and $\text{esfc}(\omega, T)$ [kg/(Nm.rad)] the *extra specific fuel consumption*.

3 Problem solution

Since this paper tries to give a deeper and analytical insight on basic optimal control of combustion engine powertrains, Pontryagin's Maximum Principle [2] is used. The analysis shows that the dependency of the extra specific fuel consumption of the engine torque T is very important. If the esfc is independent of T , an optimal control will be bang-off-bang. An optimal control trajectory is composed of several operating modes. The possible modes are: full braking, singular braking, coasting, decelerating, constant speed, singular constant speed and accelerating.

4 Test cases

Several test cases of increasing the powertrain speed are presented, for different kinds of control problems (t_e and θ_e fixed or free) and for different kinds of load functions.

If the total time and total amount of revolutions are free, the optimal torques will be relatively high and will asymptotically behave as the load function. With the total time fixed and the total amount of revolutions free, optimal torques can be lower, but the same asymptotical behavior is observed. If the total amount of revolutions is fixed, then in normal conditions there will be an evolution towards a steady state speed. For the total time free, this is the rotation speed that yields minimal consumption per rotation of the powertrain.

References

- [1] E. Hellström, "A Real-Time Fuel-Optimal Cruise Controller for Heavy Trucks Using Road Topography Information", SAE technical paper, 2006-01-0008 (2006).
- [2] D.E. Kirk, "Optimal Control Theory - An Introduction", Networks Series, Prentice-Hall, Englewood Cliffs New Jersey, 1970.
- [3] B. Saerens, M. Diehl, J. Swevers, and E. Van den Bulck, "Model Predictive Control of Automotive Powertrains - First Experimental Results", in Proc. 47th IEEE Conference on Decision and Control, Cancun, Mexico, Dec. 911 2008, pp. 5692-5697.
- [4] A.P. Stoicescu, "On Fuel-optimal Velocity Control of a Motor Vehicle", Int. J. of Vehicle Design, 16 (1995).

Controlling an active cabin suspension for commercial vehicles

Willem-Jan Evers^{**}, Arjan Teerhuis[◇], Igo Besselink^{*}, Henk Nijmeijer^{*}

^{*} Eindhoven University of Technology,
Department of Mechanical Engineering,
5600 MB Eindhoven, The Netherlands
Fax: +31 402461418
Email: W.J.E.Evers@tue.nl
Email: I.J.M.Besselink@tue.nl
Email: H.Nijmeijer@tue.nl

[◇] TNO Automotive,
Advanced Chassis and Transport Systems,
5700 AT Helmond, The Netherlands
Fax: +31 4925665666
E-mail: arjan.teerhuis@tno.nl

^{*} Corresponding author.

1 Abstract

The field of automotive suspensions is changing. Semi-active and active suspensions are starting to become viable options for vehicle designers, [2, 5, 7]. Suspension design for commercial vehicles is especially interesting given its potential, [3, 4, 8]. However, as mentioned in [1], the fields of suspension control for commercial vehicles and in particular design and control of secondary suspensions, are little addressed in literature.

In this study, an active cabin suspension is considered, consisting of four ideal actuators with parallel springs, one acting on each corner of the cabin. The main question is how to control this suspension such that it gives optimal comfort when driving in a straight line, but still follows a specified compensation strategy when cornering, braking or accelerating. The proposed controller uses modal input-output-decoupling. Each of the modes has a separate controller including: a sky-hook part for enhanced comfort; and an event part for attitude control.

The proposed control strategy is tested in simulation using a validated tractor semi-trailer model with idealized actuators. It is shown that the driver comfort can be greatly enhanced, without damaging the attitude behavior of the cabin. Furthermore, in contrast to what is known from quarter car analysis, it is shown that adding passive damping is highly desirable, see Fig. 1.

A few things can be noticed in this figure. Firstly, lowering the stiffness by replacing the steel springs of the cabin with air springs results in improved comfort. The root-mean-square value of the heave, pitch and roll accelerations are all reduced. This is also reflected in the ride comfort index [6],

$$RCI = \sqrt{\frac{1}{T} \int_0^T (\ddot{x}_{ISO}^2 + \ddot{y}_{ISO}^2 + \ddot{z}_{ISO}^2) dt}, \quad (1)$$

hence the lower the RCI value, the better the driver comfort perception. Furthermore, the significant gain using an active suspension with the proposed control

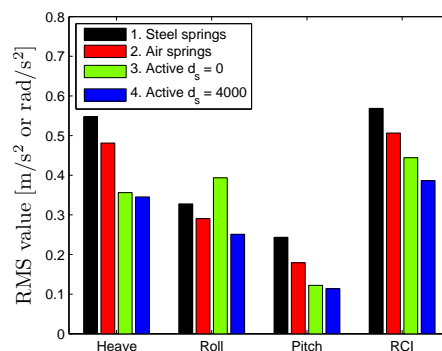


Figure 1: Overview of comfort evaluation on asphalt.

strategy is also clear. Especially for the configuration with added passive damping.

References

- [1] Cole, D.J. "Fundamental Issues in Suspension Design for Heavy Road Vehicles". *Vehicle System Dynamics*, 35(4), pp 319-360, 2007.
- [2] Evers, W.J.E., Besselink, I., van der Knaap, A.C.M. and Nijmeijer, H. "Analysis of a variable geometry active suspension". *International Symposium on Advanced Vehicle Control*, Kobe, Japan, pp. 350-355, 2008.
- [3] Fisher, D. and Isermann, R. "Mechatronic semi-active and active vehicle suspensions". *Control Engineering Practice*, 12, pp 1353-1367, 2004.
- [4] Graf, C., Maas, J. and Pflug, H-C. "Konzept für eine aktive Lkw-Fahrerhauslagerung". *AUTOREG 2008 Conference*, Baden-Baden, Germany, February 2008, (written in German).
- [5] Hrovat, D. "Survey of advanced suspension developments and related optimal control applications". *Automatica*, 33(10), pp 1781-1817, 1997.
- [6] International Standard ISO 2631-1:1997. "Evaluation of human exposure to whole-body vibration - Part 1: General requirements", 1997.
- [7] Jones, W.D. "Easy ride: Bose Corp. uses speaker technology to give cars adaptive suspension". *IEEE Spectrum*, 42(5), pp 12-14, 2005.
- [8] Nakano, K. and Suda, Y. "Combined Type Self-Powered Active Vibration Control of Truck Cabins". *Vehicle System Dynamics*, 41(6), pp 449-473, 2004.

Global Chassis Control based on Load Sensing

Mathieu Gerard, Michel Verhaegen, Edward Holweg
Delft Center for Systems and Control, Delft University of Technology
Mekelweg 2, 2628CD Delft, The Netherlands
m.p.gerard@tudelft.nl

1 Abstract

Modern cars are equipped with an increasing number of active systems [3] in order to help the driver, e.g. to better deal with unexpected changes in the vehicle dynamics. To improve the global vehicle dynamics, comfort and handling, coordination between traditionally stand-alone active systems is required. This demands for a Global Chassis Controller [2].

Thanks to the use of tyre force sensors, the controller proposed in this paper is structured on two layers which simplify the implementation and the computation.

The top layer deals with the global control and the force allocation. Thanks to the structure, the nonlinearities and uncertainties of the tyre do not appear in this layer and the allocation can be treated as a convex optimization problem. The solution to this problem taking tyre friction constraints into account is provided by a hybrid dynamical system [1].

The bottom layer features four independent local tyre controllers. These ensure, in a robust manner, that the allocated forces are realized.

A simulation example shows the performance of the method during a *split-mu braking* manoeuvre.

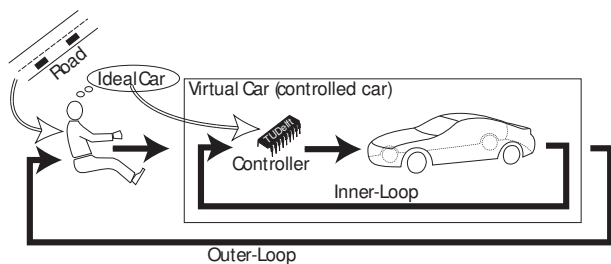


Figure 1: The vehicle motion is controlled via two feedback loops. The inner-loop, closed by the controller, renders the car easier to drive. The outer-loop, closed by the driver, maintains the trajectory.

2 Experimental Facilities

To be able to test and validate those new chassis control concepts, various experimental facilities are developed and adapted. Four facilities will constitute a consistent set for dealing with the different aspects:



Figure 2: X-Car Driving Simulator. This moving simulator is being developed with a clear focus on vehicle dynamics.

- **The Tire Test Bench.** Tyres, being nonlinear and uncertain, are playing an important role in the control design. Therefore our tyre drum has been adapted in order to allow close-loop control of the brake based on, for example, force measurement.
- **The TNO Moving Bases.** Tests are being planned on mobile robots at TNO to focus on the coupling between braking and steering at tyre level and on the interaction of the four tyres.
- **The X-Car driving simulator.** The simulator has recently been completely reprogrammed with a clear focus on vehicle dynamics. The objective is to assess the added value of new controllers when placed in the hands of a human driver. (Figure 2)
- **The BMW test vehicle.** When all the previous tests are conclusive, the final assessment and tuning will be done on our new test vehicle.

References

- [1] M. Gerard, M. Verhaegen, B. De Schutter. A Hybrid Steepest Descent Method for Constrained Convex Optimization. *Automatica*. <http://dx.doi.org/10.1016/j.automatica.2008.08.018>. 2008.
- [2] J. Andreasson. On Generic Road Vehicle Motion Modelling and Control. Doctoral Thesis in Vehicle Dynamics. Stockholm, Sweden. 2006.
- [3] M. Jonasson, S. Zetterström, A. Trigell. Autonomous Corner Modules as an Enabler for New Vehicle Chassis Solution. FISITA World Automotive Conference, Yokohama, Japan. 2006.

Development of a belt force actuator for controlled seat belt systems

Ewout van der Laan
Department of Mechanical Engineering
Technische Universiteit Eindhoven
P.O. Box 513, 5600 MB Eindhoven
The Netherlands
Email: E.P.v.d.Laan@tue.nl

Bram de Jager, Frans Veldpaus
Department of Mechanical Engineering
Technische Universiteit Eindhoven
P.O. Box 513, 5600 MB Eindhoven
The Netherlands
{A.G.de.Jager, F.E.Veldpaus}@tue.nl

1 Introduction

The loads exerted by the seat belt on a human body during a vehicle crash, are essential in the injury mechanisms of the chest [1]. Injury risk can be reduced when the seat belt load is controlled based on crash conditions, e.g., impact severity and occupant type [2]. In this study, a semi-active actuator for this control system is developed.

2 Sled setup

An experimental sled setup is developed (Fig. 1) to test the belt force actuator and to demonstrate its potential for injury reduction. A mass representing an occupants torso (4), is

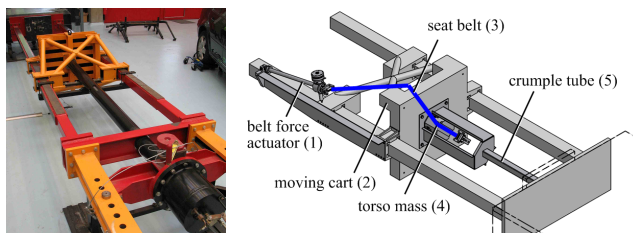


Figure 1: Picture (left) and drawing (right) of the sled setup.

mounted on a cart (2), that impacts against a deformable crumple tube (5) at high speed (12 ms^{-1}). A force actuator (1) is connected to a belt (3), and will be used to control the torso body acceleration. The sled setup is modeled, see Fig. 2, and simulations with measured cart accelerations are used to obtain actuator specifications.

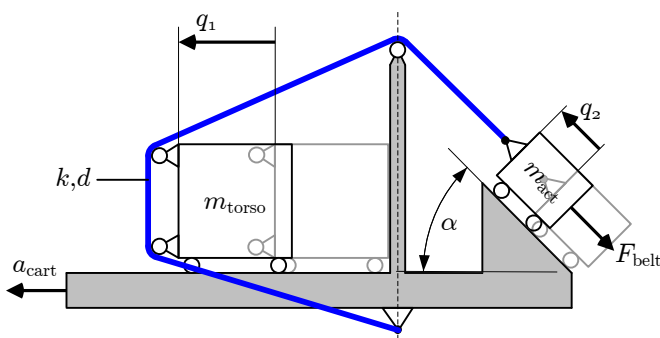


Figure 2: Simple 2D sled setup model.

3 Semi-active belt force actuator

A semi-active actuator design is chosen, comprised of an hydraulic cylinder, see Fig. 3. During impact, the belt force causes the cylinder to extend and fluid outflow is controlled by a very fast spool valve, actuated by a voice coil.

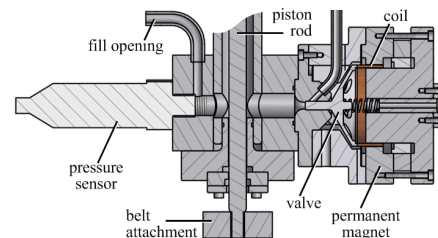


Figure 3: Semi-active hydraulic actuator.

4 Simulation results

The valve dynamics are modeled and combined with the sled model. An outer feedback controller is designed to track a desired torso acceleration. A local feedback controller calculates the current through the voice coil to track the desired force, see Fig. 4. The actuator shown in Fig. 3 has been built, and experimental results are expected early 2009.

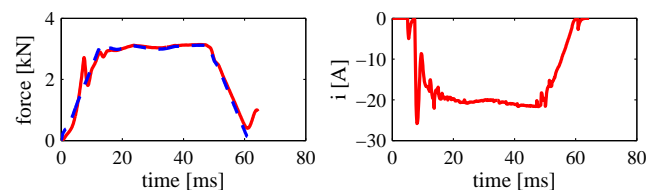


Figure 4: Desired (—) and applied (— —) belt force (left) and the required current (right)

References

- [1] J. Crandall et. al, *Limiting performance of seat belt systems for the prevention of thoracic injuries*, Journal of Automobile Engineering, 214(2), p. 127-139, 2000.
- [2] R.J. Hesseling et. al, *Feedback control of occupant motion during a crash*, International Journal of Crashworthiness, 11(1), p. 81-96, 2006.

Estimating the parameters of a Rice distribution using a Bayesian approach

Lieve Lauwers, Kurt Barbé, Wendy Van Moer and Rik Pintelon

Vrije Universiteit Brussel, dep. ELEC, Pleinlaan 2, 1050 Brussels, BELGIUM

e-mail: lieve.lauwers@vub.ac.be

Abstract - Detecting a periodic signal corrupted by zero-mean Gaussian noise is a problem that arises in various fields of engineering. The amplitude of the disturbed signal is known to follow a Rice distribution which is characterized by two parameters. A Bayesian approach is proposed to tackle this two-parameter estimation problem. The idea is to incorporate prior knowledge into a mathematical framework. The performance of the proposed Bayesian estimator is shown via simulations.

1. Introduction

In various engineering applications, the user is confronted with periodic signals that are disturbed by zero-mean Gaussian noise. It is well-known that the amplitude of the disturbed signal is distributed (in the frequency domain) according to the Rice probability density function [1]. The Rice distribution is fully described by two parameters: the amplitude A of the desired signal and the standard deviation σ of the Gaussian noise source. To estimate these two parameters from amplitude measurements only, we propose a Bayesian approach in which we make use of relevant, known information about the measured signal.

2. Rice distribution

Amplitude measurements $x = [x_1, \dots, x_N]$ of a corrupted periodic signal are Rice distributed when every sample x_i is independent and characterized by the following probability density function (pdf)

$$f(x_i|\theta) = \frac{x_i}{\sigma^2} \exp\left(-\frac{x_i^2 + A^2}{2\sigma^2}\right) I_0\left(\frac{x_i A}{\sigma^2}\right) \quad (1)$$

with $\theta = [A, \sigma]$. $I_0(x)$ denotes the zero-order modified Bessel function of the first kind [2].

3. Bayesian approach

Estimating the unknown parameters θ from N independent amplitude measurements x is classically formulated in a Maximum Likelihood (ML) framework [3]. However, using the ML approach to solve this two-parameter estimation problem is not optimal [4],[5]. To overcome the drawbacks of the ML method while keeping the good statistical properties of the ML estimator [3], we construct a Bayesian equivalent for the likelihood function of the ML framework, by using the following prior knowledge:

- A and σ are non-negative;
- A and σ are independent;
- the Rice distribution is scale invariant.

This prior information needs to be translated into a so-called prior distribution $\Pi(\theta)$ for the unknown parameters [6]. This prior distribution can be interpreted as a

description of what is known about the parameters θ in the absence of measurements x . The prior knowledge of the parameters can then be updated by taking into account the measurements x which follow the likelihood function $\mathcal{L}(x|\theta)$ [7]. This leads to the so-called posterior density function

$$f(\theta|x) = c \mathcal{L}(x|\theta) \Pi(\theta) \quad (2)$$

with c a constant. In a Bayesian framework, (2) plays a similar role as the likelihood function of the ML framework. Hence, the Maximum A Posteriori (MAP) estimator is defined as

$$\hat{\theta}_{MAP} = \arg \max_{\theta} f(\theta|x) \quad (3)$$

4. Simulation results

In Fig. 1, we compare the MAP estimator with the ML estimator in Root Mean Square (RMS) sense for different Signal-to-Noise Ratios (SNRs).

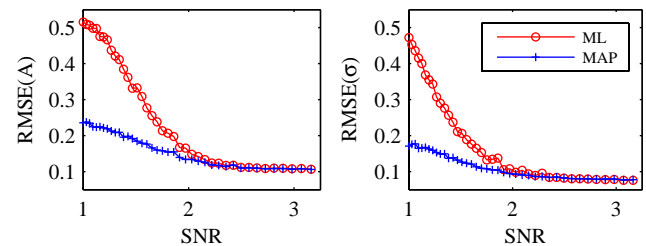


Fig. 1. The RMS error of A (left) and σ (right) as a function of the SNR for the ML (o) and the MAP (+) estimator, using 100 data points.

5. Conclusion

We have presented an alternative approach for the two-parameter estimation problem of the Rice distribution. We showed that the Bayesian estimator outperforms the ML estimator in RMS sense for low SNRs.

References

- [1] S. O. Rice, "Mathematical analysis of random noise", *Bell System Technical Journal*, Vol. 24, pp. 46 and further, 1945.
- [2] G. B. Arfken, H. J. Weber, "Mathematical Methods for Physicists", 6th edition, Harcourt: San Diego, 2005.
- [3] M. Kendall, A. Stuart, "The advanced Theory of Statistics", Griffin, Vol. 2, 4th ed., 1979.
- [4] T. R. Benedict, T. T. Soong, "The joint estimation of signal and noise from the sum envelope, *IEEE Trans. on Information Theory*, Vol. 13, No. 3, pp. 447-454, 1967.
- [5] J. Sijbers, A. J. den Dekker, et al., "Maximum-Likelihood Estimation of Rician Distribution Parameters", *IEEE Trans. on Medical Imaging*, Vol. 17, No. 3, pp. 357-361, 1998.
- [6] A. O'Hagen and J. Forster, "Kendall's Advanced Theory of Statistics: Bayesian Inference", Arnold, London, 2004.
- [7] E. L. Lehmann, G. Casella, "Theory of Point Estimation", 2nd ed., Springer-Verlag, New York, 1998.

Reverse-engineering genetic networks without prior knowledge

J. Omony*, G. van Straten*, A.J.B. van Bortel* and L.H. de Graaff**

*System and Control group, Wageningen University,

P.O. Box 17, 6700 AA Wageningen, The Netherlands.

**Laboratory of Microbiology, Wageningen University,

Dreijenplein 10, 6703HB, Wageningen.

e-mail: jimmy.omony@wur.nl

1 Introduction

The use of genetic networks is indispensable in today's highly industrialized world. The ever increasing demand for animal, agricultural and pharmaceutical products among others calls for an in-depth study of genetic networks as one of the solutions to meet the worlds' growing demands. However, intensive literature paints a picture of the complexity encountered by numerous scholars in attempts to unravel the underlying complexities encountered in studying genetic networks (especially on a genomic scale). The reconstruction of genetic networks necessitates using sophisticated mathematical computational techniques.

2 Methodology

In the simulations a system of ordinary differential equation (ODE) is set up to mimic a biochemical genetic network in a defined physiological state. The network structure is assumed to be static across time. The ODE representation is

$$\dot{\mathbf{x}}(t) = \varphi(\mathbf{x}(t), \mathbf{u}(t); \mathbf{A}, \mathbf{b}) + \mathbf{e}(t) \quad (1)$$

where the function $\varphi(\cdot) : \mathbb{R}^n \rightarrow \mathbb{R}^n$ with $\varphi = (\varphi_1, \dots, \varphi_n)^T$ is either non-linear or linear depending on the problem formulation. The Gaussian noise $\mathbf{e}(t) \sim \mathcal{N}(\mathbf{0}, \mathbf{I}_{n \times n} \sigma^2)$ in a microarray setting captures measurement and biological noise. The linearity assumption is used in the simulations. Consider a system with n genes and t_f sampling time points; where $\mathbf{x} = (x_1, \dots, x_n)^T$ and $x_i = (x_{i0}, \dots, x_{it_f})^T$ is the mRNA transcription vector. The j th entry x_{it_j} is the concentration of the i th mRNA at time t_j ; $t = (t_0, \dots, t_f)^T$ is the number of time points. The interaction coefficient matrix $\mathbf{A} = [a_{ij}]_{n \times n} \in \mathbb{R}^{n \times n}$ is considered to be sparse (especially off-diagonal elements) and Hurwitz. $\mathbf{b} = (b_1, \dots, b_n)^T \in \mathbb{R}^n$ is an external perturbation to the system. This \mathbf{b} can be viewed as a stimulus-gene interaction which can either be enhancing or inhibitory in a true biological sense; We use an input $\mathbf{u}(t)$ depended on time in the simulation. Like in Chang *et al.*, (2005) [1] the cubic splines data interpolation technique is used to whiten the simulated noisy data. A smoothing level of $p \sim 0.9995$ was used, this ensures that not all the noise effects in the data is whitened or evened out.

3 Results

Network identification aims to minimize the residuals from a fitted model in the L_2 -norm to ensure that the best linear unbiased estimates (b.l.u.e) of the ϕ_i 's are obtained.

$$\mathcal{J}(\hat{\phi}_i | b_i) = \min_{\hat{\phi}_i} \|y_i(t) - (\hat{\phi}_i \mathbf{x} + b_i \mathbf{u}(t))\|_2 \quad (2)$$

The objective is to minimize the loss function \mathcal{J} where $\hat{\phi}_i \mathbf{x} = \sum_{\ell=1}^n \hat{a}_{i\ell} x_\ell$; without loss of generality $\hat{\phi}_i = \hat{\phi}_i^{ls}$ represents the least squares parameter estimates. On fitting the model every transcript is considered one at a time. The fig.1 is an example to illustrate the reconstructed network.

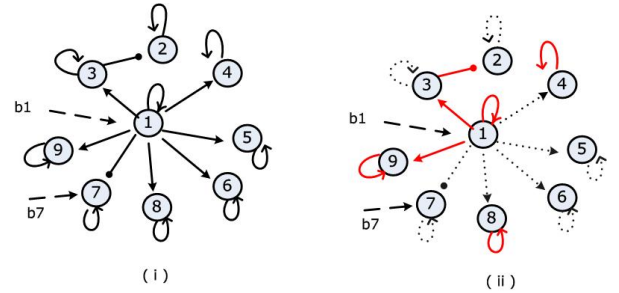


Figure 1: (i) Left is ancestral network \mathcal{G} and (ii) Right is reconstructed network \mathcal{G}^* . The dotted edges (...) are correctly identified while those in bold (red) color are not accurately identified.

4 Conclusions

It is evident from the results that the parameters are estimated with a relatively high level accuracy but still we observe that with linear parameter estimation only a fraction of the edges in the ancestral network \mathcal{G} compared to that in the reconstructed network \mathcal{G}^* . The bias of the estimated parameters was negligible (an indication of good model fit).

References

- [1] Wen-Chieh Chang, Chang-Wei Li and Bor-Sen Chen. Quantitative inference of dynamic regulatory pathways via microarray data. *BMC Bioinformatics* 2005, **6**:44.
- [2] Mukesh Bansal, Giusy Della Gatta, and Diego di Bernardo. (2006). Inference of gene regulatory networks and compound mode of action from time series gene expression profiles.

Stochastic learning of fixed-rank positive semidefinite matrices

Gilles Meyer, Silvère Bonnabel and Rodolphe Sepulchre
 Department of Electrical Engineering and Computer Science,
 GIGA Bioinformatics Platform,
 University of Liège, Belgium,

Emails : G.Meyer@ulg.ac.be, bonnabel@montefiore.ulg.ac.be and R.Sepulchre@ulg.ac.be

1 Introduction

This work presents an adaptive algorithm for learning a positive semidefinite (PSD) matrix of fixed-rank based on observed constraints between data points. The mathematical developments rely on the theory of stochastic gradient descent [1] adapted to cope with the nonlinear search space defined by fixed-rank PSD matrices.

2 Gradient based learning

In the general framework of stochastic learning [1], gradient based algorithms search the parameter matrix X that minimize the *expected risk*

$$L(X) = E_y \{l(y, X)\} = \int l(y, X) dP(y) \quad (1)$$

where $l(y, X)$ is a properly chosen loss function. The latter quantifies the error made when trying to estimate observation y with a given model parametrized by X .

Online gradient algorithms minimize this cost function by performing one gradient step in a direction that decrease the loss for each new observation,

$$X_{t+1} = X_t - \gamma \nabla_X l(y_t, X_t). \quad (2)$$

When the parameter search space is the set of PSD matrices instead of a vector space, this update formula does not guarantee that X remain in the search space. A natural framework to design algorithms that exploit the intrinsic geometry of the search space is the manifold based optimization framework presented in [2].

3 The geometry of fixed-rank PSD matrices

There exists several parameterizations of fixed-rank PSD matrices.

For example, every PSD matrix X can be factored as $X = GG^T$ where $G \in \mathbb{R}^{n \times r}$ and r is equal to the rank of the matrix. This decomposition is defined up to an orthogonal transformation right multiplying G .

As suggested in [3], it is also possible to further factorize G into $G = UW$ where U is a $n \times r$ matrix with orthogonal columns fixing the range space of X and where W is a symmetric positive definite matrix on the small dimension r .

These two parameterizations and their inherent symmetries can be exploited to derive the proper generalization of the update (2).

4 Kernel and metric learning

Two machine learning applications requiring the construction of a PSD matrix are presented as benchmark simulations for the new algorithm. The kernel learning problem [4, 5] consists in learning the kernel Gram matrix from pairwise constraints between data points. The learning of a Mahalanobis distance from data measurements is another related problem that will be discussed.

References

- [1] L. Bottou. Stochastic learning. In *Advanced Lectures on Machine Learning*, number 3176 in Lecture Notes in Artificial Intelligence, pages 146–168. Springer Verlag, Berlin, 2004.
- [2] P.-A. Absil, R. Mahony, and R. Sepulchre. *Optimization Algorithms on Matrix Manifolds*. Princeton University Press, Princeton, January 2008.
- [3] S. Bonnabel and R. Sepulchre. Geometric distance and mean for positive semi-definite matrices of fixed rank. *arXiv*, 2008.
- [4] K. Tsuda, G. Ratsch, and M. Warmuth. Matrix exponentiated gradient updates for on-line learning and bregrman projection. *Journal of Machine Learning Research*, 6:995–1018, 2005.
- [5] B. Kulis, M. Sustik, and I. Dhillon. Learning low-rank kernel matrices. In *Proc. of the 23rd International Conference on Machine Learning*, 2006.

Acknowledgments

This work was supported by the Belgian National Fund for Scientific Research (FNRS) through a Research Fellowship at the University of Liège. This paper presents research results of the Belgian Network DYSCO (Dynamical Systems, Control, and Optimization), funded by the Interuniversity Attraction Poles Programme, initiated by the Belgian State, Science Policy Office. The scientific responsibility rests with its author(s).

Metabolic Flux Interval Analysis of CHO cells

Francisca Zamorano, Alain Vande Wouwer

Service d'Automatique

Faculté Polytechnique de Mons

Boulevard Dolez 31, B-7000 Mons

Belgium

Email: francisca.zamorano, alain.vandewouwer@fpms.ac.be

Georges Bastin

CESAME

Université Catholique de Louvain

Avenue Georges Lemaitre 4, B-1348 Louvain-La-Neuve

Belgium

Email: bastin@inma.ac.be

1 Introduction

A detailed metabolic network of *CHO* – 320 is built based on available information gathered from the literature [1, 2, 3]. The fundamental assumption of quasi-steady state is applied to exponentially growing *CHO* cell cultures, and together with the measurements of the time evolution of a number of extracellular metabolites, the classical methodology of Metabolic Flux Analysis can be applied to a well constrained metabolic network [7]. However, the available measurement information is usually not sufficient and the system of equations is underdetermined. Nevertheless, this positive set of solutions can be studied and admissible ranges for the flux distribution can be defined [5] using tools of positive linear algebra, especially the algorithm METATOOL [4, 6].

2 Flux Interval Analysis

2.1 Network Structure

Based on a set of available measurements of extracellular components, alternative network configurations, corresponding to different net directions of several reversible pathways, are systematically investigated. Among the 16 candidate configurations, only 2 appear feasible, as they correspond to an admissible solution space. However, only one of them is likely to occur, depending on the level of concentration of ammonia.

2.2 Measurements Sensitivity

The influence of the availability of the measurements of the uptake or production rates of the 20 amino acids is assessed. As a result, the amino acids can be classified in two groups, one with limited influence and the other with critical influence. Considering the first group, it is possible to evaluate reasonable flux distributions, even in the situation where up to 5 measurements are missing.

2.3 Hypothetical Additional Measurements

It is of interest to consider the situation where the measurements of all 20 amino acids are available (as well as standard measurements of glucose, lactate and ammonia) and to evaluate the benefits of additional measurements such as urea uptake rate, CER, antibody production rate ($INF - \gamma$), choline and ethanolamine uptake rates. The more informative measurements appear to be CER, urea and choline uptake rates, which allow the flux intervals to be significantly reduced. Interestingly, the resulting flux ranges can be quite narrow, thus providing a very useful insight in the cell metabolism, even in the situation where some extracellular component measurements are missing and the underlying system of mass balance equations is underdetermined.

Acknowledgments This work presents research results of the Belgian Network DYSCO (Dynamical Systems, Control, and Optimization), funded by the Interuniversity Attraction Poles Programme, initiated by the Belgian State, Science Policy Office.

References

- [1] KEGG: Kyoto encyclopedia of genes and genomes. online. Metabolism Map.
- [2] C. Altamirano, A. Illanes, S. Becerra, J.J. Cairó, and F. Gòdia. Considerations on the lactate consumption by *CHO* cells in the presence of galactose. *Journal of Biotechnology*, 125:547–556, 2006.
- [3] H. P. J. Bonarius, V. Hatzimanikatis, K.P.H. Meesters, C.D. de Gooijer, G. Schmid, and J. Tramper. Metabolic flux analysis of hybridoma cells in different culture media using mass balances. *Biotechnology and Bioengineering*, 50:299–318, 1996.
- [4] T. Pfeiffer, I. Sánchez-Valdenebro, J.C. Nuño, F. Montero, and S. Schuster. METATOOL: for studying metabolic networks. *Bioinformatics*, 15(3):251–257, Mar 1999.
- [5] A. Provost. *Metabolic Design of Dynamic Bioreaction Models*. PhD thesis, Université Catholique de Louvain, 2006.
- [6] S. Schuster, T. Dandekar, and D. A. Fell. Detection of elementary flux modes in biochemical networks: a promising tool for pathway analysis and metabolic engineering. *TIBTECH*, 17:53–60, 1999.
- [7] G. N. Stephanopoulos, A. A. Aristidou, and J. Nielsen. *Metabolic Engineering: Principles and Methodologies*. 1998.

Generalized power method for sparse principal component analysis

M. Journée*, Yurii Nesterov†, Peter Richtárik† and R. Sepulchre*

*Dept. of Electrical Engineering and Computer Science, University of Liège, Belgium

†Center for Operations Research and Econometrics, Université Catholique de Louvain, Belgium

1 Sparse principal component analysis

Principal component analysis (PCA) is a well established tool for making sense of high dimensional data by reducing it to a smaller dimension. If $A \in \mathbf{R}^{p \times n}$ is a matrix encoding p samples of n variables, with n being large, PCA aims at finding a few linear combinations of these variables, called *principal components*, to explain as much of the variance in the data as possible. Principal components are, in general, combinations of all the input variables. In most applications, however, the original variables have concrete physical meaning and PCA then appears especially interpretable if the extracted components are composed only from a small number of the original variables. The objective of *sparse principal component analysis* (sparse PCA) is to find a reasonable *trade-off* between the conflicting goals of *statistical fidelity* (maximizing the variance) and *interpretability* (sparsity of the components).

Jolliffe *et al.* [1] were the first to address this issue in depth. Some further methods have been thereafter proposed [3, 2, 4, 5]. The first principal component is computed by the solution of

$$\max_{z \in S^{n-1}} z^T A^T A z,$$

which maximizes the Rayleigh quotient of the sample covariance matrix $A^T A$ and where $S^{n-1} = \{x \in \mathbb{R}^n | x^T x = 1\}$ is the unit Euclidean sphere. Penalizing the ℓ_1 -norm is well-known to enforce sparsity. Hence, the solution of

$$\phi(\gamma) = \max_{x \in S^{n-1}} z^T A^T A z - \gamma \|z\|_1, \quad (1)$$

where γ is a positive weight factor performs sparse PCA.

2 Reformulation of the problem

While the formulation (1) involves maximization of a *non-convex* function on a space of dimension involving n , the problem can be cast into the form

$$\phi^2(\gamma) = \max_{x \in S^{p-1}} \sum_{i=1}^n [|a_i^T x| - \gamma]_+^2,$$

which maximizes a *convex* function on the unit Euclidean sphere in \mathbf{R}^p and where a_i is the i th column of A . Due to the convexity of the new cost function we are able to propose and analyze the iteration-complexity of a simple gradient-type scheme, which appears to be well suited for problems of this form.

3 Generalized power method

To solve optimization problems of the form

$$\max_{x \in \mathcal{Q}} f(x)$$

where \mathcal{Q} is a compact subset of a finite-dimensional vector space and f is convex, we consider the iteration

$$x_+ \in \text{Argmax}\{f(x) + \langle f'(x), y - x \rangle \mid y \in \mathcal{Q}\}$$

where x and x_+ is the current and the new iterates, respectively. Convergence to a stationary point is guaranteed [6].

In the special case $\mathcal{Q} = S^{n-1}$ and $f(x) = x^T C x$ for some $n \times n$ symmetric positive definite matrix C , this iteration specializes to the *power method*, which aims at maximizing the Rayleigh quotient $\frac{x^T C x}{x^T x}$ and thus at computing the largest eigenvalue and the corresponding eigenvector of C . By applying this gradient scheme to the sparse PCA reformulation (1), we obtain an algorithm with per-iteration computational cost $\mathcal{O}(np)$.

References

- [1] I. T. Jolliffe, N. T. Trendafilov, and M. Uddin. A modified principal component technique based on the LASSO. 12(3):531–547, September 2003.
- [2] H. Zou, T. Hastie, and R. Tibshirani. Sparse principal component analysis, 2004.
- [3] A. d'Aspremont, L. El Ghaoui, M. I. Jordan, and G. R. G. Lanckriet. A direct formulation for sparse PCA using semidefinite programming. Technical Report UCB/CSD-04-1330, EECS Department, University of California, Berkeley, 2004.
- [4] B. Moghaddam, Y. Weiss, and S. Avidan. Spectral bounds for sparse PCA: Exact and greedy algorithms. In Y. Weiss, B. Schölkopf, and J. Platt, editors, *Advances in Neural Information Processing Systems 18*, pages 915–922. MIT Press, Cambridge, MA, 2006.
- [5] A. d'Aspremont, F. R. Bach, and L. El Ghaoui. Full regularization path for sparse principal component analysis. In *ICML '07: Proceedings of the 24th international conference on Machine learning*, pages 177–184, New York, NY, USA, 2007. ACM.
- [6] M. Journée, Y. Nesterov, P. Richtárik, and R. Sepulchre. Generalized power method for sparse principal component analysis. *ArXiv 0811.4724v1*, 2008.

An initialization procedure for parameter estimation problems using simultaneous Gauss-Newton method

Julian Bonilla^{1,2}, Moritz Diehl², Bart De Moor² and Jan Van Impe¹

¹Department of Chemical Engineering
CIT/BioTeC-Katholieke Universiteit Leuven
W. de Croylaan 46, PB 2423
Leuven-Belgium
Email: julian.bonilla@cit.kuleuven.be

²Department of Electrical Engineering
ESAT/SCD-Katholieke Universiteit Leuven
Kasteelpark Arenberg 10, bus 2446,
Leuven-Belgium
Email: moritz.diehl@esat.kuleuven.be

1 Introduction

This work introduces an initialization method for optimization tasks arisen from parameter estimation problems (PEP) with embedded parameter-affine dynamic models. Using a least squares norm, the PEP can be generally formulated as

$$\min_{p, \bar{x}(\cdot)} \frac{1}{2} \sum_{i=0}^{N-1} \sum_{j=1}^{n_x} (x_j(t_i) - \bar{x}_j(t_i))^2, \quad (1)$$

$$\begin{aligned} \text{s.t.} \quad \dot{x}(t) &= \Phi(x(t)) + \Gamma(x(t))p, \quad t \in [0, T], \\ x(t) &\in \mathbb{X}, \quad t \in [0, T], \quad p \in \mathbb{P}, \end{aligned} \quad (2)$$

where $\bar{x}_j(t_i)$ represents the j -esim process state measurement at the time instant i and p and $x(t)$ are model parameters and states respectively. \mathbb{X} and \mathbb{P} are state and parameter constraints. In this work the set defined by $\mathbb{X} \times \mathbb{P}$ is assumed convex.

2 Convex modification

Since the presented PEP is a nonconvex optimization problem, initialization is not a simple task and clearly influence the convergence to a solution. In order to provide an automatic initialization method for PEP involving parameter affine models, we propose to use the known measurement states $\bar{x}(t_i)$ as the real model state trajectory $x(t_i)$ [2]. The PEP (1)-(3) is reformulated as:

$$\min_{p, \bar{x}(\cdot)} \frac{1}{2} \sum_{i=0}^{N-1} \sum_{j=1}^{n_x} (\bar{x}_j(t_i) - \bar{x}_j(t_i))^2, \quad (4)$$

$$\begin{aligned} \text{s.t.} \quad \tilde{x}(t) &= \Phi(\bar{x}(t)) + \Gamma(\bar{x}(t))p, \quad t \in [0, T], \\ \tilde{x}(t) &\in \mathbb{X}, \quad p \in \mathbb{P}. \end{aligned} \quad (5)$$

The term $\tilde{x}(t_i) - \bar{x}(t_i)$ corresponds to the integral of the modelling errors when the states are forced to lie in the measurement trajectory, i.e. $x(t_i) = \bar{x}(t_i)$. Due to this modification, the PEP (4)-(6) becomes convex. The solution of (4)-(6) is subsequently used to initialize a simultaneous Gauss-Newton (SGN) procedure [1] on the original PEP. Figure 1

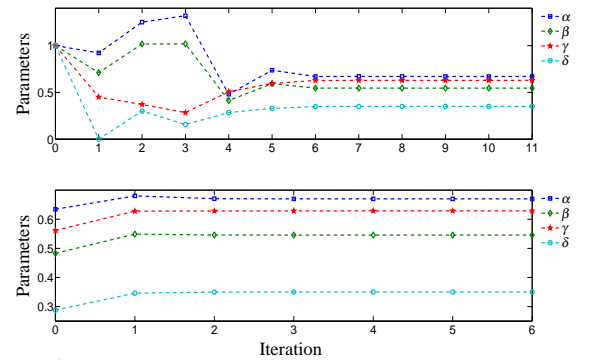


Figure 1: PEP in the Lotka-Volterra model. The optimization is performed using an arbitrary initialization (top) and the proposed convex approach (bottom).

illustrates the results for a SGN using arbitrary initialization and the proposed approach for a particular problem from the biological field.

Acknowledgements

Research supported by Research Council KUL: OT/03/30, CoE EF/05/006 (OPTec), GOA AMBioRICS, IOF-SCORES4CHEM, PhD/postdoc and fellow grants; Flemish Government: FWO: PhD/postdoc grants, projects G.0452.04, G.0499.04, G.0211.05, G.0226.06, G.0321.06, G.0302.07, G.0320.08, G.0558.08, G.0557.08, research communities (ICCoS, ANMMM, MLDM); IWT: PhD Grants, McKnow-E, Eureka-Flite; Helmholtz: viCERP; EU: ERNSI, HD-MPC; Contracts: AMINAL; Belgian Federal Science Policy Office: IUAP P6/04 (DYSCO, Dynamical systems, control and optimization, 2007-2011). The scientific responsibility is assumed by its authors.

References

- [1] Bock H, Plitt K. A multiple shooting algorithm for direct solution of optimal control problems. *In Proc. 9th IFAC world congress*, pp. 242-247, Hungary, 1984.
- [2] Bonilla J, Diehl M, De Moor B and Van Impe J. A least squares parameter estimation procedure without initial parameter guesses. *In Proc. of the 47th IEEE conference on Decision and Control*, pp. 5519-5524, Mexico, 2008.

Predictive Input Shaping Prefilters

Lieboud Van den Broeck, Moritz Diehl, Jan Swevers
Katholieke Universiteit Leuven
Celestijnenlaan 300c, 3001 Heverlee, Belgium
lieboud.vandenbroeck@mech.kuleuven.be

1 Introduction

In the last decades, a lot of effort has been put into developing efficient input shaping prefilters, see e.g. [1]. These prefilters are computed off-line and transform the reference signal such that no residual vibrations occur at the end of a motion. Input or actuator saturation is avoided by considering during the design worst case reference inputs, which is often a step reference with maximum amplitude [2]. Hence, these input filters yield conservative results with respect to the available input range and response speed if the reference input is more smooth or has a smaller amplitude. Therefore, this presentation presents a new approach to design input shaping prefilters on-line. This design is partly based on the model predictive control framework [3], hence its name: predictive prefilter. The new prefilter is both numerically and experimentally validated.

2 Predictive prefilters

Like all prefilters, the predictive prefilter transforms the reference setpoint $y_{\text{ref},l}$, i.e. the reference setpoint available at time step l , to a system input. This input has to fulfill the following three requirements; the system must drive the system output to the desired setpoint as fast as possible, the prefilter must prevent residual vibrations at the system output as much as possible, and constraints on inputs, outputs, and possibly system state variables have to be respected.

The predictive prefilter satisfies these requirements by the on-line solution of an optimization problem which results in a nonlinear mapping between the reference and the inputs of the system. The considered problem $P(\bar{x}_l, y_{\text{ref},l})$ at time step l which minimizes the time K is:

$$\begin{aligned} & \min_{x,u,y,K} K \\ \text{subject to: } & x_0 = \bar{x}_l, & (\text{starting point at time } l) \\ & x_{k+1} = f(x_k, u_k), & (\text{system dynamics (a)}) \\ & y_k = h(x_k, u_k), & (\text{system dynamics (b)}) \\ & 0 \leq g(x_k, u_k), & (\text{constraints on output, } \dots) \\ & \text{for } k = 0 \dots K \\ & x_K = f(x_K, u_K), & (\text{end point constraint (a)}) \\ & y_K \equiv y_{\text{ref},l} & (\text{end point constraint (b)}) \end{aligned}$$

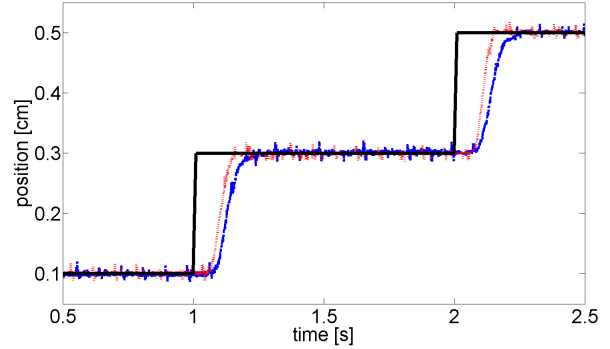


Figure 1: Experimental validation of the predictive prefilter design: desired motion (full line), and system response with a classical input shaping prefilter (dashed line) and with the predictive prefilter (dotted line).

3 Solution Strategies

Problem $P(\bar{x}_l, y_{\text{ref},l})$ has to be solved on-line in the available sampling-time. This technique is developed for mechatronic systems, hence the sampling times are in the millisecond range. Therefore, two solution techniques are developed which exploit the problem structure; the first implements an efficient search for the optimal time K^* , the second reformulates the problem more efficiently.

4 Results

The developed prefilter is implemented for a fifth-order system with a sampling time of 0.01s. Both the new prefilter and a classical linear prefilter are implemented. Tests show that gains of 30% in settling time are attainable.

References

- [1] N. C. Singer and W. P. Seering. Preshaping command inputs to reduce system vibration. *Transactions of the ASME, Journal of Dynamic Systems, Measurement, and Control*, 112:76–82, 1990.
- [2] W.E. Singhose, W. P. Seering, and N.C. Singer. Time-optimal negative input shapers. *Journal of Dynamic Systems Measurement and Control-Transactions of the ASME*, 119:198–205, 1997.
- [3] J.M. Maciejowski. *Predictive control with constraints*. Prentice Hall, 2000.

Extending iTaSC to support inequality constraints

Wilm Decré, Ruben Smits, Herman Bruyninckx and Joris De Schutter

Department of Mechanical Engineering, Division PMA

Katholieke Universiteit Leuven

Celestijnenlaan 300B box 2420, B-3001 Heverlee

Belgium

Email: Wilm.Decre@mech.kuleuven.be

1 Introduction

In [1], we presented a constraint-based programming approach, iTaSC¹, that formulates instantaneous sensor-based robot tasks as constraint sets, and subsequently solves a corresponding least-squares problem to obtain control set points. This presentation further extends this approach, (i) by explicitly supporting the inclusion of inequality constraints in the task definition, and (ii) by supporting a broader class of objective functions used when translating the task constraints into robot motion. These extensions are made while retaining a tractable mathematical problem structure (a convex program [2]). As will be illustrated by several examples, the power of the approach lies (i) at its versatility to specify a wide range of robot behaviors and the ease of making task adjustments, and (ii) at its generic nature, that permits using systematic procedures to derive the underlying control equations.

2 Method

In the presented method, the control input \mathbf{u} is obtained by solving a linearized and discrete-time version of optimization problem:

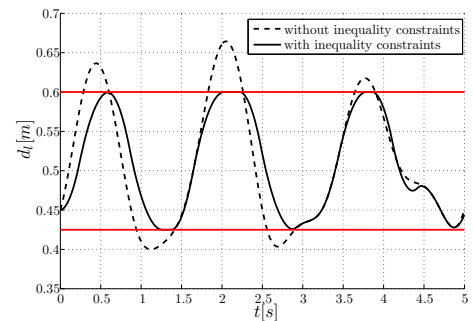
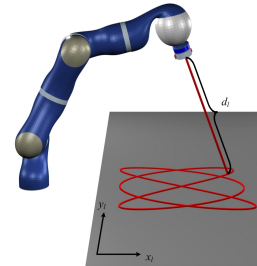
$$\begin{aligned} &\text{minimize } r(\boldsymbol{\mu}, \boldsymbol{\nu}_1, \boldsymbol{\nu}_2) \\ &\text{subject to} \\ &\quad \frac{d}{dt} \begin{pmatrix} \mathbf{q} \\ \dot{\mathbf{q}} \end{pmatrix} = \mathbf{s}(\mathbf{q}, \dot{\mathbf{q}}, \mathbf{u}) \quad (1a) \\ &\quad \mathbf{y} = \mathbf{f}(\mathbf{q}, \boldsymbol{\chi}_f) \quad (1b) \\ &\quad \mathbf{0} = \mathbf{l}(\mathbf{q}, \boldsymbol{\chi}_f) \quad (1c) \\ &\quad \mathbf{y} = \mathbf{y}_d + \boldsymbol{\mu} \\ &\quad \mathbf{y}^{(i)} \leq \mathbf{y}_{i,max} + \boldsymbol{\nu}_1 \\ &\quad \mathbf{y}^{(i)} \geq \mathbf{y}_{i,min} + \boldsymbol{\nu}_2, \end{aligned}$$

with \mathbf{q} the joint coordinates, $\boldsymbol{\chi}_f$ auxiliary coordinates that facilitate the task specification, \mathbf{y} the system output that includes all variables of control interest, (1a) the robot system's equation, (1b) the output equation, (1c) the kinematic loop closure equation, r a residual penalty function, \mathbf{y}_d the reference value of the system

output, $\mathbf{y}^{(i)}$ the i -th time derivative of \mathbf{y} , $\mathbf{y}_{i,min}$ and $\mathbf{y}_{i,max}$ lower and upper limits of $\mathbf{y}^{(i)}$, and $\boldsymbol{\mu}$, $\boldsymbol{\nu}_1$ and $\boldsymbol{\nu}_2$ residuals on the equality and inequality constraints respectively.

3 Example

The figure below depicts a laser tracing example; a laser is mounted on the end effector of a KUKA LBR 4 manipulator. The task goal is to trace a trajectory with the laser on a plane. Inequality constraints are added to constrain the laser distance d_l between 0.425 m and 0.6 m and the laser distance acceleration between $-2\frac{\text{m}}{\text{s}^2}$ and $2\frac{\text{m}}{\text{s}^2}$.



4 Acknowledgment

Research funded by a Ph.D. grant of the Institute for the Promotion of Innovation through Science and Technology in Flanders (IWT- Vlaanderen). All authors gratefully acknowledge the financial support by K.U.Leuven's Concerted Research Action GOA/05/10. This work also benefits from Research Council K.U.Leuven, CoE EF/05/006 Optimization in Engineering (OPTEC).

References

- [1] J. De Schutter, T. De Laet, J. Rutgeerts, W. Decré, R. Smits, E. Aertbeliën, K. Claes, and H. Bruyninckx, "Constraint-based task specification and estimation for sensor-based robot systems in the presence of geometric uncertainty," *The International Journal of Robotics Research*, vol. 26, no. 5, pp. 433–455, 2007.
- [2] S. Boyd and L. Vandenberghe, *Convex Optimization*. Cambridge University Press, 2004.

¹instantaneous Task Specification using Constraints

Directional repetitive control of a metrological AFM

Michael Ronde*, Roel Merry,
René van de Molengraft, Maarten Steinbuch
Department of Mechanical Engineering
Eindhoven University of Technology
P.O. Box 513, 5600 MB Eindhoven
The Netherlands
Email: * m.j.c.ronde@tue.nl

Richard Koops and Marijn van Veghel
NMi Van Swinden Laboratorium
Thijssseweg 11
2629 JA Delft
The Netherlands

1 Introduction

Metrological Atomic Force Microscopes (AFMs) are used to calibrate transfer standards for commercial AFMs. In contrast to commercial AFMs, the accuracy of the measurements is much more important than the scanning speed. However, it is desirable to increase the speed with respect to the current design [1].

In this research, repetitive control (RC) has been applied to the scanning x and imaging z -direction. Furthermore, directional repetitive control (DRC) is proposed, which is a variant of repetitive control.

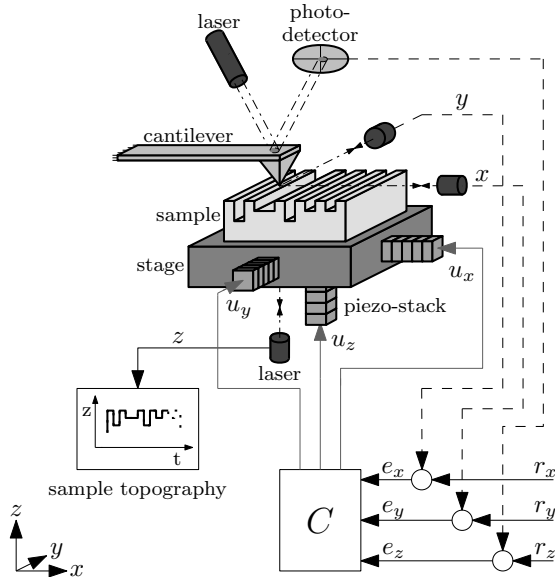


Figure 1: The AFM and the feedback control (schematic).

2 Repetitive control

A raster movement in x and y direction is used to scan the calibration samples, which have a structure that changes very little from line to line, i.e. line or checkerboard structures. Therefore, the tracking errors are largely repetitive and repetitive control techniques can be used to suppress these errors.

The error convergence of the imaging z -direction with a repetitive controller is shown in Fig. 2. In general, the sample structure is not aligned with the measurement system, i.e. the sample is rotated around the z -axis. This causes the error to become partly non-repetitive, hence the error after convergence becomes a factor 3.5 larger, see Fig. 2.

3 Directional repetitive control

To overcome this problem, we use DRC. The sample rotation is estimated using a prescan. Then, both the controller and the reference trajectory are rotated, such that the controller and reference trajectory are aligned with the sample structure. In Fig. 2, it can be observed that the same error after convergence is achieved as without rotation.

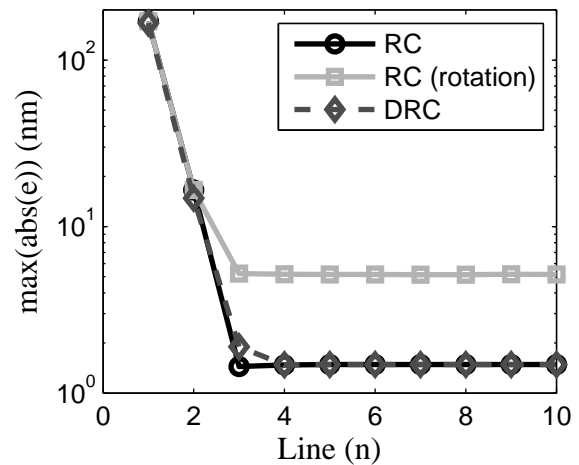


Figure 2: Error convergence of the imaging z -direction

Future research includes the MIMO control and experimental validation of the presented control strategies.

References

- [1] R. Merry, M. Uyanik, R. Koops, R. van de Molengraft, M. van Veghel, and M. Steinbuch, "Modeling, identification and control of a metrological atomic force microscope with a 3DOF stage," in *American Control Conference*, 2008, 2008, pp. 2716–2721.

Iterative Learning Control by Linear Repetitive Processes Theory

Wojciech Paszke

Department of Mechanical Engineering
Eindhoven University of Technology
P.O. Box 513, 5600 MB Eindhoven
The Netherlands
Email: W.Paszke@tue.nl

Abstract

Iterative learning control (ILC) is relatively well-known technique for controlling systems operating in a repetitive (or pass-to-pass) mode with the requirement that a given reference trajectory $y_{ref}(t)$ defined over a finite interval $0 \leq t \leq \alpha$ (where $\alpha < \infty$ and $\alpha = \text{const}$) is followed to a high precision. Examples of such systems include robotic manipulators that are required to repeat a given task, chemical batch processes or, more generally, the class of tracking systems [1].

In ILC, a major objective is to achieve convergence of the trial-to-trial error and often this has been treated as the only one that needs to be considered. In fact, it is possible that enforcing fast convergence could lead to unsatisfactory performance along the trial. One way of preventing this is to exploit the fact that ILC schemes can be modeled as linear repetitive processes and design the scheme to ensure stability along the pass (or trial). Also, since the time and trial directions in ILC are decoupled, ILC is often applied by separately designing a feedback and a learning controller. The feedback controller stabilizes the system in the time domain and suppresses unknown disturbances. The feedforward (learning) controller is designed to guarantee convergence in the trial-to-trial domain. However, currently such an integration, of the feedforward control to the feedback control, is performed separately, and may not lead to an optimal complementation of the feedback control with the feedforward control. One of the option to obtain such an optimal complementation is to exploited the inherent two-dimensional/repetitive system structure of ILC in a method that yields in a one step synthesis both a stabilizing feedback controller in the time domain and an ILC controller which guarantees convergence in the trial domain.

The contribution of this work is the development of approach to design ILC schemes with use of linear repetitive processes theory. To date most of existing works, (see, for example [4, 5]) assume that all state variables are available for measurement. In practical applications, it is not always the case. Furthermore, there is no link between these results and practical requirements for ILC schemes which are usually described by multiple frequency domain inequalities (FDIs) in (semi)finite frequency ranges. To overcome

these problems, this paper proposes to apply full order controllers (feedback and feedforward) and make extensive use of the Kalman-Yakubovich-Popov (KYP) lemma that allows us to establish the equivalence between FDIs for a transfer-function and an LMI defined in terms of its state space realization [2]. Unfortunately, it is not easy task to convert join feedback and feedforward controller design with FDI specification on transfer function of ILC scheme. Therefore the paper aims at filling this gap.

The approach to be presented is based on result [3] which states that KYP synthesis theory can be developed for direct treatment of multiple FDI specifications on closed-loop transfer functions in various frequency ranges. The problem of determining required feedback and feedforward controllers is reduced to that of checking the existence of a solution to a set of linear matrix inequalities (LMIs). Testing the resulting conditions only requires computations with a matrices and is consequently computationally attractive when compared alternatives. Finally, the theoretical findings will be validated by numerical examples.

References

- [1] D. A. Bristow, M. Tharayil, and A.G. Alleyne. A survey of iterative learning control. *IEEE Control Systems Magazine*, 26(3):96–114, 2006.
- [2] T. Iwasaki and S. Hara. Generalized KYP lemma: unified frequency domain inequalities with design applications. *IEEE Transactions on Automatic Control*, 50(1):41–59, 2005.
- [3] T. Iwasaki and S. Hara. Feedback control synthesis of multiple frequency domain specifications via generalized KYP lemma. *International Journal of Robust and Nonlinear Control*, 17:415–434, 2007.
- [4] J. E. Kurek and M. B. Zaremba. Iterative learning control synthesis based on 2-D system theory. *IEEE Transactions on Automatic Control*, 38(1):121–125, 1993.
- [5] W. Paszke, R. Merry, and R. van de Molengraft. Iterative learning control by two-dimensional system theory applied to a motion system. In *Proc. American Control Conference (ACC)*, pages 5484–5489, New York, USA, 9-13 July 2007.

A Constrained Gauss-Newton Method for Model Inversion in Iterative Learning Control

Marnix Volckaert¹, Anne Van Mulders², Moritz Diehl³, Jan Swevers¹

¹ Department of Mechanical Engineering, Katholieke Universiteit Leuven, Belgium

² Department ELEC, Vrije Universiteit Brussel, Belgium

³ Department of Electrical Engineering, Katholieke Universiteit Leuven, Belgium

Email: Marnix.Volckaert@mech.kuleuven.be

1 Introduction

This presentation introduces a new method to solve the model inversion problem that is part of model based iterative learning control (ILC) for nonlinear systems. The model inversion problem consists of finding the input signal corresponding to a given output (reference) signal. This problem is formulated as a nonlinear dynamic optimization problem in time domain and solved efficiently using a constrained Gauss-Newton algorithm. A nonlinear iterative learning controller based on this model inversion approach is validated numerically and experimentally. The considered application is an electronic circuit described by a polynomial nonlinear state-space model. The nonlinear ILC algorithm is more accurate and converges faster than an existing linear ILC approach.

2 Iterative learning control and nonlinear model inversion

A nonlinear ILC algorithm is proposed in [1], and is written as follows:

$$u^{[i+1]} = u^{[i]} + Q^{[i]} [\hat{P}^{-1}(y_r) - \hat{P}^{-1}(y^{[i]})] \quad (1)$$

with $y^{[i]} = P(u^{[i]}) + n_y$ the measured output at iteration i , with n_y the measurement noise, y_r the reference signal, and $Q^{[i]}$ the iteration gain. The crucial part of the algorithm is the calculation of the inverse signals $\hat{P}^{-1}(y_r)$ and $\hat{P}^{-1}(y^{[i]})$. If \hat{P} is a discrete time state space model, with model equations $x_{k+1} = f(x_k, u_k)$ and $y_k = h(x_k, u_k)$, the calculation of these inverse signals can be done by solving the following nonlinear least squares problem:

$$\min_{x, u} \frac{1}{2} \|h(x_k, u_k) - y_{r,k}\|^2 \quad (2a)$$

s.t.

$$f(x_k, u_k) - x_{k+1} = 0 \quad \text{for } k = 0, 1, \dots, N-1 \quad (2b)$$

$$f(x_N, u_N) - x_1 = 0 \quad (2c)$$

where the first constraint equation (2b) represents the system dynamics, and the second constraint equation (2c) is present to enforce the calculated input signal to be periodic.

3 Experimental validation

The presented nonlinear ILC algorithm is experimentally validated on an electrical circuit with a Wiener-Hammerstein structure, which is equivalent to a mass-spring-damper system with a nonlinear spring. Figure 1 shows the frequency spectra of the reference trajectory, the measurement noise, the initial tracking error and the tracking error after 10 iterations. It is clear from this figure that the tracking error is successfully reduced to the level of the measurement noise, by the nonlinear ILC algorithm. In the time domain, also shown in figure 1, it is clear that a very accurate tracking control can be reached after convergence of the ILC algorithm.

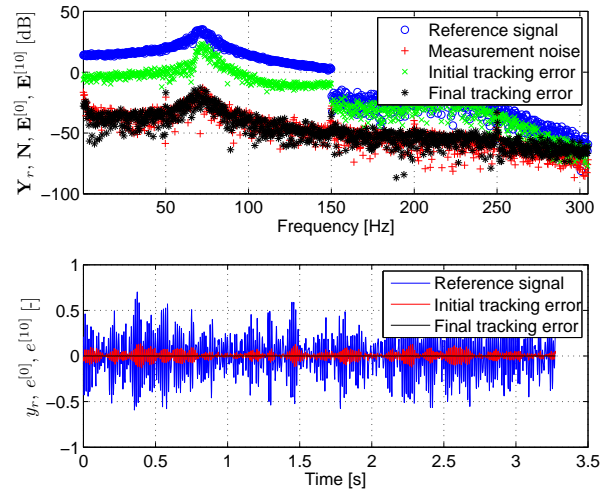


Figure 1: Results for the experimental validation of the nonlinear ILC approach in frequency and time domain

References

- [1] K. Smolders, M. Volckaert, J. Swevers, "Tracking Control of Nonlinear Lumped Mechanical Continuous-Time Systems: a Model-Based Iterative Learning Approach," *Mechanical Systems and Signal Processing*, 22-8, 2008.
- [2] A. Van Mulders, J. Schoukens, M. Volckaert, M. Diehl, "Two Nonlinear Optimization Methods for Black Box Identification Compared," *submitted to the 15th IFAC Symposium on System Identification, (SYSID 2009)*.

Iterative optimization of parameterized trajectories for complex mechatronic systems

Bruno Depraetere¹, Gregory Pinte², Wim Symens², Walter Verdonck², Jan Swevers¹

¹Department of Mechanical Engineering, Division PMA, Katholieke Universiteit Leuven

²Flanders Mechatronics Technology Centre

Celestijnenlaan 300B¹ / 300D², 3001 Heverlee, Belgium

Email: bruno.depraetere@mech.kuleuven.be

1 Introduction

Many mechatronic systems are controlled with predefined input trajectories, either in open loop or using feedback. This research considers the optimization of these trajectories, for mechatronic applications whose dynamics are difficult to model, and vary in a significant and unpredictable manner over time. For these applications, solving the trajectories with an optimal control problem requires a considerable modelling effort. In many practical applications this is avoided by parameterizing the trajectories, and estimating the optimal parameter values during an experimental calibration. Repeating the calibration at regular time intervals can compensate for system variation, but requires the machine to be taken out of production. In this research a new methodology is developed to iteratively optimize these parameterized trajectories during normal operation, hence avoiding calibrations and limiting required modelling effort.

2 Iterative optimization

Iterative methods use information from previous iterations to gradually learn the optimal trajectory, compensating for system uncertainty and variation. We will apply such iterative methods to optimize parameterized trajectories with only few parameters, which are widely used in industrial applications. Three iterative optimization approaches, following the scheme of figure 1, will be developed: (i) a model-based approach, (ii) a model-free approach and (iii) a combination of the previous two.

In the model-based approach (i) a simple, approximate system model is updated each iteration with the latest measurements. The optimal trajectory for this model is then calculated, and used for the next iteration. Since the model improves iteration by iteration and adapts to system variation, the trajectory does as well. It will be investigated to what extent the iterative procedure can compensate for the lack of an accurate system model. In contrast, no system model at all is required for the model-free, data driven approach (ii). Only experimentally obtained system responses to previous trajectories are used to directly optimize the trajectory parameters. As this happens during normal operation, convergence should be sufficiently fast to avoid

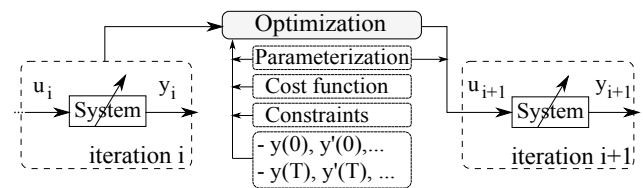


Figure 1: Iterative optimization control scheme.

long periods with poor performance. Since the number of iterations before convergence increases with the number of parameters, trajectories with a small number of parameters are especially interesting. The third approach (iii) finally attempts to combine the two previous approaches to increase the efficiency and overall performance.

3 Selected test case and future research

In the presentation we will give the general outline of the research, and report some preliminary results on the test case of a wet-plate clutch. In this test case, the goal is to optimize



Figure 2: Test setup of a transmission with wet-plate clutches.

the trajectory to the pressure valve, so the clutch engages in a smooth but fast manner. The behaviour of the clutch is non-linear and depends strongly on degradation of the friction plates and oil temperature inside the clutch. Additionally, a change in behaviour occurs when torque transfer starts.

Acknowledgement This work has been carried out within the framework of project G.0422.08 of the Research Foundation - Flanders (FWO - Vlaanderen). This work also benefits from K.U.Leuven-BOF EF/05/006 Center-of-Excellence Optimization in Engineering and from the Belgian Programme on Interuniversity Attraction Poles, initiated by the Belgian Federal Science Policy Office.

Robust Beyond-Rigid-Body Control of Next Generation Wafer Stages

Robbert van Herpen, Tom Oomen, Okko Bosgra
Technische Universiteit Eindhoven
r.m.a.v.herpen@student.tue.nl

Marc van de Wal
Philips Applied Technologies
m.m.j.van.de.wal@philips.com

Background

Increasing throughput requirements in semiconductor manufacturing demand for higher accelerations in wafer stage motion. In virtue of Newton's law, higher accelerations can be achieved if stages are lightweight. Increasing performance requirements and lightweight stage design result in flexible dynamics in the controller crossover region [2]. The goal of the present research is to enable high performance motion control for next-generation flexible stages in the presence of flexible dynamics.

Control challenges

Flexible dynamics are typically not aligned with the motion degrees-of-freedom, resulting in an inherently multi-variable plant. To enable the design of high performance controllers for such systems, model-based controller design is essential [1]. To connect experimental modeling and controller design of flexible mechanical systems, increased model complexity and accuracy is required compared to the present state-of-the-art. In addition, a classification of flexible dynamics that limit control performance and that do not affect control performance is required. These control-relevant flexible dynamics should explicitly be modeled and compensated to enable high performance motion.

Experimental results

A procedure consisting of experimental modeling, model validation, and robust control design has been developed and applied to a next-generation wafer stage. Firstly, a new basis for the choice of control relevant coprime factors $P = ND^{-1}$ has been developed, extending [3], see [4] and Fig. 1 for experimental results on a next-generation wafer stage. Clearly, the rigid-body behavior and the first resonance phenomena are control-relevant. Secondly, to confirm the extended model of the flexible behavior, model validation has been enhanced [5] to deal with both disturbances and model uncertainty in a control-relevant setting. The set of not invalidated candidate plant models is depicted in Fig. 2. Clearly, the control-relevant dynamics are modeled accurately. Finally, the optimal robust controller is depicted in Fig. 2, revealing that the worst-case performance is significantly improved and relevant resonance phenomena are explicitly compensated.

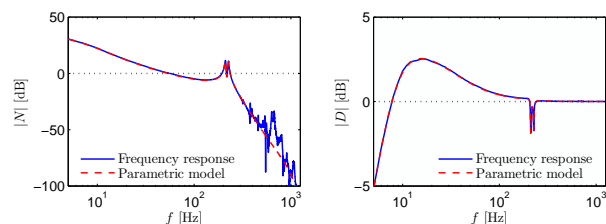


Figure 1: Control-relevant coprime factor identification.

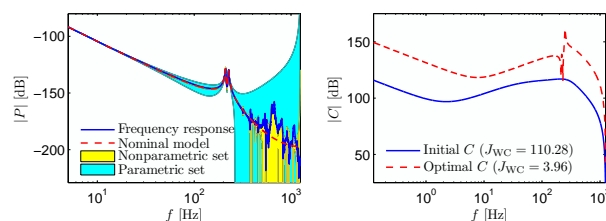


Figure 2: Left: not invalidated models, right: optimal controller.

Conclusions

A novel procedure has been presented that connects experimental modeling and robust control. Experimental results confirm improved accuracy of the extended model. In addition, the procedure enables a classification of resonance phenomena that are important to model and compensate and dynamics that are irrelevant.

References

- [1] M. van de Wal, G. van Baars, F. Sperling, and O. Bosgra. Multivariable \mathcal{H}_∞/μ feedback control design for high-precision wafer stage motion. *Contr. Eng. Pract.*, 10(7):739–755, 2002.
- [2] G. J. Balas and J. C. Doyle. Control of lightly damped, flexible modes in the controller crossover region. *AIAA Journ. Guid. Cont. Dyn.*, 17(2):370–377, 1994.
- [3] R. J. P. Schrama. Accurate identification for control: The necessity of an iterative scheme. *IEEE Trans. Automat. Contr.*, 37(7):991–994, 1992.
- [4] T. Oomen and O. Bosgra. Robust-Control-Relevant Coprime Factor Identification: A Numerically Reliable Frequency Domain Approach. *Amer. Contr. Conf.*, Seattle, WA, USA, 625–631, 2008.
- [5] T. Oomen and O. Bosgra. Estimating disturbances and model uncertainty in model validation for robust control. *Conf. Dec. Contr.*, Cancún, Mexico, 5513–5518, 2008.

Model Development for Propofol and Remifentanyl induced anesthesia in ICU patients

Ramona Hodrea, Bogdan Nour, Clara Ionescu, Robin De Keyser

Department of Electrical energy, Systems and Automation, Ghent University, Faculty of Engineering
Technologiepark 913, Gent B9052 Belgium

Email: ramona@autoctrl.UGent.be

1 Introduction

General anesthesia plays an important role in surgery and intensive care unit (ICU) and requires critical assessment of induced quantities of drugs into the patient. There are three major interactive parts in anesthesia: sedation, analgesia and neuromuscular blockade. Nowadays, drug dosing control during anesthesia is changing from manual control to automated control. Some of the advantages of automated drug dosing control are: patient safety, a significant decrease in overall costs and improved healthcare [4]. This topic captured the attention of engineers and clinicians already decades ago, starting with expert systems that offer advice to the anesthesiologist upon optimal drug infusion rate during clinical trials. Control of anesthesia poses a manifold of challenges: multivariable characteristics, variable time delays, dynamics dependent on anesthetics substances and stability issues.

This presentation shows preliminary results for identification of a MISO (multiple-input single-output) patient model for sedation and analgesia components used in ICU. The final purpose is to use this model for prediction in a model-based predictive control strategy.

2 Materials and Methods

For many control techniques, compartmental models are used to represent the drug distribution in the body for patients undergoing anesthesia. SISO patient models for control already exist in the literature for Propofol [1], as well as for neuromuscular blockade agents [3], while the analgesic effects remain one of the most difficult problems to identify. Analgesia is a very challenging aspect of general anesthesia and requires special attention, since its effects are dependent on the drug used in the patient. Some previous reports from literature consider Remifentanyl as a suitable input for inducing analgesia into the patient. Propofol and Remifentanyl are used as inputs for the model, while the effects from the neuromuscular blockade will be regarded as disturbances. The Propofol and Remifentanyl dynamics with respect to the Bispectral Index (a measure for brain activity) are taken from real-life clinical tests in patients during ICU at Ghent University Hospital. For model development and validation, data from 15 patients in closed loop (i.e. SISO

model based predictive control) and 9 patients in open loop (i.e. manual drug administration by the ICU nurse) are used.

The linear part of the model for Remifentanyl dynamics has the same structure as that of Propofol [4]: three compartments for pharmacokinetics and one effect-site compartment for pharmacodynamics. A non-linear relation between the Bispectral index and the effect of the two drugs is used [2]. Several signals are selected as useful for identification task, from real tests during ICU: Remifentanyl drug dose, electromiography, signal quality index, Remifentanyl effect site concentration. Based on the information extracted from these signals and the existing models from literature, the MISO model parameters were adjusted to capture the patient's response to the administered drugs.

3 Conclusions

The results of our model prove to be well correlated with the data from the patients, providing reliable prediction for Bispectral index evolution as a result of manipulated variables Propofol and Remifentanyl. The next step is to apply the MISO model in clinical trials.

References

- [1] C. Ionescu, R. De Keyser, B. Claure-Torrico, T. De Smet, M. Struys, J. Normey-Rico, "Robust predictive control strategy applied for Propofol using BIS as a controlled variable during Anesthesia", *IEEE Transactions on Biomedical Engineering*, **55**(9): 2161-2170, (2008).
- [2] C. Minto, T. Schnider, T. Short, K. Gregg, A. Gentilini, S. Shafer, "Response Surface Model for Anesthetic Drug Interactions", *Anesthesiology*, **92**(6), 1603-1616, (2000).
- [3] CS. Nunes, T. Mendoca, J. M. Lemos, P. Amorim, "Predictive Adaptive Control of the BIS from EEG: Exploring Electromyography as an Accesible Disturbance", *Proc. 15th Medit. Conf. on Control and Automation*, Athens, (2007).
- [4] M. Struys, T. De Smet, L. Versichelen, S. vd Velde, R. vd Broecke, E. Mortier, "Comparison of closed loop controlled administration of propofol using BIS as the controlled variable versus standard practice controlled administration", *Anesthesiology*, **95**, 6-17, (2001)

Dynamical Modeling of Micro-Assembly Systems

Bayu Jayawardhana
 Faculty of Mathematics and Natural Sciences
 Rijksuniversiteit Groningen
 9747 AG Groningen
 The Netherlands
 Email: b.jayawardhana@rug.nl

1 Introduction

It has been known that incorporating optical lenses and optical fibres into integrated circuits based on the standard Micro Systems Technology (MST) processes (e.g., various etching, molding and other semiconductor fabrication technologies) are difficult, see for example, [1, 2]. In order to perform the task, micro-assembly technology has been developed for putting the optical components into the right place [1]. Micro-assembly is also used to build a complex three-dimensional structure which can be difficult to produce by MST processes [3]. Thus, for advancing the miniaturization technology, it is important to have the ability to assemble different components with nano or micro meter size and various MST devices for building multifunctional micro machines [1, 2, 3, 4, 5, 6, 7].

In the current state-of-art technology of automatic micro-assembly, micro-mechanical arms are widely used to handle the object [1, 2, 3, 4, 5, 6, 7]. However, the dynamics of micro-mechanical arms in close contact with a surface are significantly affected by the surface forces and intermolecular forces, which include van der Waals and capillary forces. The paper [8] presents an overview of the significance of van der Waals and capillary forces when the manipulated objects have dimensions less than one millimeter. Due to these surface forces, the micro/nano components can stick to the surface and become difficult to handle. The magnitude of these forces is nonlinear with respect to the distance between the micro object and the surface [9, 10, 11].

This paper describes a one-dimensional dynamical model of a micro object moving above a surface. The object is assumed to be a solid sphere and the model uses the Lennard-Jones potential for approximating the surface forces [10]. It is assumed that the sphere can be controlled directly by external force, for example, electromagnetic force.

Based on the model, an adaptive nonlinear control strategy for tracking reference trajectories is designed and simulated. The control design is based on recent article by Jayawardhana and Weiss [12].

References

- [1] D. O. Popa and H. E. Stephanou, "Micro and mesoscale robotic assembly," *Journal of Manufacturing Processes*, vol. 6, pp. 52-71, 2004.
- [2] S. Fatikow, "Automated Nanohandling by Micro-robots," in *Springer Series in Advanced Manufacturing*, D. T. Pham, Ed. London: Springer-Verlag, 2008.
- [3] N. Dechev and M. Basha, "Robotic microassembly of 3D MEMS structure," *Proc. IEEE/RSJ Int. Conf. Int. Robots and Systems Workshop*, San Diego, USA, 2007.
- [4] D. O. Popa, "High yield automated MEMS assembly: Compliant snap-fastener design, precision robotics and assembly evaluation," *Proc. IEEE/RSJ Int. Conf. Int. Robots and Systems Workshop*, San Diego, USA, 2007.
- [5] F. Michel and W. Ehrfeld, "Mechatronic micro devices," *Proc. Int. Symp. Micromechatronics & Human Science*, Nagoya, Japan, 1999.
- [6] Q. Zhou, V. Sariola, and H. N. Koivo, "Microhandling strategies for automation," presented at *IEEE/RSJ Int. Conf. Int. Robots and Systems Workshop*, San Diego, USA, 2007.
- [7] T. Wich and H. Hulsen, "Robot-based Automated Nanohandling," in *Automated Nanohandling by Micro-robots*, Springer Series in Advanced Manufacturing, S. Fatikow, Ed.: Springer Verlag, 2008.
- [8] R. S. Fearing, "Survey of sticking effects for micro parts handling," *Proc. International Conference on Intelligent Robots and Systems*, 1995.
- [9] A. Menciassi, A. Eisinger, I. Izzo, and P. Dario, "From "Macro" to "Micro" manipulation: Models and Experiments," *IEEE/ASME Trans. Mechatronics*, vol. 9, pp. 311-320, 2004.
- [10] J. Israelachvili, *Intermolecular and Surface Forces*, Academic Press, 1991.
- [11] V.A. Parsegian, *Van der Waals Forces*, Cambridge University Press, 2005.
- [12] B. Jayawardhana, G. Weiss, "Tracking and disturbance rejection for fully actuated mechanical systems," *Automatica*, vol. 44, no. 11, pp. 2863-2868, 2008.

Modeling and Control of a Wobble Yoke Stirling Engine: Application to a Micro–Cogeneration System

Marnix Kuindersma

University of Groningen,
Faculty of Mathematics and Natural Sciences
ITM, Nijenborgh 4, 9747 AG Groningen
The Netherlands.

Email: M.Kuindersma@student.rug.nl

Eloísa García–Canseco

Eindhoven University of Technology,
Faculty of Mechanical Engineering, CST
PO Box 513, 5600 MB Eindhoven,
The Netherlands.

Email: E.Garcia.Canseco@tue.nl

Jacqueline M.A. Scherpen

University of Groningen,
Faculty of Mathematics and Natural Sciences
ITM, Nijenborgh 4, 9747 AG Groningen
The Netherlands.

Email: J.M.A.Scherpen@rug.nl

1 Introduction

In the recent decades, there has been an enormous interest in the application of heat engines for conversion of different forms of heat source into electrical energy [1]. One of the most promising applications is the micro–combined heat and power (CHP) generation, or in other words, the simultaneous production of heat and power at a small–scale [2]. A micro–CHP consist of a gas engine which drives an electrical generator. The main purpose of a micro–CHP system is to replace the conventional boiler in a central heating system.

Among the technologies that have been proposed for micro–CHP applications we can mention fuel cells, internal combustion engines and Stirling engines [2, 3].

In this work, we focus on a Whispergen micro–CHP unit with Stirling engine technology, available at the Laboratory of Technology Management at the University of Groningen. This micro–CHP unit, developed by WhisperTech Limited [4], was originally designed as a battery charger for marine applications [5]. In contrast with most Stirling engines based on free–piston mechanisms, the Whispergen micro–CHP unit comprises a “wobble–yoke Stirling engine mechanism”, that is, a four–cylinder double–acting Stirling engine configuration whose design is based on the classical spherical four–bar linkage [6].

Since the invention of the first Stirling engine by Robert Stirling in 1816, Stirling engines have been heavily studied, with an increasing interest during the last decades. Nevertheless, most of the studies rely on thermodynamics methods and intuitive design techniques. There exist few literature on the application of dynamics and control methods to investigate their stability and dynamic properties, see for instance [7, 8, 9] and the recent work [10].

This work is a part of a long term research program whose final objective is the development of control methods for micro–CHP units. We present the preliminary results on the wobble–yoke Stirling engine.

References

- [1] G. Smith and S. Barnes. Electrical power generation from heat engines. *Power Electronics for Renewable Energy (Digest No: 1997/170)*, IEE Colloquium on, pages 5/1 – 5/6, May 1997.
- [2] J. Harrison. Micro combined heat and power (CHP) for housing. In *SET 2004–3rd. Conference on Sustainable Energy Technologies*, Nottingham, UK., Jun 28–30 2004.
- [3] H. Onovwiona and V. Ugursal. Residential cogeneration systems: review of the current technology. *Renewable and Sustainable Energy Reviews*, 10:389–431, Jan 2006.
- [4] Whispergen heat and power systems. <http://www.whispergen.com/>.
- [5] D. M. Clucas and J. K. Raine. Development of a hermetically sealed stirling engine battery charger. In *Proc. of the Institution of Mechanical Engineers, IMechC*, volume 208, pages 357–366, Jan 1994.
- [6] D. M. Clucas and J. K. Raine. A new wobble drive with particular application in a Stirling engine. In *Proc. of the Institution of Mechanical Engineers, IMechE*, volume 208, pages 337–346, 1994.
- [7] R. W. Redlich and D. M. Berchowitz. Linear dynamics of a free–piston Stirling engines. In *Proc. of the Institution of Mechanical Engineers, IMechE*, volume 199, pages 203–213, 1985.
- [8] M. Kankam and J. Rauch. Controllability of free–piston Stirling engine/linear alternator driving a dynamic load. In *28th Intersociety Energy Conversion Engineering Conference*, Atlanta, Georgia, Aug 8–13 1993. ANS, SAE, ACS, IEEE, ASME, AIAA, AIChE.
- [9] I. Burrel, S. Leballois, E. Monmasson, and L. Prevond. Energy performance and stability of Stirling micro–cogeneration system. In *Power Electronics and Motion Control Conference 2006, EPE-PEMC*, pages 2057 – 2063, Portoroz, Slovenia, Aug 2006.
- [10] J. Riofrio, K. Al–Dakkan, M. Hofacker, and E. Barth. Control–based design of free–piston Stirling engines. In *American Control Conference 2008*, pages 1533 – 1538, Seattle, Washington, USA, May 2008.

Modeling the baseband output envelope of a Microwave detector

Liesbeth Gomme, Yves Rolain, Johan Schoukens and Rik Pintelon
 Vrije Universiteit Brussel (Dept. ELEC/IW); Pleinlaan 2; B-1050 Brussels (Belgium)
 Phone: +32.2.629.28.68; Fax: +32.2.629.28.50; Email: lgomme@vub.ac.be

1 Introduction

The current state-of-the-art for the calibration of wave spectra containing spectral lines that lie on a harmonic grid ($f_0, 2f_0, \dots$) relies on the well-established step recovery diode method [1]. The challenge in narrow band modulated measurements resides in the calibration of the instrument's phase distortion for such signals. A crystal detector (HP 420C, [2]) can be used as a reference element in this context, because it translates the envelope of the RF-signal to IF frequencies and induces a limited and known linear distortion of the envelope. In the case of a realistic crystal detector, the crystal detector itself will introduce phase distortion, hence the identification of a model for a realistic crystal detector was undertaken. In this work a validated parametric black-box model for a crystal detector is constructed. A black-box model is estimated from baseband data and needs to be validated for use with high frequency signals. Therefore the baseband model needs to be extrapolated to RF frequencies.

2 The crystal detector model extraction

The crystal detector was identified as a baseband block oriented nonlinear feedback model that will be used to predict the device output when excited with a modulated RF-signal. The model contains a low-pass filter in the forward path and a high-pass filter followed by the nonlinearity in the feedback loop of the block oriented structure, as shown in fig. 1 [3,4].

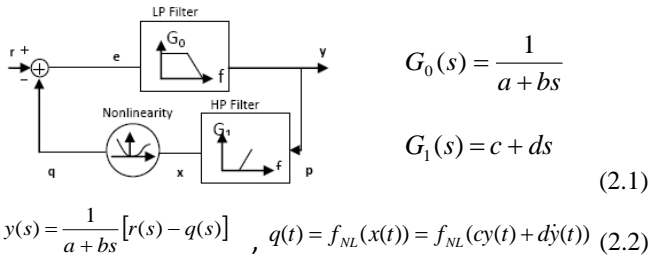


Fig. 1: Nonlinear feedback model of the crystal detector

3 Measurements for model validation

A baseband square law detector model is now available for validation in the high frequency region. To this end, an RF-signal is fed into the detector and measured at port 1 of the large-signal network analyser (LSNA). The down converted detector output is measured using an ADC of the LSNA.

4 Calculating the model output

The model output envelope can be computed by solving the differential equation adhering to the model structure in figure 1. The equivalent scheme for the model structure is depicted in figure 2.

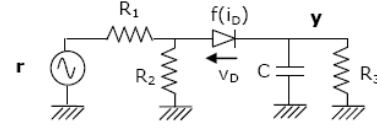


Fig. 2: Physical representation of the identified crystal detector model

The differential equation describing this scheme is

$$\left[\frac{1 + \frac{R_1}{R_1 + R_3}}{1 - \frac{R_1}{R_1 + R_2}} \right] y + \left[\frac{\frac{R_1 R_2 C}{R_2 + R_1}}{1 - \frac{R_1}{R_1 + R_2}} \right] \frac{dy}{dt} = r - \frac{v_D}{1 - \frac{R_1}{R_1 + R_2}} \quad (4.1)$$

with $i_D = \frac{y}{R_3} + C \frac{dy}{dt}$ and $v_D = f(i_D)$

R_1, R_2, R_3 and C can then be rewritten as a function of a, b, c and d , available from the model extraction. The differential equation in (4.1) is solved using a Runge-Kutta algorithm [5] when rewritten as,

$$C \frac{dy}{dt} = \frac{r}{R_1} - y \left(\frac{1}{R_1} + \frac{1}{R_2} + \frac{1}{R_3} \right) - v_D \left(\frac{1}{R_1} + \frac{1}{R_2} \right) \quad (4.2)$$

where v_D is computed iteratively using the Newton-Raphson method [5] for equation 4.3.

$$i_D = h(v_D) = \frac{r}{R_1} - y \left(\frac{1}{R_1} + \frac{1}{R_3} \right) - v_D \left(\frac{1}{R_1} + \frac{1}{R_2} \right) \quad (4.3)$$

The mean deviation in the down converted frequency band between the modelled and measured envelope equals 3.4dB. The phase of the spectral components of the modelled output coincides well with those of the measured output envelope. The difference in phase equals 10.8° between modelled and measured outputs.

5 Conclusion

Using a nonlinear feedback model for a crystal detector the output signal is computed. The physical representation of the model structure is translated into its differential equation. This approach gives good results with regard to predicting the magnitude and phase behavior of the detector output spectra.

References

- [1] W. Van Moer, Y. Rolain, A Large-Signal Network Analyzer: Why is it needed?, *IEEE Microwave Magazine*, Vol. 7, No. 6, pp. 46-62, 2006.
- [2] L. Gomme et al., On the use of a crystal detector for a phase calibration of the Large Signal Network Analyzer, *Measurement Science and Technology*, Vol.19, no.8, 2008.
- [3] S. Billing, S. Fakhouri, Identification of systems containing linear dynamic and static nonlinear elements, *Automatica* 18, 15-26, 1982.
- [4] J. Schoukens et al., Identification of a Block-Structured Nonlinear Feedback System, Applied to a Microwave Crystal Detector, *IEEE Transactions on Instrumentation and Measurement*, Vol.57, no.8, 2008.
- [5] A. Ralston, P. Rabinowitz, *A First Course in Numerical Analysis: Second Edition*, McGraw-Hill, 1978.

Identification of Low Order Model for Large Scale Systems

S.K.Wattamwar¹Siep Weiland¹Ton Backx¹

1 Introduction

Phenomenon in Fluid Dynamics are usually modeled by partial differential equations which are solved by discretization of the spatial domain. Such discretization leads to a high order systems. Despite the currently available computing power, it is difficult to use such high order models for online control and optimization applications. This motivates the search for lower dimensional models which could approximate the original high dimensional models without much loss of the original information. Such low dimensional (reduced) models should satisfy various criteria like a smaller dimension, an accurate prediction, faster computability, stability and good performance in closed loop. The problem of finding of suitable substitute model is usually referred to as model reduction.

2 Glass Manufacturing

To investigate novel model reduction ideas we are working on a Cathode Ray Tube (CRT) glass manufacturing process. This process is highly energy intensive and involves many complex phenomena. In this process raw material is fed into a melter containing molten glass. A batch blanket is formed which is heated from the top by oil/gas fired burners and by molten glass from the bottom. This process is roughly divided into four sub-processes which are melting, fining, homogenization and refining. Inhomogeneous supply of heat to the glass induces a convective flow pattern of glass in the tank which in-turn has effect on each of these sub processes. The Glass flow pattern in the tank is laminar and temperature varies between 1500-1800 K. Glass quality is highly dependent on how well each of the sub processes is carried, on the flow pattern and on the temperature distribution in the tank. Dynamic behavior of the glass tank depends on the heat input to the tank and heat exchange within the tank. Control of temperature distribution in the tank is the main control task which is very difficult due to long thermal response time of the glass. Hence it is tried to run the tank as stationary and stable as possible. A proper selection of inputs that define bubbling, electrical boosting, stirring are used to ensure proper operating conditions.

3 Recent Developments

In this paper we propose a novel procedure for obtaining a low order model of large scale non-linear process. Our approach is based on the combinations of the methods of

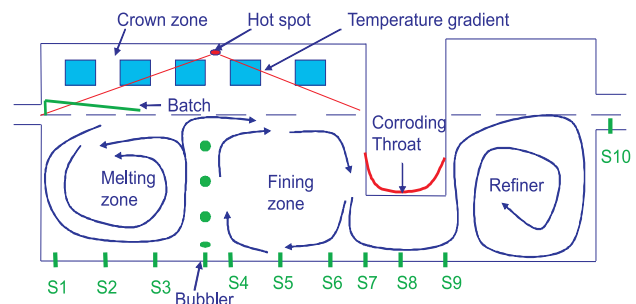


Figure 1: Glass Manufacturing Furnace

Proper Orthogonal Decomposition (*POD*), and non-linear System Identification (*SID*) techniques. In the first step *POD* is used to separate the spatial and temporal patterns and in second step a model structure and its parameters of linear and of non-linear polynomial type are identified for approximating the temporal patterns obtained by *POD*. The proposed model structure treats *POD* modal coefficients as states rather than outputs of the black-box identified model. The state space matrices which happens to be the parameters of a black-box to be identified, comes linearly in identification process. For the same reason, Ordinary Least Square (*OLS*) method is used to identify the model parameters. The simplicity and reliability of proposed method gives computationally very efficient linear and non-linear low order models for extremely large scale processes. The method is of generic nature. The efficiency of proposed approach is illustrated on a very large scale benchmark problem depicting Industrial Glass Manufacturing Process (*IGMP*). The results show good performance of proposed method. One of the disadvantage of proposed method is that for high order approximation, nonlinear polynomial model becomes unstable. It is therefore future research to impose stability in the identification process.

Acknowledgement

This work has been supported by the European union within the Marie-Curie Training Network PROMATCH under the grant number MRTN-CT-2004-512441

References

- [1] NCNG course on glass manufacturing 1997.
- [2] S. Wattamwar, "Identification of Low Dimensional Models for Geometric Parameter Variations in Industrial Glass Manufacturing Process", IEEE MSC (CCA) 2008.
- [3] P. Astrid, "Reduction of process simulation models", Phd thesis 2004.
- [4] L. Huisman, "Control of glass melting processes based on reduced CFD models", Phd thesis 2005.

¹Department of Electrical Engineering, Eindhoven University of Technology, P.O. Box 513, 5600 MB Eindhoven, The Netherlands, E-mail: s.wattamwar@tue.nl.

Efficient multiple objective optimal control: (bio)chemical engineering applications

Filip Logist, Peter M.M. Van Erdeghem, and Jan F. Van Impe
BioTeC - Chemical and Biochemical Process Technology and Control
Department of Chemical Engineering, Katholieke Universiteit Leuven
W. de Croylaan 46, B-3001 Leuven, Belgium
Email: {filip.logist, peter.vanerdeghem,jan.vanimpe}@cit.kuleuven.be

1 Introduction

In practical (bio)chemical optimal control problems multiple and conflicting objectives are often present, giving rise to a set of Pareto optimal solutions instead of one single solution. The most often exploited approaches to generate this Pareto set are (i) weighted sum approaches in which for a grid of different weights optimal control problems are solved with deterministic optimisation routines [3], or (ii) stochastic genetic algorithms in which a population of solutions is updated based on repeated cost computations in order to evolve gradually to the Pareto set [7]. Unfortunately, both approaches exhibit certain restrictions. For the weighted sum it is known that an equal distribution of weights does not necessarily lead to an even spread along the Pareto front, and that points in a non-convex part of the Pareto front cannot be obtained [1]. Stochastic approaches on the other hand (i) may become time consuming due to the repeated model simulations required, (ii) are less suited to incorporate constraints exactly, and (iii) are limited to rather low dimensional search spaces. This last aspect restricts the control parameterisations to either (i) analytical parameterisations based on expressions derived from the necessary conditions of optimality, or (ii) coarse piecewise polynomial approximations (e.g., constant or linear functions).

2 Goal

Recent techniques as Normal Boundary Intersection (NBI) [2] and Normalised Normal Constraint (NNC) [6] have been found to mitigate the disadvantages of the weighted sum for scalar multiple objective problems, while still allowing the exploitation of fast deterministic solvers. Therefore, the aim is to use NBI and NNC in a deterministic multiple shooting approach in order to efficiently solve multiple objective optimal control problems in the (bio)chemical industry.

3 Results and discussion

Several (bio)chemical applications have been successfully and efficiently optimised [4, 5]: (i) tubular chemical reactors with conflicting conversion and energy costs, (ii) fed-batch bioreactors with a production-yield conflict, as well as (iii) a periodically operated reverse flow reactor. The multiple ob-

jective optimal control problems exhibited several general features, e.g., (i) nonlinear initial as well as boundary value problems, (ii) path constraints on the controls and/or states, (iii) fixed and free end time, (iv) presence and absence of singular arcs, (v) distributed parameters In summary, the combination of NBI and NNC with multiple shooting optimal control techniques ensures an efficient and accurate treatment of multiple objective optimal control problems (i) with (bio)chemical processes described by (large sets of) ordinary differential (and algebraic) equations, and (ii) subject to a number of (in)equality constraints.

4 Acknowledgements

Work supported in part by Projects OT/03/30 and EF/05/006 (Center-of-Excellence Optimization in Engineering) of the Research Council of the Katholieke Universiteit Leuven, and by the Belgian Program on Interuniversity Poles of Attraction, initiated by the Belgian Federal Science Policy Office. The scientific responsibility is assumed by its authors.

References

- [1] I. Das and J.E. Dennis. A closer look at drawbacks of minimizing weighted sums of objectives for Pareto set generation in multicriteria optimization problems. *Structural Optimization*, 14:63–69, 1997.
- [2] I. Das and J.E. Dennis. Normal-Boundary Intersection: A new method for generating the Pareto surface in nonlinear multicriteria optimization problems. *SIAM Journal on Optimization*, 8:631–657, 1998.
- [3] F. Logist, P. Van Erdeghem, I.Y. Smets, and J.F. Van Impe. Multiple-objective optimisation of a jacketed tubular reactor. In *Procs of the European Control Conference*, pages 963–970, 2007.
- [4] F. Logist, P.M. Van Erdeghem, and J.F. Van Impe. Efficient deterministic multiple objective optimal control of (bio)chemical processes. *Chemical Engineering Science*, Accepted, 2008.
- [5] F. Logist and J.F. Van Impe. Multiple objective optimisation of cyclic chemical systems with distributed parameters. Accepted for oral presentation at the 14th IFAC Workshop on Control Applications of Optimisation, 6-8 May 2009, Jyväskylä (Finland).
- [6] A. Messac, A. Ismail-Yahaya, and C.A. Mattson. The normalized normal constraint method for generating the Pareto frontier. *Structural & Multidisciplinary Optimization*, 25:86–98, 2003.
- [7] D. Sarkar and J.M. Modak. Pareto-optimal solutions for multi-objective optimization of fed-batch bioreactors using non-dominated sorting genetic algorithm. *Chemical Engineering Science*, 60:481–492, 2005.

An Efficient Methodology for Model Predictive Control of SMB Plants Based on the Wave Theory and Reduced Order Models

Carlos Vilas

Automatic Control Laboratory
Faculté Polytechnique de Mons
31 Boulevard Dolez, 7000 Mons
Belgium

Email: carlos.vilas@fpms.ac.be

Alain Vande Wouwer

Automatic Control Laboratory
Faculté Polytechnique de Mons
31 Boulevard Dolez, 7000 Mons
Belgium

Email: Alain.VandeWouwer@fpms.ac.be

1 Introduction

The simulated moving bed (SMB) process is a chromatographic separation process. This technology is important in various industrial sectors, ranging from food to fine chemicals and pharmaceuticals. A detailed description on the process can be found on [1] and references therein.

Control of SMB plants has attracted considerable attention and many approaches have been proposed. From simple PI [2] controllers to more sophisticated techniques like model predictive control (MPC) [3]. The main limitation of simple controllers is that the operating range in which stability can be ensured is usually small for plants with highly nonlinear behavior. On the other hand, advanced control techniques might require complex implementation and/or high computational expense. In this work, we propose, for alleviating the weaknesses of each approach, to combine three different techniques -the wave theory, MPC and the proper orthogonal decomposition (POD)- for constructing the controller.

2 Outline of the Methodology

The objective of this contribution is to design a MPC strategy for the control of SMB plants. A key element in MPC is the model which, in the case of SMB, is spatially distributed. In a first attempt, the simulation was carried out using the finite element method but a comparison in terms of the purity showed that a large number of discretization points (> 100) are required to obtain good results. This implies to solve more than 3000 ODEs which makes the approach unsuitable for MPC. As an alternative, a reduced order model constructed by means of the POD method [4] was implemented. Using this technique the number of equations is reduced in more than one order of magnitude. On the other hand, on a typical implementation of MPC, an optimal profile (discretized in time) is computed for each plant input on the basis of a given optimization criteria. Only the first element of the input profiles is introduced in the plant and the procedure is repeated in the next time interval. However, for obtaining the desired plant response, usually, the number of elements in each input profile (decision variables) must be large. This fact increases the computational effort making

the method prohibitive for real time purposes (even with the POD). Instead, the wave theory [5] is used as a theoretical framework for the derivation of a PI controller following ideas developed in [2]. The MPC scheme will only search for the optimal parameters of the PI controller thus reducing drastically the number of decision variables.

The methodology was tested in a simulation experiment showing that, in the event of a perturbation, the MPC scheme is faster than a PI controller and, in the transition period, it maintains the states closer to the reference. Furthermore, for large perturbations which lead the system out of the stability range of the PI, the MPC scheme has a wider leeway for compensating their effects.

3 Acknowledgments

This paper presents research results of the Belgian Network DYSCO (Dynamical Systems, Control, and Optimization), funded by the Interuniversity Attraction Poles Program, initiated by the Belgian State, Science Policy Office. The scientific responsibility rests with its authors.

References

- [1] D. M. Ruthven and C. B. Ching. Counter-current and simulated moving bed adsorption separation processes. *Chemical Engineering Science*, 44(5):1011–1038, 1989.
- [2] H. Schramm, S. Grüner, and A. Kienle. Optimal operation of simulated moving bed chromatographic processes by means of simple feedback control. *Journal of Chromatography A*, 1006(1-2):3–13, 2003.
- [3] G. Erdem, S. Abel, M. Amanullah, M. Morari, M. Mazzotti, and M. Morbidelli. Automatic control of simulated moving beds - experimental verification. *Adsorption*, 11:573–577, 2005.
- [4] L. Sirovich. Turbulence and the dynamics of coherent structures. Part I: Coherent structures. *Quarterly of Appl. Math.*, 45(3):561–571, 1987.
- [5] F. G. Helfferich. Non-linear waves in chromatography III. multicomponent langmuir and langmuir-like systems. *Journal of Chromatography A*, 768:169–205, 1997.

The Effect of Imperfect Maintenance on Deterioration Processes

Samira S. Farahani¹

Delft Center for Systems and Control
Technische Universiteit Delft
Mekelweg 2, 2628 CD Delft
The Netherlands

Email: s.safaeifarahani@tudelft.nl

J. A. M. van der Weide

Department of Applied Mathematics
Technische Universiteit Delft
Mekelweg 4, 2628 CD Delft
The Netherlands

Email: j.a.m.vanderweide@tudelft.nl

M. J. Kallen², R. P. Nicolai³

1 Introduction

Many metal structures are subject to deterioration such as chemical corrosion, stress corrosion cracking, brittle fracture, and fatigue. Therefore, it is required to maintain these structures before they collapse or cause some damages that are not compensable. Many maintenance models have been developed to describe a deterioration process and to give optimal solutions to decrease the cost and increase the system reliability of such systems. However, most of these models are based on ideal assumptions such as perfect inspection and maintenance. This study is focused on investigating the effect of imperfect maintenance on the deterioration process of a steel structure.

2 Methodology

We are interested in representing the deterioration process with a mathematical process, in order to be able to describe the corrosion characteristics and properties under the influence of imperfect maintenance. In addition, finding a theoretical interpretation of the behavior of the time between maintenance actions is required to obtain a good decision criterion for planning the repair and replacement strategies.

To fulfill these goals, in the first case, a white-box model is designed to describe the deterioration process of a steel surface. The model specification is mainly inspired by the model proposed in [1], considering both the initiation and expansion processes as stochastic processes. The obtained results are based on the generated data before and after the 3% surface corrosion which is the maintenance threshold. In the second case-study, since the maintenance is imperfect, the inter-repair times follow a superposition process that does not have the nice properties of a renewal process and not all of these properties are known or applicable according to literature. To deal with this process, the results and assumptions presented in [2] and [3] are applied.

¹This work was done as a MSc thesis in the department of Applied mathematics, Delft University of Technology

²HKV Consultants, P.O.Box 2120, 8203 AC Lelystad, The Netherlands, Email: m.j.kallen@hkv.nl

³HKV Consultants, P.O.Box 2120, 8203 AC Lelystad, The Netherlands, Email: r.nicolai@hkv.nl

3 Results and Perspectives

The results of the simulation show that the corrosion sample path before and after imperfect maintenance follows a gamma process. This is checked according to independence assumption of the corrosion increments and the results of the K-S test which confirmed that all the increments have a gamma distribution. The parameter estimation shows that the gamma process in both cases is non-stationary with having shift in the shape parameters.

According to the approximation methods proposed in [2] and [3], the density of the inter-repair time is best fitted to a gamma distribution. Consequently, for a certain class of distributions, the superimposed process has exponential inter-arrival times when the number of pooled processes are large enough; subsequently, the inter-repair time has a gamma distribution. As a result, for a large number of repairs, the inter-repair times distribution is stationary and converges to the percentage of corroded cells multiplied by the mean value of the interarrival times.

For future studying this work can be improved by considering other factors that might influence the corrosion process since we have only considered the coating quality. Study the corrosion in three dimension is also another option of improvement.

References

- [1] Nicolai R.P., Dekker R., van Noortwijk J.M., A comparison of models for measurable deterioration: An application to coatings on steel structures, Reliability Engineering System Safety, Volume 92, Issue 12, Pages 1635-1650, December 2007.
- [2] Torab P., Kamen E. W., On Approximate Renewal Models for the Superposition of Renewal Processes, IEEE International Conference on Communications (Finland), 2001. ICC 2001., Volume 9, Pages 2901-2906.
- [3] Cox D. R., Smith W. L., On the superposition of renewal processes, Biometrika, Volume 41, Pages 91-99, 1954.

Very fast temperature pulsing: catalytic reactor design

Jasper Stolte
Postbus 513
5600 MB Eindhoven
J.Stolte@tue.nl

Ton Backx
Postbus 513
5600 MB Eindhoven
A.C.P.M.Backx@tue.nl

Okko Bosgra
Postbus 513
5600 MB Eindhoven
O.H.Bosgra@tue.nl

1 Introduction

Chemical reaction systems are mostly operated in steady state. However, these systems can be viewed as highly non-linear, coupled partial differential equations. Allowing non-steady reaction conditions allows for flexibility which can be used for optimization of the process. An earlier result in this project suggests there are reaction schemes for which it is profitable to use temperature pulsing [1]. This abstract introduces a design for a temperature pulsing reactor.

2 Design

The reactor design is based on a micro-channel flow reactor, which is modified to have a 'floor' of catalyst in the channel. This catalytic layer is made from metallic platinum, which can be subjected to a large electrical current. Ohmic losses in the catalyst will then make it heat up quickly. Figure 1 shows a schematic view (not to scale) of this reactor design.

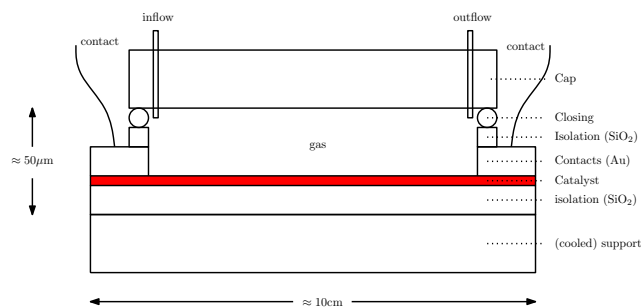


Figure 1: Schematic view of reactor design (not to scale). The red layer represents the catalyst which is heated directly.

In the design procedure the thickness of the catalytic layer and the SiO_2 layer are crucial for the shape of the temperature pulses. There exists an interplay between the ohmic heating, and cooling of the catalytic layer to the metal layer through conduction. For optimal pulse shape the heating and the cooling time constants should be roughly the same.

The current pulses are generated using an RLC resonant circuit. A capacitor is charged to a voltage of 1000 V and subsequently discharged through an inductance and the resistance of the catalytic layer. Almost all of the energy stored in the capacitor is released as heat in the catalytic layer.

3 Simulation

A simulation was created to inspect the heat distribution throughout the reactor when the catalytic layer is subjected to a current pulse. Figure 2 shows the simulated catalytic surface temperature for this design. Pulses of hundreds of Kelvin in tens of microseconds appear feasible using this design. The temperature gradients are orders of magnitude higher than any result known from literature.

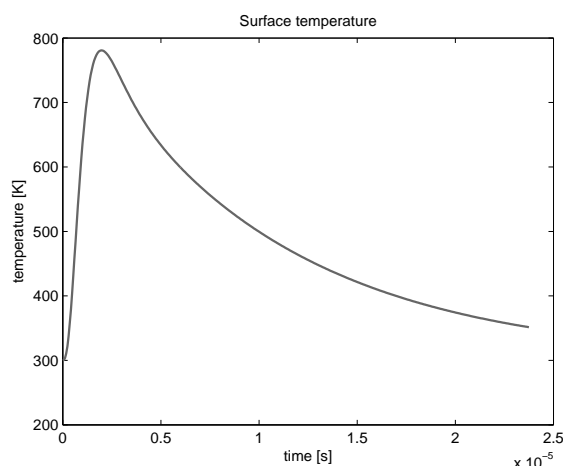


Figure 2: Simulated profile of the catalytic surface temperature. The results suggest this design is capable of temperature pulses of around 500 K which exist for only around 20 μs .

Even faster pulses can be created when the voltage that is used is higher and the layers are thinner. The required components will be significantly more expensive however.

4 Conclusion

A prototype reactor based on this design is currently being constructed. Within the next months this reactor setup will be tested, and subsequently used to investigate transient operation of heterogeneous catalytic reactions.

References

- [1] J. Stolte, J. Vissers, T. Backx, and O. Bosgra. Modeling local/periodic temperature variation in catalytic reactions. In *IEEE International Conference on Control Applications*, 2008.

Using multidimensional scaling to represent a power system according to the electric distances between nodes

Florence Fonteneau-Belmudes
University of Liège
Florence.Belmudes@ulg.ac.be

Damien Ernst
University of Liège
dernst@ulg.ac.be

Louis Wehenkel
University of Liège
L.Wehenkel@ulg.ac.be

In power systems, graphical representations of the electric networks are systematically used when designing and operating a network. Being able to visualize the elements of a power system in a two-dimensional space is of paramount importance at these two stages of power system analysis and control. The graphical representation commonly used by all the Transmission System Operators (TSOs) is based on the geographic position of each equipment of the network, which seems to be the most evident way to represent a power system.

However, we can wonder whether this representation is totally appropriate, or should be completed by another representation that would help the operators to have a better perception of the electrical phenomena that are likely to happen in their network. In current practice, system operators can only create a mental representation of the physical properties of the equipments. For example, they can associate to each transmission line the value of its impedance, or at least an approximation of it. Thanks to these indicators, they are able to figure out to which equipments an incident (such as a line overflow) is more likely to propagate. However, these conclusions are only based on the human interpretation and are therefore neither completely accurate nor perfectly reliable. This is why a dedicated tool representing the electrical properties of the equipments of a network would provide a helpful complement to the existing tools used by the transmission system operators. Whereas in-depth studies about the necessity to have user-friendly and adequate representations of a power system in order to operate it correctly have already been reported in the literature (see, e.g., [1], [2] and [3]), no alternative to the geographic coordinate system has been investigated yet.

We propose in this work to develop a graphical representation of a power system based on the impedances between nodes, and no longer on the geographic distance between them. The choice of impedances to define a “new” distance between the nodes of an electricity transportation network is based on the assumption that the impedances provide a good image of the electric proximity between nodes. To be as close as possible to the electric reality of a power system, we define here the distance between two nodes of an electric network as being the reduced impedance between these two nodes, which is computed by reducing the whole network to these only nodes.

By computing the reduced admittance between each pair of nodes of the studied system, we obtain a matrix expressing the electrical proximities between all the nodes of the network. In this context, our objective is to visualize the information contained in the n -by- n electrical proximity matrix (where n is the number of nodes of the studied electric network) in a low-dimensional space. For this purpose, we chose to use multidimensional scaling algorithms. As explained in [4], multidimensional scaling is a method that aims at representing measurements of similarity between pairs of objects as distances between points of a low-dimensional multidimensional space. This technique is therefore appropriate to extract from the electrical proximity matrix the coordinates of the nodes in a two-dimensional space.

We have implemented our approach to create an “electric” graphical representation of the IEEE 118 bus test system, vastly used in the literature as benchmark problem, and also of the Belgian electric network. The power system engineers to which these graphical representations were shown found them very informative.

References

- [1] R. Fujiwara and Y. Kohno, “User-friendly workstation for power system analysis,” *IEEE Transactions on Power Apparatus and Systems*, vol. PAS-104, No. 6, pp. 1370–76, June 1985.
- [2] P. Mahadev and R. Christie, “Envisioning power system data: Concepts and a prototype system state representation,” *IEEE Transactions on Power Systems*, vol. 8, no. 3, pp. 1084–90, August 1993.
- [3] —, “Envisioning power system data: Vulnerability and severity representations for static security assessment,” *IEEE Transactions on Power Systems*, vol. 9, no. 4, pp. 1915–20, November 1994.
- [4] I. Borg and P. J. Groenen, *Modern Multidimensional Scaling: Theory and Applications*. Springer New York, 2005.

LMI formulation for Optimal Control of coal fired Power Plants

Emile Simon and Vincent Wertz
Department of Applied Mathematics
Ecole Polytechnique de Louvain
1348 Louvain-la-Neuve
Belgium

Corresponding author: emile.simon@uclouvain.be

1 Introduction

Thermal power plants are usually controlled by classical regulations (mostly PIDs), developed with a decentralised model, splitting the system in many different SISO loops. However, multiple providers and distributed generation are more likely to cause sudden and large changes of the load demand. Improving the performance is thus a commercial commodity of great importance in the current market's state of privatised power industry. Therefore, we consider the solution of an optimal multivariable control.

The objective pursued here was already studied in a previous work [2], using the same plant and the same 2x2 transfer matrix. A simplified scheme of the plant is shown on Fig. 1. The trade-off between tracking error on the load (y_1) and low variations on the pressure (y_2) was taken as objective. The method allowed to determine the trade-off curve. A key feature was the relation between the value of the tracking cost and the delay structure of the plant.

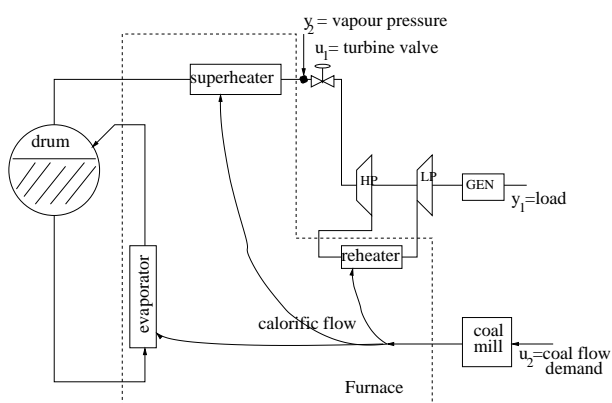


Figure 1: Simplified scheme of a coal-fired power plant.

2 Contribution

The method chosen in this paper differs from the one used in [2]. Here the problem is cast into an LMI formulation, a technique presented for instance in [1]. The same trade-off results as those in [2] are found, but now the new formulation allows one to add constraints with other LMI. Since in this paper the control energy is taken into account, a new LMI reducing the control input is developed.

Then the impact of this new constraint on the original objective is presented.

3 Results

The results provide the same trade-off as the one obtained in [2]. Using this LMI formulation allows to add new constraints formulated as new LMI. Without constraint, the coal flow input was too large. So a new LMI is introduced, allowing to reduce the norm of the optimal controller and thus the size of the input produced. This is shown to have a limited effect on the original objective, meaning a slight impact on the performance. To illustrate this we compare the responses after a step on the load, on Fig. 2.

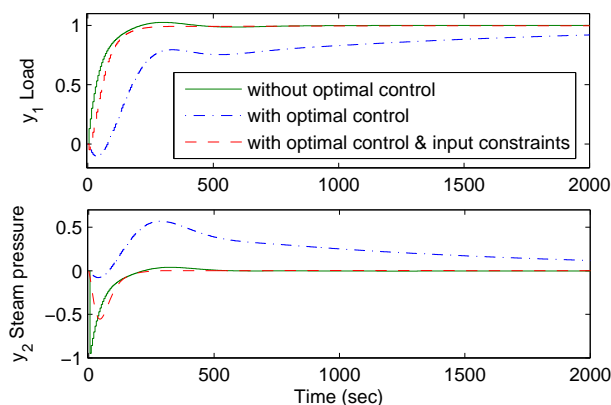


Figure 2: Step responses comparison.

We conclude from the results that the control is significantly improved, while having control inputs within their limits.

References

- [1] C. Scherer, "From mixed to multi-objective control," in *Proceedings of the 38th Conference On Decision & Control*, december 1999, pp. 3621–3626.
- [2] V. Wertz, E. Silva, G. Goodwin, and B. Codrons, "Performance limitation arising in the control of power plants," *Proceedings 17th IFAC World Congress*, 2008.

Non-centralized Model Predictive Control of Power Networks

A.C.R.M. Damoiseaux, R.M. Hermans, A. Jokić, M. Lazar, P.P.J. Van den Bosch

Department of Electrical Engineering

Eindhoven University of Technology

P.O. Box 513, 5600 MB Eindhoven

The Netherlands

Email: rhermans@tue.nl

1 Introduction

Traditional power systems are characterized by highly repetitive power flows, with a relatively small amount of uncertain power demand fluctuations, and with well-controllable, large-scale power plants on the power production side. As a consequence, a large portion of power production can be efficiently scheduled in an open-loop manner, whereas the classical Automatic Generation Control (AGC) scheme suffices for efficient real-time power balancing. Today, however, electrical power systems are going through some major restructuring processes. Firstly, from a regulated, one utility controlled operation, the system is reorganized to include many parties that compete for power production and consumption, which pushes the system towards its stability boundaries. Secondly, there has been an increasing integration of small-scale and often renewable Distributed Generation (DG). Large unpredictable power fluctuations from renewable energy sources, e.g. wind power, require efficient and fast acting controllers.

2 Model Predictive Control

Recently, it was observed that Model Predictive Control (MPC) has a potential for solving the above mentioned problems that will appear in future electrical power networks. MPC is able to guarantee optimality with respect to a desired performance objective, while explicitly taking constraints into account. Furthermore, MPC allows the usage of disturbance models that can be employed to counteract the uncertainties introduced by renewable energy sources.

Nevertheless, MPC requires solving a finite-horizon open-loop optimal control problem within each sampling period, given a model of the controlled system and measurements of the current state. As power networks are large scale systems, computationally as well as geographically, it is practically impossible to implement a centralized MPC controller.

3 Non-centralized Model Predictive Control

The problems of centralized MPC for control of large scale systems such as power networks is one of the reasons for which the non-centralized formulation and implementation of MPC receives more and more attention. Non-centralized

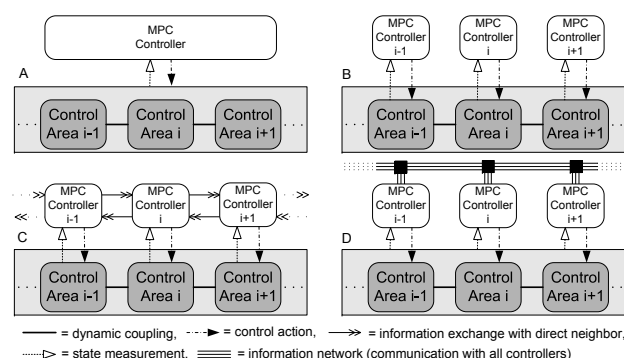


Figure 1: A schematic representation of: Centralized MPC (A), Decentralized MPC (B), Distributed MPC with communication with solely neighbors (C), Distributed MPC with communication with all subsystems (D).

MPC schemes can roughly be divided into two categories: decentralized techniques, where there is no communication in between different controllers, and distributed techniques, that allow communication between different controllers to achieve better performance.

In this talk, three non-centralized MPC techniques [1–3] are studied and the suitability for use in power networks is critically assessed with respect to relevant characteristics: performance of the closed loop system, the extent of decentralization, and the computational complexity. Furthermore, important issues such as feasibility, convergence and stability are addressed.

References

- [1] A.N. Venkat, "Distributed Model Predictive Control: Theory and applications," Ph.D. dissertation, University of Wisconsin-Madison, Wisconsin Madison, 2006.
- [2] A. Alessio, A. Bemporad, "Decentralized model predictive control of constrained linear systems," in Proceedings European Control Conference, Kos, Greece, 2007, pp. 2813-2818.
- [3] E. Camponogara, D. Jia, B.H. Krogh, and S. Talukdar "Distributed model predictive control," IEEE Control Systems Magazine, vol 22, no. 1, pp. 44-52, 2002.

Power Factor Compensation in Nonsinusoidal Systems based on Cyclodissipativity

Dunstano del Puerto-Flores, and

Jacqueline M.A. Scherpen

Dept. of Disc. Technology and Production Automation

Rijksuniversiteit Groningen

Nijenborgh 4, 9747 AG Groningen

The Netherlands

Emails: d.del.puerto.flores@rug.nl,

j.m.a.scherpen@rug.nl

Romeo Ortega

SUPELEC

Laboratoire des Signaux et Systèmes,

Plateau de Moulon, 91192, Gif-sur-Yvette,

France

Email: ortega@lss.supelec.fr

Abstract

Optimizing energy transfer from an alternating current (ac) source to a load is a classical problem in electrical engineering. In practice, the efficiency of this transfer is typically reduced due to the phase shift between voltage and current at the fundamental frequency. The power factor, defined as the ratio between the real or the active power (average of the instantaneous power) and the apparent power (the product of rms values of the voltage and current), then captures the energy-transmission efficiency for a given load. The standard approach to improving the power factor is to place a compensator between the source and the load.

If the load is scalar linear time-invariant (LTI) and the generator is ideal—that is, with negligible impedance and fixed sinusoidal voltage—it is well known that the optimal compensator minimizes the phase shift between the source voltage and current waveforms—increasing the so-called source power factor (PF), [1]. The task of designing compensators that aim at improving PF for nonlinear time-varying loads operating in non-sinusoidal regimes is far from clear.

The effectiveness of capacitive compensation in systems with nonsinusoidal voltages and currents has been widely studied by [2] and [3]. Unfortunately, in [4] it has been illustrated that the capacitive compensation may not be effective for non-sinusoidal voltages. Therefore, a more complex compensator than only a capacitor is required for the reactive power minimization in such situations. Furthermore, most of the approaches used to improve PF are based on the power definitions, [3], and a lack of a unified definition of reactive power produces misunderstanding of power phenomena in circuits with nonsinusoidal voltages and currents.

Recently, in [5] a new framework for analysis and design of (possibly nonlinear) PF compensators for electrical systems operating in non-sinusoidal (but periodic) regimes with nonlinear time-varying loads was presented. This framework is based on the cyclodissipativity property and the improvement of power factor is done independent of the re-

active power definition. This result has been applied in [6] on the practical problem of the passive compensation of a classical half-bridge controller rectifier with non-sinusoidal source voltage.

Here we illustrate the application of this framework to the passive compensation of linear loads with a non-sinusoidal source voltage. We give criteria for improvement of PF with linear capacitors, series and parallel LC filters, which determine the optimal values for the compensator parameters that depend of the spectral line of load susceptances B_n and voltage source $\hat{V}[n]$.

References

- [1] W. Shepherd and P. Zand, *Energy Flow and Power Factor in Nonsinusoidal Circuits*. Cambridge University Press, 1979.
- [2] W. Shepherd and W. Zakikhani, "Power factor correction in nonsinusoidal systems by the use of capacitance," *J. Phys. D: Appl. Phys.*, vol. 6, pp. 1850–1861, 1973.
- [3] L. S. Czarnecki, "Budeanu and fryze: Two frameworks for interpreting power properties of circuits with non-sinusoidal voltages and currents," *Electrical Engineering*, vol. 80, pp. 359–367, 1997.
- [4] L. Czarnecki, "A time-domain approach to reactive current minimization in nonsinusoidal situations," *Instrumentation and Measurement, IEEE Transactions on*, vol. 39, pp. 698–703, Oct 1990.
- [5] E. Garcia-Canseco, R. Grino, R. Ortega, M. Salichs, and A. Stankovic, "Power-factor compensation of electrical circuits," *Control Systems Magazine, IEEE*, vol. 27, pp. 46–59, April 2007.
- [6] R. Ortega, M. Hernandez-Gomez, F. Lamnabhi-Lagarrigue, and G. Escobar, "Passive power factor compensation of a controlled rectifier with non-sinusoidal generator voltage," *Conference on Decision and Control, 2008. CDC'08*, pp. 3755–3760, Dec 2008.

Using the event-driven Petri net in complex distributed systems design

Alexandre Skrylnik

Faculté Polytechnique de Mons, Energy Research Centre

Boulevard Dolez 31, B - 7000 Mons

oleksandr.skrylnyk@fpms.ac.be, <http://poleenergie.fpms.ac.be>

1 Introduction

Real-time systems stand as an assembly of hardware and software to perform a set of defined operations. Depending on the system's architecture, the communication procedure is a crucial problem that the developer faces within the system design. In many cases, the reliability of a process run of main operations is assured with appropriate software conceived to manage the system's resources in order to avoid any conflict in communication procedure. In this work we present a formal approach to conceptualize and implement the software's algorithm for distributed systems equipped with human-machine interface.

2 Case study

The conceptualising and implementation problem has been studied within a software design case for an autonomous photovoltaic system. The system is destined to simulate energy consumption by a low-energy house's heating equipment. Based on a formal approach, the appropriate software has been developed using LabVIEW and has been integrated into a real-time distributed system. The system consists of a personal computer as the human-machine interface, an industrial automation controller Compact FieldPoint, an electronic load KIKUSUI PLZ-4W and an autonomous photovoltaic installation including photovoltaic modules, storage units and a charge controller. The instrumentation subsystem includes sensors for electrical variables, temperatures and solar irradiance measurements.

The system's architecture has been referred to a complex interactive distributed class equipped with human-machine interface. The main operations to execute are the following:

- operator's commands processing;
- data acquisition;
- real-time simulation of electric energy consumer's behaviour;
- control of electronic load.

The organisation of the software's code and its communication interaction has been described using the event-driven Petri net concept. The tool stands as an extension of the ordinary Petri net [1] and is referred to as a mathematical modelling language for the description of discrete distributed systems [2]. The behaviour of the system is governed by

external and internal commands, so-called events.

The order of the main operations and their relationship is described as a 6-tuple graph $G = (P, T, A, E, R, \mu)$, where $P = \{p_i\}_{1 \leq i \leq N}$ is a finite set of positions, $T = \{t_i\}_{1 \leq i \leq M}$ is a finite set of transitions, $A : (P \times T) \cup (T \times P) \rightarrow \mathbb{N}^+$ is a multiset of arcs, $E = \{e_i\}_{1 \leq i \leq L}$ is a list of events, $R = \{r_i\}_{1 \leq i \leq K}$ is a list of priorities and $\mu : P \times E \rightarrow T$ is a multiset of functions specifying the logic of event executions.

The logic of the program code is characterized by a relation on the Petri net marking [3] $M + M' \triangleq P \rightarrow M(p) + M'(p) | p \in P$ and its execution is defined as the transition of the event logic function $M \xrightarrow{G} M' \triangleq \mu(p, e) \in \mu : M \xrightarrow{\mu(p, e)} M'$.

In order to avoid conflicts between code pages that are currently in run, the planar graph, so-called event graph, $G_e = (E, A_e)$ has been designed based on the desired properties of graph G , where every event $e \in E$ corresponds to the graph node. The nodes of graph G_e are adjacent if the events cannot be executed at the same time.

The solution of the event graph G_e colouring problem, formulated as $R : E \rightarrow \mathcal{R}(E)$, resulted in forming the priority hierarchy of event executions.

The utilization of the event-driven Petri net allowed conceptualising and implementing of a real-time algorithm for data acquisition, hardware control and user interaction.

References

- [1] Petru Eles Alej, Ro Corts and Zebo Peng. A petri net based model for heterogeneous embedded systems. In *Proceedings of NORCHIP Conference*, pages 248–255, 1999.
- [2] David Lee and Mihalis Yannakakis. Principles and methods of testing finite state machines - a survey. In *Proceedings of the IEEE*, pages 1090–1123, 1996.
- [3] T. Murata. Petri nets : Properties, analysis and applications. In *Proceedings of the IEEE*, volume 77, pages 541–580, 1989.

Biological Motion boosts the oculomotor response

Sebastien Coppe

CESAME and Lab. of Neurophysiology
Universite catholique de Louvain (UCL)
Av. G. Lemaitre 4, 1348 Louvain la Neuve
Belgium

Email: sebastien.coppe@uclouvain.be

Jean-Jacques Orban de Xivry

Biomedical Engineering Department
Johns Hopkins University
Rutland Ave 720, MD 21205 Baltimore
USA

Email: jean-jacques.orban@jhu.edu

Marcus Missal

Laboratory of Neurophysiology
Universite catholique de Louvain (UCL)
Av. Hippocrate 54, 1200 Bruxelles
Belgium

Email: marcus.missal@uclouvain.be

Philippe Lefevre

CESAME and Lab. of Neurophysiology
Universite catholique de Louvain (UCL)
Av. G. Lemaitre 4, 1348 Louvain la Neuve
Belgium

Email: philippe.lefevre@uclouvain.be

The ability to detect and perceive biologically relevant actions is particularly important for social skills [1]. Therefore, we hypothesized that the perception of biological motion could induce a different behavioral response compared with stimuli devoid of biological relevance. To check this hypothesis, we analyzed smooth eye movements during pursuit of a point-light walker, or its scrambled version.

Subjects ($n = 10$) were asked to pursue a point-light walker appearing on a tangent screen. The point-light walker was created using Cutting's algorithm [2] and consisted of a green hip dot and 10 red dots representing other body joints, like hands or feet for example. Subjects were asked to pursue the green dot representing the hip of the walker.

The scrambled control stimulus was obtained by shuffling the mean vertical position of the 10 red dots to disrupt the global form while keeping the same local motion. The green hip dot was the only dot which kept the same horizontal and vertical positions in both conditions. During a pursuit trial, the point-light walker or the control stimulus appeared and immediately started to move in a randomized heading direction for 800 ms, before disappearing behind an invisible occluder for 800 ms. After the occlusion, the stimulus reappeared and moved for an additional 800 ms period. The type of stimulus (biological motion or control), its direction of motion (leftward or rightward) and its velocity (5, 10 or 15 deg/s) were selected at random for each trial.

During smooth pursuit initiation, we found that the motor response was enhanced if the biological motion stimulus was pursued compared with the control condition. Indeed, smooth eye velocity was significantly higher during pursuit of the point-light walker 200 ms after pursuit onset ($p < 0.05$). During steady-state pursuit and during the occlusion period, the smooth pursuit response was similar for

the control and biological motion stimuli ($p > 0.05$). However, at the end of the occlusion period, a stronger smooth pursuit response to the biological motion stimulus was observed. The mean acceleration of smooth pursuit eye movements for the period from 50 to 200 ms after stimulus reappearance was significantly higher for biological motion than for the control stimulus ($p < 0.05$).

We also compared the biological motion stimulus with an upside-down walker, which is well known in the literature to completely disrupt the biological relevance of the stimulus [3]. We obtained the same kind of results with a significant advantage when tracking biological motion stimulus in comparison with the inverted walker. This was true as well as for the initiation part of the smooth pursuit and after the reappearance of the stimulus.

In summary, biological motion pursuit was stronger during movement initiation but not during steady-state and occlusion. Moreover, our results show that the biological relevance of the moving visual stimulus can enhance gradually the smooth pursuit response.

References

- [1] Blake R. and Shiffrar M. (2007) "Perception of Human Motion". *Annual Review of Psychology* 58, 47-73
- [2] Cutting J.E. (1978) "A program to generate synthetic walkers as dynamic point-light displays". *Behavior Research Methods Instruments* 10, 91-94.
- [3] Dittrich, W.H. (1993) "Action categories and the perception of biological motion". *Perception* 22, 15-22.

Controlling a moving camera setup for humanoid gaze emulation

R. Reilink[†], S. Stramigioli[‡] and F. van der Heijden[‡]

[†] IMPACT Institute, Faculty of EEMCS [‡] Signals and Systems Group, Faculty of EEMCS

University of Twente, PO Box 217, 7500 AE Enschede, The Netherlands

Email: {r.reilink,s.stramigioli,f.vanderheijden}@utwente.nl

1 Abstract

For humanoid robots, mimicking human behaviour is an important aspect to facilitate a natural interaction with humans. In order for a humanoid to be human-like, it needs head and eye movements that are similar to humans.

At the control engineering group at the University of Twente, a humanoid head-neck system has been developed [1],[2],[3]. The head is shown in figure 1, with the outer shell removed. It is a seven degree of freedom mechanical system, with two moving cameras mounted in the eye balls. The purpose of this ‘humanoid head’ is to research interaction between humanoid robots and humans in a natural way. In this work, we present the vision algorithm that determines the coordinates of the focus of attention target within the field of view. These coordinates are used to control the head and eye movements.

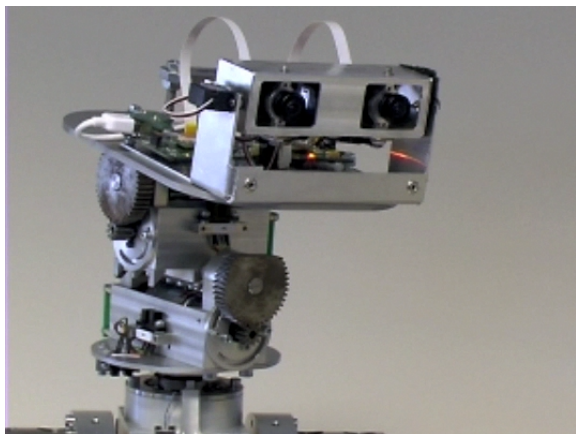


Figure 1: The Twente humanoid head

The algorithm is based on an algorithm developed by Itty et al.[4]. In the original work it was used to process static and computer generated images[5]. It has been extended to work in a system that has moving cameras.

The algorithm rates how ‘interesting’ each pixel of the input image is by determining the contrast between the foreground and background on different channels, such as color and intensity. Spatial frequency filtering is used to separate the foreground and background. This is done on multiple scales. The results are summed across the channels and across the scales, resulting in an image that is called the saliency map.

This map is used to determine where the system should look. To select this target location, it is taken into account that regions which have been looked at for a while, should be considered less interesting over time.

In order to use the saliency algorithm in a setup where the camera moves, the changing camera orientation must be accounted for. All data that originates from one frame and is used in another must be transformed according to this change.

The model of the system incorporates the pinhole projection and the lens distortion of the camera, as well as the change in orientation of the camera with respect to the world. This model was used to relate data from subsequent image frames.

The algorithm has been implemented on the humanoid head. The behaviour of the head is quite human like; people tend to associate its behaviour with human emotions and interact with the head like it were a human. Tests on a stimulus consisting of several salient dots show that the head succeeds in finding and attending the salient locations.

References

- [1] R. Reilink, S. Stramigioli, F van der Heijden and G. van Oort, "Saliency-based humanoid gaze emulation using a moving camera setup", *submitted IEEE Int. Conf. Robotics and Automation 2009*.
- [2] L.C. Visser, R. Carloni and S. Stramigioli, "Vision based motion control for a humanoid head", *submitted IEEE Int. Conf. Robotics and Automation 2009*.
- [3] D.M. Brouwer, J. Bennik, J. Leideman, H. M. J. R. Soemers and S. Stramigioli, "Mechatronic design of a fast and long range 4 degrees of freedom humanoid neck", *submitted IEEE Int. Conf. Robotics and Automation 2009*.
- [4] L. Itti, C. Koch and E. Niebur, "A Model of Saliency-Based Visual Attention for Rapid Scene Analysis", *IEEE Transactions on Pattern Analysis and Machine Intelligence*, vol 20, pp. 1254-1259, November 1998
- [5] L. Itti, N. Dhavale and F. Pighin, "Realistic Avatar Eye and Head Animation Using a Neurobiological Model of Visual Attention", *Proc. SPIE 48th Annual International Symposium on Optical Science and Technology*, B. Bosacchi, D. B. Fogel, and J. C. Bezdek, Eds., vol. 5200. Bellingham, WA: SPIE Press, Aug 2003, pp. 6478.

The visuomotor transformation of velocity signals for visually guided arm movements

Guillaume Leclercq

CESAME and Lab. Neurophysiology, Université catholique de Louvain

Avenue Georges Lemaitre 4, 1348 Louvain-la-Neuve, Belgium

Email: guillaume.leclercq@uclouvain.be

Gunnar Blohm

Centre for Neuroscience Studies, Queen's University

Stuart Street 18, Kingston, Ontario, K7L 3N6, Canada

Email: blohm@biomed.queensu.ca

Philippe Lefèvre

CESAME and Lab. Neurophysiology, Université catholique de Louvain

Avenue Georges Lemaitre 4, 1348 Louvain-la-Neuve, Belgium

Email: philippe.lefevre@uclouvain.be

Visually guided arm movements such as reaching or pointing to an object are common actions in our everyday life. Even if such movements seem easy to perform, they are the result of a complex sensorimotor transformation carried out in the brain. To achieve accurate visually-guided arm movements, humans combine feedforward information with visual and/or proprioceptive feedback about the movement. The feedforward part is especially important in the case of fast reaching movements because of the non negligible delay associated with sensory feedback. The feedforward part consists in transforming the retinal sensory input into an appropriate motor command for the arm (see [1]) before initiating the movement.

It has been shown that such a transformation accounts for the complete 3-dimensional (3D) eye-head-shoulder geometry in the case of reaching movements towards static targets [2]. It is well known that retinal position and velocity signals are processed by different neural pathways in the brain [3]. Therefore, velocity signals do not undergo the same visuomotor transformation in the brain. Here, we asked whether the visuomotor transformation of velocity signals also accounted for the 3D eye-head-shoulder linkage geometry in the arm movements framework.

To address this question, we designed a dual quaternion model describing the complete visuomotor transformation geometry for pointing, accounting for 3D eye-in-head and head-on-shoulder rotations and translations. The model predicted compensation for (1) head roll and resulting counter-roll eye movements and (2) for false ocular torsion generated by a misalignment between the retinal and spatial coordinates during oblique gaze positions.

We tested these predictions on human subjects that performed

manual tracking movements towards moving targets in darkness under different eye and head positions. To test prediction 1, subjects first had to roll their head towards one of their shoulders. Then, they pointed to the central target, which started moving 1s later towards either the left or right with an angular vertical component of -10, 0 or 10 degrees. Subjects had to track the moving target with their hand while maintaining fixation. Testing prediction 2 was similar, but now the head was maintained in an upright position and subjects instead fixated oblique targets while the same tracking task was carried out. We measured eye, hand and head movements and computed arm velocity during the open-loop period (first 100ms after movement onset). This initial movement direction was then compared to the model predictions.

Results showed that subjects compensated for both head roll and ocular counter-roll. A similar regression analysis revealed that for all but one subject, they accounted at least partially for false torsion. This suggests that for manual tracking movements, the brain makes use of 3D eye and head positions to achieve a visuomotor velocity transformation accounting for the complete eye-head-shoulder geometry.

References

- [1] Crawford JD, Medendorp WP and Marotta JJ, Spatial transformations for eye-hand coordination, *Journal of Neurophysiology*, 92, 10-19, 2004
- [2] Blohm G and Crawford JD, Computations for geometrically accurate visually guided reaching in 3-D space. *Journal of Vision*, 7(5) :4, 1-22, 2007
- [3] Krauzlis RJ, The control of voluntary eye movements : new perspectives. *Neuroscientist* 11,124-137, 2005

How To Obtain a 1 kHz Visual Servoing Setup?

Jeroen de Best, René van de Molengraft and Maarten Steinbuch

Department of Mechanical Engineering

Technische Universiteit Eindhoven

P.O. Box 513, 5600 MB Eindhoven

The Netherlands

Email: J.J.T.H.d.Best@tue.nl

Abstract

The research described here focusses on visual servoing [1] for production processes that take place on repetitive structures. The long term goal of the project is to create a setup capable of sampling with more than 1 kHz with a total time delay of less than 2 samples. It should track velocities up to 1 m/s with an accuracy in the order of 1-10 μm . As a starting point a black dot on a sheet of white paper is placed onto a two dimensional stage, where the goal is to control the black dot within the field of view at 1 kHz.

Ingredients

The setup as depicted in Fig. 1 consists of two stacked linear motors forming an xy-table. The input to the system is applied using an EtherCAT DAC module. A camera capable of reaching a frame rate of 200 Hz full frame (640 x 480), is mounted above the table. The data-acquisition is integrated in a Linux environment running a 2.6.24 real-time preemptive kernel [2]. The object of interest is a black dot on a sheet of white paper.

Pushing the limits

For achieving the goal mentioned earlier several important settings are discussed in this section. First of all, since a Gigabit Ethernet camera is used which supports jumbo frames, the maximum transfer unit of your network card should also support these jumbo frames. In that case you already re-

duce the network overhead. Furthermore, real-time priority is given to the used high resolution timers available in the preemptive kernel to decrease jitter. A region of interest (ROI) of 13 x 13 mm or equivalently of 80 x 80 pixels is used. By reading out less pixels a frame rate of 1 kHz is available. The exposure time can be set as low as 100 μs due to the use of power LEDs as illumination.

Results

The center of the black dot is detected by calculating the center of gravity and takes approximately 40 μs . The 3σ value of the measurement is 50 μm , which is still too large for the final goal. Furthermore, the position loop is closed only (!) on vision. The results of a frequency response function (FRF) measurement are given in Fig 2. Here the red line represents the measurement from input to camera coordinates. For comparison a FRF is measured from input to motor encoder, depicted in blue. Clearly different dynamics are measured in this case, caused by the place of the measurement, i.e. collocated, versus non-collocated control.

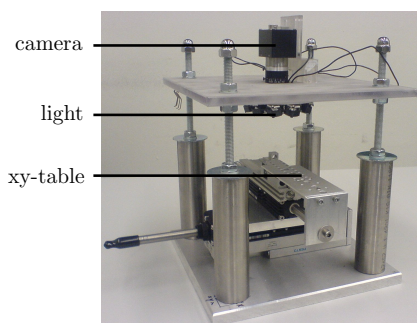


Figure 1: Visual servoing setup.

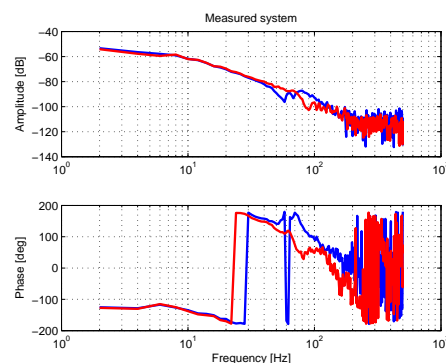


Figure 2: Measured FRFs.

References

- [1] S. Hutchinson, G.D. Hager and P.I. Corke, "A Tutorial on Visual Servo Control", Robotics and Automation, IEEE Trans., vol. 12(5), October 1996.
- [2] <http://rt.wiki.kernel.org/index.php/MainPage>, Real-Time Linux Wiki, 2008.

Active chatter control for high-speed milling using μ -synthesis

T.A.C. Verschuren, N.J.M. van Dijk, N. van de Wouw and H. Nijmeijer
 Department of Mechanical Engineering, Eindhoven University of Technology
 P.O. Box 513, 5600 MB Eindhoven, The Netherlands
 Email: t.a.c.verschuren@student.tue.nl

1 Introduction

In today's manufacturing industry, high-speed milling plays an important role. The main benefits of high-speed milling over conventional milling are the high material removal rates with relatively low cutting forces. The efficiency of high-speed milling is limited by the occurrence of regenerative chatter. Chatter is an undesired instability phenomenon, causing excessive tool vibrations, reduced product quality and rapid tool wear.

Several previous research efforts have targeted the problems of chatter control and chatter avoidance, either by modifying the spindle dynamics, e.g. [1], or by changing the process parameters (spindle speed and depth-of-cut), e.g. [2]. However, none of these efforts provide an *a priori* guarantee for chatter-free milling operation. In this work, robust control techniques are employed to systematically modify the spindle dynamics such that an *a priori* guarantee for chatter-free cutting for a predefined range of spindle speed and depth-of-cut is ensured.

2 Modelling the milling process

For the purpose of applying robust control using μ -synthesis techniques, a finite dimensional linear time-invariant (FDLTI) model of the milling process is needed. Typically, the milling process is modelled by means of a set of nonlinear delay-differential equations with time-varying coefficients. A linear time-invariant model is obtained by linearisation and averaging cutting forces over one revolution of the tool. This yields:

$$\mathbf{M}\ddot{\mathbf{v}}(t) + \mathbf{C}\dot{\mathbf{v}}(t) + \mathbf{K}\mathbf{v}(t) = a_p \bar{\mathbf{H}}[\mathbf{v}(t) - \mathbf{v}(t - \tau)], \quad (1)$$

where $\mathbf{v}(t)$ represents the tool displacements, a_p the depth-of-cut and τ the time delay which is inversely proportional to the spindle speed n . The matrices \mathbf{M} , \mathbf{C} and \mathbf{K} describe the mass-, damping- and stiffness matrix of the spindle dynamics and $\bar{\mathbf{H}}$ is a matrix containing the averaged cutting force coefficients. Furthermore, the presence of the time delay implies that the model is infinite dimensional. A finite dimensional milling model is obtained by means of a Padé approximation of the time delay. The order of the Padé approximation is chosen sufficiently large to give an accurate representation of the exact time delay τ .

3 Chatter control design using μ -synthesis

Robust control is employed using μ -synthesis techniques. Herein, two of the process parameters (spindle speed and depth-of-cut) are treated as uncertain parameters and are modelled as $a_p = \bar{a}_p(1 + r_1\Delta)$ and $n = \bar{n}(1 + r_2\Delta)$, where \bar{a}_p, \bar{n} are nominal values and r_1, r_2 define the size of the interval in which the process parameters may vary. Moreover, Δ is a scalar uncertain set satisfying $|\Delta| \leq 1$. In this way, using μ -synthesis via DK-iteration we aim to synthesize a controller which stabilises the milling process for every spindle speed and depth-of-cut in the uncertainty set for the depth-of-cut $[0, a_{p,max}]$ and the spindle speed $[n_{min}, n_{max}]$.

To illustrate the feasibility of the proposed method, stability lobes diagrams are calculated for a milling process with and without active chatter control. Stability lobes diagrams visualise the boundary between a stable cut (i.e. without chatter) and an unstable cut (i.e. with chatter) in terms of two process parameters: spindle speed and depth-of-cut. From Figure 1 it can be seen that the μ -controller has tailored the spindle dynamics such that chatter-free cutting is ensured for an *a priori* defined set of operating points (dashed box). Clearly, initially unstable operating points are stabilised by means of the active control strategy.

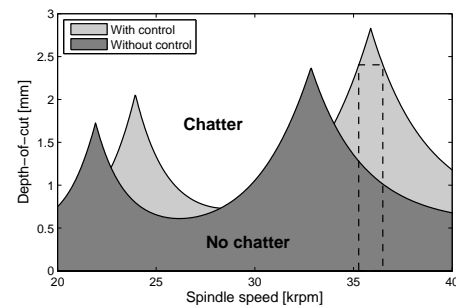


Figure 1: Stability limits with and without chatter control. The dashed box indicates the operating points to be stabilised.

References

- [1] J.L. Dohner, J.P. Lauffer et al. 'Mitigation of chatter instabilities in milling by active structural control', *Journal of Sound and Vibration*, 269(1):197-211, 2004.
- [2] Y.S. Tarng, Y.W. Hsieh and T.C. Li. 'Automatic selection of spindle speed for suppression of regenerative chatter', *Int. Journal of Advanced Manufacturing Technology*, 11(1):12-17, 1996.

A modular bearing with internal piezoshunt damping

Gregory Pinte¹, Steven Devos¹, Wim Symens¹, Bert Stallaert², Jan Swevers², Paul Sas²

¹Flanders' Mechatronics Technology Center

²Department of Mechanical Engineering, Division PMA, Katholieke Universiteit Leuven
Celestijnenlaan 300 B²/D¹, 3001 Heverlee, Belgium

Email: gregory.pinte@fmtc.be

1 Introduction

When a piezoelectric transducer is incorporated in a mechanical structure, it is possible to damp the structural vibrations of the base structure by passive energy dissipation in the electrical domain [1]. Due to the strong electromechanical coupling in piezoelectric elements, the mechanical energy can be efficiently converted to electrical energy. By shunting the piezoelectric element to a passive electric circuit, a part of the induced electrical energy can be dissipated. This principle is applied in a bearing to obtain noise and vibration reduction in rotating machinery. A ring-shaped module is developed with two perpendicular piezoelectric transducers, which can be mounted around a regular existing bearing. When the piezoelectric transducers are shunted to an appropriate electric impedance, damping will be introduced in the rotating machinery. Compared to an active solution, the increased robustness, the lower price and the ease of implementation are the main benefits of passive shunt damping.

2 Design of the piezoelectric bearing

The design of the piezoelectric bearing is shown in Figure 1. In horizontal as well as in vertical direction, a piezoelement is integrated in the bearing ring. The leaf springs and hinges allow a relative motion between the shaft and the frame while they fix the other degrees of freedom to protect the piezoelements. The piece has been produced with wire electrolytic discharge machining, such that fine details can be achieved in combination with a large thickness in the axial direction.

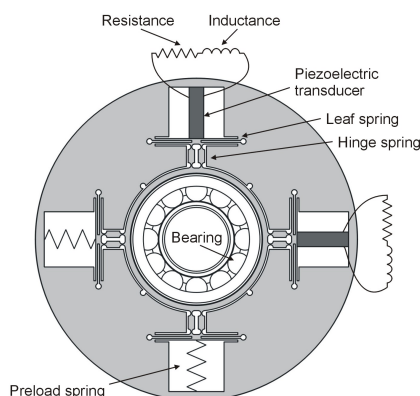


Figure 1: Design of the piezoelectric bearing

To test the potential of the developed piezoelectric module, an experimental set-up has been built (Figure 2). This set-up consists of a shaft, which is connected to a stiff frame by two bearings. The piezoelectric module is mounted around one of these bearings. Sound is radiated by a flexible panel mounted on the frame. The set-up is designed such that in the frequency range of interest, up to 1 kHz, many plate resonances, some frame resonances and the shaft resonance show up. Since this set-up efficiently radiates noise around the resonance frequency of the shaft, the objective is to select an electric impedance, which shunts the piezoelectric transducers, such that a maximal damping of the shaft resonance is obtained.

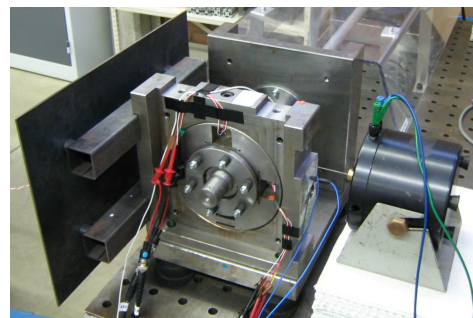


Figure 2: Test set-up

3 Shunt damping

To find the optimal shunted impedance, a mass-spring-damper model of the set-up is created, in which equivalent mechanical models are used for the piezoelectric transducers. Different types of shunt damping (resistive, inductive and inductive-resistive) have been compared in simulation and on the test set-up. The highest noise reduction (10 dB) could be obtained with an inductance (7 mH) and a resistance (20 Ohm) in series. These optimal impedance values depend on the (mechanical, electric and electromechanical) properties of the applied piezoelectric transducers as well as on the (mechanical) properties of the mechanical structure.

References

- [1] S.O.R. Moheimani. A Survey of Recent Innovations in Vibration Damping and Control Using Shunted Piezoelectric Transducers. *IEEE Transactions on Control Systems Technology*, Vol. 11, No. 4, 2003

Self-sensing actuation and damping of a Piezoelectric Tube Scanner

Stefan Kuiper

Delft Center for Systems and Control
Delft University of Technology
stefan.kuiper@tudelft.nl

Georg Schitter

Delft Center for Systems and Control
Delft University of Technology
g.schitter@tudelft.nl

1 Introduction

Atomic force microscopy (AFM) is an extensively used tool in nanotechnology for probing and imaging materials or biological features with nanometer resolution. In AFM the sample is probed with a very sharp tip measuring the interaction forces between the tip and the sample. The sample is hereby scanned simultaneously in a raster scan pattern by a piezo-driven scanning stage. One of the major drawbacks of AFM is its relatively low-imaging speed, making it impossible to capture dynamic processes on a molecular scale. Therefore, the goal of this research is to enhance the AFM imaging speed by use of modern control techniques.

2 Problem description

One of the major limitations on the AFM's imaging speed are the dynamics of the scanner stage. Undamped resonances of the scanner stage introduce oscillations when excited, which is a major source of image distortion [1]. Damping these resonances with traditional feedback control requires the use of additional position sensors to measure the tracking error. These position sensors are however expensive and limited in resolution. Therefore, in this research we are aiming to use the electromechanical coupling of the piezo-elements itself to measure and control the scanners oscillation. Using a piezo-element both as an actuator and sensor simultaneously can be done by connecting it within a capacitive bridge circuit as shown in figure 1 [2]. The oscillations of the scanner stage induce a charge within the piezo-element which can be measured as a voltage drop over the bridge circuit. The obtained measurement signal can be used for feedback control.

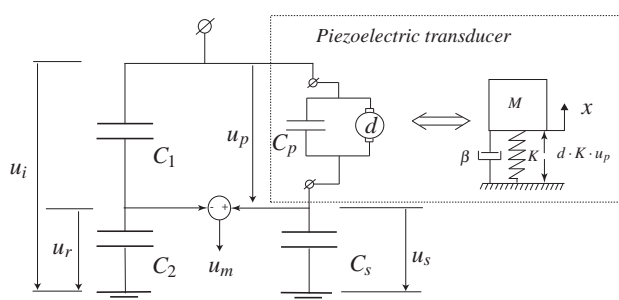


Figure 1: Schematic description of self-sensing piezo-actuation.

3 Results

The control method of figure 1 is implemented on an commercially available tube scanner (E-scanner, Veeco, Santa Barbara, CA). To compensate for circuit imbalance caused by component mismatch and hysteresis in the piezo-elements, an adaptive filter is used. The obtained measurement signal is used for feedback control of the scanners oscillations. Figure 2 shows the bode-diagram of the measured displacement of the controlled and uncontrolled tube scanner, showing a 18dB reduction of the resonance peak for the controlled case. AFM images are obtained showing a significant reduction in image distortion.

Due to the use of self-sensing actuation, implementation of this control method only requires some changes on the driving electronics of the AFM-setup. Because the use of external sensors is omitted, the scanner hardware is left unchanged, making this an effective and cost-efficient control method for increasing the imaging speed of AFM systems.

4 Acknowledgement

This work has been supported by faculty 3mE grant PAL614 and by the National Institutes of Health under Award RO1 GM 065354.

References

- [1] G. Schitter and A. Stemmer, *IEEE Trans. Control. Syst. Technol.*, vol. 12, pp 449-454, 2004.
- [2] J.J. Dosch, D.J. Inman and E. Garcia, *Journal of Intelligent Material Systems and Structures* vol. 3, p. 166, 1992.

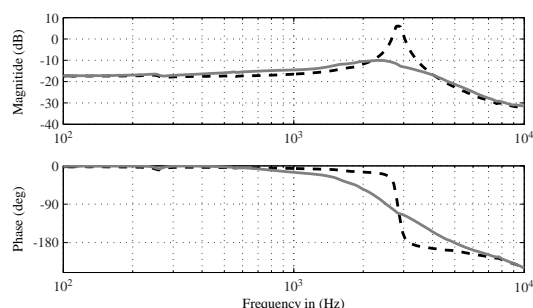


Figure 2: Bode-diagram of the measured tube scanner displacement, uncontrolled [dashed, black] and controlled [solid, grey].

Black box identification of a semi-active damper

Maarten Witters, Jan Swevers

Division PMA, Department of Mechanical Engineering,
Katholieke Universiteit Leuven, Celestijnenlaan 300B, B-3001 Heverlee, Belgium.
maarten.witters@mech.kuleuven.be

1. Introduction

This presentation discussed the identification of a continuously variable, semi-active damper for a passenger car using a black box model structure. The modeled damper is a telescopic, hydraulic damper equipped with a current controlled, electromagnetic servo-valve. A neural network based output error model structure ($NNOE$) is selected to describe the complex nonlinear damper dynamics. The identification procedure includes optimal experiment design, regression vector selection and model parameter estimation. The efficiency of the proposed procedure is demonstrated experimentally.

2. Experiment Design

Literature and insights in damper dynamics have shown that the current to the electromagnetic servo valve and the damper velocity are the two variables that mostly influence the damper response [3]. Hence, a two dimensional input space can be considered, which should be covered uniformly by the measurement data in order to be able to identify an accurate simulation model. For the excitations, periodic multisine signals are used.

The design of multisine excitation signals involves the selection of the frequency band of interest, the amplitude spectrum and the phases. The frequency band and the amplitude spectra are chosen such that the excitation approximates closely the load that the damper experiences in regular operational conditions [2]. The method to optimize the phases of the multisines is based on the *One Dimensional Homogenisation* procedure developed in [1]. This procedure chooses the phases such that the samples are spread uniformly over the achievable working range of the damper. A conventional random phase multisine excitation leads to a Gaussian distribution of the samples over the input space which is harmful for the model accuracy, as illustrated in the experimental validation.

3. Identification procedure

One of the most difficult aspects of black box modeling is the selection of the regressor variables: which variables and how many elements of each variable are necessary and sufficient to describe the systems dynamics. The authors developed an iterative identification procedure that automatically selects the regressors by alternately extending and pruning of the regression vector. For more details the interested reader is referred to [3].

4. Experimental validation

Table 1 evaluates the effectiveness of the proposed procedure by comparing the simulation accuracy of the model identified using an optimized data set ($NNOE_{OPH}$) to this of a model identified using a data set with random phase multisine excitation ($NNOE_{RPH}$), and this for validation data sets measured at 5 different excitation levels. The table clearly demonstrates that the $NNOE_{OPH}$ model is far more accurate than the $NNOE_{RPH}$ model.

	$M 1$	$M 2$	$M 3$	$M 4$	$M 5$
$NNOE_{OPH}$	9.4 %	6.0 %	5.1 %	6.9 %	7.3 %
$NNOE_{RPH}$	8.6 %	7.6 %	9.4 %	12.1 %	12.3 %

Table 1: Comparison of the simulation accuracy

Figure 1 illustrates the accuracy of the $NNOE_{OPH}$ model by comparing the simulated to the measured damper force for a medium level validation data set ($M 3$).

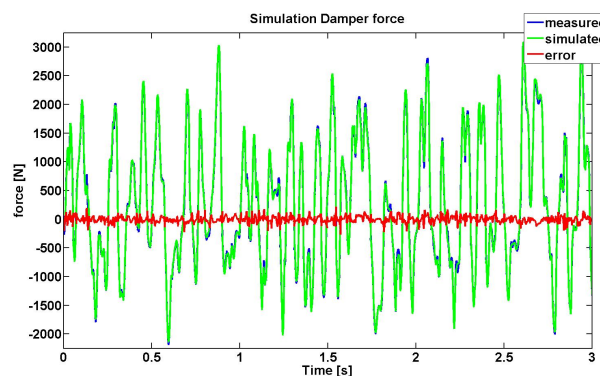


Figure 1: Simulated damper force

References

- [1] S.W.R Duym, J. Schoukens, Design of excitation signals for the restoring force surface method, *Mechanical Systems and Signal Processing*, vol. 9 (2), pp. 139-158, 1995.
- [2] J. Swevers, C. Lauwerys, B. Vandersmissen, M. Maes, K. Reybrouck, P. Sas, A model-free control structure for the on-line tuning of the semi-active suspension of a passenger car, *Mechanical Systems and Signal Processing*, vol. 21, pp. 1422-1436, 2007.
- [3] M. Witters, J. Swevers, Black-box identification of a continuously variable semi-active damper, *Proc. of the IEEE Multi-Conference on Systems and Control*, San Antonio, Texas, USA, pp. 19-24, 2008.

Stabilization & Vibration Control of Gaussmount Suspension System

C. Ding, A.A.H. Damen, and P.P.J. van den Bosch
Control Systems, Department of Electrical Engineering
Technische Universiteit Eindhoven
P.O. Box 513, 5600 MB Eindhoven, The Netherlands
Email: c.ding@tue.nl

1 Background

A suspension system is designed to inertially fix a payload, that is, to isolate it from floor vibration and simultaneously reject force disturbance exerted on the payload. When placed to work along the vertical direction, the suspension system has to compensate the payload gravity as well. Transmissibility is used to evaluate the vibration isolation performance. Current vibration isolation systems which are designed for a large payload (in scales of thousand kg), for example, the Airmount in the wafer scanner, achieve gravity compensation by means of pumping in high pressure air. However, the working bandwidth of this system is quite narrow. One possible reason is the high frequency dynamics of the high pressure air, which is very difficult to model and control accurately.

2 Gaussmount Suspension System

Gaussmount suspension system, shown in Figure 1, is a 6-DOF contactless electromagnetic suspension system. Three Gaussmount actuators are used to compensate payload gravity passively by permanent magnets and at the meanwhile to isolate the vibrations from the ground by active control. Each of the Gaussmount actuators is at least 2-DOF controllable which makes the system 6-DOF controllable. The force-current relation of a Gaussmount actuator can be described by differential equations with reasonably accuracy, which makes accurate modeling and control easier. However, due to the passive, permanent-magnet based, gravity compensation, the Gaussmount actuators are inherently unstable (proved by Earnshaw in 1842) and highly nonlinear.

3 Stabilization and Vibration Isolation

K. Nagaya and M. Ishikawa[1] built a contactless electromagnetic suspension system for a small mass. The gravity is compensated passively. The displacement with respect to an inertially fixed reference is fed back for vibration control and thus excellent transmissibility is achieved. Katsuhid Watanabe[2] built a contactless electromagnetic suspension table, which is able to lift 200 [kg] payload, incorporating four electromagnetic actuators. The feedback signal is a combination of relative position signal and acceleration signal, which is also the most possible choice for the Gauss-

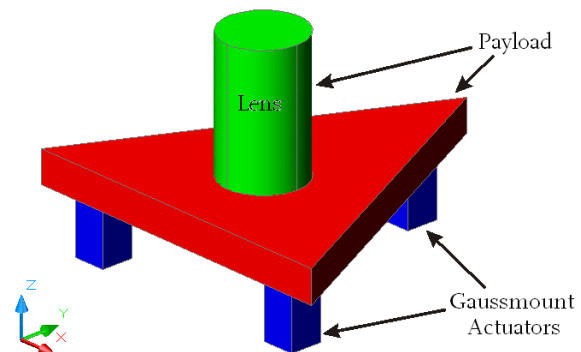


Figure 1: A Simplified View of Gaussmount Suspension System

mount suspension system because the absolute displacement signal is very difficult to obtain. Based on this choice of feedback signal, a control structure for Gaussmount suspension system is proposed.

Due to the instability and high nonlinearity of the Gaussmount actuator, the linear model derived by direct linearization has large perturbations, which may cause conflict between robust performance and stability. A simple linear parametric variable (LPV) approach is proposed and applied to a 1-DOF electromagnetic levitation system model. Simulation shows that the LPV controller stabilizes the system in a highly nonlinear range with robust performance. The application of this LPV approach on a Gaussmount actuator will be verified by simulation.

References

- [1] Kosuke Nagaya and Masashi Ishikawa, "A Noncontact Permanent Magnet Levitation Table with Electromagnetic Control and Its Vibration Isolation Method Using Direct Disturbance Cancellation Combining Optimal Regulators", IEEE Transactions on Magnetics, VOL. 31, NO. 1, January 1995.
- [2] Katsuhide WATANABE, Shinji HARA, Yoichi KANEMITSU, Takahide HAGA, Kenichi YANO, Takayuki MIZUNO, Ryuta KATAMURA, "Combination of H[∞] and PI Control for an Electromagnetically Levitated Vibration Isolation System", Proceedings of the 35th Conference on Decision and Control, Kobe, Japan, 1996.

Part 3

Plenary Lectures

*Binet-Cauchy Kernels for the Recognition of Visual
Dynamics*

René Vidal (Johns Hopkins University, USA)

Binet-Cauchy Kernels for the Recognition of Visual Dynamics

René Vidal
Center for Imaging Science
Institute for Computational Medicine
Johns Hopkins University

THE DEPARTMENT OF BIOMEDICAL ENGINEERING
The Whittaker Institute at Johns Hopkins

JHU vision lab

Modeling visual dynamical processes

- Dynamic textures: Soatto ICCV'01 • Human gaits: Bissacco CVPR'01

- Extract a set of features from the video sequence
 - Spatial filters
 - ICA/PCA
 - Wavelets
 - Intensities of all pixels
- Model spatiotemporal evolution of features as the output of a linear dynamical system (LDS): Soatto et al. '01

dynamics

$$x_{t+1} = Ax_t + Bv_t$$

images

$$y_t = Cx_t + w_t$$

appearance

Learning the model parameters

- Model is a LDS driven by IID white Gaussian noise

images

$$z(t+1) = Az(t) + v(t)$$

dynamics

appearance

$$I(t) = Cz(t) + w(t)$$
- Bilinear problem, can do EM
- Optimal solution: subspace identification (Overschee & de Moor '94)
- PCA-based solution in the absence of noise (Soatto et al. '01)
 - Can compute C and z(t) from the SVD of the images

$$[I(0) \ I(1) \ \dots \ I(F)] = C[z(0) \ z(1) \ \dots \ z(F)]$$

Given z(t) solving for A is a linear problem

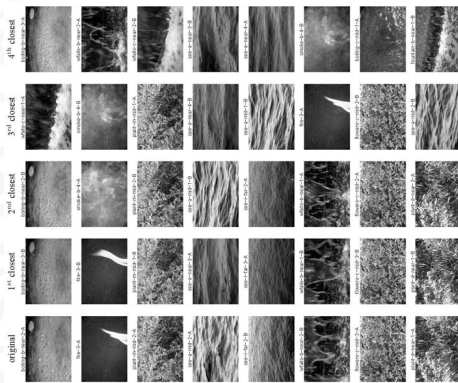
$$[z(1) \ z(2) \ \dots \ z(F)] = A[z(0) \ z(1) \ \dots \ z(F-1)]$$

Synthesizing novel sequences

- Once a model of a dynamic texture has been learned, one can use it to synthesize novel sequences:
 - Shold et al. '00, Soatto et al. '01, Doretto et al. '03, Yuan et al. '04

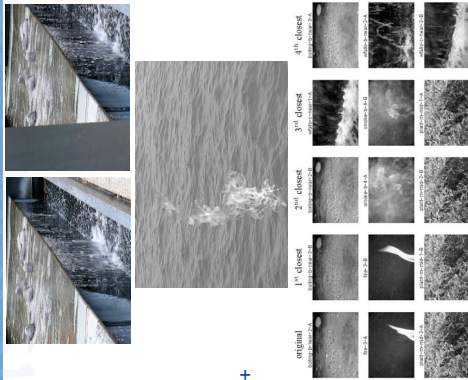
Classifying/recognizing novel sequences

- Given videos of several classes of dynamic textures, one can use their models to classify new sequences (Saisan et al. '01)
 - Identify dynamical models for all sequences in the training set
 - Identify a dynamical model for novel sequences
 - Assign novel sequences to the class of its nearest neighbor
- Requires one to compute a distance between dynamical models
 - Martin distance (Martin '00)
 - Subspace angles (De Cook '02)
 - Kulback-Leibler (Chan '07)
 - Binet-Cauchy kernels (Vishwanathan-Smolal-Vidal '07)



Talk outline

- Mosaicing (Ravichandran-Vidal '08)
 - How can we register two videos of a dynamic texture in space and time?
 - Can be reduced to image registration
- Segmentation (Choreyshi-Vidal '06)
 - How can we segment a scene containing multiple dynamic textures?
 - Variational method: dynamical models + texture descriptors + level sets
- Classification (Vishwanathan-Smolal-Vidal IJCV '07)
 - How can we recognize dynamic textures such as fire, water, etc?
 - Combine SVMs with Binet-Cauchy kernels on dynamical systems





JHU vision lab

Part I

Mosaicing Dynamic Textures

Center for Imaging Science
Institute for Computational Medicine
Johns Hopkins University



THE DEPARTMENT OF BIOMEDICAL ENGINEERING
The Whittaker Institute at Johns Hopkins



Problem statement

Given a *non-rigid dynamical* scene captured through *multiple static cameras*, we want to *register* the two sequences *spatially and temporally*

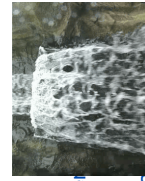


Challenges

- We are dealing with non-rigid dynamical scenes, where feature tracking and matching is very difficult.
- We are dealing with both spatial and temporal misalignment

Goal

- We would like to develop a spatial alignment technique that is invariant to the temporal alignment by reducing video registration to an image registration problem.



From image to video registration

- **Assumption:** the dynamics of the scene in the two views are the same
- The dynamic texture model can be interpreted as

$$I(\mathbf{x}, t) = \sum_{i=0}^n z_i(t) C_i(\mathbf{x}) \quad C_i(\mathbf{x}) \in \mathbb{R}^{r \times c}$$

- Video with transformed basis images

$$\tilde{I}(\mathbf{x}, t) = \sum_{i=0}^n \tilde{z}_i(t) C_i(T(\mathbf{x}))$$

$$\mathbf{z}(t) = \tilde{\mathbf{z}}(t)$$

$$\tilde{I}(x, t) = I(T(x), t).$$

Synchronized Case

$$\mathbf{z}(t - t_0) = \tilde{\mathbf{z}}(t)$$

$$\tilde{I}(x, t) = I(T(x), t - t_0).$$

Unsynchronized Case

$$\tilde{C}_i = C_i(T(\mathbf{x}))$$



Registering the video sequence is equivalent to registering n images.



Joint identification and canonical forms

- Separate identification: one dynamical model per video
 - Will produce *parameters in different basis*
 - Will not guarantee that the dynamics of the two video sequences are the same, i.e.

- Solution:

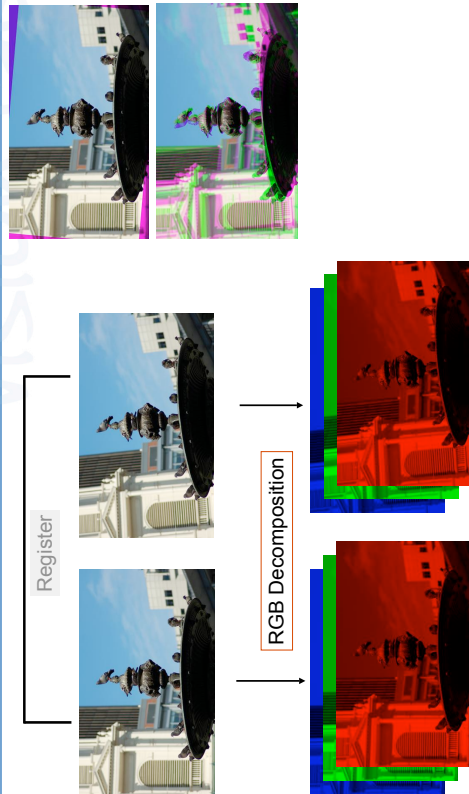
- Stacked Identification

- Jordan Canonical Form

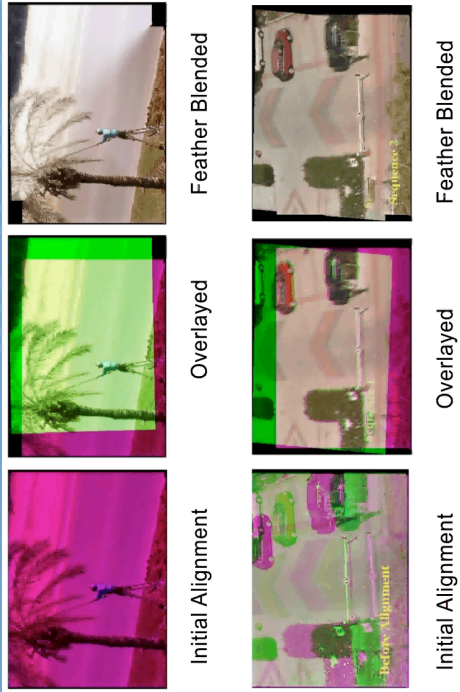
$$C_c = \begin{bmatrix} 1 & 0 & 1 & 0 & \dots & 1 & 1 \end{bmatrix} \quad A_c = \begin{bmatrix} \sigma_1 & \omega_1 & 0 & \dots & 0 & 0 \\ -\omega_1 & \sigma_1 & 0 & \dots & 0 & 0 \\ \vdots & \vdots & \ddots & \ddots & 0 & 0 \\ 0 & 0 & 0 & \lambda_{2p-n-1} & 0 & 0 \\ 0 & 0 & \dots & 0 & \lambda_{2p-n} & 0 \end{bmatrix}$$




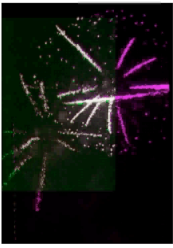
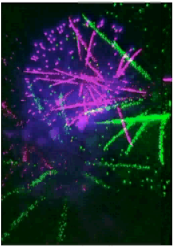
Results: format




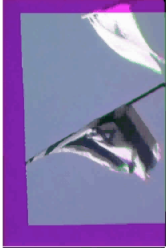
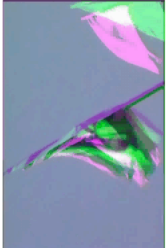
Results: rigid scenes




Results: non rigid scenes




Initial AlignmentOverlaidFeather Blended





Initial AlignmentOverlaidFeather Blended




Results: more sequences



Before AlignmentOverlaidFeather Blended




Initial AlignmentOverlaidFeather Blended



Adaptive selection of features

- **Mean vs. Dynamic Appearance**
 - Rigid sequences can be registered using the mean alone
 - Non-rigid sequences can be registered using dynamic appearance alone
 - Challenge : What to weight more?
Mean or Dynamic Appearance
- **Prior Work**
 - Register sequences using mean, dynamic appearance or both and pick the best
- **Our Work**
 - Automatically select the inliers from mean and dynamic appearance

Sequence	Dynamic
Palm	68.75
Parking	78.74
Light	84.66
Fountain	93.80
Fireworks	93.90
Flag	100.00
Wide	71.02
Multimodal	89.90



JHU vision lab

Part II

Segmenting Dynamic Textures

Center for Imaging Science
Institute for Computational Medicine
Johns Hopkins University





THE DEPARTMENT OF BIOMEDICAL ENGINEERING
The Whittaker Institute at Johns Hopkins

Level-set intensity-based segmentation

- Chan-Vese energy functional

$$E(C, c_1, c_2) = \mu|C| + \lambda_1 \int_{in(C)} (u(x, y) - c_1)^2 dx dy + \lambda_2 \int_{out(C)} (u(x, y) - c_2)^2 dx dy$$

- Implicit methods

- Represent C as the zero level set of an implicit function φ , i.e. $C = \{(x, y) : \varphi(x, y) = 0\}$



- Solution

- The solution to the gradient descent algorithm for φ is given by

$$\frac{\partial \varphi}{\partial t} = \delta(\varphi) \left(\mu \nabla \cdot \left(\frac{\nabla \varphi}{|\nabla \varphi|} \right) + \lambda_1 (u(x, y) - c_1)^2 - \lambda_2 (u(x, y) - c_2)^2 \right)$$

- c_1 and c_2 are the mean intensities inside and outside the contour C.



Dynamics & intensity-based energy

- We represent the intensities of the pixels in the images as the output of a mixture of AR models of order p

$$u(x, y, f) = a_0^j + \sum_{i=1}^p a_i^j u(x, y, f - i) + w(x, y, f)$$

- We propose an intensity spatial-temporal extension of the Chan-Vese energy functional

$$E = \mu|C| + \lambda_1 \int_{in(C)} \sum_{f=p+1}^F (u(x, y, f) - c_1(x, y, f))^2 dx dy + \lambda_2 \int_{out(C)} \sum_{f=p+1}^F (u(x, y, f) - c_2(x, y, f))^2 dx dy$$

where

$$c_j(x, y, f) = a_0^j + \sum_{i=1}^p a_i^j u(x, y, f - i) \quad j = 1, 2$$



Dynamics & intensity-based segmentation

- Given the AR parameters, we can solve for the implicit function φ by solving the PDE

$$\frac{\partial \varphi}{\partial t} = \delta(\varphi) \left(\mu \nabla \cdot \left(\frac{\nabla \varphi}{|\nabla \varphi|} \right) + \lambda_1 \sum_{f=p+1}^F (I(x, y, f) - c_1(x, y, f))^2 - \lambda_2 \sum_{f=p+1}^F (I(x, y, f) - c_2(x, y, f))^2 \right)$$

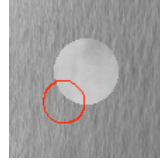
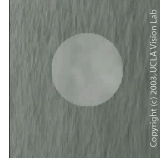
- Given the implicit function φ , we can solve for the AR parameters of the jth region by solving the linear system

$$\begin{bmatrix} 1 & \dots & \dots & 1 \\ u(x_1^j, y_1^j, f-1) & \dots & u(x_{k_j}^j, y_{k_j}^j, f-1) & u(x_1^j, y_1^j, f) \\ \vdots & \vdots & \vdots & \vdots \\ u(x_1^j, y_1^j, f-p) & \dots & u(x_{k_j}^j, y_{k_j}^j, f-p) & I(x_{k_j}^j, y_{k_j}^j, f) \end{bmatrix}^T \mathbf{a}^j = \begin{bmatrix} I(x_1^j, y_1^j, f) \\ \vdots \\ I(x_{k_j}^j, y_{k_j}^j, f) \end{bmatrix} \quad j = 1, 2$$

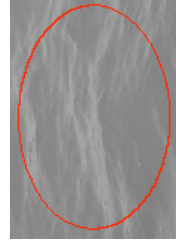


Experimental results

- Fixed boundary segmentation results and comparison



Ocean-smoke



Ocean-dynamics




Ocean-appearance




Experimental results

- Results on a real sequence

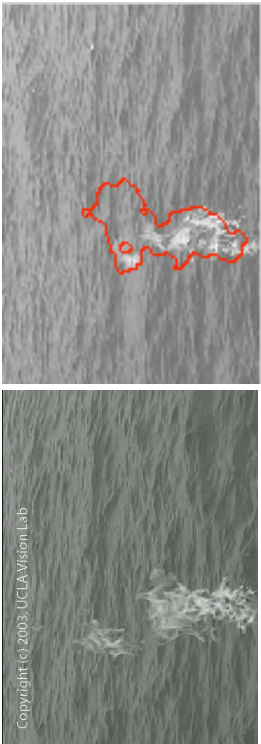


Raccoon on River




Experimental results

- Moving boundary segmentation results and comparison



Ocean-fire



JHU vision lab

Part III

Classification of Dynamic Textures

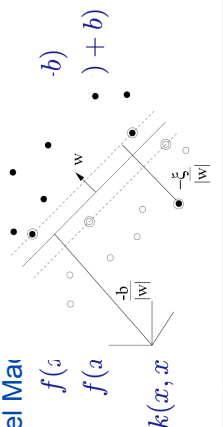
Center for Imaging Science
Institute for Computational Medicine
Johns Hopkins University





Data classification problem

- Given m observations $(x_i, y_i) \in \mathcal{X} \times \mathcal{Y}$, $\mathcal{X} \subset \mathbb{R}^D$, $\mathcal{Y} = \{-1, 1\}$ find a function $f: \mathcal{X} \rightarrow \mathcal{Y}$ that classifies observation $x \in \mathcal{X}$ into classes $+1$ and -1
- Linear classifiers (Support Vector Machines)
 - Use a classification function $f(x) = \text{sign}(\langle w, x \rangle + b)$
 - Optimal hyperplane is a linear combination of "support vectors" $w = \sum_i y_i \alpha_i x_i$
- Nonlinear classifiers (Kernel Machines)
 - Use a classification function $f(x)$
 - Optimal solution involves computing "dot products"
 - We only need a "kernel"



Can we apply kernel methods to LDS?

- Space of linear dynamical systems is non Euclidean

$$(A, B, C) \in \mathcal{M} \subset (\mathbb{R}^{n \times n}, \mathbb{R}^{n \times m}, \mathbb{R}^{p \times n})$$

$$\mathbf{x}_{t+1} = A\mathbf{x}_t + B\mathbf{v}_t$$

$$\mathbf{y}_t = C\mathbf{x}_t + \mathbf{w}_t$$

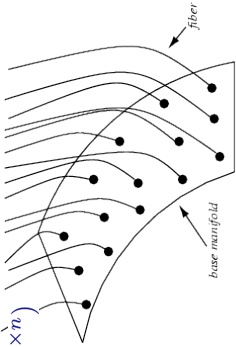
$$(A, B, C) \equiv (TAT^{-1}, TB, CT^{-1})$$

$$T \in SL(n)$$

- Need a "distance" or "kernel" for dynamical models

– Euclidean distance: does not respect the geometry of the manifold

$$d(\Sigma, \Sigma')^2 = \|A - A'\|^2 + \|B - B'\|^2 + \|C - C'\|^2$$



Existing metrics for dynamical models

- Metric based on subspace angles

– Output of noiseless AR model lies in observability subspace

$$\begin{bmatrix} y_0 & y_1 & y_2 & \dots \\ y_1 & y_2 & \dots & \dots \\ \vdots & \vdots & \ddots & \vdots \end{bmatrix} = \begin{bmatrix} C \\ CA \\ CA^2 \\ \vdots \end{bmatrix} \begin{bmatrix} x_0 & x_1 & x_2 & \dots \end{bmatrix}$$

– Metric based on principal angles between observability subspaces

$$\{\theta_i\}_{i=1}^n = \angle(\mathcal{O}, \mathcal{O}') \quad k(\Sigma, \Sigma') = \prod_{i=1}^n \cos^2(\theta_i)$$

– Several distances can be defined

$$\text{Finsler distance: } d_F(M_1, M_2) = \theta_{\max}$$

$$\text{Frobenius distance: } d_F(M_1, M_2)^2 = 2 \sum_{i=1}^{2n} \sin^2 \theta_i$$

$$\text{Martin distance: } d_M(M_1, M_2)^2 = -\ln \prod_{i=1}^{2n} \cos^2 \theta_i$$

– De Cock, D (4), 265-270, 2002



Existing metrics for dynamical models

- Euclidean metric on

– Discrete Fourier Transform: Agrawal et al. '93, Faloutsos et al. '94

– Discrete Wavelet Transform: Struzik and Sibes '99

– Principal Component Analysis: Gavrilov et al. '00

- Metric based on cepstrum coefficients (Martin metric)

– ARMA model can be expressed in terms of its transfer function

$$y_t = - \sum_{j=1}^n a_j y_{t-j} + \sum_{j=0}^m b_j v_{t-j} \iff H(z) = \frac{\sum_{j=0}^m b_j z^{-j}}{\sum_{j=0}^n a_j z^{-j}}$$

– Metric based on Euclidean distance on the cepstrum

$$\log[H(z)H^*(1/z)] = \sum_{n \in \mathbb{Z}} c_n z^{-n}$$

$$k(\Sigma, \Sigma') = \sum_{n=0}^{\infty} n c_n^* c_n'$$

– R. Martin, A metric for ARMA processes, IEEE Trans. Signal Processing, 48(4), 1164-1170, 2000



Existing metrics for dynamical models

- Metric based on the Kullback-Leibler (KL) divergence between the distributions of the output processes

– The output process is Gaussian

$$D(P_{Y_1} \| P_{Y_2}) : P_{Y_1^{1:\tau-1}} \sim \mathcal{N}(\Upsilon_1, \Phi_1) \text{ and } P_{Y_2^{1:\tau-1}} \sim \mathcal{N}(\Upsilon_2, \Phi_2);$$

– The KL divergence between two Gaussian processes can be approximated by

$$D(P_{Y_1^{1:\tau-1}} \| P_{Y_2^{1:\tau-1}}) = \frac{1}{2} \left[\log \frac{|\Phi_2|}{|\Phi_1|} + \text{trace}(\Phi_2^{-1} \Phi_1) + \|\Upsilon_1 - \Upsilon_2\|_{\Phi_2}^2 - m(\tau - 1) \right]$$

– This gives rise to the KL-kernel

$$d_{KL}(M_1, M_2) = \frac{1}{2} [D(P_{Y_1^{1:\tau-1}} \| P_{Y_2^{1:\tau-1}}) + D(P_{Y_2^{1:\tau-1}} \| P_{Y_1^{1:\tau-1}})]$$

$$k_{KL}(M_1, M_2) = e^{-\gamma(d_{KL}(M_1, M_2))}$$



– A. Chan and N. Vasconcelos, "Probabilistic kernels for the classification of autoregressive visual processes," IEEE Conference on Computer Vision and Pattern Recognition, 2005.

– T. Georgiou, "Distances between time-series and their autocorrelation statistics," LNCIS, 2007

Binet-Cauchy kernels on dynamical systems

- Propose a family of kernels on dynamical systems
 - Compute traces of compound matrices built from system trajectories
 - Use Binet-Cauchy theorem to verify properties of a kernel
- Binet-Cauchy kernels
 - Apply to multiple-input multiple-output systems
 - Depend explicitly on initial conditions
 - Can be computed in closed form for ARMA models
 - Include Martin kernel as a particular case, and can be extended to kernels on graphs (random walks, diffusion kernels, polygons, etc.)
- We present applications of our framework to
 - Clustering video shots
 - Classification of dynamic textures
 - Classification of human gaits



Binet-Cauchy theorem

Jacques Binet (1786-1856)



Augustin Cauchy (1789-1875)



Theorem 1 (Binet-Cauchy) Let $A \in \mathbb{R}^{l \times m}$ and $B \in \mathbb{R}^{l \times n}$. Then for all $q \leq \min\{m, n, l\}$

$$C_q(A^T B) = C_q(A)^T C_q(B)$$

- Particular cases
 - $q=1$ $A^T B = A^T B$
 - $q=m=n=l$ $\det(A^T B) = \det(A) \det(B)$



Compound matrices

- Let $A \in \mathbb{R}^{m \times n}$ and define the compound matrix of order $q \leq \min(m, n)$ as $C_q(A) \in \mathbb{R}^{\binom{m}{q} \times \binom{n}{q}}$

where $[C_q(A)]_{ij} = \det(A(i, j))$
 $i = (i_1, i_2, \dots, i_q)$
 $j = (j_1, j_2, \dots, j_q)$

- Particular cases
 - $q=1$ $C_1(A) = A$
 - $q=m=n$ $C_n(A) = \det(A)$



Binet-Cauchy kernels

- **Theorem:** The following is a well defined and positive-semidefinite kernel

$$k(A, B) = \text{trace}(C_q(A^T B))$$

- Particular cases
 - Trace kernels ($q=1$) $k(A, B) = \text{trace}(A^T B)$
 - Determinant kernel ($q=n$) $k(A, B) = \det(A^T B)$

- Computational complexity:

$$\text{trace}(C_q(A)) = \frac{1}{q} \sum_{j=1}^q (-1)^{j+1} \bar{C}_{q-j}(A) \bar{C}_j(A)$$

$$\bar{C}_q(A) = \sum_{j=1}^n \lambda_j^q, \quad \lambda_j = \text{eig}(A)$$



Extension to Fredholm operators

- Fredholm operator: bounded linear operator between two Hilbert spaces with closed range and finite-dimensional kernel and co-kernel

Theorem 1 Let $A : L_2(X) \rightarrow L_2(Y)$ be a Fredholm operator. There is a kernel $k_A : X \times Y \rightarrow \mathbb{R}$ such that for all $f \in L_2(X)$

$$[Af](y) = \int_X k_A(x, y) f(x) dx.$$

Theorem 2 Let $A : L_2(X) \rightarrow L_2(Y)$ and $B : L_2(Z) \rightarrow L_2(Y)$ be Fredholm operators on ordered sets X, Y, Z . Let $C_q(A)$ be the operator corresponding to $k_A^{[q]}(x, y) = \det(k_A(x_i, y_j)_{i,j=1}^q)$. Then for all $q \in \mathbb{N}$

$$C_q(A^T B) = C_q(A)^T C_q(B).$$

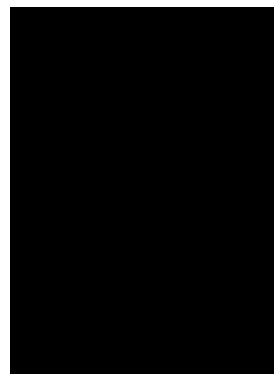


Clustering video clips

- Kill Bill: Vol 1 (2003)
- <http://www.imdb.com/title/tt0266697/>
- Randomly sample
 - 480 clips from the movie
 - 120 frames each
- Fit a linear dynamical model to each clip

$$x_{t+1} = Ax_t + v_t$$

$$y_t = Cx_t + w_t$$
- Use trace kernel to compute the k-nearest neighbors of each clip
- Use Locally Linear Embedding (LLE) for clustering the clips and embedding them in 2D space



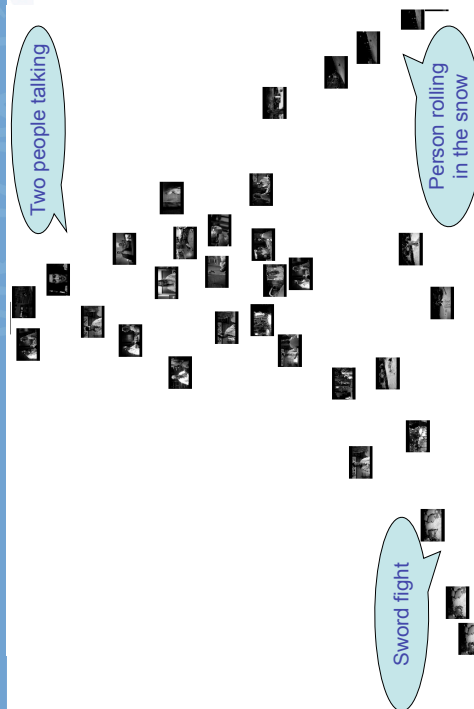
Kernels on ARMA models

- Consider two stable ARMA models
- Define an embedding
- The Binet-Cauchy kernel becomes
- Closed form expression for trace kernel

$$k((x_0, A, C), (x'_0, A', C')) = x_0^T M x'_0$$
 where M satisfies the equation

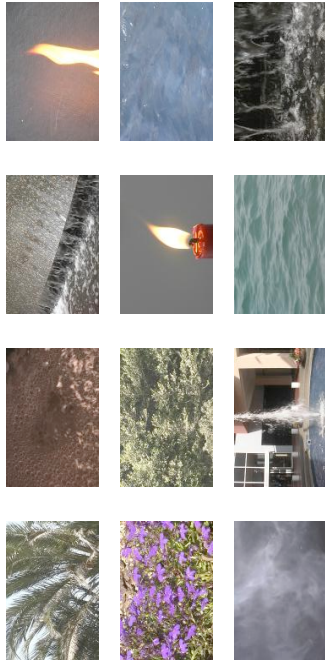


Clustering video clips



Results: dynamic texture recognition

- UCLA Dynamic Texture Database – Doretto et. al. IJCV'03
 - 50 classes including fire, smoke, steam, water, plants etc.
 - 4 sequences per class (75 frames, 160 x 110 pixels)
 - 200 sequences in total (dynamics extracted from 48 x 48 window)



Results: human gait recognition

- UCLA Database
 - 3 gaits: walking, running and climbing stairs
 - Sequences of joint angle trajectories
 - A total of 30 sequences with 10 for each gait type



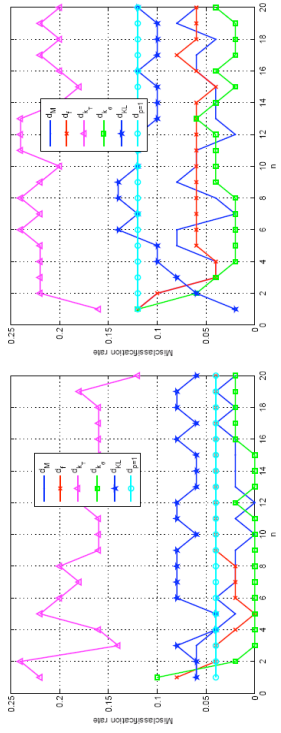
(a) UCLA - $n = 2$, 1-NN, leave one out classification

ID	Without mean			With mean		
	N4SID	PCA	EM	N4SID	PCA	EM
d_F	33	17	33	3	10	13
d_M	27	13	30	3	3	7
d_g	33	17	33	3	7	13
d_f	23	13	40	3	7	17
d_{k_M}	27	13	30	3	7	13
d_{k_T}	50	47	37	27	27	13
d_{k_s}	50	10	17	23	10	7
d_{k_d}	17	10	10	7	3	3
d_{k_e}	20	10	20	7	3	10
d_{k_L}	23	17	7	3	3	7
$d_{p=1}$				3	3	3

(b) UCLA - $n = 2$, SVM, 70% training, 30% testing

ID	Without mean			With mean		
	N4SID	PCA	EM	N4SID	PCA	EM
d_F	35 ± 3	22 ± 2	46 ± 3	4 ± 2	0 ± 0	16 ± 4
d_M	30 ± 6	16 ± 3	47 ± 6	3 ± 0	0 ± 0	18 ± 4
d_g	46 ± 5	29 ± 1	44 ± 3	3 ± 0	0 ± 0	17 ± 3
d_f	32 ± 4	18 ± 2	33 ± 6	0 ± 0	0 ± 0	12 ± 3
d_{k_M}	41 ± 7	21 ± 2	45 ± 2	3 ± 0	0 ± 0	17 ± 2
d_{k_T}	51 ± 5	32 ± 9	39 ± 4	12 ± 3	6 ± 4	8 ± 2
d_{k_s}	49 ± 4	17 ± 3	17 ± 2	15 ± 4	4 ± 1	3 ± 0
d_{k_d}	7 ± 0	4 ± 4	3 ± 0	0 ± 0	0 ± 0	3 ± 0
d_{k_e}	23 ± 2	4 ± 2	0 ± 0	7 ± 0	0 ± 0	4 ± 1
d_{k_L}	35 ± 6	15 ± 3	5 ± 2	0 ± 0	0 ± 0	4 ± 1
$d_{p=1}$				0 ± 0	0 ± 0	0 ± 0

Results: classification error vs system order



(c) SVM-RBF kernels, PCA-ID, with means

(d) 1-NN, PCA-ID, with means

Fig. 1. Misclassification rates for the dynamic textures database against system order



Results: human gait recognition

UCLA Database

(a) UCLA - $n = 2$, 1-NN, leave one out classification

ID	Without mean			With mean		
	N4SID	PCA	EM	N4SID	PCA	EM
d_F	33	17	33	3	10	13
d_M	27	13	30	3	3	7
d_g	33	17	33	3	7	13
d_f	23	13	40	3	7	17
d_{k_M}	27	13	30	3	7	13
d_{k_T}	50	47	37	27	27	13
d_{k_s}	50	10	17	23	10	7
d_{k_d}	17	10	10	7	3	3
d_{k_e}	20	10	20	7	3	10
d_{k_L}	23	17	7	3	3	7
$d_{p=1}$				3	3	3

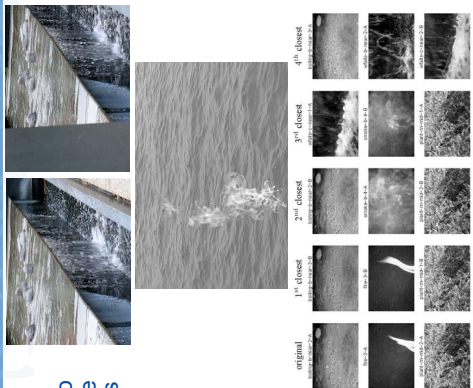
(b) UCLA - $n = 2$, SVM, 70% training, 30% testing

ID	Without mean			With mean		
	N4SID	PCA	EM	N4SID	PCA	EM
d_F	35 ± 3	22 ± 2	46 ± 3	4 ± 2	0 ± 0	16 ± 4
d_M	30 ± 6	16 ± 3	47 ± 6	3 ± 0	0 ± 0	18 ± 4
d_g	46 ± 5	29 ± 1	44 ± 3	3 ± 0	0 ± 0	17 ± 3
d_f	32 ± 4	18 ± 2	33 ± 6	0 ± 0	0 ± 0	12 ± 3
d_{k_M}	41 ± 7	21 ± 2	45 ± 2	3 ± 0	0 ± 0	17 ± 2
d_{k_T}	51 ± 5	32 ± 9	39 ± 4	12 ± 3	6 ± 4	8 ± 2
d_{k_s}	49 ± 4	17 ± 3	17 ± 2	15 ± 4	4 ± 1	3 ± 0
d_{k_d}	7 ± 0	4 ± 4	3 ± 0	0 ± 0	0 ± 0	3 ± 0
d_{k_e}	23 ± 2	4 ± 2	0 ± 0	7 ± 0	0 ± 0	4 ± 1
d_{k_L}	35 ± 6	15 ± 3	5 ± 2	0 ± 0	0 ± 0	4 ± 1
$d_{p=1}$				0 ± 0	0 ± 0	0 ± 0



Summary

- **Mosaicing**
 - Spatial-temporal registration of two videos of a dynamic texture can be reduced to registration of n images
- **Segmentation**
 - Segmentation of multiple dynamic textures can be done using level sets and dynamical models
- **Recognition**
 - Recognition of dynamic textures can be done using SVMs with Binet-Cauchy kernels on dynamic systems



Ongoing directions

- **Extending boosting to dynamical systems?**
 - DynamicBoost (Vidal-Favaro ICCV'07)
- **Making Binet-Cauchy kernels invariant to changes in**
 - Viewpoint
 - Scale
 - Illumination
- **Recognizing videos with multiple dynamic textures**
 - Metrics on hybrid systems (Petreczky-Vidal HSCC'07)



Thank You!

- **NSF CNS-0809101**
- **NSF ISS-0447739**
- **ARL Robotics-CTA**
- **ONR N00014-05-10836**
- **NSF CNS-0509101**
- **JHU APL-934652**
- **NIH RO1 HL082729**
- **WSE-APL**
- **NIH-NHLBI**

<http://www.vision.jhu.edu>



Distributed control of Robotic Networks (Part 1)

Jorge Cortés and Sonia Martínez (University of California at
San Diego, USA)

Distributed robotic networks: models, tasks, and complexity

Jorge Cortés and Sonia Martínez



Mechanical and Aerospace Engineering
University of California, San Diego
{cortes,soniamd}@ucsd.edu

28th Benelux Meeting on Systems and Control
Spa, Belgium, March 17, 2009

Acknowledgments: Francesco Bullo
Emilio Frazzoli

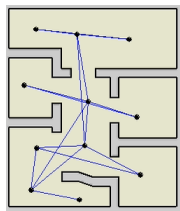
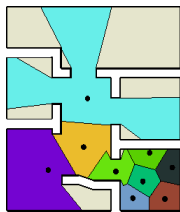
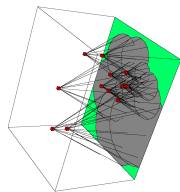
Cooperative multi-agent systems

What kind of systems?

Groups of agents with control, sensing, communication and computing

Each individual

- **senses** its immediate environment
- **communicates** with others
- **processes** information gathered
- **takes local action** in response



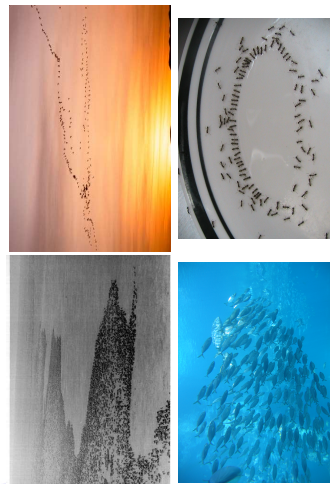
Cortés & Martínez (UCSD)

Distributed robotic networks

March 17, 2009

2 / 65

Self-organized behaviors in biological groups



Decision making in animals

Able to

- deploy over a given region
- assume specified pattern
- rendezvous at a common point
- jointly initiate motion/change direction in a synchronized way



Species achieve synchronized behavior

- with limited sensing/communication between individuals
- without apparently following group leader

(Couzin et al, Nature 05; Conradt et al, Nature 03)

Cortés & Martínez (UCSD)

Distributed robotic networks

March 17, 2009

3 / 65

Cortés & Martínez (UCSD)

Distributed robotic networks

March 17, 2009

4 / 65

Engineered multi-agent systems

Embedded robotic systems and sensor networks for

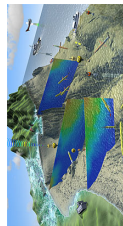
- high-stress, rapid deployment — e.g., disaster recovery networks
- distributed environmental monitoring — e.g., portable chemical and biological sensor arrays detecting toxic pollutants
- autonomous sampling for biological applications — e.g., monitoring of species in risk, validation of climate and oceanographic models
- science imaging — e.g., multispacecraft distributed interferometers flying in formation to enable imaging at microarcsecond resolution



Sandia National Labs



UCSD Scripps



MBARI AOSN



NASA

Cortés & Martínez (UCSD)

Distributed robotic networks

March 17, 2009

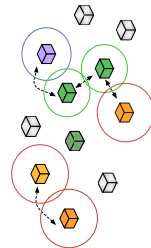
5 / 65

Research program: what are we after?

Design of provably correct coordination algorithms for basic tasks

Formal model to rigorously formalize, analyze, and compare coordination algorithms

Mathematical tools to study convergence, stability, and robustness of coordination algorithms



Coordination tasks

exploration, map building, search and rescue, surveillance, odor localization, monitoring, distributed sensing

Cortés & Martínez (UCSD)

Distributed robotic networks

March 17, 2009

7 / 65

Research challenges

What useful engineering tasks can be performed with limited-sensing/communication agents?

Feedback

rather than open-loop computation for known/static setup who knows what, when, why, how, dynamically changing

Information flow

Reliability/performance robust, efficient, predictable behavior

How to coordinate individual agents into coherent whole?

Objective: *systematic methodologies to design and analyze cooperative strategies to control multi-agent systems*

Integration of control, communication, sensing, computing

Cortés & Martínez (UCSD)

Distributed robotic networks

March 17, 2009

6 / 65

Technical approach

Optimization Methods

- resource allocation
- geometric optimization
- load balancing

Geometry & Analysis

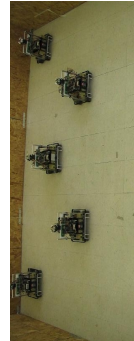
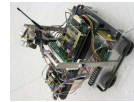
- computational structures
- differential geometry
- nonsmooth analysis

Control & Robotics

- algorithm design
- cooperative control
- stability theory

Distributed Algorithms

- adhoc networks
- decentralized vs centralized
- emerging behaviors



Cortés & Martínez (UCSD)

Distributed robotic networks

March 17, 2009

8 / 65

Outline

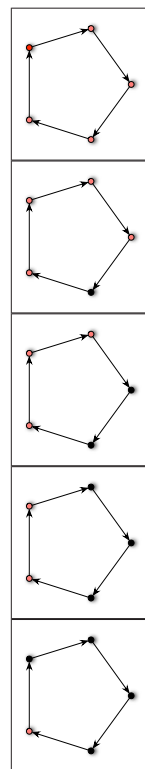
- 1 Synchronous networks
 - A motivating problem: leader election
 - Distributed algorithms
 - Complexity notions
- 2 Robotic networks
 - A motivating problem: direction agreement and equidistance
 - Proximity graphs
 - Control and communication laws
 - Coordination tasks and complexity notions
- 3 Complexity analysis of agree and pursue law
- 4 Conclusions

Cortés & Martínez (UCSD) Distributed robotic networks March 17, 2009 9 / 65

The Le Lann-Chang-Roberts (LCR) algorithm

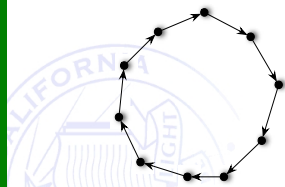
To solve the leader election problem, each agent

- sets max UID received so far to its own UID
- initially transmits its UID to neighbors
- at each **communication round**: listens to messages from other agents, and compares the received UIDs with its UID
 - ④ if max UID received is larger than own UID, declares itself a non-leader, resets max UID, and transmits it in the next communication round
 - ⑤ if max UID received is smaller than own UID, does nothing
 - ⑥ if max UID is equal to own UID, declares itself a leader



Cortés & Martínez (UCSD) Distributed robotic networks March 17, 2009 11 / 65

Leader election on a ring of processors



Network size is unknown to agents

Problem (Leader election)

Assume all processors have a state variable, say **leader**, initially set to **unknown**

A leader is elected when one and only one processor has the state variable set to **true** and all others have it set to **false**

Objective: elect a leader

Cortés & Martínez (UCSD) Distributed robotic networks March 17, 2009 10 / 65

The LCR algorithm – cont

The LCR algorithm solves the leader election problem on a ring digraph

- only agent with largest UID declares itself a leader
- all other agents declare themselves as non-leaders

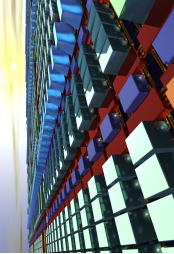
Ways to improve the algorithm?

- so that remaining agents know identity of leader at the end?
- so that leader election problem is solved differently/faster?
- so that fewer messages are transmitted?

If somebody comes up with a different algorithm, how can we tell which algorithm is better?

Cortés & Martínez (UCSD) Distributed robotic networks March 17, 2009 12 / 65

Synchronous networks



Distributed algorithms and **parallel computing** study algorithms that can be implemented in static networks of parallel processors

Synchronous network is group of processors with ability to exchange messages and perform local computations. Mathematically, a digraph (I, \mathcal{E}) ,

- 1 $I = \{1, \dots, n\}$ is the set of *unique identifiers* (*UIDs*), and
- 2 \mathcal{E} is a set of directed edges over the vertices $\{1, \dots, n\}$, called the communication links

Cortés & Martínez (UCSD) Distributed robotic networks March 17, 2009 13 / 65

Distributed algorithms

Distributed algorithm \mathcal{DA} for a network \mathcal{S} consists of the sets

- 1 L , a set containing the null element, called the *communication alphabet*; elements of L are called *messages*;
- 2 $W^{[i]}$, $i \in I$, called the *processor state sets*;
- 3 $W_0^{[i]} \subseteq W^{[i]}$, $i \in I$, sets of *allowable initial values*;

and of the maps

- 4 $\text{msg}^{[i]} : W^{[i]} \times I \rightarrow L$, $i \in I$, called *message-generation functions*;
- 5 $\text{stf}^{[i]} : W^{[i]} \times L^n \rightarrow W^{[i]}$, $i \in I$, called *state-transition functions*.

If $W^{[i]} = W$, $\text{msg}^{[i]} = \text{msg}$, and $\text{stf}^{[i]} = \text{stf}$ for all $i \in I$, then \mathcal{DA} is said to be *uniform* and is described by a tuple $(L, W, \{W_0^{[i]}\}_{i \in I}, \text{msg}, \text{stf})$

Cortés & Martínez (UCSD) Distributed robotic networks March 17, 2009 15 / 65

Outline

- 1 **Synchronous networks**
 - A motivating problem: leader election
 - **Distributed algorithms**
 - Complexity notions
- 2 **Robotic networks**
 - A motivating problem: direction agreement and equidistance
 - Proximity graphs
 - Control and communication laws
 - Coordination tasks and complexity notions
- 3 **Complexity analysis of agree and pursue law**
- 4 **Conclusions**

Cortés & Martínez (UCSD) Distributed robotic networks March 17, 2009 14 / 65

The LCR algorithm – formally

Network: Ring network
Alphabet: $L = I \cup \{\text{null}\}$
Processor State: $w = (u, \text{max-uid}, \text{leader}, \text{transmit})$, where

u	$\in I$,	initially:	$u^{[i]} = i$ for all i
max-uid	$\in I$,	initially:	$\text{max-uid}^{[i]} = i$ for all i
leader	$\in \{\text{true}, \text{unknown}\}$,	initially:	$\text{leader}^{[i]} = \text{unknown}$ for all i
transmit	$\in \{\text{true}, \text{false}\}$,	initially:	$\text{transmit}^{[i]} = \text{true}$ for all i

function $\text{msg}(w, i)$

- 1: **if** $\text{transmit} = \text{true}$ **then**
- 2: **return** max-uid
- 3: **else**
- 4: **return** null

Cortés & Martínez (UCSD) Distributed robotic networks March 17, 2009 16 / 65

The LCR algorithm – formally

```

function stif( $w, y$ )
1: if ( $y$  contains only null messages) OR (largest identifier in  $y < u$ ) then
2:   new-uid := max-uid
3:   new-leader := leader
4:   new-transmit := false
5: if (largest identifier in  $y = u$ ) then
6:   new-uid := max-uid
7:   new-leader := true
8:   new-transmit := false
9: if (largest identifier in  $y > u$ ) then
10:   new-uid := largest identifier in  $y$ 
11:   new-leader := false
12:   new-transmit := true
13: return ( $u$ , new-uid, new-leader, new-transmit)

```

Cortés & Martínez (UCSD) Distributed robotic networks March 17, 2009 17 / 65

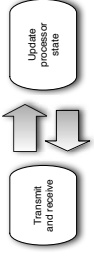
Outline

- 1 Synchronous networks
 - A motivating problem: leader election
 - Distributed algorithms
 - Complexity notions
- 2 Robotic networks
 - A motivating problem: direction agreement and equidistance
 - Proximity graphs
 - Control and communication laws
 - Coordination tasks and complexity notions
- 3 Complexity analysis of agree and pursue law
- 4 Conclusions

Cortés & Martínez (UCSD) Distributed robotic networks March 17, 2009 19 / 65

Network evolution

Execution: discrete-time communication and computation



Formally, evolution of $(\mathcal{S}, \mathcal{DA})$ from initial conditions $w_0^{[i]} \in W_0^{[i]}$, $i \in I$, is the collection of trajectories $w^{[i]}: \mathbb{T} \rightarrow W^{[i]}$, $i \in I$, satisfying

$$w^{[i]}(\ell) = \text{stf}^{[i]}(w^{[i]}(\ell-1), y^{[i]}(\ell))$$

where $w^{[i]}(-1) = w_0^{[i]}$, $i \in I$, and where the trajectory $y^{[i]}: \mathbb{T} \rightarrow L^n$ (describing the messages received by processor i) has components $y_j^{[i]}(\ell)$, for $j \in I$, given by

$$y_j^{[i]}(\ell) = \begin{cases} \text{msg}^{[j]}(w^{[j]}(\ell-1), i), & \text{if } (j, i) \in \mathcal{E}, \\ \text{null}, & \text{otherwise.} \end{cases}$$

Cortés & Martínez (UCSD) Distributed robotic networks March 17, 2009 18 / 65

Characterizing performance: complexity notions

How good is a distributed algorithm? How costly to execute?

Complexity notions characterize performance of distributed algorithms

Algorithm completion: an algorithm *terminates* when only null messages are transmitted and all processors states become constants

Time complexity: $\text{TC}(\mathcal{DA}, \mathcal{S})$ is maximum number of rounds required by execution of \mathcal{DA} on \mathcal{S} among all allowable initial states

Space complexity: $\text{SC}(\mathcal{DA}, \mathcal{S})$ is maximum number of basic memory units required by a processor executing \mathcal{DA} on \mathcal{S} among all processors and all allowable initial states

Communication complexity: $\mathcal{CC}(\mathcal{DA}, \mathcal{S})$ is maximum number of basic messages transmitted over the entire network during execution of \mathcal{DA} among all allowable initial states

until termination (basic memory unit, message contains $\log(n)$ bits)

Cortés & Martínez (UCSD) Distributed robotic networks March 17, 2009 20 / 65

Quantifying complexity

Asymptotic “order of magnitude” measures. E.g., algorithm has **time complexity of order**

- 1 $O(f(n))$ if, for all n , for all networks of order n and for all initial processor values, TC is lower than a constant factor times $f(n)$
- 2 $\Omega(f(n))$ if, for all n , \exists network of order n and initial processor values such that TC is greater than a constant factor times $f(n)$
- 3 $\Theta(f(n))$ if TC is of order $\Omega(f(n))$ and $O(f(n))$ at the same time

Similar conventions for space and communication complexity

Numerous variations of complexity definitions are possible

- 1 “Global” rather than “existential” lower bounds
- 2 Expected or average complexity notions
- 3 Complexity notions for problems, rather than for algorithms

Cortés & Martínez (UCSD) Distributed robotic networks March 17, 2009 21 / 65

Beyond leader election

Plethora of problems within distributed algorithms and parallel processing

- Distributed breadth-first and depth-first tree construction, flooding, consensus, linear algebra, optimization
- Asynchronism, processor failures, communication failures

For **robust networks**, spatial dimension introduces new problems

- mobility means changing interaction topology
- physical variables live in continuous spaces
- in addition to processing and communication, need to take control and sensing into account
- task and complexity notions have different meanings

Cortés & Martínez (UCSD) Distributed robotic networks March 17, 2009 23 / 65

Leader election by comparison

Le Lann-Chang-Roberts (LCR) algorithm **solves** leader election on a ring with **complexities**

- 1 time complexity is n
it takes n communication rounds for UID “ n ” to travel back to agent n
- 2 space complexity is 4
u, max-width, leader, transmit
- 3 communication complexity is $\Theta(n^2)$
Upper bound is *straightforward*. Initial condition that gives rise to lower bound?

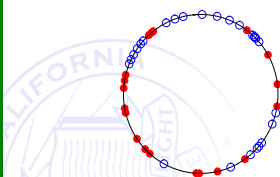
Cortés & Martínez (UCSD) Distributed robotic networks March 17, 2009 22 / 65

Outline

- 1 Synchronous networks
 - A motivating problem: leader election
 - Distributed algorithms
 - Complexity notions
- 2 Robotic networks
 - A motivating problem: direction agreement and equidistance
 - Proximity graphs
 - Control and communication laws
 - Coordination tasks and complexity notions
- 3 Complexity analysis of agree and pursue law
- 4 Conclusions

Cortés & Martínez (UCSD) Distributed robotic networks March 17, 2009 24 / 65

Direction agreement and equidistance



Network size is unknown to agents

Problem (Direction agreement & equidistance)

Assume agents move in circle according to first-order integrator dynamics. Some move clockwise, others counterclockwise

Agents talk to other agents within distance r

Objective: *agree on a common direction of motion and uniformly deploy over circle*

Cortés & Martínez (UCSD) Distributed robotic networks March 17, 2009 25 / 65

The agree-and-pursue algorithm – cont

The agree-and-pursue algorithm solves the direction agreement and equidistance problem on a circle

- all agents agree on a common direction of motion – either clockwise or counterclockwise
- network asymptotically achieves uniform, equally-spaced rotating configuration

New issues arise when considering **robotic networks**

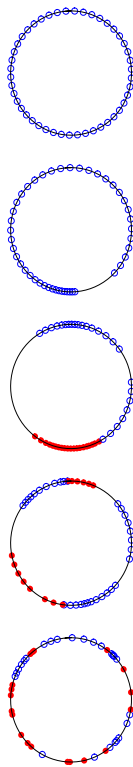
- As agents move, interconnection topology changes (e.g., network might be disconnected, and then leader election would not work)
- Tasks might not be achieved exactly, but asymptotically (e.g., equidistance)
- Need to **rethink model** and notions of **complexity** to account for **spatial component**

Cortés & Martínez (UCSD) Distributed robotic networks March 17, 2009 27 / 65

The agree-and-pursue algorithm

To solve the direction agreement and equidistance problem, each agent

- sets max UID received so far to its own UID
- initially transmits its direction of motion and UID to neighbors
- at each **communication round**: listens to messages from other agents and compares the received UIDs from agents moving toward its position with its own UID. If max UID is larger than own UID, resets UID and direction of motion
- between **communication rounds**: moves $k_{\text{prop}} \in (0, 1/2)$ times the distance to the immediately next neighbor in chosen direction, or, if no neighbors, k_{prop} times communication range r



Cortés & Martínez (UCSD) Distributed robotic networks March 17, 2009 26 / 65

Outline

- 1 Synchronous networks
 - A motivating problem: leader election
 - Distributed algorithms
 - Complexity notions
- 2 Robotic networks
 - A motivating problem: direction agreement and equidistance
 - Proximity graphs
 - Control and communication laws
 - Coordination tasks and complexity notions
- 3 Complexity analysis of agree and pursue law
- 4 Conclusions

Cortés & Martínez (UCSD) Distributed robotic networks March 17, 2009 28 / 65

Proximity graphs model interconnection topology

Proximity graph

graph whose vertex set is a set of distinct points and whose edge set is a function of the relative locations of the point set

Appear in computational geometry and topology control of wireless networks

Definition (Proximity graph)

Let X be a d -dimensional space chosen among \mathbb{R}^d , \mathbb{S}^d , and $\mathbb{R}^{d_1} \times \mathbb{S}^{d_2}$, with $d_1 + d_2 = d$. Let $\mathbb{G}(X)$ be the set of all undirected graphs whose vertex set is an element of $\mathbb{F}(X)$ (finite subsets of X)

A *proximity graph* $\mathcal{G}: \mathbb{F}(X) \rightarrow \mathbb{G}(X)$ associates to $\mathcal{P} = \{p_1, \dots, p_n\} \subset X$ an undirected graph with vertex set \mathcal{P} and edge set $\mathcal{E}_{\mathcal{G}}(\mathcal{P}) \subseteq \{(p, q) \in \mathcal{P} \times \mathcal{P} \mid p \neq q\}$.

Set of neighbors map

For proximity graph \mathcal{G} , $p \in X$, and $\mathcal{P} = \{p_1, \dots, p_n\} \in \mathbb{F}(X)$

associate set of neighbors map $\mathcal{N}_{\mathcal{G}, p}: \mathbb{F}(X) \rightarrow \mathbb{F}(X)$

$$\mathcal{N}_{\mathcal{G}, p}(\mathcal{P}) = \{q \in \mathcal{P} \mid (p, q) \in \mathcal{E}_{\mathcal{G}}(\mathcal{P} \cup \{p\})\}$$

Typically, p is a point in \mathcal{P} , but this works for any $p \in X$

When does a proximity graph provide sufficient information to compute another proximity graph?

Examples of proximity graphs

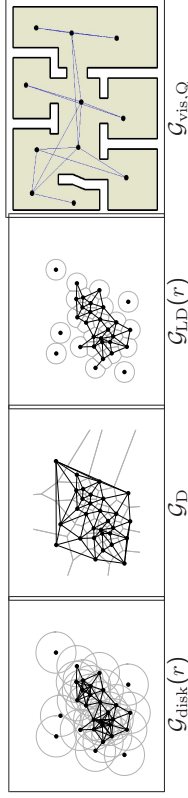
On $(\mathbb{R}^d, \text{dist}_2)$, $(\mathbb{S}^d, \text{dist}_g)$, or $(\mathbb{R}^{d_1} \times \mathbb{S}^{d_2}, (\text{dist}_2, \text{dist}_g))$

- the r -disk graph $\mathcal{G}_{\text{disk}}(r)$, for $r \in \mathbb{R}_{>0}$, with $(p_i, p_j) \in \mathcal{E}_{\mathcal{G}_{\text{disk}}(r)}(\mathcal{P})$ if $\text{dist}(p_i, p_j) \leq r$

- the Delaunay graph \mathcal{G}_{D} , with $(p_i, p_j) \in \mathcal{E}_{\mathcal{G}_{\text{D}}}(\mathcal{P})$ if $V_i(\mathcal{P}) \cap V_j(\mathcal{P}) \neq \emptyset$

- the r -limited Delaunay graph $\mathcal{G}_{\text{LD}}(r)$, for $r \in \mathbb{R}_{>0}$, with $(p_i, p_j) \in \mathcal{E}_{\mathcal{G}_{\text{LD}}(r)}(\mathcal{P})$ if $V_{i, \frac{r}{2}}(\mathcal{P}) \cap V_{j, \frac{r}{2}}(\mathcal{P}) \neq \emptyset$

- given a simple polygon Q in \mathbb{R}^2 , the visibility graph $\mathcal{G}_{\text{vis}, Q}$, with $(p_i, p_j) \in \mathcal{E}_{\mathcal{G}_{\text{vis}, Q}}(\mathcal{P})$ if the closed segment $[p_i, p_j]$ from p_i to p_j is contained in Q



Spatially distributed graphs

E.g., if a node knows position of its neighbors in the complete graph, then it can compute its neighbors with respect to any proximity graph

Formally, given \mathcal{G}_1 and \mathcal{G}_2 ,

- \mathcal{G}_1 is a subgraph of \mathcal{G}_2 , denoted $\mathcal{G}_1 \subset \mathcal{G}_2$, if $\mathcal{G}_1(\mathcal{P})$ is a subgraph of $\mathcal{G}_2(\mathcal{P})$ for all $\mathcal{P} \in \mathbb{F}(X)$

- \mathcal{G}_1 is spatially distributed over \mathcal{G}_2 if, for all $p \in \mathcal{P}$,

$$\mathcal{N}_{\mathcal{G}_1, p}(\mathcal{P}) = \mathcal{N}_{\mathcal{G}_2, p}(\mathcal{P}),$$

that is, any node equipped with the location of its neighbors with respect to \mathcal{G}_2 can compute its set of neighbors with respect to \mathcal{G}_1

\mathcal{G}_1 spatially distributed over $\mathcal{G}_2 \implies \mathcal{G}_1 \subset \mathcal{G}_2$

Converse not true: $\mathcal{G}_{\text{D}} \cap \mathcal{G}_{\text{disk}}(r) \subset \mathcal{G}_{\text{disk}}(r)$, but $\mathcal{G}_{\text{D}} \cap \mathcal{G}_{\text{disk}}(r)$ not spatially distributed over $\mathcal{G}_{\text{disk}}(r)$

Spatially distributed maps

Given a set Y and a proximity graph \mathcal{G} , a map $T: X^n \rightarrow Y^n$ is **spatially distributed over \mathcal{G}** if \exists a map $\tilde{T}: X \times \mathbb{F}(X) \rightarrow Y$ such that for all $(p_1, \dots, p_n) \in X^n$ and for all $j \in \{1, \dots, n\}$,

$$T_j(p_1, \dots, p_n) = \tilde{T}(p_j, \mathcal{N}_{\mathcal{G}, p_j}(p_1, \dots, p_n)),$$

where T_j denotes the j th-component of T

Equivalently,

the j th component of a spatially distributed map at (p_1, \dots, p_n) can be computed with the knowledge of the vertex p_j and the neighboring vertices in the undirected graph $\mathcal{G}(P)$

Cortés & Martínez (UCSD) Distributed robotic networks March 17, 2009 35 / 65

Synchronous robotic network

Definition (Robotic network)

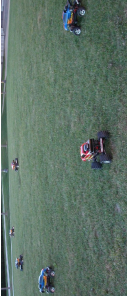
The physical components of a uniform robotic network \mathcal{S} consist of a tuple $(I, \mathcal{R}, \mathcal{E})$, where

- 1 $I = \{1, \dots, n\}$; I is called the set of unique identifiers (UIDs);
- 2 $\mathcal{R} = \{R^i\}_{i \in I} = \{(X, U, X_0, f)\}_{i \in I}$ is a set of mobile robots;
- 3 \mathcal{E} is a map from X^n to the subsets of $I \times I$; this map is called the communication edge map.

Map $x \mapsto (I, \mathcal{E}(x))$ models topology of the communication service among robots – proximity graph induced by network capabilities

Cortés & Martínez (UCSD) Distributed robotic networks March 17, 2009 35 / 65

Physical components of a robotic network



Group of robots with the ability to exchange messages, perform local computations, and control motion

Mobile robot: continuous-time continuous-space dynamical system,

- 1 X is d -dimensional space chosen among \mathbb{R}^d , \mathbb{S}^d , and the Cartesian products $\mathbb{R}^{d_1} \times \mathbb{S}^{d_2}$, for some $d_1 + d_2 = d$, called the state space;
- 2 U is a compact subset of \mathbb{R}^m containing $\mathbf{0}_n$, called the input space;
- 3 X_0 is a subset of X , called the set of allowable initial states;
- 4 $f: X \times U \rightarrow \mathbb{R}^d$ is a smooth control vector field on X

Cortés & Martínez (UCSD) Distributed robotic networks March 17, 2009 34 / 65

A couple of examples

Locally-connected first-order robots in \mathbb{R}^d : $\mathcal{S}_{\text{disk}}$ n points $x^{[1]}, \dots, x^{[n]}$ in \mathbb{R}^d , $d \geq 1$, obeying $\dot{x}^{[i]}(t) = u^{[i]}(t)$, with $u^{[i]} \in [-u_{\max}, u_{\max}]$. These are identical robots of the form

$$(\mathbb{R}^d, [-u_{\max}, u_{\max}]^d, \mathbb{R}^d, (\mathbf{0}, \mathbf{e}_1, \dots, \mathbf{e}_d))$$

Each robot can communicate to other robots within r , $\mathcal{G}_{\text{disk}}(r)$ on \mathbb{R}^d

Locally-connected first-order robots in \mathbb{S}^1 : $\mathcal{S}_{\text{circle, disk}}$ n robots $\theta^{[1]}, \dots, \theta^{[n]}$ in \mathbb{S}^1 , moving along on the unit circle with angular velocity equal to the control input. Each robot is described by

$$(\mathbb{S}^1, [-u_{\max}, u_{\max}], \mathbb{S}^1, (0, \mathbf{e}))$$

(\mathbf{e} describes unit-speed counterclockwise rotation). Each robot can communicate to other robots within r along the circle, $\mathcal{G}_{\text{disk}}(r)$ on \mathbb{S}^1

Cortés & Martínez (UCSD) Distributed robotic networks March 17, 2009 36 / 65

Robotic networks with relative sensing

Model assumes ability of each robot to know its own absolute position

Alternative setting: robots do not communicate amongst themselves, but instead

- detect and measure each other's relative position through appropriate sensors
- perform measurements of the environment without having a priori knowledge

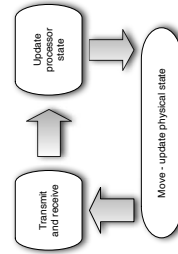
Robots do not have the ability to perform measurements expressed in a common reference frame

Cortés & Martínez (UCSD) Distributed robotic networks March 17, 2009 37 / 65

Uniform control and communication law

- 1 communication schedule
- 2 communication alphabet
- 3 processor state space
- 4 message-generation function
- 5 state-transition functions
- 6 control function

Execution: discrete-time communication
discrete-time computation
continuous-time motion



Cortés & Martínez (UCSD) Distributed robotic networks March 17, 2009 39 / 65

Outline

- 1 Synchronous networks
 - A motivating problem: leader election
 - Distributed algorithms
 - Complexity notions
- 2 Robotic networks
 - A motivating problem: direction agreement and equidistance
 - Proximity graphs
 - Control and communication laws
 - Coordination tasks and complexity notions
- 3 Complexity analysis of agree and pursue law
- 4 Conclusions

Cortés & Martínez (UCSD) Distributed robotic networks March 17, 2009 38 / 65

The agree-and-pursue algorithm – formally

Alphabet: $L = \mathbb{S}^1 \times \{c, cc\} \times I \cup \{\text{null}\}$
 Processor State: $w = (\text{dir}, \text{max-uid})$, where
 $\text{dir} \in \{c, cc\}$, initially: $\text{dir}^{[i]}$ unspecified
 $\text{max-uid} \in I$, initially: $\text{max-uid}^{[i]} = i$ for all i

```

function msg( $\theta, w, i$ )
1: return ( $\theta, w$ )

function stf( $w, y$ )
1: for each non-null message ( $\theta_{\text{rcvd}}, (\text{dir}_{\text{rcvd}}, \text{max-uid}_{\text{rcvd}})$ ) do
2:   if ( $\text{max-uid}_{\text{rcvd}} > \text{max-uid}$ ) AND ( $\text{dist}_c(\theta, \theta_{\text{rcvd}}) \leq r$  AND  $\text{dir}_{\text{rcvd}} = c$ ) OR
     ( $\text{dist}_c(\theta, \theta_{\text{rcvd}}) \leq r$  AND  $\text{dir}_{\text{rcvd}} = cc$ ) then
3:     new-dir := dirrcvd
4:     new-uid := max-uidrcvd
5:   return (new-dir, new-uid)

function ctrl( $\theta_{\text{smpld}}, w, y$ )
1:  $d_{\text{tmp}} := r$ 
2: for each non-null message ( $\theta_{\text{rcvd}}, (\text{dir}_{\text{rcvd}}, \text{max-uid}_{\text{rcvd}})$ ) do
3:   if ( $\text{dir} = cc$ ) AND ( $\text{dist}_{cc}(\theta_{\text{smpld}}, \theta_{\text{rcvd}}) < d_{\text{tmp}}$ ) then
4:      $d_{\text{tmp}} := \text{dist}_{cc}(\theta_{\text{smpld}}, \theta_{\text{rcvd}})$  and  $u_{\text{tmp}} := k_{\text{prop}} d_{\text{tmp}}$ 
5:   if ( $\text{dir} = c$ ) AND ( $\text{dist}_c(\theta_{\text{smpld}}, \theta_{\text{rcvd}}) < d_{\text{tmp}}$ ) then
6:      $d_{\text{tmp}} := \text{dist}_c(\theta_{\text{smpld}}, \theta_{\text{rcvd}})$  and  $u_{\text{tmp}} := -k_{\text{prop}} d_{\text{tmp}}$ 
7: return  $u_{\text{tmp}}$ 
  
```

$(k_{\text{prop}} \in (0, \frac{1}{2}))$

Cortés & Martínez (UCSD) Distributed robotic networks March 17, 2009 40 / 65

Evolution of a robotic network – formal definition

Evolution of (S, \mathcal{CC}) from $x_0^{[i]} \in X_0^{[i]}$ and $w_0^{[i]} \in W_0^{[i]}$, $i \in I$, is the collection of curves $x^{[i]}: \mathbb{R}_{\geq 0} \rightarrow X^{[i]}$ and $w^{[i]}: \mathbb{T} \rightarrow W^{[i]}$, $i \in I$

$$\dot{x}^{[i]}(t) = f\left(x^{[i]}(t), \text{ctrl}^{[i]}(t, x^{[i]}(\lfloor t \rfloor), w^{[i]}(\lfloor t \rfloor), y^{[i]}(\lfloor t \rfloor))\right),$$

where $\lfloor t \rfloor = \max\{\ell \in \mathbb{T} \mid \ell < t\}$, and

$$w^{[i]}(\ell) = \text{stf}^{[i]}(x^{[i]}(\ell), w^{[i]}(\ell - 1), y^{[i]}(\ell)),$$

with $x^{[i]}(0) = x_0^{[i]}$, and $w^{[i]}(-1) = w_0^{[i]}$, $i \in I$

Here, $y^{[i]}: \mathbb{T} \rightarrow L^n$ (describing the messages received by processor i) has components $y_j^{[i]}(\ell)$, for $j \in I$, given by

$$y_j^{[i]}(\ell) = \begin{cases} \text{msg}^{[ij]}(x^{[ij]}(\ell), w^{[ij]}(\ell - 1), i), & \text{if } (j, i) \in \mathcal{E}(x^{[i]}(\ell), \dots, x^{[n]}(\ell)) \\ \text{null}, & \text{otherwise} \end{cases}$$

Cortés & Martínez (UCSD) Distributed robotic networks March 17, 2009 41 / 65

Coordination tasks

What is a coordination task for a robotic network? When does a control and communication law achieve a task? And with what time, space, and communication complexity?

A **coordination task** for a robotic network \mathcal{S} is a map $\mathcal{T}: X^n \times \mathcal{W}^n \rightarrow \{\text{true}, \text{false}\}$

Logic-based: agree, synchronize, form a team, elect a leader

Motion: deploy, gather, flock, reach pattern

Sensor-based: search, estimate, identify, track, map

A control and communication law \mathcal{CC} achieves the task \mathcal{T} if, for all initial conditions $x_0^{[i]} \in X_0^{[i]}$ and $w_0^{[i]} \in W_0^{[i]}$, $i \in I$, the network evolution $t \mapsto (x(t), w(t))$ has the property

there exists $T \in \mathbb{R}_{>0}$ such that $\mathcal{T}(x(t), w(t)) = \text{true}$ for $t \geq T$

Cortés & Martínez (UCSD) Distributed robotic networks March 17, 2009 43 / 65

Outline

- 1 **Synchronous networks**
 - A motivating problem: leader election
 - Distributed algorithms
 - Complexity notions
- 2 **Robotic networks**
 - A motivating problem: direction agreement and equidistance
 - Proximity graphs
 - Control and communication laws
 - Coordination tasks and complexity notions
- 3 **Complexity analysis of agree and pursue law**
- 4 **Conclusions**

Cortés & Martínez (UCSD) Distributed robotic networks March 17, 2009 42 / 65

Task definitions via temporal logic

Loosely speaking, achieving a task means obtaining and maintaining a specified pattern in the robot physical or processor state

In other words, the task is achieved if **at some time** and **for all subsequent times** the predicate evaluates to true along system trajectories

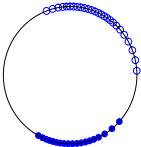
More general tasks based on more expressive predicates on trajectories can be defined through temporal and propositional logic, e.g.,
periodically visiting a desired set of configurations

Cortés & Martínez (UCSD) Distributed robotic networks March 17, 2009 44 / 65

Direction agreement and equidistance tasks

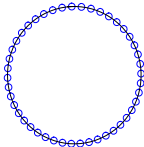
Direction agreement task $\mathcal{T}_{\text{dir}}: (\mathbb{S}^1)^n \times W^n \rightarrow \{\text{true}, \text{false}\}$

$$\mathcal{T}_{\text{dir}}(\theta, w) = \begin{cases} \text{true}, & \text{if } \text{dir}^{[1]} = \dots = \text{dir}^{[n]} \\ \text{false}, & \text{otherwise} \end{cases}$$



For $\epsilon > 0$, **equidistance task** $\mathcal{T}_{\text{eqdistnc}}: (\mathbb{S}^1)^n \rightarrow \{\text{true}, \text{false}\}$ is true iff

$$\left| \min_{j \neq i} \text{dist}_c(\theta^{[i]}, \theta^{[j]}) - \min_{j \neq i} \text{dist}_{cc}(\theta^{[i]}, \theta^{[j]}) \right| < \epsilon, \quad \text{for all } i \in I$$



Cortés & Martínez (UCSD) Distributed robotic networks March 17, 2009 45 / 65

Time complexity – formally

The **time complexity** to achieve \mathcal{T} with \mathcal{CC} from $(x_0, w_0) \in \prod_{i \in I} X_0^{[i]} \times \prod_{i \in I} W_0^{[i]}$ is

$$\text{TC}(\mathcal{T}, \mathcal{CC}, x_0, w_0) = \inf \{ \ell \mid \mathcal{T}(x(t_k), w(t_k)) = \text{true}, \text{ for all } k \geq \ell \},$$

where $t \mapsto (x(t), w(t))$ is the evolution of (S, \mathcal{CC}) from the initial condition (x_0, w_0)

The **time complexity** to achieve \mathcal{T} with \mathcal{CC} is

$$\text{TC}(\mathcal{T}, \mathcal{CC}) = \sup \left\{ \text{TC}(\mathcal{T}, \mathcal{CC}, x_0, w_0) \mid (x_0, w_0) \in \prod_{i \in I} X_0^{[i]} \times \prod_{i \in I} W_0^{[i]} \right\}.$$

The **time complexity** of \mathcal{T} is

$$\text{TC}(\mathcal{T}) = \inf \{ \text{TC}(\mathcal{T}, \mathcal{CC}) \mid \mathcal{CC} \text{ compatible with } \mathcal{T} \}$$

Cortés & Martínez (UCSD) Distributed robotic networks March 17, 2009 47 / 65

Complexity notions for control and communication laws

For network \mathcal{S} , task \mathcal{T} , and algorithm \mathcal{CC} , define **costs/complexity** control effort, communication packets, computational cost

Time complexity: maximum number of communication rounds required to achieve \mathcal{T}

Space complexity: maximum number of basic memory units required by a robot processor among all robots

Communication complexity: maximum number of basic messages transmitted over entire network

(among all allowable initial physical and processor states until termination)

basic memory unit/message contain $\log(n)$ bits

Cortés & Martínez (UCSD) Distributed robotic networks March 17, 2009 46 / 65

Communication complexity – formally

The set of all non-null messages generated during one communication round from network state (x, w)

$$\mathcal{M}(x, w) = \left\{ (i, j) \in \mathcal{E}(x) \mid \text{msg}^{[i]}(x^{[i]}, w^{[i]}, j) \neq \text{null} \right\}.$$

The **mean communication complexity** and the **total communication complexity** to achieve \mathcal{T} with \mathcal{CC} from $(x_0, w_0) \in \prod_{i \in I} X_0^{[i]} \times \prod_{i \in I} W_0^{[i]}$ are,

$$\text{MCC}(\mathcal{T}, \mathcal{CC}, x_0, w_0) = \frac{|L|_{\text{basic}}}{\lambda} \sum_{\ell=0}^{\lambda-1} |\mathcal{M}(x(\ell), w(\ell))|,$$

$$\text{TCC}(\mathcal{T}, \mathcal{CC}, x_0, w_0) = |L|_{\text{basic}} \sum_{\ell=0}^{\lambda-1} |\mathcal{M}(x(\ell), w(\ell))|,$$

where $|L|_{\text{basic}}$ is number of basic messages required to represent elements of L and $\lambda = \text{TC}(\mathcal{CC}, \mathcal{T}, x_0, w_0)$

Cortés & Martínez (UCSD) Distributed robotic networks March 17, 2009 48 / 65

Variations and extensions

Asymptotic results

Complexities in $O(f(n))$, $\Omega(f(n))$, or $\Theta(f(n))$ as $n \rightarrow \infty$

- **Infinite-horizon mean communication complexity:** mean communication complexity to maintain true the task for all times

$$cc(\mathcal{CC}, x_0, w_0) = \lim_{\lambda \rightarrow +\infty} \frac{|L|_{\text{basic}}}{\lambda} \sum_{\ell=0}^{\lambda} |\mathcal{M}(x(\ell), w(\ell))|$$

- **Communication complexity in omnidirectional networks:** All neighbors of agent receive the signal it transmits. Makes sense to count the number of transmissions, i.e., a unit cost per node, rather than a unit cost per edge of the network
- **Energy complexity**
- **Expected, rather than worst-case notions**

Cortés & Martínez (UCSD) Distributed robotic networks March 17, 2009 49 / 65

Time complexity of agree-and-pursue law

Let $r: \mathbb{N} \rightarrow]0, 2\pi[$ be a monotone non-increasing function of number of agents n – modeling wireless communication congestion

Theorem

In the limit as $n \rightarrow +\infty$ and $\epsilon \rightarrow 0^+$, the network $S_{\text{circle, disk}}$, the law $\mathcal{CC}_{\text{AGREE \& PURSUE}}$, and the tasks \mathcal{T}_{dir} and $\mathcal{T}_{\text{e-eqdstnc}}$ together satisfy:

- $\text{TC}(\mathcal{T}_{\text{dir}}, \mathcal{CC}_{\text{AGREE \& PURSUE}}) \in \Theta(r(n)^{-1})$;
- if $\delta(n) = nr(n) - 2\pi$ is lower bounded by a positive constant as $n \rightarrow +\infty$, then

$$\begin{aligned} \text{TC}(\mathcal{T}_{\text{e-eqdstnc}}, \mathcal{CC}_{\text{AGREE \& PURSUE}}) &\in \Omega(n^2 \log(n\epsilon)^{-1}), \\ \text{TC}(\mathcal{T}_{\text{e-eqdstnc}}, \mathcal{CC}_{\text{AGREE \& PURSUE}}) &\in O(n^2 \log(n\epsilon^{-1})). \end{aligned}$$

If $\delta(n)$ is lower bounded by a negative constant, then $\mathcal{CC}_{\text{AGREE \& PURSUE}}$ does not achieve $\mathcal{T}_{\text{e-eqdstnc}}$ in general.

Cortés & Martínez (UCSD) Distributed robotic networks March 17, 2009 51 / 65

Outline

- 1 Synchronous networks
 - A motivating problem: leader election
 - Distributed algorithms
 - Complexity notions
- 2 Robotic networks
 - A motivating problem: direction agreement and equidistance
 - Proximity graphs
 - Control and communication laws
 - Coordination tasks and complexity notions
- 3 Complexity analysis of agree and pursue law
- 4 Conclusions

Cortés & Martínez (UCSD) Distributed robotic networks March 17, 2009 50 / 65

Proof sketch - O bound for \mathcal{T}_{dir}

Claim: $\text{TC}(\mathcal{T}_{\text{dir}}, \mathcal{CC}_{\text{AGREE \& PURSUE}}) \leq 2\pi / (k_{\text{prop}} r(n))$

By contradiction, assume there exists initial condition such that execution has time complexity larger than $2\pi / (k_{\text{prop}} r(n))$
Without loss of generality, $\text{dir}^{[n]}(0) = c$. For $\ell \leq 2\pi / (k_{\text{prop}} r(n))$, let

$$k(\ell) = \text{argmin}\{\text{dist}_c(\theta^{[n]}(0), \theta^{[i]}(\ell)) \mid \text{dir}^{[i]}(\ell) = cc, i \in I\}$$

Agent $k(\ell)$ is agent moving counterclockwise that has smallest counterclockwise distance from the initial position of agent n

Recall that according to $\mathcal{CC}_{\text{AGREE \& PURSUE}}$

- messages with $\text{dir} = cc$ can only travel counterclockwise
- messages with $\text{dir} = c$ can only travel clockwise

Therefore, position of agent $k(\ell)$ at time ℓ can only belong to the counterclockwise interval from the position of agent $k(0)$ at time 0 to the position of agent n at time 0

Cortés & Martínez (UCSD) Distributed robotic networks March 17, 2009 52 / 65

Proof sketch - O bound for \mathcal{I}_{dir}

How fast the message from agent n travels clockwise?

For $\ell \leq 2\pi/(k_{\text{prop}}r(n))$, define

$$j(\ell) = \arg\max\{\text{dist}_c(\theta^{[n]}(0), \theta^{[i]}(\ell)) \mid \text{prior}^{[i]}(\ell) = n, i \in I\}$$

Agent $j(\ell)$

- has prior equal to n
- is moving clockwise

and is the agent furthest from the initial position of agent n in the clockwise direction with these two properties

Initially, $j(0) = n$. Additionally, for $\ell \leq 2\pi/(k_{\text{prop}}r(n))$, we claim

$$\text{dist}_c(\theta^{[j(\ell)]}(\ell), \theta^{[j(\ell+1)]}(\ell+1)) \geq k_{\text{prop}}r(n) \quad (1)$$

Cortés & Martínez (UCSD) Distributed robotic networks March 17, 2009 55 / 65

Proof sketch - O bound for $\mathcal{I}_{\text{eqdstnc}}$

Assume \mathcal{I}_{dir} has been achieved and all agents are moving clockwise

At time $\ell \in \mathbb{N}_0$, let $H(\ell)$ be the union of all the empty “circular segments” of length at least r ,

$$H(\ell) = \{x \in \mathbb{S}^1 \mid \min_{i \in I} \text{dist}_c(x, \theta^{[i]}(\ell)) + \min_{j \in I} \text{dist}_{cc}(x, \theta^{[j]}(\ell)) > r\}.$$

$H(\ell)$ does not contain any point between two agents separated by a distance less than r , and each connected component has length at least r

Let $n_H(\ell)$ be number of connected components of $H(\ell)$,

- if $H(\ell)$ is empty, then $n_H(\ell) = 0$
- $n_H(\ell) \leq n$
- if $n_H(\ell) > 0$, then $t \mapsto n_H(\ell + t)$ is non-increasing

Cortés & Martínez (UCSD) Distributed robotic networks March 17, 2009 55 / 65

Proof sketch - O bound for \mathcal{I}_{dir}

$\text{TC}(\mathcal{I}_{\text{dir}}, \mathcal{CC}_{\text{GREE}} \& \text{PURSUE}) \leq 2\pi/(k_{\text{prop}}r(n))$

Claim (1) happens because either (1) there is no agent clockwise-ahead of $\theta^{[j(\ell)]}(\ell)$ within clockwise distance r and, therefore, the claim is obvious, or (2) there are such agents. In case (2), let m denote the agent whose clockwise distance to agent $j(\ell)$ is maximal within the set of agents with clockwise distance r from $\theta^{[j(\ell)]}(\ell)$. Then,

$$\begin{aligned} \text{dist}_c(\theta^{[j(\ell)]}(\ell), \theta^{[j(\ell+1)]}(\ell+1)) &= \text{dist}_c(\theta^{[j(\ell)]}(\ell), \theta^{[m]}(\ell+1)) \\ &= \text{dist}_c(\theta^{[j(\ell)]}(\ell), \theta^{[m]}(\ell)) + \text{dist}_c(\theta^{[m]}(\ell), \theta^{[m]}(\ell+1)) \\ &\geq \text{dist}_c(\theta^{[j(\ell)]}(\ell), \theta^{[m]}(\ell)) + k_{\text{prop}}(r - \text{dist}_c(\theta^{[j(\ell)]}(\ell), \theta^{[m]}(\ell))) \\ &= k_{\text{prop}}r + (1 - k_{\text{prop}}) \text{dist}_c(\theta^{[j(\ell)]}(\ell), \theta^{[m]}(\ell)) \geq k_{\text{prop}}r \end{aligned}$$

Therefore, after $2\pi/(k_{\text{prop}}r(n))$ communication rounds, the message with prior $= n$ has traveled the whole circle in the clockwise direction, and must therefore have reached agent $k(\ell)$

Contradiction

Cortés & Martínez (UCSD) Distributed robotic networks March 17, 2009 54 / 65

Proof sketch- O bound for $\mathcal{I}_{\text{eqdstnc}}$

Number of connected components is strictly decreasing

Claim: if $n_H(\ell) > 0$, then $\exists t > \ell$ such that $n_H(t) < n_H(\ell)$

By contradiction, assume $n_H(\ell) = n_H(t)$ for all $t > \ell$. Without loss of generality, let $\{1, \dots, m\}$ be a set of agents with the properties

- $\text{dist}_{cc}(\theta^{[i]}(\ell), \theta^{[i+1]}(\ell)) \leq r$, for $i \in \{1, \dots, m\}$
- $\theta^{[1]}(\ell)$ and $\theta^{[m]}(\ell)$ belong to the boundary of $H(\ell)$
- there is no other set with the same properties and more agents

One can show that, for $\tau \geq \ell$ and $i \in \{2, \dots, m\}$

$$\begin{aligned} \theta^{[1]}(\tau+1) &= \theta^{[1]}(\tau) - k_{\text{prop}}r \\ \theta^{[i]}(\tau+1) &= \theta^{[i]}(\tau) - k_{\text{prop}} \text{dist}_c(\theta^{[i]}(\tau), \theta^{[i-1]}(\tau)) \end{aligned}$$

Cortés & Martínez (UCSD) Distributed robotic networks March 17, 2009 56 / 65

Tridiagonal and circulant linear dynamical systems

$$\text{Trid}_n(a, b, c) = \begin{bmatrix} b & c & 0 & \dots & 0 \\ a & b & c & \dots & 0 \\ \vdots & \ddots & \ddots & \ddots & \vdots \\ 0 & \dots & a & b & c \\ 0 & \dots & 0 & a & b \end{bmatrix}, \quad \text{Circ}_n(a, b, c) = \begin{bmatrix} b & c & 0 & \dots & a \\ a & b & c & \dots & 0 \\ \vdots & \ddots & \ddots & \ddots & \vdots \\ 0 & \dots & a & b & c \\ c & \dots & 0 & a & b \end{bmatrix}$$

Linear dynamical systems

$$y(\ell + 1) = Ay(\ell), \quad \ell \in \mathbb{N}_0$$

Rates of convergence to set of equilibria can be characterized – carefully look at eigenvalues. Statements of the form

if $a \geq 0$, $c \geq 0$, $b > 0$, and $a + b + c = 1$, then $\lim_{\ell \rightarrow +\infty} y(\ell) = y_{\text{ave}} \mathbf{1}$, where $y_{\text{ave}} = \frac{1}{n} \mathbf{1}^T y_0$, and maximum time required (over all initial conditions $y_0 \in \mathbb{R}^n$) for $\|y(\ell) - y_{\text{ave}} \mathbf{1}\|_2 \leq \epsilon \|y_0 - y_{\text{ave}} \mathbf{1}\|_2$ is $\Theta(n^2 \log \epsilon^{-1})$

Cortés & Martínez (UCSD) Distributed robotic networks March 17, 2009 57 / 65

Proof sketch- O bound for $\mathcal{T}_{\epsilon\text{-eqdstnc}}$

Take $\eta_1 = (nr - 2\pi)n^{-1} = \delta(n)n^{-1}$, and the contradiction follows from

$$\begin{aligned} 2\pi &\geq n_H(\ell)\eta_1 + nr - n\eta_1 \\ &= n_H(\ell)\eta_1 + nr + 2\pi - nr = n_H(\ell)\eta_1 + 2\pi \end{aligned}$$

Therefore $n_H(\ell)$ decreases by one in time $O(n \log n)$

Iterating this argument n times, in time $O(n^2 \log n)$ the set H becomes empty. At that time, resulting network obeys

$$d(\tau + 1) = \text{Circ}_n(k_{\text{prop}}, 1 - k_{\text{prop}}, 0) d(\tau)$$

In time $O(n^2 \log \epsilon^{-1})$, the error 2-norm satisfies the contraction inequality $\|d(\tau) - d_*\|_2 \leq \epsilon \|d(0) - d_*\|_2$, for $d_* = \frac{2\pi}{n} \mathbf{1}$

The conversion of this inequality into an appropriate inequality on ∞ -norms yields the result

Cortés & Martínez (UCSD) Distributed robotic networks March 17, 2009 59 / 65

Proof sketch- O bound for $\mathcal{T}_{\epsilon\text{-eqdstnc}}$ Contradiction argument

$$\begin{aligned} \text{For } d(\tau) &= (\text{dist}_{cc}(\theta^{[1]}(\tau), \theta^{[2]}(\tau)), \dots, \text{dist}_{cc}(\theta^{[m-1]}(\tau), \theta^{[m]}(\tau))), \\ d(\tau + 1) &= \text{Trid}_{m-1}(k_{\text{prop}}, 1 - k_{\text{prop}}, 0) d(\tau) + r[k_{\text{prop}}, 0, \dots, 0]^T \end{aligned}$$

Unique equilibrium point is $r(1, \dots, 1)$. For $\eta_1 \in]0, 1[$, $\tau \mapsto d(\tau)$ reaches ball of radius η_1 centered at equilibrium in $O(m \log m + \log \eta_1^{-1})$

This implies that $\tau \mapsto \sum_{i=1}^m d_i(\tau)$ is larger than $(m-1)(r - \eta_1)$ in time $O(m \log m + \log \eta_1^{-1}) = O(n \log n + \log \eta_1^{-1})$. After this time,

$$\begin{aligned} 2\pi &\geq n_H(\ell)r + \sum_{j=1}^{n_H(\ell)} (r - \eta_1)(m_j - 1) \\ &= n_H(\ell)r + (n - n_H(\ell))(r - \eta_1) = n_H(\ell)\eta_1 + n(r - \eta_1) \end{aligned}$$

Cortés & Martínez (UCSD) Distributed robotic networks March 17, 2009 58 / 65

Communication complexity of agree-and-pursue law

Theorem

In the limit as $n \rightarrow +\infty$ and $\epsilon \rightarrow 0^+$, the network $\mathcal{S}_{\text{circle, disk}}$, the law $\mathcal{CC}_{\text{AGREE \& PURSUE}}$, and the tasks \mathcal{T}_{dir} and $\mathcal{T}_{\epsilon\text{-eqdstnc}}$ together satisfy:

- if $\delta(n) \geq \pi(1/k_{\text{prop}} - 2)$ as $n \rightarrow +\infty$, then

$$\text{TCC}_{\text{unidir}}(\mathcal{T}_{\text{dir}}, \mathcal{CC}_{\text{AGREE \& PURSUE}}) \in \Theta(n^2 r(n)^{-1}),$$

otherwise if $\delta(n) \leq \pi(1/k_{\text{prop}} - 2)$ as $n \rightarrow +\infty$, then

$$\text{TCC}_{\text{unidir}}(\mathcal{T}_{\text{dir}}, \mathcal{CC}_{\text{AGREE \& PURSUE}}) \in \Omega(n^3 + nr(n)^{-1}),$$

$$\text{TCC}_{\text{unidir}}(\mathcal{T}_{\text{dir}}, \mathcal{CC}_{\text{AGREE \& PURSUE}}) \in O(n^2 r(n)^{-1});$$

- if $\delta(n)$ is lower bounded by a positive constant as $n \rightarrow +\infty$, then

$$\text{TCC}_{\text{unidir}}(\mathcal{T}_{\epsilon\text{-eqdstnc}}, \mathcal{CC}_{\text{AGREE \& PURSUE}}) \in \Omega(n^3 \delta(n) \log(n\epsilon)^{-1}),$$

$$\text{TCC}_{\text{unidir}}(\mathcal{T}_{\epsilon\text{-eqdstnc}}, \mathcal{CC}_{\text{AGREE \& PURSUE}}) \in O(n^4 \log(n\epsilon^{-1})).$$

Cortés & Martínez (UCSD) Distributed robotic networks March 17, 2009 60 / 65

Comparison with leader election

- **Leader election** task is different from, but closely related to, \mathcal{T}_{dir}
- **LCR algorithm** operates on a static ring network, and achieves leader election with time and total communication complexity, respectively, $\Theta(n)$ and $\Theta(n^2)$
- **Agree-and-pursue** law operates on robotic network with $r(n)$ -disk communication topology, and achieves \mathcal{T}_{dir} with time and total communication complexity, respectively, $\Theta(r(n))$ and $O(n^2 r(n)^{-1})$

If wireless communication congestion is modeled by $r(n)$ of order $1/n$, then identical time complexity and the LCR algorithm has better communication complexity

Computations on a possibly disconnected, dynamic network are more complex than on a static ring topology

Cortés & Martínez (UCSD) Distributed robotic networks March 17, 2009 61 / 65

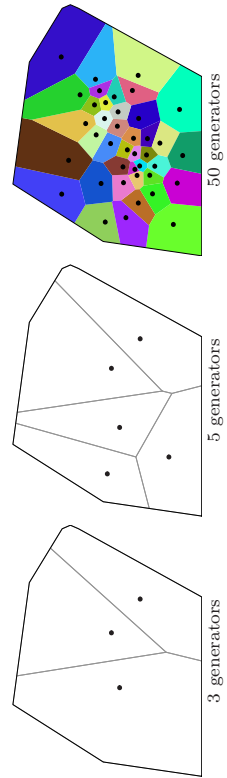
Voronoi partitions

Let $(p_1, \dots, p_n) \in Q^n$ denote the positions of n points

The **Voronoi partition** $\mathcal{V}(P) = \{V_1, \dots, V_n\}$ generated by (p_1, \dots, p_n)

$$V_i = \{q \in Q \mid \|q - p_i\| \leq \|q - p_j\|, \forall j \neq i\}$$

$$= Q \cap_j \mathcal{HP}(p_i, p_j) \quad \text{where } \mathcal{HP}(p_i, p_j) \text{ is half plane } (p_i, p_j)$$



Return

Cortés & Martínez (UCSD) Distributed robotic networks March 17, 2009 63 / 65

Conclusions

Robotic network model

- proximity graphs
- control and communication law, task, execution
- time, space, and communication complexity
- agree and pursue

Complexity analysis is **challenging** even in 1 dimension! Blend of mathematical tools required

Plenty of **open issues and problems**

- Asynchronism, quantization, delays
- What is best algorithm to achieve a task?
- What tools are useful to characterize complexity?
- How does combination of algorithms affect complexities?

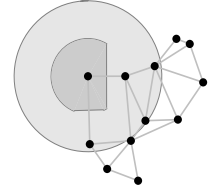
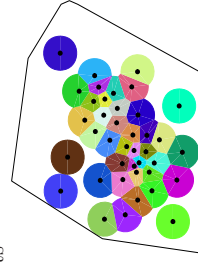
Cortés & Martínez (UCSD) Distributed robotic networks March 17, 2009 62 / 65

r -limited Voronoi partition

Let $(p_1, \dots, p_n) \in Q^n$ denote the positions of n points

The **r -limited Voronoi partition** $\mathcal{V}_r(P) = \{V_{1,r}, \dots, V_{n,r}\}$ generated by (p_1, \dots, p_n)

$$V_{i,r}(P) = V_i(P) \cap \overline{B}(p_i, r)$$

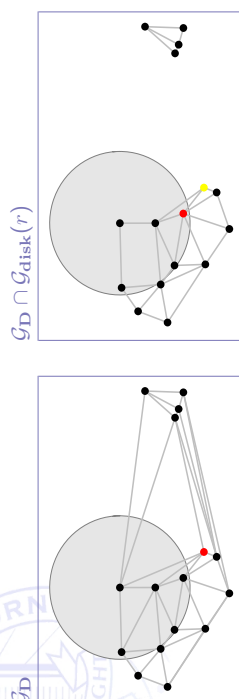


$\mathcal{G}_{LD}(r)$ is spatially distributed over $\mathcal{G}_{\text{disk}}(r)$

Return

Cortés & Martínez (UCSD) Distributed robotic networks March 17, 2009 64 / 65

\mathcal{G}_D and $\mathcal{G}_D \cap \mathcal{G}_{\text{disk}}(r)$ computation



\mathcal{G}_D and $\mathcal{G}_D \cap \mathcal{G}_{\text{disk}}(r)$ are **not** spatially distributed over $\mathcal{G}_{\text{disk}}(r)$

◀ Return

Distributed control of Robotic Networks (Part 2)

Jorge Cortés and Sonia Martínez (University of California at
San Diego, USA)

Distributed robotic networks: rendezvous, connectivity, and deployment

Jorge Cortés and Sonia Martínez



Mechanical and Aerospace Engineering
University of California, San Diego
{cortes,soniamd}@ucsd.edu

28th Benelux Meeting on Systems and Control
Spa, Belgium, March 17, 2009

Acknowledgments: Francesco Bullo
Anurag Ganguli

What we will see in this lecture

Basic motion coordination tasks:

get together at a point, stay connected, deploy over a region



Design coordination algorithms that achieve these tasks and analyze their correctness and time complexity

Expand set of math tools: invariance principles for non-deterministic systems, geometric optimization, non-smooth stability analysis

Robustness against link failures, agents' arrivals and departures, delays, asynchronism

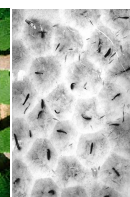


Image credits: Jupiterimages and Animal Behavior

What we have seen in the previous lecture

Cooperative robotic network model

- proximity graphs
- control and communication law, task, execution
- time, space, and communication complexity
- analysis agree and pursue algorithm

Complexity analysis is **challenging** even in 1 dimension! Blend of math

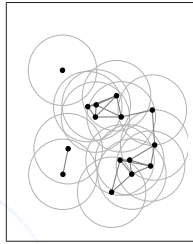
- geometric structures
- distributed algorithms
- stability analysis
- linear iterations

Outline

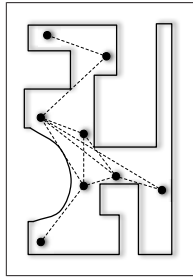
- 1 **Rendezvous and connectivity maintenance**
 - The rendezvous objective
 - Maintaining connectivity
 - Circumcenter algorithms
 - Correctness analysis via nondeterministic systems
- 2 **Deployment**
 - Expected-value deployment
 - Geometric-center laws
 - Disk-covering and sphere-packing deployment
 - Geometric-center laws
- 3 **Conclusions**

Rendezvous objective

Objective: achieve multi-robot rendezvous; i.e. arrive at the same location of space, while maintaining connectivity

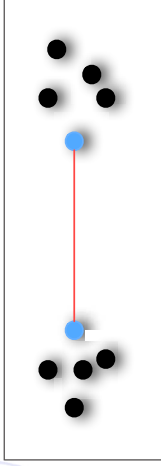


r -disk connectivity



visibility connectivity

We have to be careful...



Blindly “getting closer” to neighboring agents might break overall connectivity

Network definition and rendezvous tasks

The objective is applicable for **general robotic networks** $\mathcal{S}_{\text{disk}}$, \mathcal{S}_{LD} and $\mathcal{S}_{\infty\text{-disk}}$, and the relative-sensing networks $\mathcal{S}_{\text{disk}}^{\text{rs}}$ and $\mathcal{S}_{\text{vis-disk}}^{\text{rs}}$

We adopt the **discrete-time motion** model

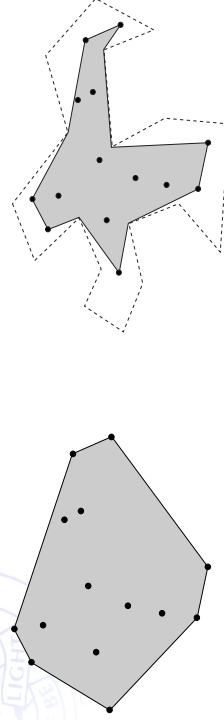
$$p^{[i]}(\ell + 1) = p^{[i]}(\ell) + u^{[i]}(\ell), \quad i \in \{1, \dots, n\}$$

Also for the **relative-sensing networks**

$$p_{\text{fixed}}^{[i]}(\ell + 1) = p_{\text{fixed}}^{[i]}(\ell) + R_{\text{fixed}}^{[i]} u_i^{[i]}(\ell), \quad i \in \{1, \dots, n\}$$

The rendezvous task via aggregate objective functions

Coordination task formulated as function minimization



Diameter convex hull

Perimeter relative convex hull

The rendezvous task formally

Let $\mathcal{S} = (\{1, \dots, n\}, \mathcal{R}, E_{\text{cmm}})$ be a uniform robotic network
 The (exact) rendezvous task $\mathcal{T}_{\text{rendezvous}} : X^n \rightarrow \{\text{true}, \text{false}\}$ for \mathcal{S} is

$$\mathcal{T}_{\text{rendezvous}}(x^{[1]}, \dots, x^{[n]}) = \begin{cases} \text{true}, & \text{if } x^{[i]} = x^{[j]}, \text{ for all } (i, j) \in E_{\text{cmm}}(x^{[1]}, \dots, x^{[n]}), \\ \text{false}, & \text{otherwise} \end{cases}$$

For $\epsilon \in \mathbb{R}_{>0}$, the ϵ -rendezvous task $\mathcal{T}_{\epsilon\text{-rendezvous}} : (\mathbb{R}^d)^n \rightarrow \{\text{true}, \text{false}\}$ is

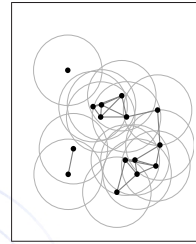
$$\begin{aligned} \mathcal{T}_{\epsilon\text{-rendezvous}}(P) &= \text{true} \\ \iff \|p^{[i]} - \text{avg}(\{p^{[j]} \mid (i, j) \in E_{\text{cmm}}(P)\})\|_2 &< \epsilon, \quad i \in \{1, \dots, n\} \end{aligned}$$

Cortés & Martínez (UCSD) Distributed robotic networks March 17, 2009 9 / 72

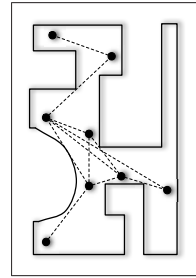
Constraint sets for connectivity

Design constraint sets with key properties

- Constraints are flexible enough so that network does not get stuck
- Constraints change continuously with agents' position



r -disk connectivity



visibility connectivity

Cortés & Martínez (UCSD) Distributed robotic networks March 17, 2009 11 / 72

Outline

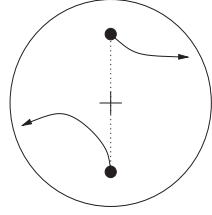
- 1 Rendezvous and connectivity maintenance
 - The rendezvous objective
 - Maintaining connectivity
 - Circumcenter algorithms
 - Correctness analysis via nondeterministic systems
- 2 Deployment
 - Expected-value deployment
 - Geometric-center laws
 - Disk-covering and sphere-packing deployment
 - Geometric-center laws
- 3 Conclusions

Cortés & Martínez (UCSD) Distributed robotic networks March 17, 2009 10 / 72

Enforcing range-limited links – pairwise

Pairwise connectivity maintenance problem:

Given two neighbors in $\mathcal{G}_{\text{disk}}(r)$, find a rich set of control inputs for both agents with the property that, after moving, both agents are again within distance r



If $\|p^{[i]}(\ell) - p^{[j]}(\ell)\| \leq r$, and remain in connectivity set,
 then $\|p^{[i]}(\ell + 1) - p^{[j]}(\ell + 1)\| \leq r$

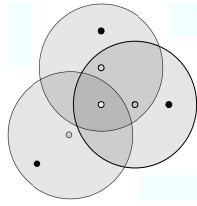
Cortés & Martínez (UCSD) Distributed robotic networks March 17, 2009 12 / 72

Enforcing range-limited links – w/ all neighbors

Definition (Connectivity constraint set)

Consider a group of agents at positions $P = \{p^{[1]}, \dots, p^{[n]}\} \subset \mathbb{R}^d$. The *connectivity constraint set* of agent i with respect to P is

$$\mathcal{X}_{\text{disk}}(p^{[i]}, P) = \bigcap \{ \mathcal{X}_{\text{disk}}(p^{[i]}, q) \mid q \in P \setminus \{p^{[i]}\} \text{ s.t. } \|q - p^{[i]}\|_2 \leq r \}$$



Same procedure over sparser graphs means fewer constraints: e.g., $\mathcal{G}_{\text{LD}}()$ has **same connected components** as $\mathcal{G}_{\text{disk}}(r)$ and is **spatially distributed** over $\mathcal{G}_{\text{disk}}(r)$

Cortés & Martínez (UCSD) Distributed robotic networks March 17, 2009 13 / 72

Enforcing range-limited line-of-sight links – w/ all neighbors

Definition (Line-of-sight connectivity constraint set)

Consider a group of agents at positions $P = \{p^{[1]}, \dots, p^{[n]}\}$ in a nonconvex allowable environment Q_δ . The *line-of-sight connectivity constraint sets* of agent i with respect to P is

$$\mathcal{X}_{\text{vis-disk}}(p^{[i]}, P; Q_\delta) = \bigcap \{ \mathcal{X}_{\text{vis-disk}}(p^{[i]}, q; Q_\delta) \mid q \in P \setminus \{p^{[i]}\} \}$$

Fewer constraints can be generated via sparser graphs with the same connected components and spatially distributed over

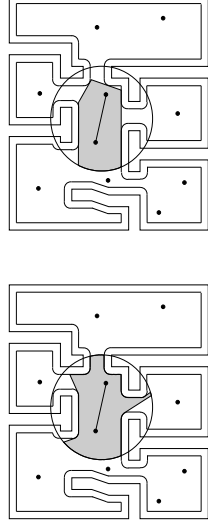
Cortés & Martínez (UCSD) Distributed robotic networks March 17, 2009 15 / 72

Enforcing range-limited line-of-sight links – pairwise

For $Q_\delta = \{q \in Q \mid \text{dist}(q, \partial Q) \geq \delta\}$ δ -contraction of compact nonconvex $Q \subset \mathbb{R}^2$

Pairwise connectivity maintenance problem:

Given two neighbors in $\mathcal{G}_{\text{vis-disk}, Q_\delta}$, find a rich set of control inputs for both agents with the property that, after moving, both agents are again within distance r and visible to each other in Q_δ



visibility region of agent i visibility pairwise constraint set

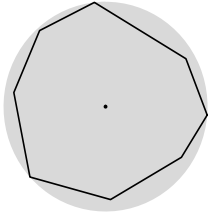
Cortés & Martínez (UCSD) Distributed robotic networks March 17, 2009 14 / 72

Outline

- 1 **Rendezvous and connectivity maintenance**
 - The rendezvous objective
 - Maintaining connectivity
 - Circumcenter algorithms
 - Correctness analysis via nondeterministic systems
- 2 **Deployment**
 - Expected-value deployment
 - Geometric-center laws
 - Disk-covering and sphere-packing deployment
 - Geometric-center laws
- 3 **Conclusions**

Cortés & Martínez (UCSD) Distributed robotic networks March 17, 2009 16 / 72

Circumcenter control and communication law



For $X = \mathbb{R}^d$, $X = \mathbb{S}^d$ or $X = \mathbb{R}^{d_1} \times \mathbb{S}^{d_2}$, $d = d_1 + d_2$, **circumcenter** $CC(W)$ of a bounded set $W \subset X$ is center of closed ball of minimum radius that contains W

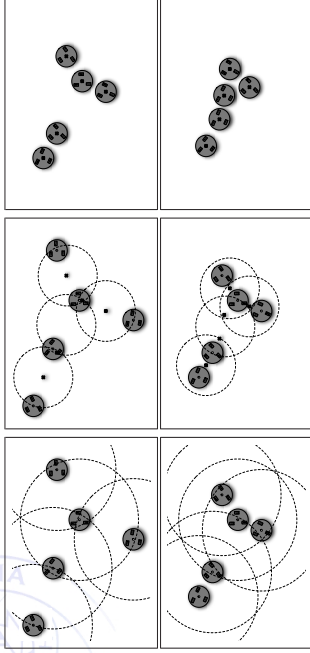
Circumradius $CR(W)$ is radius of this ball

[Informal description:]

At each communication round each agent performs the following tasks: (i) it transmits its position and receives its neighbors' positions; (ii) it computes the circumcenter of the point set comprised of its neighbors and of itself. Between communication rounds, each robot moves toward this circumcenter point while maintaining connectivity with its neighbors using appropriate connectivity constraint sets.

Circumcenter control and communication law

Illustration of the algorithm execution



Circumcenter control and communication law

Formal algorithm description

Robotic Network: $\mathcal{S}_{\text{disk}}$ with a discrete-time motion model, with absolute sensing of own position, and with communication range r , in \mathbb{R}^d

Distributed Algorithm: circumcenter

Alphabet: $L = \mathbb{R}^d \cup \{\text{null}\}$

function $\text{msg}(p, i)$

1: **return** p

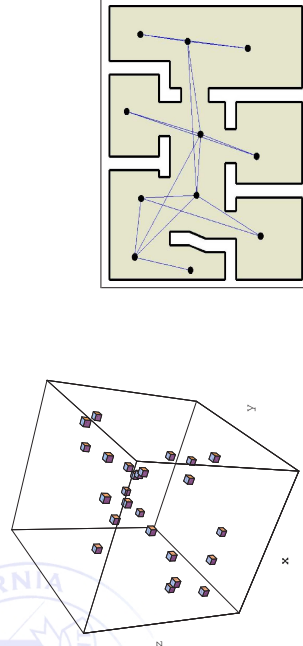
function $\text{ctrl}(p, y)$

1: $p_{\text{goal}} := CC(\{p\} \cup \{p_{\text{revd}} \mid \text{for all non-null } p_{\text{revd}} \in y\})$

2: $\mathcal{X} := \mathcal{X}_{\text{disk}}(p, \{p_{\text{revd}} \mid \text{for all non-null } p_{\text{revd}} \in y\})$

3: **return** $\text{fti}(p, p_{\text{goal}}, \mathcal{X}) - p$

Simulations



Outline

1 Rendezvous and connectivity maintenance

- The rendezvous objective
- Maintaining connectivity
- Circumcenter algorithms
- Correctness analysis via nondeterministic systems

2 Deployment

- Expected-value deployment
- Geometric-center laws
- Disk-covering and sphere-packing deployment
- Geometric-center laws

3 Conclusions

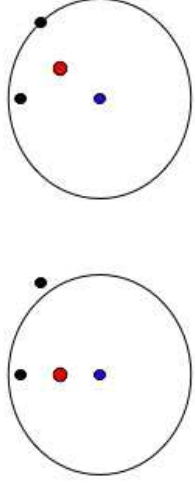
Some bad news...

Circumcenter algorithms are nonlinear discrete-time dynamical systems

$$x_{\ell+1} = f(x_\ell)$$

To analyze convergence, we need at least f continuous – to use classic Lyapunov/LaSalle results

But circumcenter algorithms are discontinuous because of changes in interaction topology

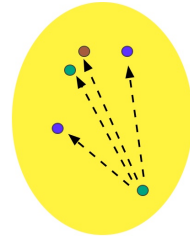


Alternative idea

Fixed undirected graph G , define **fixed-topology circumcenter algorithm**

$$f_G : (\mathbb{R}^d)^n \rightarrow (\mathbb{R}^d)^n, \quad f_{G,i}(p_1, \dots, p_n) = \text{fti}(p, p_{\text{goal}}, \mathcal{X}) - p$$

Now, there are no topological changes in f_G , hence f_G is **continuous**



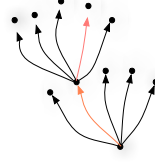
Define set-valued map $T_{fc} : (\mathbb{R}^d)^n \rightarrow \mathcal{P}((\mathbb{R}^d)^n)$

$$T_{fc}(p_1, \dots, p_n) = \{f_G(p_1, \dots, p_n) \mid G \text{ connected}\}$$

Non-deterministic dynamical systems

Given $T : X \rightarrow \mathcal{P}(X)$, a **trajectory** of T is sequence $\{x_m\}_{m \in \mathbb{N}_0} \subset X$ such that

$$x_{m+1} \in T(x_m), \quad m \in \mathbb{N}_0$$



T is **closed** at x if $x_m \rightarrow x, y_m \rightarrow y$ with $y_m \in T(x_m)$ imply $y \in T(x)$
Every continuous map $T : \mathbb{R}^d \rightarrow \mathbb{R}^d$ is closed on \mathbb{R}^d

A set C is

- **weakly positively invariant** if, for any $p_0 \in C$, there exists $p \in T(p_0)$ such that $p \in C$
- **strongly positively invariant** if, for any $p_0 \in C$, all $p \in T(p_0)$ verifies $p \in C$

A point p_0 is a **fixed point** of T if $p_0 \in T(p_0)$

LaSalle Invariance Principle – set-valued maps

$V : X \rightarrow \mathbb{R}$ is non-increasing along T on $S \subset X$ if

$$V(x') \leq V(x) \text{ for all } x' \in T(x) \text{ and all } x \in S$$

Theorem (LaSalle Invariance Principle)

For S compact and strongly invariant with V continuous and non-increasing along closed T on S
 Any trajectory starting in S converges to largest weakly invariant set contained in $\{x \in S \mid \exists x' \in T(x) \text{ with } V(x') = V(x)\}$

Cortés & Martínez (UCSD)

March 17, 2009

25 / 72

Correctness via LaSalle Invariance Principle

To recap

- T_{CC} is closed
- $V = \text{diam}$ is non-increasing along T_{CC}
- Evolution starting from P_0 is contained in $\text{co}(P_0)$ (compact and strongly invariant)

Application of **LaSalle Invariance Principle**: trajectories starting at P_0 converge to M , largest weakly positively invariant set contained in

$$\{P \in \text{co}(P_0) \mid \exists P' \in T_{CC}(P) \text{ such that } \text{diam}(P') = \text{diam}(P)\}$$

Have to **identify** M ! In fact, $M = \text{diag}((\mathbb{R}^d)^n) \cap \text{co}(P_0)$

Convergence to a point can be concluded with a little bit of extra work

Cortés & Martínez (UCSD)

March 17, 2009

27 / 72

Correctness

T_{CC} is closed and diameter is non-increasing

Recall set-valued map $T_{CC} : (\mathbb{R}^d)^n \rightarrow \mathcal{P}((\mathbb{R}^d)^n)$

$$T_{CC}(p_1, \dots, p_n) = \{f_{\mathcal{G}}(p_1, \dots, p_n) \mid \mathcal{G} \text{ connected}\}$$

T_{CC} is closed: finite combination of individual continuous maps
 Define

$$V_{\text{diam}}(P) = \text{diam}(\text{co}(P)) = \max \{\|p_i - p_j\| \mid i, j \in \{1, \dots, n\}\}$$

$$\text{diag}((\mathbb{R}^d)^n) = \{(p, \dots, p) \in (\mathbb{R}^d)^n \mid p \in \mathbb{R}^d\}$$

Lemma

The function $V_{\text{diam}} = \text{diam} \circ \text{co} : (\mathbb{R}^d)^n \rightarrow \mathbb{R}_+$ verifies:

- V_{diam} is continuous and invariant under permutations;
- $V_{\text{diam}}(P) = 0$ if and only if $P \in \text{diag}((\mathbb{R}^d)^n)$;
- V_{diam} is non-increasing along T_{CC}

Cortés & Martínez (UCSD)

March 17, 2009

26 / 72

Correctness

Theorem (Correctness of the circumcenter laws)

For $d \in \mathbb{N}$, $r \in \mathbb{R}_{>0}$ and $\epsilon \in \mathbb{R}_{>0}$, the following statements hold:

- on S_{disk} , the law $CC_{\text{circumcenter}}$ (with control magnitude bounds and relaxed \mathcal{G} -connectivity constraints) achieves $\mathcal{T}_{\text{rendezvous}}$;
- on S_{LD} , the law $CC_{\text{circumcenter}}$ achieves $\mathcal{T}_{\epsilon\text{-rendezvous}}$

Furthermore,

- if any two agents belong to the same connected component at $\ell \in \mathbb{N}_0$, then they continue to belong to the same connected component subsequently; and
- for each evolution, there exists $P^* = (p_1^*, \dots, p_n^*) \in (\mathbb{R}^d)^n$ such that:
 - the evolution asymptotically approaches P^* , and
 - for each $i, j \in \{1, \dots, n\}$, either $p_i^* = p_j^*$, or $\|p_i^* - p_j^*\|_2 > r$ (for the networks S_{disk} and S_{LD}) or $\|p_i^* - p_j^*\|_\infty > r$ (for the network $S_{\infty\text{-disk}}$).

Similar result for visibility networks in non-convex environments

Cortés & Martínez (UCSD)

March 17, 2009

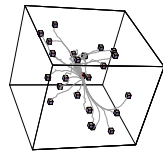
28 / 72

Correctness – Time complexity

Theorem (Time complexity of circumcenter laws)

For $r \in \mathbb{R}_{>0}$ and $\epsilon \in]0, 1[$, the following statements hold:

- on the network $\mathcal{S}_{\text{disk}}$, evolving on the real line \mathbb{R} (i.e., with $d = 1$), $\text{TC}(\mathcal{I}_{\text{rendezvous}}, \mathcal{CC}_{\text{circumcenter}}) \in \Theta(n)$;
- on the network \mathcal{S}_{LD} , evolving on the real line \mathbb{R} (i.e., with $d = 1$), $\text{TC}(\mathcal{I}_{\text{rc-rendezvous}}, \mathcal{CC}_{\text{circumcenter}}) \in \Theta(n^2 \log(n\epsilon^{-1}))$; and



Similar results for visibility networks

Cortés & Martínez (UCSD) Distributed robotic networks March 17, 2009 29 / 72

Rendezvous

Corollary (Circumcenter algorithm over $\mathcal{G}_{\text{disk}}(r)$ on \mathbb{R}^d)

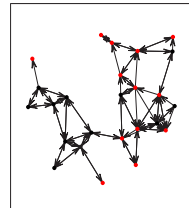
For $\{P_m\}_{m \in \mathbb{N}_0}$ synchronous execution with link failures such that union of any $\ell \in \mathbb{N}$ consecutive graphs in execution has globally reachable node

Then, there exists $(p^*, \dots, p^*) \in \text{diag}((\mathbb{R}^d)^n)$ such that

$$P_m \rightarrow (p^*, \dots, p^*) \text{ as } m \rightarrow +\infty$$

Proof uses

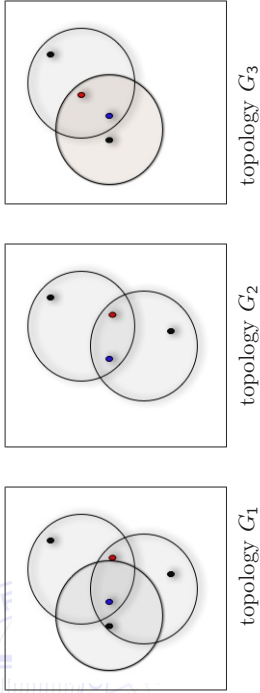
$$T_{\mathcal{CC}, \ell}(P) = \{f_{\mathcal{G}_\ell} \circ \dots \circ f_{\mathcal{G}_1}(P) \mid \cup_{s=1}^\ell \mathcal{G}_s \text{ has globally reachable node}\}$$



Cortés & Martínez (UCSD) Distributed robotic networks March 17, 2009 31 / 72

Robustness of circumcenter algorithms

Push whole idea further!, e.g., for robustness against link failures



Look at **evolution under link failures** as outcome of nondeterministic evolution under multiple interaction topologies

$$P \longrightarrow \{\text{evolution under } G_1, \text{evolution under } G_2, \text{evolution under } G_3\}$$

Cortés & Martínez (UCSD) Distributed robotic networks March 17, 2009 30 / 72

Outline

- 1 Rendezvous and connectivity maintenance
 - The rendezvous objective
 - Maintaining connectivity
 - Circumcenter algorithms
 - Correctness analysis via nondeterministic systems
- 2 Deployment
 - Expected-value deployment
 - Geometric-center laws
 - Disk-covering and sphere-packing deployment
 - Geometric-center laws
- 3 Conclusions

Cortés & Martínez (UCSD) Distributed robotic networks March 17, 2009 32 / 72

Deployment

Objective: optimal task allocation and space partitioning
optimal placement and tuning of sensors



What notion of optimality? What algorithm design?

- **top-down approach:** define aggregate function measuring “goodness” of deployment, then synthesize algorithm that optimizes function
- **bottom-up approach:** synthesize “reasonable” interaction law among agents, then analyze network behavior

Cortés & Martínez (UCSD)

Distributed robotic networks

March 17, 2009

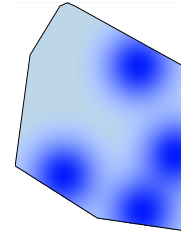
35 / 72

Expected-value multicenter function

Objective: Given sensors/nodes/robots/sites (p_1, \dots, p_n) moving in environment Q achieve **optimal coverage**

$\phi: \mathbb{R}^d \rightarrow \mathbb{R}_{\geq 0}$ density

$f: \mathbb{R}_{\geq 0} \rightarrow \mathbb{R}$ non-increasing and piecewise continuously differentiable, possibly with finite jump discontinuities



$$\text{maximize } \mathcal{H}_{\text{exp}}(p_1, \dots, p_n) = E_{\phi} \left[\max_{i \in \{1, \dots, n\}} f(\|q - p_i\|) \right]$$

Cortés & Martínez (UCSD)

Distributed robotic networks

March 17, 2009

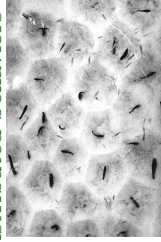
35 / 72

Coverage optimization

DESIGN of performance metrics

- how to cover a region with n minimum-radius overlapping disks?
- how to design a minimum-distortion (fixed-rate) vector quantizer? (Lloyd '57)
- where to place mailboxes in a city / cache servers on the internet?

ANALYSIS of cooperative distributed behaviors



Barlow, Hexagonal territories, *Animal Behaviour*, 1974

- how do animals share territory? what if every fish in a swarm goes toward center of own dominance region?
- what if each vehicle goes to center of mass of own Voronoi cell?
- what if each vehicle moves away from closest vehicle?

Cortés & Martínez (UCSD)

Distributed robotic networks

March 17, 2009

34 / 72

\mathcal{H}_{exp} -optimality of the Voronoi partition

Alternative expression in terms of Voronoi partition,

$$\mathcal{H}_{\text{exp}}(p_1, \dots, p_n) = \sum_{i=1}^n \int_{V_i(P)} f(\|q - p_i\|_2) \phi(q) dq$$

for (p_1, \dots, p_n) distinct

Proposition

Let $P = \{p_1, \dots, p_n\} \in \mathbb{F}(S)$. For any performance function f and for any partition $\{W_1, \dots, W_n\} \subset \mathcal{P}(S)$ of S ,

$$\mathcal{H}_{\text{exp}}(p_1, \dots, p_n, V_1(P), \dots, V_n(P)) \geq \mathcal{H}_{\text{exp}}(p_1, \dots, p_n, W_1, \dots, W_n),$$

and the inequality is strict if any set in $\{W_1, \dots, W_n\}$ differs from the corresponding set in $\{V_1(P), \dots, V_n(P)\}$ by a set of positive measure

Cortés & Martínez (UCSD)

Distributed robotic networks

March 17, 2009

36 / 72

Distortion problem

$$f(x) = -x^2$$

$$\mathcal{H}_{\text{dist}}(p_1, \dots, p_n) = -\sum_{i=1}^n \int_{V_i(P)} \|q - p_i\|_2^2 \phi(q) dq = -\sum_{i=1}^n \int_{V_i(P)} J_\phi(V_i(P), p_i)$$

($J_\phi(W, p)$ is moment of inertia). Note

$$\begin{aligned} \mathcal{H}_{\text{dist}}(p_1, \dots, p_n, W_1, \dots, W_n) \\ = -\sum_{i=1}^n \int_{V_i(P)} J_\phi(W_i, \text{CM}_\phi(W_i)) - \sum_{i=1}^n \text{area}_\phi(W_i) \phi \|p_i - \text{CM}_\phi(W_i)\|_2^2 \end{aligned}$$

Proposition

Let $\{W_1, \dots, W_n\} \subset \mathcal{P}(S)$ be a partition of S . Then,

$$\begin{aligned} \mathcal{H}_{\text{dist}}(\text{CM}_\phi(W_1), \dots, \text{CM}_\phi(W_n), W_1, \dots, W_n) \\ \geq \mathcal{H}_{\text{dist}}(p_1, \dots, p_n, W_1, \dots, W_n), \end{aligned}$$

and the inequality is strict if there exists $i \in \{1, \dots, n\}$ for which W_i has

non-vanishing area and $p_i \neq \text{CM}_\phi(W_i)$

Cortés & Martínez (UCSD) Distributed robotic networks March 17, 2009 37 / 72

Mixed distortion-area problem

$$f(x) = -x^2 \mathbf{1}_{[0,a]}(x) + b \cdot \mathbf{1}_{[a,+\infty)}(x), \text{ with } a \in \mathbb{R}_{>0} \text{ and } b \leq -a^2$$

$$\mathcal{H}_{\text{dist-area},a,b}(p_1, \dots, p_n) = -\sum_{i=1}^n \int_{V_i(P)} J_\phi(V_{i,a}(P), p_i) + b \text{area}_\phi(Q \setminus \cup_{i=1}^n \overline{B}(p_i, a)) \phi,$$

If $b = -a^2$, f is continuous, we write $\mathcal{H}_{\text{dist-area},a}$. Extension reads

$$\begin{aligned} \mathcal{H}_{\text{dist-area},a}(p_1, \dots, p_n, W_1, \dots, W_n) \\ = -\sum_{i=1}^n \left(\int_{V_i(P)} J_\phi(W_i \cap \overline{B}(p_i, a), p_i) + a^2 \text{area}_\phi(W_i \cap (S \setminus \overline{B}(p_i, a))) \phi \right). \end{aligned}$$

Proposition ($\mathcal{H}_{\text{dist-area},a}$ -optimality of centroid locations)

Let $\{W_1, \dots, W_n\} \subset \mathcal{P}(S)$ be a partition of S . Then,

$$\begin{aligned} \mathcal{H}_{\text{dist-area},a}(\text{CM}_\phi(W_1 \cap \overline{B}(p_1, a)), \dots, \text{CM}_\phi(W_n \cap \overline{B}(p_n, a)), W_1, \dots, W_n) \\ \geq \mathcal{H}_{\text{dist}}(p_1, \dots, p_n, W_1, \dots, W_n), \end{aligned}$$

and the inequality is strict if there exists $i \in \{1, \dots, n\}$ for which W_i has non-vanishing area and $p_i \neq \text{CM}_\phi(W_i \cap \overline{B}(p_i, a))$.

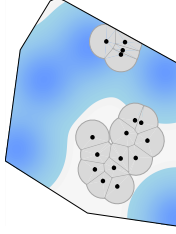
Cortés & Martínez (UCSD) Distributed robotic networks March 17, 2009 39 / 72

Area problem

$$f(x) = \mathbf{1}_{[0,a]}(x), a \in \mathbb{R}_{>0}$$

$$\begin{aligned} \mathcal{H}_{\text{area},a}(p_1, \dots, p_n) &= \sum_{i=1}^n \int_{V_i(P)} \mathbf{1}_{[0,a]}(\|q - p_i\|_2) \phi(q) dq \\ &= \sum_{i=1}^n \int_{V_i(P) \cap \overline{B}(p_i, a)} \phi(q) dq \\ &= \sum_{i=1}^n \text{area}_\phi(V_i(P) \cap \overline{B}(p_i, a)) \phi = \text{area}_\phi(\cup_{i=1}^n \overline{B}(p_i, a)) \phi, \end{aligned}$$

Area, measured according to ϕ , covered by the union of the n balls $\overline{B}(p_1, a), \dots, \overline{B}(p_n, a)$



Cortés & Martínez (UCSD) Distributed robotic networks March 17, 2009 38 / 72

Smoothness properties of \mathcal{H}_{exp}

$\text{Dscn}(f)$ (finite) discontinuities of f
 f_- and f_+ , limiting values from the left and from the right

Theorem

Expected-value multicenter function $\mathcal{H}_{\text{exp}} : S^n \rightarrow \mathbb{R}$ is

- globally Lipschitz on S^n ; and
- continuously differentiable on $S^n \setminus S_{\text{coinc}}$, where

$$\begin{aligned} \frac{\partial \mathcal{H}_{\text{exp}}}{\partial p_i}(P) &= \int_{V_i(P)} \frac{\partial}{\partial p_i} f(\|q - p_i\|_2) \phi(q) dq \\ &\quad + \sum_{a \in \text{Dscn}(f)} (f_-(a) - f_+(a)) \int_{V_i(P) \cap \partial \overline{B}(p_i, a)} n_{\text{out}, \overline{B}(p_i, a)}(q) \phi(q) dq \\ &= \text{integral over } V_i + \text{integral along arcs in } V_i \end{aligned}$$

Therefore, the gradient of \mathcal{H}_{exp} is spatially distributed over \mathcal{G}_D

Cortés & Martínez (UCSD) Distributed robotic networks March 17, 2009 40 / 72

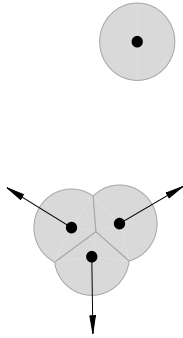
Particular gradients

Distortion problem: continuous performance,

$$\frac{\partial \mathcal{H}_{\text{dist}}}{\partial p_i}(P) = 2 \text{area}_\phi(V_i(P)) \phi(\text{CM}_\phi(V_i(P))) - p_i$$

Area problem: performance has single discontinuity,

$$\frac{\partial \mathcal{H}_{\text{area},a}}{\partial p_i}(P) = \int_{V_i(P) \cap \partial \bar{B}(p_i,a)} n_{\text{out},\bar{B}(p_i,a)}(q) \phi(q) dq$$



Mixed distortion-area: continuous performance ($b = -a^2$),

$$\frac{\partial \mathcal{H}_{\text{dist-area},a}}{\partial p_i}(P) = 2 \text{area}_\phi(V_{i,a}(P)) \phi(\text{CM}_\phi(V_{i,a}(P))) - p_i$$

Cortés & Martínez (UCSD) Distributed robotic networks March 17, 2009 41 / 72

Outline

1 Rendezvous and connectivity maintenance

- The rendezvous objective
- Maintaining connectivity
- Circumcenter algorithms
- Correctness analysis via nondeterministic systems

2 Deployment

- Expected-value deployment
- **Geometric-center laws**
- Disk-covering and sphere-packing deployment
- Geometric-center laws

3 Conclusions

Cortés & Martínez (UCSD) Distributed robotic networks March 17, 2009 43 / 72

Tuning the optimization problem

Gradients of $\mathcal{H}_{\text{area},a}$, $\mathcal{H}_{\text{dist-area},a,b}$ are distributed over $\mathcal{G}_{\text{LD}}(2a)$. Robotic agents with range-limited interactions can compute gradients of $\mathcal{H}_{\text{area},a}$ and $\mathcal{H}_{\text{dist-area},a,b}$ as long as $r \geq 2a$.

Proposition (Constant-factor approximation of $\mathcal{H}_{\text{dist}}$)

Let $S \subset \mathbb{R}^d$ be bounded and measurable. Consider the mixed distortion-area problem with $a \in]0, \text{diam}(S)]$ and $b = -\text{diam}(S)^2$. Then, for all $P \in S^n$,

$$\mathcal{H}_{\text{dist-area},a,b}(P) \leq \mathcal{H}_{\text{dist}}(P) \leq \beta^2 \mathcal{H}_{\text{dist-area},a,b}(P) < 0,$$

where $\beta = \frac{a}{\text{diam}(S)} \in [0, 1]$

Similarly, constant-factor approximations of \mathcal{H}_{exp}

Cortés & Martínez (UCSD) Distributed robotic networks March 17, 2009 42 / 72

Geometric-center laws

Uniform networks \mathcal{S}_D and \mathcal{S}_{LD} of locally-connected first-order agents in a polytope $Q \subset \mathbb{R}^d$ with the Delaunay and r -limited Delaunay graphs as communication graphs

All laws share similar structure

At each communication round each agent performs the following tasks:

- it transmits its position and receives its neighbors' positions;
- it computes a notion of geometric center of its own cell determined according to some notion of partition of the environment

Between communication rounds, each robot moves toward this center

Cortés & Martínez (UCSD) Distributed robotic networks March 17, 2009 44 / 72

VRN-CNTRD ALGORITHM

Optimizes distortion $\mathcal{H}_{\text{dlist}}$

Robotic Network: $\mathcal{S}_{\text{Din}} Q$, with absolute sensing of own position

Distributed Algorithm: VRN-CNTRD

Alphabet: $L = \mathbb{R}^d \cup \{\text{null}\}$

function msg(p, i)

1: **return** p

function ctrl(p, y)

1: $V := Q \cap (\bigcap \{H_{p, p_{\text{evd}}} \mid \text{for all non-null } p_{\text{evd}} \in y\})$

2: **return** $\text{CM}_{\phi}(V) - p$

Cortés & Martínez (UCSD)

Distributed robotic networks

March 17, 2009

45 / 72

Voronoi-centroid law on planar vehicles

Robotic Network: $\mathcal{S}_{\text{vehicles}}$ in Q with absolute sensing of own position

Distributed Algorithm: VRN-CNTRD-DYNAMCS

Alphabet: $L = \mathbb{R}^2 \cup \{\text{null}\}$

function msg($(p, \theta), i$)

1: **return** p

function ctrl($((p, \theta), (p_{\text{smpld}}, \theta_{\text{smpld}}), y)$

1: $V := Q \cap (\bigcap \{H_{p_{\text{smpld}}, p_{\text{evd}}} \mid \text{for all non-null } p_{\text{evd}} \in y\})$

2: $v := -k_{\text{prop}} (\cos \theta, \sin \theta) \cdot (p - \text{CM}_{\phi}(V))$

3: $\omega := 2k_{\text{prop}} \arctan \frac{(-\sin \theta, \cos \theta) \cdot (p - \text{CM}_{\phi}(V))}{(\cos \theta, \sin \theta) \cdot (p - \text{CM}_{\phi}(V))}$

4: **return** (v, ω)

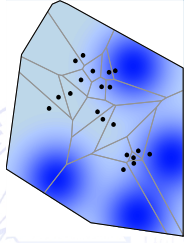
Cortés & Martínez (UCSD)

Distributed robotic networks

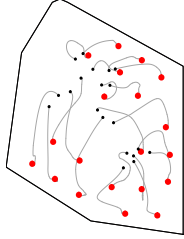
March 17, 2009

47 / 72

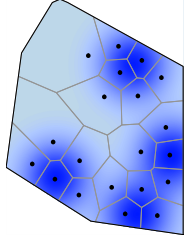
Simulation



initial configuration



gradient descent



final configuration

For $\epsilon \in \mathbb{R}_{>0}$, the ϵ -distortion deployment task

$$\mathcal{T}_{\epsilon\text{-distor-dply}}(P) = \begin{cases} \text{true,} & \text{if } \|p^{[i]} - \text{CM}_{\phi}(V^{[i]}(P))\|_2 \leq \epsilon, \ i \in \{1, \dots, n\}, \\ \text{false,} & \text{otherwise,} \end{cases}$$

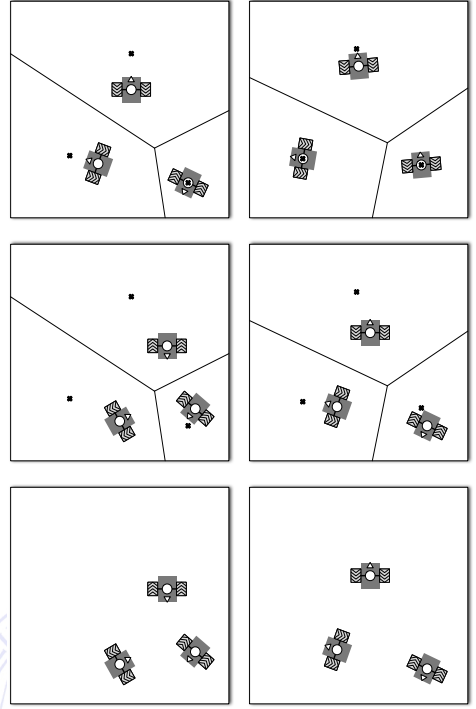
Cortés & Martínez (UCSD)

Distributed robotic networks

March 17, 2009

46 / 72

Algorithm illustration



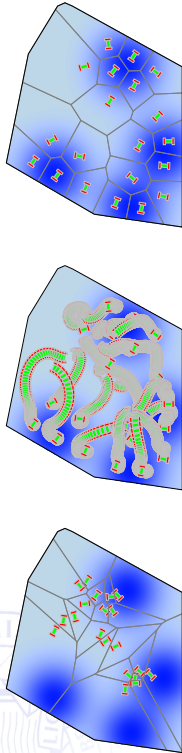
Cortés & Martínez (UCSD)

Distributed robotic networks

March 17, 2009

48 / 72

Simulation



initial configuration

gradient descent

final configuration

Cortés & Martínez (UCSD)

Distributed robotic networks

March 17, 2009

49 / 72

Simulation



initial configuration

gradient descent

final configuration

For $r, \epsilon \in \mathbb{R}_{>0}$,

$$\mathcal{T}_{\epsilon-r\text{-area-dply}}(P) = \begin{cases} \text{true,} & \text{if } \|\int_{V^{[i]}(P) \cap \partial \bar{B}(p^{[i]}, \frac{r}{2})} n_{\text{out}, \bar{B}(p^{[i]}, \frac{r}{2})} (q) \phi(q) dq\|_2 \leq \epsilon, \quad i \in \{1, \dots, n\}, \\ \text{false,} & \text{otherwise.} \end{cases}$$

Cortés & Martínez (UCSD)

Distributed robotic networks

March 17, 2009

51 / 72

LMTD-VRN-NRML algorithm

Optimizes area $\mathcal{H}_{\text{area}, \frac{r}{2}}$

Robotic Network: S_{LD} in Q with absolute sensing of own position and with communication range r

Distributed Algorithm: LMTD-VRN-NRML

Alphabet: $L = \mathbb{R}^d \cup \{\text{null}\}$

function msg(p, i)

1: **return** p

function ctrl(p, y)

1: $V := Q \cap (\bigcap \{H_{p, p_{\text{rcvd}}} \mid \text{for all non-null } p_{\text{rcvd}} \in y\})$

2: $v := \int_{V \cap \partial \bar{B}(p, \frac{r}{2})} n_{\text{out}, \bar{B}(p, \frac{r}{2})} (q) \phi(q) dq$

3: $\lambda_* := \max \left\{ \lambda \mid \delta \mapsto \int_{V \cap \bar{B}(p + \delta v, \frac{r}{2})} \phi(q) dq \text{ is strictly increasing on } [0, \lambda] \right\}$

4: **return** $\lambda_* v$

Cortés & Martínez (UCSD)

Distributed robotic networks

March 17, 2009

50 / 72

LMTD-VRN-CNTRD algorithm

Optimizes $\mathcal{H}_{\text{dist-area}, \frac{r}{2}}$

Robotic Network: S_{LD} in Q with absolute sensing of own position, and with communication range r

Distributed Algorithm: LMTD-VRN-CNTRD

Alphabet: $L = \mathbb{R}^d \cup \{\text{null}\}$

function msg(p, i)

1: **return** p

function ctrl(p, y)

1: $V := Q \cap \bar{B}(p, \frac{r}{2}) \cap (\bigcap \{H_{p, p_{\text{rcvd}}} \mid \text{for all non-null } p_{\text{rcvd}} \in y\})$

2: **return** $\text{CM}_\phi(V) - p$

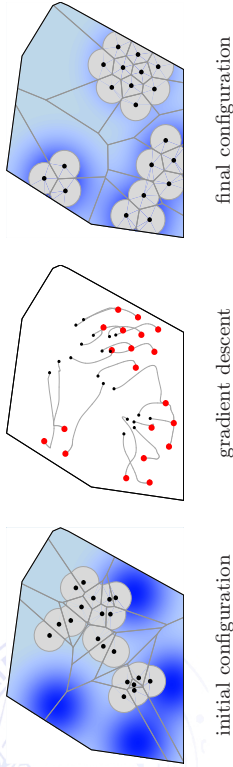
Cortés & Martínez (UCSD)

Distributed robotic networks

March 17, 2009

52 / 72

Simulation



For $r, \epsilon \in \mathbb{R}_{>0}$,

$$\mathcal{T}_{\epsilon-r\text{-distor-area-dply}}(P) = \begin{cases} \text{true,} & \text{if } \|p^{[i]} - \text{CM}_\phi(V_\frac{\epsilon}{2}^{[i]}(P))\|_2 \leq \epsilon, \quad i \in \{1, \dots, n\}, \\ \text{false,} & \text{otherwise.} \end{cases}$$

Cortés & Martínez (UCSD) Distributed robotic networks March 17, 2009 55 / 72

Correctness of the geometric-center algorithms

Theorem

For $d \in \mathbb{N}$, $r \in \mathbb{R}_{>0}$ and $\epsilon \in \mathbb{R}_{>0}$, the following statements hold.

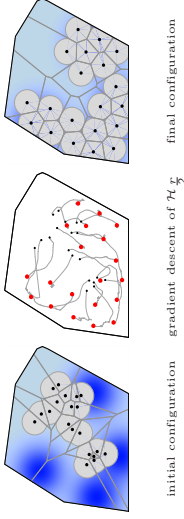
- 1 on the network \mathcal{S}_D , the law $\mathcal{CC}_{\text{VRN-CNTRD-DYNAMICS}}$ and on the network $\mathcal{S}_{\text{vehicles}}$, the law $\mathcal{CC}_{\text{VRN-CNTRD-DYNAMICS}}$ both achieve the ϵ -distortion deployment task $\mathcal{T}_{\epsilon\text{-distor-dply}}$. Moreover, any execution of $\mathcal{CC}_{\text{VRN-CNTRD-DYNAMICS}}$ monotonically optimizes the multicenter function $\mathcal{H}_{\text{dist}}$; $\mathcal{CC}_{\text{VRN-CNTRD-DYNAMICS}}$ monotonically optimizes the multicenter function $\mathcal{H}_{\text{area}, \frac{\epsilon}{2}}$; and
- 2 on the network \mathcal{S}_{LD} , the law $\mathcal{CC}_{\text{LMTD-VRN-NRML}}$ achieves the ϵ - r -area deployment task $\mathcal{T}_{\epsilon-r\text{-area-dply}}$. Moreover, any execution of $\mathcal{CC}_{\text{LMTD-VRN-NRML}}$ monotonically optimizes the multicenter function $\mathcal{H}_{\text{area}, \frac{\epsilon}{2}}$; and
- 3 on the network \mathcal{S}_{LD} , the law $\mathcal{CC}_{\text{LMTD-VRN-CNTRD}}$ achieves the ϵ - r -distortion-area deployment task $\mathcal{T}_{\epsilon-r\text{-distor-area-dply}}$. Moreover, any execution of $\mathcal{CC}_{\text{LMTD-VRN-CNTRD}}$ monotonically optimizes the multicenter function $\mathcal{H}_{\text{dist-area}, \frac{\epsilon}{2}}$.

Cortés & Martínez (UCSD) Distributed robotic networks March 17, 2009 55 / 72

Optimizing $\mathcal{H}_{\text{dist}}$ via constant-factor approximation

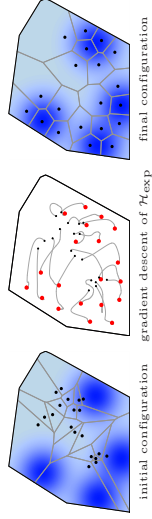
Limited range

run #1: 16 agents, density ϕ is sum of 4 Gaussians, time invariant, 1st order dynamics



Unlimited range

run #2: 16 agents, density ϕ is sum of 4 Gaussians, time invariant, 1st order dynamics



Cortés & Martínez (UCSD) Distributed robotic networks March 17, 2009 54 / 72

Time complexity of $\mathcal{CC}_{\text{LMTD-VRN-CNTRD}}$

Assume $\text{diam}(Q)$ is independent of n , r and ϵ

Theorem (Time complexity of $\mathcal{LMTD-VRN-CNTRD}$ law)

Assume the robots evolve in a closed interval $Q \subset \mathbb{R}$, that is, $d = 1$, and assume that the density is uniform, that is, $\phi \equiv 1$. For $r \in \mathbb{R}_{>0}$ and $\epsilon \in \mathbb{R}_{>0}$, on the network \mathcal{S}_{LD}

$$\text{TC}(\mathcal{T}_{\epsilon-r\text{-distor-area-dply}}, \mathcal{CC}_{\text{LMTD-VRN-CNTRD}}) \in O(n^3 \log(nc^{-1}))$$

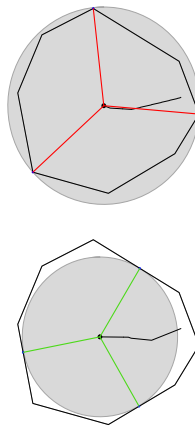
Cortés & Martínez (UCSD) Distributed robotic networks March 17, 2009 56 / 72

Outline

- 1 Rendezvous and connectivity maintenance
 - The rendezvous objective
 - Maintaining connectivity
 - Circumcenter algorithms
 - Correctness analysis via nondeterministic systems
- 2 Deployment
 - Expected-value deployment
 - Geometric-center laws
 - Disk-covering and sphere-packing deployment
 - Geometric-center laws
- 3 Conclusions

Cortés & Martínez (UCSD) Distributed robotic networks March 17, 2009 57 / 72

Deployment: 1-center optimization problems



$$\begin{aligned} \text{sm}_Q(p) &= \min\{\|p - q\| \mid q \in \partial Q\} & \text{Lipschitz} & \quad 0 \in \partial \text{sm}_Q(p) \Leftrightarrow p \in \text{IC}(Q) \\ \text{lg}_Q(p) &= \max\{\|p - q\| \mid q \in \partial Q\} & \text{Lipschitz} & \quad 0 \in \partial \text{lg}_Q(p) \Leftrightarrow p = \text{CC}(Q) \end{aligned}$$

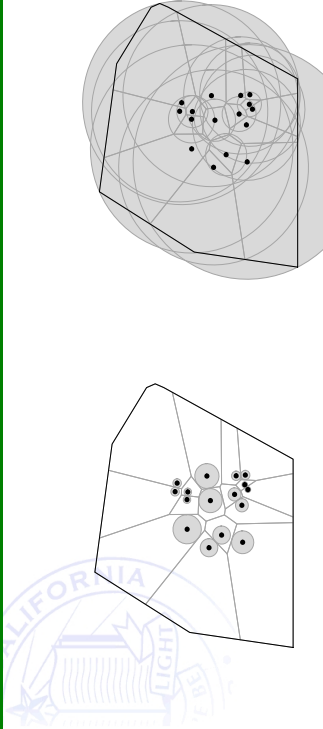
Locally Lipschitz function V are differentiable a.e.

Generalized gradient of V is

$$\partial V(x) = \text{convex closure}\left\{\lim_{i \rightarrow \infty} \nabla V(x_i) \mid x_i \rightarrow x, x_i \notin \Omega_V \cup S\right\}$$

Cortés & Martínez (UCSD) Distributed robotic networks March 17, 2009 59 / 72

Deployment: basic behaviors



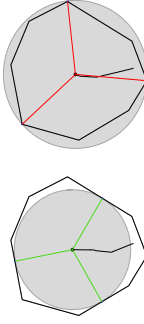
“move away from closest”

“move towards furthest”

Equilibria? Asymptotic behavior?
Optimizing network-wide function?

Cortés & Martínez (UCSD) Distributed robotic networks March 17, 2009 58 / 72

Deployment: 1-center optimization problems



$$\begin{aligned} + \text{gradient flow of } \text{sm}_Q & \quad \dot{p}_i = + \text{Ln}[\partial \text{sm}_Q](p) & \text{“move away from closest”} \\ - \text{gradient flow of } \text{lg}_Q & \quad \dot{p}_i = - \text{Ln}[\partial \text{lg}_Q](p) & \text{“move toward furthest”} \end{aligned}$$

For X essentially locally bounded, Filippov solution of $\dot{x} = X(x)$ is absolutely continuous function $t \in [t_0, t_1] \mapsto x(t)$ verifying

$$\dot{x} \in K[X](x) = \text{co}\left\{\lim_{i \rightarrow \infty} X(x_i) \mid x_i \rightarrow x, x_i \notin S\right\}$$

For V locally Lipschitz, gradient flow is $\dot{x} = \text{Ln}[\partial V](x)$
 $\text{Ln} =$ least norm operator

Cortés & Martínez (UCSD) Distributed robotic networks March 17, 2009 60 / 72

Nonsmooth LaSalle Invariance Principle

Evolution of V along Filippov solution $t \mapsto V(x(t))$ is differentiable a.e.

$$\frac{d}{dt} V(x(t)) \in \underbrace{\tilde{\mathcal{L}}_X V(x(t)) = \{a \in \mathbb{R} \mid \exists v \in K[X](x) \text{ s.t. } \zeta \cdot v = a, \forall \zeta \in \partial V(x)\}}_{\text{set-valued Lie derivative}}$$

LaSalle Invariance Principle

For S compact and strongly invariant with $\max \tilde{\mathcal{L}}_X V(x) \leq 0$

Any Filippov solution starting in S converges to largest weakly invariant set contained in $\{x \in S \mid 0 \in \tilde{\mathcal{L}}_X V(x)\}$

E.g., **nonsmooth gradient flow** $\dot{x} = -\text{Ln}[\partial V](x)$ converges to critical set

Cortés & Martínez (UCSD) Distributed robotic networks March 17, 2009 61 / 72

Deployment: multi-center optimization

Critical points of \mathcal{H}_{sp} and \mathcal{H}_{dc} (locally Lipschitz)

- If $0 \in \text{int } \partial \mathcal{H}_{sp}(P)$, then P is strict local maximum, all agents have same cost, and P is **incenter Voronoi configuration**
- If $0 \in \text{int } \partial \mathcal{H}_{dc}(P)$, then P is strict local minimum, all agents have same cost, and P is **circumcenter Voronoi configuration**

Aggregate functions **monotonically optimized** along evolution

$$\min \tilde{\mathcal{L}}_{\text{Ln}(\partial \text{sm}_{V_0})} \mathcal{H}_{sp}(P) \geq 0$$

$$\max \tilde{\mathcal{L}}_{-\text{Ln}(\partial \text{lg}_{V_0})} \mathcal{H}_{dc}(P) \leq 0$$

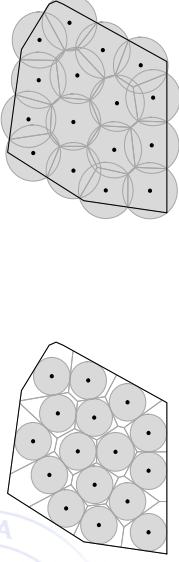
Asymptotic convergence to center Voronoi configurations via nonsmooth LaSalle

Cortés & Martínez (UCSD) Distributed robotic networks March 17, 2009 63 / 72

Deployment: multi-center optimization

sphere packing and disk covering

“move away from closest”: $\dot{p}_i = +\text{Ln}(\partial \text{sm}_{V_i(P)})(p_i)$ — at fixed $V_i(P)$
 “move towards furthest”: $\dot{p}_i = -\text{Ln}(\partial \text{lg}_{V_i(P)})(p_i)$ — at fixed $V_i(P)$



Aggregate objective functions!

$$\mathcal{H}_{sp}(P) = \min_i \text{sm}_{V_i(P)}(p_i) = \min_{i \neq j} \left[\frac{1}{2} \|p_i - p_j\|, \text{dist}(p_i, \partial Q) \right]$$

$$\mathcal{H}_{dc}(P) = \max_i \text{lg}_{V_i(P)}(p_i) = \max_{q \in Q} \left[\min_i \|q - p_i\| \right]$$

Cortés & Martínez (UCSD) Distributed robotic networks March 17, 2009 62 / 72

Outline

- 1 Rendezvous and connectivity maintenance
 - The rendezvous objective
 - Maintaining connectivity
 - Circumcenter algorithms
 - Correctness analysis via nondeterministic systems
- 2 Deployment
 - Expected-value deployment
 - Geometric-center laws
 - Disk-covering and sphere-packing deployment
 - Geometric-center laws
- 3 Conclusions

Cortés & Martínez (UCSD) Distributed robotic networks March 17, 2009 64 / 72

Voronoi-circumcenter algorithm

Robotic Network: S_D in Q with absolute sensing of own position
 Distributed Algorithm: VRN-CRCMCNTR
 Alphabet: $L = \mathbb{R}^d \cup \{\text{null}\}$
 function $\text{msg}(p, i)$
 1: **return** p
 function $\text{ctrl}(p, y)$
 1: $V := Q \cap (\bigcap \{H_{p,p_{\text{rcvd}}} \mid \text{for all non-null } p_{\text{rcvd}} \in y\})$
 2: **return** $\text{CC}(V) - p$

Cortés & Martínez (UCSD) Distributed robotic networks March 17, 2009 65 / 72

Correctness of the geometric-center algorithms

For $\epsilon \in \mathbb{R}_{>0}$, the ϵ -disk-covering deployment task

$$\mathcal{T}_{\epsilon\text{-d-dply}}(P) = \begin{cases} \text{true}, & \text{if } \|p^{[i]} - \text{CC}(V^{[i]}(P))\|_2 \leq \epsilon, i \in \{1, \dots, n\}, \\ \text{false}, & \text{otherwise,} \end{cases}$$

For $\epsilon \in \mathbb{R}_{>0}$, the ϵ -sphere-packing deployment task

$$\mathcal{T}_{\epsilon\text{-sp-dply}}(P) = \begin{cases} \text{true}, & \text{if } \text{dist}_2(p^{[i]}, \text{IC}(V^{[i]}(P))) \leq \epsilon, i \in \{1, \dots, n\}, \\ \text{false}, & \text{otherwise,} \end{cases}$$

Theorem

For $d \in \mathbb{N}$, $r \in \mathbb{R}_{>0}$ and $\epsilon \in \mathbb{R}_{>0}$, the following statements hold.

- on the network S_D , any execution of the law $\text{CC}_{\text{VRN-CRCMCNTR}}$ monotonically optimizes the multicenter function \mathcal{H}_{dc} ;
- on the network S_D , any execution of the law $\text{CC}_{\text{VRN-NCNTR}}$ monotonically optimizes the multicenter function \mathcal{H}_{sp} .

Cortés & Martínez (UCSD) Distributed robotic networks March 17, 2009 67 / 72

Voronoi-incenter algorithm

Robotic Network: S_D in Q with absolute sensing of own position
 Distributed Algorithm: VRN-NCNTR
 Alphabet: $L = \mathbb{R}^d \cup \{\text{null}\}$
 function $\text{msg}(p, i)$
 1: **return** p
 function $\text{ctrl}(p, y)$
 1: $V := Q \cap (\bigcap \{H_{p,p_{\text{rcvd}}} \mid \text{for all non-null } p_{\text{rcvd}} \in y\})$
 2: **return** $x \in \text{IC}(V) - p$

Cortés & Martínez (UCSD) Distributed robotic networks March 17, 2009 66 / 72

Summary and conclusions

Examined three basic motion coordination tasks

- **rendezvous**: circumcenter algorithms
- **connectivity maintenance**: flexible constraint sets in convex/nonconvex scenarios
- **deployment**: gradient algorithms based on geometric centers

Correctness and (1-d) complexity analysis of geometric-center control and communication laws via

- Discrete- and continuous-time nondeterministic dynamical systems
- Invariance principles, stability analysis
- Geometric structures and geometric optimization

Cortés & Martínez (UCSD) Distributed robotic networks March 17, 2009 68 / 72

Motion coordination is emerging discipline

Literature is full of exciting problems, solutions, and tools we have not covered

Formation control, consensus, cohesiveness, flocking, collective synchronization, boundary estimation, cooperative control over constant graphs, quantization, asynchronism, delays, distributed estimation, spatial estimation, data fusion, target tracking, networks with minimal capabilities, target assignment, vehicle dynamics and energy-constrained motion, vehicle routing, dynamic servicing problems, load balancing, robotic implementations,...

Too long a list to fit it here!

Cortés & Martínez (UCSD) Distributed robotic networks March 17, 2009 69 / 72

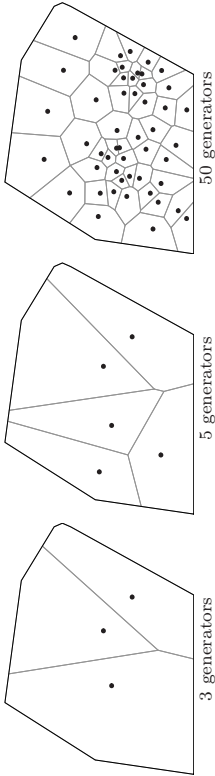
Voronoi partitions

Let $(p_1, \dots, p_n) \in Q^n$ denote the positions of n points

The **Voronoi partition** $\mathcal{V}(P) = \{V_1, \dots, V_n\}$ generated by (p_1, \dots, p_n)

$$V_i = \{q \in Q \mid \|q - p_i\| \leq \|q - p_j\|, \forall j \neq i\}$$

$$V_i = Q \cap_j \mathcal{HP}(p_i, p_j) \quad \text{where } \mathcal{HP}(p_i, p_j) \text{ is half plane } (p_i, p_j)$$



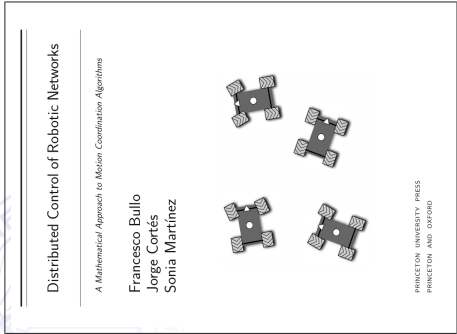
Return

Cortés & Martínez (UCSD) Distributed robotic networks March 17, 2009 71 / 72

Book coming out in June 2009

Freely available online (forever) at www.coordinationbook.info

- Self-contained exposition of graph-theoretic concepts, distributed algorithms, and complexity measures
- Detailed treatment of averaging and consensus algorithms interpreted as linear iterations
- Introduction of geometric notions such as partitions, proximity graphs, and multicenter functions
- Detailed treatment of motion coordination algorithms for deployment, rendezvous, connectivity maintenance, and boundary estimation

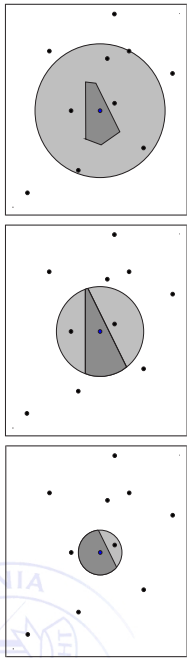


Cortés & Martínez (UCSD) Distributed robotic networks March 17, 2009 70 / 72

Distributed Voronoi computation

Assume: agent with sensing/communication radius R_i

Objective: smallest R_i which provides sufficient information for V_i



For all i , agent i performs:

- 1: initialize R_i and compute $\hat{V}_i = \bigcap_{j: \|p_i - p_j\| \leq R_i} \mathcal{HP}(p_i, p_j)$
- 2: **while** $R_i < 2 \max_{q \in \hat{V}_i} \|p_i - q\|$ **do**
- 3: $R_i := 2R_i$
- 4: detect vehicles p_j within radius R_i , recompute \hat{V}_i

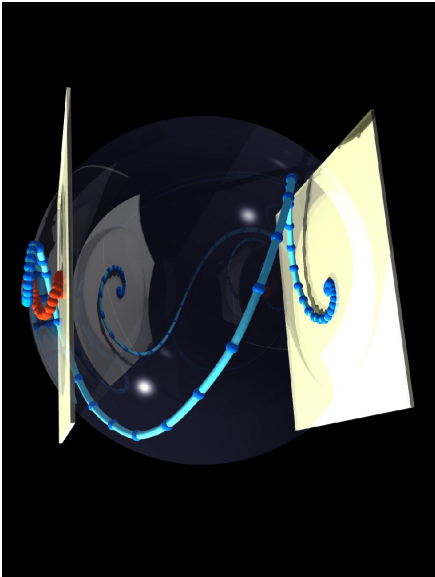
Return

Cortés & Martínez (UCSD) Distributed robotic networks March 17, 2009 72 / 72

Control of ensembles

Navin Khaneja (Harvard University, USA)

Control of Ensembles



Bilinear Control Systems and Control of Quantum Dynamics

$$\hbar \frac{d}{dt} |\psi(t)\rangle = -iH(t) |\psi(t)\rangle$$

$$\frac{dU(t)}{dt} = -i[H_d + \sum_{j=1}^m u_j H_j]U(t); \quad U(0) = I$$

$$\rho(t) = \frac{1}{N} \sum_j |\psi_j(t)\rangle \langle \psi_j(t)|$$

$$\frac{d}{dt} \rho(t) = -\frac{i}{\hbar} [H(t), \rho(t)]; \quad \rho(t) = U(t) \rho(0) U^\dagger(t)$$

$$\frac{d}{dt} \rho(t) = -i[H_0 + f(t)H_1, \rho(t)];$$

$$\frac{d}{dt} \rho(t) = -i[H_0, \rho(t)] + [H_1[H_1, \rho]]$$

“Stochastic Control of Quantum Ensembles”,
R.W. Brockett and N. Khaneja (1999)

Reachable Sets of Quantum Systems in Presence of Decoherence

$$\dot{\rho} = -i[H_d + \sum_{j=1}^n u_j H_j, \rho] + L(\rho)$$

What is the reachable set of a given initial density matrix

Time Optimal Control of Quantum Systems

$$\frac{dU(t)}{dt} = -i[H_d + \sum_{j=1}^m u_j H_j]U(t); \quad U(0) = I$$

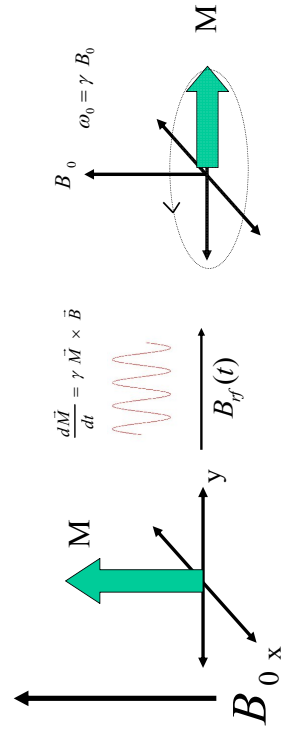
What is the minimum time required to steer the propagator to U_f

Control of Inhomogeneous Quantum Ensembles

$$H(t, s) = H_d(s) + \sum_j u_j(t) H_j(s)$$

Robust Control of Inhomogeneous Spin Ensembles

$$\frac{d}{dt} \begin{pmatrix} x \\ y \\ z \end{pmatrix} = \begin{pmatrix} 0 & -\Delta\omega & -\varepsilon u(t) \\ \Delta\omega & 0 & -\varepsilon v(t) \\ \varepsilon u(t) & \varepsilon v(t) & 0 \end{pmatrix} \begin{pmatrix} x \\ y \\ z \end{pmatrix} \quad \begin{aligned} \sqrt{u^2 + v^2} &\leq A \\ \varepsilon &\in [1 - \delta, 1 + \delta] \end{aligned}$$



Control Design by Area Generation

$$\frac{dX}{dt} = \varepsilon [u(t)\Omega_x + v(t)\Omega_y] X$$



$$U_\varepsilon(\Delta t) = \exp(-\varepsilon\Omega_y\Delta t) \exp(-\varepsilon\Omega_x\Delta t) \exp(\varepsilon\Omega_y\Delta t) \exp(\varepsilon\Omega_x\Delta t)$$

$$\approx I + (\Delta t)^2 \underbrace{[\varepsilon\Omega_x, \varepsilon\Omega_y]}_{\varepsilon^2\Omega_z}$$

$$\begin{aligned} U_\varepsilon(-\sqrt{\Delta t}) \exp(-\varepsilon\Omega_x\Delta t) U_\varepsilon(\sqrt{\Delta t}) \exp(\varepsilon\Omega_x\Delta t) \\ \approx I + (\Delta t)^2 \underbrace{[\varepsilon\Omega_x, \underbrace{[\varepsilon\Omega_x, \varepsilon\Omega_y]}_{-\varepsilon^3\Omega_y}]}_{-\varepsilon^2\Omega_z} \end{aligned}$$

Fourier Synthesis Methods for Robust Control Design

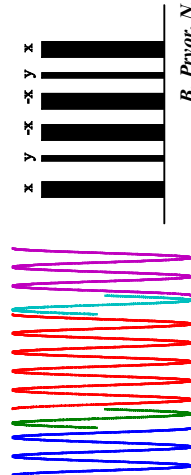
$$U_1 = \exp(k\pi\varepsilon\Omega_x) \exp(\varepsilon\frac{\beta_k}{2}\Omega_y) \exp(-k\pi\varepsilon\Omega_x)$$

$$= \exp(\varepsilon\frac{\beta_k}{2}(\cos(k\pi\varepsilon)\Omega_y + \sin(k\pi\varepsilon)\Omega_z))$$

$$U_2 = \exp(-k\pi\varepsilon\Omega_x) \exp(\varepsilon\frac{\beta_k}{2}\Omega_y) \exp(k\pi\varepsilon\Omega_x)$$

$$= \exp(\varepsilon\frac{\beta_k}{2}(\cos(k\pi\varepsilon)\Omega_y - \sin(k\pi\varepsilon)\Omega_z))$$

$$U_1 U_2 = \exp(\varepsilon\beta_k \cos(k\pi\varepsilon)\Omega_y)$$



B. Pryor, N. Khaneja *Journal of Chemical Physics* (2006).

Lie Algebras and Polynomial Approximations

Using $\varepsilon\Omega_y, \varepsilon^3\Omega_y, \dots, \varepsilon^{2k+1}\Omega_y$ as generators

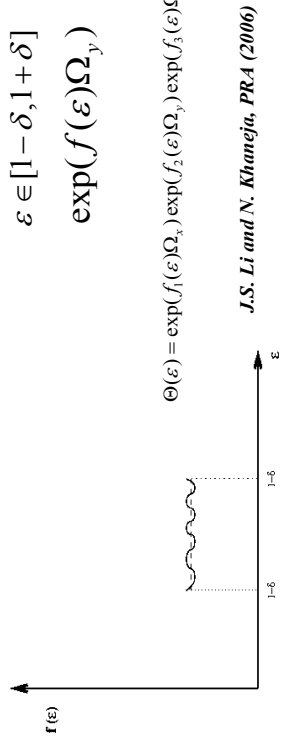
$$f(\varepsilon) = \sum_k c_k \varepsilon^{2k+1}$$

Choose $f(\varepsilon)$ such that it is approx. constant for

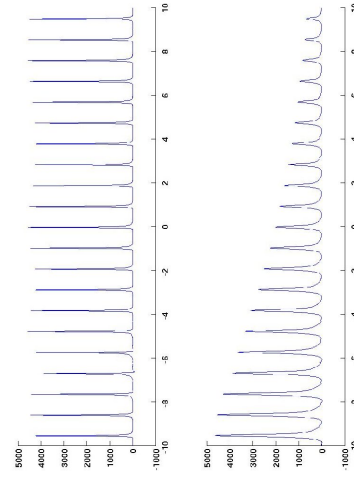
$$\varepsilon \in [1-\delta, 1+\delta]$$

$$\exp(f(\varepsilon)\Omega_y)$$

$$\Theta(\varepsilon) = \exp(f_1(\varepsilon)\Omega_x) \exp(f_2(\varepsilon)\Omega_y) \exp(f_3(\varepsilon)\Omega_x)$$



Fourier Synthesis Methods for Robust Control



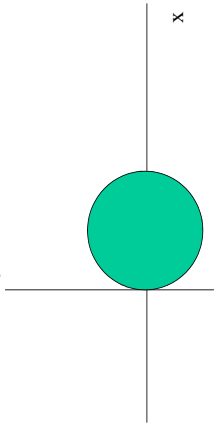
NMR spectra at proton frequency of 500 MHz

Some Negative Results

Nil-Potent Systems Cannot be Compensated

$$\frac{d}{dt} \begin{bmatrix} x \\ y \\ z \end{bmatrix} = \varepsilon u(t) \underbrace{\begin{bmatrix} 1 & 0 \\ 0 & -\gamma \end{bmatrix}}_f + \varepsilon v(t) \underbrace{\begin{bmatrix} 0 & 1 \\ 1 & x \end{bmatrix}}_g$$

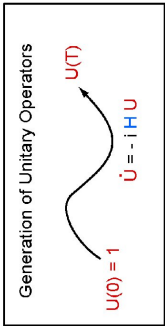
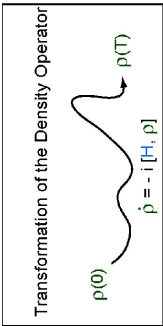
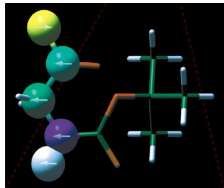
$$[f, g] = \begin{bmatrix} 0 \\ 0 \\ 1 \end{bmatrix}$$



Reachable sets of open quantum systems

$$\dot{\rho} = -i[H_d + \sum_{j=1}^n u_j H_j, \rho] + L(\rho)$$

What is the reachable set of a given initial density matrix in the presence of decoherence



$$\frac{dU(t)}{dt} = -i[H_d + \sum_{j=1}^n u_j H_j]U(t); \quad U(0) = I$$

Some Negative Results

Linear systems cannot be compensated for dispersion in control input

$$\frac{dX}{dt} = AX + \varepsilon Bu$$

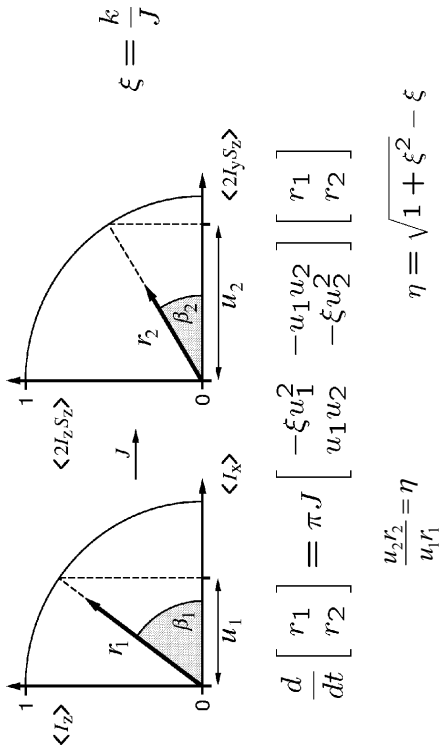
$$X(t) = e^{At} X(0) + \varepsilon \int e^{A(t-\tau)} B(\tau) u(\tau) d\tau$$

Optimal Control in the Presence of Relaxation

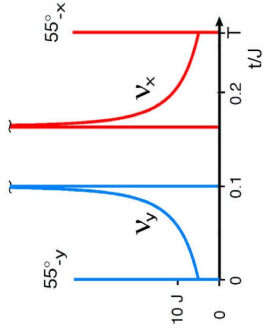
$$\frac{d}{dt} \begin{bmatrix} \langle I_z \rangle \\ \langle I_x \rangle \\ \langle 2I_y S_z \rangle \\ \langle 2I_z S_z \rangle \end{bmatrix} = \begin{bmatrix} 0 & -u(t) \\ u(t) & \boxed{\begin{matrix} -k & -J \\ J & -k \end{matrix}} \\ -v(t) & 0 \end{bmatrix} \begin{bmatrix} \langle I_z \rangle \\ \langle I_x \rangle \\ \langle 2I_y S_z \rangle \\ \langle 2I_z S_z \rangle \end{bmatrix} \quad \begin{matrix} k \\ \xi \end{matrix} = \frac{1}{J}$$

$$\begin{bmatrix} 1 & 0 & 0 & 0 \\ 0 & 0 & 0 & 0 \\ 0 & 0 & 0 & 0 \\ 0 & 0 & 0 & \eta \end{bmatrix} \rightarrow \begin{matrix} \eta = \sqrt{1 + \xi^2} - \xi \\ \frac{x_3}{x_2} = \frac{\langle 2I_y S_z \rangle}{\langle I_x \rangle} = \eta \end{matrix}$$

Reduced Control System



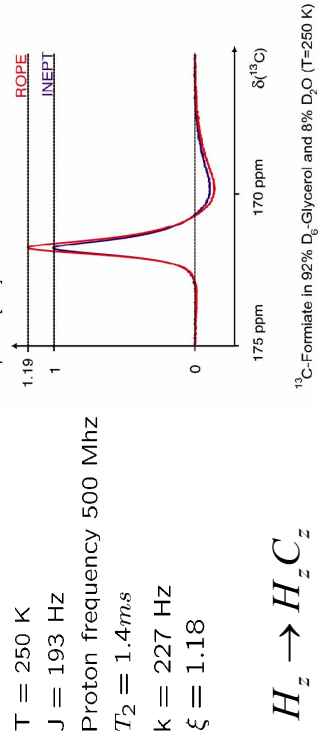
ROPE Pulse Sequence



Khaneja, Reiss, Luy, Glaser JMR(2003)

$$\frac{d}{dt} \begin{bmatrix} \langle I_z \rangle \\ \langle I_x \rangle \\ \langle I_y \rangle \\ \langle 2I_x S_z \rangle \\ \langle 2I_y S_z \rangle \end{bmatrix} = \begin{bmatrix} 0 & -u(t) & -J \\ u(t) & -k & -J \\ J & -k & -v(t) \\ v(t) & 0 & 0 \end{bmatrix} \begin{bmatrix} \langle I_z \rangle \\ \langle I_x \rangle \\ \langle I_y \rangle \\ \langle 2I_x S_z \rangle \\ \langle 2I_y S_z \rangle \end{bmatrix}$$

Experimental Results



$$H_z \rightarrow H_z C_z$$

Khaneja, Reiss, Luy, Glaser JMR(2003)

Computing Reachable Sets

$$\frac{d}{dt} \begin{bmatrix} x_1 \\ \vdots \\ x_n \end{bmatrix} = \begin{bmatrix} a_{ij} \end{bmatrix} \begin{bmatrix} x_1 \\ \vdots \\ x_n \end{bmatrix} \quad \text{A negative}$$

$$\frac{d}{dt} \begin{bmatrix} r_1 \\ \vdots \\ r_n \end{bmatrix} = \begin{bmatrix} a_{ij} u_i u_j \end{bmatrix} \begin{bmatrix} r_1 \\ \vdots \\ r_n \end{bmatrix} \quad \text{Quadratic Controls}$$

The diagram also shows a vector r_i in the z_i vs x_i plane, with a shaded sector of angle θ_i and a control input $u_i = \cos \theta_i$.

Computing Reachable Sets

$$\frac{d}{dt} \begin{bmatrix} p_1 \\ \vdots \\ p_n \end{bmatrix} = \underbrace{\begin{bmatrix} b_{ij} \end{bmatrix}}_{Am \bullet m} ; \quad b_{ij} = a_{ij} m_i m_j \quad p_i = \frac{r_i^2}{2} \quad m_i = \frac{u_i r_i}{\sqrt{(u_i r_i)^2}}$$

$$\frac{d}{dt} \begin{bmatrix} p_1 \\ \vdots \\ p_n \end{bmatrix} = Am \bullet m = \text{diag}(Am m^T) ; \quad A \leq 0$$

$$p_T - p(0) = \sum_{\alpha} \underbrace{a_{\alpha} Am_{\alpha} \bullet m_{\alpha}}_{\Re} ; a_{\alpha} > 0 ; \quad \text{diag}(AM)$$

N. Khaneja, In Preparation

Computing Reachable Sets

$$\Omega = \{ \lambda \mid \Delta A + A' \Delta \leq 0 ; \Delta = \text{diag}(\lambda) \}$$

$$\begin{bmatrix} 1 & & & \\ & \lambda_1 & & \\ & & \ddots & \\ & & & \lambda_n \end{bmatrix} A + A' \begin{bmatrix} 1 & & & \\ & \lambda_1 & & \\ & & \ddots & \\ & & & \lambda_n \end{bmatrix} \lambda_i \geq 0$$

$$P(s) = s^n + p_{n-1}(\lambda) s^{n-1} + \dots + p_1(\lambda) s + p_0(\lambda)$$

$$p_i(\lambda) \geq 0 \quad \lambda \geq 0 \quad \text{largest } \lambda_j \quad p_T - p(0) = \begin{bmatrix} -1 \\ \vdots \\ \beta_j \\ 0 \end{bmatrix} \quad \lambda_j \beta_j = 1$$

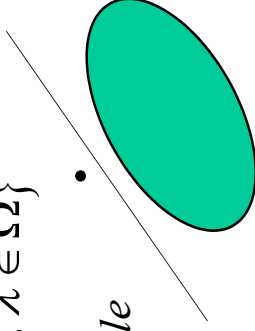
N. Khaneja, In Preparation

Hahn Banach Theorem and the Reachable Set

$$\Omega = \{ \lambda \mid \Delta A + A' \Delta \leq 0 ; \Delta = \text{diag}(\lambda) \}$$

$$\Re = \{ x \mid \langle x, \lambda \rangle \leq 0 ; \lambda \in \Omega \}$$

$$p_T - p(0) \in \Re ; \text{achievable}$$



$$\lambda' \sum_{\alpha} a_{\alpha} Am_{\alpha} \bullet m_{\alpha} = a_{\alpha} \sum_{\alpha} m'_{\alpha} (\Delta A + A' \Delta) m_{\alpha}$$

Reachable Sets

$$\Omega = \{ \lambda \mid \Delta A + A' \Delta \leq 0 ; \Delta = \text{diag}(\lambda) \}$$

$$\frac{d}{dt} \begin{bmatrix} r_1 \\ r_2 \end{bmatrix} = \pi J \begin{bmatrix} -\xi u_1^2 & -u_1 u_2 \\ u_1 u_2 & -\xi u_2^2 \end{bmatrix} \begin{bmatrix} r_1 \\ r_2 \end{bmatrix}$$

$$\begin{bmatrix} 1 & 0 \\ 0 & \lambda_1 \end{bmatrix} \begin{bmatrix} -\xi & -1 \\ 1 & -\xi \end{bmatrix} + \begin{bmatrix} -\xi & 1 \\ -1 & -\xi \end{bmatrix} \begin{bmatrix} 1 & 0 \\ 0 & \lambda_1 \end{bmatrix}$$

$$r_2^2 = \frac{1}{\lambda_1} = (\sqrt{1 + \xi^2} - \xi)^2$$

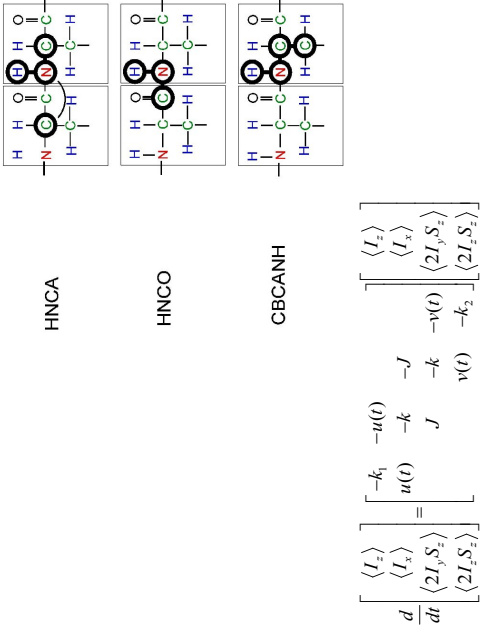
SPORTS: Relaxation optimized transfer of spin order along spin chains



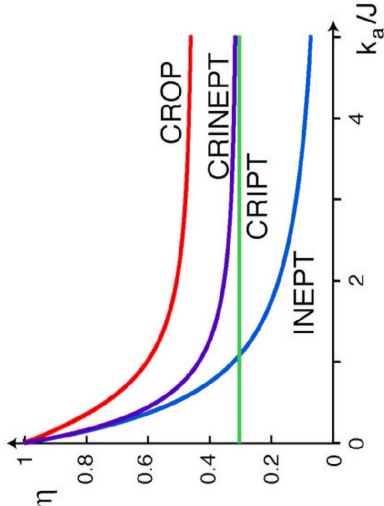
$$\sigma_{1z}\sigma_{2z} \rightarrow \sigma_{2z}\sigma_{3z} \rightarrow \dots \rightarrow \sigma_{(n-1)z}\sigma_{nz}$$
$$\frac{d}{dt} \begin{bmatrix} x_1 \\ x_2 \\ x_3 \\ x_4 \\ x_5 \end{bmatrix} = \begin{bmatrix} 0 & -u & & & \\ u & -k & -J & 0 & \\ & J & -k & -J & \\ & 0 & J & -k & -u \\ & & & u & 0 \end{bmatrix} \begin{bmatrix} x_1 \\ x_2 \\ x_3 \\ x_4 \\ x_5 \end{bmatrix}$$
$$\eta = \left(\frac{(\sqrt{\xi^2 + 2 - \xi})^2}{2} \right)$$
$$\begin{bmatrix} r_1 \\ r_2 \\ r_3 \end{bmatrix} = \begin{bmatrix} -k u_1^2 & -J u_1 u_2 & 0 \\ J u_1 u_2 & -k u_2^2 & -J u_2 u_3 \\ 0 & J u_2 u_3 & -k u_3^2 \end{bmatrix} \begin{bmatrix} r_1 \\ r_2 \\ r_3 \end{bmatrix}$$
$$\begin{bmatrix} 1 \\ \lambda_1 \\ \lambda_2 \end{bmatrix} \begin{bmatrix} -\xi & -1 & 0 \\ 1 & -\xi & -1 \\ 0 & 1 & -\xi \end{bmatrix} \begin{bmatrix} 1 \\ 0 \\ 1 \end{bmatrix} \begin{bmatrix} \lambda_1 \\ \lambda_2 \end{bmatrix}$$

Dionisis et al PRA (2005)

Spin Systems and Networks



Transfer Efficiency



Time Optimal Control of Quantum Systems

$k = \{-iH_j\}_{LA}$ $K = \exp(k)$

Minimum time to go from $U(0)$ to U_F is the same as minimum time to go from $KU(0)$ to KU_F

$\frac{dU(t)}{dt} = -i[H_d + \sum_{j=1}^m u_j H_j]U(t); \quad U(0) = I$

Khaneja, Brockett, Glaser, Physical Review A, 63, 032308, 2001

Control Systems on Coset Spaces

$$\frac{dU(t)}{dt} = -i[H_d + \sum_{j=1}^m u_j H_j]U(t); \quad U(0) = I$$

$$K_{n+1} \exp(-iHt_n) K_n \dots \exp(-iHt_2) K_2 \exp(-iHt_1) K_1$$

$$K_{n+1} \exp(-iK_n^* H K_n t_1) \dots \exp(-iK_2^* H K_2 t_2) \exp(-iK_1^* H K_1 t_1)$$

G/K is a Riemannian Symmetric Space

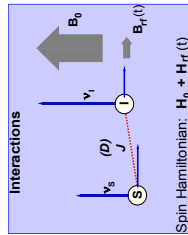
$$g = p + k; \quad p \perp k$$

$$[p, p] \subseteq k; [k, k] \subseteq k; [p, k] \subseteq p;$$

The velocities of the shortest paths
in G/K always commute!

Physical Review A , **63**, 032308 (2001)

Cartan Decompositions , Two-Spin Systems and Canonical Decomposition of SU(4)



$$\frac{dU}{dt} = -i[\sum_{\alpha,\beta} I_{\alpha\beta} I_{\alpha} S_{\beta} + u_1 I_x + u_2 I_y + u_3 S_x + u_4 S_y]U$$

$$k = \{-i I_{\alpha}, -i S_{\beta}\}; \quad p = \{-i I_{\alpha} S_{\beta}\}$$

$$G = SU(4); \quad K = SU(2) \otimes SU(2)$$

$$a = \{-i I_x S_x, -i I_y S_y, -i I_z S_z\}$$

$$G = K \exp(-i(\alpha_x I_x S_x + \alpha_y I_y S_y + \alpha_z I_z S_z)) K$$

$$\sigma_x = \frac{1}{2} \begin{pmatrix} 0 & 1 \\ 1 & 0 \end{pmatrix}; \sigma_y = \frac{1}{2} \begin{pmatrix} 0 & -i \\ i & 0 \end{pmatrix}; \sigma_z = \frac{1}{2} \begin{pmatrix} 1 & 0 \\ 0 & -1 \end{pmatrix}$$

Physical Review A , **63**, 032308 (2001)

Reachable Set

$$\frac{dU(t)}{dt} = -i[H_d + \sum_{j=1}^m u_j H_j]U(t); \quad U(0) = I$$

$$k = so(n)$$

$$K = \exp(k) = SO(n)$$

$$H_d = \begin{bmatrix} \lambda_1 & & \\ & \lambda_2 & \\ & & \ddots \\ & & & \lambda_n \end{bmatrix}$$

$$\begin{bmatrix} \mu_1 \\ \mu_2 \\ \vdots \\ \mu_n \end{bmatrix} \prec \begin{bmatrix} \lambda_1 \\ \lambda_2 \\ \vdots \\ \lambda_n \end{bmatrix} t$$

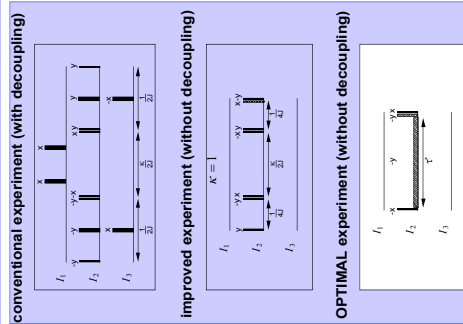
$$K_{n+1} \exp(-iK_n^* H_d K_n t_n) \dots \exp(-iK_2^* H_d K_2 t_2) \exp(-iK_1^* H_d K_1 t_1)$$

$$K \begin{bmatrix} \lambda_1 & & \\ & \lambda_2 & \\ & & \ddots \\ & & & \lambda_n \end{bmatrix} K^* = \begin{bmatrix} a_{11} & & \\ & a_{22} & \\ & & \ddots \\ & & & a_{nn} \end{bmatrix}$$

$$\begin{bmatrix} a_{11} \\ a_{22} \\ \vdots \\ a_{nn} \end{bmatrix} \prec \begin{bmatrix} \lambda_1 \\ \lambda_2 \\ \vdots \\ \lambda_n \end{bmatrix}$$

$$K_1 \exp(-i \begin{bmatrix} \mu_1 & & \\ & \mu_2 & \\ & & \ddots \\ & & & \mu_n \end{bmatrix} K_2)$$

Time Optimal Quantum Information Processing



$$\frac{SU(8)}{SU(2) \otimes SU(2) \otimes SU(2)}$$

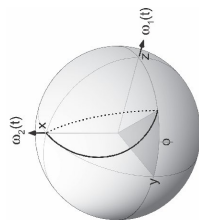
$$-iKHK^{\dagger}$$

Physical Review A , **65**, 032301 (2002)

Control of Indirectly Coupled Qubits

$$d \frac{d}{dt} \begin{bmatrix} x_1 \\ x_2 \\ x_3 \\ x_4 \end{bmatrix} = \begin{bmatrix} 0 & -1 \\ 1 & 0 & -u \\ & u & 0 & -1 \\ & & 1 & 0 \end{bmatrix} \begin{bmatrix} x_1 \\ x_2 \\ x_3 \\ x_4 \end{bmatrix}$$

$$\tan \theta = \frac{x_3}{x_2}$$



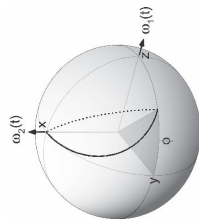
$$\theta = \omega t$$

$$\frac{(dx)^2 + (dz)^2}{1 - x^2 - z^2}$$

Control of Indirectly Coupled Qubits

$$\begin{bmatrix} x_1 & x_2 & x_3 & x_4 \\ 0 & -1 & & \\ 1 & 0 & -u & \\ & u & 0 & -k \\ & & k & 0 \end{bmatrix} = \begin{bmatrix} x_1 & x_2 & x_3 & x_4 \end{bmatrix}$$

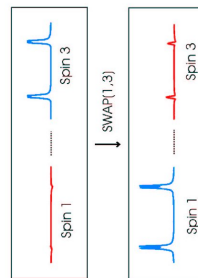
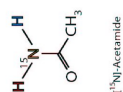
$$\tan \theta = \frac{x_3}{x_2}$$



$$\frac{d^2\theta}{dt} = (k^2 - 1)\sin\theta$$

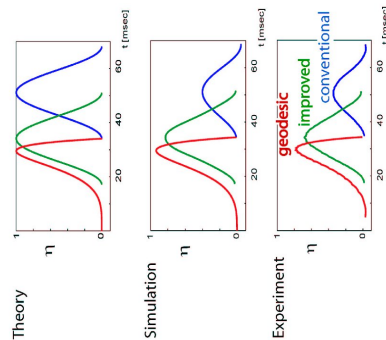
$$\frac{(dx)^2 k^2 + (dz)^2}{1 - x^2 - z^2}$$

Indirect SWAP Operation



*Reiss, Khaneja, Glaser
J. Mag. Reson. 165 (2003)*

Efficiency η of indirect SWAP sequences



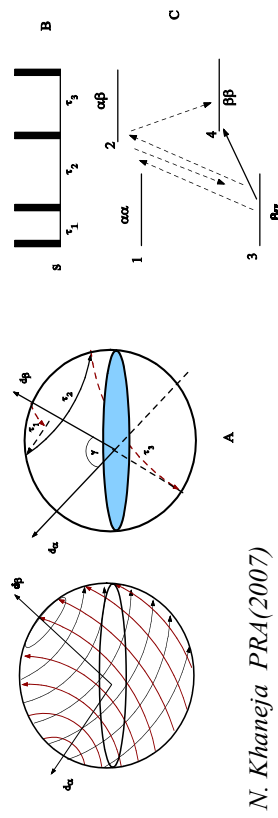
Khaneja, et. al PRA(2007)

Switched Control of Electron Nuclear Spin Systems

$$H_0 = \omega_s S_z + \omega_I I_z + S \cdot A \cdot I$$

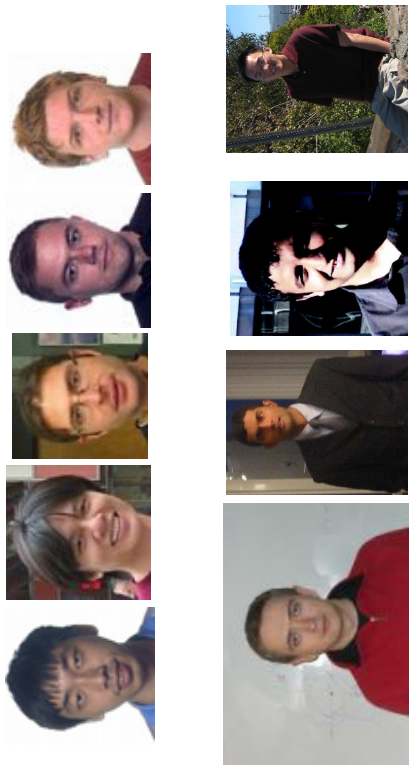
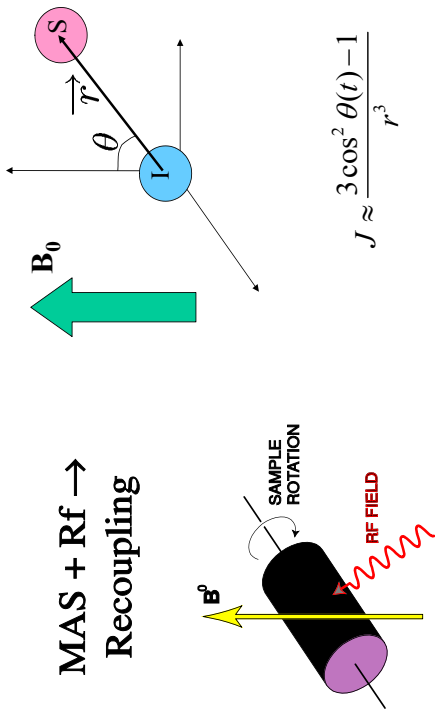
$$d_\beta = (\omega_I + A/2) \hat{z} + \frac{\hat{B}}{2} x$$

$$d_\alpha = (\omega_l - A/2) z - \frac{B}{2} x$$



N. Khaneja PRA(2007)

Anisotropy Compensated Design of Solid State
NMR experiments



NSF, Sloan, DARPA, ONR, AFOSR, Humboldt

Collaborators



Gerhard Wagner
Harvard Medical
School



Steffen Glaser
Technische Universitaet
Muenchen



Niels Nielsen
University of Aarhus

Robert G. Griffin
MIT

Part 4

List of Participants

Bouchra Abouzaid
INMA
Université catholique de Louvain
Louvain la Neuve
Belgium
bouchra.abouzaid@uclouvain.be

Pierre-Antoine Absil
INMA
Université catholique de Louvain
Louvain la Neuve
Belgium
PA.Absil@uclouvain.be

Jaron Achterberg
Electrical Engineering
TUE
Eindhoven
Netherlands
j.achterberg@tue.nl

Sisdarmanto Adinandra
Mechanical Engineering
TU Eindhoven
Eindhoven
Netherlands
s.adinandra@tue.nl

Dirk Aeyels
Systems
Universiteit Gent
Zwijnaarde
Belgium
dirk.aeyels@ugent.be

Huseyin Akcay
INMA
Université catholique de Louvain
Louvain la Neuve
Belgium
Huseyin.Akcay@uclouvain.be

Irmak Aladagli
Systems & Control
Technische Universiteit Eindhoven
Eindhoven
Netherlands
i.aladagli@student.tue.nl

Alejandro Alvarez Aguirre
Mechanical Engineering
Eindhoven University of Technology
Eindhoven
Netherlands
a.a.alvarez@tue.nl

Thibaut Andre
INMA
Université catholique de Louvain
Louvain la Neuve
Belgium
Thibaut.Andre@uclouvain.be

Bayan Babakhani
Electrical Engineering
University of Twente
Enschede
Netherlands
b.babakhani@utwente.nl

Kurt Barbe
ELEC
Vrije Universiteit Brussel
Bruxelles
Belgium
kbarbe@vub.ac.be

Georges Bastin
INMA
Université catholique de Louvain
Louvain la Neuve
Belgium
Georges.Bastin@uclouvain.be

Nicolas Bauer
Mechanical Engineering
TUE
Eindhoven
Netherlands
n.w.bauer@tue.nl

Maite Bauwens
ELEC
VUB
Bruxelles
Belgium
msbauwen@vub.ac.be

Charlotte Beauthier
Mathematics
University of Namur (Fundp)
Namur
Belgium
charlotte.beauthier@math.fundp.ac.be

Niels Besseling
Applied Mathematics
University of Twente
Enschede
Netherlands
n.c.besseling@math.utwente.nl

Bart Besselink
Mechanical Engineering
Eindhoven University of Technology
Eindhoven
Netherlands
b.besselink@tue.nl

Maarten Bezemer
Electrical Engineering
University of Twente
Enschede
Netherlands
m.m.bezemer@ewi.utwente.nl

René Boel
Systems
University of Gent
Gent
Belgium
rene.boel@ugent.be

Julian E. Bonilla Alarcon
Chemical Engineering
K.U. Leuven - Biotec
Leuven
Belgium
julian.bonilla@cit.kuleuven.be

Jan Bontsema
Greenhouse Horticulture
Wageningen University
Wageningen
Netherlands
jan.bontsema@wur.nl

Pierre Borckmans
INMA
Université catholique de Louvain
Louvain la Neuve
Belgium
pierre.borckmans@uclouvain.be

Arnaud Browet
INMA
Université catholique de Louvain
Louvain la Neuve
Belgium
arnaud.browet@uclouvain.be

Mussa Bshara
ELEC
Vrije Universiteit Brussel
Bruxelles
Belgium
mbshara@vub.ac.be

Eric Bullinger
EECS
University of Liège
Liège
Belgium
e.bullinger@ieee.org

Pieter Busschaert
Chemical Engineering
K.U. Leuven - Biotec
Leuven
Belgium
pieter.busschaert@cit.kuleuven.be

Angelo Buttafuoco
Control engineering and systems analysis
Université Libre de Bruxelles
Bruxelles
Belgium
abuttafu@ulb.ac.be

Ming Cao
Industrial technology and management
University of Groningen
Groningen
Netherlands
m.cao@rug.nl

Astrid Cappuyns
Chemical Engineering
K.U. Leuven - Biotec
Leuven
Belgium
astrid.cappuyns@cit.kuleuven.be

Raffaella Carloni
Electrical Engineering
University of Twente
Enschede
Netherlands
r.carloni@utwente.nl

Thomas Cason
INMA
Université catholique de Louvain
Louvain la Neuve
Belgium
Thomas.Cason@uclouvain.be

Sébastien Coppe
INMA
Université catholique de Louvain
Louvain la Neuve
Belgium
Sebastien.Coppe@uclouvain.be

Jorge Cortes
University of California At San Diego
United States
cortes@ucsd.edu

Daniel Coutinho
Service d'Automatique
Faculté Polytechnique de Mons
Mons
Belgium
daniel.coutinho@fpms.ac.be

Frédéric Crevecoeur
INMA
Université catholique de Louvain
Louvain la Neuve
Belgium
Frederic.Crevecoeur@uclouvain.be

Chris Criens
Mechanical Engineering
Eindhoven University of Technology
Eindhoven
Netherlands
c.h.a.criens@tue.nl

Balazs Csaji
INMA
Université catholique de Louvain
Louvain la Neuve
Belgium
balazs.csaji@uclouvain.be

Bob David
INMA
Université catholique de Louvain
Louvain la Neuve
Belgium
robert.david@uclouvain.be

Pierre Daye
INMA
Université catholique de Louvain
Louvain la Neuve
Belgium
Pierre.Daye@uclouvain.be

Jeroen de Best
Mechanical Engineering
Eindhoven University of Technology
Eindhoven
Netherlands
j.j.t.h.d.best@tue.nl

Bram de Jager
Mechanical Engineering
Technische Universiteit Eindhoven
Eindhoven
Netherlands
a.g.de.jager@tue.nl

Filip de Smet
Systems Research Group
Ghent University
Zwijnaarde
Belgium
filip.desmet@ugent.be

Coen de Visser
Control and Simulation
Delft University of Technology
Delft
Netherlands
c.c.devisser@tudelft.nl

Elwin de Weerd
Control and Simulation
Delft University of Technology
Delft
Netherlands
e.deweerd@tudelft.nl

Wilm Decre
Mechanical Engineering
Katholieke Universiteit Leuven
Heverlee
Belgium
wilm.decre@mech.kuleuven.be

Boris Defourny
EECS
University of Liège
Liège
Belgium
bdf@montefiore.ulg.ac.be

Dunstano Del Puerto Flores
Discrete Technology and Production Automation
Rijksuniversiteit Groningen
Groningen
Netherlands
d.del.puerto.flores@rug.nl

Jean-Charles Delvenne
INMA
Université catholique de Louvain
Louvain la Neuve
Belgium
Jean-Charles.Delvenne@uclouvain.be

Thomas Delwiche
Control engineering and systems analysis
Université Libre de Bruxelles
Bruxelles
Belgium
thomas.delwiche@ulb.ac.be

Arjen Den Hamer
Mechanical Engineering
Eindhoven University of Technology
Eindhoven
Netherlands
a.j.d.hamer@tue.nl

Bruno Depraetere
Mechanical Engineering
Katholieke Universiteit Leuven
Heverlee
Belgium
bruno.depraetere@mech.kuleuven.be

Laurent Dewasme
Service d'Automatique
Faculté Polytechnique de Mons
Mons
Belgium
laurent.dewasme@fpms.ac.be

Pieter-Jan D'Huys
Chemical Engineering
K.U. Leuven - Biotech
Leuven
Belgium
pieterjan.dhuys@cit.kuleuven.be

Chenyang Ding
Electrical Engineering
Eindhoven University of Technology
Eindhoven
Netherlands
c.ding@tue.nl

Daniel Dirksz
Discrete Technology and Production Automation
University of Groningen
Groningen
Netherlands
d.a.dirksz@rug.nl

Snezana Djordjevic
DCSC
TU Delft
Delft
Netherlands
s.djordjevic@tudelft.nl

Dang Doan
DCSC
TU Delft
Delft
Netherlands
m.d.doan@tudelft.nl

Tijs Donkers
Mechanical Engineering
Eindhoven University of Technology
Eindhoven
Netherlands
m.c.f.donkers@tue.nl

Guillaume Drion
EECS
University of Liège
Liège
Belgium
gdrion@ulg.ac.be

Denis Efimov
EECS
University of Liège
Liège
Belgium
efimov@montefiore.ulg.ac.be

Jacob Engwerda
Econometrics and Or
Tilburg University
Tilburg
Netherlands
engwerda@uvt.nl

Willem-Jan Evers
Mechanical Engineering
Eindhoven University of Technology
Eindhoven
Netherlands
w.j.e.evers@tue.nl

Mohammed Ezzeldin Mahdy
Electrical Engineering
Eindhoven University of Technology
Eindhoven
Netherlands
M.Ezz@tue.nl

Samira Farahani
DCSC
TU Delft
Delft
Netherlands
s.safaeifarahani@tudelft.nl

Audrey Favache
INMA
Université catholique de Louvain
Louvain la Neuve
Belgium
Audrey.Favache@uclouvain.be

Dirk Fey
EECS
University of Liège
Liège
Belgium
kybdot@hotmail.com

Raphaël Fonteneau
EECS
University of Liège
Liège
Belgium
fonteneau@montefiore.ulg.ac.be

Florence Fonteneau-Belmudes
EECS
University of Liège
Liège
Belgium
florence.belmudes@ulg.ac.be

Wim Foubert
ELEC
Vrije Universiteit Brussel
Bruxelles
Belgium
wfoubert@vub.ac.be

Michel Franken
EWI/CE
Institute of Technical Medicine
Enschede
Netherlands
michelfranken@hotmail.com

Manuel Ricardo Galvez Carrillo
Control engineering and systems analysis
Université Libre de Bruxelles
Bruxelles
Belgium
mgalvezc@ulb.ac.be

Eloisa del Carmen Garcia Canseco
Mechanical Engineering
Technische Universiteit Eindhoven
Eindhoven
Netherlands
e.garcia.canseco@tue.nl

Mathieu Gerard
DCSC
TU Delft
Delft
Netherlands
m.p.gerard@tudelft.nl

Pierre Geurts
EECS
University of Liège
Liège
Belgium
p.geurts@ulg.ac.be

Michel Gevers
INMA
Université catholique de Louvain
Louvain la Neuve
Belgium
Michel.Gevers@uclouvain.be

Rob Gielen
Electrical Engineering
Eindhoven University of Technology
Eindhoven
Netherlands
R.H.Gielen@student.tue.nl

Geert Gins
Chemical Engineering
K.U. Leuven - Biotec
Leuven
Belgium
geert.gins@cit.kuleuven.be

Guillaume Goffaux
Service d'Automatique
Faculté Polytechnique de Mons
Mons
Belgium
guillaume.goffaux@fpms.ac.be

Liesbeth Gomme
ELEC
Vrije Universiteit Brussel
Bruxelles
Belgium
lgomme@vub.ac.be

Suat Gumussoy
computer science
K.U. Leuven
Leuven
Belgium
suat.gumussoy@cs.kuleuven.be

Bart Hennen
Mechanical Engineering
Eindhoven University of Technology
Eindhoven
Netherlands
b.a.hennen@tue.nl

Ralph Hermans
Electrical Engineering
Eindhoven University of Technology
Eindhoven
Netherlands
R.Hermans@tue.nl

Peter Heuberger
DCSC
TU Delft
Delft
Netherlands
p.s.c.heuberger@tudelft.nl

Samuel Hiard
Bioinformatics and Systems
University of Liège
Liège
Belgium
s.hiard@ulg.ac.be

Ramona Hodrea
Electrical energy, Systems and Automation
Ghent University
Zwijnaarde
Belgium
ramona@autoctrl.ugent.be

Bart Huyck
ESAT/SCD
Kuleuven
Heverlee
Belgium
Bart.Huyck@esat.kuleuven.be

Tzvetan Ivanov
INMA
Université catholique de Louvain
Louvain la Neuve
Belgium
Tzvetan.Ivanov@uclouvain.be

Elias Jarlebring
computer science
K.U. Leuven
Leuven
Belgium
elias.jarlebring@cs.kuleuven.be

Bayu Jayawardhana
Discrete Technology and Production Automation
University of Groningen
Groningen
Netherlands
b.jayawardhana@rug.nl

Wassim Jouini
SCEE
Supelec / Ietr
Cesson Sevigne
France
wassim.jouini@supelec.fr

Michel Journée
EECS
University of Liège
Liège
Belgium
m.journee@ulg.ac.be

Karel Keesman
Systems and Control
Wageningen University
Wageningen
Netherlands
karel.keesman@wur.nl

Amol Khalate
DCSC
TU Delft
Delft
Netherlands
a.a.khalate@tudelft.nl

Navin Khaneja
Harvard University
United States
navin@hrl.harvard.edu

Dragan Kostic
Mechanical Engineering
Technische Universiteit Eindhoven
Eindhoven
Netherlands
d.kostic@tue.nl

Stefan Kuiper
DCSC
TU Delft
Delft
Netherlands
stefan.kuiper@tudelft.nl

Christian Lageman
EECS
University of Liège
Liège
Belgium
christian.lageman@montefiore.ulg.ac.be

Edouard Laroche
LSIIT-EAVR
University of Strasbourg
Illkirch
France
laroche@unistra.fr

John Lataire
ELEC
Vrije Universiteit Brussel
Bruxelles
Belgium
jlataire@vub.ac.be

Lieve Lauwers
ELEC
Vrije Universiteit Brussel
Bruxelles
Belgium
lieve.lauwers@vub.ac.be

Guillaume Leclercq
INMA
Université catholique de Louvain
Louvain la Neuve
Belgium
Guillaume.Leclercq@uclouvain.be

Philippe Lefèvre
INMA
Université catholique de Louvain
Louvain la Neuve
Belgium
Philippe.Lefevre@uclouvain.be

Shu Lin
DCSC
TU Delft
Delft
Netherlands
s.lin@tudelft.nl

Filip Logist
Chemical Engineering
K.U. Leuven - Biotec
Leuven
Belgium
filip.logist@cit.kuleuven.be

Gabriel Lopes
DCSC
TU Delft
Delft
Netherlands
g.a.d.lopes@tudelft.nl

Heather Maclean
INMA
Université catholique de Louvain
Louvain la Neuve
Belgium
heather.maclean@uclouvain.be

Johan Mailier
Service d'Automatique
Faculté Polytechnique de Mons
Mons
Belgium
Johan.Mailier@fpms.ac.be

Raphaël Maree
GIGA/CSEE
University of Liège
Liège
Belgium
raphael.maree@ulg.ac.be

Nicolae Marinica
systems
University of Gent
Gent
Belgium
NicolaeEmanuel.Marinica@UGent.be

Sonia Martinez
University of California At San Diego
United States
soniamd@ucsd.edu

Alexandre Mauroy
EECS
University of Liège
Liège
Belgium
alexandre.mauroy@ulg.ac.be

Ali Mesbah
DCSC
TU Delft
Delft
Netherlands
ali.mesbah@tudelft.nl

Gilles Meyer
EECS
University of Liège
Liège
Belgium
g.meyer@ulg.ac.be

Wim Michiels
computer science
K.U. Leuven
Leuven
Belgium
wim.michiels@cs.kuleuven.be

Mohammad Moradzadeh
Systems
University of Gent
Gent
Belgium
mm.moradzadeh@yahoo.com

Shah Muhammad
DIAM
TU Delft
Delft
Netherlands
s.muhammad@tudelft.nl

Mark Mutsaers
Electrical Engineering
Eindhoven University of Technology
Eindhoven
Netherlands
M.E.C.Mutsaers@tue.nl

Omar Naeem
DCSC
TU Delft
Delft
Netherlands
o.naeem@tudelft.nl

Gerrit Naus
Mechanical Engineering
Eindhoven University of Technology
Eindhoven
Netherlands
g.j.l.naus@tue.nl

Jana Nemcova
Mas 2
Cwi Amsterdam
Amsterdam
Netherlands
j.nemcova@cwi.nl

Dac Viet Ngo
Mechanical Engineering
Eindhoven University of Technology
Eindhoven
Netherlands
N.Dac.Viet@tue.nl

Toshiki Oguchi
Department of Mechanical engineering
Tokyo Metropolitan University
Tokyo
Japan
t.oguchi@tmu.ac.jp

Jimmy Omony
Systems and Control
Wageningen University
Wageningen
Netherlands
jimmy.omony@wur.nl

Victor Onclinx
INMA
Université catholique de Louvain
Louvain la Neuve
Belgium
Victor.Onclinx@uclouvain.be

Rulyue Ouyang
Discrete Technology and Production Automation
University of Groningen
Groningen
Netherlands
r.ouyang@rug.nl

Wojciech Paszke
Mechanical Engineering
Eindhoven University of Technology
Eindhoven
Netherlands
w.paszke@tue.nl

Jonatan Pena Ramirez
Mechanical Engineering
Eindhoven University of Technology
Eindhoven
Netherlands
J.Pena@tue.nl

Gregory Pinte
Flanders' Mechatronics Technology Centre
Heverlee
Belgium
gregory.pinte@fmtc.be

Rik Pintelon
ELEC
Vrije Universiteit Brussel
Bruxelles
Belgium
rik.pintelon@vub.ac.be

Douglas Plaza Guingla
Laboratory of Hydrology and water management
University of Ghent
Gent
Belgium
douglas.plazaguingla@ugent.be

Ilhan Polat
DCSC
TU Delft
Delft
Netherlands
i.polat@tudelft.nl

Herman Ramon
Biosystems / Division MeBioS
K.U. Leuven
Leuven
Belgium
herman.ramon@biw.kuleuven.be

Puduru Reddy
Econometrics and Operations
Tilburg University
Tilburg
Netherlands
p.v.reddy@uvt.nl

Rob Reilink
EE/Control Engineering
University of Twente
Enschede
Netherlands
r.reilink@utwente.nl

Quentin Rentmeesters
INMA
Université catholique de Louvain
Louvain la Neuve
Belgium
Quentin.Rentmeesters@uclouvain.be

Cristina Retamal
Control engineering and systems analysis
Université Libre de Bruxelles
Bruxelles
Belgium
cristina.retamal.reyes@ulb.ac.be

Edwin Reynders
Civil Engineering Departement
K.U. Leuven
Leuven
Belgium
edwin.reynders@bwk.kuleuven.be

David Rijlaarsdam
Mechanical Engineering
Eindhoven University of Technology
Eindhoven
Netherlands
d.j.rijlaarsdam@tue.nl

Edmundo Rocha-Cozatl
Service d'Automatique
Faculté Polytechnique de Mons
Mons
Belgium
edmundo.rocha@fpms.ac.be

Jonathan Rogge
Systems Research Group
Ghent University
Gent
Belgium
jonathan.rogge@ugent.be

Yves Rolain
ELEC
Vrije Universiteit Brussel
Bruxelles
Belgium
Yves.rolain@vub.ac.be

Michael Ronde
Mechanical Engineering
Eindhoven University of Technology
Eindhoven
Netherlands
m.j.c.ronde@tue.nl

Pierre Sacré
EECS
University of Liège
Liège
Belgium
pierre.sacre@ulg.ac.be

Bart Saerens
Mechanical Engineering
Katholieke Universiteit Leuven
Heverlee
Belgium
Bart.Saerens@mech.kuleuven.be

Chafik Samir
INMA
Université catholique de Louvain
Louvain la Neuve
Belgium
chafik.samir@uclouvain.be

Ines Saraiva
Service d'Automatique
Faculté Polytechnique de Mons
Mons
Belgium
ines@ruc.pt

Alain Sarlette
EECS
University of Liège
Liège
Belgium
alain.sarlette@ulg.ac.be

Johan Schoukens
ELEC
Vrije Universiteit Brussel
Bruxelles
Belgium
johan.schoukens@vub.ac.be

Rodolphe Sepulchre
EECS
University of Liège
Liège
Belgium
r.sepulchre@ulg.ac.be

Emile Simon
INMA
Université catholique de Louvain
Louvain la Neuve
Belgium
Emile.Simon@uclouvain.be

Alexandre Skrylnik
Energy Research Centre
Faculté Polytechnique de Mons
Mons
Belgium
oleksandr.skrylnyk@fpms.ac.be

Ilse Smets
Chemical Engineering
K.U. Leuven - Biotech
Leuven
Belgium
ilse.smets@cit.kuleuven.be

Pawel Stano
DCSC
TU Delft
Delft
Netherlands
p.m.stano@tudelft.nl

Nienke Stein
System and control group
Wetsus/Wur
Wageningen
Netherlands
nienke.stein@wetsus.nl

Maarten Steinbuch
Mechanical Engineering
Eindhoven University of Technology
Eindhoven
Netherlands
m.steinbuch@tue.nl

Erik Steur
Mechanical Engineering, dynamics and control group
Eindhoven University of Technology
Eindhoven
Netherlands
e.steur@tue.nl

Hans Stigter
Systems and Control
Wageningen University
Wageningen
Netherlands
hans.stigter@wur.nl

Jasper Stolte
Electrical Engineering
Technische Universiteit Eindhoven
Eindhoven
Netherlands
j.stolte@tue.nl

Anton Stoorvogel
Electrical Engineering, Mathematics and Computer Science
University of Twente
Enschede
Netherlands
a.a.stoorvogel@utwente.nl

Herman Sutarto
systems
University of Gent
Gent
Belgium
sutarto.sutarto@ugent.be

Jan Swevers
Mechanical Engineering
Katholieke Universiteit Leuven
Heverlee
Belgium
jan.swevers@mech.kuleuven.be

Arturo Tejada Ruiz
DCSC
TU Delft
Delft
Netherlands
a.tejadaruiz@tudelft.nl

Roland Toth
DCSC
TU Delft
Delft
Netherlands
r.toth@tudelft.nl

Ramazan Unal
Electrical Engineering
University of Twente
Enschede
Netherlands
R.Unal@ctw.utwente.nl

Patrick Van Bree
Electrical Engineering
Eindhoven University of Technology
Eindhoven
Netherlands
p.j.v.bree@tue.nl

Mattijs Van de Walle
ELEC
Vrije Universiteit Brussel
Bruxelles
Belgium
mattijs.van.de.walle@vub.ac.be

Lieboud Van Den Broeck
Mechanical Engineering
Katholieke Universiteit Leuven
Leuven
Belgium
lieboud.vandenbroeck@mech.kuleuven.be

Paul Van Den Hof
DCSC
TU Delft
Delft
Netherlands
p.m.j.vandenhof@tudelft.nl

Sara Van Der Hoeven
DCSC
TU Delft
Delft
Netherlands
s.w.vanderhoeven@tudelft.nl

Ewout Van Der Laan
Mechanical Engineering
Eindhoven University of Technology
Eindhoven
Netherlands
e.p.v.d.laan@tue.nl

Stan Van Der Meulen
Mechanical Engineering
Eindhoven University of Technology
Eindhoven
Netherlands
s.h.v.d.meulen@tue.nl

Jacob Van Der Woude
Applied Mathematics
Delft University of Technology
Delft
Netherlands
j.w.vanderwoude@tudelft.nl

Eva Van Derlinden
Chemical Engineering
K.U. Leuven - Biotec
Leuven
Belgium
eva.vanderlinden@cit.kuleuven.be

Niels Van Dijk
Mechanical Engineering
Eindhoven University of Technology
Eindhoven
Netherlands
n.j.m.v.dijk@tue.nl

Paul Van Dooren
INMA
Université catholique de Louvain
Louvain la Neuve
Belgium
Paul.Vandooren@uclouvain.be

Peter Van Erdeghe
Chemical Engineering
K.U. Leuven - Biotec
Leuven
Belgium
peter.vanerdeghem@cit.kuleuven.be

Rob Van Gils
Mechanical Engineering, dynamics and control group
Eindhoven University of Technology
Eindhoven
Netherlands
r.w.v.gils@tue.nl

Robbert Van Herpen
Mechanical Engineering
Eindhoven University of Technology
Eindhoven
Netherlands
r.m.a.v.herpen@student.tue.nl

Jan Van Hulzen
DCSC
TU Delft
Delft
Netherlands
j.r.vanhulzen@tudelft.nl

Jan Van Impe
Chemical Engineering
K.U. Leuven - Biotech
Leuven
Belgium
jan.vanimpe@cit.kuleuven.be

Erik-Jan Van Kampen
Control and Simulation
Delft University of Technology
Delft
Netherlands
e.vankampen@tudelft.nl

Thijs Van Keulen
Mechanical Engineering
Eindhoven University of Technology
Eindhoven
Netherlands
t.a.c.v.keulen@tue.nl

Wendy Van Moer
ELEC
Vrije Universiteit Brussel
Bruxelles
Belgium
wendy.vanmoer@vub.ac.be

Anne Van Mulders
ELEC
Vrije Universiteit Brussel
Bruxelles
Belgium
avmulder@vub.ac.be

Gijs Van Oort
EWI
Impact Institute/ Control Engineering
Enschede
Netherlands
g.vanoort@ewi.utwente.nl

Dennis Van Raaij
Mechanical Engineering
Eindhoven University of Technology
Eindhoven
Netherlands
d.w.j.v.raaij@tue.nl

Gerrit Van Straten
Agrotechnology and food science
Wageningen University
Wageningen
Belgium
gerrit.vanstraten@wur.nl

Gerard Van Willigenburg
Systems and Control
Wageningen University
Wageningen
Netherlands
gerard.vanwilligenburg@wur.nl

Jan-Willem Van Wingerden
DCSC
TU Delft
Delft
Netherlands
j.w.vanwingerden@tudelft.nl

Laurent Vanbeylen
ELEC
Vrije Universiteit Brussel
Bruxelles
Belgium
laurent.vanbeylen@vub.ac.be

Joris Vanbiervliet
computer science
K.U. Leuven
Leuven
Belgium
Joris.Vanbiervliet@cs.kuleuven.be

Alain Vande Wouwer
Service d'Automatique
Faculté Polytechnique de Mons
Mons
Belgium
alain.vandewouwer@fpms.ac.be

Emmanuel Vander Poorten
Mechanical Engineering
Katholieke Universiteit Leuven
Heverlee
Belgium
emmanuel.vanderpoorten@mech.kuleuven.be

Koen Vandermot
ELEC
Vrije Universiteit Brussel
Bruxelles
Belgium
koen.vandermot@vub.ac.be

Jef Vanlaer
Chemical Engineering
K.U. Leuven - Biotec
Leuven
Belgium
jef.vanlaer@cit.kuleuven.be

Joost Veenman
DCSC
TU Delft
Delft
Netherlands
j.veenman@tudelft.nl

Anke Verhulst
Chemical Engineering
K.U. Leuven - Biotec
Leuven
Belgium
anke.verhulst@cit.kuleuven.be

Tom Verschuren
Mechanical Engineering
Eindhoven University of Technology
Eindhoven
Netherlands
t.a.c.verschuren@student.tue.nl

Jonathan Verspecht
Control engineering and systems analysis
Université Libre de Bruxelles
Bruxelles
Belgium
jverspec@ulb.ac.be

René Vidal
Johns Hopkins University
United States

Carlos Vilas
Service d'Automatique
Faculté Polytechnique de Mons
Mons
Belgium
carlos.vilas@fpms.ac.be

Ludo Visser
EWI/CE
University of Twente
Enschede
Netherlands
l.c.visser@utwente.nl

Jochem Vissers
Electrical Engineering
Eindhoven University of Technology
Eindhoven
Netherlands
J.A.W.Vissers@tue.nl

Tri Vo Minh
Biosystems / Division MeBioS
K.U. Leuven
Leuven
Belgium
tri.vominh@student.kuleuven.be

Marnix Volckaert
PMA
K.U. Leuven
Heverlee
Belgium
marnix.volckaert@mech.kuleuven.be

Thomas Voss
DTPA
Rijksuniversiteit Groningen
Groningen
Netherlands
t.voss@rug.nl

Dirk Vries
DCSC
TU Delft
Delft
Netherlands
d.vries@tudelft.nl

Martin Wassink
EEMCS
University of Twente
Enschede
Netherlands
m.wassink@utwente.nl

Satyajit Wattamwar
Electrical Engineering
Technical University of Eindhoven
Eindhoven
Netherlands
s.wattamwar@tue.nl

Louis Wehenkel
EECS
University of Liège
Liège
Belgium
L.Wehenkel@ulg.ac.be

Vincent Wertz
INMA
Université catholique de Louvain
Louvain la Neuve
Belgium
Vincent.Wertz@uclouvain.be

Dhammika Widanage
ELEC
Vrije Universiteit Brussel
Bruxelles
Belgium
wwidanag@vub.ac.be

Bert Willaert
Mechanical Engineering
K.U. Leuven
Heverlee
Belgium
bert.willaert@mech.kuleuven.be

Joseph Winkin
INMA
Université catholique de Louvain
Louvain la Neuve
Belgium
isabelle.hisette@uclouvain.be

Maarten Witters
Mechanical Engineering
Kuleuven
Heverlee
Belgium
maarten.witters@mech.kuleuven.be

Gert Witvoet
Mechanical Engineering
Eindhoven University of Technology
Eindhoven
Netherlands
g.witvoet@tue.nl

Gang Xu
PMA
Katholieke Universiteit Leuven
Leuven
Belgium
wolfgang.xu@gmail.com

Hui Yu
The faculty of Aerospace engineer
Control & Simulation
Delft
Netherlands
h.yu@tudelft.nl

Francisca Zamorano
Service d'Automatique
Faculté Polytechnique de Mons
Mons
Belgium
francisca.zamorano@fpms.ac.be

Solomon Zegeye
DCSC
TU Delft
Delft
Netherlands
s.k.zegeye@tudelft.nl

Part 5

Overview Program

Monday March 16, 2009

11 :25 – 11 :30	Pierre le Grand <i>Opening</i>				
11 :30 – 12 :30	Pierre le Grand "Binet-Cauchy Kernels for the Recognition of Visual Dynamics" René Vidal (Johns Hopkins University, USA)				
12 :30 – 14 :00	Lunch				
Room	Pierre le Grand	Source de la Reine	Wellington	Pouhon Pia	Groesbeeck
MoA	MoA01 <i>Identification 1</i>	MoA02 <i>Synchronization and clustering</i>	MoA03 <i>Control for teleoperation</i>	MoA04 <i>Estimation for biochemical processes</i>	MoA05 <i>Computational methods</i>
14 :00 – 14 :25	Huyck	Oguchi	Raaij	Stein	Onclinx
14 :25 – 14 :50	Widanage	Mauroy	Barbé	Fey	Samir
14 :50 – 15 :15	Keesman	De Smet	Willaert	Rocha-Cózatl	Lageman
15 :15 – 15 :40	Blom	Steur	Vander Poorten	Van Derlinden	Vanbiervliet
15 :40 – 16 :05	Tejada	Sacré	Delwiche	Mesbah	Gumusoy
16 :05 – 16 :30	Vandermot	Drion	Franken	Verhulst	van Dijk
16 :30 – 17 :00	Coffee break				
MoB	MoB01 <i>Model reduction</i>	MoB02 <i>Model-free control</i>	MoB03 <i>Fault detection applications</i>	MoB04 <i>Humanoid robotics</i>	MoB05 <i>Distributed control</i>
17 :00 – 17 :25	Mutsaers	Fonteneau	Gins	Visser	Doan
17 :25 – 17 :50	Besselink	Aladagli	Vanlaer	Daye	Bastin
17 :50 – 18 :15	Naeem	Dewasme	Hennen	Crevecoeur	Ezzeldin
18 :15 – 18 :40		den Hamer	Gálvez	van Oort	Retamal
19 :30 –	Dinner				

Tuesday March 17, 2009

Room	Pierre le Grand	Source de la Reine	Wellington	Pouhon Pia	Groesbeeck
TuA	TuA01 <i>Stochastic estimation and decision making</i>	TuA02 <i>Nonlinear control</i>	TuA03 <i>Advanced actuation and sensing</i>	TuA04 <i>Biochemical processes</i>	TuA05 <i>Control in networks</i>
8 :30 – 8 :55	Defourny	Dirksz	van der Hoeven	Vries	Lin
8 :55 – 9 :20	Busschaert	van Gils	van Bree	Mailier	Marinica
9 :20 – 9 :45	Plaza	Abouzaid	Vo-Minh	Cappuyns	van Keulen
9 :45 – 10 :10	Jouini	Favache	van Hulzen	Bauwens	Bshara
10 :10 – 10 :35	Tejada Ruiz	Polat	Achterberg	D'Huys	Donkers
11 :00 – 12 :30	Pierre le Grand <i>"Distributed control of Robotic Networks (Part 1)"</i> Jorge Cortés and Sonia Martínez (University of California at San Diego, USA)				
12 :30 – 14 :00	Lunch				
14 :00 – 14 :15	Pierre le Grand DISC PhD Thesis Award 2008 and DISC Certificates				
14 :15 – 15 :45	Pierre le Grand <i>"Distributed control of Robotic Networks (Part 2)"</i> Jorge Cortés and Sonia Martínez (University of California at San Diego, USA)				
Room	Pierre le Grand	Source de la Reine	Wellington	Pouhon Pia	Groesbeeck
TuB	TuB01 <i>Distributed parameter systems</i>	TuB02 <i>Nonlinear control 2</i>	TuB03 <i>Aerospace</i>	TuB04 <i>Biochemical robotics</i>	TuB05 <i>Consensus and cooperative control</i>
16 :15 – 16 :40	Voss	Efimov	van Kampen	Buttafuoco	Delvenne
16 :40 – 17 :05	Van Erdeghe	Muhammad	de Weerd	Zandsteeg	Yu
17 :05 – 17 :30	Foubert	Alvarez-Aguirre	Yu	André	Viswanadha Reddy
17 :30 – 17 :55	Visiers	Khalate	de Visser	Verspecht	Kostic
17 :55 – 18 :20	Djordjevic	Coutinho	Van de Walle	Wassink	Naus
18 :20 – 18 :45	Witvoet				Rogge
19 :30 –	Dinner				

Wednesday March 18, 2009

Room	Pierre le Grand	Source de la Reine	Wellington	Pouhon Pia	Groesbeeck
WeA	WeA01 <i>Identification 2</i>	WeA02 <i>System Theory</i>	WeA03 <i>Automotive applications</i>	WeA04 <i>Methods for computational biology</i>	WeA05 <i>Optimization for learning and control</i>
8 :30 – 8 :55	Rentmeesters	Besseling	van der Meulen	Lauwers	Van den Broeck
8 :55 – 9 :20	Lataire	Nemcova	Zegeye	Omony	Decré
9 :20 – 9 :45	Vanbeylen	van Willigenburg	Saerens	Meyer	Ronde
9 :45 – 10 :10	Van Mulders	Tóth	Evers	Zamorano	Paszke
10 :10 – 10 :35	Reynders	Veenman	Gerard	Journée	Volckaert
10 :35 – 11 :00	Barbé	Engwerda	van der Laan	Bonilla	Depraetere
11 :30 – 12 :30	Pierre le Grand <i>"Control of ensembles"</i> Navin Khaneja (Harvard University, USA)				
12 :30 – 13 :50	Lunch				
Room	Pierre le Grand	Source de la Reine	Wellington	Pouhon Pia	Groesbeeck
WeB	WeB01 <i>Advanced application modeling</i>	WeB02 <i>Modeling and control of chemical processes</i>	WeB03 <i>Power systems</i>	WeB04 <i>Artificial and living vision systems</i>	WeB05 <i>Control of vibrations</i>
13 :50 – 14 :15	van Herpen	Wattamwar	Fonteneau-Belmudes	Coppe	Verschuren
14 :15 – 14 :40	Hodrea	Logist	Simon	Reilink	Pinte
14 :40 – 15 :05	Jayawardhana	Carlos	Damoiseaux	Leclercq	Kuiper
15 :05 – 15 :30	Kuindersma	Farahani	del Puerto-Flores	de Best	Witters
15 :30 – 15 :55	Gommé	Stolte	Skrylnik		Ding
16 :15 – 16 :30	Pierre le Grand Best Junior Presentation Award ceremony Closing				

